

Transactions of the ASME®

Technical Editor, **LEWIS T. WHEELER (1997)**

Department of Mechanical Engineering,
University of Houston,
Houston, TX 77204-4792

APPLIED MECHANICS DIVISION

Chairman, **C. T. HERAKOVICH**

Secretary, **T. HUGHES**

Associate Technical Editors,

R. ABEYARATNE (1997)

T. R. AKYLAS (1997)

J. L. BASSANI (1999)

R. BECKER (1998)

S. A. BERGER (1997)

I. M. DANIEL (1999)

W. J. DRUGAN (1997)

J. T. JENKINS (1999)

J. W. JU (1998)

V. KINRA (1999)

S. KYRIAKIDES (1997)

S. LICHTER (1998)

W. K. LIU (1999)

X. MARKENSCOFF (1997)

M. ORTIZ (1998)

N. C. PERKINS (1999)

J. N. REDDY (1998)

S. W. SHAW (1997)

M. SHINOZUKA (1997)

M. TAYA (1999)

BOARD ON COMMUNICATIONS

Chairman and Vice-President

R. MATES

OFFICERS OF THE ASME

President, **R. J. GOLDSTEIN**

Executive Director, **D. L. BELDEN**

Treasurer, **J. A. MASON**

PUBLISHING STAFF

Managing Director, Engineering

CHARLES W. BEARDSLEY

Director, Technical Publishing

PHILIP DI VIETRO

Managing Editor, Technical Publishing

CYNTHIA B. CLARK

Managing Editor, Transactions

CORNELIA MONAHAN

Production Coordinator

JUDITH SIERANT

Production Assistant

MARISOL ANDINO

Transactions of the ASME, Journal of Applied Mechanics
(ISSN 0021-8936) is published quarterly (Mar., June, Sept.,
Dec.) for \$210.00 per year by The American Society of
Mechanical Engineers, 345 East 47th Street, New York,
NY 10017.

Periodicals postage paid at New York, NY and additional
mailing office. POSTMASTER: Send address changes to
Transactions of the ASME, Journal of Applied Mechanics, c/o
THE AMERICAN SOCIETY OF MECHANICAL ENGINEERS,
22 Law Drive, Box 2300, Fairfield, NJ 07007-2300.

CHANGES OF ADDRESS must be received at Society
headquarters seven weeks before they are to be effective.
Please send old label and new address. PRICES: To
members, \$40.00, annually; to nonmembers, \$210.00. Add
\$30.00 for postage to countries outside the United States
and Canada.

STATEMENT from By-Laws. The Society shall not be
responsible for statements or opinions advanced in papers or
... printed in its publications (B7.1, Para. 3). COPYRIGHT ©
1997 by The American Society of Mechanical Engineers.

Authorization to photocopy material for internal or personal
use under circumstances not falling within the fair use
provisions of the Copyright Act is granted by ASME to
libraries and other users registered with the Copyright
Clearance Center (CCC), Transactional Reporting Service
provided that the base fee of \$3.00 per article is paid directly
to CCC, Inc., 222 Rosewood Drive, Danvers, MA 01923.
Request for special permission or bulk copying should be
addressed to Reprints/Permission Department. INDEXED by
Applied Mechanics Reviews and Engineering Information, Inc.
Canadian Goods & Services Tax Registration #126148048.

Journal of Applied Mechanics

Published Quarterly by The American Society of Mechanical Engineers

VOLUME 64 • NUMBER 2 • JUNE 1997

TECHNICAL PAPERS

- 257 Inverse Finite Element Characterization of Nonlinear Hyperelastic Membranes
S. K. Kyriacou, A. D. Shah, and J. D. Humphrey
- 263 Finite Element Analysis of Wrinkling Membranes
Seokwoo Kang and Seyoung Im
- 270 Weight Functions for Notches: Constructive and Variational Definition
H. O. K. Kirchner
- 275 Experimental Identification Technique of Vibrating Structures With Geometrical Nonlinearity
Kimihiro Yasuda, Keisuke Kamiya, and Munenobu Komakine
- 281 Unified Second-Order Stochastic Averaging Approach
M. Hijawi, N. Moschuk, and R. A. Ibrahim
- 292 Dynamic Substructuring of Damped Structures Using Singular Value Decomposition
R. Ohayon, R. Sampaio, and C. Soize
- 299 Exact Solutions for Simply Supported Laminated Piezoelectric Plates
P. Heyliger
- 307 On the Nonaxisymmetric Loading of Nonhomogeneous Annular Plates of Variable Thickness
Kai-yuan Yeh, Jien-huo Kue, and F. P. J. Rimrott
- 313 Wave Propagation in Poroelastic Media Saturated by Two Fluids
K. Tuncay and M. Y. Corapcioglu
- 321 Generalized Cross-Correlation Functions for Engineering Applications, Part I: Basic Theory
M. R. Belmont and A. J. Hotchkiss
- 327 Generalized Cross-Correlation, Part II: Discretization of Generalized Cross-Correlation and
Progress to Date in Its Implementation
M. R. Belmont, A. J. Hotchkiss, S. J. Maskell, and E. L. Morris
- 336 Asymptotics of Flexural Waves in Isotropic Elastic Plates
N. A. Losin
- 343 Closed-Form Forced Response of a Damped, Rotating, Multiple Disks/Spindle System
I. Y. Shen
- 353 A Comprehensive Energy Formulation for General Nonlinear Material Continua
A. Carini and O. De Donato
- 361 Simulation of Rough, Elastic Contacts
J. J. Kalker, F. M. Dekking, and E. A. H. Vollebregt
- 369 On Balance and Variational Formulations of the Equation of Motion of a Body Deploying Along
a Cable
E. B. Crellin, F. Janssens, D. Poelaert, W. Steiner, and H. Troger
- 375 Energy Release Rates for an Interface Crack Embedded in a Laminated Beam Subjected to
Three-Point Bending
M. Toya, M. Aritomi, and A. Chosa
- 383 Coefficient of Restitution for Collinear Collisions of Elastic-Perfectly Plastic Spheres
C. Thornton
- 387 Criticality of Damping in Multi-Degree-of-Freedom Systems
A. Bhaskar
- 394 Dynamic Analysis of the Axially Moving String Based on Wave Propagation
C. A. Tan and S. Ying
- 401 Nondimensional Parameters for Geometric Nonlinear Effects in Pressurized Cylinders With Axial
Cracks
H. T. Budiman and P. A. Lagace
- 408 Free-Edge Stress Singularity in a Two-Dimensional Unidirectional Viscoelastic Laminate Model
Sang Soon Lee
- 415 Shakedown Analysis for Trusses and Frames
Pham Duc Chinh
- 420 An Analysis of the Plane-Strain Compression of Viscoplastic Materials
M. J. Adams, B. J. Briscoe, G. M. Corfield, C. J. Lawrence, and T. D. Papathanasiou

(Contents continued on outside back cover)

CONTENTS (CONTINUED)

BRIEF NOTES

- | | | |
|---|------------|---|
| Contact Pressures as an Elastic Roller Crosses a Scratch
J. A. Greenwood | 425 | 435 On Pala's Method for Plastic Bending With Torsion
P. Oberweis and M. Zyczkowski |
| On the Problem of Equilibrium Length of a Bridged Crack
N. Morozov, M. Paukshto, and N. Ponikarov | 427 | 437 Elastic Tensile Stresses Beneath Perfectly Plastic Indentation Fields
D. M. Stump and V. G. Hart |
| Simultaneous Triangularization of the Coefficients of Linear Systems
W. C. Lee and F. Ma | 430 | 438 A Kelvin Theorem and Partial Work of Impulsive Forces
A. P. Ivanov |
| Stress Field Around Holes in Antiplane Shear Using Complex Variable
Boundary Element Method
S. I. Chou | 432 | 440 Finite Strain Elastostatics With Stiffening Materials: A Constrained Mini-
mization Model
S. J. Hollister, J. E. Taylor, and P. D. Washabaugh |

ERRATUM

- 374** Linear Complementary Formulations Involving Frictional Contact for Elasto-Plastic Deformable Bodies, by Maocheng Li, Desong Sha, and K. K. Tamma, and published in the March 1997 issue of the *Journal of Applied Mechanics*

ANNOUNCEMENTS AND SPECIAL NOTES

- | | |
|------------|---|
| 274 | Finite Element Books Bibliography on Internet |
| 280 | Change of Address Form |
| 443 | Worldwide Mechanics Meetings List |
| 446 | Information for Authors |

S. K. Kyriacou
Assoc. Mem. ASME.

A. D. Shah

J. D. Humphrey¹
Mem. ASME.

Department of Mechanical Engineering,
The University of Maryland,
Baltimore, MD 21250

Inverse Finite Element Characterization of Nonlinear Hyperelastic Membranes

It is advantageous in mechanics to identify experiments that correspond to tractable boundary value problems—this facilitates data reduction and interpretation. Increasingly more situations are arising, however, wherein experimentalists cannot dictate the geometry or applied loads during testing. Inverse finite element methods are, therefore, becoming essential tools for calculating material parameters. In this paper, we present numerical and experimental results that show that one such inverse finite element method is very useful in characterizing the mechanical behavior of neo-Hookean (rubber) membranes subjected to axisymmetric and nonaxisymmetric finite inflations.

Introduction

One of the final steps in any constitutive formulation is determination of the numerical values of the material parameters. Most often, parameter estimation is accomplished using data from experiments that correspond to tractable boundary value problems—this greatly facilitates data reduction and analysis. Two of the most convenient tests in finite elasticity are in-plane biaxial stretching of a thin rectangular sheet and combined extension and torsion of a solid cylindrical rod (Green and Adkins, 1970). When the material of interest can be cut or fabricated in the requisite geometry, one can perform these “preferred” tests and thereby determine material parameters in a straightforward manner.

There are, however, increasingly more situations wherein one has little or no control over the geometry of, or applied loads acting on, the material of interest. Examples include tests on biological tissues whose geometry is dictated by nature (e.g., aneurysms) as well as nondestructive evaluations of the material properties of a structure in its service environment. Hence, there is a need for nontraditional methods for characterizing the behavior of materials when the associated boundary value problem is complex. One such approach is the *inverse finite element method*, which was introduced by Kavanagh and Clough (1971). Here, we present new results from a combined numerical and experimental validation study that show that axisymmetrically and nonaxisymmetrically inflated neo-Hookean membranes can be well characterized using the inverse finite element method.

Computational and Experimental Methods

Parameter Estimation. Fundamental to determining values of material parameters from data is a good regression algorithm. Of the available approaches (e.g., steepest descent, Newton’s method), we prefer the Levenberg-Marquardt method,

which has been shown to be robust in finite strain applications in rubber elasticity and biomechanics (e.g., Twizell and Ogden, 1983; Humphrey et al., 1990, 1992). Briefly, one minimizes an objective function e , in a least-squares sense, where

$$e = \sum_{k=1}^m [(y_i(\mathbf{b}) - y_e) \cdot (y_i(\mathbf{b}) - y_e)]_k. \quad (1)$$

Herein, y_e is a vector of “experimentally measurable” quantities (e.g., surface marker positions or in-plane stress resultants), y_i contains the associated “theoretically determined” quantities, \mathbf{b} is a vector containing the (yet unknown) material parameters, and m is the number of measurements. Values of \mathbf{b} are determined via

$$(\mathbf{J}^T \mathbf{J} + \gamma \mathbf{I})(\mathbf{b}^{(i+1)} - \mathbf{b}^{(i)}) = -\mathbf{J}^T(\mathbf{y}_i - \mathbf{y}_e)^{(i)}, \quad (2)$$

where $\mathbf{J} = (\partial y_i / \partial \mathbf{b})^{(i)}$, i is an iteration counter, and γ is the Marquardt parameter. We calculated J using a forward difference method, and used a public domain routine `leasqr.m` (by R. Shrager) to perform the estimations. Determination of y_i via finite elements constitutes an inverse finite element method.

Finite Element Calculations. Our methods for solving axisymmetric and nonaxisymmetric finite inflations of isotropic and orthotropic hyperelastic membranes are described elsewhere (Kyriacou and Humphrey, 1996; Kyriacou et al., 1996). Briefly, the governing (virtual work) equation is

$$\int_{\Omega_0} (\delta w) dA - \int_{\Omega} (P \mathbf{n} \cdot \delta \mathbf{x}) da = 0, \quad (3)$$

where w is a strain-energy function defined per unit initial surface area A (and is related to W defined per unit volume by $w = WH$, where H is the undeformed thickness; Pipkin, 1968), P is the distension pressure, \mathbf{n} an outward unit normal to the membrane in the current configuration, $\delta \mathbf{x}$ the virtual changes in position, Ω_0 the original domain, and Ω the current domain. Finite element equations result from discretization of the domain and introduction of suitable interpolation functions: herein, axisymmetric and nonaxisymmetric problems were solved using isoparametric three-noded quadratic and four-noded bilinear elements, respectively, and the associated standard two and four-point quadrature rules. Because of inherent geometric and material nonlinearities, (3) yields a system of nonlinear algebraic equations, which can be represented as $\mathbf{g}(\mathbf{q}) = \mathbf{0}$, where \mathbf{q} represents the vector of (unknown) nodal positions. This equation admits an iterative Newton-Raphson solution, viz.,

¹ Address correspondence to Jay D. Humphrey, Ph.D., Department of Mechanical Engineering, University of Maryland, 1000 Hilltop Circle, Baltimore, MD 21250. Telephone: (410) 455-3309; Fax: (410) 455-1052; e-mail: humphrey@umbc2.umbc.edu.

Contributed by the Applied Mechanics Division of THE AMERICAN SOCIETY OF MECHANICAL ENGINEERS for publication in the ASME JOURNAL OF APPLIED MECHANICS.

Discussion on this paper should be addressed to the Technical Editor, Professor Lewis T. Wheeler, Department of Mechanical Engineering, University of Houston, Houston, TX 77204-4792, and will be accepted until four months after final publication of the paper itself in the ASME JOURNAL OF APPLIED MECHANICS.

Manuscript received by the ASME Applied Mechanics Division, Dec. 23, 1995; final revision, Sept. 18, 1996. Associate Technical Editor: I. M. Daniel.

$$\mathbf{K}(\mathbf{q}^{(i)})[\mathbf{q}^{(i+1)} - \mathbf{q}^{(i)}] = -\mathbf{g}(\mathbf{q}^{(i)}), \quad (4)$$

where $\mathbf{K} = \partial \mathbf{g} / \partial \mathbf{q}$ is the tangent matrix and i an iteration counter. We evaluated \mathbf{K} analytically to obtain quadratic convergence—see Kyriacou et al. (1996) for details. More important here, however, note that the finite element method yields the current position of each node, from which we can interpolate to obtain the position \mathbf{x}_i of any point on the membrane. Thus, \mathbf{y}_i in (1) is taken to be²,

$$\mathbf{y}_i = (x_{1i}^{(1)}, \dots, x_{1i}^{(n)}, x_{2i}^{(1)}, \dots, x_{2i}^{(n)}, x_{3i}^{(1)}, \dots, x_{3i}^{(n)}) \quad (5)$$

where x_{1i} is a Cartesian component and the superscript denotes a “marker” number. The x_{3i} term is identically satisfied in axisymmetric inflations and not explicitly included in those regressions.

Analytic Axisymmetric Approach. For the special case of an axisymmetric inflation, the two governing differential equations,

$$\frac{d}{dr}(rT_1) = T_2, \quad \kappa_1 T_1 + \kappa_2 T_2 = P, \quad (6)$$

can be solved for the principal Cauchy stress resultants T_α ($\alpha = 1, 2$) in terms of the experimentally measurable uniform pressure P and principal curvatures κ_α (Green and Adkins, 1970; Hsu et al., 1994):

$$T_1 = \frac{P}{2\kappa_2}, \quad T_2 = \frac{P}{\kappa_2} \left(1 - \frac{\kappa_1}{2\kappa_2} \right), \quad (7)$$

where 1 and 2 denote meridional and circumferential directions, respectively. T_α are also easily calculated for a hyperelastic membrane given a form of w and values of the principal stretch ratios λ_α (Humphrey et al., 1992), as for example,

$$\mathbf{T} = \frac{2}{\det \mathbf{F}} \mathbf{F} \cdot \frac{\partial w}{\partial \mathbf{C}} \cdot \mathbf{F}^T \quad (8)$$

where \mathbf{F} is the two-dimensional deformation gradient tensor ($\mathbf{F} = \text{diag} [\lambda_1, \lambda_2]$ here) and $\mathbf{C} = \mathbf{F}^T \cdot \mathbf{F}$. An example w for a soft biological tissue is in Humphrey et al. (1992). For the Marquardt regression, therefore, it is convenient to let

$$\mathbf{y}_i = (T_{1i}^{(1)}, \dots, T_{1i}^{(n)}, T_{2i}^{(1)}, \dots, T_{2i}^{(n)}), \quad (9)$$

wherein the superscript again denotes different locations on the membrane (which are defined by sets of markers). It is important to recognize, therefore, that except for an inflation of a perfectly spherical membrane, data from different regions of a membrane at one equilibrium configuration represent the equivalent of “different strain protocols.” For example, the inflation of a flat circular membrane clamped around its periphery yields equibiaxial stretching at the pole, strip biaxial stretching at the clamped base, and a spectrum of proportional stretching tests between (Wineman et al., 1979; Hsu et al., 1994). Hence, performing a regression based on data from one point ($n = 1$) on a membrane at, say, m pressures is very different from using data from n locations at m configurations even when nm is equivalent; indeed, using data from “multiple protocols” in a single regression can yield improved estimates of the material parameters (Humphrey et al., 1990, 1992).

Membrane Inflation Experiments. Appropriate experimental devices and techniques are essential for determining values of material parameters. We recently constructed a triplane video-based system for performing finite strain inflation tests on biomembranes (Hsu et al., 1995). Briefly, this system

consists of a computer-controlled fluid pump, pressure transducers, computer-based data acquisition system, and three synchronized CCD cameras. Two “biplane” cameras, separated by a 45 deg angle, track the motions of three to six small markers that are affixed to the surface of any inflating membrane, whereas a third camera, mounted orthogonal to the plane containing the biplane cameras, monitors “the profile” at 15 equidistant locations along axisymmetric specimens³. Marker tracking and edge detection are accomplished on-line at 15 Hz using custom correlation and threshold based algorithms, respectively. Spatial resolution was >0.05 mm. Finally, all positional data were fit (as a function of pressure) with smooth functions, from which regression data were obtained.

Two classes of experiments were performed at room temperature on thin (~ 0.18 mm) sheets of rubber taken from surgical gloves. Axisymmetric tests resulted by inflating (from underneath) initially flat, stress-free specimens through an 11 mm diameter circular orifice, whereas nonaxisymmetric tests resulted by inflating specimens through an elliptical orifice (major axis = 11 and minor axis = 6 mm); all specimens were clamped around their periphery and inflated at the same rate. Cyclic inflations were performed, using distilled water, to a maximum pressure of about 13 kPa in axisymmetric tests and 19 kPa in nonaxisymmetric tests. These inflations yielded principal stretches at the pole of about 1.3. Prior to testing, however, specimens were allowed to creep for two minutes (from an initial uniform expansion of about 1.4) at a constant pressure.

Form of the Strain Energy. The neo-Hookean W describes well the behavior of rubber over the modest range of finite stretch up to 1.3, thus it was employed herein. It is

$$W = c(I_1 - 3), \quad (10)$$

where c is a material parameter having units of stress and $I_1 = \text{tr } \mathbf{C}$ where \mathbf{C} is the three-dimensional right Cauchy-Green deformation tensor.

Axisymmetric Simulations. Prior to testing, we performed numerical simulations to identify certain preferred experimental conditions. That is, we used our finite element code to generate positional “data” for various axisymmetric inflations and a given value of the neo-Hookean parameter c . Gaussian noise was then created using a random number generator and introduced into the “data” to simulate potential experimental errors. The perturbed data were input (as \mathbf{y}_e) into the inverse finite element code which then estimated the value of c . This approach allowed comparisons of estimated and true values. For convenience, the problem was nondimensionalized: for example, the nondimensional pressure $P^* = PL/cH$, where L is a characteristic length scale (e.g., specimen radius, a), c the neo-Hookean material parameter, and H the undeformed thickness.

Results

Axisymmetric Simulations. Consider first the inflation of an initially flat circular membrane that was clamped at its periphery. Figure 1 shows the deformed configuration (solid line) for $P^* = 1.5$ and a nondimensional radius of 1. Positional data for nine “markers” (at initial radii of 0.1, 0.2, ..., 0.9; open circles) were generated by adding Gaussian noise (mean of 0.0 and standard deviation of 0.02) to a finite element solution from a ten-element mesh. Based on an initial guess of $P^* = 0.5$ (dotted line), the estimation yielded a value of $P^* = 1.510$ in seven iterations—the predicted marker positions and final deformed shape are shown by asterisks and a dashed line, respectively. All simulations yielded similar results.

² It is preferable to use positions in the objective function since they are calculated with the greatest accuracy in this “displacement”-based finite element solution.

³ Local strains can be calculated from the motions of sets of markers whereas both principal curvatures can be calculated from a single profile of an axisymmetric membrane (see Hsu et al., 1995).

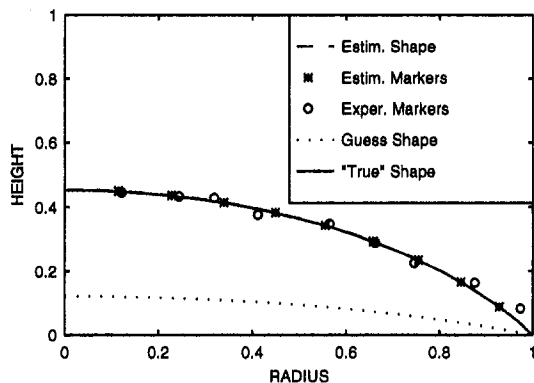


Fig. 1 Nondimensional specimen profile for an axisymmetric simulation: open circles denote marker positions (input data) that resulted from superimposing Gaussian noise on results from a standard finite element (FE) solution; the dotted line shows the FE solution based on an initial guess for c ; the dashed line shows the FE solution based on the Marquardt estimate for c ; asterisks show final predicted positions of the markers (circles); the dashed and solid lines coincide

Many studies have been based on marker positions or stretch ratios measured at only one point on an inflated membrane. Figure 2 shows predicted errors in the parameter estimation as a function of the placement of a single "marker." Each result represents a mean + SD for six estimations based on independently generated Gaussian noise, all other variables being the same as those in Fig. 1. Clearly, estimations based on a single marker were better if it was located close to the pole. It is preferable to collect data from more than one marker, however, and in general the more markers the better. Yet, experiments become more challenging as the number of markers increases, thus there is a need to identify minimum sets that yield reliable estimates. Figure 3 shows predicted errors in the parameter estimation as the number of evenly spaced markers was increased from 1 to 10 (recall that each marker supplies x_1 and x_2 information). As expected, the error decreased with increases in the number of markers, but six markers appeared sufficient in this case.

Because of material nonlinearity, the stiffness of an inflated membrane is different, in general, at each distension pressure. It is of interest, therefore, to determine how the magnitude of the pressure affects the estimation. Figure 4 shows that the error in the estimated parameter decreased with an increase in the pressure at which the data were generated (again, other variables are the same as in Fig. 2). Of course, estimations based on traditional stress-strain tests rely on data from multiple equilibrium configurations. Figure 5 shows that the error in the

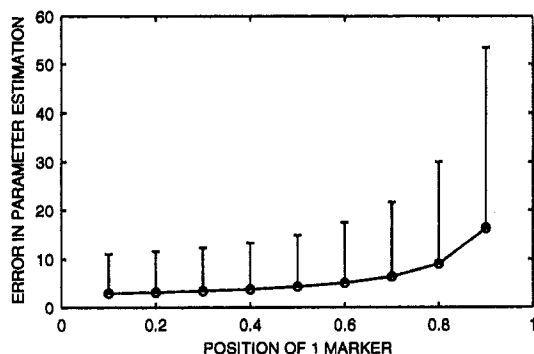


Fig. 2 Error in the estimated neo-Hookean parameter (i.e., $(c_{\text{est}} - c_{\text{true}})/c_{\text{true}}$) as a function of the position of one "tracking marker." Each result is given as mean + S.D. based on six independent simulations that resulted from superimposing different Gaussian errors on the input marker positions; position 0 denotes the pole, 1 the base.

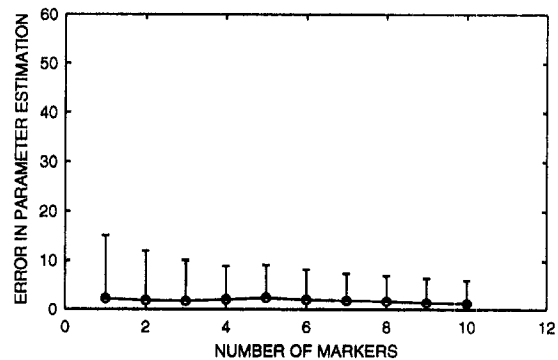


Fig. 3 Similar to Fig. 2, except for the number of markers tracked

estimated parameter tended to decrease with an increase in the number of equilibrium configurations. Nonetheless, for the case considered, one to two configurations were adequate for robust estimation; note that the maximum pressure $P^* = 1.5$ in each of these simulations.

As pointed out by Kavanagh and Clough (1971), inverse finite element methods can be very sensitive to experimental error. Hence, we performed multiple simulations (with $P^* = 1.5$ and six markers) for different levels of "experimental noise," all having a mean of 0.0 but standard deviations ranging from 0.05 to 0.0001. As expected, the error in the estimated parameter increased markedly with an increase in experimental noise (Fig. 6).

Axisymmetric Experiments. For the inverse finite element estimations we usually tracked six markers which were placed along a meridian⁴; for the analytical based estimations we tracked the entire profile plus three markers which formed a triplet (see Hsu et al., 1994, 1995). Figure 7 shows a typical result for a finite element estimation: open circles show the locations of six markers in each of two equilibrium configurations, dotted lines the predicted profiles of the membrane based on the initial parameter guess, asterisks the predicted locations of the six markers based on the final Marquardt estimated parameter, and dashed lines the associated final finite element predicted profiles. Results were similar for all seven such tests.

In contrast, estimations using the analytical approach allowed us to fit stress resultant versus principal stretch data in the traditional way. Figure 8 shows results for T_α versus λ_α for 25 successive equilibrium configurations ($P \in [0, 17.33 \text{ kPa}]$) for one representative test (note: the centroid of the triplet of markers was about 35 percent of the distance from the center). The

⁴Although it was impossible to place the markers along a single generator curve, knowledge of the three-dimensional positions allowed us to "rotate" each point to a single meridian.

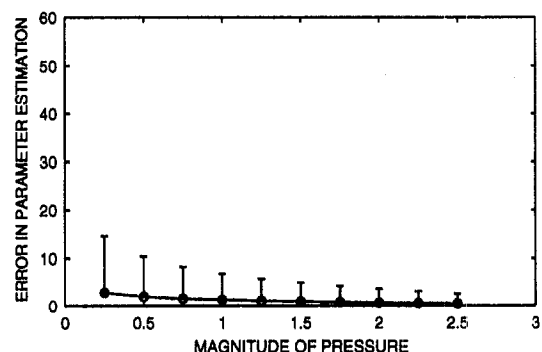


Fig. 4 Similar to Fig. 2, except for the magnitude of the nondimensional pressure P^* at which the estimation was performed

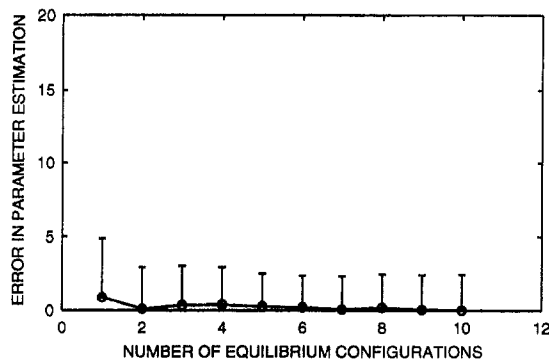


Fig. 5 Similar to Fig. 2, except for the number of equilibrium configurations used in the regression; the maximum $P^* = 1.5$ in each

initial guess for c was 2.85 kPa, and the final estimate was 200 kPa. Results were similar for all eight such experiments.

Nonaxisymmetric Experiments. For purposes of comparison, we tracked three to six markers on the initially elliptical membranes; because of nonaxisymmetry the x_1 , x_2 , and x_3 coordinate locations each gave independent information, hence tracking four markers was comparable to tracking six markers on the circular membrane. Though somewhat difficult to visualize, Figure 9 shows one-fourth of a single deformed configuration; the mesh consisted of 122 elements that were generated using the IDEAS software package. The dotted mesh shows the configuration based on the initial guess for c , whereas the dashed mesh shows the configuration corresponding to the final estimated parameter value. The five experimentally tracked markers (open circles) and their predicted positions (asterisks) are shown as well. Estimations using 17, 56, 122, and 233 elements suggested that the Marquardt solution converged with 56 to 122 elements: for example, the estimated c for one specimen was 161, 166, 167, and 167 kPa using these four meshes, respectively. For the specimen shown, the initial guess for c was 600 kPa and the final estimate was 220 kPa. Results were similar for all nine tests.

Overall, the mean values (\pm standard deviations) for all estimates of the neo-Hookean parameter c were 179 ± 8.6 kPa for the axisymmetric inverse finite element method, 185 ± 12.1 kPa for the analytic (axisymmetric) estimation, and 188 ± 18.8 kPa for the nonaxisymmetric inverse finite element method. Using standard analyses (e.g., Student's t -tests and ANOVA), we found no statistically significant difference between these three groups of results at a significance level of 0.05. As an additional check, however, we also performed a uniaxial stress-strain test on one specimen ($4 \times 40 \times 0.18$ mm in dimension) using another custom device in our laboratory. For a maximum stretch of 1.33, we found that $c = 177$ kPa, which fell within

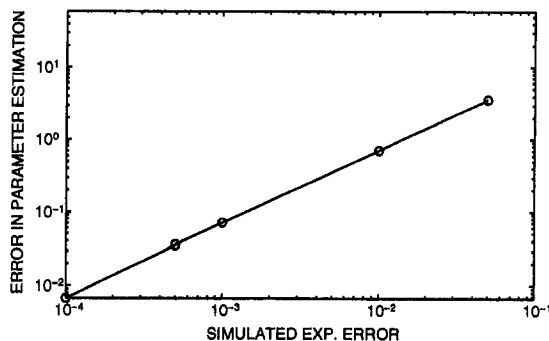


Fig. 6 Similar to Fig. 2, except for the amount of superimposed experimental error (mean of 0.0 but S.D. from 0.0001 to 0.05)

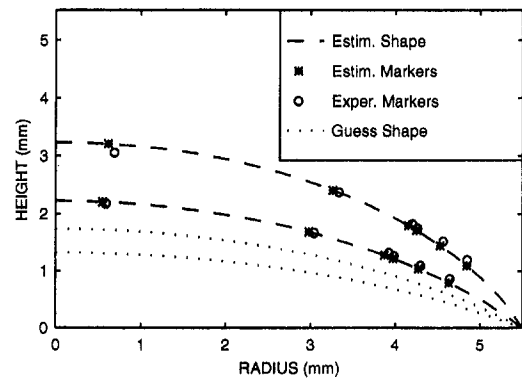


Fig. 7 Inverse finite element result based on experimental data for an axisymmetrically inflated rubber membrane; six markers were tracked and two equilibrium configurations were used. The dotted lines show deformed configurations corresponding to the guessed value of c , whereas the dashed lines reveal the predicted configuration based on the Marquardt estimate for c .

the range of values obtained using the inflation tests. Finally, it should be noted that all of these values of c were based on data collected during the loading portion of each cyclic test; because of slight hysteresis exhibited under cyclic loading, results based on data from the unloading portion were less (e.g., 157 in unloading versus 179 kPa in loading for one specimen) as expected.

Discussion

One motivation for the inverse finite element method presented herein was the need to determine membrane properties in situations wherein the boundary value problem is complex. For example, one goal in our laboratory is to quantify the mechanical behavior of intracranial saccular aneurysms, which are often irregularly shaped (Kyriacou and Humphrey, 1996). Nevertheless, a general method of parameter estimation can also be beneficial in "standard" testing situations. Recall, therefore, that axisymmetric membrane inflation tests have long been used to study the stress-strain behavior of rubber (see Treloar, 1944; Rivlin & Saunders, 1951). Yet, because of the nonuniform strain field, data are often still collected only at the pole (e.g.,

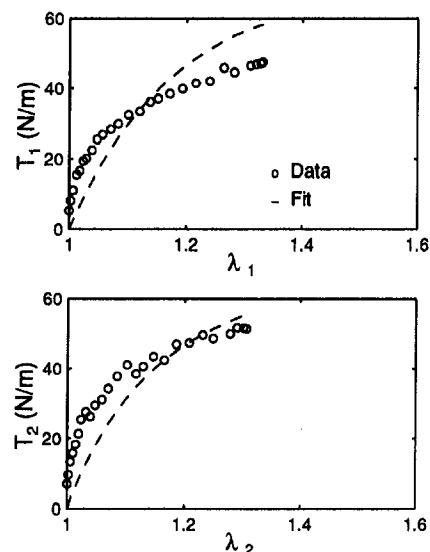


Fig. 8 Experimental data and fit for an analytic-based estimation for an axisymmetrically inflated membrane. T_1 and λ_1 are the principal stress resultants and stretch ratios, respectively. Results were similar for T_2 versus λ_2 and T_2 versus λ_1 .

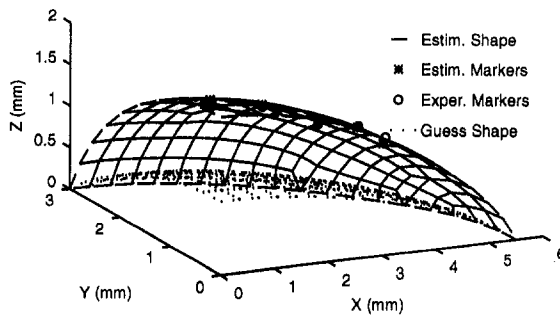


Fig. 9 One-quarter of a nonaxisymmetrically inflated membrane (initially a flat elliptical shape); the dotted line shows the FE calculated profile associated with the initial guess for c , whereas the dashed line shows the calculated profile associated with the Marquardt estimate for c . Actual data are shown by open circles.

see Xu and Mark, 1990; Ling et al., 1993), where $\lambda_1 \equiv \lambda_2$ and $T_1 \equiv T_2$. The associated parameter estimations are thus limited because one obtains “one-dimensional” information. Our simulations showed the utility of using multiple markers, and that this can be accomplished using the inverse finite element method.

One reason for collecting data only at the pole is that it is difficult to measure the principal curvatures κ_a (recall Eq. (7)) at multiple meridional locations. This is evidenced by reports wherein curvatures were inferred (during incremental tests) from multiple rods that were pushed up by the deforming membrane (Miller et al., 1979) or pictures from a single camera and multiple mirrors (Bylski et al., 1986). Although recent methods using shadow moiré (Ling et al., 1993) or computerized edge detection (Hsu et al., 1995) allow curvatures to be measured directly, this remains nontrivial and subject to experimental error—curvatures are calculated from derivatives of the measured profile. Indeed, the recent paper by Yongxiang and Jis-heng (1994) appears to be motivated, in part, by this difficulty. Hence, a major advantage of the inverse finite element method, regardless of the geometry of the membrane, is that one only needs the distension pressure and marker positions at multiple locations on the surface of the specimen, not numerically calculated derivatives based on marker positions.

For nonaxisymmetric inflations, the inverse finite element method is not just convenient, it is indispensable—there are no available analytical solutions to use in the regression algorithm. There are, however, only a few reported finite element solutions for large strain nonaxisymmetric membrane inflations (e.g., Zamani et al., 1989; Charrier et al., 1989; Nied et al., 1990; Gruttmann and Taylor, 1992; Kyriacou et al., 1996), and apparently no previous report of a fully nonlinear nonaxisymmetric finite element code that has parameter estimation capabilities. Thus, our numerical and experimental results show, for the first time, that estimation can be accomplished equally well in axisymmetric and nonaxisymmetric finite inflations, at least for neo-Hookean materials.

This study is not without limitations, however. The primary shortcoming was the need to restrict our attention to a one-parameter (neo-Hookean) material. Our test system was designed specifically to test intracranial saccular aneurysms, which have maximum biaxial extensions at the pole of about 1.3 (Kyriacou and Humphrey, 1996), thus we restricted the maximum inflations herein to the same range⁵ (to ensure maximum resolution). This, in turn, compromised our ability to test multiparameter constitutive relations like Mooney-Rivlin, Hart-Smith, etc. (see Ling et al., 1993 for different forms of W).

⁵ This moderate inflation prevented limit point instabilities, which are often observed in similar tests—e.g., see Treloar (1944) wherein maximum stretches were about 5.8 at the pole.

That is, at these moderate stretches, the neo-Hookean relation was an adequate descriptor of the observed behavior (as expected) whereas a Mooney-Rivlin relation was over-parameterized based on the correlation matrix for the parameters (Humphrey et al., 1990). Clearly, testing the robustness of multiparameter constitutive relation is a more stringent test of an estimation method, and experimental errors will likely play a more detrimental role in those cases. There is, therefore, a need for additional simulations and experiments to address this issue.

Second, it should be noted that our objective was to show the efficacy of the inverse finite element method, not to rigorously quantify the behavior of a particular rubber membrane. It was for this reason that we did not impose strict control on specimen selection (to minimize specimen-to-specimen variations). That is, specimens were obtained from either the wrist or palm region of surgical gloves taken from different boxes, albeit of the same brand. Moreover, tests were conducted over a period of months, thus specimens were of different “ages.” Although protected from direct exposure to light (except during testing), changes in lab conditions such as temperature, humidity, etc., were not controlled or recorded. Nonetheless, the aforementioned standard deviations in the estimated parameter from multiple specimens were not altogether unreasonable in comparison to variations reported in the literature—pilot experiments on the same day and the same specimen revealed only slight variations in c (e.g., 180 versus 183 kPa) due to simply removing, remounting and retesting the sample, thereby supporting that the aforementioned standard deviations primarily reflected specimen-to-specimen differences.

In summary, parameter estimation is an essential step in the formulation of a constitutive relation for a hyperelastic membrane. Although many aspects of parameter estimation were not directly addressed herein—for example, the need to limit the parameter search space so as to respect constitutive restrictions from the second law of thermodynamics and experimental inequalities, to ensure that the functional form of the final relation is not over-parameterized, to perform parameter sensitivity analyses, and to identify confidence intervals for estimations based on multiple data sets and specimens (e.g., see Humphrey et al., 1990)—we submit that the inverse finite element method is an indispensable tool for quantifying the mechanical behavior of nonlinear hyperelastic membranes and designing requisite experiments.

Acknowledgments

Financial support from the National Science Foundation (PYI:BCS 9157798) and the American Heart Association (MDSG-1395) are gratefully acknowledged.

References

- Bylski, D. I., Kriewall, T. J., Akkas, N., and Melvin, J. W., 1986, “Mechanical Behavior of Fetal Dura Mater Under Large Deformation Biaxial Tension,” *Journal of Biomechanics*, Vol. 19, pp. 19–26.
- Charrier, J. M., Shrivastava, S., and Wu, R., 1989, “Free and Constrained Inflation of Elastic Membranes in Relation to Thermoforming—Non-axisymmetric Problems,” *Journal of Strain Analysis*, Vol. 34, pp. 55–74.
- Green, A. E., and Adkins, J. E., 1970, *Large Elastic Deformations*, Clarendon Press, Oxford.
- Gruttmann, F., and Taylor, R. L., 1992, “Theory and Finite Element Formulation of Rubberlike Membrane Shells Using Principal Stretches,” *International Journal for Numerical Methods in Engineering*, Vol. 35, pp. 111–1126.
- Hsu, F. P. K., Schwab, C., Rigamonti, D., and Humphrey, J. D., 1994, “Identification of Response Functions for Nonlinear Membranes via Axisymmetric Inflation Tests: Implications for Biomechanics,” *International Journal of Solids and Structures*, Vol. 31, pp. 3375–3386.
- Hsu, F. P. K., Downs, J., Liu, A. M. C., Rigamonti, D., and Humphrey, J. D., 1995, “A Triplane Video-Based Experimental System for Studying Axisymmetrically Inflated Biomembranes,” *IEEE Transactions for Biomedical Engineering*, Vol. 42, pp. 442–449.
- Humphrey, J. D., Strumpf, R. K., and Yin, F. C. P., 1990, “Determination of a Constitutive Relation for Passive Myocardium: II. Parameter Estimation,” *ASME Journal of Biomechanical Engineering*, Vol. 112, pp. 340–346.

- Humphrey, J. D., Strumpf, R. K., and Yin, F. C. P., 1992, "A Constitutive Theory for Biomembranes: Application to Epicardium," *ASME Journal of Biomechanical Engineering*, Vol. 114, pp. 461–466.
- Kavanagh, K. T., and Clough, R. W., 1971, "Finite Element Applications in the Characterization of Elastic Solids," *International Journal of Solids and Structures*, Vol. 7, pp. 11–23.
- Kyriacou, S. K., and Humphrey, J. D., 1996, "Influence of Size, Shape, and Properties on the Mechanics of Axisymmetric Saccular Aneurysms," *Journal of Biomechanics*, Vol. 29, pp. 1015–1022.
- Kyriacou, S. K., Schwab, C., and Humphrey, J. D., 1996, "Finite Element Analysis of Nonlinear Orthotropic Hyperelastic Membranes," *Computational Mechanics*, Vol. 18, pp. 269–278.
- Ling, Y., Engel, P. A., Brodsky, W. L., and Guo, Y., 1993, "Finding the Constitutive Relation for a Specific Elastomer," *ASME Journal of Electronic Packaging*, Vol. 115, pp. 329–336.
- Miller, C. E., Lavery, J. P., and Donnelly, T. A., 1979, "Determination of Elastic Parameters for Human Fetal Membranes," *Journal of Rheology*, Vol. 23, pp. 57–78.
- Nied, H. F., Taylor, C. A., and Delorenzi, H. G., 1990, "Three-dimensional Finite Element Simulation of Thermoforming," *Polymer Engineering and Science*, Vol. 30, pp. 1314–1322.
- Pipkin, A. C., 1968, "Integration of an Equation in Membrane Theory," *ZAMP*, Vol. 19, pp. 818–819.
- Rivlin, R. S., and Saunders, D. W., 1951, "Large Elastic Deformations of Isotropic Materials. VII, Experiments on the Deformation of Rubber," *Philosophical Transactions of the Royal Society, Series A*, Vol. 243, pp. 251–288.
- Treloar, L. R. G., 1944, "Strains in an Inflated Rubber Sheet, and the Mechanism of Bursting," *Institute of Rubber Industry Transactions*, Vol. 19, pp. 201–212.
- Twizell, E. H., and Ogden, R. W., 1983, "Non-linear Optimization of the Material Constants in Ogden's Stress-deformation Function for Incompressible Isotropic Elastic Materials," *Journal of the Australian Mathematics Society*, Vol. B24, pp. 424–434.
- Wineman, A., Wilson, D., and Melvin, J. W., 1979, "Material Identification of Soft Tissue Using Membrane Inflation," *Journal of Biomechanics*, Vol. 12, pp. 841–850.
- Xu, P., and Mark, J. E., 1990, "Biaxial Extension Studies Using Inflation of Sheets of Unimodal Model Networks," *Rubber Chemistry and Technology*, Vol. 63, pp. 276–284.
- Yongxiang, G., and Jisheng, L., 1994, "The Study on Mechanical Parameters of Finite Deformation of Membranes," *ASME JOURNAL OF APPLIED MECHANICS*, Vol. 61, pp. 202–204.
- Zamani, N. G., Watt, D. F., and Esteghamatian, M., 1989, "Status of the Finite Element Method in the Thermoforming Process," *International Journal of Numerical Methods in Engineering*, Vol. 28, pp. 2681–2693.

Finite Element Analysis of Wrinkling Membranes

Seokwoo Kang
Graduate Assistant.

Seyoung Im
Professor,
Mem. ASME.

Department of Mechanical Engineering,
Korea Advanced Institute of
Science and Technology (KAIST),
Science Town, Taejeon 305-701,
South Korea

A new iterative scheme is proposed for finite element analysis of wrinkling or tension structures. The scheme is based upon the observation that there exists an invariant relationship, due to the uniaxial tensile stress state of wrinkling, between some of the strain components referred to the local frame aligned with wrinkling in a region where wrinkling occurs. This enables us to update the stress state and the internal forces correctly taking into account the existence of wrinkling. The finite element implementation of the scheme is straightforward and simple, and only minor modifications of the existing total Lagrangian finite element codes for membranes are needed. The validity of the scheme is demonstrated via numerical examples for the torsion of a membrane and the quasi-static inflation of an automotive airbag, both made of isotropic or anisotropic elastic membranes. The examples suggest that the present iterative scheme has a good convergence characteristic even for a large loading step.

1 Introduction

Analysis of wrinkling or tension structures, such as flexible membranes or fabric structures, has attracted substantial attention because of their increasing application in marine, space, and terrestrial technology, and more specifically because of the simulation of airbags as a protection mechanism for drivers and passengers in automotive industry. There have been many works, theoretical and numerical, on the analysis of such wrinkling structures (see, for example, Wagner, 1929; Reissner, 1938; Kondo et al., 1955; Wu et al., 1981; Roddeman et al., 1987; Steigmann and Pipkin, 1989).

In this work, we introduce another scheme for the wrinkling analysis that can be used in the finite element analysis of anisotropic membranes and isotropic membranes. We take into account the possibility that the membrane may have finite rotations. The scheme is based upon the observation that a local region of wrinkling is in the state of the uniaxial tension, and that the orientation and the magnitude of this uniaxial tension can be obtained from an invariant relationship between the normal strain component in the direction of the local uniaxial tension and the shear strain component in the presence of wrinkling. The scheme enables us to determine the wrinkling orientation in a straightforward manner and to reconstruct the stress state properly for wrinkled regions, so that the correct internal forces may be evaluated. We implement this scheme into a geometrically nonlinear finite element analysis using the total Lagrangian formulation. The finite element implementation of the scheme is very simple. We do not need any special finite elements, but only minor modifications of the existing total Lagrangian finite element codes for membranes are needed. We demonstrate the validity of the proposed scheme through numerical examples for an isotropic and for an orthotropic material, such as, the torsion of a membrane and the quasi-static inflation of circular airbags. Some remarks are made regarding the convergence behavior of the solution scheme depending upon the size of a loading step.

2 Basic Equations and Wrinkling Analysis

Models describing the mechanical behavior of wrinkling membranes are usually based on the assumption that membranes have zero flexural stiffness. For the analysis of membranes with wrinkled regions, it is necessary to have some fundamental assumptions as follows: (i) The configuration of the wrinkled region is controlled by negligibly small bending stiffness of the membrane. The exact shape of the membrane after wrinkling is not definable with only membrane theory. To describe the average membrane deformation that would be obtained after the wrinkles have been removed from the midplane, we define the fictitious nonwrinkled membrane which has the smooth surface as shown in Fig. 1. This fictitious nonwrinkled membrane gives only the average deformation. (ii) Because the membrane is not able to support any compressive stresses, the membrane will wrinkle at once when a negative stress is about to appear. (iii) The membrane is in the state of plane stress.

In a small material element which is under locally homogeneous deformation in the presence of wrinkling, the stress is locally in the state of the uniaxial tension, and in the deformed configuration the direction of the uniaxial tension is perpendicular to the wrinkling direction. As will be shown, the amount of wrinkling does not affect the local uniaxial tension state at all. To describe deformations of a membrane, we rely upon the Cartesian coordinate systems as shown in Fig. 1. Let (X_1, X_2, X_3) denote a Cartesian coordinate of a material point in the undeformed configuration κ_0 , and (x_1, x_2, x_3) a Cartesian coordinate of a material point in the deformed configuration $\kappa(t)$. For dealing with wrinkling, we take a local frame (\hat{X}_1, \hat{X}_2) in κ_0 such that the orientation of the \hat{X}_1 -axis is lined up with the material line element of κ_0 that is to be along the uniaxial tensile direction in the presence of wrinkling in $\kappa(t)$. Then the orientation of the \hat{X}_2 -axis is lined up with the material line element of κ_0 that is normal to the orientation of the \hat{X}_1 -axis. Moreover, we choose a local frame (\hat{x}_1, \hat{x}_2) defined on the fictitious nonwrinkled membrane in $\kappa(t)$ such that the \hat{x}_1 -axis is along the uniaxial tension direction in the presence of wrinkling and the \hat{x}_2 -axis is then aligned with the wrinkling direction. Note that a material line element along the \hat{X}_1 -axis in κ_0 is aligned with the \hat{x}_1 -axis in $\kappa(t)$. However, a material line element along the \hat{X}_2 -axis in κ_0 is not mapped to be aligned with the \hat{x}_2 -axis, which is along the wrinkling direction in $\kappa(t)$, unless the shear strain with respect to the (\hat{X}_1, \hat{X}_2) frame vanishes. Let $\mathbf{E}_I, \hat{\mathbf{E}}_I, \mathbf{e}_I$, and $\hat{\mathbf{e}}_I$ denote the unit base vectors along the coordinate axes X_I, \hat{X}_I, x_I , and \hat{x}_I , respectively. Assuming that

Contributed by the Applied Mechanics Division of THE AMERICAN SOCIETY OF MECHANICAL ENGINEERS for publication in the ASME JOURNAL OF APPLIED MECHANICS.

Discussion on this paper should be addressed to the Technical Editor, Professor Lewis T. Wheeler, Department of Mechanical Engineering, University of Houston, Houston, TX 77204-4792, and will be accepted until four months after final publication of the paper itself in the ASME JOURNAL OF APPLIED MECHANICS.

Manuscript received by the ASME Applied Mechanics Division, Feb. 8, 1996; final revision, Aug. 26, 1996. Associate Technical Editor: W. K. Liu.

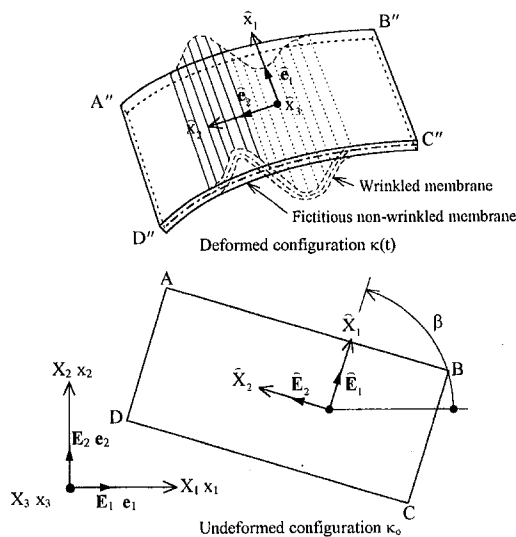


Fig. 1 The fictitious nonwrinkled membrane and coordinate systems

the Green strain \mathbf{E} is small that the second Piola-Kirchhoff stress \mathbf{S} may be approximated by the linear relationship with the Green strain, we can write the stress-strain relations referred to the $\hat{X}_1 - \hat{X}_2$ coordinate system as $S^{IJ} = C^{IJKL} E_{KL}$, or in the "collapsed representation,"

$$\begin{Bmatrix} S^{11} \\ S^{22} \\ S^{12} \end{Bmatrix} = \begin{bmatrix} C^{11} & C^{12} & C^{13} \\ C^{21} & C^{22} & C^{23} \\ C^{31} & C^{32} & C^{33} \end{bmatrix} \cdot \begin{Bmatrix} E_{11} \\ E_{22} \\ 2E_{12} \end{Bmatrix} \quad (1)$$

where C^{IJKL} is the fourth-order stiffness tensor and C^{IJ} is the component of a local "equivalent elasticity" matrix resulting from C^{IJKL} . Note that Eq. (1) is valid regardless of the magnitude of rotations as long as the strains are small.

2.1 The State of Stress and Strain in Wrinkling. Suppose a material element $\square ABCD$ in κ_0 is deformed to $\square A''B''C''D''$, as shown in Fig. 2, under a locally homogeneous plane deformation. Assume that a material line element along the \hat{X}_1 -axis in κ_0 is mapped to be aligned with the \hat{x}_1 -axis in $\kappa(t)$. Then the component of the deformation gradient \hat{F}_{21} vanishes as shown in the Appendix, and the deformation shown in Fig. 2 indeed represents a generic homogeneous plane deformation possibly including wrinkling deformations. Under the state of wrinkling, the \hat{x}_1 -axis will be the uniaxial tension direction, and the wrinkling will develop along the \hat{x}_2 -axis. Moreover, the deformation from $\square ABCD$ to $\square A''B''C''D''$ may be thought of as a series of sequential deformations: first rigid rotation from $\square ABCD$ to $\square \bar{A}\bar{B}\bar{C}\bar{D}$, next the deformation of the uniaxial tension from $\square \bar{A}\bar{B}\bar{C}\bar{D}$ to $\square A'B'C'D'$ without wrinkling, finally followed by pure wrinkling deformation from $\square A'B'C'D'$ to $\square A''B''C''D''$. Hereafter we will call the state of the uniaxial tension in the absence of wrinkling ($\square A'B'C'D'$), "the state of the natural uniaxial tension," which is to be distinguished from the state of the uniaxial tension possibly with wrinkling, which is to be the genuine final state of deformation in the presence of wrinkling. In addition, we remark that the concept of "homogeneous deformation" depicted in Fig. 2 is consistent with the discrete nature of finite element approximation wherein the strains at the discrete Gaussian points may be considered to be representative of the true inhomogeneous deformation field in some average sense.

Note that the directions of the \hat{X}_1 -axis and the \hat{x}_1 -axis, which are the uniaxial tension direction in κ_0 and $\kappa(t)$, respectively, are unknown and dependent upon a material point (X_1, X_2) . The stress-strain relation referred to the \hat{X}_1 frame may be written as

$$\begin{Bmatrix} \hat{S}^{11} \\ \hat{S}^{22} \\ \hat{S}^{12} \end{Bmatrix} = \begin{bmatrix} \hat{C}^{11} & \hat{C}^{12} & \hat{C}^{13} \\ \hat{C}^{21} & \hat{C}^{22} & \hat{C}^{23} \\ \hat{C}^{31} & \hat{C}^{32} & \hat{C}^{33} \end{bmatrix} \cdot \begin{Bmatrix} \hat{E}_{11} \\ \hat{E}_{22} \\ 2\hat{E}_{12} \end{Bmatrix} \quad (2)$$

where $\hat{C}^{IJ} = C^{KL} T^{IK} T^{JL}$ with

$$[T] = \begin{bmatrix} \cos^2 \beta & \sin^2 \beta & 2 \sin \beta \cos \beta \\ \sin^2 \beta & \cos^2 \beta & -2 \sin \beta \cos \beta \\ -\sin \beta \cos \beta & \sin \beta \cos \beta & \cos^2 \beta - \sin^2 \beta \end{bmatrix} \quad (3)$$

As \hat{x}_1 is the axis of the uniaxial tension in wrinkling, the two Cauchy stress components $\hat{\sigma}_{22}$ and $\hat{\sigma}_{12}$ should vanish, and this condition leads to $\hat{S}^{22} = \hat{S}^{12} = 0$ under plane deformations (see Appendix for proof). This condition is valid even for deformations with large strains although we limit ourselves to the small strain deformations due to the limitation of the constitutive Eq. (1). We can eliminate strains \hat{E}_{22} and \hat{E}_{12} by using these uniaxial tension conditions, $\hat{S}^{22} = \hat{S}^{12} = 0$. Then the uniaxial stress-strain relation can be obtained as

$$\hat{S}^{11} = a \cdot \hat{E}_{11} \quad \text{with}$$

$$a = \frac{l}{\hat{C}^{23}\hat{C}^{32} - \hat{C}^{22}\hat{C}^{33}} \{ \hat{C}^{11}(\hat{C}^{23}\hat{C}^{32} - \hat{C}^{22}\hat{C}^{33}) + \hat{C}^{12}(\hat{C}^{21}\hat{C}^{33} - \hat{C}^{23}\hat{C}^{31}) + \hat{C}^{13}(\hat{C}^{31}\hat{C}^{22} - \hat{C}^{21}\hat{C}^{32}) \}. \quad (4)$$

Once material data are set and the directions of the $\hat{X}_1 - \hat{X}_2$ axes are known, we can calculate the uniaxial stress at the natural uniaxial tension. Moreover, the strain components \hat{E}_{22} and \hat{E}_{12} , satisfying the uniaxial tension condition under the natural uniaxial tension can be obtained as

$$\begin{aligned} \hat{E}_{22} &= \frac{\hat{C}^{21}\hat{C}^{33} - \hat{C}^{23}\hat{C}^{31}}{\hat{C}^{23}\hat{C}^{32} - \hat{C}^{22}\hat{C}^{33}} \hat{E}_{11} \quad \text{and} \\ 2\hat{E}_{12} &= \frac{\hat{C}^{22}\hat{C}^{31} - \hat{C}^{21}\hat{C}^{32}}{\hat{C}^{23}\hat{C}^{32} - \hat{C}^{22}\hat{C}^{33}} \hat{E}_{11} \end{aligned} \quad (5a, b)$$

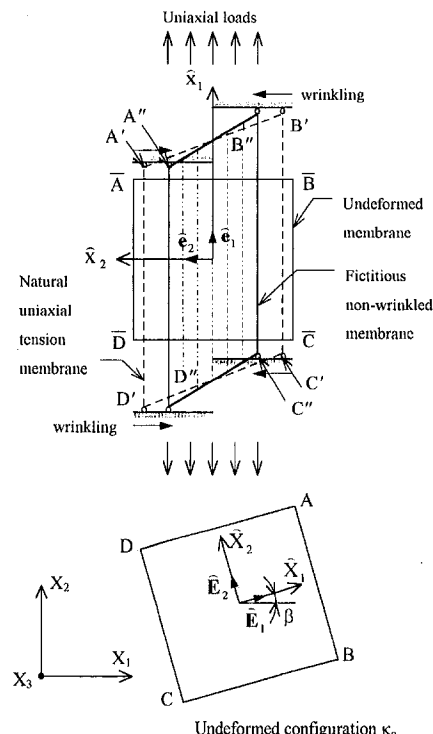


Fig. 2 Wrinkling process

Since the occurrence of wrinkling from $\square A'B'C'D'$ to $\square A''B''C''D''$ is induced by infinitesimal compressive forces due to negligible flexure stiffness of the membrane, there are no changes of the stress state due to the presence of such wrinkling, and the uniaxial stress-strain relation (4) remains valid. We now examine the change of strains during wrinkling or the deformation from $\square A'B'C'D'$ to $\square A''B''C''D''$. We recall that the deformation of the membrane is locally homogeneous in Fig. 2. Then, the deformation from $\square ABCD$ to $\square A'B'C'D'$ under the natural uniaxial tension may be written as $\hat{x}_1 = a_1 \hat{X}_2 + a_3 \hat{X}_1$ and $\hat{x}_2 = a_2 \hat{X}_2$ because $\hat{F}_{21} = 0$ (see Eq. (A-1) in Appendix). On the other hand, we have $\hat{x}_1 = b_1 \hat{X}_2 + b_3 \hat{X}_1$ and $\hat{x}_2 = b_2 \hat{X}_2$ for the locally homogeneous deformation from $\square ABCD$ to $\square A''B''C''D''$. We can then write the two Green strain tensors for the state of the natural uniaxial tension ($\square A'B'C'D'$) and for the state of wrinkling ($\square A''B''C''D''$).

$$\hat{\mathbf{E}}' = \frac{1}{2}(a_3^2 - 1)\hat{\mathbf{E}}_1 \otimes \hat{\mathbf{E}}_1 + \frac{1}{2}a_1a_3(\hat{\mathbf{E}}_1 \otimes \hat{\mathbf{E}}_2 + \hat{\mathbf{E}}_2 \otimes \hat{\mathbf{E}}_1) + (a_1^2 + a_2^2 - 1)\hat{\mathbf{E}}_2 \otimes \hat{\mathbf{E}}_2 \quad (6)$$

$$\hat{\mathbf{E}}'' = \frac{1}{2}(b_3^2 - 1)\hat{\mathbf{E}}_1 \otimes \hat{\mathbf{E}}_1 + \frac{1}{2}b_1b_3(\hat{\mathbf{E}}_1 \otimes \hat{\mathbf{E}}_2 + \hat{\mathbf{E}}_2 \otimes \hat{\mathbf{E}}_1) + (b_1^2 + b_2^2 - 1)\hat{\mathbf{E}}_2 \otimes \hat{\mathbf{E}}_2 \quad (7)$$

During the wrinkling process, points C' and D' are displaced horizontally to points C'' and D'' , respectively, and there is no change of the deformed coordinate \hat{x}_1 of a material point, while there is some change in the deformed coordinate \hat{x}_2 . Therefore we can obtain the relations $b_1 = a_1$, $b_3 = a_3$ and $b_2 \neq a_2$. From these and Eqs. (6) and (7), it follows that

$$\hat{E}'_{11} = \hat{E}''_{11} \quad \text{and} \quad \hat{E}'_{12} = \hat{E}''_{12}. \quad (8)$$

That is, during the pure wrinkling process there are no changes of the strain components \hat{E}_{11} and \hat{E}_{12} , referred to the local Cartesian frame (\hat{X}_1, \hat{X}_2) in κ_0 , wherein the \hat{X}_1 -axis is lined up along the material line element in κ_0 that is to be aligned with the direction of the uniaxial tension in $\kappa(t)$ in the presence of wrinkling. Equation (8) implies that equation (5b) remains valid regardless of the magnitude of wrinkling because the region under consideration is in the state of wrinkling or equivalently is in the state of the uniaxial tension. That is, Eq. (5b) is an invariant relation with respect to the magnitude of wrinkling, valid for wrinkled states and for the natural uniaxial tension of no wrinkling, while Eq. (5a) holds only for the natural uniaxial tension. This simple observation turns out to provide a useful clue for finding the wrinkling orientation, which is to be obtained as the direction of the uniaxial tension: that is, combining this observation with the incremental finite element scheme, we can devise an efficient scheme for searching for the wrinkling orientation, as will be shown in Section 2.3. We first examine the wrinkling criteria in Section 2.2.

2.2 Wrinkling Criterion. From given strains and appropriate constitutive equations, whether the state of the membrane is taut, wrinkled, or slack is determined based on wrinkling criteria. Up to now several wrinkling criteria have been proposed. We may categorize these into three types: the first is based upon the principal stresses; the second upon the principal strains; the third upon the principal stresses and strains. However, there have been no discussions yet regarding the effectiveness or the difficulties of each criterion. We will examine this issue in this section. Note that we may rely upon the second P.K. stress instead of the Cauchy stress for describing the wrinkling criterion for deformations with small elastic strains.

Consider first the wrinkling criterion based upon the principal stress, e.g., Contri et al. (1988) and Tabarrok et al. (1992) for a linear isotropic material; Fujikake et al. (1989) for an orthotropic material. Let S^1 and S^2 denote the principal stress components obtained from the constitutive Eq. (1) without ac-

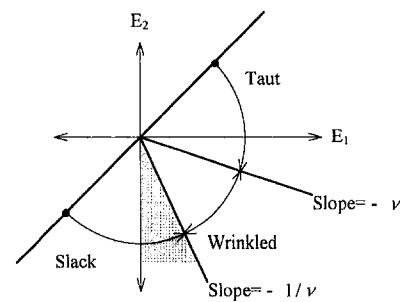


Fig. 3 The wrinkling criterion based upon stresses ($E_1 \geq E_2$) in a linear isotropic material

counting for wrinkling in the course of incremental finite element analysis. Moreover, we assume $S^1 \geq S^2$. Then the criterion is stated as (i) wrinkling does not occur (taut) if $S^2 > 0$; (ii) biaxial wrinkling occurs (slack) if $S^1 \leq 0$; (iii) uniaxial wrinkling occurs (wrinkled) if $S^1 > 0$ and $S^2 \leq 0$. This criterion has one difficulty related to the judgment of the deformation state. We may easily show the difficulty in the case of a linear isotropic material though the difficulty also occurs in an anisotropic material. We assume that strains are known at a material point of an isotropic membrane. Then we have to calculate stresses by using the constitutive equation which does not account for wrinkling like Eq. (1), because we do not know a priori the state of the membrane. Let the above criterion be represented for an isotropic membrane, as shown in Fig. 3. We assume that the principal strain E_1 is greater than or equal to the principal strain E_2 . If the given strains are in the shaded domain between the E_2 -axis and the line of slope $-1/\nu$ on the plane of the E_1 - E_2 principal strains in Fig. 3, then the following difficulty occurs: both principal stresses obtained from this strain domain will be negative in spite of the existence of the positive principal strain. According to the above criterion, the membrane should be in the slack state. In reality, however, the membrane is in the wrinkled state and the uniaxial stress of the wrinkled membrane is equal to EE_1 , where E is Young's modulus. Therefore, this criterion may cause the wrong judgment in determining whether the state of the membrane is wrinkled or slack. The finite element analysis of an inflatable circular airbag shows that the wrinkled and the slack state at the same integration point of some element repeat periodically in the iteration process and fail to converge when this criterion is applied.

Secondly for a linear isotropic material, the wrinkling criterion based upon the principal strains can be written as follows (e.g., Miller et al., 1982): first of all let E_1 and E_2 denote the principal strains, and assume that $E_1 \geq E_2$. Then the criterion is stated as (i) wrinkling does not occur (taut) if $E_1 > 0$ and $E_2 > -\nu E_1$; (ii) biaxial wrinkling occurs (slack) if $E_1 \leq 0$; (iii) uniaxial wrinkling occurs (wrinkled) if $E_1 > 0$ and $E_2 \leq -\nu E_1$. For an anisotropic material, the wrinkling criterion based upon the principal strains has not been developed.

Thirdly, consider the wrinkling criterion based upon the principal stresses and strains. This criterion was developed by Roddeman et al. (1987), which may overcome the aforementioned difficulties illustrated for isotropic materials and moreover this can be applied to anisotropic materials. For an isotropic or an anisotropic material, the wrinkling criterion based upon the principal stresses and strains can be written as follows: let $S^1 \geq S^2$ and $E_1 \geq E_2$ as before. Then

- (i) if $S^2 > 0$, wrinkling does not occur (taut),
- (ii) if $E_1 \leq 0$, biaxial wrinkling occurs (slack), and
- (iii) otherwise ($S^2 \leq 0$ and $E_1 > 0$),

uniaxial wrinkling occurs (wrinkled). (9)

The point of this criterion lies in that the stress and strain, obtained without accounting for the change in the constitutive equation due to the presence of wrinkling, can provide correct information for discriminating the taut or the slack state from a wrinkling state. If a deformation state is not taut nor slack, it must be in the state of wrinkling.

Note that the preceding wrinkling criterion in terms of the second P. K. stress can be shown to agree with the criterion in terms of the Cauchy stress (Roddeman et al., 1987) even for deformations with large strains because the condition for the taut state $S^1 > 0$ and $S^2 > 0$ in Eq. (9) is equivalent to that for $\sigma_1 > 0$ and $\sigma_2 > 0$.

2.3 Wrinkling Orientation. As discussed earlier, the wrinkled state is nothing but the state of the uniaxial tension, and the local frame \hat{x}_i for $\kappa(t)$ has been introduced for describing the wrinkling orientation such that the \hat{x}_1 -axis is along the direction of the uniaxial tension while the \hat{x}_2 -axis along the wrinkling direction. In the undeformed configuration κ_0 , the \hat{X}_I frame has been taken such that a material line element aligned with the \hat{X}_1 -axis in κ_0 is lined up with the \hat{x}_1 -axis in $\kappa(t)$ in the presence of wrinkling. Hence, the wrinkling orientation is determined by the direction of the uniaxial tension or equivalently by the orientation of the \hat{X}_I -axis for a given deformation, which is given by β (see Fig. 1 or 2). For an isotropic membrane, this orientation may be described by the condition $\hat{E}_{12} = 0$, by Eq. (5b), when \hat{E}_{11} denotes the strain component along the line of uniaxial tension. We seek the direction of $\hat{E}_{12} = 0$ for the wrinkling orientation in an isotropic membrane, and this means nothing but the direction of the principal stress, i.e., $\hat{S}_{12} = 0$ based upon Eq. (1). Hence we only have to search for the direction of the principal stress or strain to find the wrinkling orientation for an isotropic membrane. Note that the stress components are related to the strain components by Eq. (1) for this computation. For an anisotropic membrane, however, the principal direction obtained from the use of Eq. (1) will not lead to the wrinkling orientation in general; for the strain component \hat{E}_{12} in Eq. (5b) may have a nonzero value under the state of the uniaxial tension.

For an anisotropic membrane, as well as an isotropic membrane, the wrinkling orientation may be determined by exploiting the relationship (5b) between the strain components for the state of the natural uniaxial tension. Note that for all the states between $\square A'B'C'D'$ and $\square A''B''C''D''$ in Fig. 2 the two strain components \hat{E}_{11} and \hat{E}_{12} remain invariant with respect to the magnitude of wrinkling, and they are related by the condition of the natural uniaxial tension, which is given by Eq. (5b). That is, the relation (5b) remains invariant regardless of the magnitude of wrinkling when wrinkling occurs, and it is valid for the wrinkled state and for the state of the natural uniaxial tension, while Eq. (5a) holds only for the natural uniaxial tension. The consequence of this simple observation is far from being trivial: once a new displacement vector from an incremental finite element analysis corresponds to a wrinkled state in the course of iteration for equilibrium correction, Eq. (5b) enables us to determine the direction of the uniaxial tension or the wrinkling orientation, and so to reconstruct the stress state properly. We now describe this scheme in detail. As before we assume that the strain component \hat{E}_{11} is along the line of the uniaxial tension when wrinkling occurs. We first assume one value $\tilde{\beta}$ for β and transform the strain components E_{IJ} , obtained possibly in the course of equilibrium iteration in finite element analysis, to the components \hat{E}_{ij} referred to the local coordinate system (\hat{X}_1, \hat{X}_2) which takes the orientation angle $\tilde{\beta}$ from the X_I coordinate system. (The \hat{X}_I -axis is a possible candidate for the \hat{X}_I -axis and might be depicted in Fig. 1 by replacing β with $\tilde{\beta}$ and \hat{X}_I with \hat{X}_I .) That is, we have $\{\hat{E}_{11}, \hat{E}_{22}, \hat{E}_{12}\}^T = [\hat{\mathbf{T}}] \cdot \{E_{11}, E_{22}, E_{12}\}^T$ where $[\hat{\mathbf{T}}]$ indicates $[\mathbf{T}]$ of Eq. (3) with β being replaced by $\tilde{\beta}$. We next find $\beta = \tilde{\beta}$ for which the

condition of the uniaxial tension (5b) is satisfied. To insure the uniaxial tension state, we use the following procedure:

- (i) check $\hat{E}_{11} > 0$ for an assumed value of $\tilde{\beta}$,
- (ii) set $\hat{E}_{11} = \tilde{E}_{11}$,
- (iii) calculate \hat{E}_{12} and \hat{E}_{22} from Eq. (5a, b), and
- (iv) take $\beta = \tilde{\beta}$ if $\hat{E}_{12} = \tilde{E}_{12}$ and $\hat{E}_{22} \geq \tilde{E}_{22}$. (10)

The wrinkling strain E_w , which is never negative, is a measure of the "wrinkledness" of the membrane, is given by $E_w = \hat{E}_{22} - \hat{E}_{12}$. The wrinkling orientation β lies between 0 deg and 180 deg due to symmetry, and we have to check every possible direction. The key procedure for determining β is to solve the equation $f(\beta) = \hat{E}_{12} - \tilde{E}_{12} = 0$. For solving this equation, we first divide the domain of 0 deg - 180 deg into many small regions with a uniform spacing to check the sign change of the function $f(\beta)$. We then use Muller's method (Gerald et al., 1984) when the possible range of β reduces down to a smaller region. Once wrinkling occurs, there exist only one solution for β that satisfies every condition in Eq. (10).

Once the wrinkling orientation or β is determined together with the strain components $\hat{E}_{11} = \tilde{E}_{11}$, $\hat{E}_{12} = \tilde{E}_{12}$ and \hat{E}_{22} , Eq. (4) is employed for reconstruction of stress for the wrinkled state. In a finite element scheme this new stress state will be used for updating the tangent stiffness matrix and the internal forces for the next iteration.

3 Finite Element Formulation

A total Lagrangian finite element formulation based upon the principle of virtual work is used for membrane finite element analysis (Bathe, 1982), into which the foregoing scheme of the wrinkling criterion and the search for the wrinkling orientation are incorporated. We may then obtain the following secant equation:

$${}^{(n+1)}F_I(\mathbf{c}) = {}^{(n+1)}P_I \quad (11)$$

where \mathbf{c} indicates the nodal displacement vector in the global finite element equation. Equation (11) represents the balance of the internal force and the external force for each nodal degree-of-freedom, and it is nonlinear in the nodal displacement ${}^{(n+1)}\mathbf{c}$. For solution of this nonlinear equation, we rely upon a Newton-type iterative scheme via Taylor series expansion, and we can finally obtain

$${}^{(n,k)}K_{IJ} {}^{(n,k+1)}\Delta c_J = {}^{(n+1)}P_I - {}^{(n,k)}F_I \quad (12)$$

where ${}^{(n,k+1)}\Delta c_J$ is the nodal displacement increment for the $(k+1)$ th iteration, such that

$$\begin{aligned} {}^{(n,k+1)}c_J &= {}^{(n,k)}c_J + {}^{(n,k+1)}\Delta c_J \quad \text{and} \\ {}^{(n+1)}c_J &= {}^{(n)}c_J + \sum_k {}^{(n,k)}\Delta c_J = \lim_{k \rightarrow \infty} {}^{(n,k)}c_J, \\ {}^{(n,k)}K_{IJ} &= \frac{\partial {}^{(n,k)}F_I}{\partial c_J} \\ &= \int_{V^0} \frac{\partial N^\alpha}{\partial X_K} \frac{\partial {}^{(n,k)}x_m}{\partial X_L} C^{KLQP} \frac{\partial {}^{(n,k)}x_l}{\partial X_Q} \frac{\partial N^\beta}{\partial X_P} dV \\ &\quad + \int_{V^0} \delta_{ml} \frac{\partial N^\alpha}{\partial X_K} {}^{(n,k)}S^{KL} \frac{\partial N^\beta}{\partial X_L} dV. \quad (13) \end{aligned}$$

Observe that the stiffness matrix and the internal force in Eq. (12) are updated at each iteration because of the possibility of wrinkling. The wrinkling criterion (9) is applied at every iteration to check the deformation state, and the search for the wrinkling orientation and the reconstruction of the stress for a wrinkled region are carried out if the integration point under consideration is in the wrinkled state. This iteration procedure

corresponds to a quasi-Newton scheme for wrinkling structures although the stiffness is updated at every iteration; because the compressive membrane stiffness has not been relaxed in the first term of the stiffness matrix (13) in the presence of wrinkling, and the tangent stiffness is only an approximation to the first derivative of the true internal force $^{(n+1)}F_I(\mathbf{c})$.

Note that we cannot obtain a true equilibrium configuration, without updating the stress state properly for the wrinkled regions, although we may reach the convergence for a given loading step in the incremental finite element analysis; a correct internal force vector $F_I(\mathbf{c})$ is not obtained unless the stress state is properly updated for wrinkled regions. In passing, we remark that the algorithms for the proper stress update, particularly for an anisotropic membrane, as discussed in Section 2, are not reflected in most of the implicit commercial package codes currently available.

The iteration process for an equilibrium position is carried out in a two-stage procedure (Contri et al., 1988) only for the first loading step. The first stage consists in searching for an equilibrium position of the membrane with both of the compressive stresses and the tensile stresses active. Once the equilibrium position is obtained, the compressive stresses are relaxed at the next stage as follows. Given a new estimation of the nodal displacements in the processes of equilibrium correction, at each integration point of an element the judgment is made on the wrinkling criterion, whether it is taut, wrinkled, or slack. Here we use the wrinkling criterion (9) based upon the principal stresses and strains. After this decision, the following procedures will be used: In the taut situation, the stresses of the membrane are determined by the normal analysis without wrinkling. In the presence of wrinkling, the stresses are determined on the basis of the scheme for the wrinkled membrane, described in the previous section. In the slack situation, the stresses contain only zeros. When the membrane is in the wrinkled state, the special procedure discussed in Section 2.1 and 2.3 is required for the reconstruction of the stresses. Such a stress calculation is required to evaluate the stiffness matrix and the internal forces in Eq. (12) during the iterations. For loading steps except the first, the iteration process for an equilibrium correction is carried out in the one-stage procedure which corresponds to the second stage of the first loading step. Note that the present approach just follows the standard finite element analysis procedure except that it has incorporated into a finite element code the scheme for the wrinkling criterion, for the wrinkling-direction search and for the determination of the tensile uniaxial stress for the wrinkled region. It requires no special element formulation nor special treatment, and this finite element analysis can be carried out with minor modifications of the existing total Lagrangian finite element codes for membranes. For illustrating numerical examples, we have written our own membrane finite element code into which the aforementioned scheme has been incorporated.

4 Numerical Examples

4.1 Torsion of a Membrane. For the first example, we consider a circular membrane attached to a rigid disk at the inner edge and to a guard ring at the outer edge (Roddeman, 1991). Turning the rigid disk causes wrinkling of the membrane. The scheme which accounts for wrinkling should be used to calculate strains and stresses. For the finite element analysis, 120 four-node isoparametric membrane elements are used as shown in Fig. 4(a). The nodal points on the outer circle are fixed in space. The nodal points on the inner circle are rotated over ten degrees. A material behavior is assumed as follows: Young's modulus $E = 1.0 \times 10^5$ Pa and Poisson ratio $\nu = 0.3$ for a linear isotropic material; $E_{y1} = 1.0 \times 10^5$ Pa, $E_{y2} = 1.0 \times 10^6$ Pa, $\nu_{12} = 0.3$ and $G_{12} = 0.385 \times 10^5$ Pa, referred to the X_1 frame in Fig. 4, for a linear orthotropic material. It turns out

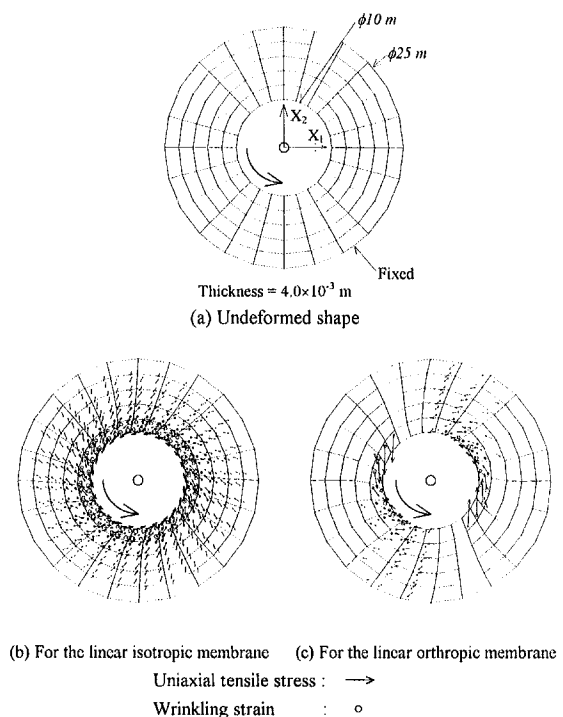


Fig. 4 Deformed shapes, the uniaxial tensile stress and the wrinkling strain on a wrinkled region for torsion of a circular membrane (144 elements)

that the full 2×2 Gaussian integration is required for obtaining a reliable solution without any possible zero-energy modes.

The deformed shapes for the linear isotropic and orthotropic membranes are shown in Fig. 4(b) and 4(c), respectively. Furthermore, the direction and the magnitude of the uniaxial tensile stress are indicated by using the direction and the length, respectively, of the arrow at each integration point in the wrinkled region. The magnitude of the wrinkling strain is also indicated by using circles of varying magnitude. Regions which are not indicated with arrows and the circles means a taut region. As expected, the isotropic problem shows itself to be rotationally symmetric. In the orthotropic membrane, wrinkling occurs mostly on the left-lower and the right-upper parts.

4.2 An Inflatable Circular Airbag (Automotive Airbag).

Now consider an inflatable circular airbag that initially consists of two flat circular pieces of fabric sewed together along the edge. In this case the unfilled (undeformed) structure exhibits a flat and stress-free surface which, when filled to a final volume, will experience stressing and wrinkling of the fabric. This wrinkling is due to the shrinkage in circumferential direction of the airbag as it is inflated. The inflatable circular airbag is modeled as two parallel circular planes using three and four-node elements as shown in Fig. 5. In the initial configuration, the two circular planes of the front and the back coincide with each other. The action of the gas inside the airbag is assumed to be a uniform pressure distribution on the inner surfaces of the bag. As before, we use the full 2×2 Gaussian integration to remove possible zero-energy modes.

Consider the airbag to be made of the same two flat isotropic membranes. By applying appropriate boundary conditions in the horizontal midplane, we need only to model one quarter of the bag. The finite element model for a quarter airbag consists of 20 total elements (four in circumferential direction and five in radial direction). A linear isotropic material behavior is assumed as follows: $E = 6.0 \times 10^7$ Pa and $\nu = 0.3$. The thickness is 0.4×10^{-3} m. The airbag is subjected to a uniform pressure from 0 to 10 kPa. Figure 6 shows the vertical displacement of

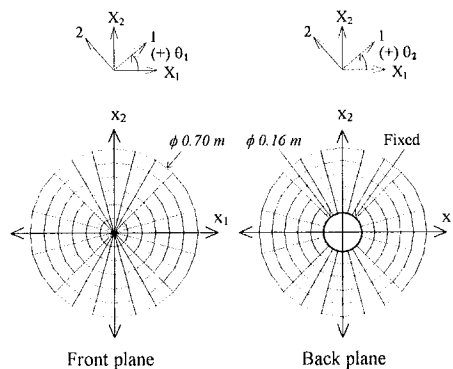
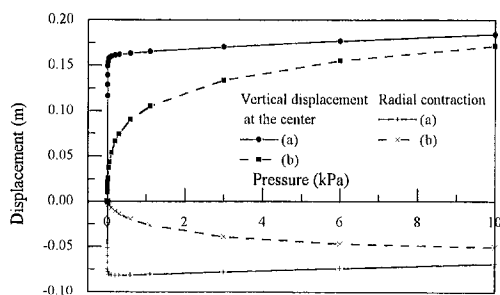


Fig. 5 The airbag model

the center point and the radial contraction of a point of the circumference with respect to the increase in the internal pressure for two cases: one obtained with wrinkling being taken into account and the other obtained from pure membrane theory with no wrinkling being taken into account. The difference between both cases is greatest in the low pressure region. As the pressure increases, the displacement difference is smaller since the wrinkled region decreases.

Consider next an airbag with front and back anisotropic membranes, modeled with 264 elements. The airbag is subjected to the uniform pressure of 5 kPa. The linear orthotropic material behavior is assumed as follows: $E_{y1} = 2.0 \times 10^8$ Pa, $E_{y2} = 2.0 \times 10^8$ Pa, $\nu_{12} = 0.1$, $G_{12} = 0.385 \times 10^5$ Pa; material principal angle $\theta_1 = 0$ deg for the front plane membrane and material principal angle $\theta_2 = 45$ deg for the back plane membrane (see Fig. 5). The thickness is 0.4×10^{-3} m. Figures 7(a)–7(d) show the overall deformed shape, the deformed shape of the front plane, the top view and the side view, respectively. Furthermore, the uniaxial tensile stress and the wrinkling strain are indicated, as in the aforementioned torsion case, at each integration point on the wrinkled region. The region with no arrows and circles means a taut region. We add that no rigorous treatment of the present anisotropic airbag problem has been reported in the literature, and that the existing commercial package codes cannot handle this problem because they are lacking in the correct stress update algorithm for wrinkling of anisotropic membranes. In passing, we point out that the most of the commercial packages rely upon the wrinkling criterion based upon the principal stresses discussed in Section 2.2, and they update the stress state for the wrinkled region by replacing the negative principal stress by zero stress. Hence, the solution process via such commercial package codes fail to converge for the present airbag problem, and no comparisons were possible.



(a) : Displacements obtained with wrinkling being taken into account
(b) : Displacements obtained from pure membrane theory with no wrinkling being taken into account

Fig. 6 The vertical displacement of the center point and the radial contraction of an inflatable circular airbag modeled with 20 elements (4×5) for a quarter plane

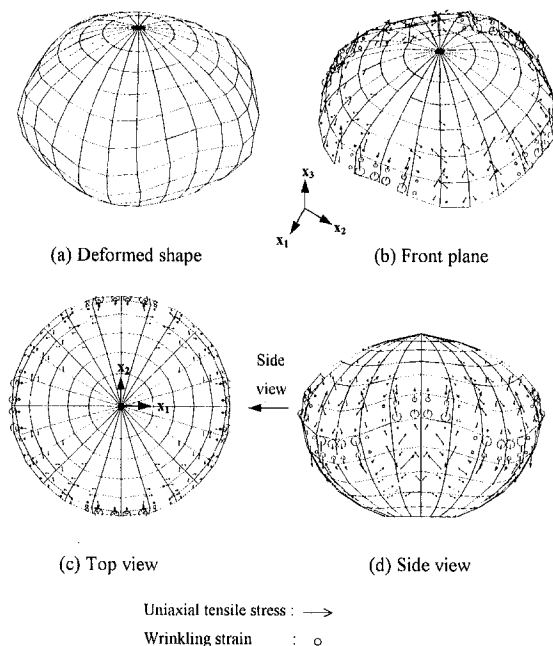


Fig. 7 Deformed shapes of an airbag ($\theta_1 = 0$ deg and $\theta_2 = 45$ deg)

To examine the convergence behavior of the present finite element scheme, we plot the total number of iterations up to convergence versus the size of the loading step in terms of the rotation angle or of the pressure in Fig. 8 wherein *only one loading step* is chosen for analysis. The maximum size of loading step is chosen to be ten degrees for the torsion of the isotropic circular membrane and 10 kPa for quasi-static inflation of the isotropic airbag, since the resulting membrane strains are no longer small beyond this loading. For both of the examples, we see that the number of iterations for convergence decreases as the size of the loading step increases. Particularly for the airbag, it is noticeable that the total number of iterations drastically decreases from the early stage as the size of the loading step increases. The abrupt drop of the total number of iterations for this case is due to the fact that the wrinkled or slack regions drastically decrease in the early stage as the pressure loading begins to increase. These numerical examples suggest that the present scheme works well for the range of small strain deformations, even for a large loading step.

5 Conclusions

With the aid of the correct stress update based upon the observation regarding the invariant relation between some of

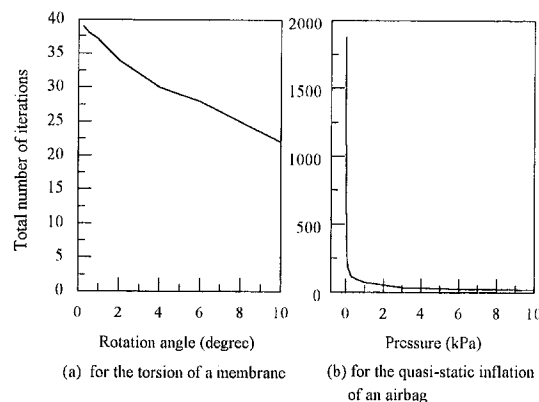


Fig. 8 Convergence behavior according to the size of a loading step for the torsion of a circular membrane and for the quasi-static inflation of an airbag (linear isotropic)

the strain components referred to a coordinate system aligned with wrinkling, a simple but efficient scheme is proposed for finite element analysis of wrinkling. This scheme is found to be applicable to an anisotropic membrane and an isotropic membrane. Moreover, it requires no special finite element development, but only minor modifications of the existing total Lagrangian finite element codes for membranes are needed. Two numerical examples have been used to demonstrate the validity of the proposed scheme: one is the torsion of a membrane and the other the inflation of an airbag used in the automotive applications. The numerical examples suggest that the present scheme retains good convergence behavior even for a large loading step within the range of small strain deformations.

References

- Bathe, K.-J., 1982, *Finite Element Procedures in Engineering Analysis*, Prentice-Hall, Englewood Cliffs, NJ.
- Contri, P., and Schrefler, B. A., 1988, "A Geometrically Nonlinear Finite Element Analysis of Wrinkled Membrane Surfaces by a No-compression Material Model," *Communications in Appl. Num. Meth.*, Vol. 4, pp. 5–15.
- Fujikake, M., Kojima, O., and Fukushima, S., 1989, "Analysis of Fabric Tension Structures," *Comput. Struct.*, Vol. 32, No. 3–4, pp. 537–547.
- Gerald, C. F., and Wheatley, P. O., 1984, *Applied Numerical Analysis*, Addison-Wesley Reading, MA.
- Kondo, K., Iai, T., Moriguri, S., and Murasaki, T., 1955, *Memoirs of the Unifying Study of the Basic Problems in Engineering by Means of Geometry*, Vol. 1, pp. 417–441.
- Miller, R. K., Hedgepeth, J. M., Weingarten, V. I., Das P., and Kahyai, S., 1982, "An Algorithm for Finite Element Analysis of Partly Wrinkled Membranes," *AIAA*, Vol. 20, pp. 1761–1763.
- Reissner, E., 1938, "On Tension Field Theory," *Proc. 5th Int. Congr. Appl. Mech.*, pp. 88–92.
- Roddeeman, D. G., Oomens, C. W. J., Janssen, J. D., and Drukker, J., 1987, "The Wrinkling of Thin Membranes: Part I—Theory," *ASME JOURNAL OF APPLIED MECHANICS*, Vol. 54, pp. 884–887.
- Roddeeman, D. G., 1991, "Finite-Element Analysis of Wrinkling Membrane," *Communications in Appl. Num. Meth.*, Vol. 7, pp. 299–307.
- Steigmann, D. J., and Pipkin, A. C., 1989, "Wrinkling of Pressurized Membranes," *ASME JOURNAL OF APPLIED MECHANICS*, Vol. 56, pp. 624–628.
- Tabarrok, B., and Qin, Z., 1992, "Nonlinear Analysis of Tension Structures," *Comput. Struct.*, Vol. 45, pp. 973–984.
- Wagner, H., 1929, "Flat Sheet Metal Girders With Very Thin Metal Web," *Z. Flugtechn. Motorluftschiffahrt*, Vol. 20, pp. 200–314.
- Wu, C. H., and Canfield, T. R., 1981, "Wrinkling in Finite Plane-Stress Theory," *Q. Appl. Math.*, pp. 179–199.

APPENDIX

We here show that the conditions $\bar{\sigma}_{22} = \bar{\sigma}_{12} = 0$ leads to the conditions $\bar{S}^{22} = \bar{S}^{12} = 0$ in terms of the second P.K. stress for homogeneous plane deformations.

Consider a locally homogeneous plane deformation $d\bar{\mathbf{X}} \rightarrow d\bar{\mathbf{x}}$. Suppose a material line element $d\bar{\mathbf{X}} = d\bar{X}_1 \bar{\mathbf{E}}_1$ in κ_0 is mapped to $d\bar{\mathbf{x}}$ in κ . Then we have $d\bar{\mathbf{x}} = \bar{\mathbf{F}} d\bar{\mathbf{X}} = d\bar{X}_1 (\bar{F}_{11} \bar{\mathbf{e}}_1 + \bar{F}_{21} \bar{\mathbf{e}}_2)$. Recall that a material line element along the \bar{X}_1 -axis is mapped into a material line element along the \bar{x}_1 -axis. Therefore we have

$$\bar{F}_{21} = 0. \quad (\text{A-1})$$

Under the present homogeneous deformation, because of Eq. (A1) the condition $\bar{\sigma}_{22} = \bar{\sigma}_{12} = 0$ leads to the two equations: $\bar{F}_{11} \bar{F}_{22} \bar{S}^{12} + \bar{F}_{12} \bar{F}_{22} \bar{S}^{22} = 0$ and $\bar{F}_{22}^2 \bar{S}^{22} = 0$. This yields $\bar{S}^{22} = \bar{S}^{12} = 0$. Similarly we can show that the conditions $\bar{S}^{22} = \bar{S}^{12} = 0$ can be transformed to the conditions $\bar{\sigma}_{22} = \bar{\sigma}_{12} = 0$ for plane deformation.

Weight Functions for Notches: Constructive and Variational Definition

H. O. K. Kirchner

Professor of Multimaterials,
Institut de Sciences des Matériaux,
Université Paris-Sud,
F-91405 Orsay, France

Weight functions for notches or cracks, which express the intensity of the stress singularity at the tip as functionals of the loadings present, can be defined either as combination of eigenfunctions or as variational derivatives of energies. The two definitions are equivalent.

1 Weight Functions

Consider the notch in the finite specimen shown in Fig. 1. It extends between the angles $\omega = 0$ and $\omega = \Omega$ around its tip, from which the radius r is counted. It is stressed suitably far away from its tip either by a line force $\mathbf{f}(r, \omega)$ or a dislocation with Burgers vector $\mathbf{b}(r, \omega)$ or both. Near the tip the displacement will vary like r^s times a function of the angle ω , giving a stress $\sigma = Kr^{s-1}F(\omega)$ near the tip. The exponent s is determined by the boundary conditions (free-free, or fixed-fixed, or fixed-free) along the flanks; it depends only on the geometry but not on the loading. The wedge with angle $\Omega = 2\pi$ is a crack; for this case $s - 1 = -\frac{1}{2}$. The angular function $F(\omega)$ is determined by equilibrium and compatibility. The stress intensity factor K , on the other hand, must be a functional of the sources $[\mathbf{b}(r, \omega), \mathbf{f}(r, \omega)]^t$,

$$K = \int_A H(r, \omega)[\mathbf{b}(r, \omega), \mathbf{f}(r, \omega)]^t dA, \quad (1)$$

the integral being taken over the specimen area A . The functional H has been called weight function by Bueckner (1970). There are two, seemingly different ways to define and compute weight functions, a variational and a constructive one.

1.1 Constructive Definition. For the special case of an isotropic wedge in antiplane strain Sham and Bueckner (1988) considered the interaction energy between two fields, with displacements varying like $u^{(1)} \cong K^{(1)}r^s$ and $u^{(2)} \cong K^{(2)}r^{-s}$, which is a quadratic form in $K^{(1)}$ and $K^{(2)}$. This approach requires proof that with the exponent s also $(-s)$ satisfies the boundary conditions. Sham and Bueckner (1988) showed this to be the case for a bimaterial wedge in antiplane strain. Belov and Kirchner (1995a, b; 1996) extended the proof to arbitrary loadings (and dislocations present) in elastically anisotropic, angularly inhomogeneous wedges. No variational argument is invoked in this type of reasoning.

1.2 Variational Definition. For the crack Bueckner (1970, 1989) considers the variation of an interaction energy between two loading systems, (1) and (2) with a virtual change δa in the crack length a . This is equal to a quadratic form in the two stress intensity factors $K^{(1)}$ and $K^{(2)}$. No change of strength of the singularity is involved, it remains $s - 1 = -\frac{1}{2}$ for the tip at a and at $a + \delta a$. Is this type of variational argument

restricted to the self-similar geometry of a crack or can variational principles also be invoked for wedges? For a wedge the virtual change in geometry to be considered is presumably a change $\delta\Omega$ in wedge angle Ω (Markenscoff, 1994). Because s is a function of geometry, such a change is associated with a change δs in the strength of the singularity.

The variational approach to weight functions for cracks was developed by Rice (1985a, b, 1989). He extended the definitions to three-dimensional situations, and dislocations and inclusions as sources of stress. He showed how the weight function becomes a crack front weight function useful for handling perturbations of the crack shape. Rice's theory was applied to practical problems of interest by Gao and Rice (1986, 1987, 1989) and by Gao (1989). Gao also extended the theory to interfacial cracks, the first step to the consideration of inhomogeneous media.

Markenscoff (1994) pointed out that, although the second definition has been used for cracks and the first one for notches, the two definitions should be equivalent, and showed explicitly that for a crack they are. In this paper it will be shown that the variational and constructive definitions of weight functions are equivalent for an angularly inhomogeneous wedge. As special cases this comprises homogeneous wedges, cracks, interfacial cracks, and cracks impinging on interfaces. The proof requires construction of the eigenfunctions of the wedge and their perturbation with changes in geometry.

2 Eigenfunctions of the Wedge

Following Kirchner (1987, 1989) and Belov and Kirchner (1995a, b; 1996) we consider a wedge where the elastic constants $C_{ijkl}(\omega)$ vary explicitly with the azimuthal angle ω . A special case would be the composite wedge of Sham and Bueckner (1988), where the elastic constants are piecewise homogeneous. The stresses σ_{ij} can be derived from the displacement vector \mathbf{u} by Hooke's law,

$$\sigma_{ij} = C_{ijkl}(\omega)\partial_k u_l, \quad (2)$$

or from a stress function vector Φ according to

$$\sigma_{i1} = \partial_2 \Phi_i, \quad \sigma_{i2} = -\partial_1 \Phi_i. \quad (3)$$

Both definitions must give the same stress, which yields a consistency condition for the entity $(\mathbf{u}\Phi)^t$:

$$\{N(\omega)\partial_r - Ir^{-1}\partial_\omega\}[\mathbf{u}(r, \omega)\Phi(r, \omega)]^t = 0, \quad (4)$$

where $N(\omega)$ is a certain combination of the elastic constants $C_{ijkl}(\omega)$. The basic idea of using a first-order differential equation for the displacement and stress function vector instead of the usual second-order differential equation in the displacement alone is well explained in Ting's book (1996). With both \mathbf{u} and Φ being vectors with three components, $[\mathbf{u}(r, \omega)\Phi(r, \omega)]^t$ has six components. The matrix N is a six-by-six matrix, I

Contributed by the Applied Mechanics Division of THE AMERICAN SOCIETY OF MECHANICAL ENGINEERS for publication in the ASME JOURNAL OF APPLIED MECHANICS.

Discussion on this paper should be addressed to the Technical Editor, Professor Lewis T. Wheeler, Department of Mechanical Engineering, University of Houston, Houston, TX 77204-4792, and will be accepted until four months after final publication of the paper itself in the ASME JOURNAL OF APPLIED MECHANICS.

Manuscript received by the ASME Applied Mechanics Division, Aug. 31, 1994; final revision, Oct. 19, 1996. Associate Technical Editor: X. Markenscoff.

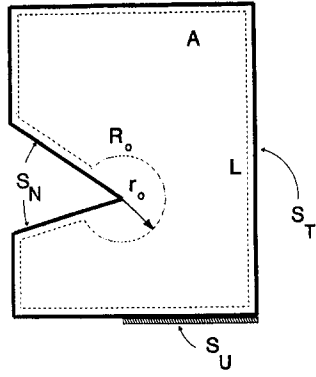


Fig. 1 Notch in a finite specimen. The tractions are prescribed on S_N and S_T , the displacements on S_U , and body forces of strength f or dislocations with Burgers vector b are present in A . The reciprocity theorem is applied to the dashed contour L .

is the six-by-six unit matrix. The solutions of the first-order differential Eq. (4) are both compatible, because the existence of a displacement \mathbf{u} was assumed, and equilibrated, because the existence of a stress function Φ was assumed. Assuming separable solutions of the form

$$[\mathbf{u}(r, \omega)\Phi(r, \omega)]^t = r^s V^{(s)}(\omega) [\mathbf{h} \mathbf{g}]^t, \quad (5)$$

where $[\mathbf{h} \mathbf{g}]^t$ is an excitation vector, the superscript t in $[\]^t$ denotes transposition and $V^{(s)}(\omega)$ is a six-by-six matrix, one finds the differential equation

$$dV^{(s)}(\omega)/d\omega = sN(\omega)V^{(s)}(\omega) \quad (6)$$

for $V^{(s)}(\omega)$ with the solution

$$V^{(s)}(\omega) = \text{Ordexp} \left\{ s \int_0^\omega N(\alpha) d\alpha \right\}. \quad (7)$$

Use of the ordered exponential, rather than a simple matrix exponential, is necessary, because in general matrices $N(\alpha)$ for two different arguments α do not commute. Because of this noncommutativity, $V^{(-s)}(\omega)$ is not the inverse of $V^{(s)}(\omega)$, and the complex number s is not an exponent but an index. The eigentensors of positive and negative index are, however, related by

$$T[V^{(s)}(\omega)]^t TV^{(-s)}(\omega) = I, \quad (8)$$

where T is a constant matrix composed of three by three identity matrices

$$T = \begin{pmatrix} 0 & I \\ I & 0 \end{pmatrix}. \quad (9a)$$

For later use we note the identity

$$TN = N^t T. \quad (9b)$$

3 Eigenvalues

If both notch faces, $\omega = 0$ and $\omega = \Omega$ are to be kept traction-free near $r = 0$, the boundary conditions are, for small r ,

$$\Phi(r, 0) = \Phi(r, \Omega) = 0. \quad (10)$$

If $V^{(s)}(\omega)$ is decomposed into three by three blocks according to

$$V^{(s)}(\omega) = \begin{pmatrix} V_1^{(s)}(\omega) & V_2^{(s)}(\omega) \\ V_3^{(s)}(\omega) & V_4^{(s)}(\omega) \end{pmatrix}, \quad (11)$$

Eq. (10) implies that the determinant of the southwest block vanishes,

$$|V_3^{(s)}(\Omega)| = 0. \quad (12)$$

This is the nonlinear eigenvalue equation for the index (s) . Belov and Kirchner (1995a) have shown that, whenever (12) is satisfied, also

$$|V_3^{(-s)}(\Omega)| = 0. \quad (13)$$

Thus, whenever (s) is an eigenvalue, also $(-s)$ is one, a fact absolutely necessary for the constructive definition of weight functions. The point is that free-free boundary conditions determine both the index (s) and the lower part of the exciting vector, $\mathbf{g} = \mathbf{0}$. Other boundary conditions are met by similar equations. For example, fixed-fixed boundary conditions, $\mathbf{u}(r, 0) = \mathbf{u}(r, \Omega) = \mathbf{0}$, are satisfied by $\mathbf{h} = \mathbf{0}$ and $|V_2^{(s)}(\Omega)| = 0$.

4 Orthogonality

Belov and Kirchner (1995a) proved the following relation between eigentensors of two different indices, $V^{(s)}(\omega)$ and $V^{(t)}(\omega)$:

$$(t+s) \int_0^\Omega [V^{(s)}(\omega)]^t TN(\omega) V^{(t)}(\omega) d\omega = \{ [V^{(s)}(\Omega)]^t TV^{(t)}(\Omega) - T \}. \quad (14)$$

This result is independent of any boundary conditions. Multiply now (14) by exciting vectors $(\mathbf{h} \mathbf{0})^t$ from the right, and $(\mathbf{h}^* \mathbf{0})$ from the left, these being of the required form for free-free boundary conditions. One obtains

$$\begin{aligned} (t+s)(\mathbf{h}^* \mathbf{0}) \int_0^\Omega [V^{(s)}(\omega)]^t TN(\omega) V^{(t)}(\omega) d\omega (\mathbf{h} \mathbf{0})^t \\ = (\mathbf{h}^* \mathbf{0}) \{ [V^{(s)}(\Omega)]^t TV^{(t)}(\Omega) - T \} (\mathbf{h} \mathbf{0})^t \\ = r^{-s} [\mathbf{u}^{*(s)}(r, \Omega) \mathbf{0}] Tr^{-t} [\mathbf{u}^{(t)}(r, \Omega) \mathbf{0}]^t - (\mathbf{h}^* \mathbf{0}) T (\mathbf{h} \mathbf{0})^t \\ = r^{-(s+t)} \mathbf{0} - \mathbf{0} = 0, \quad (15) \end{aligned}$$

where $[\mathbf{u}^{*(s)}(r, \Omega) \mathbf{0}]$ and $[\mathbf{u}^{(t)}(r, \Omega) \mathbf{0}]^t$ are the fields excited by $(\mathbf{h}^* \mathbf{0})$ and $(\mathbf{h} \mathbf{0})^t$, respectively. One concludes that, if both s and t fulfill free-free boundary conditions,

unless $(s+t) = 0$,

$$(\mathbf{h}^* \mathbf{0}) \int_0^\Omega [V^{(s)}(\omega)]^t TN(\omega) V^{(t)}(\omega) d\omega (\mathbf{h} \mathbf{0})^t = 0. \quad (16)$$

The same argument holds also for fixed-fixed, fixed-free, and free-fixed boundary conditions. For fixed-fixed ones, for example, the exciting vectors are $(\mathbf{0} \mathbf{g}^*)$ and $(\mathbf{0} \mathbf{g})^t$. Multiplication with the exciting vectors reduced the eigentensors $V^{(s)}(\omega)$ to eigenvectors $V^{(s)}(\omega)(\mathbf{h} \mathbf{0})^t$. Since for any choice of boundary conditions, with s being an eigenvalue, also $(-s)$ is an eigenvalue, there exists always one eigenvector which is not orthogonal to the one considered, but all the eigenvectors are self-orthogonal. The orthogonality situation suggests that the pairs of eigenvalues, (s) and $(-s)$ have special status, a fact already exploited by Sham and Bueckner (1988) for antiplane strain and isotropy, and that the pairs $V^{(s)}$ and $V^{(-s)}$ of eigentensors have special status, as exploited by Belov and Kirchner (1995a) for generalized plane strain and angular inhomogeneity and anisotropy.

5 Interaction Between Two Eigensystems $r^s V^{(s)}$ and $r^t V^{(t)}$

Consider now two fields, with eigenvalues (s) and (t) , being

excited by the sources $(\mathbf{h}^* \mathbf{0})'$ and $(\mathbf{h} \mathbf{0})'$, respectively. The tangential tractions of the latter are

$$[\mathbf{b} \mathbf{t}]' = r^{-1} d[\mathbf{u} \Phi]/d\omega = tr^{t-1} N(\omega) V^{(t)}(\omega) [\mathbf{h} \mathbf{0}]'. \quad (17)$$

The interaction between the s -field and the gradient of the t -field is

$$e^{(s/t)} = tr^{s+t-1} (\mathbf{h}^* \mathbf{0}) [V^{(s)}(\omega)]' TN(\omega) V^{(t)}(\omega) (\mathbf{h} \mathbf{0})', \quad (18)$$

and integrated between $\omega = 0$ and $\omega = \Omega$ over the arc element $r d\omega$,

$$E^{(s/t)} = tr^{s+t} (\mathbf{h}^* \mathbf{0}) \int_0^\Omega [V^{(s)}(\omega)]' TN(\omega) V^{(t)}(\omega) d\omega (\mathbf{h} \mathbf{0})'. \quad (19)$$

With (16) one concludes that

$$\text{unless } (s+t) = 0, \quad E^{(s/t)} = 0. \quad (20)$$

The only interaction to be considered is between $V^{(-s)}$ and $V^{(+s)}$,

$$E^{(-s/s)} = s(\mathbf{h}^* \mathbf{0}) \int_0^\Omega [V^{(-s)}(\omega)]' TN(\omega) V^{(+s)}(\omega) d\omega (\mathbf{h} \mathbf{0})'. \quad (21)$$

If the geometry of the wedge is changed, from an angle Ω to $\Omega + \delta\Omega$, only the variational change $\delta E^{(-s/s)}$ of $E^{(-s/s)}$ has to be considered, the changes of all other interactions remain zero.

6 Derivatives With Respect to the Index

By definition (6), $V^{(s)}(\omega)$ is not only a function of the argument ω , but also of the index (s) . What is its derivative with respect to this index? Try to write

$$dV^{(s)}(\omega)/ds = V^{(s)}(\omega) \int_0^\omega J(\alpha) d\alpha, \quad (22)$$

with an unknown integrand $J(\alpha)$. Forming the cross derivatives from (22) and (6) one obtains

$$\begin{aligned} d^2 V^{(s)}(\omega)/d\omega ds &= sN(\omega) V^{(s)}(\omega) \int_0^\omega J(\alpha) d\alpha + V^{(s)}(\omega) J(\omega) \\ &= N(\omega) V^{(s)} + sN(\omega) [dV^{(s)}(\omega)/ds], \end{aligned} \quad (23)$$

which leaves, by comparison,

$$J(\omega) = [V^{(s)}(\omega)]^{-1} N(\omega) V^{(s)}(\omega) \quad (24)$$

and the desired expression for the derivative

$$\begin{aligned} dV^{(s)}(\omega)/ds &= V^{(s)}(\omega) \int_0^\omega [V^{(s)}(\alpha)]^{-1} N(\alpha) V^{(s)}(\alpha) d\alpha. \end{aligned} \quad (25)$$

For $\omega = \Omega$ one obtains

$$dV^{(s)}(\Omega)/ds = V^{(s)}(\Omega) TY^{(s)}(\Omega) \quad (26)$$

with

$$Y^{(s)}(\Omega) = \int_0^\Omega [V^{(-s)}(\omega)]' TN(\omega) V^{(+s)}(\omega) d\omega. \quad (27)$$

Comparison with (21) shows that

$$E^{(-s/s)} = s(\mathbf{h}^* \mathbf{0}) Y^{(s)}(\Omega) (\mathbf{h} \mathbf{0})'. \quad (28)$$

Without realizing the connection to $dV^{(s)}/ds$, Belov and Kirchner (1995b, 1996) gave the same definition for $Y^{(s)}(\Omega)$ in their derivation of weight functions. The identity (28) will provide the link between the constructive definition of weight

functions, as given by Belov and Kirchner (1995b, 1996) and the variational one requested by Markenscoff (1994) and being developed here. The transpose of Eq. (27), written for $(-s)$ instead of (s) , reads

$$[Y^{(-s)}(\Omega)]' = \int_0^\Omega [V^{(-s)}(\omega)]' N'(\omega) T V^{(+s)}(\omega) d\omega. \quad (29)$$

Comparison of (27) with (29) shows that, because of (9b),

$$[Y^{(-s)}(\Omega)]' = Y^{(s)}(\Omega). \quad (30)$$

With (30), the transpose of Eq. (26), written for $(-s)$ instead of s , reads

$$d[V^{(-s)}(\Omega)]'/d(-s) = Y^{(s)}(\Omega) T [V^{(-s)}(\Omega)]'. \quad (31)$$

7 The Singularity s Changes With the Angle Ω

Free-free boundary conditions are satisfied by determining the eigenvalues s for the wedge angle Ω from the secular Eq. (12) and the eigenvalue $s + \delta s$ for a wedge of angle $\Omega + \delta\Omega$ from

$$|V_3^{(s+\delta s)}(\Omega + \delta\Omega)| = 0. \quad (32)$$

For fixed-fixed, fixed-free, and free-fixed boundary conditions the determinants of the other blocks have to vanish. According to the last section one has the expansion

$$\begin{aligned} V^{(s+\delta s)}(\Omega + \delta\Omega) &= V^{(s)}(\Omega) + [V^{(s)}(\Omega) TY^{(s)}(\Omega)] \delta s \\ &\quad + [sN(\Omega) V^{(s)}(\Omega)] \delta\Omega. \end{aligned} \quad (33)$$

The southwest block of (33) reads

$$V_3^{(s+\delta s)}(\Omega + \delta\Omega) = V_3^{(s)}(\Omega) + A\delta s + B\delta\Omega \quad (34a)$$

with

$$A = [V^{(s)}(\Omega) TY^{(s)}(\Omega)]_3 \quad (34b)$$

$$B = [sN(\Omega) V^{(s)}(\Omega)]_3. \quad (34c)$$

One sees that according to (32) the change δs is determined from

$$|V_3^{(s)}(\Omega) + A\delta s + B\delta\Omega| = 0, \quad (35)$$

where both δs and $\delta\Omega$ are small. This fact allows expansion of the determinant in the form

$$\begin{aligned} |V_3^{(s)}(\Omega) + A\delta s + B\delta\Omega| &= |V_3^{(s)}(\Omega)| + \{\text{cof } [V_3^{(s)}(\Omega)]_{ij}\} A_{ij} \delta s \\ &\quad + \{\text{cof } [V_3^{(s)}(\Omega)]_{ij}\} B_{ij} \delta\Omega, \end{aligned} \quad (36)$$

where cof denotes the cofactor. According to (35) and (32) the left-hand side and the first term on the right are zero. One concludes that

$$\delta s/\delta\Omega = -\{\text{cof } [V_3^{(s)}(\Omega)]_{ij}\} B_{ij} / \{\text{cof } [V_3^{(s)}(\Omega)]_{ij}\} A_{ij}. \quad (37)$$

8 Variational Derivative

We want to compute the change $\delta E^{(-s/s)}$ of the interaction $E^{(-s/s)}$ if the angle of the wedge is changed from Ω to $\Omega + \delta\Omega$. This change entails also a change in the index from s to $s + \delta s$. Formally, without specifying the operator δ for the time being,

$$\begin{aligned} \delta E^{(-s/s)} &= \delta \int_0^\Omega e^{(-s/s)}(\omega) r d\omega \\ &= \int_0^\Omega \delta \{ [V^{(-s)}(\omega)]' TN(\omega) V^{(+s)}(\omega) \} d\omega \\ &\quad + \int_\Omega^{\Omega+\delta\Omega} e^{(-s/s)}(\omega) r d\omega. \end{aligned} \quad (38)$$

The second term is simply

$$e^{(-s/s)}(\Omega)\delta\Omega, \quad (39)$$

the unchanged energy density in the newly added domain. The first term is, now being understood that no variation with Ω is necessary any more (that was taken care of by the second term),

$$\{\delta[V^{(-s)}(\Omega)]'\}TV^{(s)}(\Omega) + [V^{(-s)}(\Omega)]'T\{\delta V^{(s)}(\Omega)\}. \quad (40)$$

From (26) and (31) one has

$$\delta V^{(s)}(\Omega) = V^{(s)}(\Omega)TY^{(s)}(\Omega)\delta s, \quad (41a)$$

$$\{\delta[V^{(-s)}(\Omega)]'\} = \delta(-s)[Y^{(-s)}(\Omega)]'T[V^{(-s)}(\Omega)]'. \quad (41b)$$

Therefore,

$$\begin{aligned} \delta E^{(-s/s)}(\Omega) &= \delta(-s)Y^{(s)}(\Omega)T[V^{(-s)}(\Omega)]'TV^{(s)}(\Omega) \\ &\quad + [V^{(-s)}(\Omega)]'TV^{(s)}(\Omega)TY^{(s)}(\Omega)\delta s \\ &= Y^{(s)}\delta(-s) + Y^{(s)}\delta s = 0, \end{aligned} \quad (42)$$

where (8) and (30) have been used. This result is obtained if s is varied to $s + \delta s$ and $-s$ to $-(s + \delta s)$. As Markenscoff (1994) has shown, what has to be considered is the unchanged field against the changing field as the geometry is being changed. In other words, the variation of $(-s)$ to $-(s + \delta s)$ while (s) remains (s) . This leaves

$$\delta E^{(-s/s)} = Y^{(s)}\delta(-s). \quad (43)$$

9 Equivalency

Consider now the interaction of an (unstarred) field with index (s) and sources $K(\mathbf{h} \mathbf{0})'$, called regular, with a (starred) one with index $(-s)$ and source $K^*(\mathbf{h}^* \mathbf{0})'$, called fundamental. By adding to the starred field an expansion of all possible eigenfunctions with all other possible solutions of (12) as index, the following boundary conditions for tractions \mathbf{T}^* and displacement \mathbf{u}^* can be satisfied for the specimen of Fig. 1:

$$\mathbf{T}^* = \mathbf{0} \quad \text{on } S_T + S_N \quad (44a)$$

$$\mathbf{u}^* = \mathbf{0} \quad \text{on } S_U. \quad (44b)$$

The specimen is subjected to an external loading system which consists of body forces \mathbf{f} , prescribed surface tractions \mathbf{F} on S_T and S_N , and also of prescribed displacements \mathbf{U} at the remainder S_U of the body surface.

9.1 Constructive Definition. Apply the reciprocity theorem (without variation in the notch angle Ω) to the regular and fundamental field. For a subdomain $A' < A$, bounded, as shown in Fig. 1, by a closed contour L which consists of a circular arc R_0 of radius r_0 , the boundaries S_T and S_U , and the remaining part S_N of the notch faces, the reciprocity theorem can be written as

$$\begin{aligned} &-\int_{A'} \mathbf{u}^* \mathbf{f} dA - \int_{S_T+S_N} \mathbf{u}^* \mathbf{F} dL + \int_{S_U} \mathbf{T}^* \mathbf{U} dL \\ &= \int_{R_0} (\mathbf{T} \mathbf{u}^* - \mathbf{T}^* \mathbf{u}) dL = \\ &= \int_0^\Omega (\mathbf{u}^* \Phi^*) T \{d[\mathbf{u} \Phi]\} d\omega = E^{(-s/s)}. \end{aligned} \quad (45)$$

The latter equality follows from (19). Shrinking r_0 to zero leaves $E^{(-s/s)}$ unchanged. From comparison with (28) one has

$$E^{(-s/s)} = sK^*(\mathbf{h}^* \mathbf{0})Y^{(s)}(\mathbf{h} \mathbf{0})'K$$

$$= \left\{ -\int_A \mathbf{u}^* \mathbf{f} dA - \int_{S_T+S_N} \mathbf{u}^* \mathbf{F} dL + \int_{S_U} \mathbf{T}^* \mathbf{U} dL \right\}, \quad (46)$$

which is the constructive definition of weight function as described in Section 1.1. It is identical to Eqs. (44)–(48) of Belov and Kirchner (1996). (They define the intensity of their regular field by $-K(2\pi)^{s-1}/s$ rather than K , and take $K^* = (2\pi)^{s-1}$ as the intensity of their fundamental field.)

9.2 Variational Definition. Now take the variation of (46)

$$\begin{aligned} \delta E^{(-s/s)} &= -\int_A (\delta \mathbf{u}^*) \mathbf{f} dA - \int_{S_T+S_N} (\delta \mathbf{u}^*) \mathbf{F} dL \\ &\quad + \int_{S_U} (\delta \mathbf{T}^*) \mathbf{U} dL + \mathbf{u}^* \delta \mathbf{f} dA. \end{aligned} \quad (47)$$

According to (43) this gives, since the starred field with $(-s)$ is being varied,

$$\begin{aligned} K^*(\mathbf{h}^* \mathbf{0})Y^{(s)}(\mathbf{h} \mathbf{0})'K\delta(-s) &= -\int_A (\delta \mathbf{u}^*) \mathbf{f} dA - \int_{S_T+S_N} (\delta \mathbf{u}^*) \mathbf{F} dL \\ &\quad + \int_{S_U} (\delta \mathbf{T}^*) \mathbf{U} dL, \end{aligned} \quad (48)$$

the last term of (47) corresponding to (39). After division by δs ,

$$\begin{aligned} \delta E^{(-s/s)}/\delta s &= -K^*(\mathbf{h}^* \mathbf{0})Y^{(s)}(\mathbf{h} \mathbf{0})'K \\ &= -\int_A (\delta \mathbf{u}^*/\delta s) \mathbf{f} dA - \int_{S_T+S_N} (\delta \mathbf{u}^*/\delta s) \mathbf{F} dL \\ &\quad + \int_{S_U} (\delta \mathbf{T}^*/\delta s) \mathbf{U} dL. \end{aligned} \quad (49)$$

This equation expresses the quadratic form in K^* and K in terms of the weight function $(\delta \mathbf{u}^*/\delta s)$, which is the variational definition requested by Markenscoff (1994).

10 Discussion

The derivation presented shows that the variation δs of the singularity strength s which is induced by a change $\delta\Omega$ of the notch angle is important, the change $\delta\Omega$ itself leads only to a trivial term. Comparison of (46) with (49) shows that the variation $\delta \mathbf{u}^*$ of the eigenfunction is directly related to the eigenfunction \mathbf{u}^* by

$$\delta \mathbf{u}^*/\delta s = -\mathbf{u}^*/s, \quad \text{or} \quad \delta(\mathbf{u}^*s) = 0. \quad (50)$$

Equation (5) provides the relationship between the constructive definition of weight functions, which uses \mathbf{u}^* and the variational one, which uses $\delta \mathbf{u}^*$. The argument at the beginning of Section 9, where the boundary conditions of the finite specimen are satisfied by adding the fields of other eigenvalues implicitly assumes completeness of the eigenfunctions. For a long time completeness had not been proven, not even for homogeneous wedges, the principal difficulty being that the differential operator $\{N(\omega)\partial_r - Ir^{-1}\partial_\omega\}$ of Eq. (4) is not self-adjoint. Recently Kirchner and Alshits (1996) calculated the Green's function for the inhomogeneous wedge, and proved completeness of the eigenfunctions. Because of orthogonality the eigenfunctions do not interact, which is the reason why Markenscoff's (1994) variational derivative is finite precisely for the pair $V^{(-s)}$ and $V^{(s)}$ and zero for all others. It is also the reason why weight functions (Sham, 1989) can be defined.

References

- Belov, A., and Kirchner, H. O. K., 1995a, "Critical Angles in Bending of Rotationally Inhomogeneous Elastic Wedges," *ASME JOURNAL OF APPLIED MECHANICS*, Vol. 62, pp. 429–440.
- Belov, A., and Kirchner, H. O. K., 1995b, "Higher order weight functions in fracture mechanics of inhomogeneous anisotropic solids," *Philosophical Magazine*, Vol. A72, pp. 1471–1483.
- Belov, A., and Kirchner, H. O. K., 1996, "Universal weight functions for elastically anisotropic, angularly inhomogeneous media with notches or cracks," *Philosophical Magazine*, Vol. A73, pp. 1621–1646.
- Bueckner, H. F., 1970, "A novel principle for the computation of stress intensity factors," *Z. angew. Math. Mech.*, Vol. 50, pp. 529–546.
- Bueckner, H. F., 1989, "Observations on weight functions," *Engineering Analysis with Boundary Elements*, Vol. 6, pp. 3–18.
- Gao, H., 1989, "Application of 3-D Weight Functions—I. Formulations of Problems of Crack Interaction with Transformation Strains and Dislocations," *Journal of the Mechanics and Physics of Solids*, Vol. 37, pp. 133–153.
- Gao, H., 1992, "Weight Function Method for Interfacial Cracks in Anisotropic Bimaterials," *International Journal of Fracture*, Vol. 56, pp. 139–158.
- Gao, H., and Rice, J. R., 1986, "Shear Stress Intensity Factors for A Planar Crack With Slightly Curved Front," *ASME JOURNAL OF APPLIED MECHANICS*, Vol. 53, pp. 774–778.
- Gao, H., and Rice, J. R., 1987, "Somewhat Circular Tensile Cracks," *International Journal of Fracture*, Vol. 33, pp. 155–174.
- Gao, H., and Rice, J. R., 1989, "Application of 3-D Weight Functions—II. The Stress Field and Energy of Three Dimensional Shear Dislocation Loops at a Crack Tip," *Journal of the Mechanics and Physics of Solids*, Vol. 37, pp. 155–174.
- Kirchner, H. O. K., 1987, "Line defects along the axis of rotationally inhomogeneous media," *Philosophical Magazine*, Vol. A55, pp. 537–542.
- Kirchner, H. O. K., 1989, "Elastically anisotropic angularly inhomogeneous media. I. A new formalism," *Philosophical Magazine*, Vol. B60, pp. 423–432.
- Kirchner, H. O. K., and Alshits, V. I., 1996, "Elastically anisotropic angularly inhomogeneous media II: The Green's differential for piezoelectric, piezomagnetic and magnetoelectric media," *Philosophical Magazine*, Vol. A74, pp. 861–885.
- Markenscoff, X., 1994, "On the weight function for the wedge (or notch)," *Philosophical Magazine Letters*, Vol. 70, pp. 297–301.
- Rice, J. R., 1985a, "Three-dimensional elastic crack tip interactions with transformation strains and dislocations," *International Journal of Solids and Structures*, Vol. 21, pp. 781–791.
- Rice, J. R., 1985b, "First-Order Variation in Elastic Fields Due to Variation in Location of a Planar Crack Front," *ASME JOURNAL OF APPLIED MECHANICS*, Vol. 52, pp. 571–579.
- Rice, J. R., 1989, "Weight Function Theory for Three-Dimensional Elastic Crack Analysis," *Fracture Mechanics: Perspectives and Directions* (Twentieth Symposium), ASTM STP 1020, R. P. Wei and R. P. Gangloff, eds., American Society for Testing and Materials, Philadelphia, pp. 29–57.
- Sham, T.-L., 1989, "The theory for higher order weight functions for linear elastic plane problems," *International Journal of Solids and Structures*, Vol. 25, pp. 357–380.
- Sham, T.-L., and Bueckner, H. F., 1988, "The weight function theory for piecewise homogeneous notches in antiplane strain," *ASME JOURNAL OF APPLIED MECHANICS*, Vol. 55, pp. 596–603.
- Sham, T.-L., and Zhou, Y., 1989, "Weight functions in two-dimensional bodies with arbitrary anisotropy," *International Journal of Fracture*, Vol. 40, pp. 13–41.
- Ting, T. C. T., 1996, *Anisotropic Elasticity. Theory and Applications*, Oxford Science Publications, Oxford, UK, p. 150.

Kimihiko Yasuda
Professor.

Keisuke Kamiya
Assistant Professor.

Department of Electronic-
Mechanical Engineering,
School of Engineering,
Nagoya University,
Furo-cho, Chikusa-ku, Nagoya,
464-01, Japan

Munenobu Komakine

Production Engineer,
R & D Department 1,
Nippondenso Co., Ltd.
1-1 Showa-cho, Kariya, Aichi, 448 Japan

Experimental Identification Technique of Vibrating Structures With Geometrical Nonlinearity

A new experimental identification technique of a two-dimensional vibrating elastic structure with geometrical nonlinearity is considered. First it is shown that the governing equations given in the form of nonlinear partial differential equations can always be transformed to those given in the form of nonlinear ordinary differential equations called the modal equations, and hence identification is reduced to determination of the modal equations. Then a technique for determining the parameters of the modal equations through use of experimental data is proposed. Numerical simulation is conducted for typical cases, and applicability of the technique is confirmed.

1 Introduction

The identification of nonlinear vibrating systems through use of experimental data is of considerable importance in the applied mechanics area. Hence a number of papers have been published (Ibanez, 1973; Masri and Caughey, 1979; Udawadia and Kuo, 1981; Kirshenboim and Ewins, 1984; Masri et al., 1984; Stanway et al., 1985; Yang and Ibrahim, 1985; Busby et al., 1986; Masri et al., 1987a, b; Yasuda et al., 1988a, b; Yasuda and Kawamura, 1989; Yasuda and Kamiya, 1991). However, all these papers concern discrete systems with a relatively few degrees-of-freedom. In addition, all these papers concern cases in which the nonlinearity is expressed directly in terms of the variables of the problem. Seemingly no papers have been published which concern distributed systems. In distributed systems, cases in which the nonlinearity is not described directly by the variables of the problem are encountered. One such problem is the vibrating elastic structure with geometrical nonlinearity, in which the nonlinearity is dependent on the global deformation of the system. So apparently the identification of the system requires different approaches from those used in the existing techniques.

As a simple case of such problems, the authors considered in previous papers (Yasuda and Kamiya, 1990; Kamiya and Yasuda, 1993) a beam with geometrical nonlinearity, and proposed a technique for its identification. In the present paper, the authors consider a more general case, and propose a technique for identifying two-dimensional vibrating elastic structures. Numerical simulation is conducted for typical cases, and applicability of the proposed technique is confirmed.

2 Formulation of the Problem

Two-dimensional elastic structures such as membranes, plates and shells exhibit nonlinearity for large amplitudes, and are called systems with geometrical nonlinearity. These are the objects for which we are proposing an identification technique.

As a preparation, we consider the problem of analyzing responses of elastic structures. An orthogonal curvilinear coordinate system $O - xy$ is taken in the middle surface of a system in its equilibrium state. We denote the deflection and the stress function describing in-plane forces by w and F , respectively. Suppose that the system is subjected to external force q and viscous damping force with coefficient c . Then the equations of motion of Kármán type for the system are given by

$$\rho h \frac{\partial^2 w}{\partial t^2} + c \frac{\partial w}{\partial t} - N_0 \nabla^2 w + D \nabla^4 w = L(w, F) + \nabla_k^2 F + q$$
$$\frac{1}{Eh} \nabla^4 F = -\frac{1}{2} L(w, w) - \nabla_k^2 w \quad (1)$$

where ρ , h , N_0 , D , and E are the density, thickness, initial tension, flexural rigidity, and Young's modulus, respectively. The operators ∇^2 , ∇_k^2 , and L in Eqs. (1) are defined, for arbitrary functions f and g , as

$$\nabla^2 f = \frac{\partial^2 f}{\partial x^2} + \frac{\partial^2 f}{\partial y^2}, \quad \nabla_k^2 f = k_1 \frac{\partial^2 f}{\partial x^2} + k_2 \frac{\partial^2 f}{\partial y^2}$$
$$L(f, g) = \frac{\partial^2 f}{\partial x^2} \frac{\partial^2 g}{\partial y^2} - 2 \frac{\partial^2 f}{\partial x \partial y} \frac{\partial^2 g}{\partial x \partial y} + \frac{\partial^2 f}{\partial y^2} \frac{\partial^2 g}{\partial x^2} \quad (2)$$

where k_1 and k_2 are the curvatures in x and y -directions, respectively. For nonzero k_1 and k_2 , Eqs. (1) express equations of motion of a shell. For $k_1 = k_2 = 0$, they are reduced to those of a plate. Finally, for $D = 0$ and $k_1 = k_2 = 0$, they are reduced to those of a membrane. Our current problem is to solve Eqs. (1) under given boundary conditions.

To solve this problem, we consider, in advance, the following two eigenvalue problems. The first is the problem of determining eigenvalues and eigenfunctions of the linearized undamped system with the same boundary conditions as those of the original problem. The equations for this problem are

$$-\rho h p^2 \Phi - N_0 \nabla^2 \Phi + D \nabla^4 \Phi = \nabla_k^2 G$$
$$\frac{1}{Eh} \nabla^4 G = -\nabla_k^2 \Phi \quad (3)$$

where p denotes the eigenvalue, and Φ and G the eigenfunctions. We denote the obtained eigenvalues and the corresponding eigenfunctions by $p = p_n$ ($n = 1, 2, \dots$) and $\Phi = \Phi_n$, $G = G_n$, respectively. Note that p_n and Φ_n are the natural frequencies

Contributed by the Applied Mechanics Division of THE AMERICAN SOCIETY OF MECHANICAL ENGINEERS for publication in the ASME JOURNAL OF APPLIED MECHANICS.

Discussion on this paper should be addressed to the Technical Editor, Professor Lewis T. Wheeler, Department of Mechanical Engineering, University of Houston, Houston, TX 77204-4792, and will be accepted until four months after final publication of the paper itself in the ASME JOURNAL OF APPLIED MECHANICS.

Manuscript received by the ASME Applied Mechanics Division, Jan. 5, 1995; final revision, Sept. 20, 1996. Associate Technical Editor: M. Shinozuka.

and the modal functions of the linearized system. The second is the problem of determining the eigenvalues λ and the eigenfunctions H of equation

$$\frac{1}{Eh} \nabla^4 H = \lambda^4 H \quad (4)$$

with the same boundary conditions as those for F in the original problem. We denote the obtained eigenvalues and the corresponding eigenfunctions by $\lambda = \lambda_n$ ($n = 1, 2, \dots$) and $H = H_n$, respectively.

Now we return to solving the problem of analyzing responses. For this we expand the deflection w and the stress function F as

$$w = \sum_{n=1}^{\infty} X_n \Phi_n$$

$$F = \sum_{n=1}^{\infty} X_n G_n + \sum_{n=1}^{\infty} Y_n H_n \quad (5)$$

where X_n and Y_n are unknown functions of time, of which X_n are referred to as the modal coordinates. Since all Φ_n , G_n , and H_n satisfy the boundary conditions of the problem, w and F given by Eqs. (5) identically satisfy the same boundary conditions. Hence the remaining problem is to determine X_n and Y_n so that they satisfy Eqs. (1). Substituting Eqs. (5) into the second of Eqs. (1) and noting Eqs. (3), we obtain the conditions for w and F to satisfy the second of Eqs. (1) as follows:

$$\sum_{m=1}^{\infty} \lambda_m^4 Y_m H_m = -\frac{1}{2} L \left(\sum_{i=1}^{\infty} X_i \Phi_i, \sum_{j=1}^{\infty} X_j \Phi_j \right). \quad (6)$$

Multiplying Eq. (6) by H_n and integrating the resulting equations with respect to x and y over the region of the problem, yields, due to the orthogonality of the eigenfunctions H_n , the following equations:

$$Y_n = \sum_{i,j=1}^{\infty} a_{n,ij} X_i X_j \quad (n = 1, 2, \dots) \quad (7)$$

where

$$a_{n,ij} = -\frac{1}{2\lambda_n^4} \frac{\iint L(\Phi_i, \Phi_j) H_n dx dy}{\iint H_n^2 dx dy} \quad (8)$$

in which integration is conducted over the region of the problem. Similarly, the condition for w and F to satisfy the first of Eqs. (1) is

$$\sum_{m=1}^{\infty} (\rho h \ddot{X}_m \Phi_m + c \dot{X}_m \Phi_m + \rho h p_m^2 X_m \Phi_m)$$

$$= L \left(\sum_{i=1}^{\infty} X_i \Phi_i, \sum_{j=1}^{\infty} X_j G_j \right) + L \left(\sum_{i=1}^{\infty} X_i \Phi_i, \sum_{j=1}^{\infty} Y_j H_j \right)$$

$$+ \sum_{j=1}^{\infty} Y_j \nabla_k^2 H_j + q \quad (9)$$

where a dot means differentiation with respect to time. Multiplying Eq. (9) by Φ_n , integrating over the region of the problem, and substituting Eqs. (7) into the resulting equation, yields

$$m_n \ddot{X}_n + c_n \dot{X}_n + k_n X_n + \sum_{i,j=1}^{\infty} \alpha_{n,ij} X_i X_j + \sum_{i,j,k=1}^{\infty} \beta_{n,ijk} X_i X_j X_k = q_n$$

$$(n = 1, 2, \dots) \quad (10)$$

where

$$m_n = \iint \rho h \Phi_n^2 dx dy, \quad c_n = \iint c \Phi_n^2 dx dy$$

$$k_n = \iint \rho h p_n^2 \Phi_n^2 dx dy, \quad q_n = \iint q \Phi_n dx dy$$

$$\alpha_{n,ij} = -\iint \{ L(\Phi_i, G_j) + \sum_{m=1}^{\infty} a_{m,ij} \nabla_k^2 H_m \} \Phi_n dx dy$$

$$\beta_{n,ijk} = -\sum_{m=1}^{\infty} a_{m,jk} \iint L(\Phi_i, H_m) \Phi_n dx dy. \quad (11)$$

In the following, q_n in Eqs. (11) is referred to as the modal external force.

Equations (10) are the ordinary differential equations expressed in terms of the modal coordinates X_n , and are called the modal equations. Note that the modal equations are coupled by nonlinear terms only, and that nonlinear terms are given by polynomials of the third order of the modal coordinates. If w and F are developed in terms of other functions than those used above, the resulting equations are more complicated. Determining the modal coordinates X_n by solving Eqs. (10) and substituting them into the first of Eqs. (5), yields the deflection w . In this way the problem of analyzing responses is reduced to solving the modal equations.

We are now ready to formulate the problem of identification. As shown above, the governing Eqs. (1) can always be transformed to the modal Eqs. (10). Hence identification is reduced to the determination of the modal equations instead of Eqs. (1). Though the number of the modal equations is infinite, first few are significant in practical cases. So we may confine our problem to determining these few significant equations, and thus identification is reduced to their determination. In the following, we propose a technique for determining these equations.

3 Proposition of an Identification Technique

In identifying nonlinear systems, the task which presents most difficulty is the determination of the nonlinearity of the system. As compared with this, determination of the modal functions of the linearized system is relatively easy. They can be determined, for example, by a usual finite element method or a conventional modal analysis technique for small amplitudes. Thus, in the following, we assume that the modal functions are available. Sometimes this may be a restriction, but not vital. Furthermore, this restriction will be overcome in a similar manner as was done in a beam (Kamiya and Yasuda, 1993).

3.1 Determination of Modal Coordinates and Modal External Forces. Following the procedures required in our technique, we first consider determination of modal coordinate X_n and modal force q_n by use of the measured data of deflection w and external force q .

Suppose that the deflection is measured at N points placed on the system. The measured values of deflection are denoted by w_m ($m = 1, 2, \dots$). If we neglect, in the first expression of Eqs. (5), terms with suffix n larger than N , we have

$$\begin{Bmatrix} w_1 \\ w_2 \\ \vdots \\ w_N \end{Bmatrix} = \begin{bmatrix} \Phi_{11} & \Phi_{12} & \cdots & \Phi_{1N} \\ \Phi_{21} & \Phi_{22} & \cdots & \Phi_{2N} \\ \vdots & \vdots & \ddots & \vdots \\ \Phi_{N1} & \Phi_{N2} & \cdots & \Phi_{NN} \end{bmatrix} \begin{Bmatrix} X_1 \\ X_2 \\ \vdots \\ X_N \end{Bmatrix} \quad (12)$$

where Φ_{mn} ($m, n = 1, 2, \dots, N$) denotes the value of the n th modal function at the m th measuring point, and hence is a known quantity. Equation (12) is a simultaneous equation with respect to X_n ($n = 1, 2, \dots, N$). Unless the equation is singular, it can be solved. In this way, we can determine X_n . Among all X_n thus obtained, some may be discarded, if they are very small.

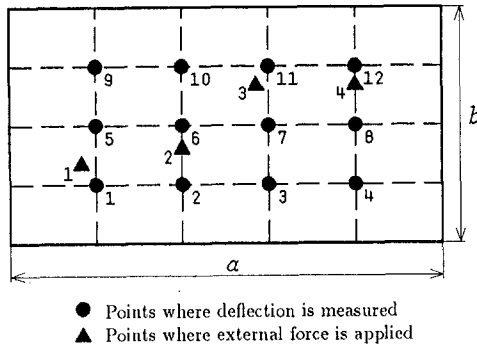


Fig. 1 Rectangular plate

In the following, we suppose that the first M of the modal coordinates are significant.

Determination of the modal external forces q_n ($n = 1, 2, \dots, M$) is easy. They can be determined through the experimental data of q , by conducting integration given in the fourth expression of Eqs. (11).

3.2 Consideration of the Form of Modal Equations. As shown in Section 2, the modal equations take the form of Eqs. (10). However, for identification, a slight modification will be desirable. First, the damping terms in Eqs. (10) may take, in practical cases, more general form. Secondly, certain coefficients of nonlinear terms such as $\alpha_{n,ij}$ and $\alpha_{n,ji}$ should be summed up as one coefficient. Thus, we put the modal equations in the form

$$m_n \ddot{X}_n + \sum_{m=1}^M c_{nm} \dot{X}_n + k_n X_n + \sum_{i,j=1 (i \leq j)}^M \alpha_{n,ij} X_i X_j + \sum_{i,j,k=1 (i \leq j \leq k)}^M \beta_{n,ijk} X_i X_j X_k = q_n \quad n = 1, 2, \dots, M \quad (13)$$

where c_{nm} ($m, n = 1, 2, \dots, M$) satisfy

$$c_{nm} = c_{mn}. \quad (14)$$

Now that the form of the modal equations have been determined, the remaining problem is to determine the unknown parameters m_n , c_{nm} , k_n , $\alpha_{n,ij}$, and $\beta_{n,ijk}$ in Eqs. (13).

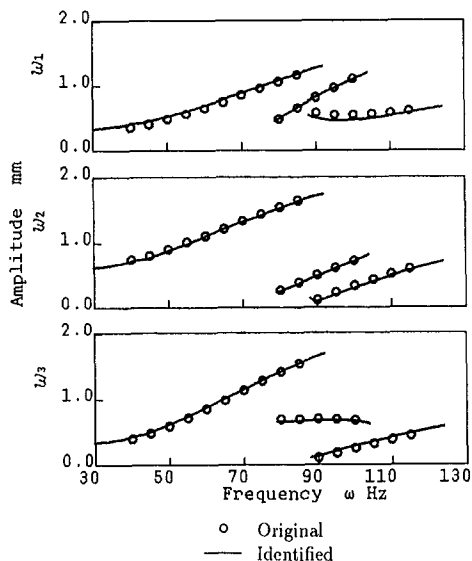


Fig. 2 Amplitudes of the deflections of the rectangular plate

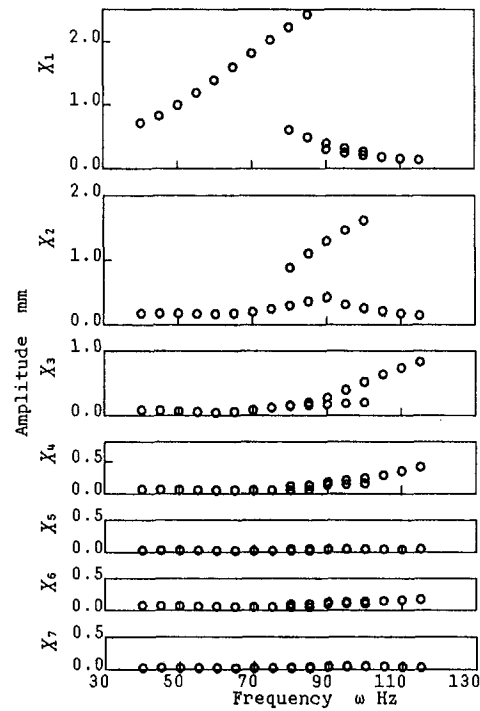


Fig. 3 Amplitudes of the modal coordinates of the rectangular plate

3.3 Determination of the Unknown Parameters. To determine the unknown parameters in Eqs. (13), various techniques in time domain may be used (Masri et al., 1984, 1987a, b; Yan and Ibrahim, 1985). However, we apply here a different technique which one of the authors proposed for simpler systems, and which may be classified as a technique in frequency domain (Yasuda et al., 1988a, b). This technique allows averaging of the data and is expected to yield more accurate results. Furthermore, the technique requires only the data of displacement, but not those of velocity and acceleration, which is very convenient in many practical cases.

We apply as external force q , a periodic one with period T . We measure the applied force q and the deflection w of the periodic response. If no periodic responses occur, we adopt other external force by varying the period or the amplitude until the periodic response occurs. Using the measured data, we determine the modal coordinates X_n and the modal external forces q_n following the procedures given above. Since X_n and q_n are periodic with the same period as that of q , they can be expanded into Fourier series

$$q_n = (q_n)_0 + (q_n)_1 \cos \omega t + (q_n)_2 \cos 2\omega t + \dots + (q_n)_1^* \sin \omega t + (q_n)_2^* \sin 2\omega t + \dots$$

$$X_n = (X_n)_0 + (X_n)_1 \cos \omega t + (X_n)_2 \cos 2\omega t + \dots + (X_n)_1^* \sin \omega t + (X_n)_2^* \sin 2\omega t + \dots \quad (15)$$

where $\omega = 2\pi/T$. The Fourier coefficients $(q_n)_0$, $(q_n)_1$, \dots and $(X_n)_0$, $(X_n)_1$, \dots in Eqs. (15) can be determined, for example, by an FFT algorithm, and are considered known quantities. Similarly, after having determined the terms $X_i X_j$, $X_i X_j X_k$ ($i, j, k = 1, 2, \dots, M$) appearing in Eqs. (13) by operation of X_n , they can be expanded into Fourier series as follows:

$$X_i X_j = (X_i X_j)_0 + (X_i X_j)_1 \cos \omega t + (X_i X_j)_2 \cos 2\omega t + \dots + (X_i X_j)_1^* \sin \omega t + (X_i X_j)_2^* \sin 2\omega t + \dots$$

Table 1 Examples of identified parameters

	Exact	Identified		Exact	Identified		Exact	Identified
m_1 kg	3.92	3.97	N/m^3	$\times 10^{11}$	$\times 10^{11}$	N/m^3	$\times 10^{11}$	$\times 10^{11}$
C_{11} Ns/m	$\times 10^2$	$\times 10^2$	1.111	1.61	1.63	1.266	0.00	1.02
C_{12}	0.00	0.00	1.112	0.00	0.00	1.333	0.00	0.14
C_{13}	0.00	0.00	1.113	-1.25	-1.30	1.334	0.00	0.38
C_{14}	0.00	0.00	1.114	0.00	0.01	1.335	0.00	0.58
C_{15}	0.00	0.01	1.115	0.00	0.08	1.336	0.00	0.77
C_{16}	0.00	0.00	1.116	0.00	0.00	1.344	0.00	0.87
			1.122	0.00	0.01	1.345	0.00	0.95
			1.123	0.00	0.00	1.346	0.00	1.04
			1.124	0.00	0.00	1.355	0.00	1.14
			1.125	0.00	0.00	1.356	0.00	1.19
k_1 N/m	$\times 10^5$	$\times 10^5$	1.126	0.00	0.00	1.366	0.00	1.26
	4.41	4.48	1.133	2.55	2.30	1.368	0.00	1.36
N/m^2	$\times 10^8$	$\times 10^8$	1.134	4.75	4.92	1.444	0.00	0.10
$\alpha_{1.11}$	0.00	0.00	1.135	0.00	0.13	1.445	0.00	0.68
$\alpha_{1.12}$	0.00	0.00	1.136	0.00	1.00	1.446	0.00	2.03
$\alpha_{1.13}$	0.00	0.00	1.138	0.00	-0.10	1.455	0.00	-1.65
$\alpha_{1.14}$	0.00	0.00	1.144	6.37	7.28	1.456	-7.93	-1.62
$\alpha_{1.15}$	0.00	0.00	1.145	0.00	-0.01	1.466	0.00	1.49
$\alpha_{1.16}$	0.00	0.00	1.146	0.00	0.00			
$\alpha_{1.22}$	0.00	0.00	1.155	0.00	0.00			
$\alpha_{1.23}$	0.00	0.00	1.156	0.00	0.00			
$\alpha_{1.24}$	0.00	0.00	1.166	0.00	0.00			
$\alpha_{1.25}$	0.00	0.00	1.222	0.00	0.00			
$\alpha_{1.26}$	0.00	0.00	1.223	1.68	1.69			
$\alpha_{1.33}$	0.00	0.00	1.224	0.00	0.04			
$\alpha_{1.34}$	0.00	0.00	1.225	0.00	-0.10			
$\alpha_{1.35}$	0.00	0.00	1.226	0.00	-0.07			
$\alpha_{1.36}$	0.00	0.00	1.233	0.00	0.06			
$\alpha_{1.44}$	0.00	0.00	1.234	0.00	-0.49			
$\alpha_{1.45}$	0.00	0.00	1.235	0.00	0.00			
$\alpha_{1.46}$	0.00	0.00	1.236	4.11	4.11			
$\alpha_{1.55}$	0.00	0.00	1.244	0.00	0.00			
$\alpha_{1.56}$	0.00	0.00	1.245	8.49	8.49			
$\alpha_{1.66}$	0.00	0.00	1.246	0.00	0.00			
			1.255	0.00	0.00			
			1.256	0.00	4.44			

$$X_i X_j X_k = (X_i X_j X_k)_0 + (X_i X_j X_k)_1 \cos \omega t + (X_i X_j X_k)_2 \cos 2\omega t + \dots + (X_i X_j X_k)_1^* \sin \omega t + (X_i X_j X_k)_2^* \sin 2\omega t + \dots \quad (16)$$

The Fourier coefficients $(X_i X_j)_0, (X_i X_j)_1, \dots$ are also considered known quantities. After substituting Eqs. (15) and (16) into Eqs. (13), we apply to the resulting equations the principle of harmonic balance, i.e., we equate the constant terms and the coefficients of $\cos \omega t, \sin \omega t, \dots$ of both sides up to an appropriate order. Then we have

$$[A]\{S\} = \{Q\} \quad (17)$$

where $\{S\}$ is an unknown vector given by

$$\{S\} = \{m_1 \dots c_{11} \dots k_1 \dots \alpha_{1,11} \dots \beta_{1,111} \dots\}^T \quad (18)$$

and $[A]$ and $\{Q\}$ are known matrix and vector, respectively, determined from the Fourier coefficients of Eqs. (15) and (16). The expressions of $[A]$ and $\{Q\}$ are omitted here, because in concrete cases they can be given easily.

Repeating the above procedures for various values of period T of the external force, we construct equations of the form of

Eq. (17) so that the number of equations exceeds that of the unknown parameters. Then the resulting equations are solved by the least square method. The result is

$$\{S\} = ([A]^T[A])^{-1}[A]^T\{Q\}. \quad (19)$$

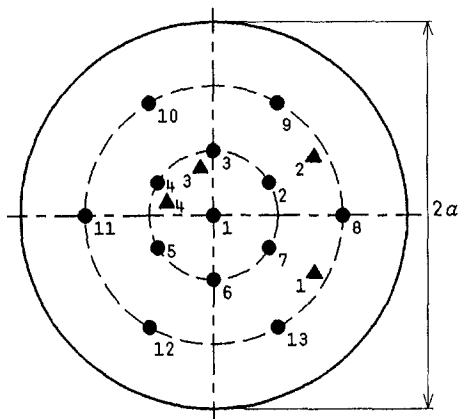
This completes the identification.

4 Numerical Simulation

To examine applicability of the proposed technique, we conduct numerical simulation. As examples of two-dimensional elastic structures, we consider plates. We obtain responses of the plates by numerical integration, and regard them as experimental data.

4.1 Rectangular Plate. First, we consider a rectangular plate with its four edges simply supported. The modal functions Φ_{mn} for this problem are given by

$$\Phi_{mn} = \sin \frac{m\pi x}{a} \sin \frac{n\pi y}{b} \quad (20)$$



● Points where deflection is measured
▲ Points where external force is applied

Fig. 4 Circular plate

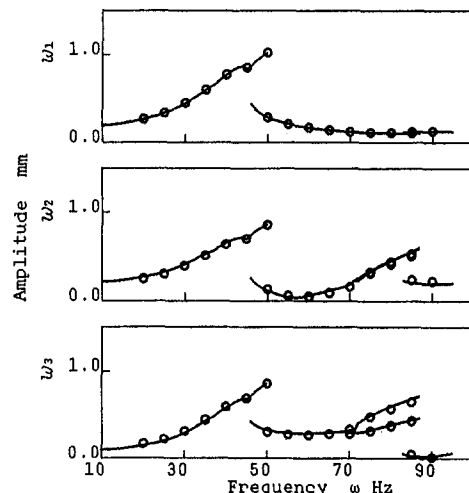


Fig. 5 Amplitudes of the deflections of the circular plate

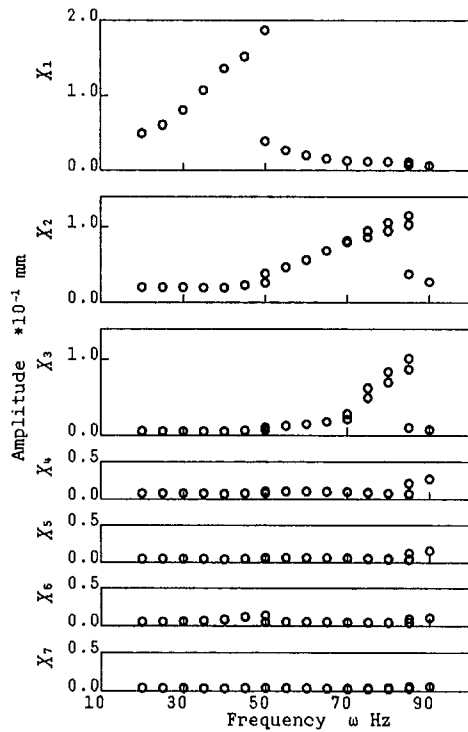


Fig. 6 Amplitudes of the modal coordinates of the circular plate

where x and y -axes are taken along the two neighboring sides of the plate, where a and b are the lengths of the two sides, and where m and n are integers denoting the order of modes (Nowacki, 1963). These modal functions are supposed to be available.

The values of the parameters are taken as

$$\begin{aligned} a &= 0.65 \text{ m}, \quad b = 0.35 \text{ m} \\ h &= 0.5 \times 10^{-3} \text{ m}, \quad \rho = 7.84 \times 10^3 \text{ kg/m}^3 \\ D &= 2.36 \text{ Nm}, \quad E = 2.06 \times 10^{11} \text{ Pa} \\ c &= 1.2 \times 10^2 \text{ Ns/m}^3, \quad N_0 = 4.0 \times 10^3 \text{ N/m}. \end{aligned} \quad (21)$$

As the external force, we adopt a concentrated harmonic force of the form

$$q = q_0 \delta(x - x_f) \delta(y - y_f) \cos \omega t \quad (22)$$

where q_0 is the magnitude of the force, and (x_f, y_f) is the excitation point at which the force is applied. The value of q_0 is taken here as 13 N . As excitation points, we select four points as shown in Fig. 1. As measuring points of deflection, we select 12 points as shown also in Fig. 1.

To make the data of deflection w , we use the first ten equations in Eqs. (10), and solve them numerically. Then the obtained periodic solutions are substituted into the first of Eqs. (5), and the values w_m ($m = 1, 2, \dots, 12$) of the deflection at the measuring points are calculated. As examples of the data, the amplitudes at the measuring points 1 to 3 when the excitation point 1 is excited, are shown by \circ in Fig. 2. The modal coordinates X_n obtained from these data are shown in Fig. 3.

From the values shown in Fig. 3 as well as those obtained when other points are excited, we see that the first six modal coordinates are significant. So we attempt to determine the first six equations of Eqs. (13).

The number of the unknown parameters contained in these equations is vast. To decrease the number, we suppose that the nonlinear terms in Eqs. (13) are derivable from a potential. In addition, since the fifth and sixth modal coordinates are small

as compared with the first four modal coordinates, we neglect, in the expression of the potential, terms which are given by products of the fifth and sixth modal coordinates with order higher than two. In applying the principle of harmonic balance, we retain terms up to the third order.

In this way, the values of all the parameters are determined. As examples, the values of parameters which appear in the first modal equations are shown in Table 1. For comparison, the original values of the parameters are also shown in the table. It is seen that the identified and original parameters agree well with each other. To see whether all the identified parameters are appropriate, we use them to predict the amplitudes of the deflection at the measuring points. The results are shown by solid line in Fig. 2, in which the original data were shown by \circ . It can be seen from this figure, that the amplitudes obtained from the identified parameters agree well with the original ones.

4.2 Circular Plate. As a second example, we consider a circular plate with its periphery clamped. The modal functions Φ_{mnc} , Φ_{mns} for this problem (Yasuda and Hayashi, 1982), expressed in polar coordinate system $O - r\theta$, are

$$\begin{aligned} \Phi_{mnc} &= \{J_m(p_{Jn}r) + \kappa_n I_m(p_{In}r)\} \cos m\theta \\ \Phi_{mns} &= \{J_m(p_{Jn}r) + \kappa_n I_m(p_{In}r)\} \sin m\theta \end{aligned} \quad (23)$$

where J_m and I_m are the Bessel function and the modified Bessel function, respectively, of order m , and p_{Jn} and p_{In} are the constants determined in terms of the eigenvalue p of the eigenvalue problem

$$-\rho h p^2 \Phi - N_0 \nabla^2 \Phi + D \nabla^4 \Phi = 0. \quad (24)$$

The modal functions of Eqs. (23) are supposed to be available.

The values of the parameters of the plate are taken as

$$\begin{aligned} a &= 0.65 \text{ m}, \quad h = 0.5 \times 10^{-3} \text{ m} \\ h &= 0.5 \times 10^{-3} \text{ m}, \quad \rho = 7.84 \times 10^3 \text{ kg/m}^3 \\ D &= 2.36 \text{ Nm}, \quad E = 2.06 \times 10^{11} \text{ Pa} \\ c &= 1.2 \times 10^2 \text{ Ns/m}^3, \quad N_0 = 4.0 \times 10^3 \text{ N/m}. \end{aligned} \quad (25)$$

As the external force q , we adopt concentrated harmonic force of the form

$$q = q_0 \delta(r - r_f) \delta(\theta - \theta_f) \cos \omega t \quad (26)$$

where q_0 is the magnitude of the force, and (r_f, θ_f) is the excitation point. The value of q_0 is taken as 3 N . As excitation points, we select four points as shown in Fig. 4. As measuring points of deflection, we select 13 points as shown also in Fig. 4.

To obtain the data of deflection, we use the first ten equations in Eqs. (10). The values w_m ($m = 1, 2, \dots, 13$) of the deflection at the measuring points are obtained similarly as above. Examples of the data are shown in Fig. 5. The modal coordinates X_n obtained from these data are shown in Fig. 6.

From the values of modal coordinates, it is seen that the first six modal coordinates are significant. We attempt to determine the first six modal equations in a similar manner as above for the rectangular plate.

The obtained results are used to predict the amplitudes of the deflection at the measuring points. They are shown by solid line in Fig. 5. It is seen from this figure, that the amplitudes obtained from the identified parameters agree well with the original ones shown by \circ .

5 Conclusion

An identification technique of a nonlinear two-dimensional vibrating elastic structure has been proposed. The technique enables one to determine the modal equations, with assuming that the modal functions of the linearized system are available.

Applicability of the proposed technique has been confirmed by numerical simulation.

References

- Busby, H. R., Nopporn, C., and Singh, R., 1986, "Experimental Modal Analysis of Non-Linear Systems: A Feasibility Study," *J. Sound Vib.*, Vol. 180, pp. 415–427.
- Ibanez, P., 1973, "Identification of Dynamic Parameters of Linear and Nonlinear Structural Models from Experimental Data," *J. Nucl. Eng. Des.*, Vol. 25, pp. 30–41.
- Kamiya, K., and Yasuda, K., 1993, "Experimental Identification of a Nonlinear Beam (Technique That Does Not Require Prior Knowledge of the Modal Functions)," 1994, *Trans. JSME*, Vol. 60, No. 573, pp. 1553–1560.
- Kirshenboim, J., and Ewins, D. J., 1984, "A Method for Recognizing Structural Nonlinearities in Steady-State Harmonic Testing," *ASME Journal of Vibration, Acoustics, Stress, and Reliability in Design*, Vol. 106, pp. 49–52.
- Masri, S. F., and Caughey, T. K., 1979, "A Nonparametric Identification Technique for Nonlinear Dynamic Problems," *ASME JOURNAL OF APPLIED MECHANICS*, Vol. 46, pp. 433–447.
- Masri, S. F., Miller, H., Sassi and Caughey, T. K., 1984, "A Method for Reducing the Order of Nonlinear Dynamic Systems," *ASME JOURNAL OF APPLIED MECHANICS*, Vol. 51, pp. 391–398.
- Masri, S. F., Miller, R. K., Saud, A. F., and Caughey, T. K., 1987a, "Identification of Nonlinear Vibrating Structures: Part I—Formulation," *ASME JOURNAL OF APPLIED MECHANICS*, Vol. 54, pp. 918–922.
- Masri, S. F., Miller, R. K., Saud, A. F., and Caughey, T. K., 1987b, "Identification of Nonlinear Vibrating Structures: Part II—Applications," *ASME JOURNAL OF APPLIED MECHANICS*, Vol. 54, pp. 923–929.
- Nowacki, W., 1963, *Dynamics of Elastic structures*, Chapman & Hall, pp. 206–212.
- Stanway, R., Sproston, J. L., and Stevens, N. G., 1985, "A Note on Parameter Estimation in Non-Linear Vibrating Systems," *Proc. Inst. Mech. Eng.*, Vol. 199, No. C1, pp. 79–84.
- Udwadia, F. E., and Kuo, Chin-Po, 1981, "Non-Parametric Identification of a Class of Non-Linear Close-Coupled Dynamic Systems," *Earthqu. Eng. Struct. Dyn.*, Vol. 9, pp. 385–409.
- Yang, Y. and Ibrahim, S. R., 1985, "A Nonparametric Identification Technique for a Variety of Discrete Nonlinear Vibrating Systems," *ASME Journal of Vibration, Acoustics, Stress, and Reliability in Design*, Vol. 107, pp. 60–66.
- Yasuda, K., Kawamura, S., and Watanabe, K., 1988a, "Identification of Nonlinear Multi-Degree-of-Freedom Systems (Presentation of an Identification Technique)," *JSME Int. J.*, Ser. III, Vol. 31, No. 1, pp. 8–14.
- Yasuda, K., Kawamura, S., and Watanabe, K., 1988b, "Identification of Nonlinear Multi-Degree-of-Freedom Systems (Identification Under Noisy Measurements)," *JSME Int. J.*, Ser. III, Vol. 31, No. 3, pp. 502–509.
- Yasuda, K., and Kawamura, S., 1989, "A Nonparametric Identification Technique for Nonlinear Vibratory Systems (Proposition of the Technique)," *JSME Int. J.*, Ser. III, Vol. 32, No. 3, pp. 365–372.
- Yasuda, K., and Kamiya, K., 1991, "Identification of Nonlinear Systems," *Proc. Asia-Pacific Vibration Conference*, pp. 2.28–2.33.
- Yasuda, K., and Kamiya, K., 1990, "Identification of a Nonlinear Beam (Proposition of an Identification Technique)," *JSME Int. J.*, Ser. III, Vol. 33, No. 4, pp. 535–540.
- Yasuda, K., and Hayashi, N., 1982, "Subharmonic Oscillations of a Prestressed Circular Plate," *Bull. JSME*, Vol. 25, No. 202, pp. 620–630.

Unified Second-Order Stochastic Averaging Approach

M. Hijawi

N. Moschuk

R. A. Ibrahim¹

Fellow ASME.

Wayne State University,
Department of Mechanical Engineering,
Detroit, MI 48202

First-order stochastic averaging has proven very useful in predicting the response statistics and stability of dynamic systems with nonlinear damping forces. However, the influence of system stiffness or inertia nonlinearities is lost during the averaging process. These nonlinearities can be recaptured only if one extends the stochastic averaging to second-order analysis. This paper presents a systematic and unified approach of second-order stochastic averaging based on the Stratonovich-Khasminskii limit theorem. Response statistics, stochastic stability, phase transition (known as noise-induced transition), and stabilization by multiplicative noise are examined in one treatment. A MACSYMA symbolic manipulation subroutine has been developed to perform the averaging processes for any type of nonlinearity. The method is implemented to analyze the response statistics of a second-order oscillator with three different types of nonlinearities, excited by both additive and multiplicative random processes. The second averaging results are in good agreement with those estimated by Monte Carlo simulation. For a special nonlinear oscillator, whose exact stationary solution is known, the second-order averaging results are identical to the exact solution up to first-order approximation.

1 Introduction

The stochastic averaging method, originally developed by Stratonovich (1963) and mathematically proved by Khasminskii (1966), has been widely used to predict the response statistics and stochastic stability of single-degree-of-freedom systems. The essence of the method is to replace the response, which contains rapid oscillations due to system nonlinearities, by a smooth response described by slowly varying amplitudes and phase shifts. Usually, the amplitude envelope of the response is uncoupled from the corresponding phase process. When considering only the stationary response of a system, high-frequency oscillations have a localized effect (in time) and do not contribute significantly to the average behavior of the system over a long period of time. The limit theorems developed by Khasminskii (1963, 1966, 1968) provide certain conditions concerning the random excitation and system parameters, such that if these conditions are satisfied, the response process converges to a diffusion Markov process. The implementation of this method to nonlinear dynamical systems with small damping is well documented by Ibrahim (1985), Roberts and Spanos (1986), Roberts (1989), and Zhu (1991). Recently, Roy (1994) extended the concept of stochastic averaging to systems excited by an arbitrary colored Gaussian process generated from multidimensional linear filters subjected to white noise.

Within the framework of first-order stochastic averaging, one can predict stochastic stability boundaries, the first-passage problem, and the response probability density function (pdf) of systems with damping nonlinearity. However, the effect of some other types of nonlinearities, such as cubic stiffness and special forms of nonlinear inertia, is lost during the averaging procedure. The effect of such nonlinearities can only be determined by performing second-order averaging. Second-order averaging

has not been widely used among dynamicists, apparently because it requires tedious mathematical manipulations. To the authors' knowledge, Baxter (1971) and Schmidt (1981) employed different forms of second-order averaging to parametrically excited systems with stiffness and inertia nonlinearities. For systems with nonlinear stiffness, alternative approaches have been proposed by Naprstek (1976), Iwan and Spanos (1978), and Roberts and Spanos (1986). These include a combination of equivalent linearization and first-order averaging (Naprstek, 1976 and Iwan and Spanos, 1978) and the stochastic averaging of the energy envelope (Roberts and Spanos, 1986). Spanos and Red-Horse (1988) and Red-Horse and Spanos (1992) extended the concept of energy envelope to problems with stiffness nonlinearity subjected to nonstationary and stationary excitations, respectively. In evaluating the diffusion parameter of the Ito equation, Red-Horse and Spanos (1992) assumed that the period of averaging to be larger than the correlation time of the white noise excitation.

The purpose of the present paper is to develop a unified second-order approach based on the same idea as in deterministic theory and the limit theorem of Khasminskii (1963). The method is systematic and is general for systems possessing stiffness, inertia, and damping nonlinearities. In addition to response statistics (pdf and response moments), the method gives conditions for phase transition and stochastic stability. A general MACSYMA symbolic algebraic subroutine is also developed to handle the algebraic manipulations of nonlinear single-degree-of-freedom systems subjected to external and/or parametric excitations. This paper is divided into two main sections. The first outlines the analytical scheme of second-order stochastic averaging, while the second is the implementation of the method to a general nonlinear system subjected to parametric random excitations in damping and stiffness and to external random excitation as well. The results are compared to those obtained using Monte Carlo simulation. The validity of the method is also verified using a special nonlinear oscillator whose exact stationary solution is known.

2 Analysis

Consider the nonlinear second-order differential equation

$$Y'' + Y = \psi(Y, Y', Y'', \xi_1(\tau), \xi_2(\tau), \dots, \epsilon) \quad (1)$$

where ϵ is a small parameter, a prime denotes differentiation

¹ To whom all correspondence should be addressed.

Contributed by the Applied Mechanics Division of THE AMERICAN SOCIETY OF MECHANICAL ENGINEERS for publication in the ASME JOURNAL OF APPLIED MECHANICS.

Discussion on this paper should be addressed to the Technical Editor, Professor Lewis T. Wheeler, Department of Mechanical Engineering, University of Houston, Houston, TX 77204-4792, and will be accepted until four months after final publication of the paper itself in the ASME JOURNAL OF APPLIED MECHANICS.

Manuscript received by the ASME Applied Mechanics Division, Jan. 5, 1995; final revision, Sept. 20, 1996. Associate Technical Editor: M. Shinozuka.

with respect to the time parameter τ , $\xi_1(\tau)$, $\xi_2(\tau)$, \dots are any zero-mean stationary bounded random processes with sufficiently well-behaved mixing properties (Ibragimov 1959, 1962). These properties require that the family of Sigma-algebra $\mathfrak{M}_{\tau_0}^{\tau}$ generated by the ω -sets of the form $\{\xi_j^{\omega}(\tau) \in \xi(\tau)\}$, $\tau_0 \leq \tau \leq \tau_1$, satisfy the two conditions:

- (i) $|P(AB) - P(A)P(B)| < R(T)P(A)$ for any τ , $A = \xi_j^{\omega}(\tau) \in \mathfrak{M}_{\tau_0}^{\tau}$, and $B = \xi_j^{\omega}(\tau) \in \mathfrak{M}_{\tau+T}^{\tau}$.
- (ii) $T^6 R(T) \downarrow 0$ as $T \rightarrow \infty$, where $R(T)$ is the autocorrelation function.

The power 6 is introduced by Khraminskii (1966) based on the proof of his limit theorem. This power also indicates that the correlation matrix of the process $\xi(\tau)$ decreases very fast as the correlation time increases.

The analysis is general for any number of random processes $\xi_i(\tau)$, however, for convenience it will be restricted to three random processes. The function Ψ includes stiffness, inertia, and damping nonlinearities, and linear damping. The random excitations $\xi_1(\tau)$, $\xi_2(\tau)$, and $\xi_3(\tau)$ can be additive or multiplicative. The motion of this system can be described by an asymptotic solution in terms of the behavior of its amplitude and phase angle. In such a system, the stationary response possesses an amplitude and phase which vary slowly about some "average" values

$$Y(\tau) = A(\tau) \cos \varphi(\tau), \quad Y'(\tau) = -A(\tau) \sin \varphi(\tau) \quad (2)$$

where $\varphi(\tau) = \tau + \theta(\tau)$

Transformation (2) can be differentiated to give the two first-order differential equations in amplitude and phase

$$A'(\tau) = \frac{Y'}{A} (Y + Y''), \quad \theta'(\tau) = -\frac{Y}{A^2} (Y + Y''). \quad (3)$$

Substituting (1) in (3) gives

$$A'(\tau) = \frac{Y'}{A} \psi(Y, Y', Y'', \xi_1(\tau), \xi_2(\tau), \xi_3(\tau), \epsilon),$$

$$\theta'(\tau) = -\frac{Y}{A^2} \psi(Y, Y', Y'', \xi_1(\tau), \xi_2(\tau), \xi_3(\tau), \epsilon) \quad (4)$$

The right-hand sides of Eqs. (4) are not explicit in A and θ . In this case Y and Y' can be replaced by using relations (2). Furthermore, the acceleration term Y'' which appears on the right-hand sides of Eqs. (4) must be eliminated by successive elimination up to any order of accuracy. The resulting equations can be written in the standard form

$$\begin{aligned} \begin{Bmatrix} A' \\ \theta' \end{Bmatrix} &= \epsilon \begin{Bmatrix} f_1(A, \theta, \tau) \\ f_2(A, \theta, \tau) \end{Bmatrix} \\ &+ \sqrt{\epsilon} \begin{bmatrix} g_{11}(A, \theta, \tau) & g_{12}(A, \theta, \tau) & g_{13}(A, \theta, \tau) \\ g_{21}(A, \theta, \tau) & g_{22}(A, \theta, \tau) & g_{23}(A, \theta, \tau) \end{bmatrix} \\ &\times \begin{Bmatrix} \xi_1(\tau) \\ \xi_2(\tau) \\ \xi_3(\tau) \end{Bmatrix} \end{aligned} \quad (5)$$

where f_1 and f_2 stand for drift terms, while the functions g_{ij} are associated with diffusion terms.

Inertia nonlinearities lead to higher-order terms in $\epsilon(\epsilon^2, \epsilon\sqrt{\epsilon}, \dots)$ which can also be included in the analysis. But for simplicity terms up to the order indicated in (5) will be retained. The nonlinear terms in f_1 and f_2 will contain numerous products of sine and cosine functions with phase angle $\varphi(\tau)$. These terms may be expanded into a series of sine and cosine functions at the multiple phase angles $n\varphi$, $n = 0, 1, 2, 3, \dots$. The functions with higher-order multiple phase angle represent rapid

oscillations or higher harmonics in the solution for the slowly varying amplitude and phase shift. When considering only the system stationary response, the high-frequency oscillations have a localized effect (in time) and do not contribute significantly to the average behavior of the system over a long period of time. We can therefore eliminate the oscillatory effects and simplify the equations of motion by introducing the near-identity transformation

$$A(\tau) = \bar{A}(\tau) + \epsilon u(\bar{A}, \bar{\theta}, \tau),$$

$$\theta(\tau) = \bar{\theta}(\tau) + \epsilon v(\bar{A}, \bar{\theta}, \tau) \quad (6)$$

where $\bar{A}(\tau)$, $\bar{\varphi}(\tau) = \bar{\theta}(\tau) + \tau$, and $\bar{\theta}(\tau)$ stand for nonoscillatory amplitude, phase angle, and phase shift, respectively. The functions u and v are expressed by the new series of functions

$$u(\bar{A}, \bar{\theta}, \tau) = \sum_{n=1}^N \epsilon^{n-1} u_n(\bar{A}, \bar{\theta}, \tau),$$

$$v(\bar{A}, \bar{\theta}, \tau) = \sum_{n=1}^N \epsilon^{n-1} v_n(\bar{A}, \bar{\theta}, \tau). \quad (7)$$

These functions are chosen in such a manner that they absorb all oscillatory terms which do not contain the random processes $\xi_1(\tau)$, $\xi_2(\tau)$, and $\xi_3(\tau)$. Representation (7) indicates that the first term leads to second-order averaging. Second and higher-order terms give rise to higher-order approximations and will not be considered. The contribution of higher-order terms beyond the first will only refine quantitative results and will not reveal new characteristics of the system. Terms containing excitation functions $\xi_1(\tau)$, $\xi_2(\tau)$, and $\xi_3(\tau)$ may also introduce oscillatory effects into the solution, however, their effect will be treated separately from the oscillatory effects of the nonexcitation terms. Accordingly, consider only the deterministic part of the Eq. (5). Differentiating relations (6) and equating each result with the corresponding drift functions from Eq. (5) gives

$$\begin{aligned} \bar{A}' + \epsilon \left\{ \frac{\partial u}{\partial \bar{A}} \bar{A}' + \frac{\partial u}{\partial \bar{\theta}} \bar{\theta}' + \frac{\partial u}{\partial \tau} \right\} &= \epsilon f_1(\bar{A} + \epsilon u, \bar{\theta} + \epsilon v, \tau) \\ \bar{\theta}' + \epsilon \left\{ \frac{\partial v}{\partial \bar{A}} \bar{A}' + \frac{\partial v}{\partial \bar{\theta}} \bar{\theta}' + \frac{\partial v}{\partial \tau} \right\} &= \epsilon f_2(\bar{A} + \epsilon u, \bar{\theta} + \epsilon v, \tau). \end{aligned} \quad (8)$$

Alternatively, these equations can be written in the matrix form

$$\begin{aligned} \begin{bmatrix} 1 + \epsilon \frac{\partial u}{\partial \bar{A}} & \epsilon \frac{\partial u}{\partial \bar{\theta}} \\ \epsilon \frac{\partial v}{\partial \bar{A}} & 1 + \epsilon \frac{\partial v}{\partial \bar{\theta}} \end{bmatrix} \begin{Bmatrix} \bar{A}' \\ \bar{\theta}' \end{Bmatrix} &= \epsilon \begin{Bmatrix} f_1(\bar{A} + \epsilon u, \bar{\theta} + \epsilon v, \tau) - \frac{\partial u}{\partial \tau} \\ f_2(\bar{A} + \epsilon u, \bar{\theta} + \epsilon v, \tau) - \frac{\partial v}{\partial \tau} \end{Bmatrix}. \end{aligned} \quad (8a)$$

Premultiplying both sides of (8a) by the inverse of the left square matrix and taking into account that

$$\begin{aligned} f_j(\bar{A} + \epsilon u, \bar{\theta} + \epsilon v, \tau) &= f_j(\bar{A}, \bar{\theta}, \tau) \\ &+ \epsilon \frac{\partial f_j}{\partial \bar{A}} u + \epsilon \frac{\partial f_j}{\partial \bar{\theta}} v + \text{H.O.T.}, \quad j = 1, 2 \end{aligned} \quad (9)$$

where H.O.T. stands for Higher Order Terms, and

$$\begin{bmatrix} 1 + \epsilon \frac{\partial u}{\partial \bar{A}} & \epsilon \frac{\partial u}{\partial \bar{\theta}} \\ \epsilon \frac{\partial v}{\partial \bar{A}} & 1 + \epsilon \frac{\partial v}{\partial \bar{\theta}} \end{bmatrix}^{-1} = \begin{bmatrix} 1 - \epsilon \frac{\partial u}{\partial \bar{A}} & -\epsilon \frac{\partial u}{\partial \bar{\theta}} \\ -\epsilon \frac{\partial v}{\partial \bar{A}} & 1 - \epsilon \frac{\partial v}{\partial \bar{\theta}} \end{bmatrix} + \text{H.O.T.} \quad (10)$$

results in the following equations

$$\begin{aligned} \bar{A}' &= \epsilon \bar{A}_1 + \epsilon^2 \bar{A}_2 + \text{H.O.T.}, \\ \bar{\theta}' &= \epsilon \bar{\theta}_1 + \epsilon^2 \bar{\theta}_2 + \text{H.O.T.} \end{aligned} \quad (11)$$

where

$$\begin{aligned} \bar{A}_1 &= f_1 - \frac{\partial u}{\partial \tau}, \\ \bar{A}_2 &= \frac{\partial f_1}{\partial \bar{A}} u + \frac{\partial f_1}{\partial \bar{\theta}} v - \frac{\partial u}{\partial \bar{A}} f_1 - \frac{\partial u}{\partial \bar{\theta}} f_2 + \frac{\partial u}{\partial \tau} \frac{\partial u}{\partial \bar{A}} + \frac{\partial v}{\partial \tau} \frac{\partial u}{\partial \bar{\theta}}, \\ \bar{\theta}_1 &= f_2 - \frac{\partial v}{\partial \tau}, \\ \bar{\theta}_2 &= \frac{\partial f_2}{\partial \bar{A}} u + \frac{\partial f_2}{\partial \bar{\theta}} v - \frac{\partial v}{\partial \bar{A}} f_1 - \frac{\partial v}{\partial \bar{\theta}} f_2 + \frac{\partial u}{\partial \tau} \frac{\partial v}{\partial \bar{A}} + \frac{\partial v}{\partial \tau} \frac{\partial v}{\partial \bar{\theta}}. \end{aligned} \quad (12)$$

The functions u and v are determined in such a manner that $f_1 - (\partial u / \partial \tau)$ and $f_2 - (\partial v / \partial \tau)$ contain only nonoscillatory terms. This can be achieved by solving the first-order differential equations

$$\frac{\partial u}{\partial \tau} = f_1 - \langle f_1 \rangle_\tau, \quad \frac{\partial v}{\partial \tau} = f_2 - \langle f_2 \rangle_\tau. \quad (13)$$

This means that the average values are subtracted from f_j , $j = 1, 2$, to make sure that u and v are oscillatory functions. Upon integrating Eqs. (13) one obtains

$$\begin{aligned} u(\bar{A}, \bar{\theta}, \tau) &= \int_0^\tau \{f_1(\bar{A}, \bar{\theta}, \bar{\tau}) - \langle f_1 \rangle_\tau\} d\bar{\tau} \\ &= \text{Osc. Terms} + z_1(\bar{A}, \bar{\theta}) \\ v(\bar{A}, \bar{\theta}, \tau) &= \int_0^\tau \{f_2(\bar{A}, \bar{\theta}, \bar{\tau}) - \langle f_2 \rangle_\tau\} d\bar{\tau} \\ &= \text{Osc. Terms} + z_2(\bar{A}, \bar{\theta}) \end{aligned} \quad (14)$$

where $z_1(\bar{A}, \bar{\theta})$ and $z_2(\bar{A}, \bar{\theta})$ are constants of integration. Having obtained functions u and v , expressions for \bar{A}_2 and $\bar{\theta}_2$ of (12) become

$$\begin{aligned} \bar{A}_2 &= \frac{\partial f_1}{\partial \bar{A}} u + \frac{\partial f_1}{\partial \bar{\theta}} v - \frac{\partial u}{\partial \bar{A}} \langle f_1 \rangle - \frac{\partial u}{\partial \bar{\theta}} \langle f_2 \rangle, \\ \bar{\theta}_2 &= \frac{\partial f_2}{\partial \bar{A}} u + \frac{\partial f_2}{\partial \bar{\theta}} v - \frac{\partial v}{\partial \bar{A}} \langle f_1 \rangle - \frac{\partial v}{\partial \bar{\theta}} \langle f_2 \rangle \end{aligned} \quad (15a)$$

where relations (13) have been used. Applying the indicated transformation to the original Eq. (5), the following stochastic differential equations in terms of the new variables \bar{A} , $\bar{\theta}$ are obtained

$$\begin{aligned} \bar{A}' &= \epsilon \bar{A}_1(\bar{A}) + \epsilon^2 \bar{A}_2(\bar{A}, \bar{\theta}, \tau) + \sqrt{\epsilon} [g_{11}(\bar{A}, \bar{\theta}, \tau) \xi_1(\tau) \\ &+ g_{12}(\bar{A}, \bar{\theta}, \tau) \xi_2(\tau) + g_{13}(\bar{A}, \bar{\theta}, \tau) \xi_3(\tau)] \end{aligned}$$

$$\begin{aligned} &+ \epsilon \sqrt{\epsilon} [\bar{g}_{11}(\bar{A}, \bar{\theta}, \tau) \xi_1(\tau) + \bar{g}_{12}(\bar{A}, \bar{\theta}, \tau) \xi_2(\tau) \\ &+ \bar{g}_{13}(\bar{A}, \bar{\theta}, \tau) \xi_3(\tau)] + \text{H.O.T.} \end{aligned} \quad (16a)$$

$$\begin{aligned} \bar{\theta}' &= \epsilon \bar{\theta}_1(\bar{A}) + \epsilon^2 \bar{\theta}_2(\bar{A}, \bar{\theta}, \tau) + \sqrt{\epsilon} [g_{21}(\bar{A}, \bar{\theta}, \tau) \xi_1(\tau) \\ &+ g_{22}(\bar{A}, \bar{\theta}, \tau) \xi_2(\tau) + g_{23}(\bar{A}, \bar{\theta}, \tau) \xi_3(\tau)] \\ &+ \epsilon \sqrt{\epsilon} [\bar{g}_{21}(\bar{A}, \bar{\theta}, \tau) \xi_1(\tau) + \bar{g}_{22}(\bar{A}, \bar{\theta}, \tau) \xi_2(\tau) \\ &+ \bar{g}_{23}(\bar{A}, \bar{\theta}, \tau) \xi_3(\tau)] + \text{H.O.T.} \end{aligned} \quad (16b)$$

where

$$\begin{aligned} \bar{g}_{11} &= -g_{11} \frac{\partial u}{\partial \bar{A}} - g_{21} \frac{\partial u}{\partial \bar{\theta}} + u \frac{\partial g_{11}}{\partial \bar{A}} + v \frac{\partial g_{11}}{\partial \bar{\theta}}, \\ \bar{g}_{12} &= -g_{12} \frac{\partial u}{\partial \bar{A}} - g_{22} \frac{\partial u}{\partial \bar{\theta}} + u \frac{\partial g_{12}}{\partial \bar{A}} + v \frac{\partial g_{12}}{\partial \bar{\theta}}, \\ \bar{g}_{13} &= -g_{13} \frac{\partial u}{\partial \bar{A}} - g_{23} \frac{\partial u}{\partial \bar{\theta}} + u \frac{\partial g_{13}}{\partial \bar{A}} + v \frac{\partial g_{13}}{\partial \bar{\theta}}, \\ \bar{g}_{21} &= -g_{11} \frac{\partial v}{\partial \bar{A}} - g_{21} \frac{\partial v}{\partial \bar{\theta}} + u \frac{\partial g_{21}}{\partial \bar{A}} + v \frac{\partial g_{21}}{\partial \bar{\theta}}, \\ \bar{g}_{22} &= -g_{12} \frac{\partial v}{\partial \bar{A}} - g_{22} \frac{\partial v}{\partial \bar{\theta}} + u \frac{\partial g_{22}}{\partial \bar{A}} + v \frac{\partial g_{22}}{\partial \bar{\theta}}, \\ \bar{g}_{23} &= -g_{13} \frac{\partial v}{\partial \bar{A}} - g_{23} \frac{\partial v}{\partial \bar{\theta}} + u \frac{\partial g_{23}}{\partial \bar{A}} + v \frac{\partial g_{23}}{\partial \bar{\theta}} \end{aligned}$$

where use has been made for the expansion

$$\begin{aligned} g_{ij}(\bar{A} + \epsilon u, \bar{\theta} + \epsilon v) \\ = g_{ij}(\bar{A}, \bar{\theta}) + \epsilon \frac{\partial g_{ij}}{\partial \bar{A}} u + \epsilon \frac{\partial g_{ij}}{\partial \bar{\theta}} v + \text{H.O.T.} \end{aligned}$$

Assume that $\xi_j(\tau)$ are stationary random processes with zero means and with correlation matrix $[R_{ij}(\tau)]$. If the coefficients of Eqs. (16) are sufficiently smooth, the processes $\xi_j(\tau)$ have sufficiently good mixing properties and its correlation matrix $[R_{ij}(\tau)]$ sufficiently quickly decreases when $\tau \rightarrow \infty$ then there is a limit Markov diffusion process, as $\epsilon \rightarrow 0$, which can be described by the well known Ito stochastic differential equations

$$d\mathbf{x} = \mathbf{a}(\mathbf{x})d\tau + \boldsymbol{\sigma}(\mathbf{x})d\mathbf{B} \quad (17)$$

where $\mathbf{x} = \{\bar{A}, \bar{\theta}\}^T$, and $\mathbf{B}(\tau) = \{B_1(\tau), B_2(\tau)\}^T$ is a two-dimensional vector of independent Brownian motion processes. The elements of the drift vector $\mathbf{a}(\mathbf{x})$ and of the diffusion matrix $\mathbf{b}(\mathbf{x}) = \boldsymbol{\sigma}(\mathbf{x})\boldsymbol{\sigma}(\mathbf{x})^T$ are given by the following expressions according to Khasminskii limit theorem:

$$\begin{aligned} a_1(\bar{A}) &= \epsilon \bar{A}_1(\bar{A}) + \epsilon^2 \frac{1}{T} \int_0^T \bar{A}_2(\mathbf{x}, \tau) d\tau \\ &+ \epsilon \sum_{j=1}^2 \sum_{k=1}^3 \sum_{l=1}^3 \frac{1}{T} \int_0^T d\bar{\tau} \int_{-\infty}^0 d\tau \frac{\partial g_{1k}}{\partial x_j}(\mathbf{x}, \bar{\tau}) \\ &\times g_{jl}(\mathbf{x}, \bar{\tau} + \tau) R_{kl}(\tau) + \epsilon^2 \sum_{j=1}^2 \sum_{k=1}^3 \sum_{l=1}^3 \frac{1}{T} \int_0^T d\bar{\tau} \\ &\times \int_{-\infty}^0 d\tau \left[\frac{\partial g_{1k}}{\partial x_j}(\mathbf{x}, \bar{\tau}) \bar{g}_{jl}(\mathbf{x}, \bar{\tau} + \tau) \right. \\ &\left. + \frac{\partial \bar{g}_{1k}}{\partial x_j}(\mathbf{x}, \bar{\tau}) g_{jl}(\mathbf{x}, \bar{\tau} + \tau) \right] R_{kl}(\tau) \end{aligned} \quad (18a)$$

$$\begin{aligned}
a_2(\bar{A}) = & \epsilon \bar{\Theta}_1(\bar{A}) + \epsilon^2 \frac{1}{T} \int_0^T \bar{\Theta}_2(\mathbf{x}, \tau) d\tau \\
& + \epsilon \sum_{j=1}^2 \sum_{k=1}^3 \sum_{l=1}^3 \frac{1}{T} \int_0^T d\tau \int_{-\infty}^0 d\tau' \frac{\partial g_{2k}}{\partial x_j}(\mathbf{x}, \tau') \\
& \times g_{jl}(\mathbf{x}, \tau' + \tau) R_{kl}(\tau) + \epsilon^2 \sum_{j=1}^2 \sum_{k=1}^3 \sum_{l=1}^3 \frac{1}{T} \int_0^T d\tau \\
& \times \int_{-\infty}^0 d\tau' \left[\frac{\partial g_{2k}}{\partial x_j}(\mathbf{x}, \tau') \bar{g}_{jl}(\mathbf{x}, \tau' + \tau) \right. \\
& \left. + \frac{\partial \bar{g}_{2k}}{\partial x_j}(\mathbf{x}, \tau') g_{jl}(\mathbf{x}, \tau' + \tau) \right] R_{kl}(\tau) \quad (18b)
\end{aligned}$$

$$\begin{aligned}
b_{ij}(\bar{A}) = & \epsilon \sum_{k=1}^3 \sum_{l=1}^3 \frac{1}{T} \int_0^T d\tau \\
& \times \int_{-\infty}^{+\infty} d\tau' g_{ik}(\mathbf{x}, \tau') g_{jl}(\mathbf{x}, \tau) R_{kl}(\tau - \tau') \\
& + \epsilon^2 \sum_{k=1}^3 \sum_{l=1}^3 \frac{1}{T} \int_0^T d\tau \int_{-\infty}^{+\infty} d\tau' [g_{ik}(\mathbf{x}, \tau') \bar{g}_{jl}(\mathbf{x}, \tau) \\
& + \bar{g}_{ik}(\mathbf{x}, \tau') g_{jl}(\mathbf{x}, \tau)] R_{kl}(\tau - \tau'). \quad (19)
\end{aligned}$$

Accordingly Eq. (17) can be written in the following form:

$$\left(\frac{\bar{A}}{\bar{\theta}} \right)' = \begin{pmatrix} a_1 \\ a_2 \end{pmatrix} + \begin{bmatrix} b_{11} & b_{12} \\ b_{21} & b_{22} \end{bmatrix}^{1/2} \begin{pmatrix} W_1(\tau) \\ W_2(\tau) \end{pmatrix} \quad (20)$$

where $\begin{bmatrix} b_{11} & b_{12} \\ b_{21} & b_{22} \end{bmatrix}^{1/2} = [\sigma_{ij}]$, $W_1(\tau) = (dB_1(\tau)/d\tau)$ and $W_2(\tau) = (dB_2(\tau)/d\tau)$ are two equivalent independent white noise processes, each with unit intensity. Generally speaking, $b_{12} = b_{21} \neq 0$. Note that the coordinate \bar{A} forms a diffusion process described by the following Ito equation:

$$\bar{A}' = a_1(\bar{A}) + \sqrt{b_{11}(\bar{A})} W(\tau)$$

and the corresponding Fokker-Planck equation for the amplitude \bar{A} is

$$\begin{aligned}
\frac{\partial p(\bar{A}, \tau)}{\partial \tau} = & - \frac{\partial}{\partial \bar{A}} (a_1(\bar{A}) p(\bar{A}, \tau)) \\
& + \frac{1}{2} \frac{\partial^2 (b_{11}(\bar{A}) p(\bar{A}, \tau))}{\partial \bar{A}^2} \quad (21)
\end{aligned}$$

with the normalization condition $\int_0^\infty p(\bar{A}, \tau) d\bar{A} = 1$. The phase is uniformly distributed on the circle $[0, 2\pi]$. The relationship between $p(A, \theta)$ and $p(\bar{A}, \bar{\theta})$ is obtained by using the well-known transformation $p(A, \theta) = p(\bar{A}, \bar{\theta}) |J|$ where $J = |\partial(\bar{A}, \bar{\theta})/\partial(A, \theta)|$ is the Jacobian given by the expression, using relations (6),

$$J = 1 - \epsilon \frac{\partial u(A, \theta, \tau)}{\partial A} - \epsilon \frac{\partial v(A, \theta, \tau)}{\partial \theta} + \text{H.O.T.}$$

and $\bar{p}(\bar{A}, \bar{\theta})$ may be represented by the asymptotic expansion

$$\begin{aligned}
\bar{p}(\bar{A}, \bar{\theta}) = & \bar{p}(A, \theta) - \epsilon u(A, \theta, \tau) \frac{\partial \bar{p}(A, \theta)}{\partial A} \\
& - \epsilon v(A, \theta, \tau) \frac{\partial \bar{p}(A, \theta)}{\partial \theta} + \text{H.O.T.}
\end{aligned}$$

Eventually $p(A, \theta)$ may be written in the form

$$\begin{aligned}
p(A, \theta) = & \bar{p}(A, \theta) - \epsilon \left[\frac{\partial}{\partial A} (\bar{p}(A, \theta) u(A, \theta, \tau)) \right. \\
& \left. + \frac{\partial}{\partial \theta} (\bar{p}(A, \theta) v(A, \theta, \tau)) \right] + \text{H.O.T.}
\end{aligned}$$

The relationship between $p(A)$ and $\bar{p}(\bar{A})$ is obtained from (23) by averaging both sides with respect to θ . It takes the form

$$p(A) = \bar{p}(\bar{A}) - \epsilon \frac{\partial}{\partial A} [\bar{p}(\bar{A}) \langle z_1(A, \theta) \rangle] + \text{H.O.T.} \quad (21a)$$

where $\langle \rangle$ means averaging with respect to θ . This result is valid provided that $p(A)$ is always positive. In other words, the expression $\epsilon(\partial/\partial A)[\bar{p}(\bar{A})\langle z_1(A, \theta) \rangle]$ in relation (21a) should not exceed 1, otherwise additional higher-order terms should be included.

The problem of noise-induced transition is examined by the qualitative change in the state of the system. This transition is not reflected in the moments of the stationary probability. The appropriate indicator of a transition are the extrema of the probability density (Horsthemke and Lefever, 1989). The extrema of the stationary probability density of the system are determined from the condition $dp(\bar{A})/d\bar{A} = 0$. This condition can be derived from the stationary Fokker-Planck equation of (21)

$$a_1(\bar{A}) - \frac{1}{2} \frac{d(b_{11}(\bar{A}))}{d\bar{A}} = 0. \quad (22)$$

Having obtained $p(\bar{A})$, one can estimate the moments of the response amplitude A

$$\begin{aligned}
E[A^n] = & \int_{\bar{\theta}=0, \bar{A}=0}^{\bar{\theta}=2\pi, \bar{A}=\infty} [\bar{A} + \epsilon u(\bar{A}, \bar{\theta})]^n p(\bar{A}, \bar{\theta}) d\bar{A} d\bar{\theta} \\
= & \int_0^\infty [\bar{A} + \epsilon z_1(\bar{A})]^n p(\bar{A}) d\bar{A}. \quad (23)
\end{aligned}$$

Note that the procedure can be reduced to first-order averaging if the functions u and v are set to zero. However, certain terms such as cubic stiffness and inertia will appear as oscillatory terms whose average values vanish. The role of the functions u and v is to bring the average values of these terms when treated as higher-order terms. This is the main rationale of second-order averaging.

3 Application

3.1 General Case. Consider the following stochastic nonlinear oscillator:

$$\begin{aligned}
Y'' + Y = & \epsilon(-\zeta Y' + \alpha_2 Y^2 + \alpha_3 Y Y' + \alpha_4 Y'^2 \\
& + \alpha_5 Y^3 + \alpha_6 Y^2 Y' + \alpha_7 Y Y'^2 + \alpha_8 Y'^3) \\
& + \sqrt{\epsilon} \gamma_1 \xi_1(\tau) + \sqrt{\epsilon} \gamma_2 Y \xi_2(\tau) + \sqrt{\epsilon} \gamma_3 Y' \xi_3(\tau). \quad (24)
\end{aligned}$$

Note that the nonlinearities include the following types: (i) nonlinear damping given by the terms $\alpha_3 Y Y' + \alpha_4 Y'^2 + \alpha_6 Y^2 Y' + \alpha_7 Y Y'^2$, (ii) nonlinear inertia given by the term $\alpha_5 Y^3$, and (iii) nonlinear stiffness given by the term $\alpha_2 Y^2$. The above system is also excited externally and parametrically as indicated by the last three terms. The state equations for the system (24) can now be written in the form (5) where

$$\begin{aligned}
f_1(A, \varphi) = & -\frac{1}{2}\zeta A + \frac{1}{8}(\alpha_6 + 3\alpha_8)A^3 + \frac{1}{2}\zeta \cos(2\varphi)A \\
& + [-\frac{1}{4}(\alpha_2 + 3\alpha_4) \sin \varphi + \frac{1}{4}\alpha_3 \cos \varphi \\
& + \frac{1}{4}(\alpha_4 - \alpha_2) \sin 3\varphi - \frac{1}{4}\alpha_3 \cos 3\varphi]A^2
\end{aligned}$$

$$\begin{aligned}
& + \left[-\frac{1}{4}(\alpha_5 + \alpha_7) \sin 2\varphi - \frac{1}{2}\alpha_8 \cos 2\varphi \right. \\
& \quad \left. + \frac{1}{8}(\alpha_7 - \alpha_5) \sin 4\varphi + \frac{1}{8}(\alpha_8 - \alpha_6) \cos 4\varphi \right] A^3 \\
f_2(A, \varphi) &= -\frac{1}{8}(3\alpha_5 + \alpha_7)A^2 - \frac{1}{2}\zeta \sin(2\varphi) \\
& + \left[\frac{1}{4}\alpha_3 \sin \varphi - \frac{1}{4}(3\alpha_2 + \alpha_4) \cos \varphi \right. \\
& + \frac{1}{4}(\alpha_4 - \alpha_2) \cos 3\varphi + \frac{1}{4}\alpha_3 \sin 3\varphi \big] A \\
& + \left[-\frac{1}{2}\alpha_5 \cos 2\varphi + \frac{1}{4}(\alpha_6 + \alpha_8) \sin 2\varphi \right. \\
& \quad \left. + \frac{1}{8}(\alpha_7 - \alpha_5) \cos 4\varphi + \frac{1}{8}(\alpha_6 - \alpha_8) \sin 4\varphi \right] A^2 \\
g_{11} &= -\gamma_1 \sin \varphi, \quad g_{12} = -\gamma_2 A \sin \varphi \cos \varphi, \\
g_{13} &= \gamma_3 A \sin^2 \varphi \\
g_{21} &= -\cos \varphi \frac{\gamma_1}{A}, \quad g_{22} = -\gamma_2 \cos^2 \varphi, \\
g_{23} &= \gamma_3 \sin \varphi \cos \varphi, \quad \varphi = \theta + \tau. \quad (25)
\end{aligned}$$

Introducing transformations (2) and (6) and following the procedure described in Section 2 to evaluate the functions u and v as defined by relations (14) the following expressions are obtained:

$$\begin{aligned}
u(\bar{A}, \bar{\varphi}) &= \frac{1}{4}\zeta \sin(2\bar{\varphi})\bar{A} + \left[\frac{1}{4}(\alpha_2 + 3\alpha_4) \cos \bar{\varphi} \right. \\
& + \frac{1}{4}\alpha_3 \sin \bar{\varphi} - \frac{1}{12}(\alpha_4 - \alpha_2) \cos(3\bar{\varphi}) - \frac{1}{12}\alpha_3 \sin(3\bar{\varphi}) \big] \bar{A}^2 \\
& + \left[\frac{1}{8}(\alpha_5 + \alpha_7) \cos(2\bar{\varphi}) - \frac{1}{4}\alpha_8 \sin(2\bar{\varphi}) \right. \\
& - \frac{1}{32}(\alpha_7 - \alpha_5) \cos(4\bar{\varphi}) + \frac{1}{32}(\alpha_8 - \alpha_6) \sin(4\bar{\varphi}) \big] \bar{A}^3 \\
& \quad \left. + z_1(\bar{A}) \right] \quad (26a)
\end{aligned}$$

$$\begin{aligned}
v(\bar{A}, \bar{\varphi}) &= \frac{1}{4}\zeta \cos(2\bar{\varphi}) + \left[-\frac{1}{4}(3\alpha_2 + \alpha_4) \sin \bar{\varphi} \right. \\
& - \frac{1}{4}\alpha_3 \cos \bar{\varphi} + \frac{1}{12}(\alpha_4 - \alpha_2) \sin(3\bar{\varphi}) - \frac{1}{12}\alpha_3 \cos(3\bar{\varphi}) \big] \bar{A} \\
& + \left[-\frac{1}{8}(\alpha_6 + \alpha_8) \cos(2\bar{\varphi}) - \frac{1}{4}\alpha_5 \sin(2\bar{\varphi}) \right. \\
& + \frac{1}{32}(\alpha_7 - \alpha_5) \sin(4\bar{\varphi}) + \frac{1}{32}(\alpha_8 - \alpha_6) \cos(4\bar{\varphi}) \big] \bar{A}^2 \\
& \quad \left. + z_2(\bar{A}) \right] \quad (26b)
\end{aligned}$$

$$\bar{\varphi} = \bar{\theta} + \tau.$$

Now substituting (26a, b) in transformation (6) and applying Khasminskii's limit theorem, the following expressions for the drift and diffusion coefficients a_1 and b_{11} are obtained:

$$\begin{aligned}
a_1 &= \epsilon \left\{ \left[-\frac{1}{2}\zeta + \frac{3}{8}\pi\gamma_2^2 S_2(2) \right. \right. \\
& + \frac{3}{8}\pi\gamma_3^2 S_3(2) + \frac{1}{4}\pi\gamma_3^2 S_3(0) \big] \bar{A} \\
& + \frac{1}{8}(3\alpha_8 + \alpha_6)\bar{A}^3 + \frac{1}{2}\gamma_1^2 \pi S_1(1)\bar{A}^{-1} \big\} \\
& + \epsilon^2 \left\{ \frac{1}{16}(9\alpha_5 + 7\alpha_7)\gamma_1^2 \pi S_1(1)\bar{A} \right.
\end{aligned}$$

$$\begin{aligned}
& + \left[\frac{1}{8}(\alpha_2\alpha_3 + \alpha_3\alpha_4 - \zeta\alpha_7) \right. \\
& + \frac{1}{64}(25\alpha_5 + 7\alpha_7)\gamma_2^2 \pi S_2(2) \\
& + \frac{1}{64}(15\alpha_5 + 17\alpha_7)\gamma_3^2 S_3(2) + \frac{1}{4}\alpha_7\gamma_3^2 \pi S_3(0) \big] \bar{A}^3 \\
& + \frac{1}{32}(\alpha_5\alpha_6 + \alpha_6\alpha_7 + \alpha_7\alpha_8 - 3\alpha_5\alpha_8)\bar{A}^5 \\
& + \frac{1}{8}[\gamma_2^2 \pi S_2(2) + \gamma_3^2 \pi S_3(2)] \left[3 \left(z_1 - \bar{A} \frac{dz_1}{d\bar{A}} \right) \right. \\
& - A^2 \frac{d^2 z_1}{d\bar{A}^2} \bigg] + \frac{1}{4}\gamma_3^2 \pi S_3(0) \left(z_1 - \bar{A} \frac{dz_1}{d\bar{A}} - A^2 \frac{d^2 z_1}{d\bar{A}^2} \right) \\
& + \frac{1}{8}(\alpha_6 + 3\alpha_8) \left(3A^2 z_1 - A^3 \frac{dz_1}{d\bar{A}} \right) \\
& - \frac{1}{2}\gamma_1^2 \pi S_1(1) \left(\bar{A}^{-2} z_1 + \bar{A}^{-1} \frac{dz_1}{d\bar{A}} + \frac{d^2 z_1}{d\bar{A}^2} \right) \\
& \quad \left. - \frac{1}{2}\zeta \left(z_1 - \bar{A} \frac{dz_1}{d\bar{A}} \right) \right\} \quad (27)
\end{aligned}$$

$$\begin{aligned}
b_{11} &= \epsilon \left\{ \gamma_1^2 \pi S_1(1) + \left[\frac{1}{4}\gamma_2^2 \pi S_2(2) \right. \right. \\
& + \frac{1}{4}\gamma_3^2 \pi S_3(2) + \frac{1}{2}\gamma_3^2 \pi S_3(0) \big] \bar{A}^2 \big\} \\
& + \epsilon^2 \left\{ \frac{1}{8}(3\alpha_5 + 5\alpha_7)\gamma_1^2 \pi S_1(1)\bar{A}^2 \right. \\
& + \left[\frac{1}{32}(5\alpha_5 + 3\alpha_7)\gamma_2^2 \pi S_2(2) \right. \\
& + \frac{1}{32}(3\alpha_5 + 5\alpha_7)\gamma_3^2 \pi S_3(2) + \frac{1}{4}\alpha_7\gamma_3^2 \pi S_3(0) \big] \bar{A}^4 \\
& + \frac{1}{2}[\gamma_2^2 \pi S_2(2) + \gamma_3^2 \pi S_3(2) + 2\gamma_3^2 \pi S_3(0)] \\
& \quad \times \left(z_1 \bar{A} - \frac{dz_1}{d\bar{A}} A^2 \right) - 2\gamma_1^2 \pi S_1(1) \frac{dz_1}{d\bar{A}} \bigg\}. \quad (28)
\end{aligned}$$

Note that all terms of order ϵ in the diffusion function b_{11} are positive definite. Terms of order ϵ^2 are guaranteed to be positive definite if the function $z_1(\bar{A})$ is selected in such a way that the \bar{A}^4 -term (which is of order ϵ^2) in the diffusion term b_{11} vanishes. This can be achieved if z_1 is a cubic function in \bar{A} as inferred from the expression $(z_1 \bar{A} - (dz_1/d\bar{A})\bar{A}^2)$, i.e.,

$$z_1(\bar{A}) = \beta \bar{A}^3$$

where

$$\beta = \frac{(5\alpha_5 + 3\alpha_7)\gamma_2^2 S_2(2) + (3\alpha_5 + 5\alpha_7)\gamma_3^2 S_3(2) + 8\alpha_7\gamma_3^2 S_3(0)}{32[\gamma_2^2 S_2(2) + \gamma_3^2 S_3(2) + 2\gamma_3^2 S_3(0)]}. \quad (29)$$

Now expressions for the drift and diffusion coefficients become

$$a_1 = C_1 \bar{A} + C_3 \bar{A}^3 + C_5 \bar{A}^5 + C_0 \frac{1}{\bar{A}},$$

$$b_{11} = 2C_0 + D_2 \bar{A}^2 \quad (30)$$

where

$$C_{01} = \frac{1}{2} \gamma_1^2 \pi S_1(1),$$

$$C_0 = \epsilon C_{01}, \quad C_1 = \epsilon C_{11} + \epsilon^2 C_{12}, \quad C_3 = \epsilon C_{31} + \epsilon^2 C_{32},$$

$$C_5 = \epsilon^2 C_{52}, \quad D_2 = \epsilon D_{21} + \epsilon^2 D_{22},$$

$$C_{11} = -\frac{1}{2} \gamma_1 + \frac{3}{8} \gamma_2^2 \pi S_2(2) + \frac{3}{8} \gamma_3^2 \pi S_3(2) + \frac{1}{4} \gamma_3^2 \pi S_3(0),$$

$$C_{12} = [\frac{1}{16}(9\alpha_5 + 7\alpha_7) - 5\beta] \gamma_1^2 \pi S_1(1)$$

$$C_{31} = \frac{1}{8}(\alpha_6 + 3\alpha_8),$$

$$C_{32} = \frac{1}{8}(\alpha_2\alpha_3 + \alpha_3\alpha_4 - \zeta\alpha_7) + \zeta\beta$$

$$+ [\frac{1}{64}(25\alpha_5 + 7\alpha_7) - \frac{3}{2}\beta] \gamma_2^2 \pi S_2(2)$$

$$+ [\frac{1}{64}(15\alpha_5 + 17\alpha_7) - \frac{3}{2}\beta] \gamma_3^2 \pi S_3(2)$$

$$+ (\frac{1}{4}\alpha_7 - 2\beta) \gamma_3^2 \pi S_3(0)$$

$$C_{52} = \frac{1}{32}(\alpha_5\alpha_6 + \alpha_6\alpha_7 + \alpha_7\alpha_8 - 3\alpha_5\alpha_8)$$

$$D_{21} = \frac{1}{4} \gamma_2^2 \pi S_2(2) + \frac{1}{4} \gamma_3^2 \pi S_3(2) + \frac{1}{2} \gamma_3^2 \pi S_3(0),$$

$$D_{22} = [\frac{1}{8}(3\alpha_5 + 5\alpha_7) - 6\beta] \gamma_1^2 \pi S_1(1) \quad (31)$$

where β should be replaced by the right-hand side of (29), and

$$S_i(\omega) = \frac{1}{2\pi} \int_{-\infty}^{\infty} \cos(\omega\tau) R_{ii}(\tau) d\tau \quad i = 1, 2.$$

It is assumed that $R_{ij} = 0$ ($i \neq j$). The drift and diffusion coefficients given by (30) establish some diffusion process $\bar{A}(\tau)$ described by the following Ito stochastic differential equation:

$$\bar{A}' = a_1(\bar{A}) + \sqrt{b_{11}(\bar{A})} W(\tau) \quad (32)$$

where $W(\tau)$ is a white noise of unit intensity. The corresponding pdf satisfies the Fokker-Planck Eq. (21) which possesses the stationary solution

$$p(\bar{A}) = K \bar{A} (2C_0 + D_2 \bar{A}^2) - \frac{3}{2} + \frac{C_1}{D_2} - \frac{2C_0 C_3}{D_2^2} + \frac{4C_0^2 C_5}{D_2^3}$$

$$\times \exp \left[\frac{C_5}{2D_2} \bar{A}^4 + \left(\frac{C_3}{D_2} - \frac{2C_0 C_5}{D_2^2} \right) \bar{A}^2 \right] \quad (33)$$

provided that $C_5 < 0$ or

$$\alpha_5\alpha_6 + \alpha_6\alpha_7 + \alpha_7\alpha_8 - 3\alpha_5\alpha_8 < 0.$$

If $C_5 = 0$ then C_3 should be negative for the existence of stationary pdf. It is convenient to write the pdf (33) in terms of the small parameter ϵ using relations (31) in the form

$$\bar{p}(\bar{A}) = K \bar{A} [2C_{01} + (D_{21} + \epsilon D_{22}) \bar{A}^{-2}] - \frac{3}{2} + \frac{C_{11} + \epsilon C_{12}}{D_{21} + \epsilon D_{22}}$$

$$- \frac{2C_{01}(C_{31} + \epsilon C_{32})}{(D_{21} + \epsilon D_{22})^2} + \epsilon \frac{4C_{01}^2 C_{52}}{(D_{21} + \epsilon D_{22})^3}$$

$$\times \exp \left\{ \left[\frac{C_{31} + \epsilon C_{32}}{D_{21} + \epsilon D_{22}} - \epsilon \frac{2C_{01} C_{52}}{(D_{21} + \epsilon D_{22})^2} \right] \bar{A}^2 \right.$$

$$\left. + \epsilon \frac{C_{52}}{2(D_{21} + \epsilon D_{22})} \bar{A}^4 \right\} \quad (33a)$$

where the normalization coefficient K depends on ϵ . As $\epsilon \rightarrow 0$ (33a) has the following limit:

$$\bar{p}_0(\bar{A}) = K_0 \bar{A} (2C_{01} + D_{21} \bar{A}^2)$$

$$- \frac{3}{2} + \frac{C_{11}}{D_{21}} - \frac{2C_{01} C_{31}}{D_{21}^2} \exp \left(\frac{C_{31}}{D_{21}} \bar{A}^2 \right) \quad (33b)$$

provided $D_{21} \neq 0$, $C_{01} \neq 0$, and either $C_{31} < 0$, or $C_{31} = 0$ and $2C_{11} < D_{21}$. The condition $2C_{11} < D_{21}$ can be written in the form

$$\pi \gamma_2^2 S_2(2) + \pi \gamma_3^2 S_3(2) < 2\zeta. \quad (34)$$

The case of external excitation only ($D_{21} = 0$) will be considered in Section 3.4. It is interesting to note that the expression of the Pdf (33b) corresponds the first-order averaging technique. If the pdf (33b) exists, the function $\bar{p}(\bar{A})$ given by (33a) can be represented in the asymptotic expansion form

$$\bar{p}(\bar{A}) = \bar{p}_0(\bar{A}) + \epsilon \bar{p}_1(\bar{A}) + \text{H.O.T.} \quad (35)$$

where

$$\bar{p}_1(\bar{A}) = \bar{p}_0(\bar{A}) (\bar{f}_1(\bar{A}) - K_1)$$

$$\bar{f}_1(\bar{A}) = \left(\frac{C_{12}}{D_{21}} - \frac{C_{11} D_{22} + 2C_{01} C_{32}}{D_{21}^2} \right.$$

$$+ \frac{4C_{01}(C_{31} D_{22} + C_{01} C_{52})}{D_{21}^3} \left. \right) \ln(2C_{01} + D_{21} \bar{A}^2)$$

$$+ \left(-\frac{3}{2} + \frac{C_{11}}{D_{21}} - \frac{2C_{01} C_{31}}{D_{21}^2} \right) \frac{D_{22} \bar{A}^2}{2C_0 + D_{21} \bar{A}^2}$$

$$+ \frac{C_{52}}{2D_{21}} \bar{A}^4 + \frac{C_{32} D_{21} - C_{31} D_{22} - 2C_{01} D_{52}}{D_{21}^2} \bar{A}^2$$

$$K_1 = K_0 \int_0^\infty \bar{p}_0(x) f_1(x) dx. \quad (36)$$

The constant K_1 guarantees that the average of $\bar{p}_1(\bar{A})$ is equal to zero. Finally the pdf of the amplitude A can be obtained using relation (21a) in the form

$$p(A) = p_0(A) + \epsilon p_1(A) + \text{H.O.T.},$$

$$p_1(A) = p_0(A) (f_1(A) - K_1), \quad p_0(A) \equiv \bar{p}_0(A)$$

$$f_1(A) = \bar{f}_1(A) - \frac{\partial}{\partial A} (z_1(A) p_0(A))$$

$$= \left(\frac{C_{12}}{D_{21}} - \frac{C_{11} D_{22} + 2C_{01} C_{32}}{D_{21}^2} \right.$$

$$+ \frac{4C_{01}(C_{31} D_{22} + C_{01} C_{52})}{D_{21}^3} \left. \right) \ln(2C_{01} + D_{21} A^2)$$

$$+ \left(-\frac{3}{2} + \frac{C_{11}}{D_{21}} - \frac{2C_{01} C_{31}}{D_{21}^2} \right)$$

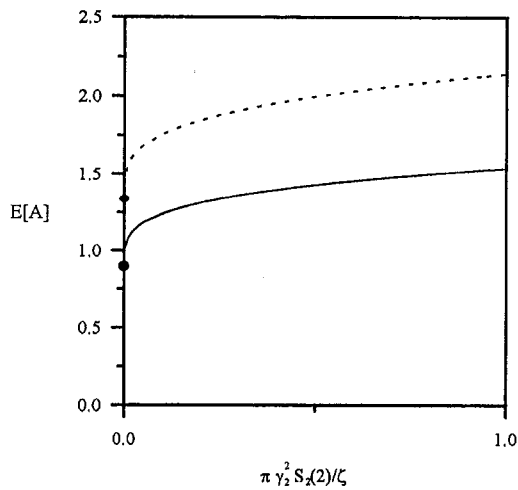


Fig. 1 Dependence of the response mean amplitude $E[A]$ on external excitation level according to first-order averaging ---, and second-order averaging —. For parametric excitation levels $\pi \gamma_1^2 S_1(1)/\zeta = \pi \gamma_2^2 S_2(2)/\zeta = \pi \gamma_3^2 S_3(0)/\zeta = \pi \gamma_3^2 S_3(2)/\zeta = 2.0$.

$$\times \frac{D_{22} - 2\beta D_{21} A^2}{2C_{01} + D_{21} A^2} A^2 + \frac{C_{52} - 4\beta C_{31}}{2D_{21}} A^4 + \left(\frac{C_{32} D_{21} - C_{31} D_{22} - 2C_{01} D_{52}}{D_{21}^2} - 4\beta \right) A^2. \quad (37)$$

The term $p_1(A)$ is due to the second-order averaging and is accounted for the effects of nonlinearities lost during first-order averaging. For the case when $p_0(A)$ exists (i.e., when the limit of (33) exists as $\epsilon \rightarrow 0$), the moments of the amplitude A as a function of the moments of the amplitude \bar{A} can be derived from (26) as follows:

$$E[A^n] = \int_0^\infty (\bar{A}^n + \epsilon n \beta \bar{A}^{n+2} + \text{H.O.T.}) p(\bar{A}) d\bar{A} = E[\bar{A}^n] + \epsilon n \beta E[\bar{A}^{n+2}] + \text{H.O.T.} \quad (38)$$

Figure 1 shows the dependence of the mean value of the response amplitude on the external excitation level $\pi \gamma_1^2 S_1(1)/\zeta$ for $\epsilon = 0.01$, $\zeta = 1$, $\alpha_2 = 4$, $\alpha_3 = -4$, $\alpha_4 = -3$, $\alpha_5 = -9$, $\alpha_6 = 2$, $\alpha_7 = -3$, $\alpha_8 = -1$, $\gamma_1 = 3$, $\gamma_2 = 1$, and $\gamma_3 = 1$. It is seen that at zero external excitation level the response begins at certain value which corresponds the response under combined parametric excitations $\pi \gamma_3^2 S_3(2)/\zeta = \pi \gamma_3^2 S_3(0)/\zeta = \pi \gamma_2^2 S_2(2)/\zeta = 2.0$. The results obtained by first and second-order averaging are shown for comparison and both are monotonically increase with the excitation level. It is clear that the first-order averaging gives higher estimate than the second-order averaging solution.

In order to gain more physical insight to the results of this analysis, it is convenient to consider the following special cases.

3.2 Parametrically Excited System in the Stiffness ($\gamma_1 = \gamma_3 = 0$, and $\gamma_2 \neq 0$). For simplicity consider only stiffness and inertia nonlinearities, i.e., $\alpha_2 = \alpha_3 = \alpha_4 = \alpha_6 = \alpha_8 = 0$. In this case $\beta = (5\alpha_5 + 3\alpha_7)/32$ and

$$\begin{aligned} C_0 &= 0, \quad C_1 = \epsilon C_{11}, \quad C_3 = \epsilon^2 C_{32}, \\ C_5 &= 0, \quad D_2 = \epsilon D_{21} \\ C_{11} &= -\frac{1}{2}\zeta + \frac{3}{8}\gamma_2^2 \pi S_2(2), \\ C_{32} &= \frac{1}{32}(5\alpha_5 - \alpha_7)[\zeta + \gamma_2^2 \pi S_2(2)], \\ D_{21} &= \frac{1}{4}\gamma_2^2 \pi S_2(2). \end{aligned} \quad (39)$$

Consequently, the averaged Eq. (32) takes the form

$$\bar{A}' = C_1 \bar{A} + C_3 \bar{A}^3 + \bar{A} \sqrt{D_2} W(\tau). \quad (40)$$

The corresponding linear system is stable (in probability) if $\gamma_2^2 \pi S_2(2)/\zeta < 2$. A stationary pdf exists only if the following conditions are satisfied:

$$\frac{C_1}{D_2} > \frac{1}{2} \quad \text{or} \quad \frac{\gamma_2^2 \pi S_2(2)}{\zeta} > 2 \quad (40a)$$

and

$$C_3 < 0, \quad \text{or} \quad 5\alpha_5 - \alpha_7 < 0 \quad (40b)$$

and is given by the formula which follows from (33),

$$p(\bar{A}) = K_N \bar{A}^{2(C_1/D_2 - 1)} \exp\left(\frac{C_3}{D_2} \bar{A}^2\right),$$

$$K_N = 2 \left(-\frac{C_3}{D_2} \right)^{(C_1/D_2 - 1/2)} / \Gamma\left(\frac{C_1}{D_2} - \frac{1}{2}\right). \quad (41)$$

The corresponding mean, mean square values and n th moment of the amplitude are

$$\begin{aligned} E[\bar{A}] &= \frac{\Gamma\left(\frac{C_1}{D_2}\right)}{\Gamma\left(\frac{C_1}{D_2} - \frac{1}{2}\right) \sqrt{-\frac{C_3}{D_2}}}, \\ E[\bar{A}^2] &= \frac{\Gamma\left(\frac{C_1}{D_2} + \frac{1}{2}\right)}{\Gamma\left(\frac{C_1}{D_2} - \frac{1}{2}\right) \left(-\frac{C_3}{D_2}\right)}, \\ E[\bar{A}^n] &= \frac{\Gamma\left(\frac{C_1}{D_2} + \frac{n-1}{2}\right)}{\Gamma\left(\frac{C_1}{D_2} - \frac{1}{2}\right) \left(-\frac{C_3}{D_2}\right)^{n/2}} \end{aligned} \quad (42)$$

and

$$E[A^n] = E[\bar{A}^n] + \epsilon n \frac{5\alpha_5 + 3\alpha_7}{32} E[\bar{A}^{n+2}] + \text{H.O.T.} \quad (42a)$$

Note that the exponent $2(C_1/D_2 - 1)$ in the expression (41) is of order 1 (with respect to ϵ) while C_3/D_2 is of order ϵ . In this case it is possible to show that $E[A^n]$ and $E[\bar{A}^n]$ are of order $\epsilon^{-n/2}$. The pdf given by (33a) can be represented in terms of ϵ in the form

$$\bar{p}(\bar{A}) = K' \epsilon^{(C_{11}/D_{21}) - (1/2)} \bar{A}^{2(C_{11}/D_{21}) - 1} \exp\left(\epsilon \frac{C_{32}}{D_{21}} \bar{A}^2\right),$$

$$K' = 2 \left(-\frac{C_{32}}{D_{21}} \right)^{(C_{11}/D_{21}) - (1/2)} / \Gamma\left(\frac{C_{11}}{D_{21}} - \frac{1}{2}\right). \quad (43)$$

As it is seen from (43) that there is no limit of $\bar{p}(\bar{A})$ as $\epsilon \rightarrow 0$. The function $\bar{p}(\bar{A})$ becomes infinite as $\epsilon \rightarrow 0$. So in this case there is no regular expansion of the form $\bar{p}_0(\bar{A}) + \epsilon \bar{p}_1(\bar{A}) + \dots$.

In terms of the original amplitude A the corresponding pdf is

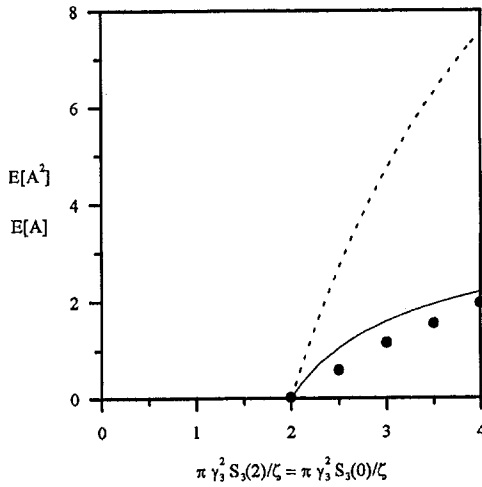


Fig. 2 Dependence of the response amplitude mean value $E[A]$ ----, and mean square $E[A^2]$ — on parametric excitation level (in stiffness) according to second-order averaging. • • • Monte Carlo simulation $E[A^2]$

$$p(A) = \bar{p}(A) - \epsilon \frac{\partial}{\partial A} [\beta \bar{p}(A) A^3] + \text{H.O.T.}$$

$$= \bar{p}(A) \left(1 - \frac{1}{8} \epsilon (5\alpha_5 + 3\alpha_7) \left(1 - \frac{\zeta}{\gamma_2^2 \pi S_2(2)} \right) A^2 \right.$$

$$\left. - \frac{1}{128} \epsilon^2 (5\alpha_5 + 3\alpha_7) (5\alpha_5 - \alpha_7) \times \left(1 + \frac{\zeta}{\gamma_2^2 \pi S_2(2)} \right) A^4 \right] + \text{H.O.T.} \quad (43a)$$

Figure 2 shows the dependence of the mean and mean square of the response amplitude on the excitation level $\pi \gamma_2^2 S_2(2)/\zeta$ for $\epsilon = 0.01$, $\zeta = 1$, $\alpha_5 = -9$, $\alpha_7 = -3$, and $\gamma_2 = 1$. It is seen that nonzero response emanates from an excitation level $\pi \gamma_2^2 S_2(2)/\zeta = 2$ which coincides with condition (40a).

The validity of the second-order averaging results has been verified using Monte Carlo simulation. The mean square amplitude as estimated by Monte Carlo simulation is plotted by solid dots in Fig. 2. It is seen that the second-order averaging is in good agreement with the numerical simulation. Note that at the bifurcation point $\pi \gamma_2^2 S_2(2)/\zeta = 2$ the response exhibits on-off intermittency. This type of intermittency takes place over an excitation level defined over the region $2 \leq \pi \gamma_2^2 S_2(2)/\zeta \leq 4$ which can be inferred from the analytical solution (39) (see Hijawi et al. (1997) for more details and other applications).

The transition of the extrema of the response probability density function can be determined from condition (22) or by setting the derivative of Eq. (39) with respect to the response amplitude to zero. This condition gives

$$C_3 \bar{A}^3 - \bar{A} (D_2 - C_1) = 0. \quad (44)$$

This equation has three solutions given by the roots

$$\bar{A}_1 = 0, \quad \bar{A}_{2,3} = \pm \sqrt{\frac{D_2 - C_1}{C_3}} \quad (44a)$$

In terms of system and excitation parameters and considering only nonlinear stiffness, these roots are

$$\bar{A}_1 = 0, \quad \bar{A}_{2,3} = \pm \sqrt{\frac{4}{5\epsilon}} \sqrt{\frac{4\zeta - \pi \gamma_2^2 S_2(2)}{\alpha_5 [\zeta + \pi \gamma_2^2 S_2(2)]}}. \quad (44b)$$

The zero root defines one peak in the response probability den-

sity function. A transition to other peaks takes place due to the multiplicative noise. The other two roots depend on whether the stiffness nonlinearity is soft $\alpha_5 > 0$, or hard $\alpha_5 < 0$. A bifurcation diagram showing the dependence of the extrema on the excitation level is shown in Fig. 3. It is seen that $\pi \gamma_2^2 S_2(2)/\zeta = 4$ separates between the extrema of soft and hard stiffness nonlinearities. Figure 3 reveals the stabilization effect of the multiplicative noise on the originally unstable system with soft stiffness nonlinearity $\alpha_5 > 0$. It is seen that as the parametric excitation increases the extrema defined by $\bar{A}_{2,3}$ decreases until it vanishes. This is only valid for systems with soft nonlinear stiffness.

3.3 Parametrically Excited System in the Damping ($\gamma_1 = \gamma_2 = 0$, and $\gamma_3 \neq 0$). Considering only stiffness and inertia nonlinearities, the following parameters are obtained:

$$\beta = \frac{(3\alpha_5 + 5\alpha_7)S_3(2) + 8\alpha_7 S_3(0)}{32[S_3(2) + 2S_3(0)]},$$

$$C_0 = 0, \quad C_1 = \epsilon \left\{ -\frac{1}{2}\zeta + \frac{3}{8}\gamma_3^2 \pi S_3(2) + \frac{1}{4}\gamma_3^2 \pi S_3(0) \right\}$$

$$C_3 = \epsilon^2 \left\{ (3\alpha_5 + \alpha_7) \frac{S_3(2)[\zeta + \pi \gamma_3^2 (S_3(2) + 3S_3(0))]}{32[S_3(2) + 2S_3(0)]} \right\},$$

$$C_5 = 0, \quad D_2 = \epsilon \left\{ \frac{1}{4}\gamma_3^2 \pi [S_3(2) + 2S_3(0)] \right\}. \quad (45)$$

The averaged equation has the same form of Eq. (40). The corresponding linear system is stable (in probability) if

$$\frac{\pi \gamma_3^2 S_3(2)}{\zeta} < 2. \quad (46)$$

The response stationary pdf exists under the two conditions: $C_1/D_2 > 1/2$ and $C_3 < 0$, or in terms of system and excitation parameters

$$\frac{\pi \gamma_3^2 S_3(2)}{\zeta} > 2 \quad \text{and} \quad 3\alpha_5 + \alpha_7 < 0. \quad (47)$$

If these conditions hold then the pdf exists and has the form (41) and the corresponding mean and mean square are given by (42) but with those coefficients defined by (45). Figure 4 shows the dependence of mean and mean square of the response amplitude on the excitation level $\pi \gamma_3^2 S_3(2)/\zeta$ or $\pi \gamma_3^2 S_3(0)/\zeta$ for $\epsilon = 0.01$, $\zeta = 1$, $\alpha_5 = -9$, $\alpha_7 = -3$, and $\gamma_3 = 1$. Again it is seen that stochastic bifurcation in moments takes place at $\pi \gamma_3^2 S_3(2)/\zeta = 2$ which coincides with the stability boundary indicated by the first condition of (47).

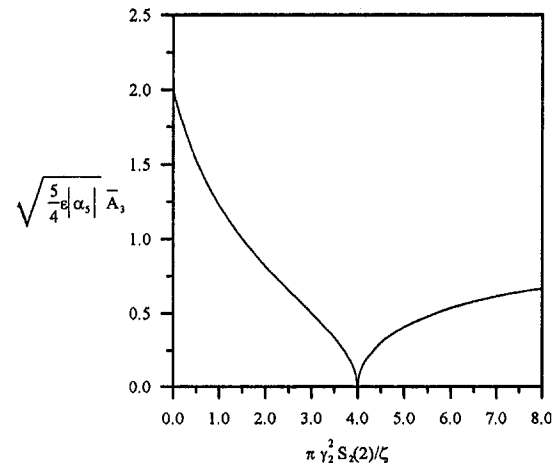


Fig. 3 Dependence of the amplitude of extrema on parametric excitation level for soft and hard stiffness nonlinearities

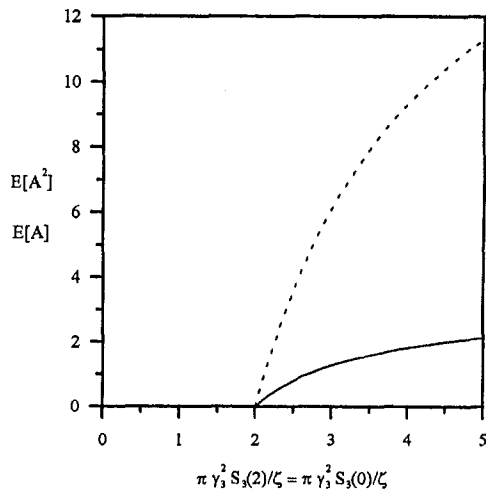


Fig. 4 Dependence of the response amplitude mean value $E[A]$ ----, and mean square $E[A^2]$ — on parametric excitation level (in damping) $\pi\gamma_2^2 S_2(2)/\zeta$ or $\pi\gamma_2^2 S_3(0)/\zeta$ according to second order averaging

Remark: If the system is subjected to both parametric excitations in stiffness and damping, then the dependence of the response on the excitation level will be different depending on the excitation level of each. In this case ($\gamma_1 = 0$, $\gamma_2 \neq 0$, $\gamma_3 \neq 0$) the parameter β is given by (29), $C_0 = C_5 = 0$ and coefficients C_1, C_3, D_2 are determined by (31). The differential equation for the \bar{A} takes the form (40) and the analysis is similar to Section 3.2. For example Fig. 5 shows the dependence of the mean and mean square of the response amplitude on $\pi\gamma_2^2 S_2(2)/\zeta$ for $\pi\gamma_2^2 S_3(2)/\zeta = \pi\gamma_2^2 S_3(0)/\zeta = 2.0$. In this case the bifurcation takes place at a lower level of $\pi\gamma_2^2 S_2(2)/\zeta$.

3.4 Externally Excited System ($\gamma_2 = \gamma_3 = 0$). If the system is subjected to additive noise, i.e., $\gamma_2 = \gamma_3 = 0$, there is no \bar{A}^4 -term in the diffusion term b_{11} and the function $z_1(\bar{A})$ is selected in such a way that the \bar{A}^2 -term in the diffusion term b_{11} vanishes. That can be achieved by choosing z_1 as a cubic function in \bar{A} with the following coefficient β :

$$\beta = \frac{3\alpha_5 + 5\alpha_7}{48}. \quad (48)$$

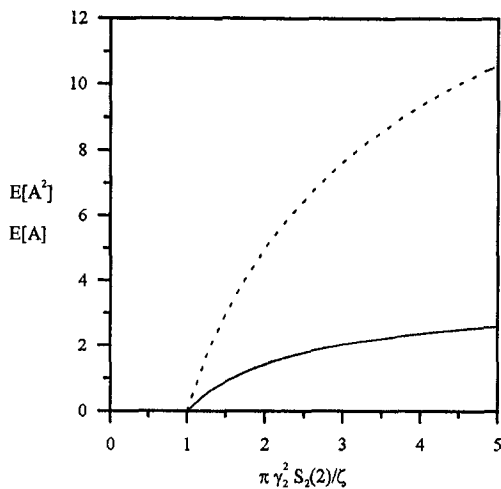


Fig. 5 Dependence of the response amplitude mean value $E[A]$ ----, and mean square $E[A^2]$ — on the parametric excitation level (in stiffness) $\pi\gamma_2^2 S_2(2)/\zeta$ according to second-order averaging for $\pi\gamma_2^2 S_3(2)/\zeta = \pi\gamma_2^2 S_3(0)/\zeta = 2.0$

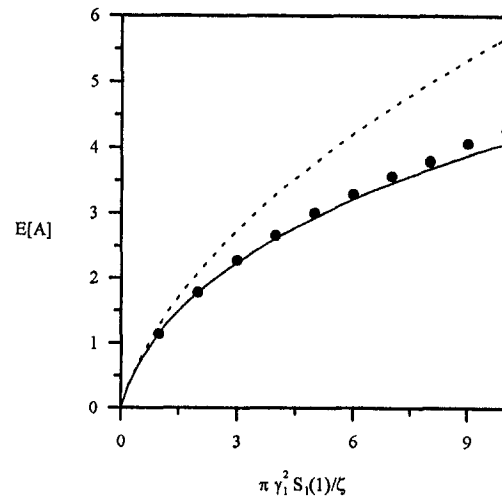


Fig. 6 Dependence of the response amplitude mean $E[A]$ on the external excitation level $\pi\gamma_1^2 S_1(1)/\zeta$ according to first-order averaging ---- and second-order averaging —. In the absence of parametric excitations, • • • Monte Carlo simulation $E[A]$.

Expressions for the drift and diffusion coefficients are

$$a_1 = C_1 \bar{A} + C_3 \bar{A}^3 + C_5 \bar{A}^5 + C_0 \frac{1}{\bar{A}}, \quad b_{11} = 2C_0 \quad (49)$$

where expressions for C_0 and C_5 remain the same as in (31) while C_1 and C_3 are given by the expressions

$$C_1 = \epsilon \left\{ -\frac{1}{2}\zeta \right\} + \epsilon^2 \left\{ \frac{1}{12}(3\alpha_5 - \alpha_7) \gamma_1^2 \pi S_1(1) \right\}$$

$$C_3 = \epsilon \left\{ \frac{1}{8}(\alpha_6 + 3\alpha_8) \right\}$$

$$+ \epsilon^2 \left\{ \frac{1}{8}\alpha_3(\alpha_2 + \alpha_4) - \frac{1}{48}(\zeta\alpha_7 - 3\zeta\alpha_5) \right\}. \quad (50)$$

The corresponding stationary pdf is

$$\begin{aligned} p(\bar{A}) &= K_N \bar{A} \exp \left(\frac{C_1}{2C_0} \bar{A}^2 + \frac{C_3}{4C_0} \bar{A}^4 + \frac{C_5}{6C_0} \bar{A}^6 \right) \\ &= K \bar{A} \exp \left(\frac{C_{11} + \epsilon C_{12}}{2C_{01}} \bar{A}^2 + \frac{C_{31} + \epsilon C_{32}}{4C_{01}} \bar{A}^4 \right. \\ &\quad \left. + \epsilon \frac{C_{52}}{6C_{01}} \bar{A}^6 \right), \quad (51) \end{aligned}$$

provided that $C_5 < 0$. If $C_5 = 0$ then the corresponding condition for existence of stationary probability density is $C_3 < 0$. Figure (6) shows the dependence of the response mean value on the excitation level $\pi\gamma_1^2 S_1(1)/\zeta$ according to first and second-order averaging solutions for $\epsilon = 0.01$, $\zeta = 1$, $\alpha_2 = 4$, $\alpha_3 = -4$, $\alpha_4 = -3$, $\alpha_5 = -9$, $\alpha_6 = 2$, $\alpha_7 = -3$, $\alpha_8 = -1$, and $\gamma_1 = 1$. The results of the second-order averaging are in an excellent agreement with those estimated by Monte Carlo simulation, indicated by solid points.

For simplicity again assume that $\alpha_2 = \alpha_3 = \alpha_4 = \alpha_6 = \alpha_8 = 0$. Then the following coefficients are obtained:

$$C_0 = \frac{1}{2}\epsilon \gamma_1^2 \pi S_1(1),$$

$$C_1 = -\frac{1}{2}\epsilon \zeta - \frac{1}{12}\epsilon^2 (\alpha_7 - 3\alpha_5) \gamma_1^2 \pi S_1(1),$$

$$C_3 = -\frac{1}{48}\epsilon^2 \zeta (\alpha_7 - 3\alpha_5), \quad C_5 = 0 \quad (52)$$

If $\alpha_7 > 3\alpha_5$ then stationary pdf exists and has the form

$$p(\bar{A}) = K_N \bar{A} \exp\left(\frac{C_1}{2C_0} \bar{A}^2 + \frac{C_3}{4C_0} \bar{A}^4\right) \\ = K_N \bar{A} \exp\left[-\frac{\zeta}{2\gamma_1^2 \pi S_1(1)} \bar{A}^2 - \frac{1}{96} \epsilon(\alpha_7 - 3\alpha_5) \right. \\ \left. \times \left(8\bar{A}^2 + \frac{\zeta}{\gamma_1^2 \pi S_1(1)} \bar{A}^4\right)\right] \quad (53)$$

where the normalization constant K_N is given by

$$K_N = \frac{4\sqrt{-\frac{C_3}{4C_0}}}{\sqrt{\pi} \exp\left(-\frac{C_1^2 C_3}{4C_0^3}\right) \left(1 - \operatorname{erf}\left(-\frac{C_1}{2\sqrt{C_0 C_3}}\right)\right)}$$

The corresponding mean square value is

$$E[\bar{A}^2] = -\frac{C_1}{C_3} \\ + \frac{1}{\sqrt{-\frac{C_3}{4C_0}} \exp\left(-\frac{C_1^2 C_3}{4C_0^3}\right) \left(1 - \operatorname{erf}\left(-\frac{C_1}{2\sqrt{C_0 C_3}}\right)\right)} \quad (54)$$

The leading term of the expression (53) corresponds to the Rayleigh distribution. Therefore it is not difficult to obtain the leading and ϵ -term for the expectation of the amplitude \bar{A} and A

$$E[\bar{A}] = \pi \gamma_1 \sqrt{\frac{S_1(1)}{2\zeta}} \left[1 - \epsilon \frac{5}{32} \frac{\pi \gamma_1^2 S_1(1)}{\zeta} (\alpha_7 - 3\alpha_5)\right] \\ + \text{H.O.T.} \quad (54a)$$

$$E[A] = \pi \gamma_1 \sqrt{\frac{S_1(1)}{2\zeta}} \left[1 + \epsilon \frac{\pi \gamma_1^2 S_1(1)}{\zeta} \frac{21\alpha_5 + 5\alpha_7}{32}\right] \\ + \text{H.O.T.} \quad (54b)$$

Note that these expressions are less accurate than those generated from Eq. (51). The asymptotic expansion of $p(A)$ for this case has the form

$$p(A) = \delta A e^{-\delta A^2/2} \left\{1 + \epsilon \left[\frac{\alpha_7 - 3\alpha_5}{4\delta} - \frac{\alpha_7}{2} A^2 \right. \right. \\ \left. \left. + \frac{3(\alpha_5 + \alpha_7)}{32} \delta A^4\right]\right\} + \text{H.O.T.}, \\ \delta = \frac{\zeta}{\gamma_1^2 \pi S_1(1)} \quad (55)$$

The validity of the pdf obtained by the proposed second-order stochastic averaging will be examined by comparing the results with those obtained with the exact solution of a special nonlinear oscillator. This will be examined in the next subsection.

3.5 Comparison With an Exact Solution. It is useful to compare the approximate solution of the pdf given by the second-order averaging with the exact pdf of a special nonlinear oscillator whose exact solution is known. We will show that

the difference between the two solutions is of order ϵ^2 . Consider the following stochastic system:

$$Y'' + Y = -\zeta Y' + \tilde{\alpha}_5 Y^3 + \tilde{\alpha}_6 Y^2 Y' + \tilde{\gamma}_1 W_1' + \tilde{\gamma}_2 Y W_2' \quad (56)$$

where ζ , $\tilde{\alpha}_5$, $\tilde{\alpha}_6$, $\tilde{\gamma}_1$, $\tilde{\gamma}_2$ are some constants and W_1' , W_2' are independent white noises of unit intensities. If $\tilde{\alpha}_5 < 0$, $\tilde{\alpha}_6 < 0$ and $(\tilde{\gamma}_1^2/\zeta) = (\tilde{\gamma}_2^2/\tilde{\alpha}_6) = 2D > 0$ then the corresponding exact solution of the stationary Fokker-Planck-Kolmogorov equation has the form

$$p(Y, Y') = K \exp\left[-\frac{1}{D} \left(\frac{Y'^2 + Y^2}{2} - \frac{\alpha_5 Y^4}{4}\right)\right] \quad (57)$$

where K is the normalization constant, $(Y'^2 + Y^2)/2 + \alpha_5 Y^4/4$ is the Hamiltonian of the system. In terms of amplitude A and angle φ expression (57) becomes

$$p(A, \varphi) = K' A \exp\left[-\frac{1}{2D} \left(A^2 - \frac{1}{2} \alpha_5 A^4 \cos^4 \varphi\right)\right] \quad (58)$$

The pdf of the amplitude A alone is

$$p(A) = K' A \exp\left(-\frac{1}{2D} A^2\right) \\ \times \left[\frac{1}{\pi} \int_0^\pi \exp\left(\frac{1}{4D} \tilde{\alpha}_5 A^4 \cos^4 \varphi\right) d\varphi\right] \quad (59)$$

This expression is valid for any values of the constants D and $\tilde{\alpha}_5$. In order to compare this result with the second-order averaging, the coefficients of Eqs. (24) and (56) have the following correspondence:

$$\zeta = \epsilon \zeta, \quad \tilde{\alpha}_5 = \epsilon \alpha_5, \quad \tilde{\alpha}_6 = \epsilon \alpha_6, \quad \tilde{\gamma}_1 = \sqrt{\epsilon} \gamma_1, \quad \tilde{\gamma}_2 = \sqrt{\epsilon} \gamma_2$$

where ϵ is a small parameter and $(\gamma_1^2/\zeta) = (\gamma_2^2/\alpha_6) = 2D$ is of order 1. In this case the pdf given by (59) can be in the form

$$p(A) = K' A \exp\left(-\frac{A^2}{2D}\right) \\ \times \left[\frac{1}{\pi} \int_0^\pi \exp\left(\epsilon \frac{1}{4D} \alpha_5 A^4 \cos^4 \varphi\right) d\varphi\right] \quad (60)$$

The main goal is to show that the exact solution (60) will yield the same leading and next term of the asymptotic expansion for pdf in terms of ϵ similar to the second-order averaging expression (33). In other words the difference between (60) and (33) is some function of order ϵ^2 . Expanding (61) in power series of ϵ gives

$$p(A) = K' A \exp\left(-\frac{A^2}{2D}\right) \left(1 + \epsilon \frac{\alpha_5}{4D} A^4 \langle \cos^4 \varphi \rangle\right) + O(\epsilon^2) \\ = K' A \exp\left(-\frac{A^2}{2D}\right) \left(1 + \epsilon \frac{3\alpha_5}{32D} A^4\right) + O(\epsilon^2). \quad (61)$$

Evaluating the normalization constant K' up to the order ϵ and substituting it in (61), we obtain

$$p(A) = \frac{A}{D} \exp\left(-\frac{A^2}{2D}\right) \\ \times \left(1 - \epsilon \frac{3\alpha_5 D}{4} + \epsilon \frac{3\alpha_5}{32D} A^4\right) + O(\epsilon^2). \quad (62)$$

Rewriting this result in the series form

$$p(A) = p_0(A) + \epsilon p_1(A) + O(\epsilon^2),$$

$$p_0(A) = \frac{A}{D} \exp\left(-\frac{A^2}{2D}\right),$$

$$p_1(A) = p_0(A) \left(-\frac{3}{4} \alpha_5 D + \frac{3\alpha_5}{32D} A^4 \right).$$

Comparing this formula with (37). In our case

$$C_{01} = \frac{\gamma_1^2}{4}, \quad C_{11} = -\frac{\zeta}{2} + \frac{3\gamma_2^2}{16}, \quad C_{12} = -\frac{7\alpha_5\gamma_1^2}{64},$$

$$C_{31} = \frac{\alpha_6}{8}, \quad C_{32} = \frac{5}{64} \alpha_5 (2\zeta + \gamma_2^2), \quad C_{52} = \frac{\alpha_5\alpha_6}{32},$$

$$D_{21} = \frac{\gamma_2^2}{8}, \quad D_{22} = -\frac{9\alpha_5\gamma_1^2}{32}.$$

These expressions reduce the coefficients listed for expression (37) to the following values:

$$\frac{C_{12}}{D_{21}} - \frac{C_{11}D_{22} + 2C_{01}C_{32}}{D_{21}^2} + \frac{4C_{01}(C_{31}D_{22} + C_{01}C_{52})}{D_{21}^3} = 0,$$

$$\frac{C_{32}D_{21} - C_{31}D_{22} - 2C_{01}C_{52}}{D_{21}^2} - 4\beta = 0$$

$$-\frac{3}{2} + \frac{C_{11}}{D_{21}} - \frac{2C_{01}C_{31}}{D_{21}^2} = 0, \quad \frac{C_{52} - 4\beta C_{31}}{2D_{21}} = \frac{3\alpha_5\zeta}{16\gamma_1^2},$$

$$K_0 = \frac{1}{D}, \quad K_1 = -\frac{3}{4} \alpha_5 D.$$

It is obvious that expressions (62) and (37) are now identical.

4 General Remarks and Conclusions

A second-order stochastic averaging scheme is developed that is capable of capturing the effects of stiffness and inertia nonlinearities which are usually lost in the first-order averaging process. Stochastic stability boundaries, response probability density functions and extrema for phase transition are obtained in closed-form expressions. Stabilization of unstable systems by multiplicative noise is also defined for systems with soft stiffness nonlinearity. The analytical procedure can be significantly facilitated by using a symbolic algebraic manipulation package, such as MACSYMA. The method has proven very powerful for general nonlinear oscillators with additive and multiplicative random excitations. The method should be extended to multi-degree-of-freedom systems with internal resonance conditions. This task is underway by the authors.

The method outlined in this paper is different from the one developed by Baxter (1971). Note that Baxter (1971) evaluated the constants of integration $z_i(\bar{A})$ in such a manner that the amplitude \bar{A} is the full amplitude of the response at the fundamental harmonic $\cos \bar{\theta}$. This can be achieved by substituting the oscillatory functions u and v into Eqs. (6) and (2) such that the coordinate $Y(\tau)$ will have no terms of order ϵ or higher that contain the fundamental harmonic, i.e.,

$$Y(\tau) = A \cos \varphi = (\bar{A} + \epsilon u) \cos (\bar{\varphi} + \epsilon v) \\ = \bar{A} \cos \bar{\varphi} + \epsilon(u \cos \bar{\varphi} - v \bar{A} \sin \bar{\varphi}) + \dots \quad (63)$$

Upon substituting for u and v from relations (14) and collecting terms of order ϵ with $\cos \varphi$ and $\sin \varphi$, one obtains z_1 and z_2 by

setting the coefficients of $\cos \bar{\varphi}$ and $\sin \bar{\varphi}$ to zero. This step is analogous to the solvability condition encountered in deterministic perturbation techniques for solving nonlinear differential equations. This procedure yields

$$z_1 = -\frac{1}{16} \bar{A}^3 (\alpha_7 + 3\alpha_5),$$

$$z_2 = \frac{1}{4} \zeta - \frac{1}{16} \bar{A}^3 (\alpha_6 + 3\alpha_8). \quad (56)$$

Final expressions for the drift and diffusion coefficients of the averaged stochastic equation for the amplitude follow from (27) and (28) after substituting for $z_i(\bar{A})$ into expressions (26a) and (26b). In this case the drift coefficient a_1 can be represented in the form (27), but b_{11} will have fourth-order term in \bar{A} , i.e., $D_4 \bar{A}^4$ and the constant D_4 is not necessary positive. Therefore in (Baxter, 1971) higher-order terms $C_5 \bar{A}^5$ and $D_4 \bar{A}^4$ were dropped.

Acknowledgment

This research is supported by grants from NSF No. MSS-9203733 and ONR No. N000149310936. Partial support has been provided by the office of Vice President for Research at Wayne State University.

References

- Baxter, G. K., 1971, "The non-linear response of mechanical systems to parametric random excitation," Ph.D. thesis, University of Syracuse.
- Gradshteyn, I. S., and Ryzhik, I. M., 1980, *Tables of Integrals, Series, and Products*, Academic Press, New York.
- Hijawi, M., Ibrahim, R. A., and Moshchuk, N., 1997, "Nonlinear Random Response of Ocean Structures Using First- and Second-Order Stochastic Averaging," *Nonlinear Dynamics*, in press.
- Horsthemke, W., and Lefever, R., 1989, "Noise-Induced Transition," *Noise in Nonlinear Dynamical Systems*, F. Moss and P. V. E. McClintock, eds., Cambridge University Press, Cambridge, UK, Vol. 2, pp. 179–208.
- Ibragimov, I. A., 1959, "Some Limit Theorems for Stochastic Processes Stationary in the Narrow Sense," *Soviet Math. Doklady* Vol. 125, No. 4, pp. 711–714.
- Ibragimov, I. A., 1962, "Some Limit Theorems for Stationary Processes," *Theory Probability and Applications*, Vol. 7, pp. 349–382.
- Ibrahim, R. A., 1985, *Parametric Random Vibration*, John Wiley and Sons, New York.
- Iwan, W. D., and Spanos, P. D., 1978, "Response Envelope Statistics for Non-linear Oscillators with Random Excitation," *ASME JOURNAL OF APPLIED MECHANICS*, Vol. 45, pp. 170–174.
- Khasminskii, R. Z., 1963, "The Averaging Principle for Parabolic and Elliptic Differential Equations and Markov Process with Small Diffusion," *Theory of Probability and Applications*, Vol. 8, pp. 121–140.
- Khasminskii, R. Z., 1966, "A Limit Theorem for Solution of Differential Equations with Random Right-Hand Side," *Theory Probability and Applications*, Vol. 11, No. 3, pp. 390–406.
- Khasminskii, R. Z., 1968, "On the Averaging Principle for Stochastic Differential Ito Equations," *Kibernetika*, Vol. 4, pp. 260–279.
- Naprstek, J., 1976, "Solution of Random Vibrations of Nonlinear Systems by Means of Markov Process," *Acta Tech. CSAV*, Vol. 21, pp. 302–345.
- Red-Horse, J. R., and Spanos, P. D., 1992, "A Generalization to Stochastic Averaging in Random Vibration," *Int. J. Nonlin. Mech.*, Vol. 27, No. 1, pp. 85–101.
- Roberts, J. B., 1989, *Averaging Methods in Random Vibration*, Technical University of Denmark, Department of Structural Engineering, Series R, No. 245.
- Roberts, J. B., and Spanos, P. D., 1986, "Stochastic Averaging: An Approximate Method of Solving Random Vibration Problems," *Int. J. Nonlinear Mech.*, Vol. 21, pp. 111–134.
- Roy, R. V., 1994, "Stochastic Averaging of Oscillators Excited by Colored Gaussian Processes," *Int. J. Nonlin. Mech.*, Vol. 29, No. 4, pp. 463–475.
- Schmidt, G., 1981, "Vibrations Caused by Simultaneous Random Forced and Parametric Excitations," *Z. Angew. Math. Mech. (ZAMM)*, Vol. 60, pp. 409–419.
- Spanos, P. D., and Red-Horse, J. R., 1988, "Nonstationary Solution in Nonlinear Random Vibration," *ASCE Journal of Engineering Mechanics*, Vol. 114, No. 11, pp. 1929–1943.
- Stratonovich, R. L., 1963, *Topics in the Theory of Random Noise*, Vol. I, Gordon and Breach, New York.
- Zhu, W. Q., 1991, "Stochastic Averaging in Random Vibration," *ASME Applied Mechanics Reviews*, Vol. 41, pp. 189–199.

R. Ohayon

Chair of Mechanics,
CNAM,
2 rue Conte,
F-75003 Paris, France
Mem. ASME

R. Sampaio

Department of Mechanical Engineering,
Pontificia Universidade
Catolica do Rio de Janeiro,
22453-900 Rio de Janeiro, RJ, Brazil

C. Soize

Structures Department,
ONERA,
BP 72,
F-92322 Châtillon Cedex,
France

Dynamic Substructuring of Damped Structures Using Singular Value Decomposition

This paper deals with the theoretical aspects concerning linear elastodynamic of damped continuum medium in the frequency domain. Eigenvalue analysis and frequency response function are studied. The methods discussed here use a dynamic substructuring approach. The first method is based on a mixed variational formulation in which Lagrange multipliers are introduced to impose the linear constraints on the coupling interfaces. A modal reduction of each substructure is obtained using its free-interface modes. A practical construction of a unique solution is carried out using the Singular Value Decomposition (SVD) related only to the frequency-independent Lagrange multiplier terms. The second method is similar to the first one replacing the free-interface modes by the fixed-interface modes and elastostatic operator on the interface of each substructure.

1 Introduction

In this paper, we are interested in eigenvalue and frequency response function calculations of a linear dynamic three-dimensional bounded damped elastic structure subjected to prescribed forces. Recall that the frequency response functions allow deterministic and stationary random analyses to be performed (Kree and Soize, 1986; Argyris and Meljnek, 1991). More precisely, this paper is devoted to theoretical aspects of structure-structure coupling by dynamic substructuring methods using modal reduction procedures. The proposed methodology can be applied to general linear coupled systems such as fluid-structure interaction problems (Morand and Ohayon, 1995; Soize, Desanti and David, 1992).

For linear structural vibrations, dynamic substructuring techniques based on the use of the fixed-interface modes or free-interface modes (completed by static boundary functions, attachment modes, residual flexibility, etc.) of each substructure have been widely developed in the literature: for conservative structures see, for example, Hurty (1965), Craig and Bampton (1968), MacNeal (1971), Rubin (1975), Flashner (1986), Min, Igusa, and Achenbach (1992), Farhat and Geradin (1994) and, for damped structures, Klein and Dowell (1974), Hale and Meirovitch (1980), Leung (1993), Farstad and Singh (1995), and Rook and Singh (1995).

Some papers are based on a mixed formulation using a Lagrange multiplier in order to impose the linear constraints on the coupling interfaces (see Klein and Dowell, 1974; Min, Igusa, and Achenbach, 1992; Farstad and Singh, 1995; Rook and Singh, 1995). Within the context of finite element discretization of linear structural dynamic problems, Farhat and Geradin (1994) have also introduced a Lagrange multiplier to take into account incompatible meshes on the interface (their analysis is devoted to undamped structures using a component mode method based on fixed-interface modes and static boundary functions).

Contributed by the Applied Mechanics Division of THE AMERICAN SOCIETY OF MECHANICAL ENGINEERS for publication in the ASME JOURNAL OF APPLIED MECHANICS.

Discussion on the paper should be addressed to the Technical Editor, Professor Lewis T. Wheeler, Department of Mechanical Engineering, University of Houston, Houston, TX 77204-4792, and will be accepted until four months after final publication of the paper itself in the ASME JOURNAL OF APPLIED MECHANICS.

Manuscript received by the ASME Applied Mechanics Division, Sept. 20, 1995; final revision, Jan. 17, 1997. Associate Technical Editor: W. K. Liu.

Below, we present an original general approach for damped structures using continuum-based variational formulations and Ritz-Galerkin projection methods using free-interface modes and fixed-interface modes of each substructure (in this paper we do not consider mathematical aspects of error estimates connected to the truncation of the modal series). For this purpose, various rigorous algebraic decompositions of admissible classes of the unknown fields are introduced and leads to several linear dynamic substructuring methods, the continuity of the displacement field on the interface being imposed through the use of a Lagrange multiplier field. As a consequence, the final system for the mixed formulation has a rank deficiency in the matrix that describes the constraints. This leads to nonuniqueness of the solution. In order to avoid this difficulty, a new constructive approach is proposed consisting in using a Singular Value Decomposition (SVD) of the frequency-independent constraint matrix and chose a "least-square" solution that is in fact the solution of the original problem. Due to a relatively small number of degrees-of-freedom in the reduced model, the use of SVD is particularly efficient. Since the problem under consideration is linear, SVD is used only once. Consequently, the SVD appears as an efficient and reliable tool to solve this rank deficiency problem. It should be noted that SVD has been used for undamped linear vibration analysis of plates using dynamic substructuring by analytical methods (Jen, Johnson and Dubois, 1995). Let us recall that SVD has also been used in the area of the nonlinear dynamical analysis of multibody systems with nonlinear constraints (Singh and Likins, 1985; Shabana, 1991; Schmidt and Müller, 1993).

Now we give a short description of the content of each section.

Section 2 deals with the displacement and mixed variational formulations for the coupled linear structure-structure problem, the Lagrange multiplier field being introduced in the mixed problem. In Section 3, we present a dynamic substructuring method using the free-interface modes of each linear substructure. The modal reduction procedure is carried out using a new explicit construction of the Lagrange multiplier admissible space. Two practical constructions of the frequency response function of the global linear damped structure and the eigenvalues of the associated conservative structure are performed using SVD once on a part of the linear system to be solved, namely on the frequency-independent Lagrange multiplier terms.

Section 4 is devoted to a dynamic substructuring method using the classical Craig and Bampton fixed-interface modes

and boundary static functions of each linear substructure, presented in an original general framework allowing various other decomposition procedures to be obtained. After having constructed the reduced matrix model of each substructure, we explain two procedures for the assemblage of the substructures and the construction of a solution, (1) in a classical manner and (2) as in Section 3 using Lagrange multiplier field and SVD.

Finally, in Section 5, some conclusions are presented.

2 Displacement and Mixed Variational Formulations for the Coupled Structure-Structure Problem

2.1 General Mechanical Hypotheses. In this section, the following hypotheses are introduced:

- One considers the linear vibrations of a three-dimensional structure about a static equilibrium configuration which is considered here as a natural state (for the sake of brevity, prestress are not considered but could be added without changing the theory).
- The structure is only submitted to prescribed external forces (no prescribed displacement).

With the above hypotheses, there are two cases.

1 The first one, which is the only case considered in this paper, corresponds to prescribed external forces which are in equilibrium at each instant. Consequently, the displacement field of the structure is defined up to an additive rigid-body displacement field. In this case, we are only interested in the part of the displacement field due to the structural deformation. We will see below how the rigid-body displacement field can be disregarded.

2 The second case corresponds to prescribed external forces which are not in equilibrium at some instants. To solve this problem, the method consists in transforming this case to the first case by adding an additional external force related to rigid-body field. For the sake of brevity, this case will not be considered in the present paper.

One presents a variational formulation of the problem (first case), taking into account an additional small structural damping based on a linear viscoelastic model with an instantaneous memory. A frequency domain formulation is used, the convention for the Fourier transform being $\mathbf{u}(\omega) = \int_{\mathbb{R}} e^{-i\omega t} \mathbf{u}(t) dt$ where ω denotes the circular frequency, $\mathbf{u}(\omega)$ is a vector in \mathbb{C}^3 and $\bar{\mathbf{u}}(\omega)$ its conjugate (\mathbb{R} and \mathbb{C} denote the set of real and complex numbers, respectively).

2.2 Notation for a Substructure Ω_r . We consider a structure formed by substructures that will be denoted by an index r . Let Ω_r be the three-dimensional bounded domain occupied at static equilibrium by the substructure labelled by index r . Let $\partial\Omega_r = \Gamma_r \cup \Gamma$ with $\Gamma_r \cap \Gamma = \emptyset$ be the boundary of Ω_r (assumed to be smooth). The boundary Γ will be the *interaction surface* with another substructure. The external prescribed volumetric and surface force fields applied to Ω_r and Γ_r are denoted by \mathbf{g}_{Ω_r} and \mathbf{g}_{Γ_r} , respectively. Let $\mathbf{u}^r = (u_1^r, u_2^r, u_3^r)$ be the displacement field at each point $\mathbf{x} = (x_1, x_2, x_3)$ in cartesian coordinates. The set of admissible displacement fields with values in \mathbb{C}^3 (resp. in \mathbb{R}^3) is denoted by C_{Ω_r} (resp. \mathcal{R}_{Ω_r}) and is used for dissipative problems (resp. associated conservative problems). For substructure Ω_r , one denotes the test function (weighted function) associated with \mathbf{u}^r as $\delta\mathbf{u}^r \in C_{\Omega_r}$ (or in \mathcal{R}_{Ω_r}). The strain tensor is defined by

$$\epsilon_{ij}(\mathbf{u}^r) = \frac{1}{2}(u_{i,j}^r + u_{j,i}^r), \quad (1)$$

in which $v_{,j}$ denotes the partial derivative of v with respect to x_j . The total stress tensor is defined by

$$\sigma_{\text{tot}}^r = \sigma^r + i\omega s^r, \quad (2)$$

where σ^r is the elastic stress tensor defined by $\sigma_{ij}^r(\mathbf{u}^r) = a_{ijkh}\epsilon_{kh}(\mathbf{u}^r)$ and $i\omega s^r$ is the viscous part of the total stress tensor such that $s_{ij}^r(\mathbf{u}^r) = b_{ijkh}\epsilon_{kh}(\mathbf{u}^r)$ (using summation over repeated indices). The mechanical coefficients a_{ijkh} and b_{ijkh} are independent of ω and verify the usual properties of symmetry and positivity (see Marsden and Hughes, 1983). The mass density is denoted by ρ^r . For the dissipative problem, three sesquilinear forms on $C_{\Omega_r} \times C_{\Omega_r}$, corresponding to the mass, stiffness, and damping operators of substructure Ω_r , are introduced as follows:

$$m^r(\mathbf{u}^r, \delta\mathbf{u}^r) = \int_{\Omega_r} \rho^r \mathbf{u}^r \cdot \overline{\delta\mathbf{u}^r} d\mathbf{x}, \quad (3)$$

$$k^r(\mathbf{u}^r, \delta\mathbf{u}^r) = \int_{\Omega_r} \sigma_{ij}^r(\mathbf{u}^r) \epsilon_{ij}(\overline{\delta\mathbf{u}^r}) d\mathbf{x}, \quad (4)$$

$$d^r(\mathbf{u}^r, \delta\mathbf{u}^r) = \int_{\Omega_r} s_{ij}^r(\mathbf{u}^r) \epsilon_{ij}(\overline{\delta\mathbf{u}^r}) d\mathbf{x}. \quad (5)$$

It should be noted that the hermitian form m^r is positive definite on $C_{\Omega_r} \times C_{\Omega_r}$. The hermitian forms k^r and d^r are semi-definite positive (degenerated forms) since rigid-body displacement fields are allowed in the present case. The set $\mathcal{R}_{\text{rig}}^r$ of \mathbb{R}^3 -valued rigid-body displacement fields (of dimension 6) is a subset of C_{Ω_r} . Consequently, for all $\delta\mathbf{u}^r$ in C_{Ω_r} , $k^r(\mathbf{u}^r, \delta\mathbf{u}^r)$ and $d^r(\mathbf{u}^r, \delta\mathbf{u}^r)$ are equal to zero for any \mathbf{u}^r in $\mathcal{R}_{\text{rig}}^r$.

We then define the following sesquilinear form z^r on $C_{\Omega_r} \times C_{\Omega_r}$:

$$z^r(\mathbf{u}^r, \delta\mathbf{u}^r) = -\omega^2 m^r(\mathbf{u}^r, \delta\mathbf{u}^r) + i\omega d^r(\mathbf{u}^r, \delta\mathbf{u}^r) + k^r(\mathbf{u}^r, \delta\mathbf{u}^r). \quad (6)$$

Finally, we define \mathbf{f}^r by the relation

$$\langle\langle \mathbf{f}^r, \overline{\delta\mathbf{u}^r} \rangle\rangle = \int_{\Omega_r} \mathbf{g}_{\Omega_r} \cdot \overline{\delta\mathbf{u}^r} d\mathbf{x} + \int_{\Gamma_r} \mathbf{g}_{\Gamma_r} \cdot \overline{\delta\mathbf{u}^r} ds. \quad (7)$$

2.3 Continuum-Based Variational Formulations for Two Coupled Substructures Ω_1 and Ω_2 . We consider a structure composed of two substructures Ω_1 and Ω_2 that interact through a common boundary Γ (the extension to the case of more than two substructures is straightforward). The notations introduced in Section 2.2 are used with $r = 1$ and $r = 2$. The linear coupling conditions on Γ are written as

$$\mathbf{u}^1 = \mathbf{u}^2 \quad \text{on } \Gamma, \quad (8)$$

$$\sigma_{\text{tot}}^1 \mathbf{n}^1 = -\sigma_{\text{tot}}^2 \mathbf{n}^2 \quad \text{on } \Gamma, \quad (9)$$

where \mathbf{n}^r is the unit normal to Γ , external to Ω^r .

2.3.1 Basic (u^1, u^2) Variational Formulation \mathcal{P}_0 . For all real ω in \mathbb{R} and prescribed $(\mathbf{f}^1, \mathbf{f}^2)$, find $(\mathbf{u}^1, \mathbf{u}^2)$ in $C_{\Omega_1} \times C_{\Omega_2}$ verifying the linear constraint $\mathbf{u}^1 = \mathbf{u}^2$ on Γ , such that, for all $(\delta\mathbf{u}^1, \delta\mathbf{u}^2)$ in $C_{\Omega_1} \times C_{\Omega_2}$ verifying the linear constraint $\delta\mathbf{u}^1 = \delta\mathbf{u}^2$ on Γ , one has

$$z^1(\mathbf{u}^1, \delta\mathbf{u}^1) + z^2(\mathbf{u}^2, \delta\mathbf{u}^2) = \langle\langle \mathbf{f}^1, \overline{\delta\mathbf{u}^1} \rangle\rangle + \langle\langle \mathbf{f}^2, \overline{\delta\mathbf{u}^2} \rangle\rangle. \quad (10)$$

From the mathematical point of view (see Dautray and Lions, 1992), by taking Sobolev space $H^1(\Omega^r, \mathbb{C}^3)$ as admissible space C_{Ω_r} , the existence and uniqueness of a solution of \mathcal{P}_0 can be proved.

2.3.2 Mixed (u^1, u^2, λ) Variational Formulation \mathcal{P}_1 . This formulation consists in relaxing the linear constraint (defined by Eq. (8)) used in \mathcal{P}_0 by the introduction of a Lagrange multiplier field λ defined on Γ . Let Λ_Γ be the admissible set of Lagrange multiplier fields defined on Γ with values in \mathbb{C}^3 .

Formulation \mathcal{P}_1 . For all real ω in \mathbb{R} and prescribed $(\mathbf{f}^1, \mathbf{f}^2)$, find $(\mathbf{u}^1, \mathbf{u}^2)$ in $C_{\Omega_1} \times C_{\Omega_2}$ and $\boldsymbol{\lambda}$ in Λ_Γ such that, for all $(\delta \mathbf{u}^1, \delta \mathbf{u}^2)$ in $C_{\Omega_1} \times C_{\Omega_2}$ and for all $\delta \boldsymbol{\lambda}$ in Λ_Γ , one has

$$z^1(\mathbf{u}^1, \delta \mathbf{u}^1) + z^2(\mathbf{u}^2, \delta \mathbf{u}^2) + b(\boldsymbol{\lambda}, \delta \mathbf{u}^1 - \delta \mathbf{u}^2) + b(\delta \boldsymbol{\lambda}, \mathbf{u}^1 - \mathbf{u}^2) = \langle \langle \mathbf{f}^1, \overline{\delta \mathbf{u}^1} \rangle \rangle + \langle \langle \mathbf{f}^2, \overline{\delta \mathbf{u}^2} \rangle \rangle, \quad (11)$$

where $b(\cdot, \cdot)$ is defined by

$$b(\boldsymbol{\lambda}, \mathbf{u}') = \int_\Gamma \boldsymbol{\lambda} \cdot \overline{\mathbf{u}'} ds. \quad (12)$$

Space of traces on Γ . The set of the traces related to the boundary Γ , is denoted by C_Γ . Therefore, if $\mathbf{u}' \in C_{\Omega_r}$, then the trace of \mathbf{u}' on Γ is denoted by $\mathbf{u}'|_\Gamma$ and belongs to C_Γ . In Eq. (11), Λ_Γ is the dual space of C_Γ .

Remark. From the mathematical point of view (see Dautray and Lions, 1992), by taking $C_{\Omega_r} = H^1(\Omega_r, \mathbb{C}^3)$, $C_\Gamma = H^{1/2}(\Gamma, \mathbb{C}^3)$ and $\Lambda_\Gamma = H^{-1/2}(\Gamma, \mathbb{C}^3)$, the existence and uniqueness of a solution of formulation \mathcal{P}_1 can be proved using the so-called LBB condition related to the sesquilinear form b (see Brezzi and Fortin, 1991). It should be noted that $H^{1/2}(\Gamma, \mathbb{C}^3)$ is dense in $H^{-1/2}(\Gamma, \mathbb{C}^3)$.

3 Dynamic Substructuring Using the Free-Interface Modes of Each Substructure

The method is based on the use of the mixed variational formulation defined by \mathcal{P}_1 . Then, a modal reduction is carried out using the Ritz-Galerkin projection on the free-interface modes of each substructure. Finally, the Singular Value Decomposition (SVD) is used for the construction of the solution.

3.1 Free-Interface Modes of a Substructure Ω_r . A free-interface mode of a substructure Ω_r (for $r = 1$ or $r = 2$) is defined as an eigenmode of the conservative problem associated with the substructure Ω_r , subject to zero forces on Γ . The real eigenvalues $\omega^2 \geq 0$ and the eigenmodes \mathbf{u}^r in \mathcal{R}_{Ω_r} are solutions of the following spectral problem: find $\omega^2 \geq 0$, $\mathbf{u}^r \in \mathcal{R}_{\Omega_r}$ ($\mathbf{u}^r \neq \mathbf{0}$) such that for all $\delta \mathbf{u}^r \in \mathcal{R}_{\Omega_r}$, one has

$$k^r(\mathbf{u}^r, \delta \mathbf{u}^r) = \omega^2 m^r(\mathbf{u}^r, \delta \mathbf{u}^r). \quad (13)$$

It can be shown that there exist six zero eigenvalues $0 = (\omega_{-5}^r)^2 = \dots = (\omega_0^r)^2$ (associated with the rigid-body displacement fields) and that the strictly positive eigenvalues (associated with the displacement field due to structural deformation) constitute the increasing sequence $0 < (\omega_1^r)^2 \leq (\omega_2^r)^2, \dots$. The six eigenvectors $\{\mathbf{u}_{-5}^r, \dots, \mathbf{u}_0^r\}$ associated with zero eigenvalues span \mathcal{R}_{rig} (space of the rigid-body displacement fields). The family $\{\mathbf{u}_{-5}^r, \dots, \mathbf{u}_0^r; \mathbf{u}_1^r, \dots\}$ of all the eigenvectors forms a complete set in \mathcal{R}_{Ω_r} . For α and β in $\{-5, \dots, 0; 1, \dots\}$, we have the orthogonality conditions

$$m^r(\mathbf{u}_\alpha^r, \mathbf{u}_\beta^r) = \delta_{\alpha\beta} \mu_\alpha^r, \quad (14)$$

$$k^r(\mathbf{u}_\alpha^r, \mathbf{u}_\beta^r) = \delta_{\alpha\beta} \mu_\alpha^r \omega_\alpha^r{}^2, \quad (15)$$

in which $\mu_\alpha^r > 0$ is the generalized mass of mode α depending on the normalization of the eigenmodes.

3.2 Modal Reduction of \mathcal{P}_1 . We introduce the subspace $C_{\Omega_r}^N$ of C_{Ω_r} , of dimension N_r , spanned by $\{\mathbf{u}_1^r, \dots, \mathbf{u}_{N_r}^r\}$ with $N_r \geq 1$. For all \mathbf{u}^r in $C_{\Omega_r}^N$, one has

$$\mathbf{u}^r = \sum_{\alpha=1}^{N_r} q_\alpha^r \mathbf{u}_\alpha^r, \quad (16)$$

in which q_α^r are complex-valued generalized coordinates. Concerning the trace of the displacement field (including rigid-body

displacement field) on Γ , the subspace spanned by the family $\{\mathbf{u}_{-5| \Gamma}^r, \dots, \mathbf{u}_{0| \Gamma}^r; \mathbf{u}_{1| \Gamma}^r, \dots\}$ is a complete set in C_Γ (for the two domains $r = 1$ and $r = 2$). Consequently, the family $\{\mathbf{u}_{1| \Gamma}^r, \dots\}$ forms a complete set of the displacement field on Γ due only to the structural deformation. Let C_Γ^N be the subspace of C_Γ spanned by the finite family $\{\mathbf{u}_{1| \Gamma}^r, \dots, \mathbf{u}_{N_r| \Gamma}^r\}$. Let \mathcal{W}_Γ^N be the subspace of C_Γ of finite dimension $N \leq N_1 + N_2$ defined by

$$\mathcal{W}_\Gamma^N = C_\Gamma^{N_1} \cup C_\Gamma^{N_2}. \quad (17)$$

The present approach is based on the fact that any $\boldsymbol{\lambda}$ in Λ_Γ can be expanded on a complete orthonormal set in C_Γ and consequently, the projection of the Lagrange multiplier $\boldsymbol{\lambda}$ is done on the subspace \mathcal{W}_Γ^N of $C_\Gamma \subset \Lambda_\Gamma$. A characterization of \mathcal{W}_Γ^N requires the construction of a basis of \mathcal{W}_Γ^N denoted by $\{\mathbf{w}_1, \dots, \mathbf{w}_N\}$. One possible method consists in extracting an independent system of N functions from the family $\{\mathbf{u}_{1| \Gamma}^1, \dots, \mathbf{u}_{N_1| \Gamma}^1, \mathbf{u}_{1| \Gamma}^2, \dots, \mathbf{u}_{N_2| \Gamma}^2\}$. Consequently, for all $\boldsymbol{\lambda}$ in \mathcal{W}_Γ^N , one has

$$\boldsymbol{\lambda} = \sum_{\gamma=1}^N p_\gamma \mathbf{w}_\gamma. \quad (18)$$

The reduced problem $\mathcal{P}_1^{\text{red}}$. We use the Ritz-Galerkin method consisting in substituting Eqs. (16) and (18) into Eq. (11). Using the orthogonality conditions defined by Eqs. (14) and (15) and introducing the vectors of generalized coordinates $\mathbf{q}^1 = (q_1^1, \dots, q_{N_1}^1)$, $\mathbf{q}^2 = (q_1^2, \dots, q_{N_2}^2)$ and $\mathbf{p} = (p_1, \dots, p_N)$, one deduces the following finite-dimension reduced problem from \mathcal{P}_1

$$\begin{bmatrix} Z^1(\omega) & 0 & \mathcal{B}_1^T \\ 0 & Z^2(\omega) & \mathcal{B}_2^T \\ \mathcal{B}_1 & \mathcal{B}_2 & 0 \end{bmatrix} \begin{bmatrix} \mathbf{q}^1 \\ \mathbf{q}^2 \\ \mathbf{p} \end{bmatrix} = \begin{bmatrix} \mathcal{F}^1 \\ \mathcal{F}^2 \\ \mathbf{0} \end{bmatrix}, \quad (19)$$

in which, for all real ω and for $r = 1$ and $r = 2$, $[Z^r(\omega)]$ is an $(N_r \times N_r)$ complex symmetric matrix, $[\mathcal{B}_r]$ a $(N \times N_r)$ real matrix which is independent of ω and \mathcal{F}^r a \mathbb{C}^{N_r} -valued vector. Matrix $[Z^r(\omega)]$ is defined by

$$[Z^r(\omega)] = -\omega^2 [\mathcal{M}^r] + i\omega [\mathcal{D}^r] + [\mathcal{K}^r], \quad (20)$$

where $[\mathcal{M}^r]$ and $[\mathcal{K}^r]$ are diagonal positive-definite matrices such that $[\mathcal{M}^r]_{\alpha\beta} = \mu_\alpha^r \delta_{\alpha\beta}$ and $[\mathcal{K}^r]_{\alpha\beta} = \mu_\alpha^r \omega_\alpha^r{}^2 \delta_{\alpha\beta}$, $[\mathcal{D}^r]$ is a full symmetric positive-definite matrix, such that $[\mathcal{D}^r]_{\alpha\beta} = d^r(\mathbf{u}_\alpha^r, \mathbf{u}_\beta^r)$. Consequently, for all real ω , matrix $[Z^r(\omega)]$ is invertible. Matrix $[\mathcal{B}_r]$ is such that for all α in $\{1, \dots, N_r\}$ and γ in $\{1, \dots, N\}$, one has

$$[\mathcal{B}_r]_{\gamma\alpha} = b(\mathbf{w}_\gamma, \mathbf{u}_\alpha^r). \quad (21)$$

Finally, vector \mathcal{F}^r is such that, for all α in $\{1, \dots, N_r\}$, one has

$$\mathcal{F}_\alpha^r = \langle \langle \mathbf{f}^r, \mathbf{u}_\alpha^r \rangle \rangle. \quad (22)$$

3.3 Practical Construction of the Frequency Response Function of the Global Structure Using Reduced Problem $\mathcal{P}_1^{\text{red}}$ and SVD. First, we introduce the $(N \times M)$ real matrix $[\mathcal{B}]$ such that

$$M = N_1 + N_2, \quad [\mathcal{B}] = [\mathcal{B}_1 \quad \mathcal{B}_2] \quad (23)$$

and write Eq. (19) as

$$\begin{bmatrix} Z(\omega) & \mathcal{B}^T \\ \mathcal{B} & 0 \end{bmatrix} \begin{bmatrix} \mathbf{q} \\ \mathbf{p} \end{bmatrix} = \begin{bmatrix} \mathcal{F} \\ \mathbf{0} \end{bmatrix}. \quad (24)$$

In order to solve Eq. (24), we use a Singular Value Decomposition (SVD) of $[\mathcal{B}]$. It is known that there exist algorithms (see Golub and Van Loan, 1989) which are very efficient for the construction of the SVD of reasonable size matrices. This is

the case for the reduced problems obtained by modal projection as Eq. (24). In the proposed approach, it should be noted that SVD will only be applied to the submatrix $[\mathcal{B}]$ in Eq. (24). The SVD of $(N \times M)$ real matrix $[\mathcal{B}]$ with $M \geq N$ (see Section 3.2) consists in constructing the following decomposition:

$$[\mathcal{B}] = [U][\Sigma][V]^T, \quad (25)$$

where $[U]$ is an $(N \times N)$ orthogonal real matrix, $[V]$ is an $(M \times M)$ orthogonal real matrix and $[\Sigma]$ is a $(N \times M)$ real matrix which is written in block form as

$$[\Sigma] = [\Sigma^+ \ 0], \quad (26)$$

in which $[0]$ is the $(N \times (M - N))$ null matrix and $[\Sigma^+]$ is the $(N \times N)$ diagonal matrix of positive or null singular values σ_k such that $\sigma_1 \geq \sigma_2 \geq \dots \geq \sigma_N \geq 0$. Let n be the integer such that $1 \leq n \leq N$ such that

$$\sigma_1 \geq \sigma_2 \geq \dots \geq \sigma_n > \sigma_{n+1} = \dots = \sigma_N = 0. \quad (27)$$

Consequently, the rank of $[\mathcal{B}]$ is equal to n and Eq. (25) yields the SVD expansion

$$[\mathcal{B}] = \sum_{k=1}^n \sigma_k \mathbf{U}^k \mathbf{V}^{kT}, \quad (28)$$

in which the vectors \mathbf{U}^k and \mathbf{V}^k are the columns of $[U]$ and $[V]$ and such that

$$\langle \mathbf{U}^j, \mathbf{U}^k \rangle = \delta_{jk}, \quad \langle \mathbf{V}^j, \mathbf{V}^k \rangle = \delta_{jk}. \quad (29)$$

The range of $[\mathcal{B}]$ is spanned by $\{\mathbf{U}^1, \dots, \mathbf{U}^n\}$ and its null space by $\{\mathbf{V}^{n+1}, \dots, \mathbf{V}^M\}$.

3.3.1 First Algebraic Stage of the Practical Construction of Solution. Equation (24) has a unique solution if the null space of $[\mathcal{B}]^T$ is reduced to $\{0\}$, or equivalently, the dimension of the null space of $[\mathcal{B}]$ is equal to $M - N$, i.e., if one has $n = N$ in Eq. (27). Generally, we have $n < N$, which means that the linear constraint equations

$$[\mathcal{B}]\mathbf{q} = 0 \quad (30)$$

are nonindependent, and consequently Eq. (24) does not have a unique solution. In that case, the SVD of $[\mathcal{B}]$ allows the construction of a unique solution \mathbf{q} of Eq. (24) in the null space of $[\mathcal{B}]$, i.e.,

$$\mathbf{q} = \sum_{k=n+1}^M \xi_k \mathbf{V}^k. \quad (31)$$

Using Eqs. (28) and (29), it can be seen that \mathbf{q} defined by Eq. (31) satisfies Eq. (30). Using Eqs. (28) and (31), Eq. (24) yields

$$\sum_{k=n+1}^M \xi_k [Z(\omega)] \mathbf{V}^k + \sum_{k=1}^n \sigma_k \eta_k \mathbf{V}^k = \mathcal{F}, \quad (32)$$

in which $\eta_k = \langle \mathbf{U}^k, \mathbf{p} \rangle$, or equivalently,

$$\sum_{k=n+1}^M \xi_k \mathbf{V}^k + \sum_{k=1}^n \sigma_k \eta_k [Z(\omega)]^{-1} \mathbf{V}^k = [Z(\omega)]^{-1} \mathcal{F}. \quad (33)$$

Equation (32) or (33) shows that ξ_k can be calculated in a unique way.

3.3.2 Second Algebraic Stage of the Practical Construction of Solution.

First procedure. The projection of Eq. (33) on $\{\mathbf{V}^1, \dots, \mathbf{V}^n\}$ yields

$$[E(\omega)]\mathbf{y} = \mathbf{e}, \quad (34)$$

in which $[E(\omega)]$ is a $(n \times n)$ complex symmetric matrix such that $[E(\omega)]_{k'k} = \langle [Z(\omega)]^{-1} \mathbf{V}^k, \mathbf{V}^{k'} \rangle$, $\mathbf{y} = (y_1, \dots, y_n)$ is a vector in \mathbb{C}^n with $y_k = \sigma_k \eta_k$ and $\mathbf{e} = (e_1, \dots, e_n)$ is a vector

in \mathbb{C}^n such that $e_k = \langle [Z(\omega)]^{-1} \mathcal{F}, \mathbf{V}^k \rangle$. Then, the projection of Eq. (33) on the remaining $\{\mathbf{V}^{n+1}, \dots, \mathbf{V}^M\}$ yields for all k in $\{n+1, \dots, M\}$,

$$\xi_k = - \sum_{k'=1}^n y_{k'} \langle [Z(\omega)]^{-1} \mathbf{V}^{k'}, \mathbf{V}^k \rangle + \langle [Z(\omega)]^{-1} \mathcal{F}, \mathbf{V}^k \rangle. \quad (35)$$

The corresponding algorithm is summarized below.

Step 0: calculating the SVD of $[\mathcal{B}]$ in order to obtain its rank n and $\mathbf{V}^1, \dots, \mathbf{V}^M$.

Then, for each real ω ,

Step 1: solving the linear equation of dimension n with $n+1$ right-hand side members $\{\mathcal{F}; \mathbf{V}^1, \dots, \mathbf{V}^n\}$

$$[Z(\omega)]\mathbf{X}^0 = \mathcal{F}, \quad [Z(\omega)]\mathbf{X}^k = \mathbf{V}^k, \quad k \in \{1, \dots, n\}; \quad (36)$$

Step 2: constructing $(n \times n)$ complex symmetric matrix $[E(\omega)]$ such that $[E(\omega)]_{k'k} = \langle \mathbf{X}^k, \mathbf{V}^{k'} \rangle$ for k and k' in $\{1, \dots, n\}$;

Step 3: constructing \mathbb{C}^n -valued vector \mathbf{e} such that $e_k = \langle \mathbf{X}^0, \mathbf{V}^k \rangle$ for k in $\{1, \dots, n\}$;

Step 4: solving Eq. (34) which has a unique solution \mathbf{y} (by construction);

Step 5: calculating ξ_{n+1}, \dots, ξ_M such that for all k in $\{n+1, \dots, M\}$,

$$\xi_k = - \sum_{k'=1}^n y_{k'} \langle \mathbf{X}^{k'}, \mathbf{V}^k \rangle + \langle \mathbf{X}^0, \mathbf{V}^k \rangle. \quad (37)$$

Step 6: calculating \mathbf{q} by using Eq. (31).

Second procedure. The projection of Eq. (32) on $\{\mathbf{V}^{n+1}, \dots, \mathbf{V}^M\}$ yields

$$[G(\omega)]\boldsymbol{\xi} = \mathbf{g}, \quad (38)$$

in which $\boldsymbol{\xi} = (\xi_{n+1}, \dots, \xi_M)$ is a vector in \mathbb{C}^{M-n} , $\mathbf{g} = (g_1, \dots, g_{M-n})$ is a vector in \mathbb{C}^{M-n} such that $g_k = \langle \mathcal{F}, \mathbf{V}^{k+n} \rangle$ and $[G(\omega)]$ is a $((M-n) \times (M-n))$ complex symmetric matrix such that

$$[G(\omega)] = -\omega^2 [\hat{\mathcal{M}}] + i\omega [\hat{\mathcal{D}}] + [\hat{\mathcal{K}}], \quad (39)$$

where $[\hat{\mathcal{M}}]$, $[\hat{\mathcal{D}}]$ and $[\hat{\mathcal{K}}]$ are $((M-n) \times (M-n))$ real symmetric positive-definite matrices defined, for all k and k' in $\{1, \dots, M-n\}$, by

$$[\hat{\mathcal{M}}]_{k'k} = \langle [\mathcal{M}] \mathbf{V}^{k+n}, \mathbf{V}^{k'+n} \rangle, \quad (40)$$

$$[\hat{\mathcal{D}}]_{k'k} = \langle [\mathcal{D}] \mathbf{V}^{k+n}, \mathbf{V}^{k'+n} \rangle, \quad (41)$$

$$[\hat{\mathcal{K}}]_{k'k} = \langle [\mathcal{K}] \mathbf{V}^{k+n}, \mathbf{V}^{k'+n} \rangle. \quad (42)$$

The corresponding algorithm is summarized below.

Step 0: calculating the SVD of $[\mathcal{B}]$ in order to obtain its rank n and $\mathbf{V}^{n+1}, \dots, \mathbf{V}^M$.

Then, for each real ω ,

Step 1: constructing $((M-n) \times (M-n))$ complex symmetric matrix $[G]$ such that $[G]_{k'k} = \langle [Z(\omega)] \mathbf{V}^{k+n}, \mathbf{V}^{k'+n} \rangle$ for k and k' in $\{1, \dots, M-n\}$;

Step 2: constructing \mathbb{C}^{M-n} -valued vector \mathbf{g} such that $g_k = \langle \mathcal{F}, \mathbf{V}^{k+n} \rangle$, $k \in \{1, \dots, M-n\}$;

Step 3: solving Eq. (38) which has a unique solution $\boldsymbol{\xi}$ (by construction);

Step 4: calculating \mathbf{q} by using Eq. (31).

Comments on the two proposed procedures.

1 Due to the fact that we have to solve a reduced size problem, N and M are small.

2 In the first procedure, Step 1 is solved substructure by substructure independently. For each substructure Ω_r , if the damping operator defined by Eq. (5) is diagonalized by the free-interface modes of this substructure, Step 1 is straightforward. If not, we have to solve a small $(N_r \times N_r)$ full complex symmetric

system for each substructure. In Step 4, one has to solve a linear system of dimension n with a full $(n \times n)$ complex symmetric matrix corresponding to the total number of independent linear constraints existing in the global structure (assemblage of all the substructures).

3 In the second procedure, Step 1 is relative to the global structure (assemblage of all the substructures) and Step 4 requires to solve a full complex symmetric linear system of dimension $M - n$.

4 For example, if there are N_S substructures (in this paper $N_S = 2$) and if the mean value of $\{N_r\}$ on the set of substructures is $N_r = (1/N_S) \sum_{r=1}^{N_S} N_r$, the order of floating operations is $N_S \times N_r^3$ for the first procedure with a damping matrix of each substructure which is not diagonalized by the free-interface modes of this substructure and, $N_S^3 \times N_r^4$ for the second procedure.

As a conclusion, the first procedure is recommended since it is more efficient (particularly, if the damping matrix of each substructure is diagonalized by the free-interface modes of this substructure).

3.4 Practical Construction of the Eigenmodes of the Global Structure Using a Reduced Spectral Problem and SVD. The conservative problem associated to Eq. (24) leads to the following spectral problem:

$$\begin{bmatrix} \mathcal{K}^1 & 0 & \mathcal{B}_1^T \\ 0 & \mathcal{K}^2 & \mathcal{B}_2^T \\ \mathcal{B}_1 & \mathcal{B}_2 & 0 \end{bmatrix} \begin{bmatrix} \mathbf{q}^1 \\ \mathbf{q}^2 \\ \mathbf{p} \end{bmatrix} = \omega^2 \begin{bmatrix} \mathcal{M}^1 & 0 & 0 \\ 0 & \mathcal{M}^2 & 0 \\ 0 & 0 & 0 \end{bmatrix} \begin{bmatrix} \mathbf{q}^1 \\ \mathbf{q}^2 \\ \mathbf{p} \end{bmatrix}, \quad (43)$$

in which the two matrices defined by blocks are real symmetric and independent of ω . Using a global notation as done in Eq. (24), Eq. (43) is rewritten as

$$\begin{bmatrix} \mathcal{K} & \mathcal{B}^T \\ \mathcal{B} & 0 \end{bmatrix} \begin{bmatrix} \mathbf{q} \\ \mathbf{p} \end{bmatrix} = \omega^2 \begin{bmatrix} \mathcal{M} & 0 \\ 0 & 0 \end{bmatrix} \begin{bmatrix} \mathbf{q} \\ \mathbf{p} \end{bmatrix}. \quad (44)$$

For this problem, we must use the second procedure defined in Section 3.3.2 (in this case, the first procedure cannot be directly used since $[\mathcal{K}] - \omega^2[\mathcal{M}]$ is not invertible for all real values of ω). Substituting Eq. (31) in the first row of Eq. (44), projecting it on $\{\mathbf{V}^{n+1}, \dots, \mathbf{V}^M\}$ and using Eq. (29), yield

$$[\hat{\mathcal{K}}]\xi = \omega^2[\hat{\mathcal{M}}]\xi, \quad (45)$$

in which $[\hat{\mathcal{M}}]$ and $[\hat{\mathcal{K}}]$ are defined by Eqs. (40) and (42).

The corresponding algorithm is summarized below.

Step 0: Calculating the SVD of $[\mathcal{B}]$ in order to obtain its rank n and $\mathbf{V}^{n+1}, \dots, \mathbf{V}^M$.

Step 1: constructing $((M - n) \times (M - n))$ real symmetric matrices $[\hat{\mathcal{M}}]$ and $[\hat{\mathcal{K}}]$;

Step 2: solving the generalized eigenvalue problem defined by Eq. (45);

Step 3: calculating the eigenmodes $\mathbf{u} = (\mathbf{u}^1, \mathbf{u}^2)$ of the structure by using Eqs. (31) and (16).

4 Dynamic Substructuring Using the Fixed-Interface Modes of Each Substructure

In this section, we present a modal reduction procedure based on formulation \mathcal{P}_1 using SVD (see Section 2.3.2) starting from a reduced matrix model for each substructure Ω_r .

4.1 Reduced Matrix Model of Substructure Ω_r .

4.1.1 Basic \mathbf{u}^r Variational Formulation for Substructure Ω_r . Consider substructure Ω_r submitted to the external applied forces \mathbf{g}_{Ω_r} in Ω_r , \mathbf{g}_Γ on Γ_r and \mathbf{g}_Γ on the interaction surface Γ .

The basic variational formulation for substructure Ω_r is written as follows.

Basic problem \mathcal{P}_1^r . For all real ω in \mathbb{R} and prescribed \mathbf{f}^r defined by Eq. (7), find \mathbf{u}^r in C_{Ω_r} such that, for all $\delta\mathbf{u}^r$ in C_{Ω_r} , one has

$$z^r(\mathbf{u}^r, \delta\mathbf{u}^r) = \langle\langle \mathbf{f}^r, \overline{\delta\mathbf{u}^r} \rangle\rangle + \langle\langle \mathbf{f}_\Gamma, \overline{\delta\mathbf{u}^r} \rangle\rangle, \quad (46)$$

in which z^r is defined by Eq. (6) and where $\langle\langle \mathbf{f}_\Gamma, \overline{\delta\mathbf{u}^r} \rangle\rangle = \int_\Gamma \mathbf{g}_\Gamma \cdot \overline{\delta\mathbf{u}^r} ds$.

4.1.2 Fixed-Interface Modes of Substructure Ω_r . A fixed-interface mode of a substructure Ω_r (for $r = 1$ or $r = 2$) is defined as an eigenmode of the conservative problem associated with the substructure Ω_r , which is fixed on Γ . Since the problem is conservative and defined in a bounded domain, all the quantities are real. Consequently, we introduce the set $\mathcal{R}_{\Omega_r}^0$ defined by

$$\mathcal{R}_{\Omega_r}^0 = \{\delta\mathbf{u}^r \in \mathcal{R}_{\Omega_r} | \delta\mathbf{u}^r = \mathbf{0} \text{ on } \Gamma\}, \quad (47)$$

in which \mathcal{R}_{Ω_r} is defined in Section 2.2. The real eigenvalues $\omega^2 > 0$ and the eigenmodes \mathbf{u}^r in $\mathcal{R}_{\Omega_r}^0$ are solution of the following spectral problem:

Find $\omega^2 > 0$, $\mathbf{u}^r \in \mathcal{R}_{\Omega_r}^0$ ($\mathbf{u}^r \neq \mathbf{0}$) such that for all $\delta\mathbf{u}^r \in \mathcal{R}_{\Omega_r}^0$, one has

$$k^r(\mathbf{u}^r, \delta\mathbf{u}^r) = \omega^2 m^r(\mathbf{u}^r, \delta\mathbf{u}^r), \quad (48)$$

in which m^r and k^r are defined by Eqs. (3) and (4), respectively. It can be shown that the eigenvalues constitute an increasing sequence $0 < (\omega_1^r)^2 \leq (\omega_2^r)^2, \dots$. The family $\{\mathbf{u}_1^r, \mathbf{u}_2^r, \dots\}$ of the eigenvectors associated with the eigenvalues, forms a complete set in $\mathcal{R}_{\Omega_r}^0$. For α and β in $\{1, 2, \dots\}$, we have the orthogonality conditions similar to Eqs. (14) and (15).

4.1.3 Introduction of the Elastostatic Lifting Operator S^r . We consider the solution $\mathbf{u}_{\text{stat}}^r$ of the elastostatic problem of substructure Ω_r subjected to a prescribed displacement field \mathbf{u}_Γ^r on Γ . Let \mathcal{R}_Γ and $\mathcal{R}_{\Omega_r}^{\text{u}_\Gamma^r}$ be the sets of functions such that

$$\mathcal{R}_\Gamma = \{\mathbf{x} \mapsto \mathbf{u}_\Gamma(\mathbf{x}), \quad \forall \mathbf{x} \in \Gamma\}, \quad (49)$$

$$\mathcal{R}_{\Omega_r}^{\text{u}_\Gamma^r} = \{\mathbf{u}^r \in \mathcal{R}_{\Omega_r} | \mathbf{u}^r = \mathbf{u}_\Gamma^r \text{ on } \Gamma\}. \quad (50)$$

The field $\mathbf{u}_{\text{stat}}^r$ satisfies the following variational formulation:

$$k^r(\mathbf{u}_{\text{stat}}^r, \delta\mathbf{u}^r) = 0, \quad \mathbf{u}_{\text{stat}}^r \in \mathcal{R}_{\Omega_r}^{\text{u}_\Gamma^r}, \quad \forall \delta\mathbf{u}^r \in \mathcal{R}_{\Omega_r}^0 \quad (51)$$

where $\mathcal{R}_{\Omega_r}^0$ is the space $\mathcal{R}_{\Omega_r}^{\text{u}_\Gamma^r}$ obtained for $\mathbf{u}_\Gamma^r = \mathbf{0}$. The solution $\mathbf{u}_{\text{stat}}^r$ of Eq. (51) defines the linear operator S^r from \mathcal{R}_Γ into \mathcal{R}_{Ω_r} (called lifting operator in mathematics), such that

$$\mathbf{u}_\Gamma^r \mapsto \mathbf{u}_{\text{stat}}^r = S^r(\mathbf{u}_\Gamma^r). \quad (52)$$

We denote the range space of operator S^r as $\mathcal{R}_{\Omega_r}^\Gamma \subset \mathcal{R}_{\Omega_r}$ such that $\mathcal{R}_{\Omega_r}^\Gamma = S^r(\mathcal{R}_\Gamma)$. It should be noted that the discretization of S^r by the finite element method is obtained by a classical static condensation procedure (sometimes called the Schur complement) of the stiffness matrix of substructure Ω_r with respect to degrees of freedom on Γ .

4.1.4 Conjugate Relationships Between \mathbf{u}_α^r and $\mathbf{u}_{\text{stat}}^r$. Taking $\delta\mathbf{u}^r = \mathbf{u}_\alpha^r$ in Eq. (51), for $\mathbf{u}_{\text{stat}}^r$ satisfying Eq. (51) yields

$$k^r(\mathbf{u}_{\text{stat}}^r, \mathbf{u}_\alpha^r) = 0. \quad (53)$$

For a given mode $(\omega_\alpha^r, \mathbf{u}_\alpha^r \in \mathcal{R}_{\Omega_r}^0)$, the modal reaction forces $\mathbf{F}_\alpha^r = \sigma^r(\mathbf{u}_\alpha^r)\mathbf{n}^r$ on Γ is defined by the variational property

$$k'(\mathbf{u}_\alpha^r, \delta \mathbf{u}^r) - (\omega_\alpha^r)^2 m'(\mathbf{u}_\alpha^r, \delta \mathbf{u}^r) = \int_\Gamma \mathbf{F}_\alpha^r \cdot \delta \mathbf{u}^r ds, \quad \forall \delta \mathbf{u}^r \in \mathcal{R}_{\Omega_r}. \quad (54)$$

Using Eqs. (48) and (53), Eq. (54) yields

$$m'(\mathbf{u}_{\text{stat}}^r, \mathbf{u}_\alpha^r) = - \frac{1}{(\omega_\alpha^r)^2} \int_\Gamma \mathbf{F}_\alpha^r \cdot \mathbf{u}_{|\Gamma}^r ds. \quad (55)$$

Consequently, for all field $\mathbf{u}_{|\Gamma}^r$ in \mathcal{R}_Γ and \mathbf{u}_α^r in $\mathcal{R}_{\Omega_r}^0$, one has

$$k'(S^r(\mathbf{u}_{|\Gamma}^r), \mathbf{u}_\alpha^r) = 0, \quad (56)$$

$$m'(S^r(\mathbf{u}_{|\Gamma}^r), \mathbf{u}_\alpha^r) = - \frac{1}{(\omega_\alpha^r)^2} \int_\Gamma \mathbf{F}_\alpha^r \cdot \mathbf{u}_{|\Gamma}^r ds. \quad (57)$$

4.1.5 Decomposition of \mathcal{R}_{Ω_r} and \mathcal{C}_{Ω_r} . Due to the fact that the trace of $\mathbf{u}^r - \mathbf{u}_{\text{stat}}^r$ is zero on Γ , we have the following decomposition:

$$\mathcal{R}_{\Omega_r} = \mathcal{R}_{\Omega_r}^\Gamma \oplus \mathcal{R}_{\Omega_r}^0, \quad (58)$$

$$\mathbf{u}^r = S^r(\mathbf{u}_{|\Gamma}^r) + \sum_{\alpha=1}^{\infty} q_\alpha^r \mathbf{u}_\alpha^r. \quad (59)$$

Let $\mathcal{C}_{\Omega_r}^\Gamma$ and $\mathcal{C}_{\Omega_r}^0$ be the complexified vector spaces of $\mathcal{R}_{\Omega_r}^\Gamma$ and $\mathcal{R}_{\Omega_r}^0$, respectively. One then has

$$\mathcal{C}_{\Omega_r} = \mathcal{C}_{\Omega_r}^\Gamma \oplus \mathcal{C}_{\Omega_r}^0, \quad (60)$$

and Eq. (59) holds with $\mathbf{u}_{|\Gamma}^r$ being a \mathbb{C}^3 -valued field and q_α^r complex numbers.

4.1.6 Construction of the Reduced Matrix Model. We introduce the subspace $\mathcal{C}_{\Omega_r}^{0,N_r}$ of $\mathcal{C}_{\Omega_r}^0$, of dimension N_r , spanned by $\{\mathbf{u}_1^r, \dots, \mathbf{u}_{N_r}^r\}$ with $N_r \geq 1$ and the subspace $\mathcal{C}_{\Omega_r}^{\Gamma,N_r}$ of $\mathcal{C}_{\Omega_r}^\Gamma$, such that

$$\mathcal{C}_{\Omega_r}^{\Gamma,N_r} = \mathcal{C}_{\Omega_r}^\Gamma \oplus \mathcal{C}_{\Omega_r}^{0,N_r}. \quad (61)$$

For all \mathbf{u}^r and $\delta \mathbf{u}^r$ in $\mathcal{C}_{\Omega_r}^{N_r}$, one has

$$\mathbf{u}^r = S^r(\mathbf{u}_{|\Gamma}^r) + \sum_{\alpha=1}^{N_r} q_\alpha^r \mathbf{u}_\alpha^r, \quad (62)$$

$$\delta \mathbf{u}^r = S^r(\delta \mathbf{u}_{|\Gamma}^r) + \sum_{\alpha=1}^{N_r} \delta q_\alpha^r \mathbf{u}_\alpha^r. \quad (63)$$

We use the Ritz-Galerkin method related to space $\mathcal{C}_{\Omega_r}^0$ consisting in substituting Eqs. (62) and (63) into Eq. (46). Using the conjugate relations (56) and (57) and the orthogonality properties (14) and (15) for fixed-interface modes, we obtain in abstract operator notation

$$\begin{bmatrix} \mathbf{Z}_\Gamma^r(\omega) & \mathcal{A}^r(\omega) \\ \mathcal{A}^r(\omega) & \mathbf{Z}^r(\omega) \end{bmatrix} \begin{bmatrix} \mathbf{u}_\Gamma^r \\ \mathbf{q}^r \end{bmatrix} = \begin{bmatrix} \mathbf{f}_\Gamma^r \\ \mathcal{F}^r \end{bmatrix}, \quad (64)$$

in which $\mathbf{q}^r = (q_1^r, \dots, q_{N_r}^r)$ is the vector of generalized coordinates related to the fixed-interface modes, $\mathcal{F}^r = (\mathcal{F}_1, \dots, \mathcal{F}_{N_r})$ is the vector whose components are given by Eq. (22) using the fixed-interface modes and \mathbf{f}_Γ^r is defined in Section 4.1.1.

1 For all real ω , linear operator $\mathbf{Z}_\Gamma^r(\omega)$ is defined by the following sesquilinear form on $\mathcal{C}_{\Omega_r}^\Gamma \times \mathcal{C}_{\Omega_r}^\Gamma$:

$$\langle\langle \mathbf{Z}_\Gamma^r(\omega) \mathbf{u}_{|\Gamma}^r, \overline{\delta \mathbf{u}_{|\Gamma}^r} \rangle\rangle = z^r(S^r(\mathbf{u}_{|\Gamma}^r), S^r(\delta \mathbf{u}_{|\Gamma}^r)). \quad (65)$$

From Eq. (6), we deduce the following abstract operator equation:

$$\mathbf{Z}_\Gamma^r(\omega) = -\omega^2 \mathbf{M}_\Gamma^r + i\omega \mathbf{D}_\Gamma^r + \mathbf{K}_\Gamma^r, \quad (66)$$

in which the mass, damping, and stiffness operators \mathbf{M}_Γ^r , \mathbf{D}_Γ^r , and \mathbf{K}_Γ^r are defined by

$$\langle\langle \mathbf{M}_\Gamma^r \mathbf{u}_{|\Gamma}^r, \overline{\delta \mathbf{u}_{|\Gamma}^r} \rangle\rangle = m^r(S^r(\mathbf{u}_{|\Gamma}^r), S^r(\delta \mathbf{u}_{|\Gamma}^r)), \quad (67)$$

$$\langle\langle \mathbf{D}_\Gamma^r \mathbf{u}_{|\Gamma}^r, \overline{\delta \mathbf{u}_{|\Gamma}^r} \rangle\rangle = d^r(S^r(\mathbf{u}_{|\Gamma}^r), S^r(\delta \mathbf{u}_{|\Gamma}^r)), \quad (68)$$

$$\langle\langle \mathbf{K}_\Gamma^r \mathbf{u}_{|\Gamma}^r, \overline{\delta \mathbf{u}_{|\Gamma}^r} \rangle\rangle = k^r(S^r(\mathbf{u}_{|\Gamma}^r), S^r(\delta \mathbf{u}_{|\Gamma}^r)), \quad (69)$$

where m^r , k^r , and d^r are defined by Eqs. (3), (4), and (5), respectively. It should be noted that these operators are related to surface Γ and correspond to the static condensation on Γ of the mass, stiffness (Guyan, 1965) and damping operators using the elastostatic operator S^r defined in Section 4.1.3.

2 For all real ω , the $(N_r \times N_r)$ complex symmetric matrix $[\mathbf{Z}^r(\omega)]$ is defined by Eq. (20) using the fixed-interface modes. It should be noted that if the damping operator defined by Eq. (5) is diagonalized by the fixed-interface modes, matrix $[\mathbf{Z}^r(\omega)]$ is diagonal.

3 For all real ω , the linear operator $\mathcal{A}^r(\omega)$ is defined by the following sesquilinear form on $\mathcal{C}_{\Omega_r}^\Gamma \times \mathbb{C}^{N_r}$.

$$\langle\langle \mathcal{A}^r(\omega) \mathbf{u}_{|\Gamma}^r, \overline{\delta \mathbf{q}^r} \rangle\rangle = \sum_{\alpha=1}^{N_r} z^r(S^r(\mathbf{u}_{|\Gamma}^r), \mathbf{u}_\alpha^r) \overline{\delta q_\alpha^r}, \quad (70)$$

in which $\delta \mathbf{q}^r = (\delta q_1^r, \dots, \delta q_{N_r}^r)$. From Eq. (6), we deduce the following abstract operator equation:

$$\mathcal{A}^r(\omega) = -\omega^2 \mathcal{A}_m^r + i\omega \mathcal{A}_d^r, \quad (71)$$

in which \mathcal{A}_m^r and \mathcal{A}_d^r are operators defined by

$$\langle\langle \mathcal{A}_m^r \mathbf{u}_{|\Gamma}^r, \overline{\delta \mathbf{q}^r} \rangle\rangle = \sum_{\alpha=1}^{N_r} m^r(S^r(\mathbf{u}_{|\Gamma}^r), \mathbf{u}_\alpha^r) \overline{\delta q_\alpha^r}, \quad (72)$$

$$\langle\langle \mathcal{A}_d^r \mathbf{u}_{|\Gamma}^r, \overline{\delta \mathbf{q}^r} \rangle\rangle = \sum_{\alpha=1}^{N_r} d^r(S^r(\mathbf{u}_{|\Gamma}^r), \mathbf{u}_\alpha^r) \overline{\delta q_\alpha^r}, \quad (73)$$

in which Eq. (56) has been used. The quantities $m^r(S^r(\mathbf{u}_{|\Gamma}^r), \mathbf{u}_\alpha^r)$ are calculated using Eq. (57) and $d^r(S^r(\mathbf{u}_{|\Gamma}^r), \mathbf{u}_\alpha^r)$ using Eqs. (5), (51), and (52). Finally, operator $\mathcal{A}^r(\omega)$ is defined by the following sesquilinear form on $\mathbb{C}^{N_r} \times \mathcal{C}_{\Omega_r}^\Gamma$, such that

$$\langle\langle \mathcal{A}^r(\omega) \mathbf{q}^r, \overline{\delta \mathbf{u}_{|\Gamma}^r} \rangle\rangle = \sum_{\alpha=1}^{N_r} q_\alpha^r z^r(\mathbf{u}_\alpha^r, S^r(\delta \mathbf{u}_{|\Gamma}^r)). \quad (74)$$

In conclusion, the matrix (of operators) in the left-hand side of Eq. (64) is called the “reduced matrix model” of substructure Ω_r relative to the displacement field $\mathbf{u}_{|\Gamma}^r$ on Γ and the N_r generalized coordinates (which can be viewed as “internal generalized degrees-of-freedom”). We refer to Morand and Ohayon (1995) for the particular case of an undamped structure.

4.2 Frequency Response Function and Eigenmodes Constructions for the Global Structure Using the Mixed Variational Formulation and SVD.

4.2.1 Modal Reduction of Mixed Problem \mathcal{P}_1 . The reduction of \mathcal{P}_1 defined in Section 2.3.2 is obtained using the reduced matrix model defined by Eq. (64) for each substructure. Recall that the projection of Lagrange multiplier $\boldsymbol{\lambda}$ must be done on the subspace \mathcal{W}_Γ^N of $\mathcal{C}_\Gamma \subset \Lambda_\Gamma$. A characterization of \mathcal{W}_Γ^N requires the construction of a basis of \mathcal{W}_Γ^N denoted by $\{\mathbf{w}_1, \dots, \mathbf{w}_N\}$. Consequently, for all $\boldsymbol{\lambda}$ in \mathcal{W}_Γ^N , one has Eq. (18). Substituting Eqs. (62), (63), (18) and $\delta \boldsymbol{\lambda} = \sum_{\gamma=1}^N \delta p_\gamma \mathbf{w}_\gamma$ into Eq. (11), we obtain

$$\begin{bmatrix} Z_1^1(\omega) & \mathcal{A}^1(\omega) & 0 & 0 & \mathcal{B}_1 \\ \mathcal{A}^1(\omega) & [Z^1(\omega)] & 0 & 0 & 0 \\ 0 & 0 & Z_1^2(\omega) & \mathcal{A}^2(\omega) & \mathcal{B}_2 \\ 0 & 0 & \mathcal{A}^2(\omega) & [Z^2(\omega)] & 0 \\ \mathcal{B}_1 & 0 & \mathcal{B}_2 & 0 & 0 \end{bmatrix} \begin{bmatrix} \mathbf{u}_\Gamma^1 \\ \mathbf{q}^1 \\ \mathbf{u}_\Gamma^2 \\ \mathbf{q}^2 \\ \mathbf{p} \end{bmatrix} = \begin{bmatrix} 0 \\ \mathcal{F}^1 \\ 0 \\ \mathcal{F}^2 \\ 0 \end{bmatrix}, \quad (75)$$

in which we can recognize the reduced model of each substructure (see Eq. (64)). Using Eq. (12), for $r = 1, 2$ and γ in $\{1, \dots, N\}$, operators \mathcal{B}_1 and \mathcal{B}_2 are defined by

$$[\mathcal{B}_r]_\gamma = b(\mathbf{w}_\gamma, \mathbf{u}_\Gamma^r). \quad (76)$$

4.2.2 Practical Construction of the Frequency Response Function Using SVD. Since \mathcal{B}_1 and \mathcal{B}_2 are independent of ω , Eq. (75) can be rewritten as

$$\begin{bmatrix} Z(\omega) & \mathcal{B} \\ \mathcal{B} & 0 \end{bmatrix} \begin{bmatrix} \mathbf{Q} \\ \mathbf{p} \end{bmatrix} = \begin{bmatrix} \mathcal{F} \\ 0 \end{bmatrix}, \quad (77)$$

where $\mathbf{Q} = (\mathbf{u}_\Gamma^1, \mathbf{q}^1, \mathbf{u}_\Gamma^2, \mathbf{q}^2)$. Equation (77) being similar to Eq. (24), the practical construction is carried out as described in Section 3.3.

4.2.3 Practical Construction of the Eigenmodes Using SVD. The conservative problem associated to Eq. (75) leads to the following spectral problem:

$$\begin{bmatrix} \mathbf{K}_\Gamma^1 & 0 & 0 & 0 & \mathcal{B}_1 \\ 0 & [\mathcal{K}^1] & 0 & 0 & 0 \\ 0 & 0 & \mathbf{K}_\Gamma^2 & 0 & \mathcal{B}_2 \\ 0 & 0 & 0 & [\mathcal{K}^2] & 0 \\ \mathcal{B}_1 & 0 & \mathcal{B}_2 & 0 & 0 \end{bmatrix} \begin{bmatrix} \mathbf{u}_\Gamma^1 \\ \mathbf{q}^1 \\ \mathbf{u}_\Gamma^2 \\ \mathbf{q}^2 \\ \mathbf{p} \end{bmatrix} = \omega^2 \begin{bmatrix} \mathbf{M}_\Gamma^1 & \mathcal{A}_m^1 & 0 & 0 & 0 \\ \mathcal{A}_m^1 & [\mathcal{M}^1] & 0 & 0 & 0 \\ 0 & 0 & \mathbf{M}_\Gamma^2 & \mathcal{A}_m^2 & 0 \\ 0 & 0 & \mathcal{A}_m^2 & [\mathcal{M}^2] & 0 \\ 0 & 0 & 0 & 0 & 0 \end{bmatrix} \begin{bmatrix} \mathbf{u}_\Gamma^1 \\ \mathbf{q}^1 \\ \mathbf{u}_\Gamma^2 \\ \mathbf{q}^2 \\ \mathbf{p} \end{bmatrix}. \quad (78)$$

Equation (78) is rewritten using the global notation introduced in Eq. (77) and is then similar to Eq. (44). Consequently, we can use the method presented in Section 3.4 for solving this spectral problem.

4.2.4 General Comments. In the case of a finite element discretization with incompatible mesh on Γ , the method presented in Section 4.3 (Eqs. (75) and (78)) is efficient because, since \mathcal{B}_1 and \mathcal{B}_2 are independent of ω , the SVD is carried out once and for all (even if the sizes of the matrices of the discretized operators \mathcal{B}_1 and \mathcal{B}_2 are important).

5 Conclusion

Within a general continuum-based approach, we have presented two dynamic substructuring procedures by modal reduction methods in order to calculate the frequency response function of linear damped structures and the eigenmodes of the associated conservative systems. The free-interface and fixed-interface modes of each substructure are used within a mixed variational formulation involving Lagrange multiplier fields defined on the coupling interfaces. Generally, the introduction of a Lagrange multiplier field associated with kinematic linear constraints induces some difficulties for the construction of the

solution due to the rank deficiency of the obtained linear system. In the present paper, the Singular Value Decomposition (SVD) method is applied to the frequency-independent Lagrange multiplier terms. The use of SVD is particularly efficient due to a relatively small number of degrees-of-freedom in the reduced model and is used once. Therefore, the SVD appears as an efficient and reliable tool for this problem.

References

- Argyris, J., and Meljnek, H. P., 1991, *Dynamics of Structures*, North-Holland, Amsterdam.
- Brezzi, F., and Fortin, M., 1991, *Mixed and Hybrid Finite Element Methods*, Springer, Berlin.
- Craig, R. R., Jr., 1985, "A Review of Time Domain and Frequency Domain Component Mode Synthesis Method," *Combined Experimental-Analytical Modeling of Dynamic Structural Systems*, D. R. Martinez and A. K. Miller, eds., ASME, New York.
- Craig, R. R., Jr., and Bampton, M. C. C., 1968, "Coupling of Substructures for Dynamic Analysis," *AIAA Journal*, Vol. 6, pp. 1313–1319.
- Dautray, R., and Lions, J.-L., 1992, *Mathematical Analysis and Numerical Methods for Science and Technology*, Springer-Verlag, Berlin.
- Farhat, C., and Geradin, M., 1994, "On a Component Mode Method and its Application to Incompatible Substructures," *Computer and Structures*, Vol. 51, No. 5, pp. 459–473.
- Farstad, J. E., and Singh, R., 1995, "Structurally Transmitted Dynamic Power in Discretely Joined Damped Component Assemblies," *J. Acoust. Soc. Am.*, Vol. 97, No. 5, pp. 2855–2865.
- Flashner, H., 1986, "An Orthogonal Decomposition Approach to Modal Synthesis," *Int. J. Num. Meth. Eng.*, Vol. 23, No. 3, pp. 471–493.
- Golub, G. H., and Van Loan, C. F., 1989, *Matrix Computations*, 2nd ed., The John Hopkins University Press, Baltimore.
- Guyon, R. J., 1965, "Reduction of Stiffness and Mass Matrices," *AIAA Journal*, Vol. 3, pp. 185–203.
- Hale, A. L., and Meirovitch, L., 1980, "A General Substructure Synthesis Method for the Dynamic Simulation of Complex Structures," *Journal of Sound and Vibration*, Vol. 69, No. 2, pp. 309–326.
- Hurty, W. C., 1965, "Dynamic Analysis of Structural Systems Using Component Modes," *AIAA Journal*, Vol. 3, No. 4, pp. 678–685.
- Jen, C. W., and Johnson, D. A., and Dubois, F., 1995, "Numerical Modal Analysis of Structures Based on a Revised Substructure Synthesis Approach," *Journal of Sound and Vibration*, Vol. 180, No. 2, pp. 185–203.
- Klein, L. R., and Dowell, E. H., 1974, "Analysis of Modal damping by Component Modes Method Using Lagrange Multipliers," *ASME JOURNAL OF APPLIED MECHANICS*, Vol. 39, pp. 727–732.
- Kree, P., and Soize, C., 1986, *Mathematics of Random Phenomena*, Reidel, Dordrecht.
- Leung, A. Y. T., 1993, *Dynamic Stiffness and Substructures*, Springer-Verlag, New York.
- MacNeal, R. H., 1971, "A Hybrid Method of Component Mode Synthesis," *Computers and Structures*, Vol. 1, pp. 581–601.
- Marsden, J. E., and Hughes, T. J. R., 1983, *Mathematical Foundations of Elasticity*, Prentice-Hall, Englewood Cliffs, NJ.
- Min, K. W., Igusa, T., and Achenbach, J. D., 1992, "Frequency Window Method for Strongly Coupled and Multiply Connected Structural Systems: Multiple-Mode Windows," *ASME JOURNAL OF APPLIED MECHANICS*, Vol. 59, pp. 244–252.
- Morand, H. J. P., and Ohayon, R., 1995, *Fluid Structure Interaction*, John Wiley and Sons, New York.
- Rubin, S., 1975, "Improved Component Mode Representation for Structural Dynamic Analysis," *AIAA Journal*, Vol. 18, No. 8, pp. 995–1006.
- Rook, T. E., and Singh, R., 1995, "Power Flow Through Multidimensional Compliant Joints Using Mobility and Modal Approaches," *J. Acoust. Soc. Am.*, Vol. 97, No. 5, pp. 2882–2891.
- Schmidt, Th., and Müller, P. C., 1993, "A Parameter Estimation Method for Multibody Systems with Constraints," *Advanced Multibody System Dynamics*, W. Schiehlen, ed., Kluwer Academic Publishers, Dordrecht, pp. 427–433.
- Shabana, A. A., 1991, "Constrained Motion of Deformable Bodies," *Int. J. Num. Meth. Eng.*, Vol. 32, pp. 1813–1831.
- Singh, R. P., and Likins, P. W., 1985, "Singular Value Decomposition for Constrained Dynamical Systems," *ASME JOURNAL OF APPLIED MECHANICS*, Vol. 52, pp. 943–948.
- Soize, C., Desanti, A., and David, J. M., 1992, "Numerical Methods in Elastodynamics for Low and Medium Frequency Ranges," *La Recherche Aéronautique* (English Edition), Vol. 5, pp. 25–44.

Exact Solutions for Simply Supported Laminated Piezoelectric Plates

P. Heyliger

Department of Civil Engineering,
Colorado State University,
Fort Collins, CO 80523

Exact solutions are presented for the static behavior of laminated piezoelectric plates with simple support. The upper and lower surfaces of the laminate can be subjected to a number of applied loadings, confined in this study to an applied transverse load or a specified surface potential. Each layer of the laminate can be piezoelectric, elastic/dielectric, or conducting, with perfect bonding assumed between each interface. Expressions are obtained for the components of displacement, stress, electric displacement, and potential through the thickness of the laminate. Representative examples are shown to demonstrate the fundamental behavior, and the influence of the piezoelectric coefficients and internal electrodes are discussed.

1 Introduction

Following the initial theoretical developments of piezoelectric solids documented in the works of Voight (1928), Mason (1950), Cady (1964), and Nye (1972), a number of significant studies have appeared considering the analysis of laminated piezoelectric plates. The fundamental work of Tiersten (1969) gave much of the necessary theoretical development for the static and dynamic behavior of a single-layer piezoelectric plate. Lee and Moon (1989), Lee (1990), and Lee and co-workers (1991) used the assumptions of Kirchhoff plate theory to derive a simple theory for piezoelectric plates, used primarily for the design of piezoelectric laminates for bending and torsional control. Lazarus and Crawley (1989) developed pin-force and consistent plate models for the design of induced strain actuators. Dimitriadis and co-workers (1989) and Wang and co-workers (1989) developed a two-dimensional model for rectangular plates to represent the behavior induced by piezoceramic patches bonded to the bottom and top surfaces of a laminate. Wang and Rogers (1991) used the assumptions of classical lamination theory combined with inclusion of the effects of spatially distributed, small-sized induced strain actuators embedded at any location of the laminate.

In most previous studies, an attempt was made to represent the behavior of piezoelectric laminates under mechanical and electrical loading using some type of approximation to the elastic and electric fields. Ray (1993) studied the behavior of an elastic layer bonded to a piezoelectric layer in a more exact sense, but included the assumption that the through-thickness piezoelectric coefficient e_{33} was zero. This constraint results in solutions of significantly different form than those where this constant is included (Heyliger, 1995). In this study, the static behavior of laminated, piezoelectric plates as modeled by the linear theory of piezoelectricity is studied using an exact solution for simply supported plates. The solution strategy follows similar work of Pagano (1970) for laminated elastic plates and Heyliger and Brooks (1995) for piezoelectric laminates under cylindrical bending. The results obtained using the solution

methodology presented here should provide a useful means of comparison for approximate piezoelectric plate theories.

2 Exact Solution

Governing Equations. The geometrical configuration of the laminate is such that the thin or thickness dimension of the laminate coincides with the z -direction, with the lengths of the plate in the x and y -directions denoted as L_x and L_y , respectively. The total plate thickness is denoted as H . Each layer of the laminate can be elastic or piezoelectric. The general problem considered in this study is to determine the behavior of the elastic and electric field components throughout the laminate under an applied mechanical or electrical loading. The forcing function is introduced through either an applied surface displacement, traction, potential, or electric charge. It is also possible to consider internally applied quantities in this formulation.

A single piezoelectric layer has the constitutive equations given in compressed notation as (Tiersten, 1969)

$$\begin{aligned}\sigma_p &= C_{pq}S_q - e_{kp}E_k \\ D_i &= e_{iq}S_q + \epsilon_{ik}E_k\end{aligned}\quad (1)$$

where p and q take the values $1, \dots, 6$ and i and k take the values $1, \dots, 3$, σ_p are the components of the stress tensor, C_{pq} are the elastic stiffness components, S_q are the components of infinitesimal strain, e_{iq} are the piezoelectric coefficients, E_k are the components of the electric field, D_i are the components of the electric displacement, and ϵ_{ik} are the dielectric constants. The poling direction is coincident with the x_3 or z -axis.

The displacement components u_i , where $u_1 = u$, $u_2 = v$, and $u_3 = w$, are related to the strain components through the relations

$$S_{ik} = \frac{1}{2} \left(\frac{\partial u_i}{\partial x_k} + \frac{\partial u_k}{\partial x_i} \right) \quad (2)$$

where $S_{ik} = S_p$ when $i = k$ and $p = 1, 2, 3$ and $2S_{ik} = S_p$ when $i \neq k$ and $p = 4, 5, 6$ (Tiersten, 1969). The electric field components can be related to the electrostatic potential ϕ using the relation

$$E_i = - \frac{\partial \phi}{\partial x_i} \quad (3)$$

For the materials used in this study, it is assumed that the nonzero components of the rotated piezoelectric tensor e_{kp} are e_{31} , e_{32} , e_{33} , e_{24} , and e_{15} . The elastic stiffnesses C_{pq} are those

Contributed by the Applied Mechanics Division of THE AMERICAN SOCIETY OF MECHANICAL ENGINEERS for publication in the ASME JOURNAL OF APPLIED MECHANICS.

Discussion on the paper should be addressed to the Technical Editor, Professor Lewis T. Wheeler, Department of Mechanical Engineering, University of Houston, Houston, TX 77204-4792, and will be accepted until four months after final publication of the paper itself in the ASME JOURNAL OF APPLIED MECHANICS.

Manuscript received by the ASME Applied Mechanics Division, Sept. 3, 1993; final revision, Dec. 9, 1996. Associate Technical Editor: M. Taya.

of an orthotropic material, and the dielectric constants are given by ϵ_{11} , ϵ_{22} , and ϵ_{33} .

The equilibrium equations in the absence of body forces are given in terms of the uncontracted stresses as

$$\sigma_{ij,j} = 0, \quad (4)$$

The charge equation of electrostatics is given as

$$D_{i,i} = 0. \quad (5)$$

Substituting in the constitutive relations, the stress-strain relations, and the field-potential relations gives the governing equations of the problem in terms of the displacement components u , v , and w and the electrostatic potential ϕ as

$$\begin{aligned} C_{11} \frac{\partial^2 u}{\partial x^2} + C_{12} \frac{\partial^2 v}{\partial x \partial y} + C_{13} \frac{\partial^2 w}{\partial x \partial z} \\ + e_{31} \frac{\partial^2 \phi}{\partial x \partial z} + C_{66} \left(\frac{\partial^2 u}{\partial y^2} + \frac{\partial^2 v}{\partial x \partial y} \right) \\ + C_{55} \left(\frac{\partial^2 u}{\partial z^2} + \frac{\partial^2 w}{\partial x \partial z} \right) + e_{15} \frac{\partial^2 \phi}{\partial x \partial z} = 0 \end{aligned} \quad (6)$$

$$\begin{aligned} C_{12} \frac{\partial^2 u}{\partial x \partial y} + C_{22} \frac{\partial^2 v}{\partial y^2} + C_{23} \frac{\partial^2 w}{\partial y \partial z} \\ + e_{32} \frac{\partial^2 \phi}{\partial y \partial z} + C_{44} \left(\frac{\partial^2 v}{\partial z^2} + \frac{\partial^2 w}{\partial y \partial z} \right) \\ + C_{66} \left(\frac{\partial^2 u}{\partial x \partial y} + \frac{\partial^2 v}{\partial x^2} \right) + e_{24} \frac{\partial^2 \phi}{\partial y \partial z} = 0 \end{aligned} \quad (7)$$

$$\begin{aligned} C_{13} \frac{\partial^2 u}{\partial x \partial z} + C_{23} \frac{\partial^2 v}{\partial y \partial z} + C_{33} \frac{\partial^2 w}{\partial z^2} \\ + C_{23} \frac{\partial^2 v}{\partial y \partial z} + e_{24} \frac{\partial^2 \phi}{\partial y^2} + C_{44} \left(\frac{\partial^2 w}{\partial y^2} + \frac{\partial^2 v}{\partial y \partial z} \right) \\ + C_{55} \left(\frac{\partial^2 u}{\partial x \partial z} + \frac{\partial^2 w}{\partial x^2} \right) + e_{33} \frac{\partial^2 \phi}{\partial z^2} = 0 \end{aligned} \quad (8)$$

$$\begin{aligned} -e_{11} \frac{\partial^2 \phi}{\partial x^2} + e_{31} \frac{\partial^2 u}{\partial x \partial z} + e_{32} \frac{\partial^2 v}{\partial y \partial z} + e_{33} \frac{\partial^2 w}{\partial z^2} \\ + e_{32} \frac{\partial^2 v}{\partial y \partial z} - e_{22} \frac{\partial^2 \phi}{\partial y^2} + e_{24} \left(\frac{\partial^2 w}{\partial y^2} + \frac{\partial^2 v}{\partial y \partial z} \right) \\ - e_{15} \left(\frac{\partial^2 u}{\partial x \partial z} + \frac{\partial^2 w}{\partial x^2} \right) - e_{33} \frac{\partial^2 \phi}{\partial z^2} = 0. \end{aligned} \quad (9)$$

These represent the governing equation for a single piezoelectric layer. For a layer with no piezoelectric effects, these equations reduce to the three-dimensional equations of elasticity and, assuming $\epsilon_{11} = \epsilon_{22} = \epsilon_{33}$, the Laplace equation for electrostatics.

For the problems considered in this study, an arbitrary number of laminae are assumed to be perfectly bonded together. At the top and bottom surface of the laminate, a specified load, displacement, potential, or charge can be specified. Of primary

interest here are the cases in which either a known normal traction or potential are imposed on the top and/or bottom surfaces. These are the cases considered in this study, with the shear tractions specified to be zero on the top and bottom surfaces in both cases. The laminate is assumed to be simply supported, and the vertical edges of the laminate are assumed to be grounded. Hence along a plate edge, the normal stress, tangential displacement, transverse displacement, and potential are specified to be zero.

Both the applied load and potential can be expressed in the form of a Fourier series. These functions are represented in the form

$$q(x, y) = q_o \sin px \sin qy \quad (10)$$

$$\phi(x, y) = \phi_o \sin px \sin py \quad (11)$$

where

$$p = p(n) = \frac{n\pi}{L_x} \quad (12)$$

$$q = q(m) = \frac{m\pi}{L_y} \quad (13)$$

where the expressions can be used either for the top or bottom of the laminate.

At each interface between layers, continuity conditions of displacement, traction, potential, and electric displacement must be enforced. Using an indexing scheme, the conditions for the i th layer can be expressed as, for example,

$$U^i \left(y, \frac{-h_i}{2} \right) = U^{i+1} \left(y, \frac{h_{i+1}}{2} \right). \quad (14)$$

Here i represents the layer number, with $i = 1$ the top layer, each layer has an individual coordinate system with the origin at the left end in the center of the layer, and h_i is the thickness of the i th layer. Similar interface conditions exist for V , W , ϕ , σ_z , τ_{xz} , τ_{yz} , and D_z . At a single interface of a laminate with n plies, there are six conditions related to the elastic variables and two conditions related to the electrostatic variables for a total of $8(n - 1)$ conditions. At both the top and bottom surfaces, there are three elastic boundary conditions and one electric condition for a total of eight conditions. Enforcing all conditions leads to $8n$ equations relating the variables within all layers of the laminate.

Method of Solution. Solutions for the displacement components and the electrostatic potential are sought in the form

$$u(x, y, z) = U(z) \cos px \sin qy = \bar{U} \exp(sz) \cos px \sin qy$$

$$v(x, y, z) = V(z) \sin px \cos qy = \bar{V} \exp(sz) \sin px \cos qy$$

$$w(x, y, z) = W(z) \sin px \sin qy = \bar{W} \exp(sz) \sin px \sin qy$$

$$\phi(x, y, z) = \Phi(z) \sin px \sin qy = \bar{\Phi} \exp(sz) \sin px \sin qy. \quad (15)$$

Here the overbarred terms are constants and s is an unknown number. Substitution of these expressions into the equilibrium and charge equations results in the system of equations

$$\begin{bmatrix} C_{11}p^2 + C_{66}q^2 - C_{55}s^2 & pq(C_{12} + C_{66}) & -ps(C_{13} + C_{55}) & -(e_{31} + e_{15})ps \\ pq(C_{12} + C_{66}) & C_{66}p^2 + C_{22}q^2 - C_{44}s^2 & -qs(C_{23} + C_{44}) & -qs(e_{32} + e_{24}) \\ ps(C_{13} + C_{55}) & qs(C_{23} + C_{44}) & C_{55}p^2 + C_{44}q^2 - C_{33}s^2 & e_{15}p^2 + e_{24}q^2 - e_{33}s^2 \\ ps(e_{15} + e_{31}) & qs(e_{24} + e_{32}) & e_{15}p^2 + e_{24}q^2 - e_{33}s^2 & -e_{11}p^2 - e_{22}q^2 + e_{33}s^2 \end{bmatrix} \begin{bmatrix} \bar{U} \\ \bar{V} \\ \bar{W} \\ \bar{\Phi} \end{bmatrix} = \begin{bmatrix} 0 \\ 0 \\ 0 \\ 0 \end{bmatrix}. \quad (16)$$

Setting the determinant of this matrix to zero results in the characteristic equation

$$As^8 + Bs^6 + Cs^4 + Ds^2 + E = 0. \quad (17)$$

Expressions for the coefficients of this polynomial are lengthy and are not given here. This characteristic equation can be written as the fourth-order equation

$$r^4 + cr^3 + dr^2 + er + f = 0 \quad (18)$$

where

$$r = s^2 \quad c = \frac{B}{A} \quad d = \frac{C}{A} \quad (19)$$

$$e = \frac{D}{A} \quad f = \frac{E}{A}. \quad (20)$$

The roots of this equation are a function of the material properties and the form of the applied load and potential as represented by p and q . They can be real, imaginary, or complex. Regardless of the nature of the roots, the solutions for a given s are based on and initial construction of the solution for $U(z)$. The remaining components can then be computed using Eq. (16), which is rearranged in terms of the unknown constants as

$$\begin{bmatrix} C_{66}p^2 + C_{22}q^2 - C_{44}s^2 & -qs(C_{23} + C_{44}) & -qs(e_{32} + e_{24}) \\ qs(C_{23} + C_{44}) & C_{55}p^2 + C_{44}q^2 - C_{33}s^2 & e_{15}p^2 + e_{24}q^2 - e_{33}s^2 \\ qs(e_{32} + e_{24}) & e_{15}p^2 + e_{24}q^2 - e_{33}s^2 & -\epsilon_{11}p^2 - \epsilon_{22}q^2 + \epsilon_{33}s^2 \end{bmatrix} \begin{Bmatrix} \bar{V} \\ \bar{W} \\ \bar{\Phi} \end{Bmatrix} = \bar{U} \begin{Bmatrix} -pq(C_{12} + C_{66}) \\ ps(C_{13} + C_{55}) \\ ps(e_{15} + e_{31}) \end{Bmatrix}. \quad (21)$$

General expressions for the constants \bar{V} , \bar{W} , and $\bar{\Phi}$ can be constructed as a function of the real, imaginary, or complex roots. These are

$$\bar{V}(s) = \frac{f_{11}s^4 + f_{12}s^2 + f_{13}}{\bar{D}(s)} \quad (22)$$

$$\bar{W}(s) = \frac{s(f_{21}s^4 + f_{22}s^2 + f_{23})}{\bar{D}(s)} \quad (23)$$

$$\bar{\Phi}(s) = \frac{s(f_{31}s^4 + f_{32}s^2 + f_{33})}{\bar{D}(s)} \quad (24)$$

$$\bar{D}(s) = d_1s^6 + d_2s^4 + d_3s^2 + d_4. \quad (25)$$

The constants d_i and f_{ij} are given in Heyliger, Pei, and Ramirez (1993).

The solutions for the elastic and electric field components corresponding to each type of root are developed separately below.

Case 1: Real Roots for r . Given n real roots for r , the $2n$ roots for s can be obtained using Eq. (19). These roots are either real or imaginary depending on the sign of r . Following the nomenclature used in Pagano (1970) and Heyliger and Brooks (1995), the solution for the displacement components and electrostatic potential corresponding to these roots can be written as

$$\begin{aligned} U(z) &= \sum_{j=1}^n U_j(z) & V(z) &= \sum_{j=1}^n L_j U_j(z) \\ W(z) &= \sum_{j=1}^n M_j W_j(z) & \phi(z) &= \sum_{j=1}^n N_j W_j(z) \end{aligned} \quad (26)$$

where

$$\begin{aligned} U_j &= F_j C_j(z) + G_j S_j(z) \\ W_j &= G_j C_j(z) + \alpha_j F_j S_j(z). \end{aligned} \quad (27)$$

Here F_j and G_j are real constants, there is no sum on j , and the functions C and S and the value m are defined as

$$C_j = \cosh(m_j z) \quad S_j(z) = \sinh(m_j z) \quad \alpha_j = 1 \quad (\gamma > 0) \quad (28)$$

$$\begin{aligned} C_j &= \cos(m_j z) \quad S_j(z) = \sin(m_j z) \\ \alpha_j &= -1 \quad (\gamma < 0) \quad m_j = |s_j|. \end{aligned} \quad (29)$$

The coefficients L_j , M_j , and N_j are more specific representations of the parameters given in Eqs. (21)–(24), and are given in this case as

$$L_j = \frac{1}{D_j} (f_{11}m_j^4 + f_{12}\alpha_j m_j^2 + f_{13}) \quad (30)$$

$$M_j = \frac{m_j}{D_j} (f_{21}m_j^4 + f_{22}\alpha_j m_j^2 + f_{23}) \quad (31)$$

$$N_j = \frac{m_j}{D_j} (f_{31}m_j^4 + f_{32}\alpha_j m_j^2 + f_{33}) \quad (32)$$

where the determinant D_j is given by

$$D_j = d_1\alpha_j m_j^6 + d_2m_j^4 + d_3\alpha_j m_j^2 + d_4. \quad (33)$$

Using the constitutive equations in (1), the corresponding

expressions for the stress and electric displacement can be computed as

$$\begin{aligned} \sigma_i &= \sin px \sin qy \sum_{j=1}^n \left[-pC_{i1} - qC_{i2}L_j \right. \\ &\quad \left. + C_{i3}\alpha_j \frac{m_j^2}{D_j} (f_{21}m_j^4 + f_{22}m_j^2\alpha_j + f_{23}) \right. \\ &\quad \left. + e_{3i}\alpha_j \frac{m_j^2}{D_j} (f_{31}m_j^4 + f_{32}m_j^2\alpha_j + f_{33}) \right] U_j(z) \end{aligned} \quad (34)$$

$$\tau_{yz} = \sin px \cos qy \sum_{j=1}^n [C_{44}(L_j m_j + qM_j) + e_{24}N_j q] W_j(z) \quad (35)$$

$$\tau_{xz} = \cos px \sin qy \sum_{j=1}^n [C_{55}(m_j + pM_j) + e_{24}N_j q] W_j(z) \quad (36)$$

$$\tau_{xy} = \cos px \cos qy \sum_{j=1}^n C_{66}(q + pL_j) U_j \quad (37)$$

$$\begin{aligned} D_i &= \sin px \sin qy \sum_{j=1}^n \left[-e_{31}p - e_{32}qL_j \right. \\ &\quad \left. + e_{33}\alpha_j \frac{m_j^2}{D_j} (f_{21}m_j^4 + f_{22}m_j^2\alpha_j + f_{23}) \right. \\ &\quad \left. + e_{33}\alpha_j \frac{m_j^2}{D_j} (f_{31}m_j^4 + f_{32}m_j^2\alpha_j + f_{33}) \right] W_j(z) \end{aligned} \quad (38)$$

Here $i = 1, 2, 3$ corresponds to x, y , and z for the stress and electric displacement components.

A special case in which there are real roots for r is the nonpiezoelectric elastic layer. The $e_{ij} = 0$ in this case and the elastic and electric fields uncouple. The elastic solution has been given by Pagano (1970), and the results are not repeated here except to note that the elastic field behavior is represented

by six roots and six unknown constants within the layer. This corresponds to the six interface/boundary conditions (three displacements and the σ_{iz} stress components) for a single layer. The electrostatic behavior in this case is represented using the two roots

$$n_{1,2} = \sqrt{\frac{\epsilon_{11}p^2 + \epsilon_{22}q^2}{\epsilon_{33}}} \quad (39)$$

The potential and transverse electric displacement components in this case are given by

$$\phi(x, y, z) = \sin px \sin qy \sum_{j=1}^2 B_j \exp(n_j z) \quad (40)$$

$$D_z = -\epsilon_{33} \sin px \sin qy \sum_{j=1}^2 B_j n_j \exp(n_j z). \quad (41)$$

Case 2: Complex Roots for r . The elastic, electric, and geometric properties for some laminae yield complex roots. These occur in conjugate pairs, which result in the final roots for s in the form $\pm(a \pm ib)$, where $i = \sqrt{-1}$ and a and b are positive constants. The solution for $U(z)$ in this case can be expressed as

$$U(z) = c_1 e^{az} \cos bz + c_2 e^{az} \sin bz + c_3 e^{-az} \cos bz + c_4 e^{-az} \sin bz \quad (42)$$

where c_1 – c_4 are real constants. Following some algebraic manipulations and using Eqs. (21)–(24), the solution for $V(z)$ can be expressed as

$$V(z) = c_1 e^{az} (\Gamma_1 \cos bz - \Omega_1 \sin bz) + c_2 e^{az} (\Omega_1 \cos bz + \Gamma_1 \sin bz) + c_3 e^{-az} (\Gamma_1 \cos bz + \Omega_1 \sin bz) + c_4 e^{-az} (-\Omega_1 \cos bz + \Gamma_1 \sin bz). \quad (43)$$

Here $\Gamma_1 = \Re[\tilde{V}(a + ib)]$ and $\Omega_1 = \Im[\tilde{V}(a + ib)]$. Similarly, the final expression for $W(z)$ can be expressed as

$$W(z) = c_1 e^{az} [(a\Gamma_2 - b\Omega_2) \cos bz + (-b\Gamma_2 - a\Omega_2) \sin bz] + c_2 e^{az} [(b\Gamma_2 + a\Omega_2) \cos bz + (a\Gamma_2 - b\Omega_2) \sin bz] + c_3 e^{-az} [(b\Omega_2 - a\Gamma_2) \cos bz + (-b\Gamma_2 - a\Omega_2) \sin bz] + c_4 e^{-az} [(b\Gamma_2 + a\Omega_2) \cos bz + (-a\Gamma_2 + b\Omega_2) \sin bz] \quad (44)$$

where $\Gamma_2 = \Re[\tilde{W}(a + ib)]$ and $\Omega_2 = \Im[\tilde{W}(a + ib)]$. The final expression for ϕ can be obtained in similar fashion to yield

$$\phi(z) = c_1 e^{az} [(a\Gamma_3 - b\Omega_3) \cos bz + (-b\Gamma_3 - a\Omega_3) \sin bz] + c_2 e^{az} [(b\Gamma_3 + a\Omega_3) \cos bz + (a\Gamma_3 - b\Omega_3) \sin bz] + c_3 e^{-az} [(b\Omega_3 - a\Gamma_3) \cos bz + (-b\Gamma_3 - a\Omega_3) \sin bz] + c_4 e^{-az} [(b\Gamma_3 + a\Omega_3) \cos bz + (-a\Gamma_3 + b\Omega_3) \sin bz] \quad (45)$$

where $\Gamma_3 = \Re[\tilde{\phi}(a + ib)]$ and $\Omega_3 = \Im[\tilde{\phi}(a + ib)]$.

The expressions for the stress and electric displacement components can be obtained by the appropriate differentiation and combination with the constitutive equations as given in Eq. (1). These expressions are omitted here for brevity.

Solution for the Laminate. The elastic and electric field components within each layer are expressed in terms of eight unknown constants. These are determined using the interface and continuity conditions at the upper and lower surfaces of each lamina. For an elastic/dielectric layer, there are six constants corresponding to the elastic part of the solution and two

Table 1 Elastic, piezoelectric, and dielectric properties of piezoelectric materials

Property	PZT-4	PVDF
C_{11} (GPa)	238.0	139.0
C_{22}	23.6	139.0
C_{33}	10.6	115.0
C_{12}	3.98	77.8
C_{13}	2.19	74.3
C_{23}	1.92	74.3
C_{44}	2.15	25.6
C_{55}	4.4	25.6
C_{66}	6.43	30.6
e_{24} (C/m ²)	-0.01	12.72
e_{31}	-0.13	-5.20
e_{32}	-0.14	-5.20
e_{33}	-0.28	15.08
$\frac{\epsilon_{11}}{\epsilon_0}$	12.5	1475
$\frac{\epsilon_{22}}{\epsilon_0}$	11.98	1475
$\frac{\epsilon_{33}}{\epsilon_0}$	11.98	1300

constants for the electrostatic solution. For most common piezoelectric materials, however, the roots fall into one of two categories. For some piezoelectric materials with orthotropic behavior such as PVDF, the four roots for r are real. Correspondingly, there are eight constants (F_1 – F_4 and G_1 – G_4 in Eq. (26)) that uniquely define the fields within the layer. For piezoelectric materials with transverse isotropy such as PZT-4, there are two real roots and two complex conjugate roots for r . Hence the eight constants are F_1 , F_2 , G_1 , and G_2 from Eq. (26) and c_1 – c_4 from Eqs. (43)–(46). Following the solution of the total system of equations for the constants, the solution for any component can be computed at any location within the laminate.

3 Numerical Examples

Several examples are considered in this section. A two-layer plate of dissimilar piezoelectric materials is studied first and compared with an approximate discrete-layer plate theory. In the second example, the influence of the piezoelectric coefficients e_{ip} is examined by studying a single layer of piezoelectric material. The third example considers the influence of an internal electrode in a single piezoelectric layer. Finally, a three-layer square cross-ply of PVDF is considered. The material properties are listed for each material in Table 1. These are taken from Berlincourt and co-workers (1964) for the PZT-4 and adapted from Tashiro and co-workers (1981) for the PVDF.

Two-Layer Laminate of Dissimilar Piezoelectric Materials. We first consider a rectangular laminated plate composed of PZT-4 on the top and PVDF on the bottom. Both layers have the thickness fixed at 0.0025 m with $L_x = 2L_y$. The two aspect ratios of $L_x/H = 4$ and $L_x/H = 10$ were studied. For each geometry, two load cases are considered: an applied sinusoidal transverse load ($q_0 = 1.0$, $m = n = 1$) at the top surface with top and bottom surfaces held at zero potential and zero shear tractions, and an applied sinusoidal potential on the top surface with both top and bottom surfaces traction free. These are termed applied load case and applied potential case, respectively.

The objective of this example is to provide representative values for the elastic and electric fields at specific locations in the laminate and to compare the results with the discrete-layer theory developed by Heyliger and co-workers (Heyliger, Pei,

Table 2 Comparison of exact and discrete-layer values for applied load case

	$L_x/H=4$				$L_x/H=10$			
	z_t		z_b		z_t		z_b	
	Exact	DL	Exact	DL	Exact	DL	Exact	DL
U	-6.2574e-14	-6.2554e-14	3.5524e-14	3.5498e-14	-8.7000e-13	-8.6989e-13	7.0679e-13	7.0666e-13
V	9.5134e-14	9.5079e-14	-9.6408e-14	-9.6371e-14	-1.1186e-12	-1.1184e-12	2.0057e-12	2.0053e-12
W	2.8503e-13	2.8496e-13	3.2885e-13	3.2879e-13	6.6004e-12	6.5996e-12	6.5167e-12	6.5158e-12
σ_x	-1.4347	-1.4303	3.2246	3.2228	13.142	13.140	-11.463	-11.457
σ_y	-.71755	-.71592	4.4761	4.4728	18.397	18.393	-6.0339	-6.0312
τ_{xy}	.16785	.16740	-1.0649	-1.0638	-5.4961	-5.4949	1.3814	1.3807
D_z	-1.7048e-11	-1.7019e-11	23.409e-11	23.444e-11	.20111e-9	.20137e-9	.82096e-11	.82092e-11

a. Values at top and bottom surfaces.

	$L_x/H=4$		$L_x/H=10$	
	Exact	DL	Exact	DL
ϕ	.11147e-2	.11154e-2	.011675	.011675
σ_z	.23228	.23183	.35705	.35681
τ_{xz}	.35629	.35664	1.1491	1.1501
τ_{yz}	.39776	.39877	1.3367	1.3385

b. Values at mid-plane.

and Ramirez 1993). A total of 64 layers of equal thickness are used to divide the thickness direction of the laminate. The results for the applied load case are shown in Table 2, with those for the applied potential case shown in Table 3. The maximum values for the displacements, in-plane stresses, and normal electric displacement components are given at the top and bottom of the laminate with the potential and transverse stresses given at the center of the laminate. The exact solution explicitly provides the values at these locations. For the discrete-layer theory, the stresses and electric displacement are computed at the center of each discrete layer. Hence the values at the top and bottom are linearly extrapolated from the values at $z = \pm 0.0024609375$. The values at the center of the plate are extrapolated from the two adjoining layers and then averaged.

The results from the two formulations are in excellent agreement. Several of the effects of thickness and the difference in

material properties can be observed. For example, the transverse displacement W has a much wider variability for the thicker plate geometry, while the thinner plate yields a more constant distribution through the thickness. The potential also strongly depends on the aspect ratio of the plate, with the thinner plate resulting in a much higher midplane potential for the applied potential case.

Influence of e_{ij} . A square plate composed of a single layer of PZT-4 is considered next to study the effect of the piezoelectric coefficients on the resulting displacements and electrostatic potential. The total thickness is fixed at 0.025 m, with $L_x = L_y = L$. The aspect ratios of $L/H = 4, 6, 10, 25$, and 50 were considered. The influence of the e_{kp} was sought through calculation of the parameters $\beta_{kp} = (\partial\phi/\partial e_{kp})$ for the case of the applied load and $\eta_{kp} = (\partial W/\partial e_{kp})$ and $\zeta_{kp} = (\partial U/\partial e_{kp})$ for the applied potential.

Table 3 Comparison of exact and discrete-layer values for applied potential case

	$L_x/H=4$				$L_x/H=10$			
	z_t		z_b		z_t		z_b	
	Exact	DL	Exact	DL	Exact	DL	Exact	DL
U	-6.7845e-10	-6.7811e-11	-1.8380e-11	-1.8386e-11	-3.5347e-11	-3.5334e-11	-1.6402e-11	-1.6411e-11
V	-1.3885e-10	-1.3879e-10	-4.5792e-14	-4.5815e-11	-7.6708e-11	-7.6692e-11	-4.2402e-11	-4.2429e-11
W	-2.3409e-10	-2.3421e-10	-1.6239e-13	-1.6249e-10	-2.0111e-10	-2.0120e-10	-2.0599e-10	-2.0607e-10
σ_x	-1941.7	-1942.9	721.50	720.03	-364.25	-364.42	237.96	238.00
σ_y	74.713	72.161	325.25	324.87	89.578	89.292	95.501	95.551
τ_{xy}	-1319.6	-1318.6	-83.379	-83.249	-283.40	-283.31	-30.384	-30.392
D_z	-.46248e-5	-.46236e-5	-.26329e-7	-.26322e-7	-.95036e-6	-.95032e-6	-.41175e-7	-.41174e-7

a. Values at top and bottom surfaces.

	$L_x/H=4$		$L_x/H=10$	
	Exact	DL	Exact	DL
ϕ	0.65943	0.65941	0.92243	0.92243
σ_z	-66.387	-66.587	-3.7377	-3.7486
τ_{xz}	-40.090	-40.037	-6.9023	-6.9095
τ_{yz}	-45.704	-45.857	-4.5247	-4.5102

b. Values at the mid-plane.

Table 4 Influence of piezoelectric coefficients on displacement and potential fields

L/H	kp		
	31	33	15
4	1	.036	.581
6	1	.188	.236
10	1	.256	.0820
25	1	.285	0.0127
50	1	.290	0.00318

a. β_{kp} (applied load case).

L/H	kp		
	31	33	15
4	0.000935	0.514	1
6	0.0415	0.432	1
10	0.0637	0.389	1
25	0.0743	0.368	1
50	0.0758	0.365	1

b. η_{kp} (applied potential case).

L/H	kp		
	31	33	15
4	1	0.514	0.501
6	1	0.577	0.256
10	1	0.618	0.0997
25	1	0.638	0.0166
50	1	0.644	0.00417

c. ζ_{kp} (applied potential case).

The normalized absolute values of β_{kp} , η_{kp} , and ζ_{kp} are shown in Table 4(a)–(c). Table 4(a) shows the influence of the three independent constants on the midplane potential for the applied load case, while Tables 4(b)–(c) show the analogous influence on U and W at the top surface of the plate for the applied potential case.

In the applied load case, the coefficient e_{31} plays the dominant role in generating the midplane potential, being over three times as influential as the other constants for relatively thin plates. As the plate becomes thick, the influence of e_{15} becomes larger in part because of the higher electric field component E_x . This influence lessens as the plate becomes thin, with the coefficient e_{33} still having a fairly large effect even for thin plates.

For the applied potential case, the influence of the coefficient e_{15} dominates the transverse behavior, with η_{15} being at least twice as high as for the other η_{33} and η_{31} . The coefficient e_{31} has little influence for this purpose. In generating the displacement U , e_{31} is dominant, with e_{33} and e_{15} being about half as influential for thick plates. As the plate becomes thin, the influence of e_{15} once again dissipates, with e_{33} maintaining its influence.

An Internal Electrode. Piezoelectric elements or layers can act as actuators to generate a specific response of a solid. In this example, this type of situation is simulated. A potential is specified along the top surface of a piezoelectric layer, but in addition an internal electrode with a specified potential is specified within the thickness of the plate. A single square layer

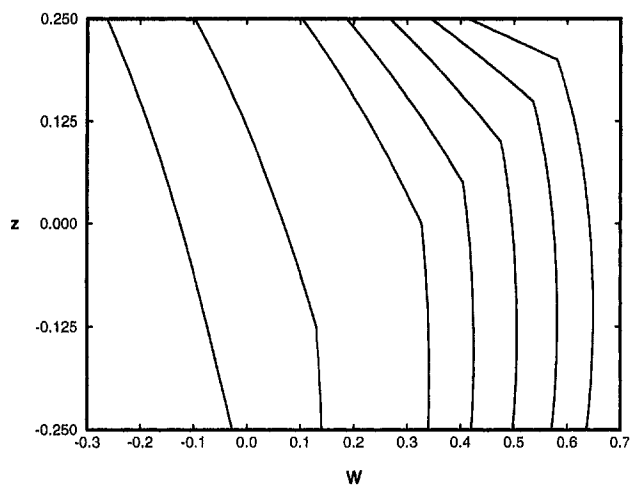


Fig. 1 Through-thickness transverse displacement for single layer with embedded electrodes

of PZT-4 is studied, with the dimensions fixed at $L = 0.02$ m and $H = 0.005$ m. A sinusoidal potential of peak amplitude of one is applied to the upper surface, with the bottom surface fixed at zero potential. In addition, a surface simulating an internal electrode with zero total thickness is located within the plate and held at zero potential. The objective of this example is to study the effects of moving the electrode location and assess the nature of the through-thickness potential and transverse displacement distributions.

The plate is modeled as two layers with thicknesses h_1 and h_2 , with the ratio h_1/H varied as 0.1, 0.2, 0.3, 0.4, 0.5, 0.75, and 1. The last case is a single layer with no internal electrode. For this specific case, the continuity and interface conditions must be modified at the location of the electrode. The six continuity conditions on the displacement and stress components remain the same as before, but the two remaining conditions are now $\phi_1(y, -h_1/2) = \phi_2(y, h_2/2) = 0$. The normal electric displacement component is no longer continuous across this interface. The resulting distributions for W and ϕ through the thickness are shown in Figs. 1 and 2, respectively. The values for W have been multiplied by 10^9 and those of z by 100.

As the actuating layer becomes thin, the electric field increases and generally yields larger values of the transverse displacement as shown in Fig. 1. The break in the slope of W indicates the location of the electrode for all cases except the

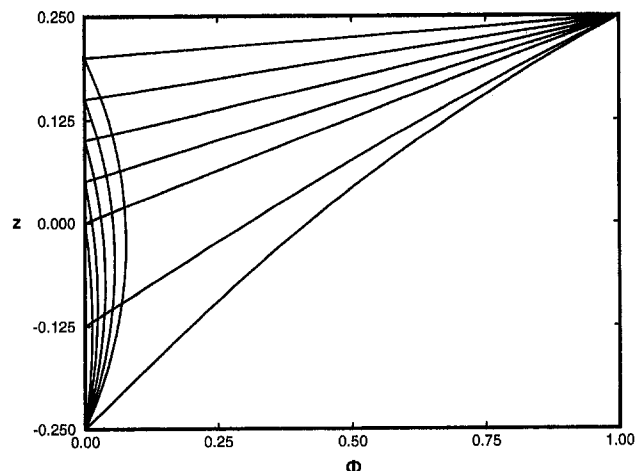


Fig. 2 Through-thickness electrostatic potential for single layer with embedded electrodes

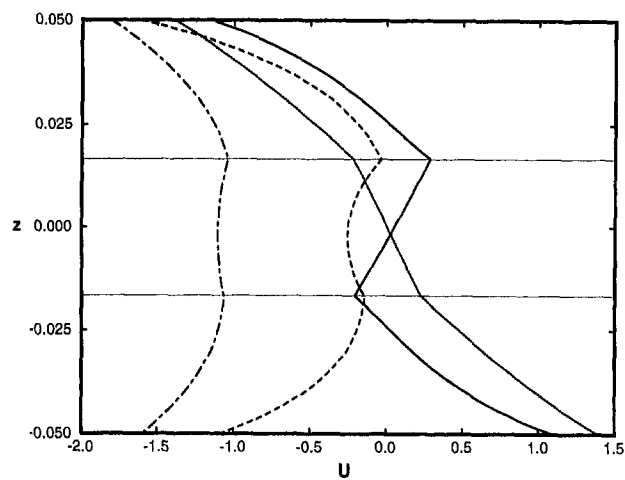


Fig. 3(a) Displacement in x-direction

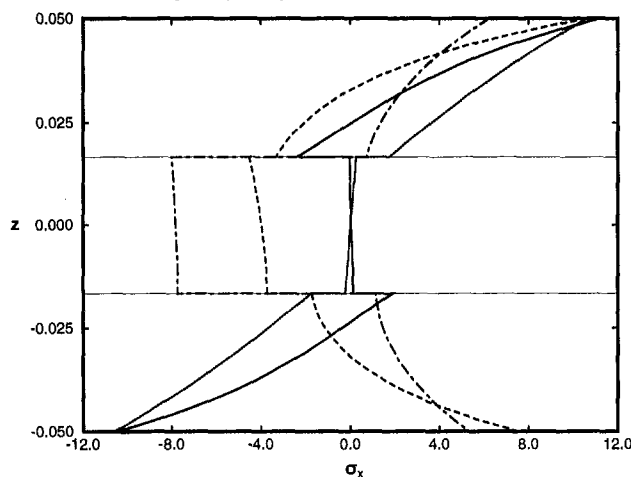


Fig. 3(b) Normal stress in x-direction

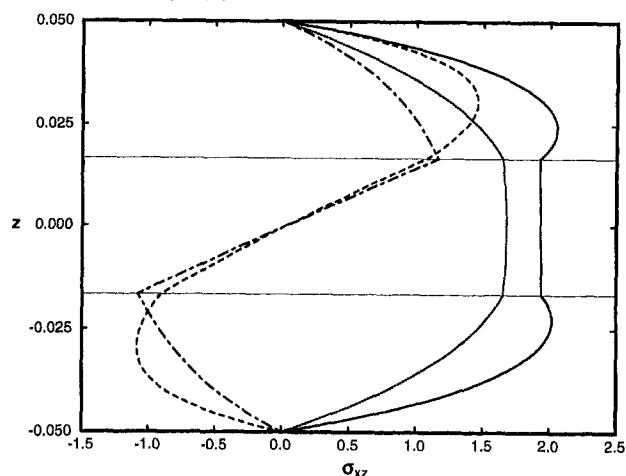


Fig. 3(c) Shear stress σ_{xz}

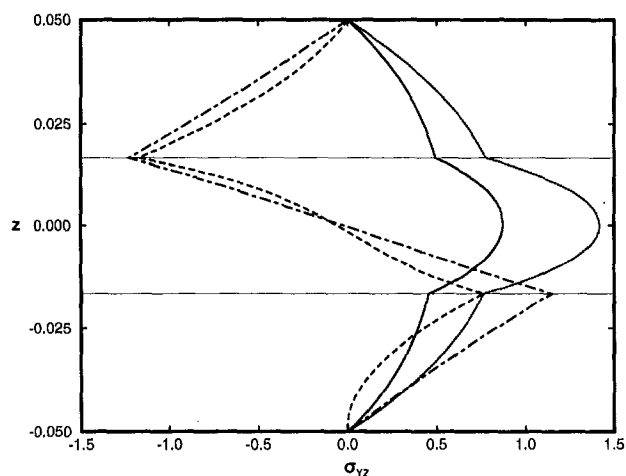


Fig. 3(d) Shear stress σ_{yz}

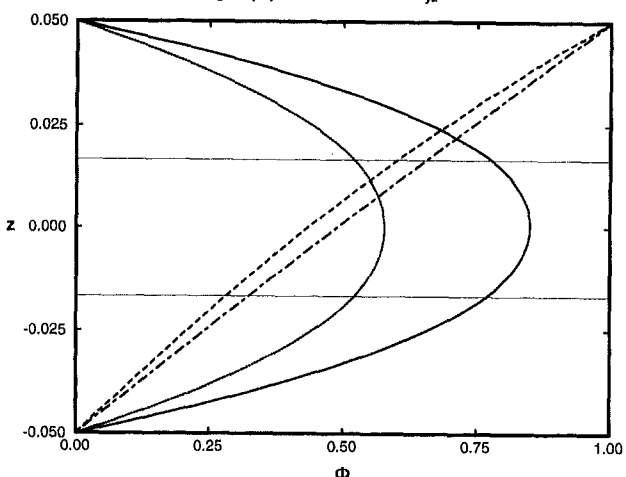


Fig. 3(e) Electrostatic potential

Fig. 3 Through-thickness distributions for cross-ply square plate

single layer. The transverse displacement varies much more strongly in the upper actuated layer than the lower layer. This is in part because of the e_{33} term and the fact that the electric field component E_z is much smaller in the lower layer.

In the analysis of piezoelectric systems, it is often assumed that the transverse electric field is a constant within an actuating layer. Figure 2 shows that this assumption is valid even for relatively large actuating thicknesses. Even for $h_1/H = 1$, the distribution is only slightly nonlinear. For this particular exam-

ple, decreasing the actuating layer thickness results in larger potentials of the same sign within the lower layer.

Cross-Ply of PVDF. A three-layer cross-ply square ($L_x = L_y = L$) plate with the stacking sequence $[0/90/0]$ is constructed of PVDF. The total laminate thickness is fixed at 0.01 m. Two lengths are considered: 0.04 m and 0.1 m. There are two conditions applied on the top surface: an applied sinusoidal transverse load and an applied sinusoidal surface potential. For the applied load, the top and bottom surfaces are grounded and the remaining surface tractions are zero. For the applied potential, only the bottom surface is grounded and both faces are traction-free.

Cases 1 and 2 are defined as the applied load with $L = 0.04$ m and $L = 0.1$ m, respectively. Cases 3 and 4 denote the applied potential case for $L = 0.04$ m and $L = 0.1$ m, respectively. The results are shown in Figure 3(a)–(e). In all plots, the solid lines represent case 1, the dotted line case 2, the dashed line case 3, and the dot-dashed line case 4. To facilitate plots on the same graphs, the field distributions are scaled. The factors by which the distributions have been multiplied for cases (1, 2, 3, 4) are as follows: U (0.2, 0.02, 1, 1) $\times 10^{12}$, σ_x (1, 0.2, 0.5, 1), τ_{xz} (2, 0.5, 10, 30), τ_{yz} (1, 1, 10, 20), and ϕ (20000, 5000, 1, 1). These are all plotted against the thickness coordinate z . All plots show the maximum field distributions for a given quantity.

Increasing the L/H ratio has the effect of smoothing out the axial displacements as shown in Fig. 3(a). The results for the

applied load cases are similar to the behavior found for elastic laminates by Pagano (1970). For the applied potential, the displacement field is significantly different and indicates that approximations for these displacements in laminated piezoelectric plate theories need to be sufficiently variable to account for this type of behavior.

Similar trends are observed for the stress distributions, with the increase in L/H resulting in less variability of the stresses within each layer. The shear stresses are self-equilibrating for cases 3 and 4, and balance the applied loading for cases 1 and 2. The potential distribution becomes more linear as L/H increases in the applied potential case, but remains effectively parabolic for the case of the applied load. Both distributions are clearly affected by the relative values of the dielectric constants for each of the layers, which were nearly identical in this case. Again, approximate plate theories would need to be able to represent the different types of response depending on the loading condition if they are to accurately depict the actual fields within the laminate for a variety of conditions.

References

- Berlincourt, D. A., Curran, D. R., and Jaffe, H., 1964, "Piezoelectric and Piezomagnetic Materials and Their Function in Transducers," in *Physical Acoustics*, W. P. Mason, ed., Vol. 1, pp. 169–270.
- Cady, W. G., 1964, *Piezoelectricity*, rev. ed., Vols. I and II, Dover Publications, New York.
- Dimitriadis, E. K., Fuller, C. R., and Rogers, C. A., 1989, "Piezoelectric Actuators for Distributed Noise and Vibration Excitation of Thin Plates," *Proceedings of ASME Failure Prevention and Reliability Conference*, Montreal, pp. 223–233.
- Heyliger, P. R., Pei, K. C., and Ramirez, G., 1994, "Discrete-Layer Piezoelectric Plate and Shell Models for Active Tip Clearance Control," NASA Contractor Report 195383.
- Heyliger, P., 1994, "Static Behavior of Laminated Elastic/Piezoelectric Plates," *AIAA Journal*, Vol. 32, pp. 2481–2484.
- Heyliger, P., and Brooks, S., 1996, "Exact Solutions for Laminated Piezoelectric Plates in Cylindrical Bending," *ASME JOURNAL OF APPLIED MECHANICS*, Vol. 63, pp. 903–910.
- Lazarus, K. B., and Crawley, E. F., 1989, "Induced Strain Actuation of Composite Plates," GTL Report No. 197, M.I.T., Cambridge, MA.
- Lee, C.-K., and Moon, F. C., 1989, "Laminated Piezopolymer Plates for Torsion and Bending Sensors and Actuators," *Journal of the Acoustical Society of America*, Vol. 85, pp. 2432–2439.
- Lee, C.-K., 1990, "Theory of Laminated Piezoelectric Plates for the Design of Distributed Sensors/Actuators. Part I: Governing Equations and Reciprocal Relationships," *Journal of the Acoustical Society of America*, Vol. 87, pp. 1144–1158.
- Lee, C.-K., Chiang, W.-W., and O'Sullivan, T. C., 1991, "Piezoelectric Modal Sensor/Actuator Pairs for Critical Active Damping Vibration Control," *Journal of the Acoustical Society of America*, Vol. 90, pp. 374–384.
- Mason, W. P., 1950, *Piezoelectric Crystals and Their Applications to Ultrasonics*, D. Van Nostrand, New York.
- Nye, N. Y., 1972, *Physical Properties of Crystal: Their Representation by Tensors and Matrices*, Oxford University Press, Oxford, UK.
- Pagano, N. J., 1970, "Exact Solutions for Rectangular Bidirectional Composites and Sandwich Plates," *Journal of Composite Materials*, Vol. 4, pp. 20–34.
- Tiersten, H. F., 1969, *Linear Piezoelectric Plate Vibrations*, Plenum, New York.
- Ray, M. C., Bhattacharya, R., and Samanta, B., 1993, "Exact Solutions for Static Analysis of Intelligent Structures," *AIAA Journal*, Vol. 31, pp. 1684–1691.
- Tashiro, K., Tadokoro, H., and Kobayashi, M., 1981, "Structure and Piezoelectricity of Poly(Vinylidene Fluoride)," *Ferroelectrics*, Vol. 32, pp. 167–175.
- Voigt, W., 1928, *Lehrbuch der Kristallphysik*, 2nd ed., B. G. Teubner, Leipzig.
- Wang, B. T., Dimitriadis, E. K., and Fuller, C. R., 1989, "Active Control of Panel Related Noise Using Multiple Piezoelectric Actuators," *Journal of the Acoustical Society of America*, Vol. 86, No. S1, p. S84.
- Wang, B.-T., and Rogers, C. A., 1991, "Laminate Plate Theory for Spatially Distributed Induced Strain Actuators," *Journal of Composite Materials*, Vol. 25, pp. 433–452.

Kai-yuan Yeh

Visiting Professor,
Department of Mechanical Engineering,
University of Toronto,
Toronto, ON M5S 1A4, Canada

Jien-huo Kue

Southwestern Research and Design Center
for Nuclear Reactor Engineering,
Zhengtu, P. R. China

F. P. J. Rimrott

Professor,
Department of Mechanical and
Industrial Engineering,
University of Toronto,
Toronto, ON M5S 3G8, Canada
Fellow ASME

On the Nonaxisymmetric Loading of Nonhomogeneous Annular Plates of Variable Thickness

In this paper, the stepped reduction method is used to find general solutions for the nonaxisymmetric bending of arbitrary axisymmetric nonhomogeneous annular plates of variable thickness under an arbitrary nonaxisymmetric temperature field and an arbitrary nonaxisymmetric distributed load. In spite of a large number of steps, eventually only two simultaneous algebraic linear equations with two unknowns have to be solved. As an example, the bending of a circular plate, whose solution is known, is carried out by the proposed approach, and it is shown that results obtained by the proposed method compare well with previous solutions obtained by other methods and hence prove the accuracy of the proposed method.

1 Introduction

Using a sufficient number of steps, any arbitrary nonhomogeneous annular plate of continuously varying thickness, subjected to arbitrary and not necessarily axisymmetric bending due to transverse loads and temperature variations can be treated by reducing it into a stepped one. The solution of such a problem is, however, not easy, as it requires the solution of simultaneous linear equations with many unknowns. Using the new method suggested by Yeh (see Yeh and Hsu, 1979a), we readily overcome these difficulties. In spite of an initially large number of steps, the problem eventually reduces to the solution of a set of two simultaneous linear algebraic equations with two unknowns. As an example, the bending of a circular plate of continuously varying thickness, whose solution is known, is studied. Results, obtained with our method, compare well with previous ones (see Picher, 1928; Yeh, 1955) obtained by different methods and thus prove the accuracy of the new approach.

2 General Solution of a Bending Problem

Consider a nonhomogeneous, variable thickness plate as shown in Fig. 1, whose outer radius is a , inner radius b , and the distribution of flexural rigidity D is as shown in the figure, we choose polar coordinates (r, θ) and the center of the plate at origin. First we discretize the continuous distribution curve of D by a stepped one (see Fig. 1). The value of D for each step is defined as the following:

$$\begin{aligned} D_0 &= D(b) \quad \text{when} \quad b \leq r < \xi_1 \\ D_1 &= D(\xi_1) \quad \text{when} \quad \xi_1 \leq r < \xi_2 \\ &\dots \\ D_i &= D(\xi_i) \quad \text{when} \quad \xi_i \leq r < \xi_{i+1} \\ &\dots \\ D_n &= D(\xi_n) \quad \text{when} \quad \xi_n \leq r \leq a. \end{aligned} \quad (2.1)$$

This plate is subjected to the four load types:

- 1 arbitrarily distributed transverse load $q(r, \theta)$ with the following properties:

$$\left. \begin{aligned} q(r, \theta) &= q(r, \theta) \quad \text{when} \quad r \geq c \\ &= 0 \quad \text{when} \quad r < c \end{aligned} \right\}, \quad (2.2)$$

- 2 circular arbitrarily linearly distributed moment per unit length $M(\theta)$, the radius of the circle being d ,
- 3 circular arbitrarily linearly distributed force per unit length $Q(\theta)$, the radius of the circle being f , and
- 4 arbitrarily distributed temperature field $\Theta(r, \theta)$.

The annular plate and the loads applied to it after this simplification are shown in Fig. 2, where $c \geq \xi_c$, $d \geq \xi_d$, $f \geq \xi_f$ and ξ_c, ξ_d, ξ_f are the radii of the steps adjacent to c, d, f .

In order to change the fundamental equations, (Yeh and Hsu, 1979a; Yeh and Hsu, 1979b; Timoshenko, 1959; Yeh and Han, 1994) into dimensionless form, we introduce the following dimensionless quantities:

$$\left. \begin{aligned} W &= \frac{w}{a}, \quad x = \frac{r}{a}, \quad \alpha_c = \frac{c}{a}, \quad \alpha_d = \frac{d}{a}, \quad \alpha_f = \frac{f}{a} \\ \beta_i &= \frac{\xi_i}{a}, \quad \beta_c = \frac{\xi_c}{a}, \quad \beta_d = \frac{\xi_d}{a}, \quad \beta_f = \frac{\xi_f}{a} \\ p &= qa^3/D_0, \quad M^* = Ma/D_0, \quad Q^* = Qa^2/D_0, \\ \alpha &= \frac{b}{a}, \quad \bar{M}_r = aM_r/D_0, \quad \bar{V}_r = a^2V_r/D_0, \quad \bar{Q}_r = a^2Q_r/D_0 \\ \bar{Q}_\theta &= a^2Q_\theta/D_0, \quad \bar{M}_{r\theta} = aM_{r\theta}/D_0, \quad \bar{M}_\theta = aM_\theta/D_0, \quad T = a\Theta \end{aligned} \right\} \quad (2.3)$$

where w is the deflection; M_r is the radial bending moment per unit length; M_θ is the circumferential bending moment per unit length; $M_{r\theta}$ is the twist moment per unit length; $D(r) = E(r)h(r)^3/(12(1-\nu^2))$ is the flexural rigidity of the plate; $E(r)$ is Young's modulus; ν is Poisson's ratio; $h(r)$ is the thickness of the plate; t is the temperature; $\Theta = \alpha^*\lambda_2 t$, $\lambda_1 = 1 - \nu$, $\lambda_2 = 1 + \nu$; α^* is the coefficient of linear thermal expansion; V_r is the radial reactive force per unit length; Q_r is the radial shearing force per unit length; and Q_θ is the circumferential shearing force per unit length. The problem of bending of

Contributed by the Applied Mechanics Division of THE AMERICAN SOCIETY OF MECHANICAL ENGINEERS for publication in the ASME JOURNAL OF APPLIED MECHANICS.

Discussion on the paper should be addressed to the Technical Editor, Professor Lewis T. Wheeler, Department of Mechanical Engineering, University of Houston, Houston, TX 77204-4792, and will be accepted until four months after final publication of the paper itself in the ASME JOURNAL OF APPLIED MECHANICS.

Manuscript received by the ASME Applied Mechanics Division, Oct. 3, 1995; final revision, May 22, 1995. Associate Technical Editor: J. N. Reddy.

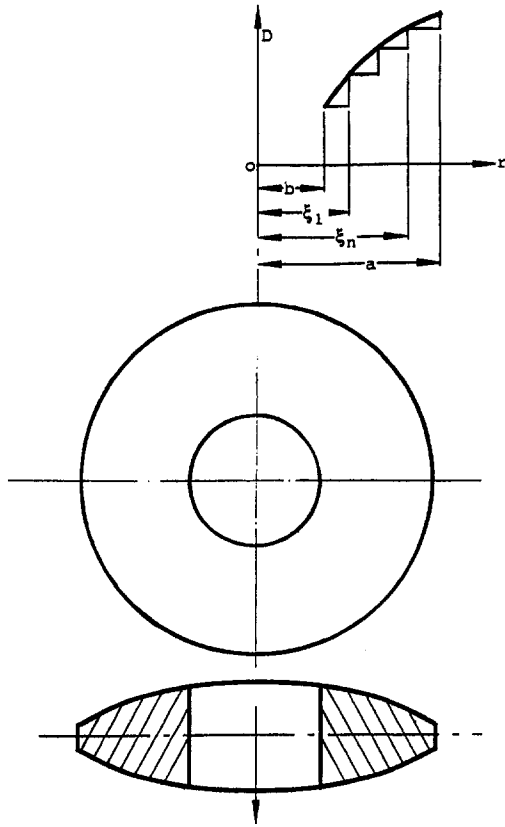


Fig. 1 Dimensions of the annular plate and discrete curve of flexural rigidity

the above-mentioned simplified annular plate is changed into the following boundary value problem, whose fundamental equation is

$$\nabla^2 \nabla^2 W = \{x - \alpha_c\}^0 p \times [\delta_c + \sum_{i=c+1}^n \{x - \beta_i\}^0 (\delta_i - \delta_{i-1})] - \nabla^2 T \quad (2.4)$$

where $\{x - \alpha_c\}^0$, $\{x - \beta_i\}^0$ are Heaviside functions, whose definition is

$$\begin{cases} \{x - \alpha_c\}^0 = 1, & \text{when } x \geq \alpha_c, \\ = 0, & \text{when } \alpha < \alpha_c \end{cases} \quad (2.5)$$

$$\nabla^2 = \frac{\partial^2}{\partial x^2} + \frac{1}{x} \frac{\partial}{\partial x} + \frac{1}{x^2} \frac{\partial^2}{\partial \theta^2} \quad (2.6)$$

$$\delta_i = D_0/D_i, \quad \delta_0 = 1, \quad \delta_c = D_0/D(\xi_c). \quad (2.7)$$

Relations between reduced deflection, temperature, and reduced bending moment, shearing force, twisting moment, and reaction force are

$$\bar{M}_r = -k_n(x) \left(\lambda_1 \frac{\partial^2 W}{\partial x^2} + \nu \nabla^2 W + T \right) \quad (2.8a)$$

$$\bar{M}_\theta = k_n(x) \frac{\partial}{\partial x} \left(\nabla^2 W - \lambda_1 \frac{\partial^2 W}{\partial x^2} \right) \quad (2.8b)$$

$$\bar{Q}_r = -k_n(x) \frac{\partial}{\partial x} (\nabla^2 W + T) \quad (2.8c)$$

$$\bar{Q}_\theta = k_n(x) \frac{1}{x} \frac{\partial}{\partial \theta} (\nabla^2 W + T) \quad (2.8d)$$

$$\bar{M}_{r\theta} = k_n(x) \lambda_1 \frac{\partial}{\partial x} \left(\frac{1}{x} \frac{\partial W}{\partial \theta} \right) \quad (2.8e)$$

$$\bar{V}_r = -k_n(x) \left[\frac{\partial}{\partial x} (\nabla^2 W + T) + \frac{\lambda_1}{x} \frac{\partial}{\partial x} \left(\frac{1}{x} \frac{\partial^2 W}{\partial \theta^2} \right) \right] \quad (2.8f)$$

where

$$k_n(x) = 1 + \sum_{i=1}^n \{x - \beta_i\}^0 \left(\frac{D_i}{D_0} - \frac{D_{i-1}}{D_0} \right). \quad (2.9)$$

The following continuity conditions should be satisfied at each step junction:

$$\left. \begin{aligned} W(\beta_i - \epsilon) &= W(\beta_i) & \frac{\partial W(\beta_i - \epsilon)}{\partial x} &= \frac{\partial W(\beta_i)}{\partial x} \\ \bar{M}_r(\beta_i - \epsilon) &= \bar{M}_r(\beta_i) & \bar{V}_r(\beta_i - \epsilon) &= \bar{V}_r(\beta_i) \end{aligned} \right\} \quad (i = 1, 2, \dots, n) \quad (2.10)$$

where ϵ is an infinitesimal quantity.

Boundary conditions usually are represented by the following three cases, taking the edge $x = \alpha$ (or $x = 1$) as an example:

1 Fixed edge

$$W = 0, \quad \frac{\partial W}{\partial x} = 0 \quad \text{as } x = \alpha \text{ (or } x = 1) \quad (2.11)$$

2 Simply supported edge

$$W = 0, \quad \bar{M}_r = 0 \quad \text{as } x = \alpha \text{ (or } x = 1) \quad (2.12)$$

3 Free edge

$$\bar{M}_r = 0, \quad \bar{V}_r = 0 \quad \text{as } x = \alpha \text{ (or } x = 1) \quad (2.13)$$

Now we treat the boundary value problem; under boundary conditions (2.11)–(2.13) and continuity conditions (2.10), we have to solve Eq. (2.4). First, we expand $p(x, \theta)$, $T(x, \theta)$, $M^*(\theta)$, $Q^*(\theta)$ into Fourier series

$$A(x, \theta) = \sum_{m=0}^{\infty} A_m(x) \cos m\theta + \sum_{m=1}^{\infty} \bar{A}_m(x) \sin m\theta \quad (2.14)$$

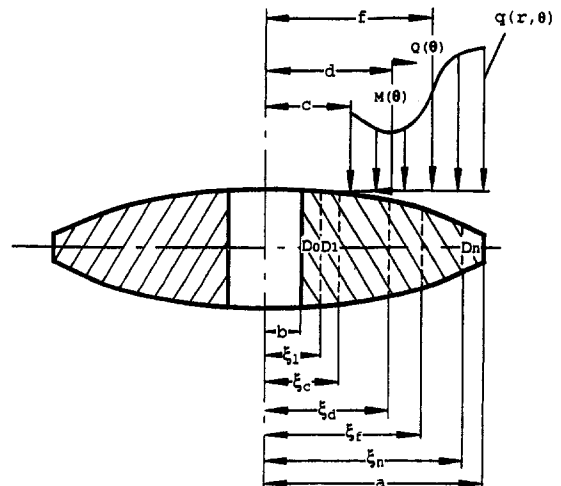


Fig. 2 Discrete dimensions of the annular plate and its loads

where

$$\left. \begin{aligned} A(x, \theta) &= (p(x, \theta), T(x, \theta), M^*(\theta), Q^*(\theta)) \\ (p_0, T_0, M_0, Q_0) &= \frac{1}{2\pi} \int_0^{2\pi} (p, T, M^*, Q^*) d\theta \\ (p_m, T_m, M_m, Q_m) &= \frac{1}{2\pi} \int_0^{2\pi} (p, T, M^*, Q^*) \cos m\theta d\theta \\ (\bar{p}_m, \bar{T}_m, \bar{M}_m, \bar{Q}_m) &= \frac{1}{2\pi} \int_0^{2\pi} (p, T, M^*, Q^*) \sin m\theta d\theta \end{aligned} \right\} \quad (2.15)$$

Then we put W, \bar{M}_r, \bar{V}_r into the following form:

$$B = \sum_{m=0}^{\infty} B_m(x) \cos m\theta + \sum_{m=0}^{\infty} \bar{B}_m(x) \sin m\theta \quad (2.16)$$

where

$$\left. \begin{aligned} B &= (W, \bar{M}_r, \bar{V}_r) \\ B_m &= (W_m(x), M_m(x), V_m(x)) \\ \bar{B}_m &= (\bar{W}_m(x), \bar{M}_m(x), \bar{V}_m(x)) \end{aligned} \right\} \quad (2.17)$$

Substituting Eqs. (2.14) and (2.16) into (2.4), and using continuity conditions (2.10) and boundary conditions (2.11)–(2.13) for W_m ($m = 0, 1, 2, \dots$), we have the following boundary value problem:

$$\Delta_m^2 \Delta_m^2 W_m = \{x - \alpha_c\}^0 p_m \times [\delta_c + \sum_{i=c+1}^m \{x - \beta_i\}^0 (\delta_i - \delta_{i-1})] - \Delta_m^2 T_m \quad (2.18)$$

where

$$\Delta_m^2 = \frac{d^2}{dx^2} + \frac{1}{x} \frac{d}{dx} - \frac{m^2}{x^2} \quad (2.19)$$

Continuity conditions corresponding to (2.10a, b) are

$$W_m(\beta_i - \epsilon) = W_m(\beta_i), \quad \frac{dW_m(\beta_i - \epsilon)}{dx} = \frac{dW_m(\beta_i)}{dx}, \quad (2.20)$$

$$M_{rm}(\beta_i - \epsilon) = M_{rm}(\beta_i), \quad V_{rm}(\beta_i - \epsilon) \quad (i = 1, 2, 3, \dots, n) \quad (2.21)$$

where

$$\left. \begin{aligned} M_{rm} &= -k_n(x) \left(\lambda_1 \frac{d^2 W_m}{dx^2} + \nu \Delta_m^2 W_m + T_m \right) \\ V_{rm} &= -k_n(x) \left[\frac{d}{dx} (\Delta_m^2 W_m + T_m) - \frac{m^2 \lambda_1}{x} \frac{d}{dx} \left(\frac{W_m}{x} \right) \right] \end{aligned} \right\} \quad (2.22)$$

Boundary conditions corresponding to (2.11)–(2.13) are

1 Fixed edge

$$W_m = 0, \quad \frac{dW_m}{dx} = 0, \quad \text{as } x = \alpha \text{ (or } x = 1) \quad (2.23)$$

2 Simply supported edge

$$W_m = 0, \quad M_{rm} = 0, \quad \text{as } x = \alpha \text{ (or } x = 1) \quad (2.24)$$

3 Free edge

$$M_{rm} = 0, \quad V_{rm} = 0, \quad \text{as } x = \alpha \text{ (or } x = 1). \quad (2.25)$$

For \bar{W}_m , we have a similar boundary value problem, only

changing $W_m, p_m, T_m, M_{rm}, V_{rm}$ into $\bar{W}_m, \bar{p}_m, \bar{T}_m, \bar{M}_{rm}, \bar{V}_{rm}$, as well as M_m, Q_m into \bar{M}_m, \bar{Q}_m in Eq. (2.18), continuity conditions (2.20), (2.21) and boundary conditions (2.23)–(2.25), with $m \neq 0$. Solutions of W_m and \bar{W}_m are the same but different constants are to be determined. In the following we only discuss how to solve W_m and do not take into account \bar{W}_m .

According to Yeh and Hsu (see Yeh and Hsu, 1979a; Yeh and Hsu, 1979b), it is not difficult to find the solutions of W_m .

$$\begin{aligned} W_m(x) &= W_m(\alpha) \{f_1^{(m)}(x, \alpha) \\ &+ \sum_{i=1}^n \{x - \beta_i\}^0 f_{mi}^{(1)} f_3^{(m)}(x, \beta_i) \\ &+ \sum_{i=1}^n \{x - \beta_i\}^0 g_{mi}^{(1)} f_4^{(m)}(x, \beta_i) \\ &+ \frac{dW_m(\alpha)}{dx} \{f_2^{(m)}(x, \alpha) \\ &+ \sum_{i=1}^n \{x - \beta_i\}^0 f_{mi}^{(2)} f_3^{(m)}(x, \beta_i) \\ &+ \sum_{i=1}^n \{x - \beta_i\}^0 g_{mi}^{(2)} f_4^{(m)}(x, \beta_i) \\ &+ M_{rm}(\alpha) \{f_3^{(m)}(x, \alpha) + \sum_{i=1}^n \{x - \beta_i\}^0 f_{mi}^{(3)} f_3^{(m)}(x, \beta_i) \\ &+ \sum_{i=1}^n \{x - \beta_i\}^0 g_{mi}^{(3)} f_4^{(m)}(x, \beta_i) \\ &+ V_{rm}(\alpha) \{f_4^{(m)}(x, \alpha) + \sum_{i=1}^n \{x - \beta_i\}^0 f_{mi}^{(4)} f_3^{(m)}(x, \beta_i) \\ &+ \sum_{i=1}^n \{x - \beta_i\}^0 g_{mi}^{(4)} f_4^{(m)}(x, \beta_i) \\ &+ \{x - \alpha_d\}^0 \delta_d M_{rm} f_3^{(m)}(x, \alpha_d) \\ &+ \sum_{i=d+1}^n \{x - \beta_i\}^0 \delta_d M_{rm} f_{mi}^{(5)} f_3^{(m)}(x, \beta_i) \\ &+ \sum_{i=d+1}^n \{x - \beta_i\}^0 \delta_d M_{rm} g_{mi}^{(5)} f_4^{(m)}(x, \beta_i) \\ &- \{x - \alpha_f\}^0 \delta_f Q_m f_4^{(m)}(x, \alpha_d) \\ &- \sum_{i=f+1}^n \{x - \beta_i\}^0 \delta_f Q_m f_{mi}^{(6)} f_3^{(m)}(x, \beta_i) \\ &- \sum_{i=f+1}^n \{x - \beta_i\}^0 \delta_f Q_m g_{mi}^{(6)} f_4^{(m)}(x, \beta_i) \\ &+ \{x - \alpha_c\}^0 W_m^*(x) + \sum_{i=c+1}^n \{x - \beta_i\}^0 f_{mi}^{(7)} f_3^{(m)}(x, \beta_i) \\ &+ \sum_{i=c+1}^n \{x - \beta_i\}^0 g_{mi}^{(7)} f_4^{(m)}(x, \beta_i) - W_m^{**}(x) \\ &+ \sum_{i=1}^n \{x - \beta_i\}^0 f_{mi}^{(8)} f_3^{(m)}(x, \beta_i) \\ &+ \sum_{i=1}^n \{x - \beta_i\}^0 g_{mi}^{(8)} f_4^{(m)}(x, \beta_i). \end{aligned} \quad (2.26)$$

In expression (2.26), $f_i^{(m)}(x, y)$ ($i = 1, 2, 3, 4$) and their derived formulae $[f_i^{(m)}(x, y)]^{(j)}$ ($j = I, II, III$) are complicated expressions not presented here.

As $m = 0$,

$$f_{0i}^{(1)} = g_{0i}^{(1)} = g_{0i}^{(2)} = g_{0i}^{(3)} = g_{0i}^{(5)} = g_{0i}^{(8)} = 0. \quad (2.27)$$

As $m = 1$,

$$W_1^*(x) = \frac{1}{x} \int_{\alpha_c}^x x dx \int_{\alpha_c}^x \frac{dx}{x} \int_{\alpha_c}^x x dx \int_{\alpha_c}^x p_1 \\ \times [\delta_c + \sum_{i=c+1}^n \{x - \beta_i\}^0 (\delta_i - \delta_{i-1})] dx \quad (2.28)$$

$$W_1^{**}(x) = \frac{1}{x} \int_{\alpha_c}^x x dx \int_{\alpha_c}^x T_1 dx. \quad (2.29)$$

As $m = 0$ and $m > 1$,

$$W_m^*(x) = x^m \int_{\alpha_c}^x \frac{dx}{x^{2m+1}} \int_{\alpha_c}^x x^{2m+1} dx \int_{\alpha_c}^x \frac{dx}{x^{2m+1}} \int_{\alpha_c}^x x^{m+1} \\ \times p_m [\delta_c + \sum_{i=c+1}^n \{x - \beta_i\}^0 (\delta_i - \delta_{i-1})] dx \quad (2.30)$$

$$W_m^{**}(x) = x^m \int_{\alpha_c}^x \frac{dx}{x^{2m+1}} \int_{\alpha_c}^x x^{2m+1} T_m dx. \quad (2.31)$$

In expression (2.26), constants to be determined are found by continuity condition (2.21) as follows:

$$f_{mi}^{(k)} = \{[f_k^{(m)}(\beta_i, f_{mj}^{(k)}[f_3^{(m)}(\beta_i, \beta_j)]^{(m)}(\beta_i, \beta_j))]^{(II)}\} \psi_i \\ g_{mi}^{(k)} = \{f_k^{(m)}(\beta_i, f_{mj}^{(k)}[f_3^{(m)}(\beta_i, \beta_j)]^{(III)} \\ + g_{mj}^{(m)}[f_4(\beta_i, \beta_j)]^{(III)}\} \psi_i \quad (k = 1, 2, 3, 4); \\ f_{mi}^{(5)} = \{[f_3^{(m)}(\beta_i, \alpha_d)]^{(II)} + \sum_{j=d+1}^{i-1} f_{mj}^{(5)}[f_3^{(m)}(\beta_i, \beta_j)]^{(II)} \\ + \sum_{j=d+1}^{i-1} g_{mj}^{(5)}[f_4^{(m)}(\beta_i, \beta_j)]^{(II)}\} \psi_i \\ g_{mi}^{(5)} = \{[f_3^{(m)}(\beta_i, \alpha_d)]^{(III)} + \sum_{j=d+1}^{i-1} f_{mj}^{(5)}[f_3^{(m)}(\beta_i, \beta_j)]^{(III)} \\ + \sum_{j=d+1}^{i-1} g_{mj}^{(5)}[f_4^{(m)}(\beta_i, \beta_j)]^{(III)}\} \psi_i \\ (i = d + 1, d + 2, d + 3, \dots, n) \\ f_{mi}^{(6)} = \{[f_4^{(m)}(\beta_i, \alpha_f)]^{(II)} + \sum_{j=f+1}^{i-1} f_{mj}^{(6)}[f_3^{(m)}(\beta_i, \beta_j)]^{(II)} \\ + \sum_{j=f+1}^{i-1} g_{mj}^{(6)}[f_4^{(m)}(\beta_i, \beta_j)]^{(II)}\} \psi_i \\ g_{mi}^{(6)} = \{[f_4^{(m)}(\beta_i, \alpha_f)]^{(III)} + \sum_{j=f+1}^{i-1} f_{mj}^{(6)}[f_3^{(m)}(\beta_i, \beta_j)]^{(III)} \\ + \sum_{j=f+1}^{i-1} g_{mj}^{(6)}[f_4^{(m)}(\beta_i, \beta_j)]^{(III)}\} \psi_i \\ (i = f + 1, f + 2, f + 3, \dots, n). \quad (2.32)$$

As $m = 0$ and $m > 1$,

$$f_{mi}^{(7)} = \left\{ -m(m-1) \lambda_1 \beta_i^{m-2} \int_{\alpha_c}^{\beta_i} \frac{dx}{x^{2m+1}} \right. \\ \times \int_{\alpha_c}^x x^{2m+1} dx \int_{\alpha_c}^x \frac{dx}{x^{2m+1}} \int_{\alpha_c}^x x^{m+1} p_m \\ \times [\delta_c + \sum_{j=c+1}^{i-1} \{x - \beta_j\}^0 (\delta_i - \delta_{i-1})] dx \\ \left. + \frac{\lambda_1}{\beta_i^{m+2}} \int_{\alpha_c}^{\beta_i} x^{2m+1} dx \int_{\alpha_c}^x \frac{dx}{x^{2m+1}} \int_{\alpha_c}^x x^{m+1} p_m \right.$$

$$\times [\delta_c + \sum_{j=c+1}^{i-1} \{x - \beta_j\}^0 (\delta_j - \delta_{j-1})] dx \\ - \beta_i^m \int_{\alpha_c}^{\beta_i} \frac{dx}{x^{2m+1}} \int_{\alpha_c}^x x^{m+1} p_m \\ \times [\delta_c + \sum_{j=c+1}^{i-1} \{x - \beta_j\}^0 (\delta_j - \delta_{j-1})] dx \\ + \sum_{j=c+1}^{i-1} f_{mj}^{(7)} [f_3^{(m)}(\beta_i, \beta_j)]^{(II)} \\ + \sum_{j=c+1}^{i-1} g_{mj}^{(7)} [f_4^{(m)}(\beta_i, \beta_j)]^{(II)} \} \psi_i$$

$$g_{mi}^{(7)} = \left\{ m^2(m-1) \lambda_1 \beta_i^{m-3} \int_{\alpha_c}^{\beta_i} \frac{dx}{x^{2m+1}} \right. \\ \times \int_{\alpha_c}^x x^{2m+1} dx \int_{\alpha_c}^x \frac{dx}{x^{2m+1}} \int_{\alpha_c}^x x^{m+1} p_m \\ \times [\delta_c + \sum_{j=c+1}^{i-1} \{x - \beta_j\}^0 (\delta_j - \delta_{j-1})] dx \\ + \frac{m^2 \lambda_1}{\beta_i^{m+3}} \int_{\alpha_c}^{\beta_i} x^{2m+1} dx \int_{\alpha_c}^x \frac{dx}{x^{2m+1}} \int_{\alpha_c}^x x^{m+1} p_m \\ \times [\delta_c + \sum_{j=c+1}^{i-1} \{x - \beta_j\}^0 (\delta_j - \delta_{j-1})] dx \\ - m \beta_i^{m-1} \int_{\alpha_c}^{\beta_i} \frac{dx}{x^{2m+1}} \int_{\alpha_c}^x x^{m+1} p_m \\ \times [\delta_c + \sum_{j=c+1}^{i-1} \{x - \beta_j\}^0 (\delta_j - \delta_{j-1})] dx \\ - \frac{1}{\beta_i^{m+1}} \int_{\alpha_c}^{\beta_i} x^{m+1} p_m [\delta_c + \sum_{j=c+1}^{i-1} \{x - \beta_j\}^0 (\delta_j - \delta_{j-1})] dx \\ + \sum_{j=c+1}^{i-1} f_{mj}^{(7)} [f_3^{(m)}(\beta_i, \beta_{sbj})]^{(III)} \\ + \sum_{j=c+1}^{i-1} f_{mj}^{(7)} \sum_{j=c+1}^{i-1} g_{mj}^{(7)} [f_4^{(m)}(\beta_i, \beta_j)]^{(III)} \} \psi_i \\ (i = c + 1, c + 2, c + 3, \dots, n)$$

$$f_{mi}^{(8)} = \left\{ m(m-1) \lambda_1 \beta_i^{m-2} \int_{\alpha_c}^{\beta_i} \frac{dx}{x^{2m+1}} \int_{\alpha_c}^x x^{m+1} T_m dx \right. \\ - \frac{\lambda_1}{\beta_i^{m+2}} \int_{\alpha_c}^{\beta_i} x^{m+1} T_m dx + \sum_{j=1}^{i-1} f_{mj}^{(8)} [f_3^{(m)}(\beta_i, \beta_j)]^{(II)} \\ + \sum_{j=1}^{i-1} g_{mj}^{(8)} [f_4^{(m)}(\beta_i, \beta_j)]^{(II)} \} \psi_i \\ g_{mi}^{(8)} = \left\{ -m^2(m-1) \lambda_1 \beta_i^{m-3} \int_{\alpha_c}^{\beta_i} \frac{dx}{x^{2m+1}} \int_{\alpha_c}^x x^{m+1} T_m dx \right. \\ - \frac{m^2 \lambda_1}{\beta_i^{m+3}} \int_{\alpha_c}^{\beta_i} x^{m+1} T_m dx + \sum_{j=1}^{i-1} f_{mj}^{(8)} [f_3^{(m)}(\beta_i, \beta_j)]^{(III)} \\ + \sum_{j=1}^{i-1} g_{mj}^{(8)} [f_4^{(m)}(\beta_i, \beta_j)]^{(III)} \} \psi_i. \quad (2.33)$$

As $m = 1$,

$$\begin{aligned}
 f_{li}^{(7)} = & \left\{ -\frac{1}{\beta_i} \int_{\alpha_c}^{\beta_i} x dx \int_{\alpha_c}^x p_1 \right. \\
 & \times [\delta_c + \sum_{j=c+1}^{i-1} \{x - \beta_j\}^0 (\delta_j - \delta_{j-1})] dx \\
 & + \frac{\lambda_1}{\beta_i} \int_{\alpha_c}^{\beta_i} \frac{dx}{x} \int_{\alpha_c}^x x dx \int_{\alpha_c}^x p_1 \\
 & \times [\delta_c + \sum_{j=c+1}^{i-1} \{x - \beta_j\}^0 (\delta_j - \delta_{j-1})] dx \\
 & - \frac{2\lambda_1}{\beta_i^3} \int_{\alpha_c}^{\beta_i} x dx \int_{\alpha_c}^x \frac{dx}{x} \int_{\alpha_c}^x x dx \int_{\alpha_c}^x p_1 [\delta_c \\
 & + \sum_{j=c+1}^{i-1} \{x - \beta_j\}^0 (\delta_j - \delta_{j-1})] dx + \sum_{j=c+1}^{i-1} f_{lj}^{(7)} \\
 & \left. \times [f_3^{(1)}(\beta_i, \beta_j)]^{(m)} + \sum_{j=c+1}^{i-1} g_{lj}^{(7)} [f_4^{(1)}(\beta_i, \beta_j)]^{(m)} \right\} \psi_i \\
 g_{li}^{(7)} = & \left\{ -\int_{\alpha_c}^{\beta_i} p_1 [\delta_c + \sum_{j=c+1}^{i-1} \{x - \beta_j\}^0 (\delta_j - \delta_{j-1})] dx \right. \\
 & + \frac{1}{\beta_i^2} \int_{\alpha_c}^{\beta_i} x dx \int_{\alpha_c}^x p_1 [\delta_c + \sum_{j=c+1}^{i-1} \{x - \beta_j\}^0 (\delta_j - \delta_{j-1})] dx \\
 & + \frac{\lambda_1}{\beta_i^2} \int_{\alpha_c}^{\beta_i} \frac{dx}{x} \int_{\alpha_c}^x x dx \int_{\alpha_c}^x p_1 \\
 & \times [\delta_c + \sum_{j=c+1}^{i-1} \{x - \beta_j\}^0 (\delta_j - \delta_{j-1})] dx \\
 & - \frac{2\lambda_1}{\beta_i^4} \int_{\alpha_c}^{\beta_i} x dx \int_{\alpha_c}^x \frac{dx}{x} \int_{\alpha_c}^x x dx \int_{\alpha_c}^x p_1 \\
 & \times [\delta_c + \sum_{j=c+1}^{i-1} \{x - \beta_j\}^0 (\delta_j - \delta_{j-1})] dx + \sum_{j=c+1}^{i-1} f_{lj}^{(7)} \\
 & \left. \times [f_3^{(1)}(\beta_i, \beta_j)]^{(m)} + \sum_{j=c+1}^{i-1} g_{lj}^{(7)} [f_4^{(1)}(\beta_i, \beta_j)]^{(m)} \right\} \psi_i \\
 & (i = c + 1, c + 2, c + 3, \dots, n) \\
 f_{li}^{(8)} = & \left\{ \frac{2\lambda_1}{\beta_i^3} \int_{\alpha_c}^{\beta_i} x dx \int_{\alpha_c}^x T_1 dx - \frac{\lambda_1}{\beta_i} \int_{\alpha_c}^{\beta_i} T_1 dx + \sum_{j=1}^{i-1} f_{lj}^{(8)} \right. \\
 & \left. \times [f_3^{(1)}(\beta_i, \beta_j)]^{(m)} + \sum_{j=1}^{i-1} g_{lj}^{(8)} [f_4^{(1)}(\beta_i, \beta_j)]^{(m)} \right\} \psi_i \\
 g_{li}^{(8)} = & \left\{ -\frac{\lambda_1}{\beta_i^2} \int_{\alpha_c}^{\beta_i} T_1 dx + \frac{2\lambda_1}{\beta_i^4} \int_{\alpha_c}^{\beta_i} x dx \int_{\alpha_c}^x T_1 dx + \sum_{j=1}^{i-1} f_{lj}^{(8)} \right. \\
 & \left. \times [f_3^{(1)}(\beta_i, \beta_j)]^{(m)} + \sum_{j=1}^{i-1} g_{lj}^{(8)} [f_4^{(1)}(\beta_i, \beta_j)]^{(m)} \right\} \psi_i \quad (2.34)
 \end{aligned}$$

where

$$\psi_i = (D_{i-1} - D_i)/D_i. \quad (2.35)$$

3 Example

Let us study an example to explain the calculation procedure and examine the exactness of our method. Assume the thickness of a circular plate varies according to the relationship $h = h_0 e^{-(\beta/6)/(r/a)^2}$ where h_0 is the thickness at the center of the plate,

β is an arbitrary parameter (here we put $\beta = 2$) and the edge of the plate is fixed. The plate is subjected to a uniformly distributed load q . The central deflection W_{\max} and the edge radial stress $\sigma_r(a)$ (see Fig. 3) are to be determined.

Picher (1928) and Yeh (1955) have investigated this continuously variable thickness circular plate problem by different methods. Yeh was the first to discretize the continuously variable thickness circular plate into stepped thicknesses, either circumscribed or inscribed, and called one case A and the other case B (see Fig. 3). The bending is symmetrical, therefore $m = 0$. Putting $m = 0$, $\alpha = 0$, $n = 9$ and $\nu = 0.3$ in Eqs. (2.26), boundary conditions (2.23) at $x = 1$, (2.27), (2.33) and (2.34) we obtain,

in case A,

$$M_{r0}(0) = 0.15952 p_0, \quad W(0) = W_{\max} = 0.02370 p_0.$$

Notice that

$$W_{\max} = \frac{W_{\max}}{a}, \quad p_0 = \frac{a^3 q}{D_0}, \quad D_0 = \frac{E h_0^3}{12(1 - \nu^2)}$$

Substituting into the above expression, we obtain

$$w_{\max} = 0.04740 \frac{6a^4(1 - \nu^2)}{E h_0^3} q$$

while the exact solution (see Picher, 1928; Yeh, 1955) gives

$$w_{\max} = 0.0505 \frac{6a^4(1 - \nu^2)}{E h_0^3} q.$$

Thus, the error is

$$\frac{0.0505 - 0.04740}{0.0505} = 6.14 \text{ percent.}$$

In case B,

$$M_{r0}(0) = 0.16810 p_0, \quad W(0) = 0.02567 p_0$$

$$D_0 = \frac{E h_0^3 e^{-0.01}}{12(1 - \nu^2)}$$

giving

$$w_{\max} = 0.05186 \frac{6a^4(1 - \nu^2)}{E h_0^3} q$$

and an error of

$$\frac{0.0505 - 0.05186}{0.0505} = -2.70 \text{ percent.}$$

Taking the average value of the results in cases A and B, we obtain

$$w_{\max} = 0.04963 \frac{6a^4(1 - \nu^2)}{E h_0^3} q$$

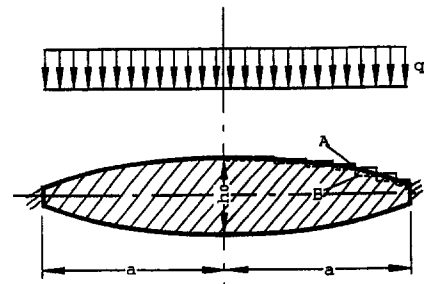


Fig. 3 Continuously variable thickness plate of the example

and an error of

$$\frac{0.0505 - 0.04963}{0.0505} = 1.72 \text{ percent.}$$

Now let us to find out the edge radial stress $\sigma_r(a)$. From Eq. (2.22a), we obtain the expression for $M_{r0}(1)$. Then from the numerical data, we can compute the value of $M_{r0}(1)$ and the results obtained may be written in the form

$$M_{r0}(1) = \alpha' \frac{D_0}{D_0} \frac{qa^3}{D_0}$$

$$\sigma_r(a) = \gamma \frac{3qa^2}{h_0^2}.$$

Comparing the above two expressions, we have

$$\gamma = 2 \frac{h_0}{h_0} \alpha'.$$

For case A, we have

$$\gamma = \mp 2e^{-0.27} \alpha' = \mp 0.3841,$$

with an error of

$$\frac{0.4125 - 0.3841}{0.4125} = 6.89 \text{ percent.}$$

For case B, we have

$$\gamma = \mp 2e^{-0.33} \alpha' = \mp 0.4223$$

with an error of

$$\frac{0.4125 - 0.4223}{0.4125} = -2.37 \text{ percent.}$$

Taking the average of both cases, we obtain

$$\gamma = \mp 0.4032$$

and an error of

$$\frac{0.4125 - 0.4032}{0.4125} = 2.25 \text{ percent.}$$

For other examples on structural optimization by the approach presented in this paper, the reader is referred to Yeh (1988); Yeh, Yu, and Liu (1987); Yu and Yeh (1987); and Yu and Yeh (1988).

5 Conclusion

For a stepwise nonhomogeneous variable thickness plate, solutions obtained by the stepped reduction method are exact solutions.

In solving the problem of a continuous nonhomogeneous variable thickness plate by changing it into a stepped nonhomogeneous variable thickness plate (discretization), from the present example, we see that results obtained by the present method are accurate enough even for only $n = 9$, and it is very easy to estimate the error by computing the upper and lower bounds of

the solutions. Therefore, the method can be extended to other kinds of nonhomogeneous variable thickness structural problems.

From the above example, we also see that unlike the conventional method of discretization which results in a system of algebraic equations and thus requiring a numerical approach for solution, this technique produces only a single algebraic equation, regardless of the number of discrete annular plates used in the model. This is achieved by expressing the continuity conditions between any two annular plates in terms of the boundary conditions for the overall problem using the Heaviside function, and this is done successively for all junctions. The main advantage of the stepped reduction method is that it permits an analytical formulation for handling the problem of nonhomogeneity and variable thickness in annular plates. The accuracy of using this procedure depends on the discretization scheme used: as the number of annular plates increases to infinity, the discretized plates tend towards the continuous plate and the approximate solution approaches the exact solution.

The small parameter method, used by Yeh (1955) still has a certain superiority, so it can be used together with the present method.

If we want to increase the accuracy in the present example, we can increase the number of steps. There is no difficulty in principle, only an increase in the labour of computation.

The convergence conditions of the present method were discussed by Ji (1988).

This method has solutions in analytic form, so it can be used for inverse problems (see Yeh (1989) and Yeh and Han (1994)), such as structural optimization, flexible robotics, etc.

References

- Ji, Zhen-yi, 1988, "The convergent condition and united formula of step reduction method," *Applied Mathematics and Mechanics* (English ed.), Vol. 9, No. 12, pp. 1183-1193.
- Edited by Olszak, W., ed., 1959, *Non-Homogeneity in Elasticity and Plasticity, Proceedings of the I.U.T.A.M. Symposium*, Pergamon Press, New York.
- Picher, O., 1928, "Die Biegung kreissymmetrischer Platten von veränderlicher Dicke," Dissertation, Berlin, Germany, (also refer to Timoshenko, S., 1959).
- Timoshenko, S., 1959, *Theory of Plates and Shells*, McGraw-Hill, New York, pp. 257-260.
- Yeh, Kai-yuan, 1955, "Bending of a thin elastic plate of variable thickness," *Acta Physica Sinica*, Vol. 11, No. 3, pp. 15-32.
- Yeh, Kai-yuan, 1988, "Recent investigation of structural optimization by analytic method," *Structural Optimization*, G. I. N. Rozvany and B. L. Karihaloo, eds., Kluwer Academic Publishers, pp. 379-386.
- Yeh, Kai-yuan, and Hsu, Chin-yun, 1979a, "General solutions on certain problems of elasticity with non-homogeneity and variable thickness I. Elastic and plastic stress analyses of high speed rotating disc with non-homogeneity and variable thickness under non-homogeneous steady temperature field," *Journal of Lanzhou University (Natural Sciences)*, Special Number of Mechanics, No. 1, pp. 60-74.
- Yeh, Kai-yuan, and Hsu, Chin-yun, 1979b, "General solutions of bending of ring-shaped elastic thin plates under arbitrary transverse loads and several problems," *Journal of Lanzhou University (Natural Sciences)*, Special Number of Mechanics, No. 1, pp. 202-225.
- Yeh, Kai-yuan, and Han, R. P. S., 1994, "Thermoelastic Analysis of High-Speed Rotating Disks With Variable Thickness and Inhomogeneity," *ASME JOURNAL OF APPLIED MECHANICS*, Vol. 61, pp. 186-191.
- Yu, Huan-ran, and Yeh, Kai-yuan, 1987, "Optimal design of minmax deflection of an annual plate," *International Conference on Optimization: Technique and Applications*, Singapore, pp. 1087-1095.
- Yu, Huan-ran, and Yeh, Kai-yuan, 1988, "Optimal design of minmax deflection of an annual Plate," *Applied Mathematics and Mechanics*, (English ed.), Vol. 9, No. 1, pp. 13-18.

Wave Propagation in Poroelastic Media Saturated by Two Fluids

K. Tuncay¹

M. Y. Corapcioglu

Department of Civil Engineering,
Texas A&M University,
College Station, TX 77843-3136

A theory of wave propagation in isotropic poroelastic media saturated by two immiscible Newtonian fluids is presented. The macroscopic constitutive relations, and mass and momentum balance equations are obtained by volume averaging the microscale balance and constitutive equations and assuming small deformations. Momentum transfer terms are expressed in terms of intrinsic and relative permeabilities assuming the validity of Darcy's law. The coefficients of macroscopic constitutive relations are expressed in terms of measurable quantities in a novel way. The theory demonstrates the existence of three compressional and one rotational wave. The third compressional wave is associated with the pressure difference between the fluid phase and dependent on the slope of the capillary pressure-saturation relation.

Introduction

Dynamics of porous media is of interest in various diversified areas of science and engineering. This phenomena has been studied extensively in soil mechanics, seismology, acoustics, earthquake engineering, geophysics, and many other disciplines. The importance of the inertial effects, which cause wave propagation, were shown by Zienkiewicz et al. (1980) and Bowen and Lockett (1983). Although wave propagation in porous media has been studied for quite some time, Biot's (1956a, 1956b) work appears to be the first one employing the fundamentals of transport phenomena in porous media. Biot's theory is an extension of a consolidation theory developed earlier (Biot, 1941). Although the theory is developed in a heuristic manner, it is well accepted and still forms a base for wave propagation in porous media. The theory predicts an additional compressional wave which was first confirmed experimentally by Plona (1980) (also see Berryman, 1980). Because of its highly dissipative behavior, this wave is very difficult to observe but contributes the energy losses which effect the characteristics of other types of body waves. The physical interpretations of the elastic constants in Biot's theory were given by Biot and Willis (1957). Fatt (1959) calculated Biot's constants for sandstone. The elastic coefficients were also studied by Geertsma and Smith (1961), Berryman (1981, 1986), and Pride et al. (1992).

Mixture theory has been used extensively in the formulation of wave propagation in porous media. In this approach, phases are viewed as overlapping media simultaneously existing everywhere and occupying the whole space. The theory does not require the description of the pore structure. Disadvantage of this theory is the lack of information about the interaction terms. Hence, even if the pore structure can be described, there is no systematic way to obtain the interaction terms. There is a vast literature on the use of mixture theory among which one can note; Drumheller (1978), Jenkins (1980), Katsube and Carroll (1987), Garg et al. (1971, 1975, 1986), Berryman (1986), Prevost (1980), and Santos (1990a, 1990b). An extensive literature survey is given by Bowen (1976) and Bedford and Drumheller (1983).

Another approach of formulating multiphase equations is the use of the volume-averaging technique. Mass and momentum balance equations as well as the constitutive relations are obtained by volume averaging the equations and relations expressed at the microscopic scale. The volume-averaging technique has been employed after the development of the theorem for volume average of a gradient (Slattery, 1967; Anderson and Jackson, 1967; Marle, 1967; Whitaker, 1967). Although the volume-averaging technique has been used extensively to formulate the flow problems in rigid porous media (Slattery, 1967, 1968; Whitaker, 1967), it has been recently applied to deformable media (e.g., Bear et al., 1984). De la Cruz and Spanos (1985) made the first attempt to formulate the constitutive relations and balance equations of wave propagation in saturated porous media. In a subsequent paper, de la Cruz and Spanos (1989) extended their theory to include the thermodynamic considerations. Pride et al. (1992) obtained Biot's (1941, 1956a) equations for saturated porous media by employing the volume-averaging technique. The resulting constitutive relations of Pride et al. (1992) contained the same parameters as of Biot and Willis (1957).

An alternative derivation to the volume averaging technique is the two-space method. In this approach, the unknown field quantities are considered to be functions of two sets of space variables. This extends the definitions of the field quantities from a three to six-dimensional space. These two sets are related by the ratio of the characteristic length of the microscale to the characteristic length of macroscale. The two-space method was first developed and studied by Sanchez-Palencia (1980) and Keller (1977). The two-space method was applied to wave propagation phenomena by Burridge and Keller (1981), Levy (1979), Auriault (1980), and Auriault et al. (1985). In principle both the volume averaging and two-space method yield the same results. However, application of volume averaging is simpler and enables physical interpretations of the averaged equations.

In contrast to porous media saturated by a single fluid, wave propagation in porous media saturated by multiphase fluids received very limited attention from researchers. The general trend is to extend Biot's formulation developed for a saturated medium by replacing model parameters with the ones modified for the fluid-fluid or fluid-gas mixture (Domenico, 1974; Mochizuki, 1982; Berryman, 1985; Murphy, 1984). Brutsaert (1964) who extended Biot's theory appears to be the first one to predict three compressional waves. The third compressional wave arises due to presence of a second fluid phase in the pores. Brutsaert and Luthin (1964) provided experimental data which agrees with the results of Brutsaert's (1964) theory. The third compressional wave was also predicted by Garg and Nayfeh

¹ Current address: Department of Chemistry, Indiana University, Bloomington, IN 47405.

Contributed by the Applied Mechanics Division of THE AMERICAN SOCIETY OF MECHANICAL ENGINEERS for publication in the ASME JOURNAL OF APPLIED MECHANICS.

Discussion on the paper should be addressed to the Technical Editor, Professor Lewis T. Wheeler, Department of Mechanical Engineering, University of Houston, Houston, TX 77204-4792, and will be accepted until four months after final publication of the paper itself in the ASME JOURNAL OF APPLIED MECHANICS.

Manuscript received by the ASME Applied Mechanics Division, Nov. 30, 1994; final revision, Aug. 15, 1996. Associate Technical Editor: J. T. Jenkins.

(1986) and Santos et al. (1990a). Garg and Nayfeh (1986) used the mixture theory and solved the one-dimensional equations by Laplace transformation for two limiting values of viscous coupling. Santos et al. (1990a) derived the governing equations by using the principle of virtual complementary work. In a companion paper, Santos et al. (1990b) presented a method to determine the elastic constants for isotropic porous media saturated by two fluids. In all these works, the momentum transfer between the solid and fluid phases are approximated by Darcy-type expressions. We refer the reader to Corapcioglu and Tuncay (1996) for a comprehensive discussion of wave propagation in porous media saturated by multiphase fluids.

In this paper, we apply the volume-averaging technique to explore the wave propagation characteristics of a linearly elastic porous medium saturated by two immiscible Newtonian fluids. The paper will start with a brief review of volume-averaging theorems. The macroscale mass and momentum balance equations and constitutive relations will be obtained by volume averaging the corresponding microscale equations. In the microscale, the grains will be assumed to be linearly elastic and the fluids are Newtonian. The coefficients of macroscopic constitutive relations will be expressed in terms of measurable quantities in a novel way. These constitutive relations can be reduced to those given by Biot and Willis (1957) for porous medium saturated by a single fluid phase. Momentum transfer terms will be formulated in terms of intrinsic and relative permeabilities assuming the validity of Darcy's law.

Volume-Averaging Theorems

Let L , l , and r be the characteristic lengths of the macroscopic scale, averaging volume, and pore scale, respectively. The required condition for the volume averaging is (Slattery, 1981)

$$r \ll l \ll L. \quad (1)$$

In this study, we assume that this requirement is satisfied, and furthermore, if λ is the wavelength of the wave, we assume $l \ll \lambda$. In other words, we limit the present study to low-frequency waves. We continue with the definitions used in the volume-averaging literature. Let B_i be a field quantity of phase i , then the volume average of B_i is defined as

$$\langle B_i \rangle = \frac{1}{V} \int_{R_i} B_i dV \quad (2)$$

where V is the averaging volume and R_i is the region occupied by phase i . The intrinsic volume average of B_i , i.e., the mean value of B_i in R_i , is given by

$$\overline{B_i} = \frac{1}{V_i} \int_{R_i} B_i dV \quad (3)$$

where V_i is the volume of phase i in the averaging volume. These two averages are related by

$$\langle B_i \rangle = \alpha_i \overline{B_i} \quad (4)$$

where α_i is the volume fraction of phase i . Now, we set the volume average theorem for a gradient and a time derivative (Slattery, 1967, 1968, 1981)

$$\langle \nabla B_i \rangle = \nabla \langle B_i \rangle + \frac{1}{V} \int_{S_{ij}} B_i n_i dA \quad i \neq j, \quad j = 1, \dots, N \quad (5)$$

$$\left\langle \frac{\partial B_i}{\partial t} \right\rangle = \frac{\partial \langle B_i \rangle}{\partial t} - \frac{1}{V} \int_{S_{ij}} B_i u \cdot n_i dA$$

$$i \neq j, \quad j = 1, \dots, N \quad (6)$$

where S_{ij} is the interface between phase i and phase j , n_i is the outward normal of S_{ij} , and $u \cdot n_i$ is the speed of displacement

of S_{ij} into other phases. The theorem of a volume average of a divergence is stated as

$$\langle \nabla \cdot B_i \rangle = \nabla \cdot \langle B_i \rangle + \frac{1}{V} \int_{S_{ij}} B_i \cdot n_i dA \quad i \neq j, \quad j = 1, \dots, N. \quad (7)$$

If B_i is taken to be a constant, Eqs. (5) and (6) take the following forms:

$$\nabla \alpha_i = - \frac{1}{V} \int_{S_{ij}} n_i dA \quad i \neq j, \quad j = 1, \dots, N \quad (8)$$

$$\frac{\partial \alpha_i}{\partial t} = + \frac{1}{V} \int_{S_{ij}} u \cdot n_i dA \quad i \neq j, \quad j = 1, \dots, N. \quad (9)$$

Microscopic Constitutive Relations, Mass, and Momentum Balance Equations

In this study, the compressible porous medium consists of compressible solid grains, and two immiscible viscous compressible fluids. We assume that there is no mass exchange between the phases. The solid phase is assumed to be initially at rest, linearly elastic, isotropic, and experiencing small deformations. Then the constitutive relations are given by

$$\tau_s = K_s \nabla \cdot u_s I + G_s (\nabla u_s + (\nabla u_s)^T - \frac{2}{3} \nabla \cdot u_s I) \quad (10)$$

where u_s , τ_s , K_s , G_s , I are the displacement, incremental stress tensor, bulk modulus, shear modulus of the solid phase and the unit tensor, respectively. The superscript T denotes the transpose of a tensor. We assume that both fluid phases are Newtonian with constitutive relations

$$\tau_i = -P_i I + \mu_i (\nabla v_i + (\nabla v_i)^T - \frac{2}{3} \nabla \cdot v_i I) \quad i = 1, 2 \quad (11)$$

where v_i , τ_i , P_i and μ_i are the velocity, incremental stress tensor, incremental pore fluid pressure and shear viscosity of fluid phase i , respectively. In Eq. (11), the bulk viscosity of fluids is assumed to be negligible. The state equations of fluid phases are assumed to be in the form of

$$\frac{1}{K_i} \frac{dP_i^*}{dt} = \frac{1}{\rho_i} \frac{d\rho_i}{dt} \quad i = 1, 2 \quad (12)$$

where K_i , ρ_i and P_i^* are the bulk modulus, mass density, and pressure of phase i . The mass balance equations are expressed as

$$\frac{1}{\rho_i} \frac{d\rho_i}{dt} = -\nabla \cdot v_i \quad i = 1, 2. \quad (13)$$

By combining Eqs. (12) and (13), we obtain

$$\frac{1}{K_i} \frac{dP_i^*}{dt} = -\nabla \cdot v_i \quad i = 1, 2. \quad (14)$$

The pressure increment P_i can be written as

$$-P_i = K_i \nabla \cdot u_i \quad i = 1, 2 \quad (15)$$

where u_i is the displacement of the fluid phase i from a reference position, i.e., incremental displacement. We continue with the momentum balance equation in terms of incremental stresses and velocities

$$\nabla \cdot \tau_j = \rho_j \frac{dv_j}{dt} \quad j = s, 1, 2. \quad (16)$$

We can rewrite Eq. (16) by using the mass balance Eqs. (13) as

$$\nabla \cdot \tau_j = \frac{\partial(\rho_j v_j)}{\partial t} + \nabla \cdot (\rho_j v_j v_j) \quad j = s, 1, 2. \quad (17)$$

We note that the body forces do not appear in Eqs. (16) and (17) because equations are expressed in terms of incremental stresses. The boundary conditions at the solid-fluid interfaces are expressed as

$$v_s = v_i \quad \text{and} \quad \tau_s \cdot n_s + \tau_i \cdot n_i = 0 \quad \text{on} \quad S_{si} \quad i = 1, 2 \quad (18)$$

where the subscript (*si*) denotes the interface between the solid phase and fluid phase *i* and n_j is the unit outward vector normal to the interface. The boundary conditions at the fluid-fluid interfaces are (Slattery, 1981)

$$v_1 = v_2 \quad \text{and} \quad \tau_1 \cdot n_1 + \tau_2 \cdot n_2 = \nabla_\sigma \gamma - 2H\gamma n \quad \text{on} \quad S_{12} \quad (19)$$

where ∇_σ , γ , H are the surface gradient operator, interfacial tension, and mean curvature of the interface, respectively. The terms on the right-hand side of Eq. (19) may be interpreted as the rate of momentum production per unit area of the phase interphase. The first term on right-hand side incorporates the position dependency of surface tension upon the interface. Therefore the surface gradient operator incorporates the spatial variation of the surface tension along the phase interface because of impurities in the fluids and temperature variations. The second term on the right-hand side is known as the Laplace formula. This results from the fact that a discontinuity in fluid pressures exists across a curved interface separating the two immiscible fluids. The behavior of the interface is similar to that of a stretched membrane (Bear and Bachmat, 1990). The Laplace formula is obtained under the conditions of force equilibrium at the microscopic level by stating the balance of force components normal to an infinitesimal element of a curved interface. H is expressed depending on the geometry of the interface curvature.

Macroscopic Constitutive Relations

Our next step is to obtain macroscopic constitutive relations by averaging the microscopic relations over a representative elementary volume (Bear, 1972). Volume averaging of Eq. (10) yields

$$\begin{aligned} \frac{1}{V} \int_{R_s} \tau_s dV &= K_s \left(\nabla \cdot (\alpha_s \bar{u}_s) + \frac{1}{V} \int_{S_{si}} u_s \cdot n_s dA \right) I \\ &+ G_s (\nabla(\alpha_s \bar{u}_s) + (\nabla(\alpha_s \bar{u}_s))^T - \frac{2}{3} \nabla \cdot (\alpha_s \bar{u}_s) I + K_{si}) \end{aligned} \quad i = 1, 2 \quad (20)$$

where

$$K_{si} = \frac{1}{V} \int_{S_{si}} (u_s n_s + n_s u_s - \frac{2}{3} u_s \cdot n_s I) dA \quad i = 1, 2 \quad (21)$$

is a second-order tensor with zero trace. Since there is no mass exchange between the phases, the velocity of the interface is equal to the velocity of a point at the interface, i.e., material surface. Hence, by employing Eq. (9), the integral in Eq. (20) can be expressed as

$$\frac{1}{V} \int_{S_{si}} u_s \cdot n_s dA = (\alpha_s - \alpha_s^0) = \Delta \alpha_s \quad i = 1, 2 \quad (22)$$

where the superscript (0) refers to the reference configuration. Since the displacements are assumed to be small, by definition $\bar{u}_j \cdot \nabla \alpha_j \approx 0$. However, $\alpha_j \nabla \bar{u}_j$ cannot be neglected since α_j is a finite number. Then volume averaged constitutive relations for the solid phase can be expressed as

$$\begin{aligned} \alpha_s \bar{\tau}_s &= K_s (\alpha_s \nabla \cdot \bar{u}_s + \Delta \alpha_s) I + G_s (\alpha_s \nabla \bar{u}_s \\ &+ \alpha_s (\nabla \bar{u}_s)^T - \frac{2}{3} \alpha_s \nabla \cdot \bar{u}_s I + K_{si}) \quad i = 1, 2 \end{aligned} \quad (23)$$

where $\bar{\tau}_s$ is the intrinsic averaged incremental stress of the solid phase. Similarly, the volume averaged constitutive relations for fluid phases are

$$\begin{aligned} \alpha_i \bar{\tau}_i &= K_i (\alpha_i \nabla \cdot \bar{u}_i + \Delta \alpha_i) I + \mu_i (\alpha_i \nabla \bar{v}_i + \alpha_i (\nabla \bar{v}_i)^T \\ &- \frac{2}{3} \alpha_i \nabla \cdot \bar{v}_i I + J_{is} + J_{ik}) \quad i \neq k, \quad i = 1, 2 \end{aligned} \quad (24)$$

where

$$J_{ij} = \frac{1}{V} \int_{S_{ij}} (v_i n_i + n_i v_i - \frac{2}{3} v_i \cdot n_i I) dA. \quad (25)$$

Under the small deformations assumption, the interfaces of the phases are not allowed to experience large deformations. Then by using Eqs. (21) and (25), and assuming $\partial u_i / \partial t \gg v_i \cdot \nabla u_i$, we can write

$$J_{ij} = \frac{\partial K_{ij}}{\partial t}. \quad (26)$$

Furthermore, employing the no slip conditions (Eqs. (18)–(19)), we can write $K_{jk} = -K_{kj}$ and $J_{jk} = -J_{kj}$. K_{ij} and J_{ij} couple the shear deformation of the phases. However, we must note that physical meanings of the shear modulus of the solid phase and viscosity of the fluid phases are totally different. In almost all studies associated with the deformation of the solid matrix, these coupling terms are neglected assuming that all shear resistance is provided by the matrix only.

The microscopic boundary condition at the fluid-fluid interface (Eq. (19)) shows that there is a jump in the stresses of the immiscible fluids because of the presence of interfacial tension and curvature of the interface. Assuming that smooth pressure variations within the averaging volume and viscous shear in Eq. (11) is negligible and can be neglected, we can write

$$\bar{P}_1^* - \bar{P}_2^* = P_{\text{cap}} = P_{\text{cap}}(S_1) \quad (27)$$

where \bar{P}_1^* and \bar{P}_2^* are the intrinsic averaged pressures. P_{cap} also known as macroscopic capillary pressure is assumed to be a function of S_1 (saturation of the nonwetting phase) only. This assumption results from the right-hand side of Eq. (19) which can be interpreted as the rate of production of linear momentum per unit area of the interface (Bear and Bachmat, 1990). This concept introduces the molecular level effects between the two fluids as a force (per unit length) tangent to the interface. At the macroscopic level, we assume that the right-hand side of Eq. (19) can be expressed as a function of the degree of saturation of the nonwetting phase. In a more general level, it will be a function of temperatures and concentrations of chemical compounds in the two fluids. In the literature this function is known as the capillary pressure-saturation relation. From now on fluid phase 1 will be considered as the nonwetting phase and fluid phase 2 as the wetting phase. S_1 is related to the volume fractions by

$$S_i = \frac{\alpha_i}{1 - \alpha_s} \quad i = 1, 2. \quad (28)$$

Then $S_1 + S_2 = 1$. Noting that fluid pressures we work with are the incremental pressures, as a first-order approximation we can write

$$\bar{P}_1 - \bar{P}_2 = \frac{dP_{\text{cap}}}{dS_1} \Delta S_1, \quad (29)$$

provided that change in saturation, ΔS_1 is small.

Deformation of a porous medium can be investigated by independently considering the volume change behavior (non-

zero trace) and shear deformation behavior (zero trace). In the following, we first consider the part of constitutive relations associated with the volume changes. After examining the shear deformations, we combine these two to finalize the macroscopic constitutive relations.

To explore the constitutive relations associated with the volume changes, we start by introducing \bar{P}_j

$$-\alpha_j \bar{P}_j = \frac{1}{3} \text{tr}(\alpha_j \bar{\epsilon}_j) = K_j(\alpha_j \nabla \cdot \bar{u}_j + \Delta \alpha_j) \quad j = s, 1, 2. \quad (30)$$

Equation (30) does not contain any rotational deformations. For an elastic porous medium saturated by a single fluid, we can write (see Appendix A for details)

$$\nabla \cdot \bar{u}_s = -\alpha_s \frac{(\bar{P}_s - \bar{P}_f)}{K_{fr}} - \frac{\bar{P}_f}{K_s} \quad (31)$$

where K_{fr} is defined as the "frame" or "drained" bulk modulus. We assume that in case of two fluids \bar{P}_f is given by

$$\bar{P}_f = S_1 \bar{P}_1 + (1 - S_1) \bar{P}_2. \quad (32)$$

Then, we can rewrite Eq. (31) as

$$\nabla \cdot \bar{u}_s = -\alpha_s \frac{(\bar{P}_s - S_1 \bar{P}_1 - (1 - S_1) \bar{P}_2)}{K_{fr}} - \frac{(S_1 \bar{P}_1 + (1 - S_1) \bar{P}_2)}{K_s} \quad (33)$$

We can express the change in volume fraction of the nonwetting phase from Eq. (31) as

$$\begin{aligned} \Delta \alpha_1 &= \Delta(S_1(1 - \alpha_s)) = S_1(1 - \alpha_s) - S_1^0(1 - \alpha_s^0) \\ &= (1 - \alpha_s^0) \Delta S_1 - S_1^0 \Delta \alpha_s - \Delta \alpha_s \Delta S_1 \\ &\approx (1 - \alpha_s) \Delta S_1 - S_1 \Delta \alpha_s \end{aligned} \quad (34)$$

and the change in volume fraction of the wetting phase as

$$\begin{aligned} \Delta \alpha_2 &= \Delta((1 - S_1)(1 - \alpha_s)) \\ &= (1 - S_1)(1 - \alpha_s) - (1 - S_1^0)(1 - \alpha_s^0) \\ &= -(1 - \alpha_s^0) \Delta S_1 - (1 - S_1^0) \Delta \alpha_s + \Delta \alpha_s \Delta S_1 \\ &\approx -(1 - \alpha_s) \Delta S_1 - (1 - S_1) \Delta \alpha_s. \end{aligned} \quad (35)$$

Since we have already assumed that ΔS_1 and $\Delta \alpha_s$ are small, the product of these terms can be neglected. Equations (29), (30), and (33) can be rewritten in the matrix form as

$$\begin{bmatrix} 0 & -\frac{dP_{cap}}{dS_1} & 0 & 1 & -1 \\ 0 & 0 & -\frac{\alpha_s}{K_{fr}} & S_1 \left(\frac{\alpha_s}{K_{fr}} - \frac{1}{K_s} \right) & (1 - S_1) \left(\frac{\alpha_s}{K_{fr}} - \frac{1}{K_s} \right) \\ -\frac{1}{\alpha_s} & 0 & -\frac{1}{K_s} & 0 & 0 \\ \frac{1}{1 - \alpha_s} & -\frac{1}{S_1} & 0 & -\frac{1}{K_1} & 0 \\ \frac{1}{1 - \alpha_s} & \frac{1}{1 - S_1} & 0 & 0 & -\frac{1}{K_2} \end{bmatrix} \begin{bmatrix} \Delta \alpha_s \\ \Delta S_1 \\ \bar{P}_s \\ \bar{P}_1 \\ \bar{P}_2 \end{bmatrix} = \begin{bmatrix} 0 \\ \nabla \cdot \bar{u}_s \\ \nabla \cdot \bar{u}_s \\ \nabla \cdot \bar{u}_1 \\ \nabla \cdot \bar{u}_2 \end{bmatrix} \quad (36)$$

Solutions for the unknowns, $\Delta \alpha_s$, ΔS_1 , \bar{P}_s , \bar{P}_1 , and \bar{P}_2 are obtained by inverting the coefficient matrix as

$$\Delta \alpha_s = b_1 \nabla \cdot \bar{u}_s + b_2 \nabla \cdot \bar{u}_1 + b_3 \nabla \cdot \bar{u}_2 \quad (37)$$

$$\Delta S_1 = c_1 \nabla \cdot \bar{u}_s + c_2 \nabla \cdot \bar{u}_1 + c_3 \nabla \cdot \bar{u}_2 \quad (38)$$

$$-\alpha_s \bar{P}_s = a_{11} \nabla \cdot \bar{u}_s + a_{12} \nabla \cdot \bar{u}_1 + a_{13} \nabla \cdot \bar{u}_2 \quad (39)$$

$$-(1 - \alpha_s) S_1 \bar{P}_1 = a_{21} \nabla \cdot \bar{u}_s + a_{22} \nabla \cdot \bar{u}_1 + a_{23} \nabla \cdot \bar{u}_2 \quad (40)$$

$$\begin{aligned} -(1 - \alpha_s)(1 - S_1) \bar{P}_2 \\ = a_{31} \nabla \cdot \bar{u}_s + a_{32} \nabla \cdot \bar{u}_1 + a_{33} \nabla \cdot \bar{u}_2 \end{aligned} \quad (41)$$

where the constants are obtained as

$$b_1 A_3 = -K_s A_1 (1 - \alpha_s) (K_1 (1 - S_1) + A_2 + K_2 S_1);$$

$$b_2 A_3 = A_1 K_1 S_1 (1 - \alpha_s) (A_2 + K_2) \quad (42)$$

$$b_3 A_3 = A_1 K_2 (1 - S_1) (1 - \alpha_s) (A_2 + K_1);$$

$$c_1 A_3 = A_1 K_s S_1 (1 - S_1) (K_2 - K_1) \quad (43)$$

$$c_2 A_3 = -K_1 S_1 (1 - S_1) [-K_s^2 (1 - \alpha_s) + K_2 A_1];$$

$$c_3 A_3 = K_2 S_1 (1 - S_1) [K_s^2 (1 - \alpha_s) + K_1 A_1] \quad (44)$$

$$a_{11} A_3 = K_s [A_1 \alpha_s (K_1 A_2 S_1 + K_2 K_1 + K_2 A_2 (1 - S_1))$$

$$+ K_s K_{fr} (1 - \alpha_s) (K_1 (1 - S_1) + S_1 K_2 + A_2)] \quad (45)$$

$$a_{12} A_3 = K_1 K_s A_1 S_1 (1 - \alpha_s) (A_2 + K_2);$$

$$a_{13} A_3 = K_2 K_s A_1 (1 - S_1) (1 - \alpha_s) (A_2 + K_1) \quad (46)$$

$$a_{21} = a_{12};$$

$$a_{22} A_3 = K_1 S_1^2 (1 - \alpha_s) [K_s^2 (1 - \alpha_s) (K_2 + A_2/S_1)$$

$$+ K_2 A_2 A_1 (1 - S_1)/S_1] \quad (47)$$

$$a_{23} A_3 = -K_1 K_2 S_1 (1 - S_1) (1 - \alpha_s) [-K_s^2 (1 - \alpha_s) + A_2 A_1];$$

$$a_{31} = a_{13} \quad (48)$$

$$a_{32} = a_{23};$$

$$a_{33} A_3 = K_2 (1 - S_1)^2 (1 - \alpha_s) [K_s^2 (1 - \alpha_s)$$

$$\times (K_1 + A_2/(1 - S_1)) + K_1 A_2 A_1 S_1/(1 - S_1)] \quad (49)$$

where

$$A_1 = \alpha_s K_s - K_{fr}; \quad A_2 = \frac{dP_{cap}}{dS_1} S_1 (1 - S_1) \quad (50)$$

$$A_3 = A_1 (K_1 A_2 S_1 + K_1 K_2 + K_2 A_2 (1 - S_1))$$

$$+ K_s^2 (1 - \alpha_s) (K_1 (1 - S_1) + A_2 + K_2 S_1). \quad (51)$$

Our next step is the evaluation of the solid matrix's shear

$$\begin{aligned}\tau_e &= \alpha_s \bar{\tau}_s^D + \alpha_1 \bar{\tau}_1^D + \alpha_2 \bar{\tau}_2^D \\ &\approx \alpha_s \bar{\tau}_s = G_{fr} (\nabla \bar{u}_s + (\nabla \bar{u}_s)^T - \frac{2}{3} \nabla \cdot \bar{u}_s I) \quad (52)\end{aligned}$$

where τ_j^D is the deviatoric stress of phase j . In other words, the fluids are viscous but the mechanical shear response of the porous medium is provided by the solid matrix only. Fluid viscosities will be taken into consideration later when we discuss the momentum transfers between the phases as they contribute the energy losses in the system. We can rewrite the complete constitutive relations by introducing Eq. (52) into Eq. (39) and definitions of incremental stress tensor of phase 1 and phase 2 into Eqs. (40) and (41),

$$\begin{aligned}\langle \tau_s \rangle &= \alpha_s \bar{\tau}_s = (a_{11} \nabla \cdot \bar{u}_s + a_{12} \nabla \cdot \bar{u}_1 + a_{13} \nabla \cdot \bar{u}_2) I \\ &\quad + G_{fr} (\nabla \bar{u}_s + (\nabla \bar{u}_s)^T - \frac{2}{3} \nabla \cdot \bar{u}_s I) \quad (53)\end{aligned}$$

$$\begin{aligned}\langle \tau_1 \rangle &= S_1 (1 - \alpha_s) \bar{\tau}_1 \\ &= (a_{21} \nabla \cdot \bar{u}_s + a_{22} \nabla \cdot \bar{u}_1 + a_{23} \nabla \cdot \bar{u}_2) I \quad (54)\end{aligned}$$

$$\begin{aligned}\langle \tau_2 \rangle &= (1 - S_1) (1 - \alpha_s) \bar{\tau}_2 \\ &= (a_{31} \nabla \cdot \bar{u}_s + a_{32} \nabla \cdot \bar{u}_1 + a_{33} \nabla \cdot \bar{u}_2) I. \quad (55)\end{aligned}$$

As in the case of single phase fluid, the cross terms appearing in the expressions are symmetric, i.e., $a_{ij} = a_{ji}$. Similar conclusions were reached previously by Santos et al. (1990a, 1990b) and Brutsaert (1964) by using energy principles. However, Garg and Nayfeh (1986) noted that cross terms are symmetric only in the absence of capillary effects. These equations can be reduced to a case with a single fluid phase by setting $A_2 = S_1 = 0$. In that case, the definitions of the material constants are identical to those given by Biot and Willis (1957). Usually, bulk modulus of the solid grains is very large in comparison to the frame bulk modulus. Then, coefficients of the macroscopic constitutive relations (Eq. (42)–(49)) take the following simplified forms:

$$b_1 = -\alpha_s; \quad b_2 = b_3 = 0 \quad (56)$$

$$\begin{aligned}c_1 &= \frac{\alpha_s S_1 (1 - S_1) (K_2 - K_1)}{(1 - \alpha_s) (K_1 (1 - S_1) + A_2 + K_2 S_1)}; \\ c_2 &= \frac{K_1 S_1 (1 - S_1)}{K_1 (1 - S_1) + A_2 + K_2 S_1}; \\ c_3 &= \frac{K_2 S_1 (1 - S_1)}{K_1 (1 - S_1) + A_2 + K_2 S_1} \quad (57)\end{aligned}$$

$$\begin{aligned}a_{11} &= K_{fr}; \quad a_{12} = \frac{K_1 \alpha_s S_1 (A_2 + K_2)}{K_1 (1 - S_1) + A_2 + K_2 S_1}; \\ a_{13} &= \frac{K_2 \alpha_s (1 - S_1) (A_2 + K_1)}{K_1 (1 - S_1) + A_2 + K_2 S_1} \quad (58)\end{aligned}$$

$$\begin{aligned}a_{21} &= a_{12}; \quad a_{22} = \frac{K_1 S_1^2 (1 - \alpha_s) (K_2 + A_2 / S_1)}{K_1 (1 - S_1) + A_2 + K_2 S_1}; \\ a_{23} &= \frac{K_1 K_2 S_1 (1 - S_1) (1 - \alpha_s)}{K_1 (1 - S_1) + A_2 + K_2 S_1} \quad (59)\end{aligned}$$

$$\begin{aligned}a_{31} &= a_{13}; \quad a_{32} = a_{23}; \\ a_{33} &= \frac{K_2 (1 - S_1)^2 (1 - \alpha_s) (K_1 + A_2 / (1 - S_1))}{K_1 (1 - S_1) + A_2 + K_2 S_1} \quad (60)\end{aligned}$$

Macroscopic Momentum Balance Equations

Employing the averaging theorems (Eqs. (5)–(7)), the volume average of Eq. (17) is obtained as

$$\begin{aligned}\frac{\partial \langle \rho_j v_j \rangle}{\partial t} + \nabla \cdot (\langle \rho_j v_j v_j \rangle) + \frac{1}{V} \int_{S_{ji}} \rho_j v_j (v_j - u) \cdot n_j dA \\ = \nabla \cdot \langle \tau_j \rangle + \frac{1}{V} \int_{S_{ji}} \tau_j \cdot n_j dA \quad j \neq i, \quad i = s, 1, 2. \quad (61)\end{aligned}$$

The integral on the left-hand side of Eq. (61) vanishes since the velocity of the interface is equal to the velocity of a point at the interface, i.e., no mass exchange between the phases. We assume that the second term on the left-hand side can be neglected under the small deformation assumption. Average velocities and displacements for all phases are related by

$$\begin{aligned}\langle v_j \rangle &= \left\langle \frac{\partial u_j}{\partial t} \right\rangle = \frac{\partial \langle u_j \rangle}{\partial t} - \frac{1}{V} \int_{S_{ji}} u_j v_j \cdot n_j dA \\ j &\neq i, \quad i = s, 1, 2. \quad (62)\end{aligned}$$

Since we are interested in the low frequency wave propagation, i.e., characteristic length of the microscopic scale is smaller than the wavelength, the displacements appearing in the integrand in Eq. (62) can be assumed to be constant. Then, Eq. (62) can be rewritten by employing Eqs. (4) and (9) as

$$\begin{aligned}\langle v_j \rangle &\approx \alpha_j \frac{\partial \bar{u}_j}{\partial t} + \bar{u}_j \frac{\partial \alpha_j}{\partial t} - \frac{\bar{u}_j}{V} \int_{S_{ji}} v_j \cdot n_j dA = \alpha_j \frac{\partial \bar{u}_j}{\partial t} \\ j &\neq i, \quad i = s, 1, 2. \quad (63)\end{aligned}$$

Substitution of Eq. (63) in Eq. (61) and linearization of $\langle \rho_j \rangle$ in the resulting equations yield

$$\begin{aligned}\langle \rho_j \rangle \frac{\partial^2 \bar{u}_j}{\partial t^2} = \nabla \cdot \langle \tau_j \rangle + \frac{1}{V} \int_{S_{ji}} \tau_j \cdot n_j dA \\ j \neq i, \quad i = s, 1, 2. \quad (64)\end{aligned}$$

Momentum Transfer (Interaction Terms)

One of the difficulties in mechanics of porous media is the momentum transfer terms appearing in volume averaged momentum balance equations. Since the integral is over a representative volume of the microstructure, it requires the characterization and solution of the pore-scale equations. This is usually done by assuming a simple periodic microstructure. After solving the pore-scale equations, the solutions are related to the macroscopic variables (Biot, 1956a). A alternative approach is the use of empirical relations. In this study, due to the complexity of the pore-scale problem, we approximate the interaction terms by assuming the validity of Darcy's law. Since the theory is formulated for low frequency wave propagation, the assumption of laminar flow is a reasonable one. Biot (1956a, 1956b) suggests that the laminar flow will break at a critical frequency defined by $f_{cr} = \pi \mu_f / 4 d^2 \rho_f$ where ρ_f , d , μ_f are the density of the fluid, characteristic dimension of the pores and dynamic viscosity, respectively. Critical frequency concept has been used effectively for saturated porous media. For frequencies higher than the critical frequency, Biot (1956b) proposed frequency-dependent viscosity terms. In the presence of a second fluid phase, one can expect to have a lower critical frequency because of various factors. For example, the capillary pressure-saturation relation (Eq. (27)) is obtained under static conditions rather than dynamic conditions. The effect of the frequency on the capillary pressure-saturation curve which is beyond the scope of this paper, needs further study. Hence, we strictly limit our study to low-frequency waves. Boundary conditions at the solid-fluid interfaces given by Eq. (18) imply that

for fluid phase 1

$$\frac{1}{V} \int_{S_{s1}} \tau_s \cdot n_s dA = - \frac{1}{V} \int_{S_{1s}} \tau_1 \cdot n_1 dA, \quad (65)$$

for fluid phase 2

$$\frac{1}{V} \int_{S_{s2}} \tau_s \cdot n_s dA = -\frac{1}{V} \int_{S_{s2}} \tau_2 \cdot n_2 dA. \quad (66)$$

Because of boundary conditions at the fluid-fluid interfaces (Eq. (19)), we can write

$$\frac{1}{V} \int_{S_{12}} \tau_1 \cdot n_1 dA \neq -\frac{1}{V} \int_{S_{21}} \tau_2 \cdot n_2 dA. \quad (67)$$

These terms result in the cross permeabilities known as Yuster effect in the literature (Yuster, 1953; Scott and Rose, 1953). The Yuster effect can be neglected for practical purposes (Bear, 1972). Then, assuming the validity of Darcy's law

$$\frac{1}{V} \int_{S_{s1}} \tau_s \cdot n_s dA = \frac{(1 - \alpha_s)^2 S_1^2 \mu_1}{K k_{r1}} (\bar{v}_1 - \bar{v}_s) \quad (68)$$

$$\frac{1}{V} \int_{S_{s2}} \tau_s \cdot n_s dA = \frac{(1 - \alpha_s)^2 (1 - S_1)^2 \mu_2}{K k_{r2}} (\bar{v}_2 - \bar{v}_s) \quad (69)$$

where K is the intrinsic permeability of the medium and k_{ri} is the relative permeability of phase i . Similar expressions were also used by Garg and Nayfeh (1986) and Santos et al. (1990a, 1990b).

Final Set of Equations

Substitution of the constitutive relations (Eqs. (53)–(55)) and the interaction terms (Eqs. (68)–(69)) in the averaged momentum balance equations (Eq. (64)) yield

$$\langle \rho_s \rangle \frac{\partial^2 \bar{u}_s}{\partial t^2} = \nabla \cdot \left(\left(a_{11} + \frac{G_{fr}}{3} \right) \nabla \cdot \bar{u}_s + a_{12} \nabla \cdot \bar{u}_1 + a_{13} \nabla \cdot \bar{u}_2 \right) + \nabla \cdot (G_{fr} \nabla \bar{u}_s) + C_1 (\bar{v}_1 - \bar{v}_s) + C_2 (\bar{v}_2 - \bar{v}_s) \quad (70)$$

$$\langle \rho_1 \rangle \frac{\partial^2 \bar{u}_1}{\partial t^2} = \nabla \cdot (a_{21} \nabla \cdot \bar{u}_s + a_{22} \nabla \cdot \bar{u}_1 + a_{23} \nabla \cdot \bar{u}_2) - C_1 (\bar{v}_1 - \bar{v}_s) \quad (71)$$

$$\langle \rho_2 \rangle \frac{\partial^2 \bar{u}_2}{\partial t^2} = \nabla \cdot (a_{31} \nabla \cdot \bar{u}_s + a_{32} \nabla \cdot \bar{u}_1 + a_{33} \nabla \cdot \bar{u}_2) - C_2 (\bar{v}_2 - \bar{v}_s) \quad (72)$$

where

$$C_1 = \frac{(1 - \alpha_s)^2 S_1^2 \mu_1}{K k_{r1}} \quad (73)$$

$$C_2 = \frac{(1 - \alpha_s)^2 (1 - S_1)^2 \mu_2}{K k_{r2}} \quad (74)$$

Equations (70)–(72) are the governing equations for low-frequency wave propagation in a poroelastic medium saturated by two immiscible fluids with unknowns: \bar{u}_s , \bar{u}_1 , and \bar{u}_2 . These equations are hyperbolic with dissipation terms due to the momentum transfer. Equations (70) and (72) reduce to Biot's (1956a) equations for a single fluid phase by setting S_1 and A_2 to zero.

The formulation for the compressional waves is obtained by applying the divergence operator to Eqs. (70)–(72)

$$\langle \rho_s \rangle \frac{\partial^2 \epsilon_s}{\partial t^2} = a_{11}^* \nabla^2 \epsilon_s + a_{12} \nabla^2 \epsilon_1 + a_{13} \nabla^2 \epsilon_2 + C_1 \left(\frac{\partial \epsilon_1}{\partial t} - \frac{\partial \epsilon_s}{\partial t} \right) + C_2 \left(\frac{\partial \epsilon_2}{\partial t} - \frac{\partial \epsilon_s}{\partial t} \right) \quad (75)$$

$$\langle \rho_1 \rangle \frac{\partial^2 \epsilon_1}{\partial t^2} = a_{21} \nabla^2 \epsilon_s + a_{22} \nabla^2 \epsilon_1 + a_{23} \nabla^2 \epsilon_2 - C_1 \left(\frac{\partial \epsilon_1}{\partial t} - \frac{\partial \epsilon_s}{\partial t} \right) \quad (76)$$

$$\langle \rho_2 \rangle \frac{\partial^2 \epsilon_2}{\partial t^2} = a_{31} \nabla^2 \epsilon_s + a_{32} \nabla^2 \epsilon_1 + a_{33} \nabla^2 \epsilon_2 - C_2 \left(\frac{\partial \epsilon_2}{\partial t} - \frac{\partial \epsilon_s}{\partial t} \right) \quad (77)$$

where $\epsilon_j = \nabla \cdot \bar{u}_j$ and $a_{11}^* = a_{11} + 4G_{fr}/3$. The dilatational plane harmonic waves propagating along the z -direction are given by

$$\epsilon_j = B_j e^{i(\xi z - \omega t)} \quad (78)$$

where B_j is the wave amplitude, ξ is the wave number, ω is the frequency, and i is the imaginary number. In general, ξ is a complex number. For convenience we rewrite Eq. (78) as

$$\epsilon_j = B_j e^{-\xi_i z} e^{i(\xi_r z - \omega t)} \quad (79)$$

where ξ_i and ξ_r are the imaginary and real parts of ξ , respectively. The imaginary part of the wave number ξ_i , is usually called the attenuation coefficient. The phase velocity is defined as $c = \omega/\xi_r$. Substitution of Eq. (78) in Eqs. (75)–(77) yields

$$\begin{bmatrix} -\omega^2 & 0 & 0 \\ 0 & \langle \rho_1 \rangle & 0 \\ 0 & 0 & \langle \rho_2 \rangle \end{bmatrix} + \xi^2 \begin{bmatrix} a_{11}^* & a_{12} & a_{13} \\ a_{21} & a_{22} & a_{23} \\ a_{31} & a_{32} & a_{33} \end{bmatrix} + i\omega \begin{bmatrix} -C_1 - C_2 & C_1 & C_2 \\ C_1 & -C_1 & 0 \\ C_2 & 0 & -C_2 \end{bmatrix} \begin{bmatrix} B_s \\ B_1 \\ B_2 \end{bmatrix} = \begin{bmatrix} 0 \\ 0 \\ 0 \end{bmatrix} \quad (80)$$

which implies that for nonzero solutions the determinant of the coefficient matrix must be equal to zero. This equation is known as the dispersion equation in wave mechanics. The determinant can be expressed as

$$Z_1 X^3 + Z_2 X^2 + Z_3 X + Z_4 = 0 \quad (81)$$

where $X = \omega^2/\xi^2$. The complex coefficients of Eq. (81) are given by

$$Z_1 = \frac{C_1 C_2 (\langle \rho_1 \rangle + \langle \rho_2 \rangle + \langle \rho_s \rangle) - \langle \rho_s \rangle \langle \rho_1 \rangle \langle \rho_2 \rangle \omega^2}{\omega^2} - i \frac{C_2 \langle \rho_1 \rangle (\langle \rho_2 \rangle + \langle \rho_s \rangle) + C_1 \langle \rho_2 \rangle (\langle \rho_1 \rangle + \langle \rho_s \rangle)}{\omega} \quad (82)$$

$$Z_2 = -\frac{a_{11}^* (C_1 C_2 - \langle \rho_1 \rangle \langle \rho_2 \rangle \omega^2) + 2C_1 C_2 (a_{12} + a_{13} + a_{23}) + a_{22} (C_1 C_2 - \langle \rho_s \rangle \langle \rho_2 \rangle \omega^2) + a_{33} (C_1 C_2 - \langle \rho_s \rangle \langle \rho_1 \rangle \omega^2)}{\omega^2} - i \frac{a_{11} (C_2 \rho_1 + C_1 \rho_2) + 2a_{12} C_1 \rho_2 + 2a_{13} C_2 \rho_1 + a_{22} (C_2 (\rho_2 + \rho_s) + C_1 \rho_2) + a_{33} (C_2 \rho_1 + C_1 (\rho_s + \rho_1))}{\omega} \quad (83)$$

$$Z_3 = -a_{11}^* (a_{22} \langle \rho_2 \rangle + a_{33} \langle \rho_1 \rangle) - a_{12}^2 \langle \rho_2 \rangle - a_{13}^2 \langle \rho_1 \rangle + \langle \rho_s \rangle (a_{22} a_{33} - a_{23}^2) - i \frac{a_{11} (a_{22} C_2 + a_{33} C_1) - a_{12}^2 C_2 - 2a_{12} (a_{23} C_2 - a_{33} C_1) - a_{13}^2 C_1 + 2a_{13} (a_{22} C_2 - a_{23} C_1) + (C_1 + C_2) (a_{22} a_{33} - a_{23}^2)}{\omega} \quad (84)$$

$$Z_4 = a_{11}^*(a_{22}a_{33} - a_{23}^2) - a_{12}^2a_{33} + a_{13}(2a_{12}a_{23} - a_{13}a_{22}) \quad (85)$$

In general, for a given frequency ω , the polynomial in Eq. (81) has three complex roots and the wave number ξ , has six roots. However, only three of these roots are physically possible, i.e., the amplitudes of waves should decrease so that the imaginary part of ξ must be greater than zero. This implies the existence of three compressional waves in a poroelastic medium saturated by two immiscible fluids. When we set $A_2 = 0$, we find $Z_4 = 0$, which indicates that one of the compressional waves is associated with the pressure difference between two fluid phases, i.e., capillary pressure.

The formulation for the rotational waves is obtained by applying the curl operator to Eqs. (70)–(72)

$$\langle \rho_s \rangle \frac{\partial^2 \Omega_s}{\partial t^2} = G_{fr} \nabla^2 \Omega_s + C_1 \left(\frac{\partial \Omega_l}{\partial t} - \frac{\partial \Omega_s}{\partial t} \right) + C_2 \left(\frac{\partial \Omega_2}{\partial t} - \frac{\partial \Omega_s}{\partial t} \right) \quad (86)$$

$$\langle \rho_1 \rangle \frac{\partial^2 \Omega_l}{\partial t^2} = -C_1 \left(\frac{\partial \Omega_l}{\partial t} - \frac{\partial \Omega_s}{\partial t} \right) \quad (87)$$

$$\langle \rho_2 \rangle \frac{\partial^2 \Omega_2}{\partial t^2} = -C_2 \left(\frac{\partial \Omega_2}{\partial t} - \frac{\partial \Omega_s}{\partial t} \right) \quad (88)$$

where $\Omega_j = \nabla \times \vec{u}_j$. The substitution of harmonic waves as given by Eq. (78) in Eqs. (86)–(88) yields

$$\left\{ -\omega^2 \begin{bmatrix} \langle \rho_s \rangle & 0 & 0 \\ 0 & \langle \rho_1 \rangle & 0 \\ 0 & 0 & \langle \rho_2 \rangle \end{bmatrix} + \xi^2 \begin{bmatrix} G_{fr} & 0 & 0 \\ 0 & 0 & 0 \\ 0 & 0 & 0 \end{bmatrix} + i\omega \begin{bmatrix} -C_1 - C_2 & C_1 & C_2 \\ C_1 & -C_1 & 0 \\ C_2 & 0 & -C_2 \end{bmatrix} \right\} \begin{bmatrix} B_s \\ B_l \\ B_2 \end{bmatrix} = \begin{bmatrix} 0 \\ 0 \\ 0 \end{bmatrix} \quad (89)$$

The dispersion equation is the determinant of the coefficient matrix and is in the form of

$$X^2(Z_1 X + Z_2) = 0 \quad (90)$$

where

$$Z_1 = \frac{C_1 C_2 (\langle \rho_1 \rangle + \langle \rho_2 \rangle + \langle \rho_s \rangle) - \langle \rho_s \rangle \langle \rho_1 \rangle \langle \rho_2 \rangle \omega^2}{\omega^2} - i \frac{C_2 \langle \rho_1 \rangle (\langle \rho_2 \rangle + \langle \rho_s \rangle) + C_1 \langle \rho_2 \rangle (\langle \rho_1 \rangle + \langle \rho_s \rangle)}{\omega} \quad (91)$$

$$Z_2 = - \frac{G_{fr} (C_1 C_2 - \langle \rho_1 \rangle \langle \rho_2 \rangle \omega^2)}{\omega^2} + i \frac{G_{fr} (C_2 \langle \rho_1 \rangle + C_1 \langle \rho_2 \rangle)}{\omega} \quad (92)$$

Equation (90) shows the existence of a single rotational wave in porous medium saturated by two immiscible fluids.

Conclusions

A dynamic theory of a linearly elastic, isotropic porous medium saturated by two immiscible Newtonian fluids is presented. The macroscopic equations are obtained by volume averaging the microscale mass and momentum balance equations, and constitutive relations and assuming small deformations. In the microscale, the grains are assumed to be linearly elastic and the fluids are Newtonian. Two macroscopic parameters, i.e., frame bulk modulus and frame shear modulus are introduced

to finalize the macroscopic constitutive relations. The capillary pressure effects are taken into account by assuming the validity of the relationship between capillary pressure and saturation. The coefficients of macroscopic constitutive relations are expressed in terms of measurable quantities in a novel way. As in the saturated porous media, we show the existence of symmetry in the macroscopic constitutive relations. Momentum transfer terms are expressed in terms of intrinsic and relative permeabilities assuming the validity of Darcy's law. Since Darcy's law is valid for laminar flow, the theory is limited to low frequency waves. Another constitutive relation limited to low frequencies is the capillary pressure-saturation relation. The effect of the frequency on the capillary pressure-saturation curve needs further study. The final set of equations has an hyperbolic behavior with dissipation due to momentum transfer. We find three compressional and one rotational waves in an infinite porous medium. The third compressional wave arises due to the presence of a second fluid phase. We show that the third compressional wave is associated with the pressure difference between the fluids and dependent on the slope of the capillary pressure-saturation relation. A further study of the subject by the authors (Tuncay and Corapcioglu, 1996) shows that an analysis of governing equations reveals significant reductions in phase velocities of the first and second compressional waves in the presence of a gas phase. The third compressional wave has the lowest phase velocity and the highest attenuation coefficient which make it very difficult to observe, if not impossible.

References

- Anderson, T. B., and Jackson, R., 1967, "A fluid mechanical description of fluidized beds," *I&EC Fundamentals*, Vol. 6, pp. 527–539.
- Auriault, J. L., 1980, "Dynamic behaviour of a porous medium saturated by a Newtonian fluid," *Int. J. Eng. Sci.*, Vol. 18, pp. 775–785.
- Auriault, J. L., Borne, L., and Chambon, R., 1985, "Dynamics of porous saturated media: Checking of the generalized law of Darcy," *J. Acoust. Soc. Am.*, Vol. 77, pp. 1641–1650.
- Bear, J., 1972, *Dynamics of Fluids in Porous Media*, Elsevier, New York.
- Bear, J., and Bachmat, Y., 1990, *Introduction to Modeling of Transport Phenomena in Porous Media*, Kluwer, Dordrecht, The Netherlands.
- Bear, J., Corapcioglu, M. Y., and Balakrishna, J., 1984, "Modeling of centrifugal filtration in unsaturated deformable porous media," *Adv. Water Resources*, Vol. 7, pp. 150–167.
- Bedford, A., and Drumheller, D. S., 1983, "Theories of immiscible and structured mixtures," *Int. J. Eng. Sci.*, Vol. 21, pp. 863–960.
- Berryman, J. G., 1980, "Confirmation of Biot's theory," *Appl. Phys. Lett.*, Vol. 37, pp. 382–384.
- Berryman, J. G., 1981, "Elastic wave propagation in fluid-saturated porous media," *J. Acoust. Soc. Am.*, Vol. 69, pp. 416–424.
- Berryman, J. G., 1986, "Effective medium approximation for elastic constants of porous solids with microscopic heterogeneity," *J. Appl. Phys.*, Vol. 59, pp. 1136–1140.
- Biot, M. A., 1941, "General theory of three-dimensional consolidation," *J. Appl. Physics*, Vol. 12, pp. 155–164.
- Biot, M. A., 1956a, "Theory of propagation of elastic wave in a fluid saturated porous solid, I. Low frequency range," *J. Acoust. Soc. Am.*, Vol. 28, pp. 168–178.
- Biot, M. A., 1956b, "Theory of propagation elastic waves in a fluid saturated porous solid, II. Higher frequency range," *J. Acoust. Soc. Am.*, Vol. 28, pp. 169–191.
- Biot, M. A., and Willis, D. G., 1957, "The Elastic Coefficients of the Theory of Consolidation," *ASME JOURNAL OF APPLIED MECHANICS*, Vol. 24, pp. 594–601.
- Bowen, R. M., 1976, "The theory of mixtures," *Continuum Physics*, Vol. 3, A. C. Eringen, ed., Academic Press, New York.
- Bowen, R. M., and Lockett, R. R., 1983, "Inertial effects in poroelasticity," *ASME JOURNAL OF APPLIED MECHANICS*, Vol. 50, pp. 334–342.
- Brutsaert, W., 1964, "The propagation of elastic waves in unconsolidated unsaturated granular mediums," *J. Geophys. Res.*, Vol. 69, pp. 243–257.
- Brutsaert, W., and Luthin, J. N., 1964, "The velocity of sound in soils near the surface as a function of the moisture content," *J. Geophys. Res.*, Vol. 69, pp. 643–652.
- Burridge, R., and Keller, J. B., 1981, "Poroelasticity equations derived from microstructure," *J. Acoust. Soc. Am.*, Vol. 70, pp. 1140–1146.
- Corapcioglu, M. Y., and Tuncay, K., 1996, "Propagation of waves in porous media," *Advances in Porous Media*, Vol. 3, M. Y. Corapcioglu, ed., Elsevier, Amsterdam, pp. 361–440.
- de la Cruz, V., and Spanos, T. J. T., 1985, "Seismic wave propagation in a porous medium," *Geophysics*, Vol. 50, pp. 1556–1565.

de la Cruz, V., and Spanos, T. J. T., 1989, "Thermomechanical coupling during seismic wave propagation in a porous medium," *J. Geophysical Res.*, Vol. 94, pp. 637–642.

Domenico, S. N., 1974, "Effects of water saturation of sand reservoirs encased in shales," *Geophysics*, Vol. 29, pp. 759–769.

Drumheller, D. J., 1978, "Theoretical treatment of a porous solid using a mixture theory," *Int. J. Solids and Structures*, Vol. 14, pp. 441–456.

Fatt, I., 1959, "The Biot-Willis Elastic Coefficients for a Sandstone," *ASME JOURNAL OF APPLIED MECHANICS*, Vol. 26, pp. 296–297.

Garg, S. K., 1971, "Wave propagation effects in a fluid saturated porous solid," *J. Geophys. Res.*, Vol. 76, pp. 7947–7962.

Garg, S. K., Brownell, C. H., Pritchett, and Herrman, R. G., 1975, "Shock wave propagation in fluid saturated porous media," *J. Appl. Phys.*, Vol. 46, pp. 702–713.

Garg, S. K., and Nayfeh, A. H., 1986, "Compressional wave propagation in liquid and/or gas saturated elastic porous media," *J. Appl. Phys.*, Vol. 60, pp. 3045–3055.

Geertsma, J., and Smith, D. C., 1961, "Some aspects of elastic wave propagation in fluid saturated porous solids," *Geophysics*, Vol. 26, pp. 160–180.

Jenkins, J. T., 1980, "Static Equilibrium of a Fluid-Saturated Porous Solid," *ASME JOURNAL OF APPLIED MECHANICS*, Vol. 47, pp. 493–495.

Katsube, N., and Carrol, M. M., 1987, "The Modified Mixture Theory for Fluid-Filled Porous Materials: Theory," *ASME JOURNAL OF APPLIED MECHANICS*, Vol. 54, pp. 35–40.

Keller, J. B., 1977, "Effective behavior of heterogeneous media," *Statistical Mechanics and Statistical Methods in Theory and Applications*, U. Landman, ed., Plenum, New York, pp. 631–644.

Levy, T., 1979, "Propagation of waves in a fluid-saturated porous elastic solid," *Int. J. Eng. Sci.*, Vol. 17, pp. 1005–1014.

Marle, C. M., 1967, "Ecoulements monophasiques en milieu poreux," *Rev. Inst. Francais du Pétrole*, Vol. 22, pp. 1471–1509.

Mochizuki, S., 1982, "Attenuation in partially saturated rocks," *J. Geophysical Res.*, Vol. 87, pp. 8598–8604.

Murphy, W. F., 1982, "Effects of partial water saturation on attenuation in Massillon sandstone and Vycor porous glass," *J. Acoust. Soc. Am.*, Vol. 71, pp. 1458–1468.

Plona, T. J., 1980, "Observation of a second bulk compressional wave in a porous medium at ultrasonic frequencies," *App. Phys. Lett.*, Vol. 36, pp. 259–261.

Pride, S. R., Gangi, A. F., and Morgan, F. D., 1992, "Deriving the equations of motion for isotropic media," *J. Acoust. Soc. Am.*, Vol. 92, pp. 3278–3290.

Prevost, J. H., 1980, "Mechanics of continuous porous media," *Int. J. Eng. Sci.*, Vol. 18, pp. 787–800.

Sanchez-Palencia, E., 1980, *Non-Homogeneous Media and Vibration Theory*, Springer-Verlag, New York.

Santos, J. E., and Corbero, J. M., and Douglas, J., 1990a, "Static and dynamic behaviour of a porous solid," *J. Acoust. Soc. Am.*, Vol. 87, pp. 1428–1438.

Santos, J. E., Douglas, J., Corbero, J. M., and Lovera, O. M., 1990b, "A model for wave propagation in a porous medium saturated by a two-phase fluid," *J. Acoust. Soc. Am.*, Vol. 87, pp. 1439–1448.

Scott, P. H., and Rose, W., 1953, "An explanation of the Yuster effect," *J. Petr. Technol.*, Vol. 5, pp. 19–20.

Slattery, J. C., 1967, "Flow of viscoelastic fluids through porous media," *AIChE J.*, Vol. 13, pp. 1066–1071.

Slattery, J. C., 1968, "Multiphase viscoelastic fluids through porous media," *AIChE J.*, Vol. 14, pp. 50–56.

Slattery, J. C., 1981, *Momentum, Energy and Mass Transfer in Continua*, Krieger, New York.

Tuncay, K., and Corapcioglu, M. Y., 1996, "Body waves in poroelastic media saturated by two immiscible fluids," *J. Geophysical Research-Solid Earth*, Vol. 101, pp. 25,149–25,159.

Whitaker, S., 1967, "Diffusion and dispersion in porous media," *AIChE J.*, Vol. 13, pp. 420–427.

Yuster, S. T., 1953, "Theoretical considerations of multiphase flow in idealized capillary system," *Proc. Third World Petr. Cong.*, The Hague, Vol. 2, pp. 436–445.

Zienkiewicz, O. C., Chang, C. T., and Battess, P., 1980, "Drained, undrained, consolidating, and dynamic behaviour assumptions in soils: Limits of validity," *Geotechnique*, Vol. 30, pp. 385–395.

$\nabla \cdot \bar{u}_s$ when \bar{P}_s and \bar{P}_f are simultaneously present. Superposition is justified by the linearity of the system.

In the first case, we consider a drained porous medium, i.e., $\bar{P}_f = 0$. Introducing the drained bulk modulus of the fractured porous medium K_{fr} , we write

$$-\alpha_s \bar{P}_s = K_{fr} \nabla \cdot \bar{u}_s. \quad (A1)$$

K_{fr} can be evaluated experimentally by testing a drained porous sample.

In the second case, we consider a stress state where $\bar{P}_s = \bar{P}_f$. This case corresponds to a porous medium immersed in a fluid subjected to external pressure. Because of the homogeneity and isotropy of the medium, all volume fractions remain constant and Eq. (30) yields

$$-\bar{P}_s = K_s \nabla \cdot \bar{u}_s. \quad (A2)$$

The stress states can be summarized as

$$\text{Case 1: } \bar{P}_s = P_1 \quad \bar{P}_f = 0$$

$$\text{Case 2: } \bar{P}_s = P_2 \quad \bar{P}_f = P_2 \quad (A3)$$

where subscripts 1 and 2 refer to case 1 and case 2, respectively. Since we seek expressions when \bar{P}_s and \bar{P}_f are simultaneously present in the system, P_1 and P_2 are obtained as

$$P_1 = \bar{P}_s - \bar{P}_f; \quad P_2 = \bar{P}_f. \quad (A4)$$

The dilatation of the solid matrix is obtained by superposing Eqs. (A1) and (A2) as

$$\nabla \cdot \bar{u}_s = -\frac{\alpha_s P_1}{K_{fr}} - \frac{P_2}{K_s}. \quad (A5)$$

Substitution of Eq. (A4) in (A5) yields

$$\nabla \cdot \bar{u}_s = -\alpha_s \frac{(\bar{P}_s - \bar{P}_f)}{K_{fr}} - \frac{\bar{P}_f}{K_s}. \quad (A6)$$

The total stress is the sum of the volume averaged stresses of individual phases

$$\langle \tau_i \rangle = \alpha_s \bar{\tau}_s + \alpha_f \bar{\tau}_f. \quad (A7)$$

Employing the definition of total stress given in Eq. (A7), Eq. (A6) can be rewritten as

$$\frac{\text{trace}(\langle \tau_i \rangle)}{3} + \beta \bar{P}_f = K_{fr} \nabla \cdot \bar{u}_s \quad (A8)$$

where

$$\beta = 1 - \frac{K_{fr}}{K_s}. \quad (A9)$$

We recall that K_{fr} is the drained bulk modulus of the porous medium. Thus, we can write the following equation for a drained porous medium:

$$\frac{\text{trace}(\langle \tau_i \rangle)}{3} = K_{fr} \nabla \cdot \bar{u}_s. \quad (A10)$$

Comparing (A8) and (A10), we conclude that the effective stress is given by

$$\frac{\text{trace}(\langle \tau_{\text{eff}} \rangle)}{3} = \frac{\text{trace}(\langle \tau_i \rangle)}{3} + \beta \bar{P}_f. \quad (A11)$$

Equation (A11) is referred as the effective stress principle for saturated porous media in literature (Biot and Willis, 1957; Nur and Byerle, 1971). Hence, Eq. (A6) (Eq. (31) in the text) is an alternative form of the effective stress principle.

APPENDIX A

Effective Stress Expression

In this Appendix, we analyze two different stress state conditions individually to incorporate \bar{P}_s and \bar{P}_f in the effective stress expression (Eq. (31)). In each of these cases, we obtain an expression for the dilatation of the solid matrix $\nabla \cdot \bar{u}_s$ by introducing macroscopic material coefficients when necessary. Then we will superpose these expressions to obtain a relation for

Generalized Cross-Correlation Functions for Engineering Applications, Part I: Basic Theory

M. R. Belmont

School of Engineering,
University of Exeter,
Harrison Engineering Building,
North Park Road,
Exeter EX4 4QF, UK

A. J. Hotchkiss

Sun Electric Europe Research.

Traditional cross-correlation considers situations where two functions or data sets are linked by a constant shift either in time or space. Correlation provides estimates of such shifts even in the presence of considerable noise corruption. This makes the technique valuable in applications like sonar, displacement or velocity determination and pattern recognition. When regions are decomposed into patches in applications such as Particle Image Velocimetry it also allows estimates to be made of whole displacement/flow fields. The fundamental problem with traditional correlation is that patch size and hence statistical reliability must be compromised with resolution. This article develops a natural generalization of cross-correlation which removes the need for such compromises by replacing the constant shift with a function of time or space. This permits correlation to be applied globally to a whole domain retaining any long-range coherences present and dramatically improves statistical reliability by using all the data present in the domain for each estimate.

1 Introduction

The cross-correlation of two function or data sets f_1 and f_2 (Weiner, 1949, 1964) is a very common tool in applications as diverse as sonar, flow determination, and pattern recognition in badly corrupted data (Trahey et al., 1969; Coupland and Halliwell, 1992; Richards and Roberts, 1971; Lee, 1960; Matic et al., 1991; Berryman and Blair, 1986; Dejong et al., 1991; Gonzalez and Woods, 1992). Conventional cross-correlation typically applies to situations where the quantities of interest f_1 and f_2 are related by a simple constant shift τ :

$$f_2(\xi) = f_1(\xi + \tau) \quad (1)$$

and the aim is to obtain a statistically reliable estimate of what will be termed here the transformation parameter τ . In time series work ξ is the time t and τ a time delay while in spatial applications ξ and τ define N dimensional displacement vectors, rotations, or some combination of these (Gonzalez and Woods, 1992; Kamachi, 1989).

For applications like particle image velocimetry (Willert and Gharib, 1991; Utami et al., 1991; Adrian, 1986), where a whole flow field is characterized, cellular correlation has been developed (Kamachi, 1989; Leese et al., 1971; Ninnis et al., 1986). The displacement/flow field is made visible in some way with f_1 and f_2 being consecutive images of the displacement/flow. The images are segmented into patches and cross-correlation is then applied essentially to each patch in turn to determine an average displacement/flow velocity for each such cell.

The main problem with this approach is that increasing spatial resolution means reducing the patch size. As typical applications involve digitized noise corrupted data this reduces the information available in each patch for correlation and thus degrades

the reliability of the estimates. If the noise is Gaussian variance of the sample estimate is inversely proportional to patch size. Furthermore, treating each cell independently loses the information theoretic advantages stemming from intercellular coherence in the displacement/flow field. These problems could be avoided if cross-correlation could be generalized to allow spatial or temporal variation of the shift τ and the present article is concerned with developing such a Generalized Cross-Correlation (denoted as GC-C).

The range of uses of conventional cross-correlation extends far beyond the description of displacement/flow problems cited here in both practical and analytical areas, and consequently the scope of GC-C is expected to be even wider.

The treatment here in Part I is in terms of continuous variables while issues associated with discretisation are addressed in the companion work Part II, Belmont et al. (1997).

2 The Properties Required of a Cross-Correlation Function

The first step in developing the GC-C is to specify those features which a cross-correlation function of any kind should exhibit. These are natural extensions of the characteristics exhibited by conventional cross-correlation (Weiner, 1949, 1964):

1 Cross-correlation should operate upon a pair of functions, or data sets, (in its discrete form), denoted as f_1 and f_2 .

2 If f_1 and f_2 are connected by some transformation of their independent variables, then the cross-correlation function should exhibit an absolute maximum when a matching transformation is induced by cross-correlation processes. A corollary of this is that the location of the maximum should allow the computation of any parameters associated with the transformation, e.g., τ in Eq. (1).

3 The cross-correlation function should approach the absolute maximum smoothly.

4 Points 2 and 3 should hold even if f_1 and f_2 are contaminated by extraneous additive components that are uncorrelated between f_1 and f_2 .

Contributed by the Applied Mechanics Division of THE AMERICAN SOCIETY OF MECHANICAL ENGINEERS for publication in the ASME JOURNAL OF APPLIED MECHANICS.

Discussion on the paper should be addressed to the Technical Editor, Professor Lewis T. Wheeler, Department of Mechanical Engineering, University of Houston, Houston, TX 77204-4792, and will be accepted until four months after final publication of the paper itself in the ASME JOURNAL OF APPLIED MECHANICS.

Manuscript received by the ASME Applied Mechanics Division, Sept. 27, 1995; final revision, Oct. 28, 1996. Associate Technical Editor: S. Lichter.

3 A Generalized Cross-Correlation Function

3.1 Parameterizing the Shift Function. To be useful it is preferable that the variable shift should be generated from a parameterized set of known functions, then determining the shift is achieved by estimating the so-called transformation parameters. Consequently the GC-C function must contain correlation parameters that, in effect, are varied to match the transformation parameters.

Such a generalized cross-correlation function of m correlation parameters, $\mu_1 \dots \mu_m$, derived from two multidimensional functions f_1 and f_2 will be denoted as $K_{1,2}(\mu_1 \dots \mu_m)$. The development of such functions begins with a consideration of the simplest case denoted as $K_{1,2}(\mu)$, i.e., where the shift function depends upon only the single parameter μ and the data functions $f_1(\zeta)$ and $f_2(\zeta)$ are one-dimensional. This means that $f_1(\zeta)$ and $f_2(\zeta)$ are related by

$$f_2(\zeta) = f_1(\zeta + S\{\zeta, \mu_0\}) \quad (2)$$

where the variable shift function $S\{\zeta, \mu_0\}$ is a member of the family of functions, $S\{\zeta, \mu\}$, that are continuous over Γ in both ζ and μ up to their second derivatives.

3.2 The Approach Used to Develop GC-C. GC-C will be developed via an extension of the technique used by Wiener to prove that a conventional correlation function exhibits a smooth absolute maximum (Weiner, 1949, 1964). A special case of this treatment has been employed in the development of the Dilation Correlation Function (Belmont, 1990; Belmont et al., 1991), which is related to Wavelets and Melin transforms and measures stretching transformations. The Dilation Correlation has been used to investigate expansion effects in combustion gases (Belmont et al., 1991).

The present method establishes an inequality, whose LHS is positive and is independent of the correlation parameter μ , and also reduces to an equality when the correlation parameter μ equals the transformation parameter μ_0 . The RHS side of this inequality serves to define the GC-C function. Such an inequality is¹

$$\int_{\Gamma} \{f_1(\zeta + S\{\zeta, \mu\})R(\zeta, \mu) - W(\zeta, \mu)f_2(\zeta)\}^2 d\zeta \geq 0 \quad (3)$$

where now R and W are as yet unassigned.

Expanding (3) produces

$$\begin{aligned} & \int_{\Gamma} f_1(\zeta + S\{\zeta, \mu\})^2 R(\zeta, \mu)^2 d\zeta \\ & + \int_{\Gamma} f_2(\zeta)^2 W(\zeta, \mu)^2 d\zeta \\ & \geq 2 \int_{\Gamma} f_1(\zeta + S\{\zeta, \mu\})f_2(\zeta)R(\zeta, \mu)W(\zeta, \mu) d\zeta. \end{aligned} \quad (4)$$

$R(\zeta, \mu)$ and $W(\zeta, \mu)$ must now be chosen so that the LHS is independent μ and exhibits an absolute maximum when $\mu = \mu_0$.

3.3 Assignment Options for R and W . The fact that R and W should remove the dependence of the LHS in inequality (4) on μ and thus on the form of $S(\zeta, \mu)$, suggests that R and W are acting as Jacobians of the transformations. Recalling conventional cross-correlation implies, if possible, they should

map the LHS integrals into the form $\int_{\Gamma+S(\Gamma, \mu)} f_1 \text{ or } 2(u)^2 du$. These factors suggest

$$R(\zeta, \mu) = \sqrt{1 + \frac{\partial S\{\zeta, \mu\}}{\partial \zeta}} \quad (5)$$

and

$$W(\zeta, \mu) = R(\zeta, \mu).$$

Hence (12) becomes

$$\begin{aligned} & \int_{\Gamma} f_1(\zeta + S\{\zeta, \mu\})^2 \left(1 + \frac{\partial S\{\zeta, \mu\}}{\partial \zeta}\right) d\zeta \\ & + \int_{\Gamma} f_2(\zeta)^2 \left(1 + \frac{\partial S\{\zeta, \mu\}}{\partial \zeta}\right) d\zeta \\ & \geq 2 \int_{\Gamma} f_1(\zeta + S\{\zeta, \mu\})f_2(\zeta) \left(1 + \frac{\partial S\{\zeta, \mu\}}{\partial \zeta}\right) d\zeta. \end{aligned} \quad (6)$$

The first LHS term is independent of μ , provided

(A) $f_1(\zeta + S\{\zeta, \mu\})$ is square integrable over Γ and

(B) $f_1(\zeta + S\{\zeta, \mu\})$ is zero outside Γ .

Condition (A) and a special case of (B) also apply to conventional cross-correlation. Unfortunately, the second LHS term in (6) varies with μ . One way to remove this dependence is to reassign W as

$$W(\zeta, \mu_0) = \sqrt{1 + \frac{\partial S\{\zeta, \mu_0\}}{\partial \zeta}}. \quad (7)$$

This means that any GC-C definition will explicitly contain the transformation parameter μ_0 . As a major application of GC-C is the determination of μ_0 such an assignment for W is generally unrealistic. This option is viable for certain analytic approximations taken at the correlation maximum akin to the perturbation method described in Section 7. However, as the basis for a general definition, the explicit presence of μ_0 is unacceptable.

An alternative is to simply take the second LHS term over to the RHS then (6) becomes

$$\begin{aligned} & \int_{\Gamma} f_1(\zeta + S\{\zeta, \mu\})^2 \left(1 + \frac{\partial S\{\zeta, \mu\}}{\partial \zeta}\right) d\zeta \\ & \geq 2 \int_{\Gamma} f_1(\zeta + S\{\zeta, \mu\})f_2(\zeta) \left(1 + \frac{\partial S\{\zeta, \mu\}}{\partial \zeta}\right) d\zeta \\ & \quad - \int_{\Gamma} f_2(\zeta)^2 \left(1 + \frac{\partial S\{\zeta, \mu\}}{\partial \zeta}\right) d\zeta. \end{aligned} \quad (8)$$

The inequality now exhibits all the desired features and thus the RHS provides the definition for GC-C:

$$\begin{aligned} K_{1,2}(\mu) = & 2 \int_{\Gamma} f_1(\zeta + S\{\zeta, \mu\})f_2(\zeta) \left(1 + \frac{\partial S\{\zeta, \mu\}}{\partial \zeta}\right) d\zeta \\ & - \int_{\Gamma} f_2(\zeta)^2 \left(1 + \frac{\partial S\{\zeta, \mu\}}{\partial \zeta}\right) d\zeta. \end{aligned} \quad (9)$$

4 Multidimensional Multiparameter Form

The extension to a multiparameter shift $S(\zeta, \mu_{1,0} \dots \mu_{m,0})$ is immediate, i.e.,

¹ The present treatment concerns real functions, to extend the result to complex quantities a conjugate product replaces the squaring operation.

$$\begin{aligned}
K_{1,2}(\mu_1 \dots \mu_m) &= 2 \int_{\Gamma} f_1(\zeta + S\{\zeta, \mu_1 \dots \mu_m\}) f_2(\zeta) \\
&\times \left(1 + \frac{\partial S\{\zeta, \mu_1 \dots \mu_m\}}{\partial \zeta} \right) d\zeta \\
&- \int_{\Gamma} f_2(\zeta)^2 \left(1 + \frac{\partial S\{\zeta, \mu_1 \dots \mu_m\}}{\partial \zeta} \right) d\zeta. \quad (10)
\end{aligned}$$

Using the analysis in Section 3 shows that $K_{1,2}(\mu_1 \dots \mu_m)$ satisfies the requirements of a cross-correlation function.

Further generalization of Eq. (10) to accommodate multidimensional functions $f_1(\zeta)$ and $f_2(\zeta)$ is almost as immediate. It is achieved by recalling that R^2 and W^2 behave as Jacobians J_R and J_W in the LHS integrals.

4.1 Multidimensional form of J . In the one-dimensional case the Jacobian is simply $(1 + \partial S\{\zeta, \mu\}/\partial \zeta)$; however, in n dimensions it becomes the much more complicated determinant

$$J = \begin{vmatrix} \frac{\partial \beta_1}{\partial \zeta_1} & \dots & \frac{\partial \beta_1}{\partial \zeta_n} \\ \vdots & \ddots & \vdots \\ \frac{\partial \beta_n}{\partial \zeta_1} & \dots & \frac{\partial \beta_n}{\partial \zeta_n} \end{vmatrix} \quad (11)$$

which defines a transformation between the variables $\zeta_1 \dots \zeta_n$ and $\beta_1 \dots \beta_n$. J is conventionally written in the compact form

$$J = \frac{\partial(\beta_1, \dots, \beta_n)}{\partial(\zeta_1, \dots, \zeta_n)}. \quad (12)$$

The variables $\beta_1 \dots \beta_n$ are defined by

$$\beta_i = \zeta_i + S_i\{\zeta, \mu\} \quad (13)$$

where S_i is the i th component of the transformation vector \mathbf{S} and the nomenclature μ is shorthand for the multiparameter set, i.e., μ implies the set μ_1, \dots, μ_m .

Consequently in vector notation the expression for an n dimensional generalized cross-correlation function in m correlation parameters operating on n dimensional functions $f_1(\zeta)$ and $f_2(\zeta)$ takes the form

$$\begin{aligned}
K_{1,2}(\mu) &= 2 \int_{\Gamma_1} \dots \int_{\Gamma_n} f_1(\zeta + \mathbf{S}\{\zeta, \mu\}) f_2(\zeta) J d\zeta_1 \dots d\zeta_n \\
&- \int_{\Gamma_1} \dots \int_{\Gamma_n} f_2^2(\zeta) J d\zeta_1 \dots d\zeta_n \quad (14)
\end{aligned}$$

i.e.,

$$\begin{aligned}
K_{1,2}(\mu) &= 2 \int_{\Gamma_1} \dots \int_{\Gamma_n} f_1(\zeta + \mathbf{S}\{\zeta, \mu\}) f_2(\zeta) \\
&\times \frac{\partial(\zeta_1 + S_1, \dots, \zeta_n + S_n)}{\partial(\zeta_1, \dots, \zeta_n)} d\zeta_1 \dots d\zeta_n \\
&- \int_{\Gamma_1} \dots \int_{\Gamma_n} f_2^2(\zeta) \frac{\partial(\zeta_1 + S_1, \dots, \zeta_n + S_n)}{\partial(\zeta_1, \dots, \zeta_n)} \\
&\times d\zeta_1 \dots d\zeta_n. \quad (15)
\end{aligned}$$

Using the analysis in Section 3 shows this multidimensional multiparameter form satisfies all the requirements of a cross-correlation function.

4.2 Using $|J|$ Rather than J . The discussion of the mapping from ζ to $\zeta + S\{\zeta, \mu\}$ and its generalization in the integrals has been rather informal. In general to effect the required trans-

formation of variables within integrals it is the modulus of J which is needed and thus $|J|$ will be employed subsequently. However, in most anticipated applications of GC-C it is expected that the transformations of interest are unlikely to be severe and thus J has values close to unity. This means $|J| = J$ and the modulus requirement can usually be dropped.

5 Two-Dimensional Case

Due to its practical importance the subsequent analysis will concentrate on the two-dimensional case. In which case Eq. (15) becomes

$$\begin{aligned}
K_{1,2}(\mu) &= 2 \int_{\Gamma_1} \int_{\Gamma_2} f_1(\zeta_1 + S_1\{\zeta_1, \zeta_2, \mu\}, \zeta_2 + S_2\{\zeta_1, \zeta_2, \mu\}) \\
&\times f_2(\zeta_1, \zeta_2) \left| \left(1 + \frac{\partial S_1}{\partial \zeta_1} \right) \left(1 + \frac{\partial S_2}{\partial \zeta_2} \right) - \frac{\partial S_1}{\partial \zeta_2} \frac{\partial S_2}{\partial \zeta_1} \right| d\zeta_1 d\zeta_2 \\
&- \int_{\Gamma_1} \int_{\Gamma_2} f_2^2(\zeta_1, \zeta_2) \left| \left(1 + \frac{\partial S_1}{\partial \zeta_1} \right) \left(1 + \frac{\partial S_2}{\partial \zeta_2} \right) \right. \\
&\quad \left. - \frac{\partial S_1}{\partial \zeta_2} \frac{\partial S_2}{\partial \zeta_1} \right| d\zeta_1 d\zeta_2 \quad (16)
\end{aligned}$$

where $S_1\{\zeta_1, \zeta_2, \mu\}$ and $S_2\{\zeta_1, \zeta_2, \mu\}$ are the ζ_1 and ζ_2 components of the displacement vector \mathbf{S} .

6 Small Change Approximation

For a variety of well-accepted reasons in flow-field determination the velocities should only induce small changes between $f_1(\zeta)$ and $f_2(\zeta)$ (Kamachi, 1989; Willert and Gharib, 1991; Utami, 1991; Adrian, 1986; Leese, 1971; Ninnis et al., 1986). One of the most obvious reasons is simplicity so that to a good approximation $\mathbf{S}(\zeta, \mu_0)$ is proportional to the local velocity $\mathbf{v}(\zeta)$ i.e.,

$$\mathbf{S}(\zeta, \mu_0) \simeq \mathbf{v}(\zeta) \delta t, \quad (17)$$

where the parameter δt is the time between images f_1 and f_2 .

In any computational procedure aimed at determining the components of μ_0 the ranges of the m correlation parameters as represented by the components of μ , must sensibly be chosen so as to reflect those of the transformation parameters, μ_0 . Therefore, unless extremely pathological circumstances prevail $\mathbf{S}(\zeta, \mu)$ will be of the same order as $\mathbf{S}(\zeta, \mu_0)$. Hence not only are $f_1(\zeta)$ and $f_2(\zeta)$ very similar but so are $f_1\{\zeta + \mathbf{S}(\zeta, \mu)\}$ and $f_2(\zeta)$.

This permits a short Taylor's series approximation of $f_1(\zeta + \mathbf{S}(\zeta, \mu))$:

$$\begin{aligned}
f_1(\zeta + \mathbf{S}(\zeta, \mu)) &\simeq f_1(\zeta) + \frac{\partial f_1}{\partial \zeta_1} S_1(\zeta, \mu) + \frac{\partial f_1}{\partial \zeta_2} S_2(\zeta, \mu) \\
&+ \frac{1}{2!} \left\{ \frac{\partial^2 f_1}{\partial \zeta_1^2} S_1^2(\zeta, \mu) + \frac{\partial^2 f_1}{\partial \zeta_2^2} S_2^2(\zeta, \mu) \right. \\
&\quad \left. + 2 \frac{\partial^2 f_1}{\partial \zeta_1 \partial \zeta_2} S_1(\zeta, \mu) S_2(\zeta, \mu) \right\} + O(S^3) \quad (18)
\end{aligned}$$

where $\mathcal{O}(S^3)$ denotes the order of the error.

Using Eq. (18) in Eq. (16) and retaining terms up to quadratic in the S functions or their spatial derivatives produces a second-order² approximation for $K_{1,2}(\boldsymbol{\mu})$. At the maximum of $K_{1,2}(\boldsymbol{\mu})$, i.e., at $K_{1,2}(\boldsymbol{\mu}_0)$, the following system of equations hold:

$$\left. \frac{\partial K_{1,2}(\boldsymbol{\mu})}{\partial \mu_i} \right|_{\mu_{i,0}} = 0 \quad (19)$$

where $1 \leq i \leq m$. This system can be solved for the m values of the parameters $\mu_{i,0}$. As will be shown in Section 8 the equation system defined by (19) is linear in the $\mu_{i,0}$. Determining the $\mu_{i,0}$ by solving such a system of linear equations is clearly much more efficient than performing a computationally expensive and potentially unreliable multiparameter hill-climb maximum search or optimization processes to estimate these parameters by finding the maximum of $K_{1,2}(\boldsymbol{\mu})$. To proceed further it is clearly necessary to define the functional form of $S(\boldsymbol{\zeta}, \boldsymbol{\mu})$.

6.1 Boundary Conditions on $f_i(\boldsymbol{\zeta})$. Conditions (A) and (B) in Section 3.3 imply that certain boundary conditions will apply and possibly restrictions exist on the displacement function $S(\boldsymbol{\zeta}, \boldsymbol{\mu})$. In the small perturbation case on a rectangular domain $[0, L][0, L]$, these issues can be addressed analytically.

After manipulation, including use of Greens Theorem, it can be shown, up to quadratic terms in the Taylor Expansion, that as $S(\boldsymbol{\zeta}, \boldsymbol{\mu}) \rightarrow S(\boldsymbol{\zeta}, \boldsymbol{\mu}_0)$ the $\lim_{\boldsymbol{\mu} \rightarrow \boldsymbol{\mu}_0} K_{1,2}(\boldsymbol{\mu})$ is given by

$$\begin{aligned} K_{1,2}(\boldsymbol{\mu}) \rightarrow & \int_0^L \int_0^L f^2 d\zeta_1 d\zeta_2 \\ & + \oint_C \{ (f^2 S_{1,0} + f f_{\zeta_1} S_{1,0}^2 + 2 f f_{\zeta_2} S_{1,0} S_{2,0}) d\zeta_2 \\ & - (f^2 S_{2,0} + f f_{\zeta_2} S_{2,0}^2) d\zeta_1 \} \\ & + \int_0^L \{ [f S_{1,0} S_{2,0_{\zeta_2}}]_{\zeta_1=0}^{\zeta_1=L} \} d\zeta_2 \\ & - \int_0^L \{ [f S_{1,0} S_{2,0_{\zeta_1}}]_{\zeta_2=0}^{\zeta_2=L} \} d\zeta_1 + \mathcal{O}(S^3) \quad (20) \end{aligned}$$

where C is the boundary contour of the domain and f is equivalent to $f_1(\boldsymbol{\zeta})$. The symbols $S_{1,0}$ and $S_{2,0}$ denote the S values corresponding to $\boldsymbol{\mu} = \boldsymbol{\mu}_0$ and the subscripts, ζ_1 and ζ_2 have the conventional meaning of partial differentiation. Equation (3) reveals the boundary conditions upon the various quantities and their spatial derivatives. As would be expected from the lack of any special distinction between the ζ_1 and ζ_2 -axes, it is also possible to derive an alternate form of Eq. (20) in which the roles of S_1 and S_2 are reversed.

Examination of Eq. (20) and its alternate form shows that conditions (A) and (B) in Section 3.3 are satisfied if any of the following six requirements hold:

$$\lim_{\boldsymbol{\mu} \rightarrow \boldsymbol{\mu}_0} K_{1,2}(\boldsymbol{\mu}) \rightarrow \int_0^L \int_0^L f_1^2(\zeta_1, \zeta_2) d\zeta_1 d\zeta_2.$$

Condition 1. The most important case for applications is that data function, $f_1(\boldsymbol{\zeta})$, is zero on the boundary. The ability to impose an appropriate window function on f_1 means that this condition can always be forced if it is not present naturally. It is very important to note that in this case no restrictions arise wrt the displacement function $S(\boldsymbol{\zeta}, \boldsymbol{\mu})$ and consequently the velocity \mathbf{v} .

² The need for $K_{1,2}(\boldsymbol{\mu})$ to exhibit a maximum for some $S(\boldsymbol{\mu}, \boldsymbol{\zeta})$ means that a first-order approximation is inadmissible.

Condition 2. If either $S_{1,0}$ or both $S_{2,0_{\zeta_1}}$ and $S_{2,0_{\zeta_2}}$ are zero on the boundary.

Condition 3. If f_1 and $S_{1,0}$ and $S_{2,0_{\zeta_1}}$ and $S_{2,0_{\zeta_2}}$ are periodic over the domain.

Condition 4. The alternate form of Eq. (20) shows that conditions 2 and 3 also hold with $S_{1,0}$ replaced by $S_{2,0}$. This produces the two further conditions.

Condition 6. Various interrelationships between the f_1 , and the values and derivatives of $S_{1,0}$ and $S_{2,0}$ on the boundaries can also be found; however, these are not expected to be of much practical value.

While these results are formally limited to the case of a rectangular domain, intuition does suggest that this condition will also apply to other shaped regions.

7 A Specific Model for $S(\boldsymbol{\zeta}, \boldsymbol{\mu})$

In order to implement $K_{1,2}(\boldsymbol{\mu})$ in any particular case, whether in general or as the small change form, a sensible choice must be made for the mathematical form of $S(\boldsymbol{\zeta}, \boldsymbol{\mu})$. In the present context "a sensible choice" is one which will adequately describe the situation at hand to the required precision using the least number of parameters, with some attention being paid to analytic simplicity.

Many anticipated applications will be for "localized flow process," e.g., flow within the cylinder of an internal combustion engine, or more open problems like cyclonic weather systems. The "rotational" nature of such flows suggests a set of two-dimensional sinusoids of various, i.e., implying a trigonometric polynomial model would appear to be "a sensible choice." Thus

$$S(\boldsymbol{\zeta}, \boldsymbol{\mu}) = \sum_{l=-\text{Max}}^{\text{Max}} \sum_{r=-\text{Max}}^{\text{Max}} \boldsymbol{\mu}_{l,r} e^{j\mathbf{k}_{l,r} \cdot \boldsymbol{\zeta}}. \quad (21)$$

The coefficient vectors $\boldsymbol{\mu}_{l,r}$ have components, $\mu_{1,l,r}$ and $\mu_{2,l,r}$, which are complex numbers

$$\boldsymbol{\mu}_{l,r} = \mu_{1,l,r} \hat{\boldsymbol{\mu}}_1 + \mu_{2,l,r} \hat{\boldsymbol{\mu}}_2, \quad (22)$$

and the wave vector $\mathbf{k}_{l,r}$ is

$$\mathbf{k}_{l,r} = k_{1,l} \hat{\mathbf{k}}_1 + k_{2,r} \hat{\mathbf{k}}_2, \quad (23)$$

where $\hat{\mathbf{k}}_1$ and $\hat{\mathbf{k}}_2$ are the unit basis vectors for $\mathbf{k}_{l,r}$. The unit vectors $\hat{\boldsymbol{\mu}}_1$ and $\hat{\boldsymbol{\mu}}_2$ are the basis for $\boldsymbol{\mu}$, these typically but not exclusively correspond to those for $\boldsymbol{\zeta}$.

The trigonometric choice is further endorsed by the work on Proper Orthogonal Decomposition for describing turbulent shear flows (Moser, 1990; Lumley, 1967, 1970). However, such functions may not be parametrically parsimonious in other applications. An obvious example is in elastic deformation problems where orthogonal polynomials normally be a far more efficient choice for $S(\boldsymbol{\zeta}, \boldsymbol{\mu})$.

Equations (21) and (23) place no restrictions upon the frequencies present and thus $S(\boldsymbol{\zeta}, \boldsymbol{\mu})$ is an Almost Periodic Function, Bohr (1947, 1968). This is the obvious form to use if there is additional information available concerning the values of the important spatial frequencies present in the problem. However, if these are not known in advance, then it is probably sensible to restrict Eq. (21) and (23) to having integer multiples of some fundamental wavelength in which case

$$\mathbf{k}_{l,r} \cdot \boldsymbol{\zeta} = 2\pi \left(\frac{\zeta_1 l}{L_1} + \frac{\zeta_2 r}{L_2} \right) \quad (24)$$

where L_1 and L_2 are the longest wavelength components in the ζ_1 and ζ_2 directions, respectively. In the absence of additional information L_1 and L_2 would normally be set to the bounding dimensions of the system thus making Eq. (21) a conventional two-dimensional Fourier Series.

The word, normally, is italicized to emphasize the importance of incorporating any prior knowledge about the problem of interest into Eq. (21) as this can considerably improve the efficiency of the transformation model in terms of the number of components required. This is the case for the partially forced vortex examined in Part II (Belmont et al., 1997), which has one spatial rotation in the domain of interest and falls to zero towards the walls and the center. Modeling even the main features of such a flow with a conventional Fourier Series based upon a fundamental spatial wavelength L requires many harmonics. However, making the fundamental $2L$, i.e., a half-period over the domain³, means that $\text{Max} = 2$ in Eq. (21) is sufficient to described all the major aspects of this flow.

8 Determination of the Parameters

Determining a set of parameter values which maximize a function is a common computational problem. It can be treated as a hill-climb process or, more indirectly, as an optimization process with Eq. (19) defining the cost function. Typically such procedures are computationally expensive if a large number of parameters must be determined. However, for typical applications when the small change approximation described in Section 7 holds, the problem reduces to solving a system of equations which, as shown in Section 8.1, are linear in the m complex $\mu_{i,0}$ parameters.

8.1 Evaluation Algorithm for the Small Change Approximation Case. Substituting the trigonometric polynomial model for $S(\zeta, \mu)$ described in Section 8.0 into the system of Eq. (19) produces a set of integral equations in the $\mu_{0,i}$ parameters. Invoking the small change approximation (18) for $f_1(\zeta + S(\zeta, \mu))$, expanding out and retaining only terms up to quadratic in S and its spatial derivatives leads to a system which is linear in the $\mu_{0,i}$.

Extensive but elementary manipulation yields the following two equations in $\mu_{1,l,m}$ and $\mu_{2,l,m}$:

$$0 = \frac{j2\pi}{L_1} p \Theta_1(-p, -q) + \Theta_2(-p, -q) + \sum_{l=-\text{Max}}^{\text{Max}} \sum_{m=-\text{Max}}^{\text{Max}} \left[\mu_{1,l,m} \left\{ j \frac{2\pi}{L_1} (l+p) \Theta_2 \times \{-p-l, -q-m\} + \Theta_4\{-p-l, -q-m\} \right\} + \mu_{2,l,m} \left\{ \frac{2\pi^2}{L_1 L_2} (-pm + ql) \Theta_1\{-p-l, -q-m\} + j \frac{2\pi}{L_2} m \Theta_2\{-p-l, -q-m\} + j \frac{2\pi}{L_1} p \Theta_3\{-p-l, -q-m\} + \Theta_6\{-p-l, -q-m\} \right\} \right] \quad (25)$$

and

$$0 = j \frac{2\pi}{L_2} q \Theta_1(-p, -q) + \Theta_3(-p, -q) + \sum_{l=-\text{Max}}^{\text{Max}} \sum_{m=-\text{Max}}^{\text{Max}} \left[\mu_{1,l,m} \left\{ + \frac{2\pi^2}{L_1 L_2} (-ql + pm) \Theta_1 \times \{-p-l, -q-m\} + j \frac{2\pi}{L_2} q \Theta_2\{-p-l, -q-m\} + j \frac{2\pi}{L_1} l \Theta_3\{-p-l, -q-m\} + \Theta_6(-p-l, -q-m) \right\} + \mu_{2,l,m} \left\{ \frac{j2\pi}{L_2} (m+q) \Theta_3\{-p-l, -q-m\} + \Theta_5\{-p-l, -q-m\} \right\} \right] \quad (26)$$

For each pair of p, q values Eqs. (25) and (26) each give rise to two equations in terms of the real and imaginary parts of $\mu_{1,l}$ and $\mu_{2,l}$. The quantities $\Theta\{p, q\}$ are produced from the functions $f_1(\zeta)$ and $f_2(\zeta)$ via the Finite Interval Fourier Transform shown in Eq. (27). Such integrals are typified by that for $\Theta_1\{p, q\}$, which is given by

$$\Theta_1\{-p, -q\} = \int_{\Gamma_1} \int_{\Gamma_2} \{ 2f_1(\zeta) f_2(\zeta) - f_2^2(\zeta) \} e^{-j2\pi(\zeta_1 p / L_1 + \zeta_2 q / L_2)} d\zeta_1 d\zeta_2 \quad (27)$$

where Γ_1 and Γ_2 denote the domains of ζ_1 and ζ_2 , respectively.

Using the symbol \Leftrightarrow to denote an integral transform pair the six Θ functions are given by

$$\Theta_1\{-p, -q\} \Leftrightarrow 2f_1(\zeta) f_2(\zeta) - f_2^2(\zeta) \quad (28)$$

$$\Theta_2\{-p, -q\} \Leftrightarrow \frac{2\partial f_1}{\partial \zeta_1} f_2(\zeta) \quad (29)$$

$$\Theta_3\{-p, -q\} \Leftrightarrow \frac{2\partial f_1}{\partial \zeta_2} f_2(\zeta) \quad (30)$$

$$\Theta_4\{-p, -q\} \Leftrightarrow \frac{2\partial^2 f_1}{\partial \zeta_1^2} f_2(\zeta) \quad (31)$$

$$\Theta_5\{-p, -q\} \Leftrightarrow \frac{2\partial^2 f_1}{\partial \zeta_2^2} f_2(\zeta) \quad (32)$$

$$\Theta_6\{-p, -q\} \Leftrightarrow \frac{2\partial^2 f_1}{\partial \zeta_1 \partial \zeta_2} f_2(\zeta). \quad (33)$$

The equation system (25)–(33) uses integer-related sinuoids as this is probably the form of most practical interest. However, with no extra difficulty above the results can be derived in terms of arbitrary noninteger spatial frequencies.

8.2 Relationship to Conventional Cross-Correlation and the Consequences. For a constant shift S the analysis in Section 3 allows $K_{1,2}(\mu)$ to have the same form as the conventional cross-correlation function. This raises the very tempting speculation as to whether a generalisation of the Wiener Khintchine theorem can be found implying the existence of some very general and potentially powerful new class of integral transforms.

If this were the case then it may open up the route to very efficient evaluation of the μ_0 in the same way as spectral routes are efficient in conventional cross correlation work. Thus, be-

³ This means that Eq. (21) has much of the character of a cosine transform whose origin lies at the center of the domain.

yond the purely applications driven viewpoint are much wider mathematical horizons.

Resume and Concluding Comments

The definition of a cross-correlation function has been extended so as to allow the underlying coordinate shift processes operating to vary from point to point over the region of interest. As the parameters in the shift function are computed from global data the usual compromises between resolution and reliability encountered when a region is correlated in a set of patches (Kamachi, 1989; Leese, 1971; Ninnis, 1986) is completely avoided. This issue is of particular importance in view of the central role that patch-based correlation has come to play in techniques like Particle Image Velocimetry (Willert and Gharib, 1991; Utami et al., 1991; Adrian, 1986).

An approximate scheme has been developed which allows efficient calculation of the correlation parameters when the changes in the objects of interest are small. As the vast majority of applications are likely to be of this kind, such an approach is probably the preferred one in practice. The form used for the displacement function in the small change scheme is that of a trigonometric polynomial. This choice was made partly for mathematical utility and partly because such functions tend to rather naturally reflect flows in closed regions. However, it is important to recognise that it is a very straightforward matter to employ any desired set of functions to describe the displacement $S(\xi, \mu)$. The only real change that occurs is in the form of the integral in Eq. (27) and hence of the functions $\Theta_i\{k_{1,p}, k_{2,q}\}$.

The emphasis here has been mainly upon establishing the basis for Generalized Cross-Correlation Functions, all of the results have been developed in terms of continuous variables. The consequences of using sampled data sets for f_1 and f_2 are dealt with in Part II, Belmont et al. (1997).

References

- Adrian, R. J., 1986, "Multi-point optical measurement of simultaneous vectors in unsteady flow—A review," *Int. J. of Heat and Fluid Flow*, Vol. 7, No. 2, pp. 127–145.
- Belmont, M. R., 1990, "Dilation Correlation Functions and Their Applications," *I.E.E. Proc.*, Vol. 137, Pt. F, No. 5.
- Belmont, M. R., Hotchkiss, A. J., Maskell, S. J., and Morris, E. L., 1997, "Generalized Cross-Correlation, Part II: Discretization of Generalized Cross-Correlation and Progress to Date in Its Implementation," *ASME JOURNAL OF APPLIED MECHANICS*, Vol. 64, pp. 327–335.
- Belmont, M. R., Thurley, R., Thomas, J., Haviland, J. S., Morris, E. L., and Pourzanjani, M. A., 1991, "Two dimensional dilation correlation functions," *Proc. Sixth Int. I.E.E. Conf. On Processing of Signals*, Loughborough Sept.
- Belmont, M. R., Thurley, R., Thomas, J., Morris, E. L., Hacohen, J., Buckingham, D. J., and Haviland, J. S., 1991, "A new technique capable of measurement of flame temperature in I.C. engines prior to significant heat release," *Proc. I. Mech. E. Seminar. Experimental methods in engine research and development*, I. Mech. E., London, Dec, pp. 41–50.
- Berryman, J. G., and Blair, S. C., 1986, "Use of digital image analysis to estimate fluid permeability of porous materials—Application of 2-point correlation-functions," *J. Appl. Phys.*, Vol. 60, No. 6, pp. 1930–1938.
- Bohr, H., 1947, *Almost Periodic Functions*, Chelsea, New York; also Corduneau, C., 1968, *Almost Periodic Functions*, Wiley Interscience, New York.
- Coupland, J. M., and Halliwell, N. A., 1992, "Particle image velocimetry—3-dimensional fluid velocity-measurements using holographic recording and optical correlation," *Applied Optics*, Vol. 31, No. 8, pp. 1005–1007.
- Dejong, P. G. M., Arts, T., Hoeks, A. P. G., and Reneman, R. S., 1991, "Experimental Evaluation of the Correlation Interpolation Technique to Measure Regional Tissue Velocity," *Ultrasonic Imaging*, Vol. 13, No. 2, pp. 145–161.
- Gonzalez, R. G., and Woods, R. E., 1992, *Digital Image Processing*, Addison-Wesley.
- Kamachi, M., 1989, "Advective surface velocities derived from sequential images for rotational flow field—Limitations and applications of maximum cross-correlation method with rotational registration," *J. Geophysical Research-Oceans*, Vol. 94, NC12, pp. 18,227–18,233.
- Lee, Y. W., 1960, *Statistical Theory of Communication*, John Wiley and Sons, New York.
- Leese, J. A., Novak, C. S., and Clark, B. B., 1971, "An automated technique for obtaining Cloud Motion from Geosynchronous Satellite Data using Cross-Correlation," *J. Appl. Met.*, Vol. 10, No. 1, pp. 118–132.
- Lumley, J. L., 1967, "The structure of inhomogeneous turbulent flows," *Atmospheric turbulence and Radio Wave Propagation*, A. M. Yaglom and I. Tatarsky, eds. NAUKA, Moscow, p. 166.
- Lumley, J. L., 1970, *Stochastic Tools in Turbulence*, Academic press, New York.
- Matic, P., Kirby, G. C., Jolles, M. I., and Father, P. R., 1991, "Ductile alloy constitutive response by correlation of iterative finite-element simulation with laboratory video images," *Eng. Fract. Mech.*, Vol. 40, No. 2, pp. 395–419.
- Moser, R. D., 1990, "Statistical analysis of near-wall structures in turbulent channel flow," *Near-Wall Turbulence*, S. J. Kline and N. H. Afgan, eds., pp. 46–62. The International Centre for Heat and Mass Transfer, Hemisphere, pp. 46–62.
- Ninnis, R. M., Emery, W. J., and Collins, M. J., 1986, "Automated extraction of Pack Ice Motion from Advanced Very High Resolution Radiometer Imagery," *J. Geophys. Res.* Vol. 91, No. C9, pp. 10,725–10,734.
- Richards, R. L., and Roberts, G. T., 1969, "Correlator Applications Nos. 1 to 10," *Hewlett-Packard Journal*, Vol. 21, No. 3, pp. 1–20.
- Trahey, G. E., Hubbard, S. M., and Vonramm, O. T., 1988, "Angle independent ultrasonic blood-flow detection by frame-to-frame correlation of B-mode images," *Ultrasonics*, Vol. 26, No. 5, pp. 271–276.
- Utami, T., Blackwelder, R. F., and Ueno, T., 1991, "A Cross-Correlation technique for Velocity Field extraction from particulate visualisation," *Experiments in Fluids*, Vol. 10, No. 4, pp. 213–223.
- Wiener, N., 1949, *Extrapolation, Interpolation, and Smoothing of Stationary Time Series with Engineering Applications*, M.I.T., Cambridge, MA; also Wiener, N., 1964, *Generalised Harmonic Analysis and Tauberian theorems*, M.I.T., Cambridge, MA.
- Willert, C. E., and Gharib, M., 1991, "Digital Particle Image Velocimetry," *Experiments in Fluids*, Vol. 10, No. 4, pp. 181–193.

M. R. Belmont
School of Engineering,
University of Exeter,
Harrison Engineering Building,
North Park Road,
Exeter EX4 4QF, UK

A. J. Hotchkiss
Glaxo

S. J. Maskell

E. L. Morris
School of Engineering,
University of Exeter,
Harrison Engineering Building,
North Park Road,
Exeter EX4 4QF, UK

Generalized Cross-Correlation, Part II: Discretization of Generalized Cross-Correlation and Progress to Date in Its Implementation

The companion article, "Generalised Cross-Correlation Functions, Part I," introduced a generalization of cross-correlation in which the constant shift used in traditional cross-correlation is replaced by a function of time or space. This allows correlation to be applied globally to the whole domain of interest avoiding the need to compromise spatial resolution with statistical reliability. The development in Part I was entirely in terms of continuous variables. This article examines the issues that arise when Generalized Cross-Correlation is applied to discrete variable situations. Topics discussed include sampling rate requirements, noise rejection, and efficient approximate algorithms, with special attention being paid to the condition number for the system.

1 Introduction

Part I (Belmont and Hotchkiss, 1997), develops the basic theory for generalizing the well-known cross-correlation function. The properties of the Generalized Cross-Correlation function, (abbreviated to GC-C), were discussed together with its advantages in applications. While GC-C has a wide range of uses the specific problems discussed concern the determination of displacement or flow fields, usually from pairs of images (Leese et al., 1971; Ninnis et al., 1986; Willert and Gharib, 1991; Utami et al., 1991; Adrian, 1986). The development in Part I (Belmont and Hotchkiss, 1997) is entirely in terms of continuous functions whereas almost all the practical situations of interest will involve sampled data sets. Consequently, it is necessary to examine the effects that discretization has on GC-C and this is the main role of the present article.

In order to avoid duplication the required definitions and results of the continuous variable GC-C theory are all quoted directly from Part I. A convention is adopted that a primed equation number refers to the corresponding numbers in Part I. Consequently, this article must be read in conjunction with Part I.

It is important to note that examining the effects of discretizing GC-C is not the same as considering the details of applications. The focus of attention here is on aspects such as spatial sampling, noise, and numerical issues associated with the reliable determination of parameters. While consideration is given to the effects these factors have on applications this article is not concerned explicitly with actual experimental data. All the numerical studies employ simulation.

The problem of identifying the parameters in the GC-C which characterize the situation of interest is in general terms the same as for any cross-correlation technique, i.e., a search is required for those parameters which maximize the value of the GC-C

function. There are many different ways of tackling this problem but they are all computationally intensive. For this reason what is essentially a second-order small perturbation approach to GC-C was developed in Part I that produces a set of linear equations from which the parameters can be determined. This Part II article is mainly concerned with the small perturbation method implementation of GC-C.

The small perturbation approach is very attractive in terms of computing resources. However, the process of solving systems of equations based upon such approximation schemes is notoriously sensitive to the condition number of the system (Golub and Van Loan, 1989). Crudely speaking, for the parameter estimates to be reliable, the product of the condition number κ and the coefficient error bound Δ must be small compared to the smallest parameter value (Golub and Van Loan, 1989). As this article focuses upon the small perturbation method the examination of condition number and its effects on the applications forms an important part of Part II.

1.1 The Approach to Considering Discretization. It is unrealistic to attempt a general analytical application of the Nyquist Sampling Theorem directly to the GC-C problem due to the inherent need in GC-C to invert a substantial equation system. Thus the approach adopted here is to explore archetypal cases derived from continuous functions which are sampled so as to generate the required discrete data sets. Where required, controlled synthetic noise is added to such data to examine the noise sensitivity of the technique. Examples of the use of actual experimental data in GC-C will be reported on subsequently.

2 The GC-C Results Needed for Two-Dimensional Implementation

In its most general form GC-C as developed in Part I (Belmont and Hotchkiss, 1997) applies to arbitrary dimensional systems. However, the main interest here will be with two-dimensional cases as these reflect the important practical problem of extracting displacement/flow-field information from sequences of images. One-dimensional GC-C, which is valuable in applications such as the rapid-scan sonar or radar, is simply a special case of the present work and will therefore not be

Contributed by the Applied Mechanics Division of THE AMERICAN SOCIETY OF MECHANICAL ENGINEERS for publication in the ASME JOURNAL OF APPLIED MECHANICS.

Discussion on this paper should be addressed to the Technical Editor, Professor Lewis T. Wheeler, Department of Mechanical Engineering, University of Houston, Houston, TX 77204-4792, and will be accepted until four months after final publication of the paper itself in the ASME JOURNAL OF APPLIED MECHANICS.

Manuscript received by the ASME Applied Mechanics Division, Sept. 25, 1995; final revision, Oct. 28, 1996. Associate Technical Editor: S. Lichter.

examined explicitly. The target problem will be the determination of displacement/flow fields from pairs of consecutive images.

3 The Spatial Sampling Frequency Required and Number of Parameters Needed

From a purely algebraic standpoint the bare minimum number of spatial samples needed is equal to the number of parameters. However, this view loses sight of physical issues and it is more fruitful to employ the Nyquist Sampling Theorem. This requires that the spatial sampling frequency of all the quantities concerned is at least twice the highest spatial frequency present in the GC-C process, otherwise aliasing errors will be present. Clearly the bandwidth W_s of the displacement functions S_1 and S_2 must also match that of the displacement/velocity field. This is reflected in the changes wrought between f_1 and f_2 , and as will be shown in Section 3.1.3 introduces some interesting and rather surprising issues.

If the information used for f_1, f_2 , etc., were obtained in analogue form, then it is possible to satisfy the sampling theorem for f_1 and f_2 via anti-alias filtering prior to the sampling process. However, in practice images are typically obtained by CCD cameras which directly sample images into pixels. Filtration is only possible via the properties of the optical system¹. Hence knowledge of the spatial bandwidth of the problem is necessary for choosing the pixel density for the optical sensor.

3.1.1 The Sampling Rate Requirements of the Initial Image $f_1(\zeta_1, \zeta_2)$. The minimum spatial sampling interval $\delta\zeta$ for f_1 is $\delta\zeta = 1/(2W_{f_1})$ where W_{f_1} is the spatial bandwidth of f_1 . In mechanical strain applications the image f_1 can be induced (e.g., as a pattern painted on the material) prior to applying the loads that deform the domain changing f_1 into f_2 ; thus f_1 and hence W_{f_1} are arbitrary. However, in flow-field determinations it is unlikely that the image-forming attribute can be introduced sufficiently rapidly for this to be possible. Consequently in flow problems, f_1 will reflect at least in part the spatial bandwidth of the flow field.

3.1.2 The Sampling Rate Requirements of the Transformation Functions S_1 and S_2 and M the Number of Parameters Needed. The bandwidth W_s of the displacement functions S_1 and S_2 is that of the displacement/flow field. Hence the upper frequency index Max in Eq. (21') is the nearest integer above LW_s , thus according to Eq. (21') in the absence of a uniform displacement/flow component GC-C requires $16 \cdot \text{Max}^2$ real parameters.

3.1.3 The Sampling Rate Requirements of the Transformed Image $f_2(\zeta_1, \zeta_2)$. Interestingly if f_1 is band limited then f_2 must be a wideband function. This is because Eqs. (3) and (4) define f_2 as f_1 being frequency (or phase) modulated by the trigonometric functions S_1 and S_2 . Such FM modulated functions have infinite bandwidth.

This appears to question the legitimacy of describing f_2 purely as a coordinate transformation of f_1 because there is nothing special about the choice of f_1 and f_2 and at least in flow problems both will have similar spectral characteristics. The reason why f_2 is wideband is easily recognized by considering a Taylor Series expansion of f_2 about f_1 with S_1 and S_2 as small parameters. Applying the appropriate multiple angle trigonometrical relationships shows that each extra new term in Taylor Series expansion increases the bandwidth. In the small perturbation form of GC-C only quadratic terms are retained so in the context of the present analysis the spectrum of f_2 remains band limited.

3.1.4 Quadratic Factors Containing the Displacement Functions and Their Derivatives. The coefficients in the basic equation system 25' and 26' are derived from Fourier Trans-

forms of factors such as $f_1(\zeta_1, \zeta_2, \mu_0)f_{1,\zeta_1}(\zeta_1, \zeta_2, \mu_0)S_1^2(\zeta_1, \zeta_2, \mu_0)$. Given that the small perturbation form of GC-C only retains terms up to quadratic powers in the S functions or their derivatives such products produce a finite maximum frequency of $2\{W_s + W_{f_1}\}$. This is the highest frequency encountered in the sampling rate discussion in Sections 3.1.1 \rightarrow 3.1.4 and hence serves to define the spatial sampling rate as $4\{W_s + W_{f_1}\}$ sample m^{-1} .

3.2 Differentiation. The equation system coefficients require spatial derivatives of the initial image f_1 which are determined analytically in the simulation work. Applications using discrete noise² corrupted data require a combination of minimum bandwidth and a band limited differentiating digital filter. The appropriate techniques are standard practice in two dimensional discrete linear systems work and the key elements involved are summarised in the appendix.

4 The Properties of the Equation System

4.1 Spectral Symmetries and Redundancies. The displacement/flow functions S_1 and S_2 are real, hence the well-known symmetries of Fourier Transforms mean that only half of the μ_0 values are unique. Consequently only half of the $4(2\text{Max} + 1)^2$ equations comprising the system are required to solve for these unique parameters. The other half of the system must be removed otherwise it introduces linear dependencies which lead to singularity.

4.2 The Condition Number κ and Sensitivity. The small perturbation GC-C implementation is second-order accurate, hence there are inevitably errors in the system coefficients. Denoting the scale of such coefficient errors by Δ , the contribution of such errors to the solution is magnified by a factor of κ (Golub and Van Loan, 1989). Thus it is necessary that the scale ϵ of S_1 and S_2 satisfies

$$\epsilon \gg \kappa \Delta. \quad (1)$$

However, ϵ must also remain small enough for f_2 to be legitimately treated as a perturbation of f_1 .

5 Overview of Numerical Work

Section 1.2 indicated that it is unrealistic to develop a general treatment of the discretisation errors in GC-C and hence the approach adopted is to employ continuous functions with known μ_0 parameters to model typical examples. These are then sampled to provide the discrete data. Using this methodology four key issues will be explored:

First, the state of conditioning of the system and its consequences. Closely linked to this is, how precisely can the $\mu_{0,i}$ be estimated by the perturbation method? Third, the robustness of the technique is assessed by determining its ability to estimate the $\mu_{0,i}$ in the presence of uncorrelated noise. Fourth, does discretization introduce new boundary condition constraints and any other additional requirements?

5.1 Windowing the Images. To avoid leakage errors it is standard practice to window space or time series data (Brigham, 1988). The window functions employed (e.g., Hamming, 1977) typically have both zero value and derivative at boundaries. In terms of the present coordinates ζ_1, ζ_2 over the L_1 by L_2 domain one of the simplest window functions $w(\zeta_1, \zeta_2, L_1, L_2)$ is

$$w(\zeta_1, \zeta_2, L_1, L_2) = \frac{1}{4} \left\{ 1 - \cos \left(\frac{2\pi\zeta_1}{L_1} \right) \right\} \left\{ 1 - \cos \left(\frac{2\pi\zeta_2}{L_2} \right) \right\}. \quad (2)$$

² Any uncorrelated differences between f_1 and f_2 are treated as noise. In two-dimensional applications such as image work these include out-of-plane displacements.

¹ The simplest approach is to use defocusing.

The distortions introduced by such a window can always be compensated for, except very close to the boundaries.

Such a function automatically satisfies the boundary requirements on f_1 and it thus appears that windowing offers a way of making arbitrary systems available to GCC. Unfortunately the corresponding window needed for f_2 must be shifted by \mathbf{S} which is clearly not known in advance. However, by extending the basic window concept, it is possible to employ a development of this approach because the small perturbation GCC also applies to systems where f_1 and f_2 are periodic over the domain. A simple way to make f_1 and f_2 periodic is to analytically continue both functions by mirroring them along the ζ_1 and ζ_2 boundaries. This does increase the domain size, doubling the fundamental spatial wavelength, but due to the symmetries does not increase the number of unique coefficients needed.

This technique is termed an extension of the windowing technique because the most general way of avoiding leakage is actually to make a function periodic over the domain (Brigham, 1988). The traditional method of forcing it to be zero at the boundaries is simply a special case of this.

5.2 The Local Zoom Technique. The use of the analytical continuation form of windowing suggests the possibility of a Local Zoom technique to extract a ΔL_1 by ΔL_2 region of interest to which GC-C can be legitimately applied with largest wavelengths scaled to ΔL_1 , ΔL_2 . This avoids modeling the displacement/flow field on an unnecessarily fine scale over the whole domain.

This Local Zoom technique has obvious applications as a general purpose tool. However, it also has the potential to be a very powerful method when employed specifically to examine the self-similarity aspects (Mandelbrot, 1983) of complicated evolving flow fields. The key issue here is how the same dynamical processes operate on a range of length scales. The Zoom facility means that the flow fields can be analyzed at progressively smaller length scales using the same class of spectral model. Operating GC-C in this manner it is almost certain that the displacement functions S_1 and S_2 should be modeled by Wavelet Expansions rather than the trigonometric forms predominantly considered here.

5.3 Noise-Free Simulations. The simplest and most natural nontrivial example of an image satisfying the boundary conditions for small perturbation GC-C is where f_1 has the form of the window function in Eq. (2), i.e.,

$$f_1(\zeta_1, \zeta_2) = \frac{1}{4} \left\{ 1 - \cos \left(\frac{2\pi\zeta_1}{L_1} \right) \right\} \left\{ 1 - \cos \left(\frac{2\pi\zeta_2}{L_2} \right) \right\}. \quad (3)$$

In the examples considered subsequently the domain is taken to be square so $L_1 = L_2 = L$. Sensible choices for the displacement/flow field are the simplest forms which exhibit the full range of different types of boundary conditions. For each dimension three distinguishable cases occur: (i) zero value, finite derivative (ii) finite value, zero derivative, i.e., a maximum (iii) finite value and finite derivative. The case where both value and slope are zero is a combination of (ii) with a constant and thus is not treated separately.

The following are the simplest forms that describe the various zero value/slope cases in two dimensions:

$$\begin{aligned} S_1 &= \epsilon_1 \frac{1}{4} \frac{\sin \left(\frac{2\pi\zeta_1}{L} \right)}{\cos \left(\frac{2\pi\zeta_1}{L} \right)} \frac{\sin \left(\frac{2\pi\zeta_2}{L} \right)}{\cos \left(\frac{2\pi\zeta_2}{L} \right)} \\ S_2 &= \epsilon_2 \frac{1}{4} \frac{\sin \left(\frac{2\pi\zeta_1}{L} \right)}{\cos \left(\frac{2\pi\zeta_1}{L} \right)} \frac{\sin \left(\frac{2\pi\zeta_2}{L} \right)}{\cos \left(\frac{2\pi\zeta_2}{L} \right)} \end{aligned} \quad (4)$$

where sin/cos means the different combinations of sin or cos which give different boundary conditions. There are only five

such possibilities as $\sin(2\pi\zeta_1/L) \cos(2\pi\zeta_2/L)$ does not exhibit a different type of behavior to $\cos(2\pi\zeta_1/L) \sin(2\pi\zeta_2/L)$. The finite value and slope situation is representable by

$$\begin{aligned} S_1 &= \epsilon_1 \frac{1}{4} \sin \left(\frac{2\pi\zeta_1}{L} + \Psi_1 \right) \sin \left(\frac{2\pi\zeta_2}{L} + \Psi_2 \right) \\ S_2 &= \epsilon_2 \frac{1}{4} \sin \left(\frac{2\pi\zeta_1}{L} + \Psi_3 \right) \sin \left(\frac{2\pi\zeta_2}{L} + \Psi_4 \right). \end{aligned} \quad (5)$$

The attraction of these forms for S_1 and S_2 is that they can all be described exactly by the trigonometric models given in Eq. (21') and thus are ideally suited for testing the precision of the small perturbation technique as implemented in discrete form in the absence of any other confounding factors.

The results of error versus size of displacement (the scale of S_1 and S_2) are presented in Fig. 1(a). The domain size L was set equal to 2π for convenience and 13 samples were used in each direction which is a little oversampled as the Nyquist requirement as defined in Section 3.1.4 is eight samples. The phase shifts $\Psi_1 \rightarrow \Psi_4$ in Eq. (5) were set to $\pi/4$ with the displacement scales set equal, i.e., $\epsilon_1 = \epsilon_2 = \epsilon$. The ordinate in Fig. 1(a) shows the percentage RMS error in the estimates of the model coefficients while the abscissa is the displacement scale parameter ϵ as a fraction of the total domain size of 2π .

The behavior of the condition number κ for the equation system described in Section 4 is shown in Figs. 1(b) and 1(c). These plots indicate the variation of κ with displacement scale and also the manner in which the RMS error depends on κ .

5.3.1 Discussion of Noise-Free Results. The form of the RMS error is as expected for the small perturbation method, i.e., zero error for infinitely small displacements with an increasing error as the displacement scale increases. There is some variation in precision depending upon the type of displacement boundary conditions but no evidence of any pathological cases. The manner with which the condition number κ varies with displacement scale in Fig. 1(b) together with the error dependence on κ in Fig. 1(c) confirms this.

5.3.2 A Pathological Image Form. Unlike the zero slope and value requirement for leakage error reduction, continuous variable GC-C only needs a zero image value at the boundary. Hence, for completeness it was decided to investigate the behavior of such image forms. The simplest type of f_1 function that exhibits this behavior is

$$f_1(\zeta) = \sin \left(\frac{2\pi\zeta_1}{L} \right) \sin \left(\frac{2\pi\zeta_2}{L} \right). \quad (6)$$

Clearly this function cannot be a physical image because of the negative intensities present, nonetheless its simplicity justifies its use.

The RMS error and condition number plots paralleling those for the image in Eq. (3) are presented in Figs. 2(a) and 2(b). These show markedly different condition number behavior, both in value and form, which are also reflected in very erratic error behavior. Given the approximate nature of the method condition number behavior of this type generally leads to unreliable solution estimates (Golub and Van Loan, 1989).

That condition number is responsible for this pathology, rather than any other type of error, is confirmed by substituting the μ_0 parameters into the system and evaluating the right-hand side vector. The equations are then found to be adequately satisfied. Further exploration of this case reveals that the coefficient matrix becomes singular in the limit of small displacements.

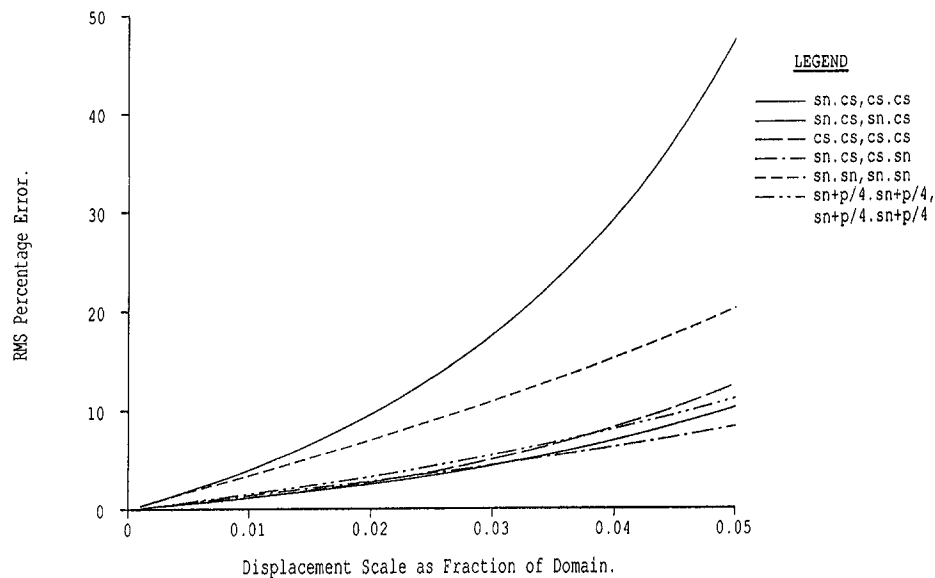


Fig. 1(a) The RMS percentage errors in the parameter estimates are plotted against the size of the displacement under noise-free conditions. The types of displacement/flow field used are given by the abbreviations in the legend and correspond to Eqs. (4) and (5). The initial image f_1 was as defined by Eq. (3) and 13 spatial samples were used per dimension.

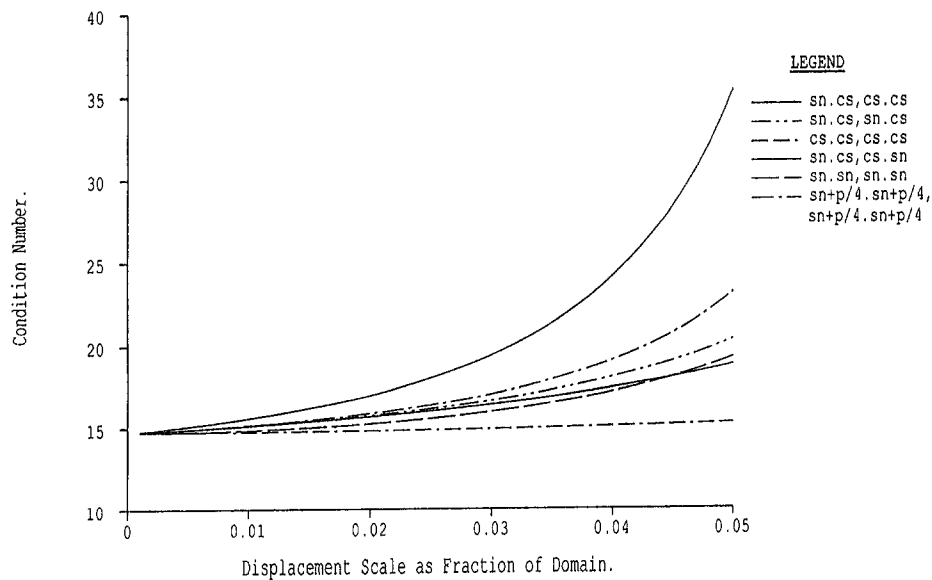


Fig. 1(b) Condition number versus the size of displacement for the conditions given in Fig. 1(a)

Clearly this form of image is pathological and it would be of academic interest to pursue the specific reasons for such behavior in more depth. However, in view of the nonphysical nature of this type of function, such effort is not considered to be justifiable and it is sufficient to highlight the special nature of this type of example.

5.4 Noise Rejection Capabilities of GC-C. A fundamental feature of cross-correlation is its ability to reject noise that is uncorrelated with the data of interest. In order to examine this aspect of GC-C, calculations were performed with wideband noise added to the displacement functions S_1 and S_2 . This simulated noise in the displacement/velocity field.

The computational procedure was to add wideband random noise with a uniform probability density to the displacement functions S_1 and S_2 then to estimate the model parameters and hence the error as in the noise-free case. This procedure was then repeated 100 times and the RMS error over the set of 100 runs was determined. As with the noise-free case, 13 spatial

samples were used in each dimension. The results are presented for the most general type of boundary condition i.e., both finite value and derivative. Figure 3(a) shows the results for various-sized displacement scale values. The behavior is as expected with the error asymptoting to the noise-free limit in each case. Even for the modest number of samples used the noise rejection is good.

To assess the effects of data corruption during the image capture process noise was added directly to the image f_1 . Using the same conditions as in Fig. 3(a) with a specific displacement scale fraction of 0.005 the results presented in Fig. 3(b) were obtained. These show that there is very little difference between the effects of noise addition to either the flow field or the image.

Finally, in order to illustrate the effect of sample number size on noise rejection, the 0.005 displacement scale case in Fig. 3(a) was repeated for a modest range of sample values. Figure 3(c) shows that for moderate signal-to-noise ratios, as expected the noise rejection improves as the number of samples increases. The results with a signal to noise ratio of 1 show a large scatter

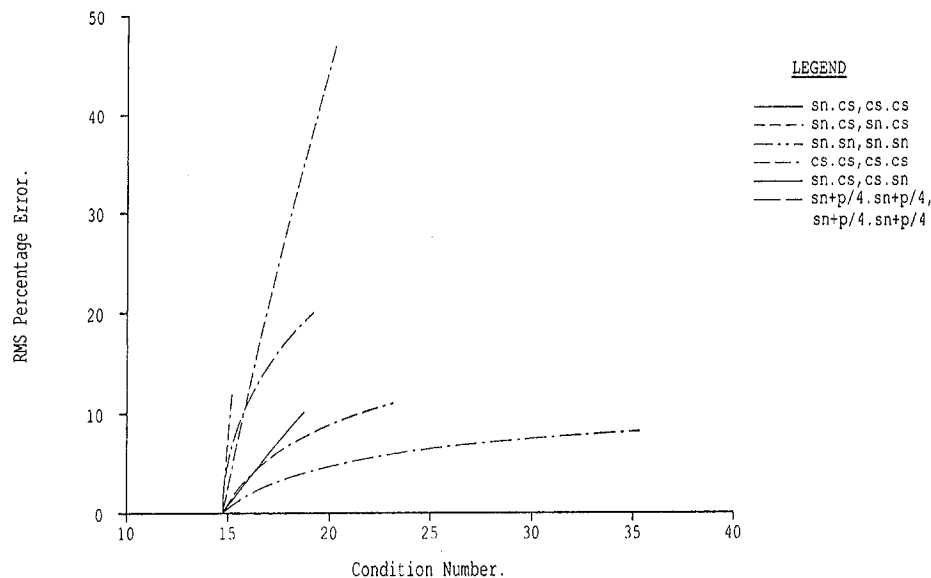


Fig. 1(c) Percentage RMS error in the parameter estimates plotted against condition number for conditions given in Fig. 1(a)

which reflects the poor statistical quality obtained at high signal-to-noise ratios when only 100 averages are used.

5.5 Larger Systems and Conditioning Effects. The examples presented above use 16 real parameters and show that reasonable precision can be achieved with condition numbers up to the order of 10^2 . The next obvious question is how the condition number behaves as the required number of parameters increases.

Doubling the spatial resolution for the above systems means that the number of real parameters needed is increased to 32 parameters. This causes the condition number to rise dramatically, typically to several thousand, depending in detail as would be expected on the exact form of S_1 and S_2 . The criterion given in Section 4.2 predicts that this is likely to produce unacceptable errors. Numerical experimentation with a range of displacement functions confirms this to be the case.

5.6 Condition Number Versus System Size. The present findings indicate that the class of linear equations with spectral coefficients that are of interest here have poor conditioning properties as the size of the equation system increases. To probe their behavior more closely some of the coefficients were set to zero allowing an arbitrary variation in the size of the equation system as opposed to the steps of 16×2^n as used in the cases described so far. This showed that for a wide variety of forms of S_1 and S_2 the condition number κ rose smoothly with increasing system size up to values of $\kappa \approx 100$ which as expected gave sensible parameter estimates. For even small increases in system size beyond this point a discontinuous jump would occur in κ to values of several thousand. For most cases examined this jump occurs in the range 20–30 parameters. In general, the larger κ is the smaller must be both the error associated with the quadratic approximation (and hence the smaller the displacements) and the error induced by noise effects (Golub and Van Loan, 1989).

The consequences that this condition number behavior has for applications are examined in Section 6.

5.7 Numerical Techniques. The results presented here employed direct matrix inversion to solve the parameter equation system. Given that Singular Value Decomposition is often found to be valuable where systems have poor condition number behavior, this method was also explored. However, it showed no advantage over direct inversion.

In analytical terms an equation system with $\kappa \geq 1$ behaves as an expansive rather than contracting mapping of the parameter vector, thus it would be expected that substituting the known values of the parameters into the system should produce a good estimate of the right-hand side vector. This was found to be the case confirming that the condition number behavior was directly responsible for the unreliability of the parameter estimates.

Given this type of condition number behavior and the fact that evaluation of the RHS vector using the known solutions was acceptably precise, it appears that the most effective numerical technique would be a recursive approximation method. This would exploit the fact that the equation system behaves as a contractive mapping for the forward substitution process involved in such techniques, in contrast to the expansive behavior manifest in attempts to *solve*, i.e., invert, the system. As in essence the present numerical task is an optimization problem, i.e., maximizing the GC-C function, this suggests using either traditional linear programming methods or the more recently developed genetic algorithms (Goldberg, 1989). The results of such a study will form the basis of a future report.

6 Consequences of Condition Number Behavior on Applications

The main thrust of this work has been to discover the consequences of discretizing CG-C, mainly in its small perturbation form, and not to explicitly consider implementations for applications. However, given the limits which the condition number behavior imposes on the number of parameters which can be reliably calculated, it is clearly necessary to at least consider the consequences of this particular constraint on potential applications.

The main finding of the condition number work is that typically at most 20 parameters in the S_1 and S_2 displacement functions can be reliably determined with the numerical techniques employed here. For one-dimensional cases such as rapid scanning sonar this restriction is unlikely to present a serious problem. However, until numerical techniques can be determined which circumvent the condition number behavior, the two-dimensional applications of GC-C to experimental data will have to be approached in a much more circumspect manner. The basic requirement is to make the best possible use of the parameters available.

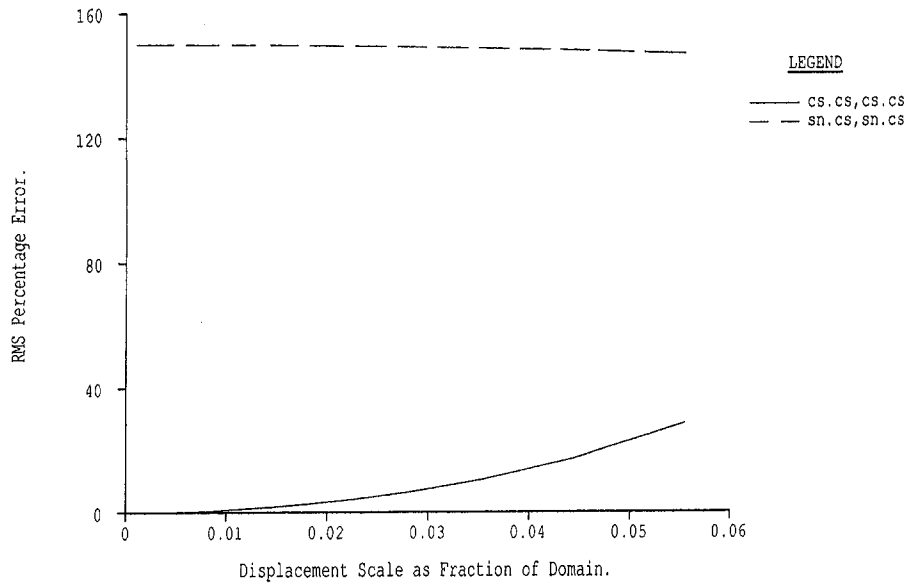


Fig. 2(a) The RMS percentage errors in the parameter estimates are plotted against the size of the displacement under noise free conditions under the same conditions as Fig. 1(a) but with using the pathological image form of Eq. (6) for the initial image f_1

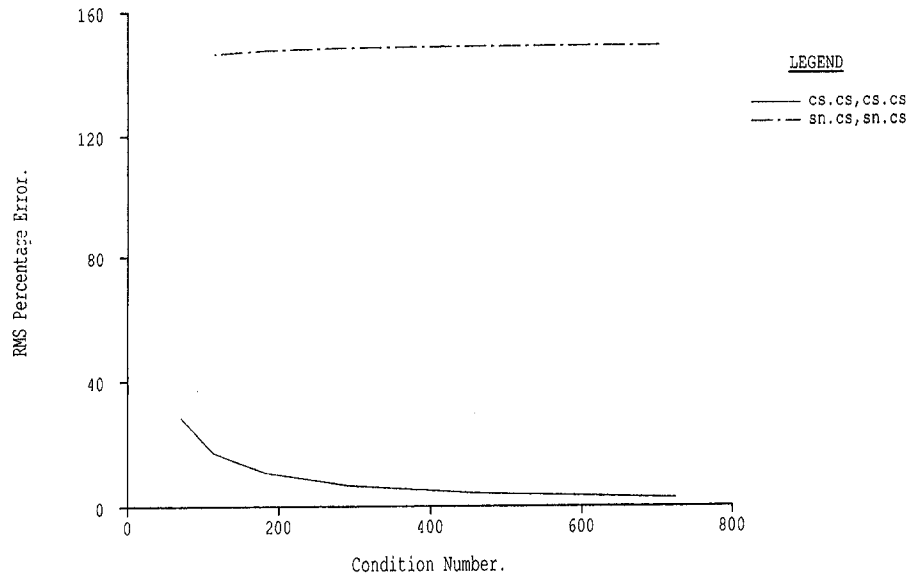


Fig. 2(b) Condition number versus the size of displacement for the conditions given in Fig. 2(a)

6.1 Systems With Zero Flow/Displacement on the Boundary. The number of length scales that the available number of parameters can represent will obviously depend upon the context. The most sensible situations to examine first are those whose properties motivated the choice of the trigonometric polynomials employed to model S_1 and S_2 . Such systems are characterized by zero displacement/flow velocity on the boundary and represent problems such as flows in closed regions, cyclonic weather systems, strain in regions clamped at the boundary, etc.

Analytically this boundary condition requires that only the sin terms in S_1 and S_2 are nonzero. Thus Eq. (4) in vector form becomes

$$S(\zeta, \mu) = \sum_{l=1}^{\text{Max}} \sum_{r=1}^{\text{Max}} \mu_{l,r} \sin\left(2\pi \frac{\zeta_{1l}}{L_1}\right) \sin\left(2\pi \frac{\zeta_{2r}}{L_2}\right), \quad (7)$$

i.e., the size of the system has fallen by a factor of four. A common feature of such cases is the presence of global rotation

which means that the longest lengthscale present is twice the size of the domain. As an example of this case a simulation was made of a very simple model of a cyclonic weather system. The defining equations are

$$S_1(\zeta, \eta) = V_x \delta_t \sin\left(\frac{\pi \zeta}{L}\right) \sin\left(\frac{2\pi \eta}{L}\right) \quad (8)$$

and

$$S_2(\zeta, \eta) = -V_y \delta_t \sin\left(\frac{2\pi \zeta}{L}\right) \sin\left(\frac{\pi \eta}{L}\right), \quad (9)$$

where V_x and V_y are the maximum flow speeds in each coordinate and δ_t is the time between images. A vector plot of the flow field produced by Eqs. (8) and (9) is shown in Fig. 4.

The initial image $f_1(\zeta, \eta)$ used is described by Eq. (3) and varying amounts of wideband noise were added to the flow

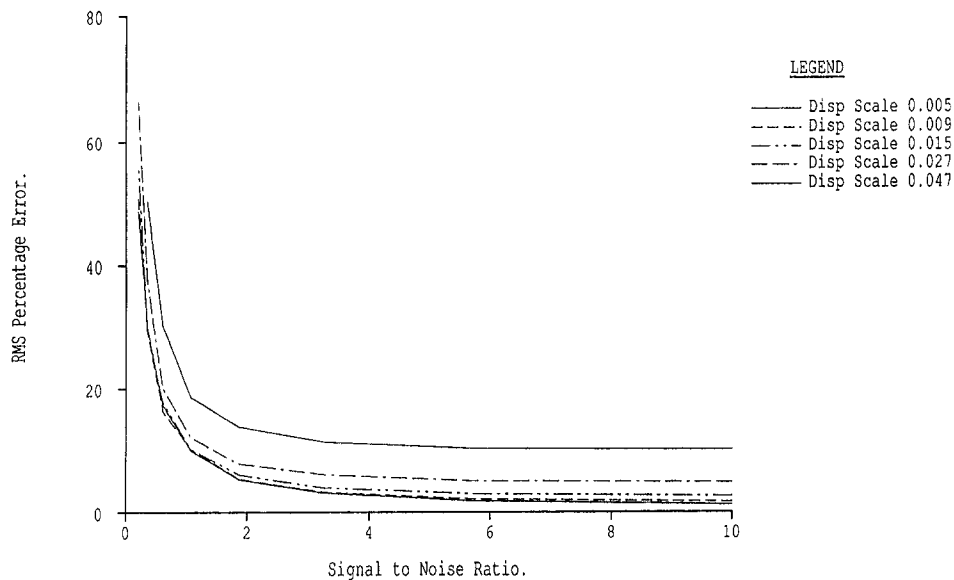


Fig. 3(a) The RMS percentage errors in the parameter estimates plotted against signal-to-noise ratio. The displacement field was given by Eq. 5 with $\Psi = \pi/4$. Wideband noise was added to the displacement values. The legend indicates the displacement scale. The initial image f_1 was as defined by Eq. (3) and 13 spatial samples were used per dimension. Results were the average of 100 separate runs.

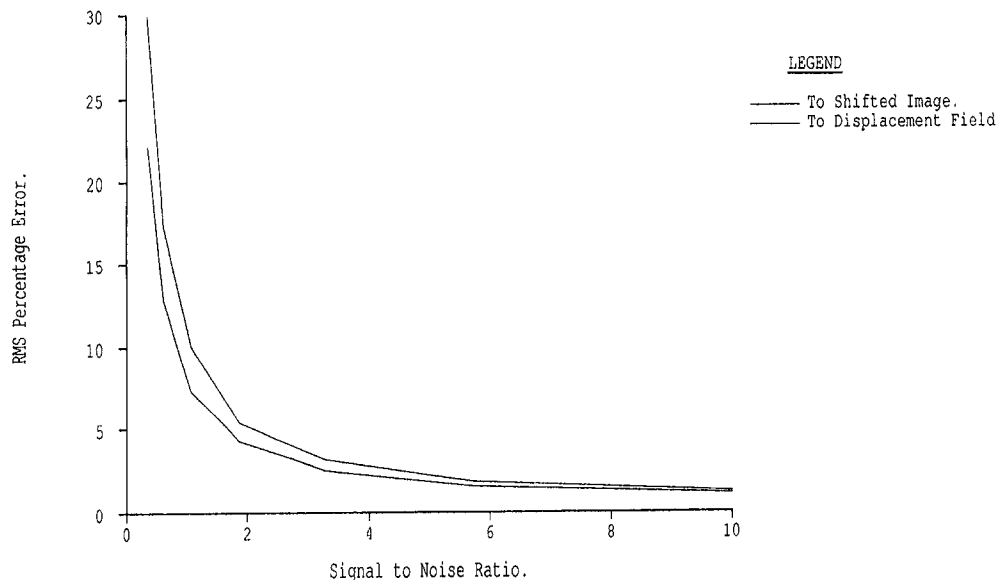


Fig. 3(b) A comparison of the effects of adding noise to the displacement field with adding noise to the image for the case of a displacement scale of 0.5 percent. The conditions were as for Fig. 3(a).

field. The fractional RMS errors in the estimated coefficients 10 are presented in Table 1.

6.3 Use of GC-C in Conjunction With Cellular Correlation. If approximate values are available for the dominant components of the displacement/flow field then it is possible to select just these in GC-C. This suggests that a combination of conventional cellular cross correlation and currently available numerical implementation of GC-C could provide a powerful tool.

The approach would be as follows:

- 1 Make an assessment of the displacement/flow field with cellular technique correlation (Kamachi, 1989; Leese et al., 1971; Utami et al., 1991) at a cell size L_m .
- 2 Determine the spatial spectrum of this estimate and identify the key terms in the displacement/flow field as represented by S_1 and S_2 formulation.

If step 2 leads to less than roughly 20 GC-C parameters, then these two steps are repeated with a smaller value of L_m .

- 3 Perform a GC-C estimation of the chosen parameters.

This results in a global displacement/flow-field model with all the advantages of the GC-C technique.

6.4 Strip Correlation. A halfway house between full GC-C and conventional cellular correlation is to segment the domain into strips of width δr and perform one-dimensional GC-C on each separate strip. This clearly loses the fully two-dimensional coherence of GC-C but does provide long-range coherence along each strip and allows all the parameters to be employed in modeling the behavior along every individual strip.

Clearly δr must be small enough to ensure negligible change in the coordinate normal to the strip and thus $\delta r \ll \lambda_{\min}$ where λ_{\min} is the smallest spatial wavelength of interest. A sensible check on precision is to perform a second strip GC-C calculation

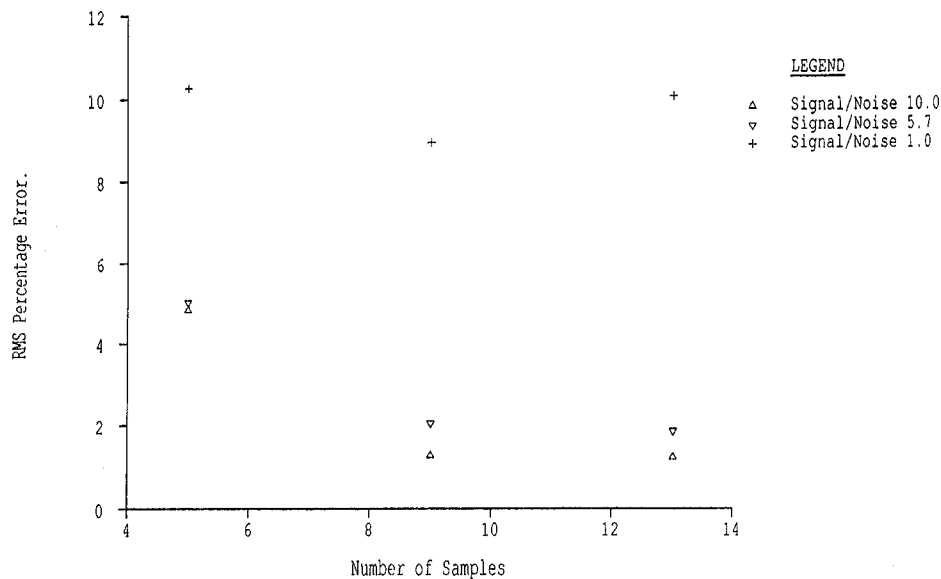


Fig. 3(c) To show the effect of the number of spatial samples per dimension on noise rejection with conditions as in Fig. 3(b) with noise added to the displacement field

along the coordinate normal to that in the first analysis. This provides an overall measure of self-consistency and will also highlight any specific local anomalies.

The strip technique is the simplest current numerical GC-C option to implement and it is felt that until appropriate numerical methods are found for the full two-dimensional GC-C this strip method will probably find the most use in application. As this approach is very obvious and does not require any additional new results, explicit illustrations are not presented here.

7 Conclusions

Discrete implementation has been performed of the small perturbation form of Two-Dimensional Generalized Cross-Correlation (Belmont and Hotchkiss, 1997), where the intention was to recover a spatially varying transformation between successive image-like functions. Typical applications are expected

to be the recover of displacement/flow-field data from successive images. For a moderate number of parameters the technique achieves its desired aim and rejects additive noise in the anticipated manner.

For a large number of parameters the conditioning of the equation system used to extract the parameters becomes very poor. The properties of the equation system used to calculate the parameters suggests that this restriction can be overcome by using optimisation rather than inversion-based solution methods. Genetic Algorithms (Goldberg, 1989) appear to be attractive in this respect. The consequences for applications are that most one-dimensional problems such as rapid scan sonar can be tackled in a relatively routine way, but that at present two-dimensional applications GC-C must be used in a more thoughtful manner. A direct approach is viable for cases with a few dominant length scales or in conjunction with other methods which provide a preliminary exploration of the problem. A compromise form of GC-C can be set up which does yield a very large number of model parameters in a routine manner. This preserves long-range coherence in one rather than two dimensions.

So far only a trigonometric representation of the displacement/flow-field model version of discretized GC-C has been examined in detail in terms of its condition number behavior. There are a limitless number of other possible representations (Belmont and Hotchkiss, 1997) to explore and given the analytic difficulties it will almost certainly be necessary to investigate each of these in turn.

8 Results Update

The above work employed the lowest possible bandwidth image, i.e., one cycle over the domain. This has recently been

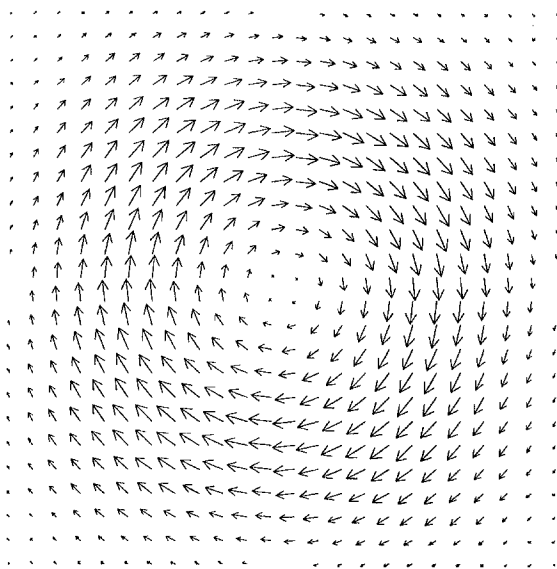


Fig. 4 A vector plot of the flow field as defined by Eqs. (8) and (9). The initial image f , was given by Eq. (3). Noise was added to the displacement and 50 samples were used per spatial dimension. Results were averaged over 15 separate runs.

Table 1 Effects of wideband noise added to the flow field in Fig. 4

Percentage RMS Noise Added to Velocity	Percentage RMS Error Coefficients
0.0	0.03
1	0.33
10	3.3
100	32

shown to be very much a worst-case situation and findings for wider band images, much more typical of real experimental data, show that the condition number problems are far less for such images. This allows the full two-dimensional form of GC-C can be applied over many length scales with usually more than 100 nonzero parameters. The reasons for this are almost certainly because the width of any type of correlation object is a reducing function of the bandwidth of the data. Hence: (i) in this case, a slowly changing image can be approximated by a proportionately wider range of "wrong parameters" than a wider bandwidth image, and (ii) for a given size of shift a much larger change will be introduced in the wideband case. While the formal position concerning the current state of development of the Discrete Implementation of GC-C must still remain that described for the worst case those potential users wishing to implement the technique in the nonanalytic form on typical experimentally derived images can expect with some degree of confidence to press the method far beyond the most pessimistic position.

References

- Adrian, R. J., 1986, "Multi-point optical measurement of simultaneous vectors in unsteady flow—A review," *Int. J. of Heat and Fluid Flow*, Vol. 7, No. 2, pp. 127–145.
- Belmont, M. R., and Hotchkiss, A. J., 1997, "The Generalized Cross-Correlation Functions for Engineering Applications, Part I: Basic Theory," *ASME JOURNAL OF APPLIED MECHANICS*, Vol. 64, pp. 321–326.
- Brigham, E. O., 1988, *The Fast Fourier Transform and its Applications*, Prentice-Hall, Englewood Cliffs, NJ.
- Goldberg, D. E., 1989, *Genetic Algorithms in Search, Optimisation and Machine Learning*, Addison-Wesley; also Z. Michalewicz, 1992, *Genetic Algorithms + Data Structures = Evolutionary Programs*, Springer-Verlag, New York.
- Golub, G., and Van Loan, C. F., 1989, *Matrix Computations*, 2nd ed., The Johns Hopkins Univ. Press.
- Hamming, R. W., 1977, *Digital Filters*, Prentice-Hall, Englewood Cliffs, NJ.
- Kamachi, M., 1989, "Advective surface velocities derived from sequential images for rotational flow field—Limitations and applications of maximum cross-correlation method with rotational registration," *J. Geophysical Research-Oceans*, Vol. 94, NC12, pp. 18,227–18,233.
- Leese, J. A., Novak, C. S., and Clark, B. B., 1971, "An automated technique for Obtaining Cloud Motion from Geosynchronous Satellite Data Using Cross-Correlation," *J. Appl. Met.* Vol. 10, No. 1, pp. 118–132.
- Mandelbrot, B. B., 1983, *The Fractal Geometry of Nature*, W. H. Freeman and Co., San Francisco, CA.
- Ninnis, R. M., Emerey, W. J., and Collins, M. J., 1986, "Automated extraction of Pack Ice Motion from Advanced Very High Resolution Radiometer Imagery," *J. Geophys. Res.*, Vol. 91, No. C9, pp. 10,725–10,734.
- Press, W. H., et al., 1987, *Numerical Recipes*, Cambridge University Press, Cambridge, U.K.
- Utami, T., Blackwelder, R. F., and Ueno, T., 1991, "A cross-correlation technique for Velocity Field extraction from particulate visualisation," *Experiments in Fluids*, Vol. 10, No. 4, pp. 213–223.
- Willert, C. E., and Gharib, M., 1991, "Digital Particle Image Velocimetry," *Experiments in Fluids*, Vol. 10, No. 4, pp. 181–193.

APPENDIX

This appendix lists the discrete convolutions needed to compute the $\Theta[p, q]$ functions in the equation system coefficients, (28')–(33').

Defining the following Fourier Series coefficients,

$$P_1[p, q] \Leftrightarrow f_1(\zeta_1, \zeta_2) \quad (A1)$$

$$P_2[p, q] \Leftrightarrow f_2(\zeta_1, \zeta_2), \quad (A2)$$

the terms Θ_1 to Θ_6 are given by $\Theta_1[p, q]$ as previously stated in (28'), and

$$\begin{aligned} \Theta_2[p, q] = & \frac{2}{N^2} j \frac{2\pi}{L_1} \sum_{r=0}^N \sum_{s=0}^N r \Phi[r, s] \\ & \times P_1[r, s] P_2[(r-p), (s-q)] \quad (A3) \end{aligned}$$

$$\begin{aligned} \Theta_3[p, q] = & \frac{2}{N^2} j \frac{2\pi}{L_2} \sum_{r=0}^N \sum_{s=0}^N s \Phi[r, s] \\ & \times P_1[r, s] P_2[(r-p), (s-q)] \quad (A4) \end{aligned}$$

$$\begin{aligned} \Theta_4[p, q] = & -\frac{2}{N^2} \left(\frac{2\pi}{L_1} \right)^2 \sum_{r=0}^N \sum_{s=0}^N r^2 \Phi[r, s] \\ & \times P_1[r, s] P_2[(r-p), (s-q)] \quad (A5) \end{aligned}$$

$$\begin{aligned} \Theta_5[p, q] = & -\frac{2}{N^2} \left(\frac{2\pi}{L_2} \right)^2 \sum_{r=0}^N \sum_{s=0}^N s^2 \Phi[r, s] \\ & \times P_1[r, s] P_2[(r-p), (s-q)] \quad (A6) \end{aligned}$$

$$\begin{aligned} \Theta_6[p, q] = & -\frac{2}{N^2} \frac{(2\pi)^2}{L_1 L_2} \sum_{r=0}^N \sum_{s=0}^N rs \Phi[r, s] \\ & \times P_1[r, s] P_2[(r-p), (s-q)] \quad (A7) \end{aligned}$$

where the index N must be optimized in a given application in order to minimize discrete convolution end effect errors, and $\Phi[r, s]$ is a low pass filter function whose roll-off is set just outside the bandwidth of the $\Theta[p, q]$ coefficients. The roll-off of $\Phi[r, s]$ must be chosen so as a compromise between minimizing that portion of the differentiator bandwidth beyond that of the $\Theta[p, q]$ coefficients while also minimizing Gibbs Phenomenon errors.

This approach obviously entails more computational effort than direct differencing and should only be invoked when significant uncorrelated high-frequency differences, considered as noise, exist between f_1 and f_2 .

Asymptotics of Flexural Waves in Isotropic Elastic Plates

N. A. Losin

10834 N. 32nd Lane,
Phoenix, AZ 85029

The long and short-wave asymptotics of order $O(k^6 h^6)$ for the flexural vibrations of an infinite, isotropic, elastic plate are studied. The differential equation for the flexural motion is derived from the system of three-dimensional dynamic equations of linear elasticity. All coefficients of the differential operator are presented as explicit functions of the material parameter $\gamma = c_s^2/c_L^2$, the ratio of the velocities squared of the flexural (shear) and extensional (longitudinal) waves. Relatively simple frequency and velocity dispersion equations for the flexural waves are deduced in analytical form from the three-dimensional analog of Rayleigh-Lamb frequency equation for plates. The explicit formulas for the group velocity are also presented. Variations of the velocity and frequency spectrums depending on Poisson's ratio are illustrated graphically. The results are discussed and compared to those obtained and summarized by R. D. Mindlin (1951, 1960), Tolstoy and Usdin (1953, 1957), and Achenbach (1973).

1 Introduction

The problem of elastic wave motion in infinite plates, because of its technical importance, has been the subject of many investigations. We list here just a few original works, reviews, and summaries that contain extensive bibliographies on this topic, reflect the main achievements, and describe some basic methods of investigation: Achenbach (1973) through Brekhovskikh and Goncharov (1994); Davis (1988) through Kolsky (1963); Miklowitz (1966) through Ufland (1948). According to some early and relatively recent publications: (Redwood, 1960; Bedford and Drumheller, 1994; Bland, 1988; Brekhovskikh and Goncharov, 1994; Doyle, 1989; Reismann, 1988), no simple direct relations between velocity-frequency and wave numbers

analysis of the corresponding dynamic boundary value problem is employed. This method was initially applied for solution of wave problems for thin-shelled structures in Protchenko (1980). Later, it was used for the computer-generated derivation of the propagation equations and numerical analysis of normal waves motion in cylindrical shells (Losin and Protchenko, 1984).

2 Formulation

Consider free wave motion in an isotropic plate of thickness $2h$, bounded by two planes $z = \pm h$, and infinite in (x, y) directions. We formulate the corresponding dynamic boundary value problem of linear elasticity in matrix form

$$\left\{ \begin{pmatrix} \mu & 0 & 0 \\ 0 & \mu & 0 \\ 0 & 0 & \lambda + 2\mu \end{pmatrix} \partial_z^2 + \begin{pmatrix} 0 & 0 & (\lambda + \mu)\partial_x \\ 0 & 0 & (\lambda + \mu)\partial_y \\ (\lambda + \mu)\partial_x & (\lambda + \mu)\partial_y & 0 \end{pmatrix} \partial_z \right. \\ \left. + \begin{pmatrix} (\lambda + 2\mu)\partial_x^2 + \mu\partial_y^2 & (\lambda + \mu)\partial_{xy}^2 & 0 \\ (\lambda + \mu)\partial_{yx}^2 & \mu\partial_x^2 + (\lambda + 2\mu)\partial_y^2 & 0 \\ 0 & 0 & \mu(\partial_x^2 + \partial_y^2) \end{pmatrix} - \rho I \partial_t^2 \right\} \mathbf{U} = \mathbf{0}, \quad (1)$$

for infinite plates are available at the present time. The asymptotic expansion of the frequency equation for flexural waves in plates generated by the Rayleigh-Lamb equation does not give an adequate approximation, even for velocities $v < c_s$. Moreover, three-dimensional wave propagation is possible at velocities $v > c_s$. All this motivates the search for some different approaches for the solution to the problem. This article is an attempt to find a relatively simple explicit frequency and velocity dispersion relations from the three-dimensional analog of the Rayleigh-Lamb frequency equation that would be adequate for flexural and extensional waves. The asymptotic method for

$$\mathcal{T} = \left\{ \begin{pmatrix} \mu & 0 & 0 \\ 0 & \mu & 0 \\ 0 & 0 & \lambda + 2\mu \end{pmatrix} \partial_z \right. \\ \left. + \begin{pmatrix} 0 & 0 & \mu\partial_x \\ 0 & 0 & \mu\partial_y \\ \lambda\partial_x & \lambda\partial_y & 0 \end{pmatrix} \right\} \mathbf{U} = \mathbf{0}, \quad z = \pm h, \quad (2)$$

where (1) is the system of Navier's equations written in terms of Lamé's constants λ, μ ; the boundary conditions (2) express the absence of stresses at the free plate's surfaces $z = \pm h$; $\mathbf{U} = \mathbf{U}(x, y, z, t) = \{U_x, U_y, U_z\}'$ is the displacement vector; $\mathcal{T} = \{\tau_{xz}, \tau_{yz}, \tau_{zz}\}'$ is the stress vector; ρ is the density of the plate; and I is the identity matrix.

We seek solutions in the form of an harmonic wave

$$\mathbf{U}(x, y, z, t) = \mathbf{u}(z)e^{-i(k_x x + k_y y - \omega t)}, \quad (3)$$

where $\mathbf{u}(z) = \{u_x(z), u_y(z), u_z(z)\}'$ is the amplitude vector;

Contributed by the Applied Mechanics Division of THE AMERICAN SOCIETY OF MECHANICAL ENGINEERS for publication in the ASME JOURNAL OF APPLIED MECHANICS.

Discussion on the paper should be addressed to the Technical Editor, Professor Lewis T. Wheeler, Department of Mechanical Engineering, University of Houston, Houston, TX 77204-4792, and will be accepted until four months after final publication of the paper itself in the ASME JOURNAL OF APPLIED MECHANICS.

Manuscript received by the ASME Applied Mechanics Division, Sept. 13, 1995; final revision, Nov. 27, 1996. Associate Technical Editor: D. M. Barnett.

$\omega = \omega(\mathbf{k})$ is the circular frequency depending on \mathbf{k} (dispersion relation); $\mathbf{k} = \{k_x, k_y\}$ is the wave vector. Differentiating (3) with respect to x, y, t , and replacing partial derivatives by their symbols

$$\begin{aligned}\partial_x &\rightarrow -ik_x, \quad \partial_y \rightarrow -ik_y, \quad \partial_t \rightarrow i\omega, \\ \partial_x^2 &\rightarrow -k_x^2, \quad \partial_y^2 \rightarrow -k_y^2, \quad \partial_t^2 \rightarrow -\omega^2,\end{aligned}\quad (4)$$

we may reduce (1) and (2) to the form

$$D\mathbf{u}'' - B_0(k)\mathbf{u}' - C_0(k)\mathbf{u} = \mathbf{0}, \quad -h < z < h, \quad (5)$$

$$\mathcal{T}(z, k) = D\mathbf{u}' - A_0(k)\mathbf{u} = \mathbf{0}, \quad z = \pm h, \quad (6)$$

$$B_0(k) = ik \begin{pmatrix} 0 & 0 & (\lambda + \mu)n_1 \\ 0 & 0 & (\lambda + \mu)n_2 \\ (\lambda + \mu)n_1 & (\lambda + \mu)n_2 & 0 \end{pmatrix},$$

$$A_0(k) = ik \begin{pmatrix} 0 & 0 & \mu n_1 \\ 0 & 0 & \mu n_2 \\ \lambda n_1 & \lambda n_2 & 0 \end{pmatrix},$$

$$C_0(k) = k^2 \begin{pmatrix} (\lambda + 2\mu)n_1^2 + \mu n_2^2 - \rho v^2 & (\lambda + \mu)n_1 n_2 & 0 \\ (\lambda + \mu)n_2 n_1 & \mu n_1^2 + (\lambda + 2\mu)n_2^2 - \rho v^2 & 0 \\ 0 & 0 & \mu(n_1^2 + n_2^2) - \rho v^2 \end{pmatrix},$$

$$D = \text{diag} \{ \mu, \mu, \lambda + 2\mu \}, \quad B_0(k) = A_0(k) + A_0'(k),$$

$$\mathbf{u}' = d\mathbf{u}(z)/dz, \quad v(\mathbf{k}) = \omega(\mathbf{k})/k, \quad (7)$$

$$v(\mathbf{k}) = |\mathbf{v}(\mathbf{k})|, \quad k = |\mathbf{k}| = \sqrt{k_x^2 + k_y^2}, \quad \mathbf{k} = |\mathbf{k}|\mathbf{n} = k\mathbf{n},$$

$$\mathbf{n} = \{n_1, n_2\}, \quad n_1 = k_x/k, \quad n_2 = k_y/k,$$

where \mathbf{v} is the phase velocity and v is the phase speed of a traveling wave; \mathbf{n} is the unit direction vector; and n_1, n_2 are direction cosines of \mathbf{n} . Then, we multiply (5), (6) by the diagonal matrix D^{-1} from the left, eliminate the Lamé's constants λ, μ , and express matrix coefficients through the unique parameter γ , the ratio of the velocities squared of the shear and extensional waves. Introducing the modified stress vector \mathcal{T}_c , we finally formulate the boundary value problem in matrix form as the following system of ordinary differential equations:

$$\mathbf{u}'' = \hat{B}(k)\mathbf{u}' + \hat{C}(k)\mathbf{u}, \quad -h < z < h, \quad (8)$$

$$\mathcal{T}_c(z, k) = \rho(\mathbf{u}' - \hat{A}(k)\mathbf{u}) = \mathbf{0}, \quad z = \pm h, \quad (9)$$

$$\hat{B}(k) = D^{-1}B_0(k) = kB, \quad \hat{C}(k) = D^{-1}C_0(k) = k^2C,$$

$$\hat{A}(k) = D^{-1}A_0(k) = kA,$$

$$D^{-1} = \text{diag} \{ \mu^{-1}, \mu^{-1}, (\lambda + 2\mu)^{-1} \},$$

$$B = i \begin{pmatrix} 0 & 0 & (\gamma^{-1} - 1)n_1 \\ 0 & 0 & (\gamma^{-1} - 1)n_2 \\ (1 - \gamma)n_1 & (1 - \gamma)n_2 & 0 \end{pmatrix},$$

$$A = i \begin{pmatrix} 0 & 0 & n_1 \\ 0 & 0 & n_2 \\ (1 - 2\gamma)n_1 & (1 - 2\gamma)n_2 & 0 \end{pmatrix},$$

$$C = \begin{pmatrix} \gamma^{-1}n_1^2 + n_2^2 - v_s^2 & (\gamma^{-1} - 1)n_1 n_2 & 0 \\ (\gamma^{-1} - 1)n_2 n_1 & n_1^2 + \gamma^{-1}n_2^2 - v_s^2 & 0 \\ 0 & 0 & \gamma(1 - v_s^2) \end{pmatrix},$$

where $\mathcal{T}_c(z, k) = \rho D^{-1}\mathcal{T}(z, k) = \{\tau_{xz}/c_s^2, \tau_{yz}/c_s^2, \tau_{zz}/c_L^2\}$ is the modified stress vector; c_s, c_L are velocities (speeds) of the shear and extensional waves, respectively,

$$c_s^2 = \mu/\rho, \quad c_L^2 = (\lambda + 2\mu)/\rho, \quad v_s = v/c_s, \quad v_L = v/c_L,$$

$$\gamma = c_s^2/c_L^2 = \mu/(\lambda + 2\mu), \quad c_s^2 = \gamma c_L^2, \quad v_L^2 = \gamma v_s^2.$$

3 Asymptotic Boundary Value Problem

Assuming that $\mathcal{T}_c(z, k)$ has a finite asymptotic expansion of the form $\mathcal{T}_c(z, k) = \sum_{n=0}^N \hat{\mathcal{T}}_c^{(n)}(\zeta)\epsilon^n + o(\epsilon^N)$, $\zeta = z/h$, $\epsilon = kh$, we approximate it by the partial sum of Taylor series in $z(-h < z < h)$, about $z = 0$

$$\mathcal{T}_c(z) = \rho(\mathbf{u}' - \hat{A}(k)\mathbf{u}) = \sum_{n=0}^N \mathcal{T}_c^{(n)}(0)z^n/n! + o(z^N),$$

where the second argument of \mathcal{T}_c is omitted for convenience.

Denoting $\mathcal{T}_c^+ = \mathcal{T}_c(h)$, $\mathcal{T}_c^- = \mathcal{T}_c(-h)$, and combining them as

$$\mathcal{T}_c^+ + \mathcal{T}_c^- = \mathbf{0}, \quad \mathcal{T}_c^+ - \mathcal{T}_c^- = \mathbf{0},$$

we obtain the boundary conditions in the asymptotic form

$$\mathcal{T}_c(0) + \frac{h^2}{2} \mathcal{T}_c''(0) + \frac{h^4}{24} \mathcal{T}_c^{(4)}(0) \approx \mathbf{0} \quad (10)$$

$$\mathcal{T}_c'(0) + \frac{h^2}{6} \mathcal{T}_c'''(0) + \frac{h^4}{120} \mathcal{T}_c^{(5)}(0) \approx \mathbf{0}. \quad (11)$$

The approximate equality signs here are due to the truncated infinite series on the left-hand sides of (10) and (11). Differentiating $\mathcal{T}_c(z)$ in z five times,

$$\mathcal{T}_c^{(n)}(z) = \rho(\mathbf{u}^{(n+1)} - \hat{A}(k)\mathbf{u}^{(n)}), \quad (n = 1, \dots, 5), \quad (12)$$

and substituting (12) at $z = 0$ into (10), (11), we arrive at the asymptotic boundary value problem in terms of the displacement vector \mathbf{u} :

$$\mathbf{u}'' = \hat{B}(k)\mathbf{u}' + \hat{C}(k)\mathbf{u}, \quad -h < z < h, \quad (13)$$

$$\begin{aligned}\mathbf{u}'(0) - \hat{A}(k)\mathbf{u}(0) + \frac{h^2}{2}(\mathbf{u}'''(0) - \hat{A}(k)\mathbf{u}''(0)) \\ + \frac{h^4}{24}(\mathbf{u}^{(5)}(0) - \hat{A}(k)\mathbf{u}^{(4)}(0)) \approx \mathbf{0},\end{aligned}\quad (14)$$

$$\begin{aligned}\mathbf{u}''(0) - \hat{A}(k)\mathbf{u}'(0) + \frac{h^2}{6}(\mathbf{u}^{(4)}(0) - \hat{A}(k)\mathbf{u}'''(0)) \\ + \frac{h^4}{120}(\mathbf{u}^{(6)}(0) - \hat{A}(k)\mathbf{u}^{(5)}(0)) \approx \mathbf{0}.\end{aligned}\quad (15)$$

Equations (14) and (15) are valid at the free surfaces, i.e., at the boundaries of a plate $z = \pm h$.

4 Resolving Operator Equation

The asymptotic boundary value problem, i.e., the system (13)–(15), can be reduced to one resolving operator equation written in terms of lambda matrices (Lancaster, 1966). First, we differentiate Eq. (13) four times:

$$\mathbf{u}^{(n+2)} = \hat{B}(k)\mathbf{u}^{(n+1)} + \hat{C}(k)\mathbf{u}^{(n)}, \quad (n = 1, \dots, 4).$$

Then, using Eq. (13) again, we express derivatives $\mathbf{u}^{(n)}(0)$,

($n = 2, \dots, 6$), in (14), (15) through $\mathbf{u}(0)$ and $\mathbf{u}'(0)$ with some new matrix coefficients

$$\left(I + \frac{k^2 h^2}{2} G + \frac{k^4 h^4}{24} E\right) \mathbf{u}'(0) - k \left(A - \frac{k^2 h^2}{2} H - \frac{k^4 h^4}{24} F\right) \mathbf{u}(0) \approx \mathbf{0} \quad (16)$$

$$k \left(B - A + \frac{k^2 h^2}{6} K + \frac{k^4 h^4}{120} P\right) \mathbf{u}'(0) + k^2 \left(C + \frac{k^2 h^2}{6} L + \frac{k^4 h^4}{120} Q\right) \mathbf{u}(0) \approx \mathbf{0}, \quad (17)$$

$$G = C + (B - A)B, \quad H = (B - A)C, \\ K = H + GB, \quad (18)$$

$$L = GC, \quad E = L + KB, \quad F = KC,$$

$$P = EB + F, \quad Q = EC.$$

The system (8)–(9), and, consequently, the system (16)–(17), can be simplified by rotating the coordinate system, i.e., considering the waves propagating along one of the coordinate axes, for example, the OX-axis. In this case, the matrices G and E have the diagonal structure $G = \text{diag} \{g_{11}, g_{22}, g_{33}\}$, $E = \text{diag} \{e_{11}, e_{22}, e_{33}\}$, as well as the matrix coefficient $M = \text{diag} \{m_{11}, m_{22}, m_{33}\}$ in front of $\mathbf{u}'(0)$ in (16),

$$M = I + \frac{k^2 h^2}{2} G + \frac{k^4 h^4}{24} E,$$

$$m_{jj} = 1 + \frac{k^2 h^2}{2} g_{jj} + \frac{k^4 h^4}{24} e_{jj}, \quad (j = 1, 2, 3),$$

$$m_{11} = 1 + k^2 h^2 / 2 (3 - 2\gamma - v_s^2) \\ + k^4 h^4 / 24 (v_s^4 - 2(2 - \gamma^2)v_s^2 + 5 - 4\gamma), \\ m_{22} = 1 + k^2 h^2 / 2 (1 - v_s^2) + k^4 h^4 / 24 (1 - v_s^2)^2, \\ m_{33} = 1 + k^2 h^2 / 2 (2\gamma - 1 - \gamma v_s^2) \\ + k^4 h^4 / 24 (\gamma^2 v_s^4 + 2(1 - \gamma - \gamma^2)v_s^2 - 3 + 4\gamma).$$

The diagonal matrix M is easily invertible,

$$M^{-1} = \text{diag} \{m_{11}^{-1}, m_{22}^{-1}, m_{33}^{-1}\}, \quad m_{jj} \neq 0,$$

and Eq. (16) can be solved for $\mathbf{u}'(0)$ as

$$\mathbf{u}'(0) \approx k M^{-1} \left(A - \frac{k^2 h^2}{2} H - \frac{k^4 h^4}{24} F\right) \mathbf{u}(0). \quad (19)$$

Substituting (19) into (17), we finally come to the resolving operator of the form

$$T \mathbf{u}(0) = \left(T_0 + \frac{k^2 h^2}{6} T_2 + \frac{k^4 h^4}{120} T_4\right) \mathbf{u}(0) \approx \mathbf{0} \quad (20)$$

$$T_0 = C + (B - A)M^{-1}A,$$

$$T_2 = L + KM^{-1}A - 3(B - A)M^{-1}H$$

$$T_4 = Q + PM^{-1}A - 10KM^{-1}H - 5(B - A)M^{-1}F.$$

The matrix of the operator T has a diagonal block structure (in general case) where the blocks governing flexural (T_s) and in-plane (T_L) motion are separated:

$$T \mathbf{u}(0) = \begin{pmatrix} t_{11} & t_{12} & 0 \\ t_{21} & t_{22} & 0 \\ 0 & 0 & t_{33} \end{pmatrix} \begin{bmatrix} u_x(0) \\ u_y(0) \\ u_z(0) \end{bmatrix} \approx \mathbf{0}, \quad (21)$$

$$T_L = \begin{pmatrix} t_{11} & t_{12} \\ t_{21} & t_{22} \end{pmatrix}, \quad T_s \equiv t_{33}. \quad (22)$$

We regard the system (21) as a homogeneous system of linear algebraic equations $T \mathbf{u}(0) = \mathbf{0}$. Such a system has non-trivial solutions if its determinant vanishes, i.e., if

$$\det T = \det T_L \cdot \det T_s = 0 \quad (23)$$

$$\det T_L = 0 \quad (24)$$

$$\det T_s = 0, \quad \text{or} \quad t_{33} = 0. \quad (25)$$

Equation (23) is the three-dimensional analog of the Rayleigh-Lamb frequency equation for a plate. Equations (24) and (25) are the corresponding frequency equations for extensional and flexural vibrations, respectively.

5 Flexural Motion of a Plate

Equation (25) is the third equation of the system (21) that governs the flexural vibrations, since the operator $T_s = t_{33}$ affects the displacement $u_z \equiv w$ only. This equation generates the dispersion equation, the velocity equation, and the differential equation of a plate's flexural motion. According to the structure (20) of the operator T , Eq. (25) has the form

$$t_{33}^{(0)} + \frac{k^2 h^2}{6} t_{33}^{(2)} + \frac{k^4 h^4}{120} t_{33}^{(4)} = 0, \quad (26)$$

$$t_{33}^{(0)} = -\gamma k^2 v_s^2 / m_{11}, \quad t_{33}^{(2)} = \gamma k^2 (a_0 v_s^4 - a_1 v_s^2 + a_2) / m_{11}, \quad (27)$$

$$t_{33}^{(4)} = -\gamma k^2 (b_0 v_s^6 - b_1 v_s^4 + b_2 v_s^2 - b_3) / m_{11},$$

$$a_0(\gamma) = (3 + \gamma), \quad a_1(\gamma) = 4(3 - 2\gamma),$$

$$a_2(\gamma) = 8(1 - \gamma), \quad (28)$$

$$b_0(\gamma) = 5 + 10\gamma + \gamma^2, \quad b_1(\gamma) = 4(9 + 3\gamma - 4\gamma^2),$$

$$b_2(\gamma) = 16(4 - 2\gamma - \gamma^2),$$

$$b_3(\gamma) = 32(1 - \gamma) = 4a_2(\gamma),$$

where $v_s = v/c_s$ is the dimensionless phase velocity of a wave. The substitution of (27) into (26) gives the desired result

$$b_0 v_s^6 - \left(b_1 + \frac{20}{k^2 h^2} a_0\right) v_s^4 + \left(b_2 + \frac{20}{k^2 h^2} a_1 + \frac{120}{k^4 h^4}\right) v_s^2 \\ - b_3 \left(1 + \frac{5}{k^2 h^2}\right) = 0. \quad (29)$$

Equation (29) is the final velocity equation for the flexural vibrations of a plate. The substitution $v_s = \omega_s/k$ turns the velocity Eq. (29) into the frequency equation

$$b_0 \omega_s^6 - \left(b_1 k^2 + \frac{20}{h^2} a_0\right) \omega_s^4 + \left(b_2 k^4 + \frac{20}{h^2} a_1 k^2 + \frac{120}{h^4}\right) \omega_s^2 \\ - b_3 \left(k^6 + \frac{5}{h^2} k^4\right) = 0. \quad (30)$$

Equation (30) is the dispersion equation for the flexural motion of a plate with respect to the ratio $\omega_s = \omega/c_s$. Rearranging terms in Eq. (30) and substituting symbols (4) backward by the corresponding partial derivatives, (where $\nabla^4 \rightarrow k^4$), we

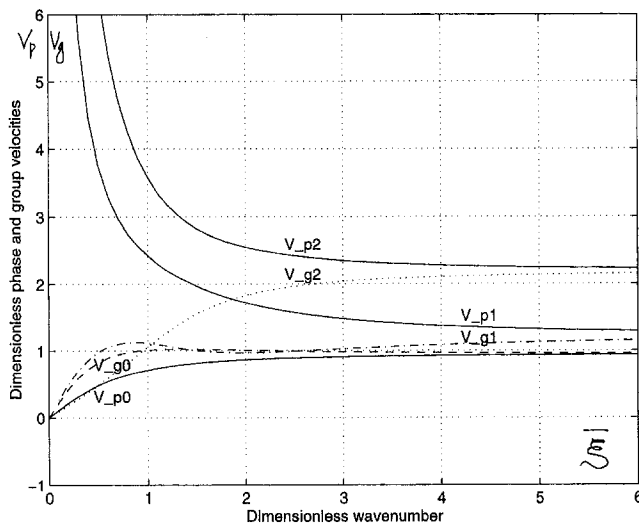


Fig. 1 Phase V_{pi} and group V_{gi} , ($i = 0, 1, 2$), velocity spectrums of flexural modes for $\nu = \frac{1}{2}$ ($\gamma = 0$)

finally obtain the differential equation for the flexural motion of a plate in the form

$$\left\{ \partial_t^2 + \frac{h^2}{6} (a_0 \partial_t^4 - a_1 \partial_t^2 \nabla^2 + a_2 \nabla^4) + \frac{h^4}{120} (b_0 \partial_t^6 - b_1 \partial_t^4 \nabla^2 + b_2 \partial_t^2 \nabla^4 - b_3 \nabla^6) \right\} w = 0, \quad (31)$$

where the coefficients $a_i(\gamma)$, $b_i(\gamma)$, ($i = 0, 1, 2; j = 0, 1, 2, 3$), of the differential operator are functions (28) of the dimensionless material parameter $\gamma = c_s^2/c_L^2$, or Poisson's ratio ν since $\gamma = (1 - 2\nu)/(2(1 - \nu))$.

6 Velocity and Frequency Spectrums

The phase velocities of a propagating wave are roots of the bicubic algebraic Eq. (29) with coefficients depending on two parameters kh and γ . The solutions of (29) give the phase velocities v_s of three wave modes (in general case) as functions of kh and γ . Their graphs corresponding to Poisson's ratios $\nu = \frac{1}{4}$ and $\nu = 0$, are shown in Figs. 2 and 3. For incompressible materials ($\nu = \frac{1}{2}$), the same equation is valid, and the velocities distribution can be obtained by solving Eq. (29) with $\gamma = 0$ (Fig. 1).

The wave motion under consideration is dispersive and the dispersion relation is given by Eq. (30). Its roots represent the frequency spectrum of vibrations depending on k , h , and γ . Differentiating Eq. (30) with respect to k , where $\omega_s = \omega_s(k)$, we obtain the following expressions for the group velocity $V_g(k) = d\omega(k)/dk$ of the flexural motion in terms of the frequency ω_s :

$$V_g = \frac{b_1 \omega_s^4 k - 2\omega_s^2 (b_2 k^3 + k 10a_1/h^2) + b_3 (3k^5 + 10k^3/h^2)}{3b_0 \omega_s^5 - 2\omega_s^3 (b_1 k^2 + 20a_0/h^2) + \omega_s (b_2 k^4 + k^2 20a_1/h^2 + 120/h^4)},$$

or in terms of the velocity $v_s(k) = \omega_s(k)/k$

$$V_g = \frac{b_1 v_s^4 - 2v_s^2 (b_2 + 10a_1/k^2 h^2) + b_3 (3 + 10/k^2 h^2)}{3b_0 v_s^5 - 2v_s^3 (b_1 + 20a_0/k^2 h^2) + v_s (b_2 + 20a_1/k^2 h^2 + 120/k^4 h^4)}. \quad (32)$$

The velocity and the frequency spectrums are shown in Figs. 1–6.

7 Long and Short-Wave Approximations

Both long and short-wave approximations are available from Eqs. (29), (30). For long waves, the wavelength is very large compared to the thickness $2h$ of the plate, i.e., $kh \rightarrow 0$. The limiting form of Eq. (30) is

$$\omega_s^2 (b_0 \omega_s^4 - 20a_0 \omega_s^2/h^2 + 120/h^4) = 0, \quad (33)$$

which obviously has one trivial solution $\omega_s = 0$. The corresponding phase velocity is also equal to zero. The biquadratic equation in (33) with coefficients depending on h and γ , (or ν), gives two more roots in general case. These two roots are real and different practically in all the physical domain of Poisson's ratio ($0.02 \leq \nu \leq 0.5$) and for the thickness range $2h = \frac{1}{10} - \frac{1}{20}$. They are values of the cut-off frequencies for the first and second modes with the corresponding phase velocities tending to infinity (see Figs. 1 and 2). The exception is a very small neighborhood of the origin ($0 \leq \nu < 0.02$) where the biquadratic equation has a pair of complex-conjugate roots.

For the short-wave approximation, the wavelength is very small compared to the thickness of a plate. The substitution of $kh \rightarrow \infty$ into (29) gives the limiting form of the velocity equation

$$b_0 v_s^6 - b_1 v_s^4 + b_2 v_s^2 - b_3 = 0. \quad (34)$$

The roots of this bicubic equation are phase velocities of short-wave modes depending on the material parameter γ only. Equation (34) has three finite real roots that correspond to the velocities of the first three wave modes. The fundamental mode approaches to the velocity of Rayleigh's surface wave c_R . The first mode tends to the velocity c_s of the shear wave ($v/c_s \rightarrow 1$, or, $\nu \rightarrow c_s$). The second mode approaches to the limit which is very close to the thin-plate analog of the bar velocity $c_p = \sqrt{E/(\rho(1 - \nu^2))} = 2\sqrt{1 - \gamma}$.

8 Discussion of Results

1 Equation (31) is the asymptotic approximation of the order $O(k^6 h^6)$ to the differential equation for the flexural motion of a plate. The third term with coefficient $h^4/120$ in (31) is due to the high order effects. By omitting this term, the Eq. (31) is turned into the known standard form of the differential equation for the flexural vibrations of the order $O(k^4 h^4)$

$$\{D_c \nabla^4 - D_{12} \nabla^2 \partial_t^2 + D_{22} \partial_t^4 + \rho 2h \partial_t^2\} w = 0,$$

$$D_c = E(2h)^3/(12(1 - \nu^2)).$$

Here, the first and the last terms on the left-hand side of the differential equation are from the classical plate theory. The second and the third terms are due to the effects of the rotary inertia and the transverse shear deformations (Mindlin, 1951; Timoshenko, 1955).

All coefficients of the differential operator (31) are expressed as explicit functions (28) of the material parameter γ . Equations (29), (30) are velocity and frequency dispersion relations for

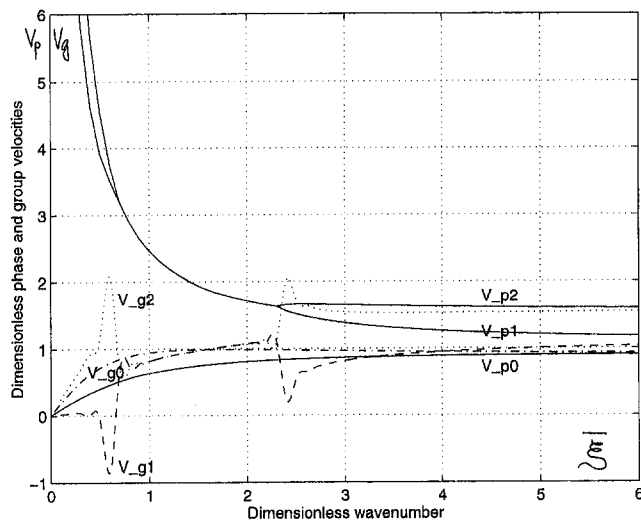


Fig. 2 Phase V_{pi} and group V_{gi} , ($i = 0, 1, 2$), velocity spectrums of flexural modes for $\nu = \frac{1}{4}$ ($\gamma = \frac{1}{3}$)

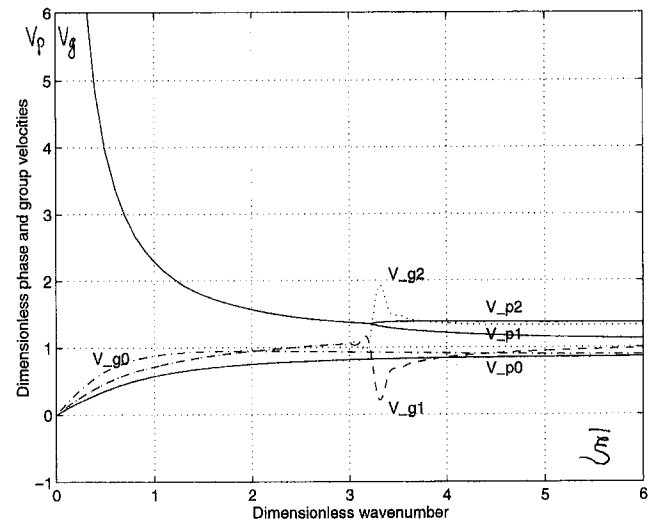


Fig. 3 Phase V_{pi} and group V_{gi} , ($i = 0, 1, 2$), velocity spectrums of flexural modes for $\nu = 0$ ($\gamma = \frac{1}{2}$)

flexural motion of a plate that are valid for any long or short-wave asymptotics, and for any materials ($0 \leq \nu \leq \frac{1}{2}$).

2 In order to improve the results, the method used in (Protsenko, 1980) was modified. Instead of the approximate matrix inversion by means of Neumann's series (Courant and Hilbert, 1962), the actual matrix inversion was applied for the solution of the boundary value problem. Both ways were tested and compared. The results of numerical experiments did clearly show the advantage of the new approach. This modification was found critical and very effective. It eliminated restrictions due to the convergence interval for the infinite matrix series, and permitted us to create the universal model applicable for both long and short-wave asymptotics, and for any materials.

3 The velocity and frequency spectrums depending on Poisson's ratio are shown in Figs. 1–3 and 4–6, respectively, in dimensionless coordinates

$$\bar{\xi} = \frac{\pi}{2} \xi, \quad \bar{\Omega} = \frac{\pi}{2} \Omega, \quad v_s = \frac{v}{c_s}, \quad \xi = \frac{2}{\pi} kh, \quad \Omega = \frac{2}{\pi c_s} \omega h.$$

There, the subscript $i = 0$ indicates the fundamental (lowest) flexural mode; $i = 1$ corresponds to the first equivoluminal mode, and $i = 2$ is associated with the first dilatational mode.

Comparing these graphs and the corresponding curves from Tolstoy and Usdin (1953, 1957), Mindlin (1951, 1960), and Achenbach (1973), we can see that the graphs of the phase and group velocities for the fundamental wave mode are perfectly approximated by the curves V_{p0} and V_{g0} , respectively, including incompressible materials (Fig. 1). They increase from the origin for long waves, and tend to the common limit c_R for short waves, as predicted by the exact plate theory. The accuracy of the approximation is impressive at this stage.

The phase velocities for the first mode are also in good agreement, except for the fact that the curve V_{p1} (Figs. 2, 3) is piecewise smooth. Both curves V_{p1} in Fig. 2 and the second antisymmetric mode M_{22} in Fig. 4 (Tolstoy and Usdin, 1953) decrease continuously from infinity for long waves, and approach the velocity c_s for short waves.

The correspondence between the group velocities is not so good. At high frequencies, the limit of V_{g1} is slightly greater than c_s , that is probably due to the approximation error. Although the curve V_{g1} in Fig. 2 is not smooth, it is similar to the graph M_{22} despite of the scaling factor used in Fig. 2 (Tolstoy and Usdin,

1957), while the curve V_{g2} only reminds the corresponding result in Fig. 4 (Tolstoy and Usdin, 1953).

4 One more wave mode is available in general case from the bicubic Eq. (29) with the phase velocity V_{p2} , the group velocity V_{g2} , and the frequency branch m_2 in Figs. 1–6. Its phase velocity $V_{p2} \rightarrow \infty$, as $kh \rightarrow 0$; V_{p2} coincides with V_{p1} for the intermediate wavelengths (see Figs. 2, 5), and V_{p2} is very close to the velocity c_p , as $kh \rightarrow \infty$. This last result indicates to some symmetric motion of a plate at high frequencies. It was mentioned by Tolstoy and Usdin (1957) for high modes, and confirmed experimentally by Evans et al., (1954).

The coupling of the first flexural and the first longitudinal modes in both velocity and frequency spectrums occurs over the interval $\nu < 0.37$ in Figs. 2, 3, 5, and 6. For high modes, this phenomenon was described by Mindlin (1960) and Tolstoy and Usdin (1957), but it was not reported for low ($i = 1$) equivoluminal or dilatational branches of the infinite plate with traction-free boundaries (Achenbach, 1973, p. 232). The credibility of this result is to be verified.

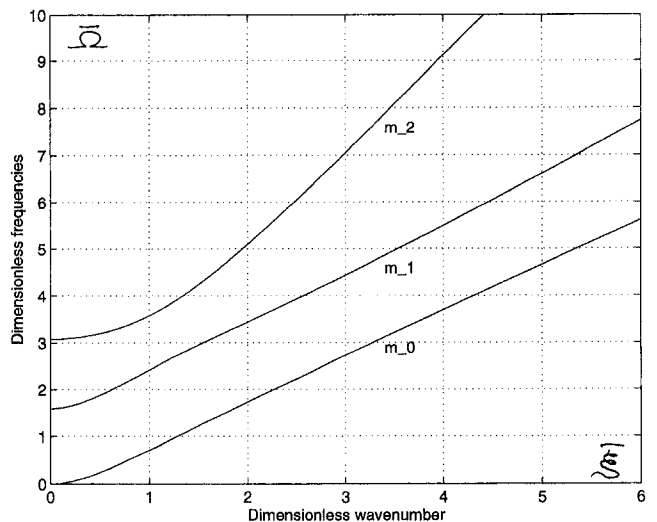


Fig. 4 Frequency spectrum of flexural modes m_i , ($i = 0, 1, 2$), for $\nu = \frac{1}{2}$ ($\gamma = 0$)

5 The interesting point is that the number of different branches in the frequency and velocity spectrums depends on Poisson's ratio and the wave number range in Figs. 1–6. The perturbations in the group velocities V_{g1} , V_{g2} are due to the bifurcation points of the corresponding phase velocities V_{p1} , V_{p2} . It should be separately noticed the appearance of the negative group velocity V_{g1} in a small neighborhood of the left bifurcation point in Fig. 2. This effect was detected by Tolstoy and Usdin (1957), and mentioned by some authors (Mindlin, 1960; Redwood, 1960).

Conclusion

The flexural wave motion in infinite isotropic elastic plates was studied by means of the asymptotic method applied to thin-shelled structures in (Protsenko, 1980). This method allowed the reduction of the boundary value problem to the corresponding asymptotic operator equation that generated the equations of propagation and the three-dimensional analog of Raleigh-Lamb frequency equation for flexural waves in plates. Some modification of the initial technique permitted development of the universal asymptotic model applicable for any long or short-wave approximations, and for any materials.

The three-dimensional analog of Rayleigh-Lamb frequency equation for plates was obtained and used to generate the approximations for dispersion relations. A relatively simple explicit frequency and velocity dispersion equations, the group velocity formulas, and the differential equation of flexural vibrations for plates were derived. The coefficients of all equations and formulas were presented as explicit functions of the material parameter γ .

The comparison of spectrums in Figs. 1–6 and the corresponding results in Mindlin (1951, 1960), Tolstoy and Usdin (1953, 1957), and Achenbach (1973) did show that the approximations given by formulas (29), (30), and (32) were obviously close to well-known results for flexural waves in plates. Variations of the velocity and frequency spectrums depending on Poisson's ratio were illustrated graphically. The velocity and frequency branches of the first two flexural modes were approximated well with some minor exceptions. Some discrepancies in graphs of velocities and frequencies were detected. A number of interesting features, such as negative group velocity, were observed. Some of these notable effects are still to be interpreted correctly.

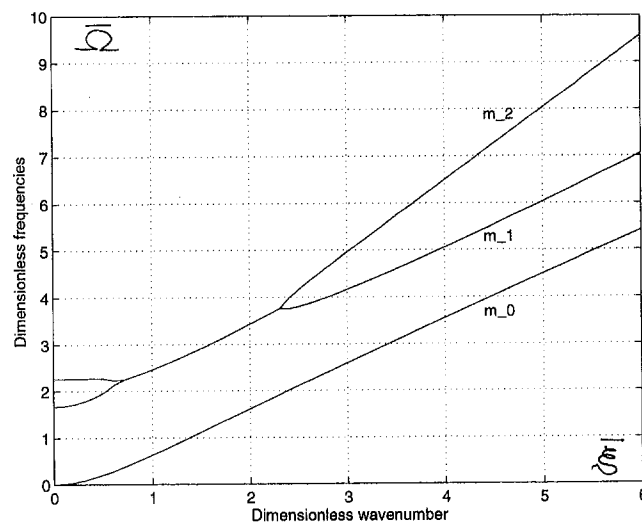


Fig. 5 Frequency spectrum of flexural modes m_i , ($i = 0, 1, 2$), for $\nu = \frac{1}{4}$ ($\gamma = \frac{1}{3}$)

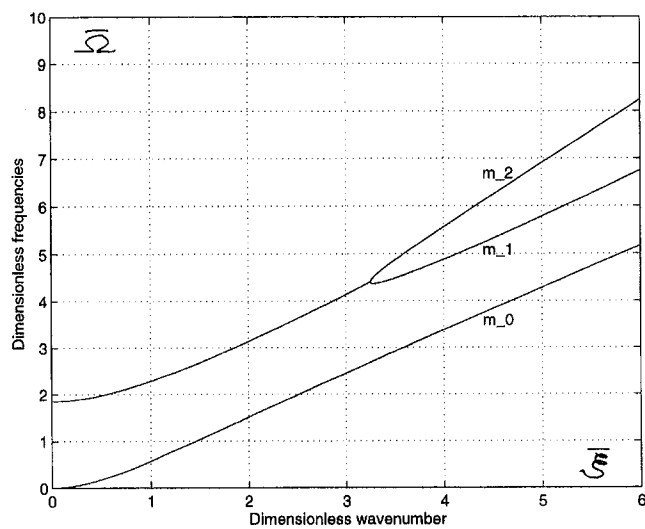


Fig. 6 Frequency spectrum of flexural modes m_i , ($i = 0, 1, 2$), for $\nu = 0$ ($\gamma = \frac{1}{2}$)

The derived dispersion relations give good approximations for the first two frequency and velocity modes without any correction factors, as in the Reissner-Mindlin theory.

The asymptotic analysis of extensional waves in plates is the subject of a separate publication.

Acknowledgment

The author is grateful to Prof. A. M. Protsenko, Moscow, Russia, for the statement of the problem and initial guidance; and to Prof. Basil Nicolaenko, Arizona State University, for moral and technical support.

References

- Achenbach, J. D., 1973, *Wave Propagation in Elastic Solids*, North-Holland, Amsterdam.
- Bache, T. C., and Hegemier, G. A., 1974, "On Higher-Order Elastodynamic Plate Theories," *ASME JOURNAL OF APPLIED MECHANICS*, Vol. 41, pp. 423–428.
- Bedford, A., and Drumheller, D. S., 1994, *Introduction to Elastic Wave Propagation*, John Wiley and Sons, New York.
- Bland, D. R., 1988, *Wave Theory and Applications*, Oxford University Press, New York.
- Brekhovskikh, L. M., and Goncharov, V., 1994, *Mechanics of Continua and Wave Dynamics*, Springer-Verlag, New York.
- Courant, R., and Hilbert, D., 1962, *Methods of Mathematical Physics*, Vol. 1, Wiley Interscience, New York.
- Davis, J. L., 1988, *Wave Propagation in Solids and Fluids*, Springer-Verlag, New York.
- Doyle, J. F., 1989, *Wave Propagation in Structures*, Springer-Verlag, New York.
- Eringen, A. C., and Suhubi, E. S., 1975, *Elastodynamics*, Vol. 2, Academic Press, New York.
- Evans, J. F., Hadley, C. F., Eisler, J. D., and Silverman, D., 1954, "A Three-Dimensional Seismic Wave Model with Both Electrical and Visual Observation of Waves," *Geophysics*, Vol. 19, pp. 220–236.
- Ewing, W. M., Jardetzky, W. S., and Press, F., 1957, *Elastic Waves in Layered Media*, McGraw-Hill, New York.
- Goldenveizer, A. L., Kaplunov, J. D., and Nold, E. V., 1993, "On Timoshenko-Reissner Type Theories of Plates and Shells," *International Journal of Solids and Structures*, Vol. 30, No. 5, pp. 675–694.
- Graff, K. F., 1991, *Wave Motion in Elastic Solids*, Dover, New York.
- Kolsky, H., 1963, *Stress Waves in Solids*, Dover, New York.
- Lancaster, P., 1966, *Lambda-Matrices and Vibrating Systems*, Pergamon Press, New York.
- Losin, N. A., and Protsenko, A. M., 1984, "Spectrum of Normal Waves in a Cylindrical Shell (Izvestia AN SSSR)," *Mechanics of Solids*, Vol. 19, No. 3, pp. 186–189.
- Miklowitz, J., 1966, "Elastic Wave Propagation," *Applied Mechanics Surveys*, H. N. Abramson, H. Liebowitz, J. N. Crowley, and S. Juhasz, eds., Spartan Books, Washington, pp. 809–839.

- Miklowitz, J., 1978, *The Theory of Elastic Waves and Waveguides*, North-Holland, Amsterdam.
- Mindlin, R. D., 1951, "Influence of Rotatory Inertia and Shear on Flexural Vibrations of Isotropic, Elastic Plates," *ASME JOURNAL OF APPLIED MECHANICS*, Vol. 18, pp. 31–38.
- Mindlin, R. D., 1960, "Waves and Vibrations in Isotropic, Elastic Plates," *Structural Mechanics*, J. N. Goodier and N. J. Hoff, eds., Pergamon Press, New York, pp. 199–232.
- Mindlin, R. D., and Onoe, M., 1957, "Mathematical Theory of Vibrations of Elastic Plates," *Proceedings of the 11th Annual Symposium on Frequency Control*, U.S. Army Signal Engineering Laboratories, Fort Monmouth, NJ, pp. 17–40.
- Protsenko, A. M., 1980, "Asymptotics of Wave Problems for a Cylindrical Shell (Izvestia AN SSSR)," *Applied Mathematics and Mechanics*, Vol. 44, No. 3, pp. 507–515.
- Redwood, M., 1960, *Mechanical Waveguides*, Pergamon Press, New York.
- Reismann, H., 1988, *Elastic Plates*, John Wiley and Sons, New York.
- Segel, L. A., 1987, *Mathematics Applied to Continuum Mechanics*, Dover, New York.
- Timoshenko, S. P., 1955, *Vibration Problems in Engineering*, D. Van Nostrand, New York.
- Tolstoy, I., and Usdin, E., 1953, "Dispersive Properties of Stratified Elastic and Liquid Media: A Ray Theory," *Geophysics*, Vol. 18, pp. 844–870.
- Tolstoy, I., and Usdin, E., 1957, "Wave Propagation in Elastic Plates: Low and High Mode Dispersion," *Journal of the Acoustical Society of America*, Vol. 29, No. 1, pp. 37–42.
- Ufland, Y. S., 1948, "The Propagation of Waves in the Transverse Vibrations of Bars and Plates," *Applied Mathematics and Mechanics*, Vol. 12, pp. 287–300 (in Russian).
-

Closed-Form Forced Response of a Damped, Rotating, Multiple Disks/Spindle System

I. Y. Shen

Department of Mechanical Engineering,
University of Washington,
Seattle, WA 98195
Mem. ASME

This paper is to study forced vibration response of a rotating disk/spindle system consisting of multiple flexible circular disks clamped to a rigid spindle supported by two flexible bearings. In particular, the disk/spindle system is subjected to prescribed translational base excitations and externally applied loads. Because of the bearing flexibility, the rigid spindle undergoes infinitesimal rigid-body rocking and translation simultaneously. To model real vibration response that has finite resonance amplitudes, the disks and the bearings are assumed to be viscously damped. Equations of motion are then derived through use of Rayleigh dissipation function and Lagrange's equation. The equations of motion include three sets of matrix differential equations: one for the rigid-body rocking of the spindle and one-nodal-diameter disk modes, one for the axial translation of the spindle and axisymmetric disk modes, and one for disk modes with two or more nodal diameters. Each matrix differential equation contains either a gyroscopic matrix or a damping matrix or both. The causal Green's function of each matrix differential equation is determined explicitly in closed form through use of matrix inversion and inverse Laplace transforms. Closed-form forced response of the damped rotating disk/spindle system is then obtained from the causal Green's function and the generalized forces through convolution integrals. Finally, responses of a disk/spindle system subjected to a concentrated sinusoidal load or an impulsive load are demonstrated numerically as an example.

1 Introduction

Recent advances of electronic and manufacturing technology have made mechanics of computer hard disk drives a major area of intensive research. Currently, most high capacity hard disk drives support ten disks and have track density of 6000 tracks per inch. Moreover, the disk drive industry doubles the track density almost every other year. Increased track density implies increased data storage per disk as well as reduced cost. With current hard drives, the radial spacing between the annular data tracks is about $6\text{ }\mu\text{m}$. The allowable misregistration between the read/write head and the data track is about $0.6\text{ }\mu\text{m}$. Mechanical vibration exceeding this allowable misregistration may cause errors in data storage and retrieval processes.

A major vibration problem encountered in hard disk drives is the unbalanced $(0, 1)$ mode (Fig. 1), predicted by Shen and Ku (1995) and experimentally verified by Low and Shen (1996). For the unbalanced $(0, 1)$ mode, the spindle is whirling conically about the disk/spindle centroid. In the meantime, the disks oscillate with the whirling frequency and undergo an in-phase deflection of zero nodal circle and one nodal diameter. (The description above for the unbalance $(0, 1)$ mode is for a ground-based observer.) In general, the unbalanced $(0, 1)$ mode has low resonance frequency ($<500\text{ Hz}$) and large in-plane vibration amplitude because of the spindle rocking. Moreover, this mode is very lightly damped if the supporting bearings have small damping capacity (e.g., ball bearings). The combination of the low resonance frequency and small damping make the unbalanced $(0, 1)$ mode very susceptible to external excita-

tions, which often result in excessive in-plane vibrations exceeding the allowable misregistration.

Traditionally, hard disk drives have been modeled as flexible disks mounted on a rigid spindle with rigid bearings (Mote, 1970; Iwan and Stahl, 1973; Chen and Bogy, 1992). This model, however, fails to predict the resonance of the unbalanced $(0, 1)$ mode, because this model doesn't take into account the rigid-body rocking of the spindle. A more elaborate model, borrowed from rotordynamics, consists of flexible disks and flexible spindles (Dopkin and Shoup, 1974; Chivens and Nelson, 1975; Flowers and Ryan, 1993). This model, however, becomes somewhat impractical and excessive for hard disk drives, because disk drives all have very short and fairly rigid spindles. To modify this model for disk drive applications, Shen and Ku (1995) presented a formulation that considered multiple flexible disks clamped to a rigid spindle supported by elastic bearings. With this new model, Shen and Ku (1995) successfully predicted the resonance of the unbalanced $(0, 1)$ mode. This model is also verified experimentally by Low and Shen (1996) through experimental modal analysis for a ten-disk hard drive. Shen and Ku (1995), however, assumed no damping in their model and did not study the forced response of the disk/spindle system. An accurate model for forced response will substantially reduce the time and number of tests needed in the design phase of a disk drive.

To predict the forced response analytically, there are three major difficulties to overcome: damping, gyroscopic effect, and closed-form solution. To model real vibration responses that have finite resonance amplitudes, the mathematical model proposed by Shen and Ku (1995) needs to be augmented to include damping of the disks and the bearings¹. Because the disk/spindle system is damped and spinning, gyroscopic terms and damping terms will appear simultaneously in the equations of motion.

Contributed by the Applied Mechanics Division of THE AMERICAN SOCIETY OF MECHANICAL ENGINEERS for publication in the ASME JOURNAL OF APPLIED MECHANICS.

Discussion on the paper should be addressed to the Technical Editor, Professor Lewis T. Wheeler, Department of Mechanical Engineering, University of Houston, Houston, TX 77204-4792, and will be accepted until four months after final publication of the paper itself in the ASME JOURNAL OF APPLIED MECHANICS.

Manuscript received by the ASME Applied Mechanics Division, Dec. 23, 1995; final revision, Oct. 7, 1996. Associate Technical Editor: N. C. Perkins.

¹ The magnitude of damping virtually determines the magnitude of the resonance peaks. When damping is absent from the model, the resonance peaks become unbounded.

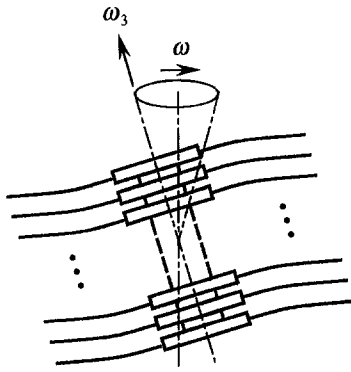


Fig. 1 Unbalanced (0, 1) mode with multiple flexible disks and a rigid spindle

As a result, the method of modal analysis for gyroscopic systems proposed by Meirovitch (1974, 1975), D'Eleuterio and Hughes (1984), or Hughes and D'Eleuterio (1986) will no longer be feasible. In particular, closed-form solutions are difficult to obtain.

The objective of this paper is to derive a closed-form forced response of a damped, rotating disk/spindle system containing arbitrary number of disks. The mathematical model proposed by Shen and Ku (1995), which consists of N linearly elastic disks, a rigid spindle, and two elastic bearings, is augmented in this paper with viscous disk and bearing dampings. The assumption of viscous damping is a crude approximation for preliminary analysis. In reality, damping mechanisms in disk drives can include material damping of disk/spindle systems, aerodynamic drag, frictional loss in bearings and at disk/spacer interface. Most of the damping mechanisms in disk drives are, in fact, nonlinear. Detail modeling of each damping mechanisms will make the already complicated equations of motion more involved, and their solutions will become extremely unwieldy. Also, the external excitations in this augmented model will only include prescribed base motion of the disk/spindle system and time varying loads applied to the disks. Follower excitations that depend on the motion of the disks and the spindle (such as spring and inertial loading from the recording head assembly) are not considered in this paper, because follower excitations will fundamentally change the dynamics of disk/spindle systems and result in instability (Iwan and Stahl, 1973).

The availability of the closed-form solutions results from the particular format that couples the gyroscopic terms and the damping terms in the equations of motion. This coupling format allows the causal Green's function of the equation of motion to be determined in closed-form through use of matrix inversion and inverse Laplace transform. The closed-form forced response of the damped rotating disk/spindle system is then obtained from the causal Green's function and the generalized forces through convolution integrals.

2 Formulation

Consider a disk/spindle system E that contains N elastic circular disks and a rigid spindle as shown in Fig. 2. Let \mathbf{R}_G be the position vector from a fixed reference point O to the centroid G of the disk/spindle system, and let $\boldsymbol{\omega}$ be the angular velocity of the disk/spindle system E .

The rigid spindle rotates with a constant angular speed ω_3 and is simply supported by two bearings A and B (not shown in Fig. 2). The bearing A , which is distance z_a from the centroid G , has transverse stiffnesses k_{ax} , k_{ay} and axial stiffness k_{az} . In addition, the bearing has isotropic transverse viscous damping coefficient c_a and axial damping coefficient c_{az} . The bearing B can be described in the same manner with the subscript a replaced by b .

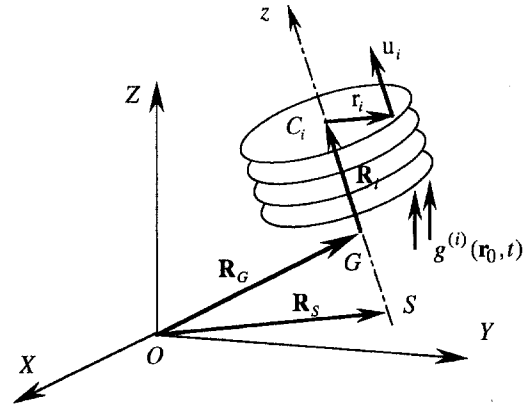


Fig. 2 A disk/spindle system with N flexible disks and a rigid spindle

Consider the i th disk. The disk is rigidly attached to the spindle through the center C_i (Fig. 2), which is distance z_i away from the centroid G of the disk/spindle system. In the following, a subscript i or a superscript (i) will refer to quantities of the i th disk. The subscript i will sometimes be dropped to simplify the notation. In addition, the i th disk has inner radius a_i , outer radius b_i , thickness h_i , density ρ_i , flexural rigidity D_i , Poisson ratio ν_i , and viscous damping coefficient c_i . Also, let $I_i^{(i)}$ be the mass moment of inertia of the disk with respect to its diameter.

The motion of the disk/spindle system is described in terms of the following coordinate systems. Figure 3 shows the Euler angles θ_x , θ_y , and ψ together with a set of rocking coordinates xyz with unit vectors \mathbf{i} , \mathbf{j} , and \mathbf{k} . The rocking coordinate system is related to the inertia frame XYZ through the coordinate transformation

$$\begin{pmatrix} \mathbf{i} \\ \mathbf{j} \\ \mathbf{k} \end{pmatrix} = \begin{bmatrix} \cos \theta_y & \sin \theta_x \sin \theta_y & -\cos \theta_x \sin \theta_y \\ 0 & \cos \theta_x & \sin \theta_x \\ \sin \theta_y & -\sin \theta_x \cos \theta_y & \cos \theta_x \cos \theta_y \end{bmatrix} \begin{pmatrix} \mathbf{I} \\ \mathbf{J} \\ \mathbf{K} \end{pmatrix} \quad (1)$$

where \mathbf{I} , \mathbf{J} , and \mathbf{K} are unit vectors of the inertia frame XYZ . Also note that $x''y''z''$ is a set of coordinates attached to the disk, and $x'y'z'$ is an intermediate coordinate system to define the rocking coordinates xyz .

Under these coordinate systems,

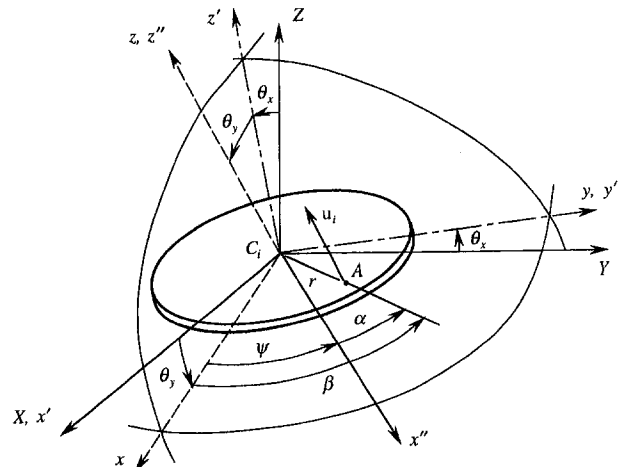


Fig. 3 Euler angles of the spinning elastic disk

$$\mathbf{R}_G = (a_x + R_x)\mathbf{I} + (a_y + R_y)\mathbf{J} + (a_z + R_z)\mathbf{K} \quad (2)$$

where

$$\mathbf{a}(t) \equiv a_x(t)\mathbf{I} + a_y(t)\mathbf{J} + a_z(t)\mathbf{K} \quad (3)$$

is the prescribed motion of the disk/spindle housing, and R_x , R_y , and R_z are rigid-body translation of the disk/spindle centroid relative to the housing. In addition, the transverse vibration of the i th disk is

$$\mathbf{u}_i = w_i(r, \beta, t)\mathbf{k} \quad (4)$$

where $w_i(r, \beta, t)$ is the deflection of the i th disk measured from an observer rocking with xyz . Moreover, the disk deflection w_i is discretized through an eigenfunction expansion

$$w_i(r, \beta, t) = \sum_{m=0}^{\infty} \sum_{n=-\infty}^{\infty} w_{mn}^{(i)}(r, \beta) q_{mn}^{(i)}(t) \quad (5)$$

where $w_{mn}^{(i)}(r, \beta)$ is the mode shape (or eigenfunctions) of the i th elastic disk subjected to the axisymmetric membrane stresses from rotation, i.e., $w_{mn}^{(i)}(r, \beta)$ are the eigenfunctions of the following eigenvalue problem:

$$\begin{aligned} \mathcal{L}[w_{mn}^{(i)}] &\equiv D_i \nabla^4 w_{mn}^{(i)} - \frac{h_i}{r} \frac{\partial}{\partial r} \left(r \sigma_{rr}^{(i)} \frac{\partial w_{mn}^{(i)}}{\partial r} \right) \\ &\quad - \frac{h_i \sigma_{\theta\theta}^{(i)}}{r^2} \frac{\partial^2 w_{mn}^{(i)}}{\partial \theta^2} = \rho_i h_i [\omega_{mn}^{(i)}]^2 w_{mn}^{(i)} \end{aligned} \quad (6)$$

where $\sigma_{rr}^{(i)}$ and $\sigma_{\theta\theta}^{(i)}$ are membrane stresses of the i th disk from rotation, and $\omega_{mn}^{(i)}$ is the natural frequency of the i th disk from a plate-based observer. Note that $\omega_{mn}^{(i)}$ is a function of the rotational speed ω_3 , because the membrane stresses $\sigma_{rr}^{(i)}$ and $\sigma_{\theta\theta}^{(i)}$ depend on ω_3 . Besides, $w_{mn}^{(i)}(r, \beta)$ satisfy fixed-end boundary conditions at the inner rim and free-end boundary conditions at the outer rims. From separation of variables, (6) implies that

$$w_{mn}^{(i)}(r, \beta) = \begin{cases} R_{mn}^{(i)}(r) \cos n\beta, & n \geq 0 \\ R_{m|n|}^{(i)}(r) \sin |n|\beta, & n < 0 \end{cases} \quad (7)$$

where $R_{mn}^{(i)}(r)$ satisfies the fixed-free boundary conditions at the inner and outer rims. Because (6) and the fixed-free boundary conditions form a self-adjoint eigenvalue problem, the mode shapes $w_{mn}^{(i)}$ satisfy the following orthonormality conditions:

$$\int w_{mn}^{(i)} w_{pq}^{(i)} dm_i = I_1^{(i)} \delta_{mp} \delta_{nq} \quad (8)$$

$$\int \mathcal{L}[w_{mn}^{(i)}] w_{pq}^{(i)} dv_i = I_1^{(i)} [\omega_{mn}^{(i)}]^2 \delta_{mp} \delta_{nq}. \quad (9)$$

In summary, the coupled motion of the disk/spindle system is described by the following generalized coordinates: infinitesimal rigid-body translation $R_x(t)$, $R_y(t)$, and $R_z(t)$ of the disk/spindle centroid, infinitesimal rigid-body rocking $\theta_x(t)$ and $\theta_y(t)$ of the spindle, and generalized coordinates $q_{mn}^{(i)}(t)$ of the transverse vibration of the i th disk. The Rayleigh dissipation function and the generalized forces will be derived in terms of these generalized coordinates in the next two sections. Then the equations of motion of the damped disk/spindle system will be derived through use of Lagrange's equation.

3 Rayleigh Dissipation Function

The Rayleigh dissipation function of the damped disk/spindle system is

$$\begin{aligned} \mathcal{F} &= \frac{1}{2} \sum_{\alpha=a,b} [c_{\alpha} (v_{\alpha x}^2 + v_{\alpha y}^2) + c_{\alpha z} v_{\alpha z}^2] \\ &\quad + \frac{1}{2} \sum_{i=1}^N c_i \int \left(\frac{dw_i}{dt} \right)^2 dA_i \end{aligned} \quad (10)$$

where the first sum results from the bearing damping and the second sum results from the disk damping. In (10), $v_{\alpha x}\mathbf{i} + v_{\alpha y}\mathbf{j} + v_{\alpha z}\mathbf{k}$, ($\alpha = a, b$) are the velocities of the spindle relative to the disk/spindle housing evaluated at the bearing supports, and dw_i/dt is the material derivative of the disk vibration. Substitution of the explicit expressions of the relative velocities and dw_i/dt found by Shen and Ku (1995) into (10) results in

$$\begin{aligned} \mathcal{F} &= \frac{1}{2} \sum_{i=1}^N \zeta_i I_1^{(i)} \left[\sum_{m=0}^{\infty} \sum_{n=-\infty}^{\infty} (\dot{q}_{mn}^{(i)} + n\dot{\psi} q_{m,-n}^{(i)})^2 \right] \\ &\quad + \frac{1}{2} \sum_{\alpha=a,b} c_{\alpha} [(\dot{R}_x + z_{\alpha} \dot{\theta}_y \cos \theta_y)^2 \\ &\quad + (\dot{R}_y - z_{\alpha} \dot{\theta}_x \cos \theta_x \cos \theta_y + z_{\alpha} \dot{\theta}_y \sin \theta_x \sin \theta_y)^2] \\ &\quad + \frac{1}{2} \sum_{\alpha=a,b} c_{\alpha z} (\dot{R}_z - z_{\alpha} \dot{\theta}_x \sin \theta_x \cos \theta_y \\ &\quad - z_{\alpha} \dot{\theta}_y \cos \theta_x \sin \theta_y)^2 \end{aligned} \quad (11)$$

where

$$\zeta_i = \frac{c_i}{\rho_i h_i}. \quad (12)$$

4 Generalized Forces

In this paper, the external loads applied to the i th disk are assumed to take the form of $g^{(i)}(\mathbf{r}_0, t)\mathbf{K}$. In other words, both the orientation of the load (\mathbf{K}) and the point of application ($\mathbf{r}_0 \equiv x_0\mathbf{I} + y_0\mathbf{J}$) are fixed in the space; see Fig. 2. The virtual work done by $g^{(i)}(\mathbf{r}_0, t)\mathbf{K}$ is

$$\delta W = \sum_{i=1}^N \int g^{(i)}(\mathbf{r}_0, t) \delta \Delta_i(\mathbf{r}_0, t) dA_0^{(i)} \quad (13)$$

where $\Delta_i(\mathbf{r}_0, t)\mathbf{K}$ is the deflection of the i th disk measured from a *ground-based* observer located at \mathbf{r}_0 . According to Shen and Ku (1995),

$$\begin{aligned} \Delta_i(\mathbf{r}_0, t) &= R_z - x_0 \theta_y + y_0 \theta_x \\ &\quad + \sum_{m=0}^{\infty} \sum_{n=-\infty}^{\infty} w_{mn}^{(i)}(r_0, \beta_0) q_{mn}^{(i)}(t) \end{aligned} \quad (14)$$

where r_0 and β_0 are the polar coordinates of \mathbf{r}_0 . After (14) is substituted into (13) and the variation is carried out, the generalized forces are the coefficients of $\delta\theta_x$, $\delta\theta_y$, δR_z , and $\delta q_{mn}^{(i)}$.

5 Equations of Motion

With the Rayleigh dissipation function and the generalized forces, the equations of motion are derived through use of Lagrange's equation (Shen and Ku, 1995) followed by a linearization assuming constant $\dot{\psi} = \omega_3$, $\theta_x \ll 1$, and $\theta_y \ll 1$. The θ_x equation is

$$\begin{aligned} I_1 \ddot{\theta}_x + I_3 \omega_3 \dot{\theta}_y &+ \sum_{i=1}^N I_1^{(i)} \left[\sum_{m=0}^{\infty} a_m^{(i)} (\ddot{q}_{m,-1}^{(i)} - 2\omega_3 \dot{q}_{m1}^{(i)}) \right] \\ &+ z_a k_{ay} (z_a \theta_x - R_y) + z_b k_{by} (z_b \theta_x - R_y) - z_a c_a (\dot{R}_y - z_a \dot{\theta}_x) \\ &- z_b c_b (\dot{R}_y - z_b \dot{\theta}_x) = \sum_{i=1}^N \int g^{(i)}(\mathbf{r}_0, t) y_0 dA_0^{(i)} \end{aligned} \quad (15)$$

where

$$a_m^{(i)} = \frac{\pi \rho_i h_i}{I_1^{(i)}} \int_{a_i}^{b_i} R_{m1}^{(i)}(r) r^2 dr \quad (16)$$

and \bar{I}_1 and \bar{I}_3 are centroidal mass moment of inertia of the disk/spindle system with respect to the x and z -axes, respectively. The θ_y equation is

$$\begin{aligned} \bar{I}_1 \ddot{\theta}_y - \bar{I}_3 \omega_3 \dot{\theta}_x - \sum_{i=1}^N I_1^{(i)} \left[\sum_{m=0}^{\infty} a_m^{(i)} (\dot{q}_{m1}^{(i)} + 2\omega_3 \dot{q}_{m,-1}^{(i)}) \right] \\ + z_a k_{ax} (z_a \dot{\theta}_y + \dot{R}_x) + z_b k_{bx} (z_b \dot{\theta}_y + \dot{R}_x) + z_a c_a (z_a \dot{\theta}_y + \dot{R}_x) \\ + z_b c_b (z_b \dot{\theta}_y + \dot{R}_x) = - \sum_{i=1}^N \int g^{(i)}(\mathbf{r}_0, t) x_0 dA_0^{(i)}. \quad (17) \end{aligned}$$

The R_x equation is

$$\begin{aligned} M \ddot{R}_x + k_{ax} (R_x + z_a \dot{\theta}_y) + k_{bx} (R_x + z_b \dot{\theta}_y) \\ + c_a (\dot{R}_x + z_a \dot{\theta}_y) + c_b (\dot{R}_x + z_b \dot{\theta}_y) = -M \ddot{a}_x(t) \quad (18) \end{aligned}$$

where M is the mass of the disk/spindle system. The R_y equation is

$$\begin{aligned} M \ddot{R}_y + k_{ay} (R_y - z_a \dot{\theta}_x) + k_{by} (R_y - z_b \dot{\theta}_x) \\ + c_a (\dot{R}_y - z_a \dot{\theta}_x) + c_b (\dot{R}_y - z_b \dot{\theta}_x) = -M \ddot{a}_y(t). \quad (19) \end{aligned}$$

The R_z equation is

$$\begin{aligned} M \ddot{R}_z + \sum_{i=1}^N I_1^{(i)} \left[\sum_{m=0}^{\infty} b_m^{(i)} \dot{q}_{m0}^{(i)} \right] + (k_{az} + k_{bz}) R_z + (c_{az} + c_{bz}) \dot{R}_z \\ = \sum_{i=1}^N \int g^{(i)}(\mathbf{r}_0, t) dA_0^{(i)} - M \ddot{a}_z(t) \quad (20) \end{aligned}$$

where

$$b_m^{(i)} = \frac{2\pi \rho_i h_i}{I_1^{(i)}} \int_{a_i}^{b_i} R_{m0}^{(i)}(r) r dr. \quad (21)$$

The $q_{mn}^{(i)}$ equation is

$$\begin{aligned} I_1^{(i)} \{ \ddot{q}_{mn}^{(i)} + 2n\omega_3 \dot{q}_{m,-n}^{(i)} + ([\omega_{mn}^{(i)}]^2 - n^2 \omega_3^2) q_{mn}^{(i)} + \ddot{R}_z b_m^{(i)} \delta_{n0} \\ + a_m^{(i)} \delta_{n,-1} (\ddot{\theta}_x + 2\omega_3 \dot{\theta}_y) - a_m^{(i)} \delta_{n1} (\ddot{\theta}_y - 2\omega_3 \dot{\theta}_x) \\ + \zeta_i (\dot{q}_{mn}^{(i)} + n\omega_3 \dot{q}_{m,-n}^{(i)}) \} \\ = \int g^{(i)}(\mathbf{r}_0, t) w_{mn}^{(i)}(\mathbf{r}_0) dA_0^{(i)} - I_1^{(i)} b_m^{(i)} \delta_{n0} \ddot{a}_z(t). \quad (22) \end{aligned}$$

6 Isotropic Disk/Spindle Systems

In most applications, all N disks are identical and the bearing stiffnesses are isotropic, i.e., $k_{ax} = k_{ay} = k_a$ and $k_{bx} = k_{by} = k_b$. (In the following, the subscript i or superscript (i) will be dropped when it is obvious.) As a result, the complex representations

$$\theta \equiv \theta_x + j\theta_y, \quad R \equiv R_x + jR_y, \quad Q_{mn}^{(i)} \equiv q_{m,-n}^{(i)} - j q_{mn}^{(i)}, \quad (23)$$

where $j = \sqrt{-1}$, substantially simplify the equations of motion (15) to (22). In addition, vibration modes with one or more nodal circles are not significant in practical applications. Therefore, only zero-nodal-circle modes will be retained in the equations of motion. In this case, the equations of motion split into three sets of matrix equation of motion: one for rigid-body rocking of the spindle and the (0, 1) disk modes, one for axial rigid-body translation of the spindle and the (0, 0) disk mode, and one for disk modes with two or more nodal diameters. They are explained in detail as follows.

6.1 Equations for Spindle Rocking and Disk (0, 1) Modes. The matrix equation coupling the rigid-body rocking of the spindle and the disk (0, 1) modes is obtained from (15), (17), (18), (19), and (22) with $m = 0$ and $n = \pm 1$ resulting in

$$\mathbf{M}_1 \ddot{\mathbf{q}}_1(t) + (\mathbf{C}_1 + \mathbf{G}_1) \dot{\mathbf{q}}_1(t) + (\mathbf{K}_1 + \mathbf{Q}_1) \mathbf{q}_1(t) = \mathbf{f}_1(t) \quad (24)$$

where \mathbf{M}_1 is a Hermitian mass matrix, \mathbf{C}_1 is a Hermitian damping matrix, \mathbf{G}_1 is an anti-Hermitian gyroscopic matrix, \mathbf{K}_1 is a Hermitian stiffness matrix, \mathbf{Q}_1 is an anti-Hermitian oscillatory matrix, \mathbf{q}_1 is a displacement vector, and \mathbf{f}_1 is a generalized excitation vector. The subscript 1 implies that the quantities are related to (0, 1) modes. Moreover, define

$$\eta_1 \equiv \bar{I}_1 / I_1^{(i)}, \quad \eta_3 \equiv \bar{I}_3 / I_1^{(i)}, \quad \eta_0 \equiv M / I_1^{(i)} \quad (25)$$

$$c_{rr} \equiv \frac{c_a z_a^2 + c_b z_b^2}{I_1^{(i)}}, \quad c_{rt} \equiv \frac{c_a z_a + c_b z_b}{I_1^{(i)}}, \quad c_{tt} \equiv \frac{c_a + c_b}{I_1^{(i)}} \quad (26)$$

and

$$\begin{aligned} k_{rr} \equiv \frac{k_a z_a^2 + k_b z_b^2}{I_1^{(i)}}, \quad k_{rt} \equiv \frac{k_a z_a + k_b z_b}{I_1^{(i)}}, \quad k_{tt} \equiv \frac{k_a + k_b}{I_1^{(i)}}, \\ \omega_r^2 = [\omega_{01}^{(i)}]^2 - \omega_3^2. \end{aligned} \quad (27)$$

Then the matrices and vectors in (24) are

$$\mathbf{q}_1 = (\theta, R, Q_{01}^{(1)}, Q_{01}^{(2)}, \dots, Q_{01}^{(N)})^T \quad (28)$$

$$\mathbf{M}_1 = \begin{bmatrix} \eta_1 & 0 & a_0 & a_0 & \dots & a_0 \\ 0 & \eta_0 & 0 & 0 & \dots & 0 \\ a_0 & 0 & 1 & 0 & \dots & 0 \\ a_0 & 0 & 0 & 1 & \dots & 0 \\ \vdots & \vdots & \vdots & \vdots & \ddots & \vdots \\ a_0 & 0 & 0 & 0 & \dots & 1 \end{bmatrix} \quad (29)$$

$$\mathbf{C}_1 = \begin{bmatrix} c_{rr} & j c_{rt} & 0 & 0 & \dots & 0 \\ -j c_{rt} & c_{tt} & 0 & 0 & \dots & 0 \\ 0 & 0 & \zeta & 0 & \dots & 0 \\ 0 & 0 & 0 & \zeta & \dots & 0 \\ \vdots & \vdots & \vdots & \vdots & \ddots & \vdots \\ 0 & 0 & 0 & 0 & \dots & \zeta \end{bmatrix} \quad (30)$$

$$\mathbf{G}_1 = -j\omega_3 \begin{bmatrix} \eta_3 & 0 & 2a_0 & 2a_0 & \dots & 2a_0 \\ 0 & 0 & 0 & 0 & \dots & 0 \\ 2a_0 & 0 & 2 & 0 & \dots & 0 \\ 2a_0 & 0 & 0 & 2 & \dots & 0 \\ \vdots & \vdots & \vdots & \vdots & \ddots & \vdots \\ 2a_0 & 0 & 0 & 0 & \dots & 2 \end{bmatrix} \quad (31)$$

$$\mathbf{K}_1 = \begin{bmatrix} k_{rr} & j k_{rt} & 0 & 0 & \dots & 0 \\ -j k_{rt} & k_{tt} & 0 & 0 & \dots & 0 \\ 0 & 0 & \omega_r^2 & 0 & \dots & 0 \\ 0 & 0 & 0 & \omega_r^2 & \dots & 0 \\ \vdots & \vdots & \vdots & \vdots & \ddots & \vdots \\ 0 & 0 & 0 & 0 & \dots & \omega_r^2 \end{bmatrix} \quad (32)$$

$$\mathbf{Q}_1 = -j\omega_3 \begin{bmatrix} 0 & 0 & 0 & 0 & \dots & 0 \\ 0 & 0 & 0 & 0 & \dots & 0 \\ 0 & 0 & \zeta & 0 & \dots & 0 \\ 0 & 0 & 0 & \zeta & \dots & 0 \\ \vdots & \vdots & \vdots & \vdots & \ddots & \vdots \\ 0 & 0 & 0 & 0 & \dots & \zeta \end{bmatrix} \quad (33)$$

and

$$\mathbf{f}_1 = -\frac{1}{I_1} \begin{pmatrix} j \sum_{i=1}^N \int g^{(i)}(\mathbf{r}_0, t) r_0 e^{j\beta_0} dA_0^{(i)} \\ M[\ddot{a}_x(t) + j\ddot{a}_y(t)] \\ j \int g^{(1)}(\mathbf{r}_0, t) R_{01}(r_0) e^{j\beta_0} dA_0^{(1)} \\ \vdots \\ j \int g^{(N)}(\mathbf{r}_0, t) R_{01}(r_0) e^{j\beta_0} dA_0^{(N)} \end{pmatrix}. \quad (34)$$

6.2 Equations for Axial Translation and (0, 0) Mode. The matrix equation coupling the axial translation of the spindle and the (0, 0) disk mode is obtained from (20) and (22) with $m = 0$ and $n = 0$ resulting in

$$\mathbf{M}_0 \ddot{\mathbf{q}}_0(t) + \mathbf{C}_0 \dot{\mathbf{q}}_0(t) + \mathbf{K}_0 \mathbf{q}_0(t) = \mathbf{f}_0(t) \quad (35)$$

where \mathbf{M}_0 is a symmetric mass matrix, \mathbf{C}_0 is a symmetric damping matrix, \mathbf{K}_0 is a symmetric stiffness matrix, \mathbf{q}_0 is a displacement vector, and \mathbf{f}_0 is a generalized excitation vector. The subscript 0 implies that the quantities are related to the disk (0, 0) mode. Moreover, define

$$k_{zz} \equiv \frac{k_{az} + k_{bz}}{I_1^{(i)}}, \quad c_{zz} \equiv \frac{c_{az} + c_{bz}}{I_1^{(i)}}. \quad (36)$$

Then the matrices and vectors in (35) are

$$\mathbf{q}_0 = (R_z, q_{00}^{(1)}, q_{00}^{(2)}, \dots, q_{00}^{(N)})^T \quad (37)$$

$$\mathbf{M}_0 = \begin{bmatrix} \eta_0 & b_0 & b_0 & \cdots & b_0 \\ b_0 & 1 & 0 & \cdots & 0 \\ b_0 & 0 & 1 & \cdots & 0 \\ \vdots & \vdots & \vdots & \ddots & \vdots \\ b_0 & 0 & 0 & \cdots & 1 \end{bmatrix} \quad (38)$$

$$\mathbf{C}_0 = \text{diag} [c_{zz}, \zeta, \zeta, \dots, \zeta] \quad (39)$$

$$\mathbf{K}_0 = \text{diag} [k_{zz}, \omega_{00}^2, \omega_{00}^2, \dots, \omega_{00}^2] \quad (40)$$

and

$$\mathbf{f}_0 = \frac{1}{I_1} \begin{pmatrix} \sum_{i=1}^N \int g^{(i)}(\mathbf{r}_0, t) dA_0^{(i)} \\ \int g^{(1)}(\mathbf{r}_0, t) R_{00}(r_0) dA_0^{(1)} \\ \vdots \\ \int g^{(N)}(\mathbf{r}_0, t) R_{00}(r_0) dA_0^{(N)} \end{pmatrix} - \ddot{a}_z(t) \begin{pmatrix} \eta_0 \\ b_0 \\ \vdots \\ b_0 \end{pmatrix}. \quad (41)$$

6.3 Equations for (0, 2) Modes and Above. The complex equations governing the disk (0, 2) modes and above are obtained from (22) with $m = 0$ and $n = \pm 2, 3, \dots$ resulting in

$$\begin{aligned} \ddot{Q}_{mn}^{(i)} + (\zeta - 2n\omega_3 j) \dot{Q}_{mn}^{(i)} + [\omega_{mn}^2 - n^2\omega_3^2 - j\zeta n\omega_3] Q_{mn}^{(i)} \\ = f_{mn}^{(i)}(t) \equiv -\frac{j}{I_1} \int g^{(i)}(\mathbf{r}_0, t) R_{mn}(r_0) e^{jn\beta_0} dA_0^{(i)}, \\ i = 1, 2, \dots, N. \end{aligned} \quad (42)$$

7 Green's Functions of Disk/Spindle Systems

According to the governing equations derived above, an isotropic, damped, rotating disk/spindle system manifests itself as a damped gyroscopic system. A careful inspection of all $[\cdot]_1$ matrices shows that all (0, 1) disk modes are coupled to one another only through the rigid-body rocking of the spindle. Similarly, an inspection of all $[\cdot]_0$ matrices show that all (0, 0) disk modes are coupled through the axial translation of the spindle. This special form of coupling suggests that the forced response be obtained in *closed-form* through use of causal Green's functions and the convolution integral.

Take Laplace transforms (denoted by overbars) of (24) and (35) with zero initial conditions to obtain

$$[s^2 \mathbf{M}_i + s(\mathbf{C}_i + \mathbf{G}_i) + (\mathbf{K}_i + \mathbf{Q}_i)] \bar{\mathbf{q}}_i(s) = \bar{\mathbf{f}}_i(s), \quad i = 1, 0 \quad (43)$$

where $\mathbf{G}_0 = \mathbf{Q}_0 \equiv \mathbf{0}$. Inverting (43) to obtain

$$\bar{\mathbf{q}}_i(s) = \bar{\mathbf{H}}_i(s) \bar{\mathbf{f}}_i(s) \equiv \mathbf{P}_i^{-1}(s) \bar{\mathbf{f}}_i(s), \quad i = 1, 0 \quad (44)$$

where

$$\mathbf{P}_i(s) \equiv s^2 \mathbf{M}_i + s(\mathbf{C}_i + \mathbf{G}_i) + (\mathbf{K}_i + \mathbf{Q}_i) \quad (45)$$

The convolution theorem of Laplace transforms implies that forced responses of (24) and (35) are

$$\mathbf{q}_i(t) = \int_0^t \mathbf{H}_i(t - \tau) \mathbf{f}_i(\tau) d\tau, \quad i = 1, 0 \quad (46)$$

where $\mathbf{H}_i(t)$, $i = 1, 0$, are known as the causal Green's matrices.

7.1 Spindle Rocking and (0, 1) Disk Modes.

For $i = 1$,

$$\mathbf{P}_1(s) = \begin{bmatrix} A_1 & D_1 & B_1 & B_1 & \cdots & B_1 \\ -D_1 & E_1 & 0 & 0 & \cdots & 0 \\ B_1 & 0 & C_1 & 0 & \cdots & 0 \\ B_1 & 0 & 0 & C_1 & \cdots & 0 \\ \vdots & \vdots & \vdots & \vdots & \ddots & \vdots \\ B_1 & 0 & 0 & 0 & \cdots & C_1 \end{bmatrix} \quad (47)$$

where

$$A_1(s) = \eta_1 s^2 + (c_{rr} - j\omega_3 \eta_3) s + k_{rr} \quad (48)$$

$$B_1(s) = a_0 s(s - 2j\omega_3) \quad (49)$$

$$C_1(s) = s^2 + (\zeta - 2j\omega_3) s + \omega_r^2 - j\omega_3 \zeta \quad (50)$$

$$D_1(s) = j(c_{rs} s + k_{rs}) \quad (51)$$

and

$$E_1(s) = \eta_0 s^2 + c_{rr} s + k_{rr}. \quad (52)$$

A direct matrix inversion of (47) results in

$$\begin{aligned} \mathbf{P}_1^{-1}(s) = \frac{\mathbf{p}_1(s) \mathbf{h}_1^T(s)}{F_1(s) C_1(s) E_1(s)} + \frac{1}{E_1(s)} \text{diag} [0, 1, 0, \dots, 0] \\ + \frac{1}{C_1(s)} \text{diag} [0, 0, 1, 1, \dots, 1] \end{aligned} \quad (53)$$

where

$$F_1(s) = (A_1 C_1 - N B_1^2) E_1 + C_1 D_1^2 \quad (54)$$

and

$$\mathbf{p}_1(s) = \begin{pmatrix} -C_1 E_1 \\ -C_1 D_1 \\ B_1 E_1 \\ \vdots \\ B_1 E_1 \end{pmatrix}, \quad \mathbf{h}_1(s) = \begin{pmatrix} -C_1 E_1 \\ C_1 D_1 \\ B_1 E_1 \\ \vdots \\ B_1 E_1 \end{pmatrix}. \quad (55)$$

To reveal the physical meaning of $\mathbf{P}_1^{-1}(s)$, substitute (34) and (53) into (44) and obtain

$$\begin{aligned} \begin{pmatrix} \bar{\theta} \\ \bar{R} \\ \bar{Q}_{01}^{(1)} \\ \vdots \\ \bar{Q}_{01}^{(N)} \end{pmatrix} = \frac{\mathbf{h}_1^T(s) \bar{\mathbf{f}}_1(s)}{F_1(s) C_1(s) E_1(s)} \mathbf{p}_1(s) - \frac{\eta_0 s^2}{E_1(s)} \begin{pmatrix} 0 \\ \bar{a}_x + j\bar{a}_y \\ 0 \\ \vdots \\ 0 \end{pmatrix} \\ - \frac{j}{I_1 C_1(s)} \begin{pmatrix} 0 \\ 0 \\ \int \bar{g}^{(1)}(\mathbf{r}_0, s) R_{01}(r_0) e^{j\beta_0} dA_0^{(1)} \\ \vdots \\ \int \bar{g}^{(N)}(\mathbf{r}_0, s) R_{01}(r_0) e^{j\beta_0} dA_0^{(N)} \end{pmatrix}. \end{aligned} \quad (56)$$

Both resonant and nonresonant motion can occur. Consider the resonant motion first. Let $p_j^{(1)}$, $j = 1, \dots, 6$, be the zeros of $F_1(s)$ satisfying

$$F_1(s) = (\eta_1 - Na_0^2)\eta_0 \prod_{j=1}^6 (s - p_j^{(1)}). \quad (57)$$

The residue of (56) corresponding to $s = p_k^{(1)}$ ($k = 1, \dots, 6$) is

$$\text{Res}(p_k^{(1)}) = \left\{ \frac{\mathbf{h}_1^T(s) \bar{\mathbf{F}}_1(s)}{F_1'(s) C_1(s) E_1(s)} \mathbf{p}_1(s) \right\}_{s=p_k^{(1)}}, \quad k = 1, 2, \dots, 6 \quad (58)$$

where

$$\begin{aligned} \{F_1'(s)\}_{k=p_k^{(1)}} &\equiv \left\{ \frac{d}{ds} F_1(s) \right\}_{k=p_k^{(1)}} \\ &= (\eta_1 - Na_0^2)\eta_0 \prod_{\substack{j=1 \\ j \neq k}}^6 (p_k^{(1)} - p_j^{(1)}). \end{aligned} \quad (59)$$

According to (58), $\text{Res}(p_k^{(1)})$ is proportional to $\mathbf{p}_1(p_k^{(1)})$, which implies from (55) that the system response at resonances will have nonzero rigid-body rocking $\bar{\theta} = -C_1 E_1$ and translation $\bar{R} = -C_1 D_1$ of the spindle. At the same time, all N disks will vibrate in-phase through disk (0, 1) modes with magnitude $B_1 E_1$. This type of resonance is known as unbalanced (0, 1) modes (Shen and Ku, 1995), because the inertia force of the (0, 1) disk modes and the restoring forces from the bearings result in a net moment about the centroid causing steady precession of the disk/spindle system; see Fig. 1. There are two things worth noting. Firstly, the poles $p_j^{(1)}$, $j = 1, 2, \dots, 6$, imply that there are six unbalanced (0, 1) modes. Each unbalanced (0, 1) mode will have a shape similar to that in Fig. 1 but with a different frequency. Secondly, the prescribed base motion $a_x(t) + ja_y(t)$ and the applied force $g^{(i)}(\mathbf{r}_0, t)$, $i = 1, 2, \dots, N$, that are not in self-equilibrium can excite the unbalanced (0, 1) mode to resonance.

Likewise, let $p_j^{(1)}$, $j = 7, 8$, be the zeros of $C_1(s)$ satisfying

$$C_1(s) = (s - p_7^{(1)})(s - p_8^{(1)}). \quad (60)$$

The residue of (56) corresponding to $s = p_k^{(1)}$ ($k = 7, 8$) can be found as

$$\begin{aligned} \text{Res}(p_k^{(1)}) &= \frac{j}{I_1 C_1'(p_k^{(1)})} \\ &\times \left\{ \frac{1}{N} \sum_{i=1}^N \int \bar{g}^{(i)}(\mathbf{r}_0, s) R_{01}(r_0) e^{j\beta_0} dA_0^{(i)} \begin{pmatrix} 0 \\ 0 \\ 1 \\ 1 \end{pmatrix} \right. \\ &\quad \left. - \begin{pmatrix} 0 \\ 0 \\ \int \bar{g}^{(1)}(\mathbf{r}_0, s) R_{01}(r_0) e^{j\beta_0} dA_0^{(1)} \\ \vdots \\ \int \bar{g}^{(N)}(\mathbf{r}_0, s) R_{01}(r_0) e^{j\beta_0} dA_0^{(N)} \end{pmatrix} \right\}_{s=p_k^{(1)}}, \quad k = 7, 8 \quad (61) \end{aligned}$$

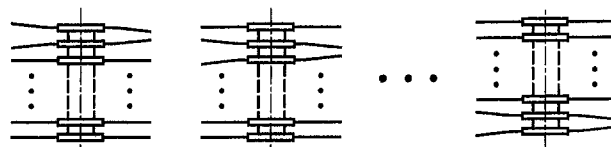


Fig. 4 Balanced (0, 1) mode with multiple flexible disks and a rigid spindle

where

$$\begin{aligned} C_1'(p_k^{(1)}) &\equiv \left\{ \frac{d}{ds} C_1(s) \right\}_{s=p_k^{(1)}} \\ &= \prod_{\substack{j=7 \\ j \neq k}}^8 (p_k^{(1)} - p_j^{(1)}) = 2p_k^{(1)} + \zeta - 2j\omega_3, \\ &\quad k = 7, 8. \end{aligned} \quad (62)$$

Notice that $\text{Res}(p_k^{(1)})$ in (61) can be represented as a combination of the following $N - 1$ resonant modes

$$\begin{pmatrix} 0 \\ 0 \\ 1 \\ -1 \\ 0 \\ \vdots \\ 0 \end{pmatrix}, \begin{pmatrix} 0 \\ 0 \\ 0 \\ 1 \\ -1 \\ \vdots \\ 0 \end{pmatrix}, \dots, \begin{pmatrix} 0 \\ 0 \\ 0 \\ 0 \\ 1 \\ \vdots \\ -1 \end{pmatrix}. \quad (63)$$

Each of these $N - 1$ shapes implies that two adjacent disks vibrate with out-of-phase (0, 1) disk modes while other disks remain undeformed. In the meantime, the spindle undergoes no rigid-body rocking nor translation. These $N - 1$ shapes are called balanced (0, 1) modes, because the inertia force associated with the disks are balanced to zero; see Fig. 4. Also note that these $N - 1$ modes have the same frequency; they are $(N - 1)$ -fold repeated. As a result, any linear combination of the modes in (63) is also a balanced (0, 1) modes. For example, disks 1 and 3 vibrating out of phase while other disks remain undeformed is a balanced (0, 1) mode, because it is a linear combination of the modes in (63). According to (61), the prescribed base motion $a_x(t) + ja_y(t)$ cannot excite the balanced (0, 1) modes at resonances. Neither can the balanced (0, 1) modes be excited when the applied forces $g^{(i)}(\mathbf{r}_0, t)$ to each disk are identical.

Finally, let $p_j^{(1)}$, $j = 9, 10$, be the zeros of $E_1(s)$ satisfying

$$E_1(s) = \eta_0(s - p_9^{(1)})(s - p_{10}^{(1)}). \quad (64)$$

The residue of (56) corresponding to $s = p_j^{(1)}$ ($j = 9, 10$) is, in fact, zero. This implies that $p_9^{(1)}$ and $p_{10}^{(1)}$ are not system poles. In other words, the spindle will never undergo purely lateral rigid-body translation in any resonances. This is because the lateral rigid-body translation is coupled to the rigid-body rocking and is part of the unbalanced (0, 1) modes.

When $D_1 = 0$, translation and rocking of the disk/spindle system are decoupled. In this case,

$$F_1(s) = (A_1 C_1 - NB_1^2) E_1 \quad (65)$$

and the zeros of $E_1(s)$ become system poles. As a result, unbalanced (0, 1) modes only consist of spindle rocking and disk (0, 1) modes. Also, the number of unbalanced (0, 1) modes is reduced to four.

For the nonresonant motion, the response $\bar{\mathbf{q}}_1(s)$ can always be represented in terms of a linear combination of unbalanced and balanced (0, 1) modes, because they are linearly independent and form a set of basis. The method of modal analysis, however, is not feasible, because the unbalanced and balanced (0, 1) modes do not diagonalize \mathbf{M}_1 , \mathbf{C}_1 , \mathbf{G}_1 , \mathbf{K}_1 , and \mathbf{Q}_1 simul-

taneously. A much simpler way to find nonresonant response is to use (56). According to (56), the prescribed base motion $a_x(t)$ and $a_y(t)$ will excite both unbalanced (0, 1) modes through $\bar{\mathbf{f}}_1(s)$ and the rigid-body translation through $\bar{a}_x + j\bar{a}_y$. In addition, the force $g^{(i)}(\mathbf{r}_0, t)$ applied to the i th disk will result in combination of the unbalanced (0, 1) modes of the system through $\bar{\mathbf{f}}_1(s)$ and the vibration of the i th disk through $\int \bar{g}^{(i)}(\mathbf{r}_0, s) R_{01}(r_0) e^{j\beta_0} dA_0^{(i)}$.

To obtain the causal Green's matrix, expand $\mathbf{P}_1^{-1}(s)$ into a partial fraction

$$\bar{\mathbf{H}}_1(s) = \mathbf{P}_1^{-1}(s) = \sum_{j=1}^8 \frac{\mathbf{A}_j^{(1)}}{s - p_j^{(1)}} \quad (66)$$

where

$$\mathbf{A}_j^{(1)} = \left\{ \frac{\mathbf{p}_1(s) \mathbf{h}_1^T(s)}{F_0'(s) C_1(s) E_1(s)} \right\}_{s=p_j^{(1)}}, \quad j = 1, 2, \dots, 6 \quad (67)$$

and

$$\mathbf{A}_j^{(1)} = \frac{1}{C_1'(p_j^{(1)})} \left\{ \begin{array}{l} \text{diag} [0, 0, 1, \dots, 1] \\ -\frac{1}{N} \begin{pmatrix} 0 \\ 0 \\ 1 \\ \vdots \\ 1 \end{pmatrix} \begin{pmatrix} 0 \\ 0 \\ 1 \\ \vdots \\ 1 \end{pmatrix}^T \end{array} \right\}, \quad j = 7, 8. \quad (68)$$

The inverse Laplace transform of (66) gives

$$\mathbf{H}_1(t) = \sum_{j=1}^8 \mathbf{A}_j^{(1)} e^{p_j^{(1)} t}. \quad (69)$$

7.2 Axial Spindle Translation and (0, 0) Modes. For $i = 0$,

$$\mathbf{P}_0(s) = \begin{bmatrix} A_0 & B_0 & B_0 & \cdots & B_0 \\ B_0 & C_0 & 0 & \cdots & 0 \\ B_0 & 0 & C_0 & \cdots & 0 \\ \vdots & \vdots & \vdots & \ddots & \vdots \\ B_0 & 0 & 0 & \cdots & C_0 \end{bmatrix} \quad (70)$$

where

$$A_0(s) = \eta_0 s^2 + c_{zz} s + k_{zz} \quad (71)$$

$$B_0(s) = b_0 s^2 \quad (72)$$

and

$$C_0(s) = s^2 + \zeta s + \omega_{00}^2. \quad (73)$$

A direct matrix inversion of (70) gives

$$\mathbf{P}_0^{-1}(s) = \frac{\mathbf{p}_0(s) \mathbf{p}_0^T(s)}{F_0(s) C_0(s)} + \frac{1}{C_0(s)} \text{diag} [0, 1, 1, \dots, 1] \quad (74)$$

where

$$F_0(s) = A_0 C_0 - N B_0^2 \quad (75)$$

and

$$\mathbf{p}_0(s) = (C_0, -B_0, \dots, -B_0)^T. \quad (76)$$

To explain the physical meaning of $\mathbf{P}_0^{-1}(s)$, substitute (41) and (74) into (44) and obtain

$$\begin{pmatrix} \bar{R}_z \\ \bar{q}_{00}^{(1)} \\ \vdots \\ \bar{q}_{00}^{(N)} \end{pmatrix} = \frac{\mathbf{p}_0^T(s) \bar{\mathbf{f}}_0(s)}{F_0(s) C_0(s)} \mathbf{p}_0(s) + \frac{1}{C_0(s)} \left\{ \frac{1}{I_1} \begin{pmatrix} 0 \\ \int \bar{g}^{(1)}(\mathbf{r}_0, s) R_{00}(r_0) dA_0^{(1)} \\ \vdots \\ \int \bar{g}^{(N)}(\mathbf{r}_0, s) R_{00}(r_0) dA_0^{(N)} \end{pmatrix} - b_0 s^2 \bar{a}_z(s) \begin{pmatrix} 0 \\ 1 \\ \vdots \\ 1 \end{pmatrix} \right\}. \quad (77)$$

Both resonant and nonresonant motion can occur. Consider the resonant motion first. Let $p_j^{(0)}, j = 1, \dots, 4$, be the zeros of $F_0(s)$ satisfying

$$F_0(s) = (\eta_0 - N b_0^2) \prod_{j=1}^4 (s - p_j^{(0)}). \quad (78)$$

The residue of (77) corresponding to $s = p_k^{(0)} (k = 1, \dots, 4)$ is

$$\text{Res}(p_k^{(0)}) = \left\{ \frac{\mathbf{p}_0^T(s) \bar{\mathbf{f}}_0(s)}{F_0'(s) C_0(s)} \mathbf{p}_0(s) \right\}_{s=p_k^{(0)}}, \quad k = 1, \dots, 4 \quad (79)$$

where

$$\begin{aligned} \{F_0'(s)\}_{s=p_k^{(0)}} &\equiv \left\{ \frac{d}{ds} F_0(s) \right\}_{s=p_k^{(0)}} \\ &= (\eta_0 - N b_0^2) \prod_{\substack{j=1 \\ j \neq k}}^4 (p_k^{(0)} - p_j^{(0)}). \end{aligned} \quad (80)$$

According to (79), $\text{Res}(p_k^{(0)})$ is proportional to $\mathbf{p}_0(p_k^{(0)})$, which implies from (76) that the spindle undergoes an axial translation $\bar{R}_z = C_0$. In the meantime, all disks undergo in-phase vibration of (0, 0) mode with magnitude $-B_0$. Consequently, the total inertia force associated with the disks and the axial restoring forces from the bearings result in a net axial force causing the axial rigid-body motion of the spindle. This type of motion is known as unbalanced (0, 0) mode. Note that both the prescribed base motion $a_z(t)$ and applied forces $g^{(i)}(\mathbf{r}_0, t), i = 1, 2, \dots, N$, that are not in self-equilibrium can excite the unbalanced (0, 0) mode to resonance. Also, there are four unbalanced (0, 0) modes.

Likewise, let $p_j^{(0)}, j = 5, 6$, be the zeros of $C_0(s)$ satisfying

$$C_0(s) = (s - p_5^{(0)})(s - p_6^{(0)}). \quad (81)$$

The residue of (77) corresponding to $s = p_k^{(0)} (k = 5, 6)$ is

$$\text{Res}(p_k^{(0)}) = \frac{1}{I_1 C_0'(p_k^{(0)})} \times \left\{ -\frac{1}{N} \sum_{i=1}^N \int \bar{g}^{(i)}(\mathbf{r}_0, s) R_{00}(r_0) dA_0^{(i)} \begin{pmatrix} 0 \\ 1 \\ \vdots \\ 1 \end{pmatrix} \right\}$$

$$+ \left(\begin{array}{c} 0 \\ \int \bar{g}^{(1)}(\mathbf{r}_0, s) R_{00}(r_0) dA_0^{(1)} \\ \vdots \\ \int \bar{g}^{(N)}(\mathbf{r}_0, s) R_{00}(r_0) dA_0^{(N)} \end{array} \right) \Bigg\}_{s=p_k^{(0)}} \quad k = 5, 6 \quad (82)$$

where

$$C_0'(p_k^{(0)}) \equiv \left\{ \frac{d}{ds} C_0(s) \right\}_{s=p_k^{(0)}} = \prod_{\substack{j=5 \\ j \neq k}}^6 (p_k^{(0)} - p_j^{(0)}) \\ = 2p_k^{(0)} + \zeta, \quad k = 5, 6. \quad (83)$$

Notice that (82) can be represented as a combination of the following $N - 1$ modes

$$\begin{pmatrix} 0 \\ 1 \\ -1 \\ 0 \\ \vdots \\ 0 \end{pmatrix}, \begin{pmatrix} 0 \\ 0 \\ 1 \\ -1 \\ \vdots \\ 0 \end{pmatrix}, \dots, \begin{pmatrix} 0 \\ 0 \\ 0 \\ \vdots \\ 1 \\ -1 \end{pmatrix}. \quad (84)$$

Each of the $N - 1$ shapes implies that two adjacent disks vibrate with out-of-phase (0, 0) modes while other disks remain undeformed. In the meantime, the spindle undergoes no axial motion, because the inertia force associated with each of the $N - 1$ shapes are balanced to zero. Therefore, they are called balanced (0, 0) modes. Again, all these $N - 1$ modes have the same frequency. According to (82), the prescribed motion cannot excite the balanced (0, 0) modes at resonances. Neither can the balanced (0, 0) modes be excited when the applied forces $g^{(i)}(\mathbf{r}_0, t)$ to each disk are identical.

For nonresonant motion, the response $\bar{\mathbf{q}}_0$ can always be represented as a linear combination of unbalanced and balanced (0, 0) modes, because they form a set of basis. Again, the method of modal analysis is not feasible, because the unbalanced and balanced (0, 0) modes do not diagonalize \mathbf{M}_0 , \mathbf{C}_0 , and \mathbf{K}_0 simultaneously. Nevertheless, (77) gives a much simpler way to predict nonresonant response. According to (77), the prescribed base motion $a_z(t)$ will excite the unbalanced (0, 0) mode through $\bar{\mathbf{f}}_0(s)$ and the disk (0, 0) modes of all disks through $\bar{a}_z(s)$. In addition, the force $g^{(i)}(\mathbf{r}_0, t)$ applied to the i th disk will result in combination of the unbalanced (0, 0) modes of the system through $\bar{\mathbf{f}}_0(s)$ and the vibration of the i th disk through $\int \bar{g}^{(i)}(\mathbf{r}_0, s) R_{00}(r_0) dA_0^{(i)}$.

To obtain the causal Green's matrix, expand $\mathbf{P}_0^{-1}(s)$ into a partial fraction

$$\mathbf{H}_0(s) = \mathbf{P}_0^{-1}(s) = \sum_{j=1}^6 \frac{\mathbf{A}_j^{(0)}}{s - p_j^{(0)}} \quad (85)$$

where

$$\mathbf{A}_j^{(0)} = \left\{ \begin{array}{c} \mathbf{p}_0(s) \mathbf{p}_0^T(s) \\ F_0'(s) C_0(s) \end{array} \right\}_{s=p_j^{(0)}}, \quad j = 1, \dots, 4 \quad (86)$$

and

$$\mathbf{A}_j^{(0)} = \frac{1}{C_0'(p_j^{(0)})} \left\{ \text{diag} [0, 1, \dots, 1] - \frac{1}{N} \begin{pmatrix} 0 \\ 1 \\ \vdots \\ 1 \end{pmatrix} \begin{pmatrix} 0 \\ 1 \\ \vdots \\ 1 \end{pmatrix}^T \right\}, \quad j = 5, 6. \quad (87)$$

The inverse Laplace transform of (66) gives

$$\mathbf{H}_0(t) = \sum_{j=1}^6 \mathbf{A}_j^{(0)} e^{p_j^{(0)} t}. \quad (88)$$

7.3 Disk (0, 2) Modes and Above. For disk modes with two or more nodal diameters, the solution of (42) is

$$Q_{mn}^{(i)}(t) = \int_0^t h_{mn}(t - \tau) f_{mn}^{(i)}(\tau) d\tau \quad (89)$$

where

$$h_{mn}(t) = \frac{e^{p_{mn} t} - e^{p_{m,-n} t}}{p_{mn} - p_{m,-n}}. \quad (90)$$

In (90), p_{mn} and $p_{m,-n}$ are the roots of

$$P_{mn}(s) = s^2 + (\zeta - 2n\omega_3 j)s + [\omega_{mn}^2 - n^2\omega_3^2 - j\zeta n\omega_3] = 0. \quad (91)$$

8 An Example

This numerical example demonstrates the frequency response function and the impulse response function of a disk/spindle system with four identical disks under arbitrary rotational speed ω_3 . Table 1 shows the properties of the disk/spindle system. When the disk/spindle system is stationary, the natural frequencies of the disk (without the bearings and spindle) are $\omega_{00}^{(0)} = 632.50$ Hz, $\omega_{01}^{(0)} = 618.75$ Hz, and $\omega_{02}^{(0)} = 732.50$ Hz. The disk damping coefficient c is assumed to be 2.721×10^{-5} N-s/mm³ (0.1 lbf-s/in.³), and the bearing damping coefficients c_a , c_b , c_{az} , and c_{bz} are assumed to be 1.756×10^{-2} N-s/mm (0.1 lbf-s/in.).

Consider a concentrated load applied to the fourth disk at $r = b$ and $\beta = 0$ deg with

$$g^{(1)}(\mathbf{r}_0, t) = g^{(2)}(\mathbf{r}_0, t) = g^{(3)}(\mathbf{r}_0, t) = 0, \\ g^{(4)}(\mathbf{r}_0, t) = -\delta(\mathbf{r}_0 - b\mathbf{I})f(t). \quad (92)$$

Two types of loading will be considered: impulsive loading with $f(t) \equiv \delta(t)$ and harmonic loading with $f(t) \equiv \cos \omega t$. The numerical simulation demonstrates the response of the fourth disk from a ground-based observer at the driving point (i.e., $r = b$ and $\beta = 0$ deg).

To obtain generalized forces, substitute (92) into (34), (41), and (42) to obtain

$$\mathbf{f}_1 = \frac{j}{I} [b, 0, 0, 0, 0, R_{01}(b)]^T f(t) \quad (93)$$

$$\mathbf{f}_0 = -\frac{1}{I} [1, 0, 0, 0, 0, R_{00}(b)]^T f(t) \quad (94)$$

and

$$f_{mn}^{(i)} = \begin{cases} 0, & i = 1, 2, 3 \\ (j/I) R_{mn}(b) f(t), & i = 4. \end{cases} \quad (95)$$

For the case of harmonic loading, (44) gives

$$\mathbf{q}_1(t) = \frac{j}{2I} [\mathbf{P}_0^{-1}(j\omega) e^{j\omega t} + \mathbf{P}_0^{-1}(-j\omega) e^{-j\omega t}] \\ \times [b, 0, 0, 0, 0, R_{01}(b)]^T \quad (96)$$

$$\mathbf{q}_0(t) = -\frac{1}{2I} [\mathbf{P}_0^{-1}(j\omega) e^{j\omega t} + \mathbf{P}_0^{-1}(-j\omega) e^{-j\omega t}] \\ \times [1, 0, 0, 0, 0, R_{00}(b)]^T \quad (97)$$

Table 1 Properties of the disk/spindle system used in the numerical simulation

Disk				Spindle		Bearings	
b	47.50 mm	z_1	-3.712 mm	I_1^I	3.941 kg-mm ²	k_a, k_b	2.021×10^4 N/mm
a	16.51 mm	z_2	-0.9747 mm	I_3^I	4.739 kg-mm ²	k_{az}, k_{bz}	8.666×10^3 N/mm
I_1^d	8.827 kg-mm ²	z_3	1.762 mm	m_s	3.189×10^{-2} kg	z_a	-8.077 mm
I_3^d	17.65 kg-mm ²	z_4	4.601 mm			z_b	5.131 mm
m	1.371×10^{-2} kg						

and

$$Q_{mn}^{(i)}(t) = \begin{cases} 0, & i = 1, 2, 3 \\ (j/2I)R_{mn}(b)[P_{mn}^{-1}(j\omega)e^{j\omega t} + P_{mn}^{-1}(-j\omega)e^{-j\omega t}], & i = 4. \end{cases} \quad (98)$$

For impulse response, (44) gives

$$\mathbf{q}_1(t) = \frac{j}{I} \mathbf{H}_1(t)[b, 0, 0, 0, R_{01}(b)]^T \quad (99)$$

$$\mathbf{q}_0(t) = -\frac{1}{I} \mathbf{H}_0(t)[1, 0, 0, 0, R_{00}(b)]^T \quad (100)$$

and

$$Q_{mn}^{(i)}(t) = \begin{cases} 0, & i = 1, 2, 3 \\ (j/I)R_{mn}(b)h_{mn}(t), & i = 4. \end{cases} \quad (101)$$

The real and imaginary parts of $\mathbf{q}_1(t)$, $\mathbf{q}_0(t)$, and $Q_{mn}^{(i)}(t)$ give the generalized coordinates (e.g., θ_x and θ_y). Then (14) gives the lateral vibration response.

Calculation of the response requires the knowledge of ω_{mn} , $R_{mn}(r)$, a_0 , and b_0 at the rotational speed ω_3 . Since the exact values of these quantities are unknown, they need to be estimated in the simulation. ω_{mn} is estimated by the sensitivity approach (Chen and Boggy, 1992) as

$$\omega_{mn} \approx \omega_{mn}^{(0)} + \frac{\omega_3^2 A_{mn}}{2\omega_{mn}^{(0)}} \quad (102)$$

where $\omega_{mn}^{(0)}$ is the disk natural frequency at zero rotational speed, and A_{mn} is the contribution from centrifugal membrane stresses. The detail formulation of A_{mn} can be found in Shen and Ku (1995). $R_{mn}(r)$, $n \neq 0$, are approximated by

$$R_{mn}(r) \approx \sqrt{\frac{15(b^4 - a^4)}{2(b-a)^5(5b+a)}} (r-a)^2, \quad n \neq 0. \quad (103)$$

Notice that $R_{mn}(r)$ in (103) are chosen so that they satisfy the orthonormality condition (8). Similarly, $R_{00}(r)$ is approximated by

$$R_{00}(r) \approx \sqrt{\frac{15(b^4 - a^4)}{4(b-a)^5(5b+a)}} (r-a)^2 \quad (104)$$

and $R_{00}(r)$ in (104) also satisfies the orthonormality condition (8). a_0 and b_0 are obtained by substituting (103) and (104) into (16) and (21), respectively.

In this numerical simulation, the following five types of modes are retained as a first approximation: unbalanced (0, 1) modes, balanced (0, 1) modes, unbalanced (0, 0) modes, balanced (0, 0) modes, and (0, 2) modes. Figure 5 shows the amplitude of the frequency response function of the disk/spindle system at $\omega_3 = 120$ Hz from a ground-based observer at the driving point (i.e., $r = b$ and $\beta = 0$ deg). The resolution of the frequency axis in this simulation is 0.25 Hz. According to the calculated frequency response function, the lowest two unbalanced (0, 1) modes are at 449.75 Hz and 689.5 Hz. The balanced (0, 1) modes are at 521 Hz and 761 Hz. The lowest

unbalanced (0, 0) mode is at 639.75 Hz. The balanced (0, 0) mode is at 652.0 Hz. The lower frequency of (0, 2) disk modes resulting from the backward travelling wave is 517.75 Hz. Note that the (0, 1) balanced modes follow the usual mode splitting rule of $2\omega_3$ in rotating disks, i.e., 761 Hz - 521 Hz = 240 Hz, which is twice of the rotational speed. The splitting of (0, 1) unbalanced modes, given by $689.5 - 449.75 = 239.75$ Hz is almost twice of the rotational speed. Theoretically, the $2\omega_3$ splitting rule does not apply to (0, 1) unbalanced modes, because the (0, 1) unbalanced modes are coupled motion of the spindle and the disks. Therefore, the splitting of (0, 1) unbalanced modes cannot be explained by forward and backward traveling waves of the circular disks alone, as in (0, 1) balanced modes. An exact and complete analysis on frequency splitting of rocking modes is yet to be developed. Finally, Fig. 6 shows the impulse response function from $t = 0$ to $t = 0.1$ second corresponding to the frequency response function in Fig. 5. Notice that the response is negative when the motion is initiated, because the applied force is negative.

9 Some Remarks

Although this paper presents a closed-form solution, one must realize that the solution is not exact. The approximation appears because finite terms in eigenfunctions are retained in order to obtain (24) and (35). As a result, (47) and (70) are valid only when disk modes with zero nodal circle are retained in the approximation. When more disk modes with one or more nodal circles are retained, (47) and (70) will take different forms. Nevertheless, the off-diagonal terms will be coupled through the spindle rocking in the same way allowing the procedures of causal Green's function and inverse Laplace transform for closed-form solution.

Although this paper assumes space-fixed load $g^{(i)}(\mathbf{r}_0, t)\mathbf{K}$, it is able to handle the moving load problem. For example, if a concentrated load is moving along the circle $r = b$ with velocity v on the i th disk, then

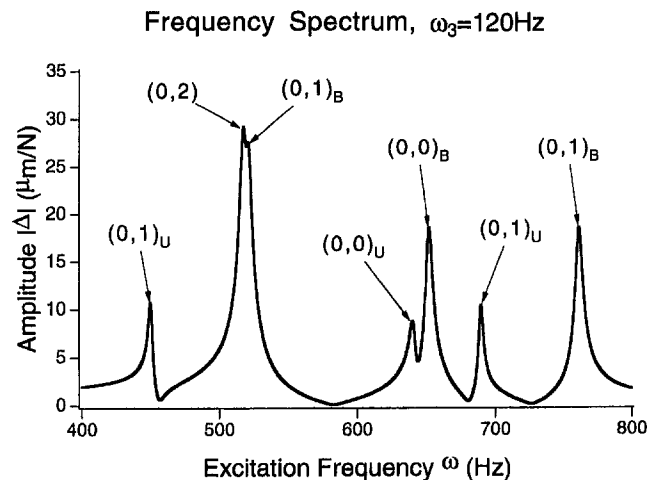


Fig. 5 The amplitude of the frequency response function of the disk/spindle system at $\omega_3 = 20$ Hz

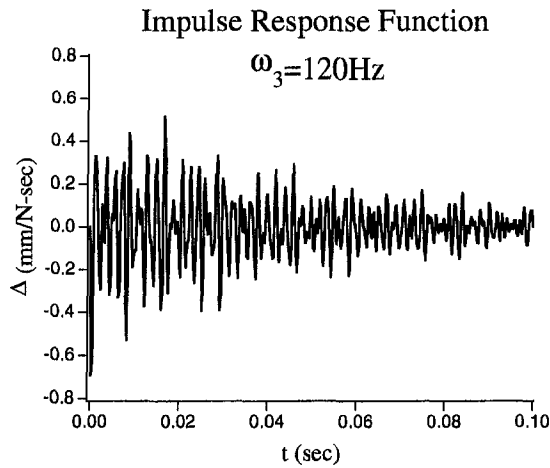


Fig. 6 The impulse response function of the disk/spindle system from $t = 0$ to $t = 0.1$ second

$$g^{(i)}(r_0, \beta_0, t) = \delta(r_0 - b)\delta(\beta_0 - vt). \quad (105)$$

Viscoelasticity of the disks can also be incorporated in this disk/spindle model. Let $\eta(\omega)$ be the loss factor of the disk material subjected to sinusoidal tensile or compressive strain with frequency ω . Then the frequency response function can be obtained through the same analysis, provided that $[\omega_{mn}^{(i)}]^2$ is replaced by $[\omega_{mn}^{(i)}]^2 \{1 + i\eta(\omega)\}$. Note that the transient time response cannot be obtained this way, because the loss factor is a concept of the frequency domain.

10 Conclusions

1 Forced response of a rotating, damped disk/spindle system with multiple disks is derived in this paper. Responses in the time domain and in the frequency domain have both been predicted explicitly in closed form.

2 Prescribed base motion will excite unbalanced (0, 1) and (0, 0) modes, but not other modes.

3 If the applied forces are in self-equilibrium, then the forces will not excite the unbalanced (0, 1) and (0, 0) modes to resonance. If the applied forces are identical to each disk, the forces will not excite the balanced (0, 1) and (0, 0) modes to resonances. Otherwise, applied forces will excite both the unbalanced and balanced modes to resonances.

Acknowledgments

The material is based upon work supported by the National Science Foundation under Grant No. CMS-9634557.

References

- Chen, J.-S. and Boggy, D. B., 1992, "Effects of Load Parameters on the Natural Frequencies and Stability of a Flexible Spinning Disk with a Stationary Load System," *ASME JOURNAL OF APPLIED MECHANICS*, Vol. 59, pp. S230-S235.
- Chivens, D. R., and Nelson, H. D., 1975, "The Natural Frequencies and Critical Speeds of a Rotating, Flexible Shaft-Disk System," *ASME Journal of Engineering for Industry*, pp. 881-886.
- D'Eleuterio, G. M. T., and Hughes, P. C., 1984, "Dynamics of Gyroelastic Continua," *ASME JOURNAL OF APPLIED MECHANICS*, Vol. 51, pp. 415-422.
- Dopkin, J. A., and Shoup, T. E., 1974, "Rotor Resonant Speed Reduction Caused by Flexibility of Disks," *ASME Journal of Engineering for Industry*, pp. 1328-1333.
- Flowers, G. T., and Ryan, S. G., 1993, "Development of a Set of Equations for Incorporating Disk Flexibility Effects in Rotordynamic Analyses," *ASME Journal of Engineering for Gas Turbines and Power*, Vol. 115, pp. 227-233.
- Hughes, P. C., and D'Eleuterio, G. M. T., 1986, "Modal Parameter Analysis of Gyroelastic Continua," *ASME JOURNAL OF APPLIED MECHANICS*, Vol. 53, pp. 919-924.
- Iwan, W. D., and Stahl, K. J., 1973, "The Response of an Elastic Disk with a Moving Mass System," *ASME JOURNAL OF APPLIED MECHANICS*, Vol. 40, pp. 445-451.
- Low, M., and Shen, I. Y., 1996, "Experimental Modal Analysis of a Spinning Rigid Shaft Carrying Multiple Elastic Disks," *Proceedings of the Sixth International Symposium on Transport Phenomena and Dynamics of Rotating Machinery (ISROMAC-6)*, Vol. 1, pp. 187-194.
- Meirovitch, L., 1974, "A New Method of Solution of the Eigenvalue Problem for Gyroscopic Systems," *AIAA Journal*, Vol. 12, No. 10, pp. 1337-1342.
- Meirovitch, L., 1975, "A Modal Analysis for the Response of Linear Gyroscopic Systems," *ASME JOURNAL OF APPLIED MECHANICS*, Vol. 42, pp. 446-450.
- Mote, C. D., Jr., 1970, "Stability of Circular Plates Subjected to Moving Loads," *Journal of the Franklin Institute*, Vol. 290, No. 4, pp. 329-344.
- Shen, I. Y., and Ku, Roger C.-P., 1995, "On the Vibration Analysis of Multiple Rotating Flexible Disks," *Advances in Information Storage and Processing Systems*, ISPS-Vol. 1, pp. 259-270; also as "A Non-classical Vibration Analysis of a Multiple Rotating Disk and Spindle Assembly," *ASME JOURNAL OF APPLIED MECHANICS*, accepted for publication.

A Comprehensive Energy Formulation for General Nonlinear Material Continua

A. Carini

Assistant Professor,
Department of Civil Engineering,
University of Brescia,
via Branze 38,
25123 Brescia, Italy

O. De Donato

Professor,
Department of Structural Engineering,
Politecnico di Milano,
piazza Leonardo da Vinci 32,
20133 Milano, Italy

By specialization to the continuum problem of a general formulation of the initial/boundary value problem for every nonpotential operator (Tonti, 1984) and by virtue of a suitable choice of the "integrating operator," a comprehensive energy formulation is established. Referring to the small strain and displacement case in the presence of any inelastic generally nonlinear constitutive law, provided that it is differentiable, this formulation allows us to derive extensions of well-known principles of elasticity (Hu-Washizu, Hellinger-Reissner, total potential energy, and complementary energy). An illustrative example is given. Peculiar properties of the formulation are the energy characterization of the functional and the use of Green functions of the same problem in the elastic range for every inelastic, generally nonlinear material considered.

1 Introduction

The present paper is framed within the context of the studies of the so-called "inverse problem" of variational calculus, i.e., the problem of finding "extended" variational formulations of linear or nonlinear problems with a nonpotential operator.

A fundamental contribution, which allowed subsequent important progress in the field, was given by Gurtin (1964) who introduced the convolution product for the variational formulation of the linear initial-value problem. In subsequent papers, Tonti (1972, 1973) emphasized the role of the bilinear form, and in particular of the convolutive form, giving a "potentiality criterium" in the search of variational principles for nonlinear problems. Then Magri (1974) introduced a bilinear, not necessarily symmetric, mapping for the variational formulation of linear initial-value problems.

More recently Tonti (1982, 1984) established a general method for the variational formulation of any nonlinear problem on the basis of the choice of an integrating operator.

In this paper, making a suitable choice of Tonti's integrating operator and using the above quoted recent results, a general variational formulation is given for a generally nonlinear differentiable operator and, by application to the continuum problem, extensions of the classical elasticity principles (Hu-Washizu, Hellinger-Reissner, total potential energy, complementary energy) are found to the material nonlinear case.

In the frame of the approaches that derive the solution of the nonlinear problem from the superposition of the elastic response to the given load and of the elastic response to the unknown inelastic strains (see Colonnetti, 1918; Ceradini, 1966; Maier, 1968, 1969; De Donato and Franchi, 1973; Zarka, 1979; Mura, 1991; Yu, 1992), the nonlinear constitutive law is suitably decomposed into an elastic and inelastic (remaining part) and, as Tonti's integrating operator, the inverse of the elastic operator (including boundary conditions) is adopted.

In this way the extended principles proved herein specialize to the corresponding elastic ones when the nonlinear part of the

constitutive law is ignored. Finally the energy character of the functionals is briefly discussed.

Two of the above four theorems had been established by Carini (1996) but using another approach based on Colonnetti's principle (Colonnetti, 1918).

2 Mathematical Preliminaries

In the following, the basic definitions and notations adopted for the representation both of a general nonlinear problem and of the corresponding variational formulations are briefly summarized.

Let a nonlinear problem be written in the following form:

$$\mathbf{N}(w) - P = 0 \quad (2.1)$$

where \mathbf{N} (the so-called *problem operator*) denotes any nonlinear differentiable operator and w is a function or a set of functions (of a given vector space W) satisfying prescribed linear initial or boundary conditions, while P is a known function or a set of known functions. The round brackets in (2.1) are customary in the theory of nonlinear operators, just as in the notation $f(x) = 0$. When the operator is linear the round brackets are omitted.

Let $\mathcal{D}(\mathbf{N})$ be the domain of the problem operator \mathbf{N} , conceived as a subset of the vector space W ; the set of elements $v = \mathbf{N}(w)$ constitutes the *range* of the problem operator and will be denoted by $\mathcal{R}(\mathbf{N})$ and conceived as a subset of a vector space V .

As it is well known, if a functional F exists such that its first variation δF is given by

$$\delta F[w] = \langle \mathbf{N}(w) - P, \delta w \rangle \quad (2.2)$$

where $\langle \cdot, \cdot \rangle$ is a bilinear nondegenerate functional, i.e. (being $w, w' \in W$ and $v, v' \in V$):

$$\text{if } \langle v, w' \rangle = 0 \text{ for every } v \in V \text{ then } w' = 0$$

$$\text{if } \langle v', w \rangle = 0 \text{ for every } w \in W \text{ then } v' = 0, \quad (2.3)$$

then the operator \mathbf{N} is the *gradient* of F and the functional F is the *potential* of \mathbf{N} (and \mathbf{N} is called a *potential operator*). In this case the original problem (2.1) is equivalent to the stationarity of

Contributed by the Applied Mechanics Division of THE AMERICAN SOCIETY OF MECHANICAL ENGINEERS for publication in the ASME JOURNAL OF APPLIED MECHANICS.

Discussion on this paper should be addressed to the Technical Editor, Professor Lewis T. Wheeler, Department of Mechanical Engineering, University of Houston, Houston, TX 77204-4792, and will be accepted until four months after final publication of the paper itself in the ASME JOURNAL OF APPLIED MECHANICS.

Manuscript received by the ASME Applied Mechanics Division, June 19, 1995; final revision, May 2, 1996. Associate Technical Editor: W. K. Liu.

$$F[w] = F[w_0] + \int_{\lambda=0}^{\lambda=1} \left\langle (\mathbf{N}(\eta(\lambda)) - P), \frac{\partial \eta}{\partial \lambda} \right\rangle d\lambda \quad (2.4)$$

where $\eta(\lambda)$ denotes a one-parameter family of functions with $\eta(0) = w_0$ and $\eta(1) = w$. However, for a general nonlinear operator \mathbf{N} , the original problem (2.1) does not have a variational formulation in a classical sense.

Nevertheless Tonti (1984) showed that a corresponding *extended* variational formulation may be given provided that a suitable bilinear form may be found so that an integrating operator \mathbf{K} , symmetric with respect to the bilinear form itself, exists. In this case the problem (2.1) (with \mathbf{N} even nonpotential operator) is equivalent to the stationarity of the following *extended* functional:

$$F_{\text{ext}}[w] = \frac{1}{2} \langle \mathbf{N}(w) - 2P, \mathbf{K}\mathbf{N}(w) \rangle \quad (2.5)$$

under the assumption that (a) the solution of the problem exists and (b) it is unique, (c) $\mathcal{D}(\mathbf{N})$ is simply connected, (d) the Gateaux derivative \mathbf{N}' of \mathbf{N} exists, (e) $\mathcal{D}(\mathbf{N}')$ is dense in W , (f) the adjoint operator \mathbf{N}'^* of \mathbf{N}' is invertible for every $w \in \mathcal{D}(\mathbf{N})$, (g) \mathbf{K} is linear and invertible, (h) $\mathcal{D}(\mathbf{K}) \supset \mathcal{R}(\mathbf{N})$, (i) $\mathcal{R}(\mathbf{K}) \subset \mathcal{D}(\mathbf{N}'^*)$.

The above results were obtained by Tonti with reference to linear *homogeneous* boundary conditions. In the following, however, reference will be made to nonhomogeneous boundary conditions and far less assumptions will be required than the original (a) to (f) made by Tonti. Besides, it will be more useful to rewrite the original problem (2.1) in a form in which the linear boundary conditions are explicitly represented, i.e.,

$$N(w) = f \quad \text{in } \Omega \times T \quad (2.6)$$

$$Bw = g \quad \text{on } \Gamma \times T \quad (2.7)$$

where N is the *formal* nonlinear operator corresponding to the *problem operator* \mathbf{N} while B is the linear operator of the boundary conditions and $T = [t_0, t_1]$ is the time interval considered. For the sake of simplicity in the following, vanishing initial conditions are assumed, i.e.,

$$w \equiv 0 \quad \text{on } \Omega \times (-\infty, t_0). \quad (2.8)$$

3 Problem Position

Consider a solid which occupies a region Ω , in a triaxial orthogonal Cartesian reference system x_i ($i = 1, 2, 3$), with the boundary Γ being Γ_u and Γ_p the parts of the surface Γ where displacements and surface tractions are prescribed, respectively. The external actions on the solid, i.e., volume forces $\bar{F}_i(t)$, prescribed displacements $\bar{u}_i(t)$ on Γ_u and surface forces $\bar{p}_i(t)$ on Γ_p , are given for any instant $t_0 \leq t \leq t_1$ through known time functions (all stresses, strains, displacements, and external actions for $t < t_0$ vanishing). The stresses, strains, and displacements space-time functions $\sigma_{ij}(x_k, t)$, $\epsilon_{ij}(x_k, t)$ and $u_i(x_k, t)$, are to be determined in the volume Ω and in the time interval T .

The governing equations of the general nonlinear continuum problem in the presence of small displacements and strains, i.e., equilibrium, compatibility, direct and inverse constitutive law are, respectively (the repeated index summation convention is adopted):

$$\sigma_{ij,j} + \bar{F}_i = 0 \quad \text{in } \Omega \times T \quad (3.1)$$

$$\sigma_{ijn_j} = \bar{p}_i \quad \text{on } \Gamma_p \times T \quad (3.2)$$

$$\epsilon_{ij} = \frac{1}{2}(u_{i,j} + u_{j,i}) \quad \text{in } \Omega \times T \quad (3.3)$$

$$u_i = \bar{u}_i \quad \text{on } \Gamma_u \times T \quad (3.4)$$

$$\sigma_{ij} = \Psi(\epsilon_{ij}) \quad \text{in } \Omega \times T \quad (3.5)$$

$$\epsilon_{ij} = \Phi(\sigma_{ij}) \quad \text{in } \Omega \times T \quad (3.6)$$

where Ψ and Φ are differential or integral or generally nonlinear operators and $(\cdot)_{,j} = \partial(\cdot)/\partial x_j$ while n_j are the components of the outward normal unit vector to surface Γ .

The form (3.5) of the direct constitutive law is able to take different kinds of time histories of the strain into account. However, due to the differentiability assumption of the operator \mathbf{N} of Eq. (2.1), the operator Ψ has to be differentiable and then only the time histories of the strain amenable to differentiable operators Ψ can be considered. This implies, for example, the exclusion of the elastic-plastic behavior while the viscoelastic case can be fully considered. In this last case the direct constitutive law (3.5) would have, under the assumption of linearity, the following form (see, e.g., Christensen, 1982):

$$\sigma_{ij}(\mathbf{x}; t) = H_{ijkl}(\mathbf{x}; 0)\epsilon_{hk}(\mathbf{x}; t) + \int_{t_0}^t \frac{\partial H_{ijkl}(\mathbf{x}; t - \tau)}{\partial(t - \tau)} \epsilon_{hk}(\mathbf{x}; \tau) d\tau \quad (3.7)$$

where the time integral represents the time history of the strain being H_{ijkl} the relaxation viscous kernel.

Let's assume in the following that both the direct and the inverse constitutive laws are of the additive type, that is, that they can be written splitting each of the above operators Ψ and Φ into two parts, the first of which is representative of the linear elastic behavior, while the second (the residual part) is representative of the deviation of the inelastic nonlinear behavior with respect to the linear elastic part. In other words, the assumption is that (3.5) and (3.6) can be written in the form:

$$\sigma_{ij} = D_{ijkl}\epsilon_{hk} + \Psi_r(\epsilon_{ij}) \quad \text{in } \Omega \times T \quad (3.8)$$

$$\epsilon_{ij} = D_{ijkl}^{-1}\sigma_{hk} + \Phi_r(\sigma_{ij}) \quad \text{in } \Omega \times T \quad (3.9)$$

where D_{ijkl} is the linear elastic modulus tensor. For instance, in the case of the linear viscoelastic constitutive law (3.7)

$$D_{ijkl}(\mathbf{x}) = H_{ijkl}(\mathbf{x}; 0) \quad (3.10)$$

represents the elastic instantaneous modulus tensor, while

$$\Psi_r(\epsilon_{ij}) = \int_{t_0}^t \frac{\partial H_{ijkl}(\mathbf{x}; t - \tau)}{\partial(t - \tau)} \epsilon_{hk}(\mathbf{x}; \tau) d\tau \quad (3.11)$$

represents the inelastic viscous part. With the above notation all the known inelastic linear or nonlinear material behaviors (history dependent or not) amenable to *differentiable* operators Ψ and Φ may be considered (such as viscoelastic, viscoelastoplastic, etc.).

Defining the equilibrium operator E and the compatibility operator C such that $E\sigma_{ij} = \sigma_{ij,j}$ and $Cu_i = \frac{1}{2}(u_{i,j} + u_{j,i})$, the preceding (3.1) to (3.6) relations can be summarized in the following three and two-field operatorial formulations (with a clear meaning of identity operator I and null operator O):

(a) Three-Field Operatorial Formulation ($u_i, \epsilon_{ij}, \sigma_{ij}$).

$$\begin{bmatrix} O & O & -E \\ O & \Psi(\cdot) & -I \\ C & -I & O \end{bmatrix} \cdot \begin{bmatrix} u_i \\ \epsilon_{ij} \\ \sigma_{ij} \end{bmatrix} = \begin{bmatrix} \bar{F}_i \\ 0 \\ 0 \end{bmatrix} \quad \text{in } \Omega \times T \quad (3.12)$$

$$\begin{bmatrix} O & O & n_j \\ O & O & O \\ -n_j & O & O \end{bmatrix} \cdot \begin{bmatrix} u_i \\ \epsilon_{ij} \\ \sigma_{ij} \end{bmatrix} = \begin{bmatrix} \bar{p}_i \\ 0 \\ -n_j \bar{u}_i \end{bmatrix} \quad \begin{matrix} \text{on } \Gamma_p \times T \\ \text{on } \Gamma_u \times T \end{matrix} \quad (3.13)$$

which may be written in the more compact form (in the unknowns $u_i, \epsilon_{ij}, \sigma_{ij}$):

$$N_{hw}(w) = f_{hw} \quad \text{in } \Omega \times T \quad (3.14)$$

$$B_{hw}w = g_{hw} \quad \text{on } \Gamma \times T \quad (3.15)$$

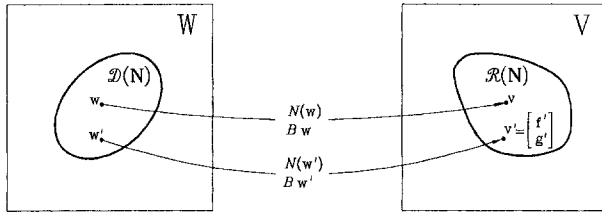


Fig. 1 Mapping of the element w, w' of the domain $\mathcal{D}(\mathbf{N})$ in the vector space W with the corresponding elements v, v' of the range $\mathcal{R}(\mathbf{N})$ in the vector space V relevant to the nonlinear initial/boundary value problem (2.6)–(2.7)

where $\tilde{w} = [u_i, \epsilon_{ij}, \sigma_{ij}]$, $\tilde{f}_{hw} = [\bar{F}_i, 0, 0]$, $\tilde{g}_{hw} = [\bar{p}_i, 0, -n_j \bar{u}_i]$, while N_{hw} and B_{hw} are the matrices of the operators in the first members of Eqs. (3.12), (3.13) and a tilde means transposition.

(b) Two-Field Operatorial Formulation (u_i, σ_{ij}).

$$\begin{bmatrix} O & E \\ -C & \Phi(\cdot) \end{bmatrix} \cdot \begin{bmatrix} u_i \\ \sigma_{ij} \end{bmatrix} = \begin{bmatrix} -\bar{F}_i \\ 0 \end{bmatrix} \quad \text{in } \Omega \times T \quad (3.16)$$

$$\begin{bmatrix} O & -n_j \\ n_j & O \end{bmatrix} \cdot \begin{bmatrix} u_i \\ \sigma_{ij} \end{bmatrix} = \begin{bmatrix} -\bar{p}_i \\ n_j \bar{u}_i \end{bmatrix} \quad \begin{matrix} \text{on } \Gamma_p \times T \\ \text{on } \Gamma_u \times T \end{matrix} \quad (3.17)$$

i.e.,

$$N_{hr}(w) = f_{hr} \quad \text{in } \Omega \times T \quad (3.18)$$

$$B_{hr}w = g_{hr} \quad \text{on } \Gamma \times T \quad (3.19)$$

where $\tilde{w} = [u_i, \sigma_{ij}]$, $\tilde{f}_{hr} = [-\bar{F}_i, 0]$, $\tilde{g}_{hr} = [-\bar{p}_i, n_j \bar{u}_i]$, while N_{hr} and B_{hr} are the matrices of the operators in the first members of Eqs. (3.16), (3.17) and a tilde means transposition.

4 The Choice of the Bilinear Form

Let's adopt for both the operatorial formulations (3.14)–(3.15) and (3.18)–(3.19) the common notation (2.6)–(2.7) or, in compact form, the notation (2.1). Let's associate the following bilinear form (see Fig. 1) to the problem (3.1)–(3.6):

$$\langle w, v' \rangle = \int_T \left\{ \int_{\Omega} w f' d\Omega + \int_{\Gamma} w g' d\Gamma \right\} dt \quad (4.1)$$

or using the operator \mathbf{N} :

$$\langle w, \mathbf{N}(w') \rangle = \int_T \left\{ \int_{\Omega} w \mathbf{N}(w') d\Omega + \int_{\Gamma} w B w' d\Gamma \right\} dt \quad (4.2)$$

being $w, w' \in \mathcal{D}(\mathbf{N}) \subset W$ and $v, v' \in \mathcal{R}(\mathbf{N}) \subset V$ where W and V are linear vector spaces which can be defined when the constitutive law is given. It is worth noting that the problem operator \mathbf{N} , in general, is not symmetric with respect to the bilinear form (4.2). However, it is always possible to transform the bilinear form (4.2) in a new one in order to obtain the symmetry of \mathbf{N} with respect to the new bilinear form. To this aim let the operator \mathbf{N} be split as follows:

$$\mathbf{N} = \mathbf{S} + \mathbf{R} \quad (4.3)$$

where \mathbf{S} is the linear elastic part of \mathbf{N} , with the same boundary conditions of \mathbf{N} , and \mathbf{R} is the remaining inelastic part (linear or nonlinear) of the original operator without boundary conditions (this means that \mathbf{R} coincide with its formal operator R). \mathbf{S} may be interpreted as the operator relevant to the following continuum problem:

$$S w^s = f \quad \text{in } \Omega \times T \quad (4.4)$$

$$B w^s = g \quad \text{on } \Gamma \times T \quad (4.5)$$

or in compact form:

$$\mathbf{S} w^s = P \quad (4.6)$$

corresponding to the original inelastic generally nonlinear problem where the material properties are assumed linear elastic. This allows to introduce and to understand the meaning of operator \mathbf{S}^{-1} as the linear operator which gives the elastic response of the above solid for any assigned external load P , that is

$$w^s = \mathbf{S}^{-1} P. \quad (4.7)$$

The symmetry of \mathbf{S} , and that of \mathbf{S}^{-1} , with respect to the bilinear form $\langle w, v' \rangle$ (Eq. (4.1)), being $w \in \mathcal{D}(\mathbf{S}) \subset W$, $v' \in \mathcal{R}(\mathbf{S}) \subset V$, may be easily proved. The above symmetry of \mathbf{S}^{-1} allows to recognize the new bilinear form (with respect to which the nonlinear operator \mathbf{N} will always be symmetric) as the following:

$$\langle \mathbf{S}^{-1} v, v' \rangle = \langle \mathbf{S}^{-1} \mathbf{N}(w), \mathbf{N}(w') \rangle. \quad (4.8)$$

Finally it is worth noting that \mathbf{S}^{-1} may be expressed in terms of Green functions of the original solid in the elastic range.

5 A General Principle for Nonlinear Continuum Problem

The new bilinear form (4.1) and the symmetry of the linear and invertible operator \mathbf{S}^{-1} are all the elements required, according to Tonti's approach, in order to find extended variational formulations of nonlinear problems of the kind (3.14)–(3.15) or (3.18)–(3.19). Simply choosing

$$\mathbf{K} \equiv \mathbf{S}^{-1}, \quad (5.1)$$

the general extended functional (2.5) becomes

$$F_{\text{ext}}[w] = \frac{1}{2} \langle \mathbf{N}(w) - 2P, \mathbf{S}^{-1} \mathbf{N}(w) \rangle \quad (5.2)$$

i.e., being $\mathbf{S}^{-1} \mathbf{N}(w) = \mathbf{S}^{-1}(\mathbf{S} + \mathbf{R})(w) = w + \mathbf{S}^{-1} \mathbf{R}(w) = w + \hat{w}$,

$$F_{\text{ext}}[w] = \frac{1}{2} \langle \mathbf{N}(w) - 2P, w + \hat{w} \rangle \quad (5.3)$$

where \hat{w} is the solution of the elastic auxiliary problem:

$$S \hat{w} = R(w) \quad \text{in } \Omega \times T \quad (5.4)$$

$$B \hat{w} = 0 \quad \text{on } \Gamma \times T. \quad (5.5)$$

This solution \hat{w} may be represented through the so-called Green's functions relative to the considered elastic auxiliary solid. Using the formal operators N and B , the functional (5.2) becomes

$$F_{\text{ext}}[w] = \int_T \left\{ \frac{1}{2} \int_{\Omega} N(w)(w + \hat{w}) d\Omega + \frac{1}{2} \int_{\Gamma} B w(w + \hat{w}) d\Gamma - \int_{\Omega} f(w + \hat{w}) d\Omega - \int_{\Gamma} g(w + \hat{w}) d\Gamma \right\} dt. \quad (5.6)$$

Theorem. At any solution (if at least one exists) w of the problem (3.1)–(3.6) the functional (5.2) is stationary and assumes the value

$$F^o = -\frac{1}{2} \langle P, w^s \rangle. \quad (5.7)$$

Conversely, any field w (if at least one exists), at which the functional (5.2) is stationary and assumes the above value F^o , is the (or a) solution of the problem.

Proof. Let us write the functional (5.2) in the following more expanded form:

$$F_{\text{ext}} = \frac{1}{2} \langle \mathbf{N}(w) - P, \mathbf{S}^{-1}(\mathbf{N}(w) - P) \rangle - \frac{1}{2} \langle P, w^s \rangle \quad (5.8)$$

whose first variation is (due to the symmetry of \mathbf{S}^{-1} with respect to the adopted bilinear form (4.1))

$$\delta F_{\text{ext}} = \langle \mathbf{N}(w) - P, \mathbf{S}^{-1} \delta \mathbf{N}(w) \rangle. \quad (5.9)$$

If w is a solution of the problem (3.1)–(3.6), then $\mathbf{N}(w) = P$ and δF_{ext} of Eq. (5.9) vanishes (this means stationarity of F_{ext} at w). Meanwhile, since w is a solution, $F_{\text{ext}}[w]$ assumes the value F^o (see Eq. (5.8)). The first part of the theorem is proved.

Conversely, let us assume F_{ext} stationary at w ; this implies, since $\delta F_{\text{ext}}[w] = 0$ and by virtue of property (2.3), one of the following three possibilities: (1) $\mathbf{N}(w) - P = 0$ and $\delta \mathbf{N}(w) \neq 0$, (2) $\delta \mathbf{N}(w) = 0$ and $\mathbf{N}(w) - P \neq 0$, (3) $\mathbf{N}(w) - P = 0$ and $\delta \mathbf{N}(w) = 0$. In cases (1) and (3) w must be a solution and from (5.8) the value assumed by the functional at w becomes F^o . In case (2) w is not a solution but, despite the stationarity at w , $F_{\text{ext}}[w] \neq F^o$. This proves the second part of the theorem. \square

Under the only restriction that $\mathcal{D}(\mathbf{S}^{-1}) \supset \mathcal{R}(\mathbf{N})$ the above result is to be considered general, that is, valid for any kind of nonlinear differentiable operator \mathbf{N} (i.e., operator for which the Gateaux derivative \mathbf{N}' exists) even relevant to problems for which uniqueness and existence of solution may not be asserted.

A more useful form of the functional (5.6) may be derived using the principle of virtual work which gives

$$\int_{\Omega} R(w) w d\Omega = \int_{\Omega} S w \hat{w} d\Omega + \int_{\Gamma} B w \hat{w} d\Gamma \quad \forall t \in T. \quad (5.10)$$

Using Eq. (5.10) the functional (5.6) becomes

$$\begin{aligned} F_{\text{ext}}[w] = & \int_T \left\{ \frac{1}{2} \int_{\Omega} (S w - 2f) w d\Omega \right. \\ & + \frac{1}{2} \int_{\Gamma} (B w - 2g) w d\Gamma + \int_{\Omega} R(w) w d\Omega \\ & \left. + \frac{1}{2} \int_{\Omega} (R(w) - 2f) \hat{w} d\Omega - \int_{\Gamma} g \hat{w} d\Gamma \right\} dt. \quad (5.11) \end{aligned}$$

It is worth noting that if the external actions $r = R(w)$ of the problem (5.4)–(5.5) are assumed as known, the last two terms of (5.11) become constant with respect to w and then the functional assumes the more compact form

$$\begin{aligned} F_{\text{ext}}[w] = & \int_T \left\{ \frac{1}{2} \int_{\Omega} (S w - 2f) w d\Omega \right. \\ & \left. + \frac{1}{2} \int_{\Gamma} (B w - 2g) w d\Gamma + \int_{\Omega} r w d\Omega \right\} dt, \quad (5.12) \end{aligned}$$

which is of the Colonnetti type (Colonnetti, 1918) in the sense that the functional is constituted by an elastic part (the first two terms) and a term representing the work done by known imposed external actions $r = R(w)$, by the corresponding dual variables w .

Remarks. The particular choice of the integrating operator \mathbf{K} made with Eq. (5.1), substantially transformed the original problem into the sum of the elastic response to the external

loads and of the elastic response (the elastic auxiliary problem) to distortions corresponding to the inelastic deformations. This approach to inelastic problems (the so-called Colonnetti's approach) had numerous developments and applications in literature, among others, by Ceradini (1966), Maier (1968, 1969), and De Donato and Franchi (1973) in elastoplasticity; by Mura (1987) in micromechanics (eigenstrain approach); and by Zarka (1979) in shakedown analysis (operator split approach). However, a larger range of approaches than Eq. (5.1) appear available when different choices of the integrating operator \mathbf{K} are adopted. The wide range of possibilities given by this choice would be worth exploring in the authors' opinion.

6 Extension of Elasticity Principles to General Nonlinear Materials

On the basis of the above general functional (5.6) or (5.11) it is easy to derive the following family of functionals of the linear elasticity theory extended to the general nonlinear case simply by using operators S, R, B defined in Sections 3, 4, and 5.

6.1 Extension of Hu-Washizu Principle. In this case the unknowns of the problem are the displacements u_i , the strains ϵ_{ij} and the stresses σ_{ij} , and the functional (5.11), where $\hat{w} = [u_i, \epsilon_{ij}, \sigma_{ij}]$, takes the form

$$\begin{aligned} F_{hw}[w] = & \frac{1}{2} \langle \mathbf{N}_{hw}(w) - 2P_{hw}, w + \hat{w} \rangle \\ = & \int_T \left\{ \frac{1}{2} \int_{\Omega} (-\sigma_{ij,j} u_i + D_{ijk} \epsilon_{ij} \epsilon_{hk} - 2\sigma_{ij} \epsilon_{ij} \right. \\ & + \sigma_{ij} \frac{1}{2} (u_{i,j} + u_{j,i})) d\Omega - \int_{\Omega} \bar{F}_i u_i d\Omega + \frac{1}{2} \int_{\Gamma_p} n_j \sigma_{ij} u_i d\Gamma \\ & - \frac{1}{2} \int_{\Gamma_u} n_j \sigma_{ij} u_i d\Gamma - \int_{\Gamma_p} \bar{p}_i u_i d\Gamma + \int_{\Gamma_u} n_j \sigma_{ij} \bar{u}_i d\Gamma \\ & + \int_{\Omega} \Psi_r(\epsilon_{ij}) \epsilon_{ij} d\Omega + \frac{1}{2} \int_{\Omega} \Psi_r(\epsilon_{ij}) \hat{\epsilon}_{ij} d\Omega - \int_{\Omega} \bar{F}_i \hat{u}_i d\Omega \\ & \left. - \int_{\Gamma_p} \bar{p}_i \hat{u}_i d\Gamma + \int_{\Gamma_u} n_j \hat{\sigma}_{ij} \bar{u}_i d\Gamma \right\} dt. \quad (6.1) \end{aligned}$$

When $\Psi_r \equiv 0$ and the external actions are time independent, the functional (6.1) trivially specializes in the well-known classical Hu-Washizu functional of elasticity.

6.2 Extension of Hellinger-Reissner Principle. In this case the unknowns of the problem are the displacements u_i and the stresses σ_{ij} and the functional (5.11) where $\hat{w} = [u_i, \sigma_{ij}]$ takes the form

$$\begin{aligned} F_{hr}[w] = & \frac{1}{2} \langle \mathbf{N}_{hr}(w) - 2P_{hr}, w + \hat{w} \rangle \\ = & \int_T \left\{ \frac{1}{2} \int_{\Omega} (\sigma_{ij,j} u_i + D_{ijk}^{-1} \sigma_{ij} \sigma_{hk} - \sigma_{ij} \frac{1}{2} (u_{i,j} + u_{j,i})) d\Omega \right. \\ & + \int_{\Omega} \bar{F}_i u_i d\Omega - \frac{1}{2} \int_{\Gamma_p} n_j \sigma_{ij} u_i d\Gamma + \frac{1}{2} \int_{\Gamma_u} n_j \sigma_{ij} u_i d\Gamma \\ & + \int_{\Gamma_p} \bar{p}_i u_i d\Gamma - \int_{\Gamma_u} n_j \sigma_{ij} \bar{u}_i d\Gamma + \int_{\Omega} \Phi_r(\sigma_{ij}) \sigma_{ij} d\Omega \\ & + \frac{1}{2} \int_{\Omega} \Phi_r(\sigma_{ij}) \hat{\sigma}_{ij} d\Omega + \int_{\Omega} \bar{F}_i \hat{u}_i d\Omega \\ & \left. + \int_{\Gamma_p} \bar{p}_i \hat{u}_i d\Gamma - \int_{\Gamma_u} n_j \hat{\sigma}_{ij} \bar{u}_i d\Gamma \right\} dt. \quad (6.2) \end{aligned}$$

When $\Phi_r \equiv 0$ and the external actions are time independent, the

functional (6.2) trivially specializes in the well-known classical Hellinger-Reissner functional of elasticity.

6.3 Extension of Total Potential Energy Principle. This extension may be simply derived from the extended Hu-Washizu functional (6.1) taking into account that between the components of the vector $\tilde{w} = [u_i, \epsilon_{ij}, \sigma_{ij}]$ the compatibility (3.3)–(3.4) and the constitutive (3.8) equations hold. This leads to the functional

$$F_{pe}[u_i] = \int_T \left\{ \frac{1}{2} \int_{\Omega} D_{ijk} \epsilon_{ij} \epsilon_{hk} d\Omega - \int_{\Omega} \bar{F}_i u_i d\Omega - \int_{\Gamma_p} \bar{p}_i u_i d\Gamma + \int_{\Omega} \Psi_r(\epsilon_{ij}) \epsilon_{ij} d\Omega + \frac{1}{2} \int_{\Omega} D_{ijk} \hat{\epsilon}_{ij} \hat{\epsilon}_{hk} d\Omega - \int_{\Omega} \bar{F}_i \hat{u}_i d\Omega - \int_{\Gamma_p} \bar{p}_i \hat{u}_i d\Gamma + \int_{\Gamma_u} n_j \hat{\sigma}_{ij} \bar{u}_i d\Gamma \right\} dt. \quad (6.3)$$

As in the case of the Hu-Washizu functional, when $\Psi_r \equiv 0$ and the external actions are time independent, the functional (6.3) trivially specializes in the well-known classical total potential energy functional of elasticity.

6.4 Extension of Complementary Energy Principle. As in the previous case this extension may be derived from the extended Hellinger-Reissner functional (6.2) taking into account that between the components of the vector $\tilde{w} = [u_i, \sigma_{ij}]$ the equilibrium (3.1)–(3.2) and constitutive (3.9) equations hold. This leads to the functional

$$F_{ce}[\sigma_{ij}] = \int_T \left\{ \frac{1}{2} \int_{\Omega} D_{ijk}^{-1} \sigma_{ij} \sigma_{hk} d\Omega - \int_{\Gamma_u} n_j \sigma_{ij} \bar{u}_i d\Gamma + \int_{\Omega} \Phi_r(\sigma_{ij}) \sigma_{ij} d\Omega + \frac{1}{2} \int_{\Omega} D_{ijk}^{-1} \hat{\sigma}_{ij} \hat{\sigma}_{hk} d\Omega + \int_{\Omega} \bar{F}_i \hat{u}_i d\Omega + \int_{\Gamma_p} \bar{p}_i \hat{u}_i d\Gamma - \int_{\Gamma_u} n_j \hat{\sigma}_{ij} \bar{u}_i d\Gamma \right\} dt. \quad (6.4)$$

As in the case of the Hellinger-Reissner functional, when $\Phi_r \equiv 0$ and the external actions are time independent, the functional (6.4) trivially specializes in the well-known classical complementary energy functional of elasticity.

6.5 Remarks.

1 According to the theorem of Section 5, the problem (3.1)–(3.6) has at least one solution if and only if the functionals (6.1) and (6.3) assume, at least in one of the stationarity points, the following value (see Eq. (5.7))

$$F^o = -\frac{1}{2} \langle P, w^s \rangle = \frac{1}{2} \int_T \left\{ - \int_{\Omega} \bar{F}_i u_i^s d\Omega - \int_{\Gamma_p} \bar{p}_i u_i^s d\Gamma + \int_{\Gamma_u} \bar{u}_i n_j \sigma_{ij}^s d\Gamma \right\} dt \quad (6.5)$$

while the functionals (6.2) and (6.4) assume, at the stationarity the following value

$$F^o = -\frac{1}{2} \langle P, w^s \rangle = \frac{1}{2} \int_T \left\{ \int_{\Omega} \bar{F}_i u_i^s d\Omega + \int_{\Gamma_p} \bar{p}_i u_i^s d\Gamma - \int_{\Gamma_u} \bar{u}_i n_j \sigma_{ij}^s d\Gamma \right\} dt. \quad (6.6)$$

2 It is worth noting that in the case of the Hu-Washizu and of the total potential energy functionals the stresses $\hat{\sigma}_{ij}$, strains $\hat{\epsilon}_{ij}$, and displacements \hat{u}_i of the elastic auxiliary problem are the

stresses, strains, and displacements of the original problem under the following assumptions: (a) linear elastic material behavior, (b) homogeneous boundary conditions, (c) external actions given only by the imposed non equilibrated stresses σ_{ij}^o corresponding (through the inelastic part Ψ_r of the constitutive law (3.8)) to the real strains ϵ_{ij} solution of the nonlinear original problem. In other words, denoting with σ_{ij}^{so} and with ϵ_{ij}^{so} the elastic stresses and strains induced in the elastic auxiliary problem by the above mentioned stresses σ_{ij}^o , the following relations hold:

$$\begin{cases} \hat{\sigma}_{ij} = \sigma_{ij}^{so} + \sigma_{ij}^o \\ \hat{\epsilon}_{ij} = \epsilon_{ij}^{so} \end{cases}, \quad \begin{cases} \sigma_{ij}^{so} = D_{ijk} \epsilon_{hk}^{so} \\ \epsilon_{ij}^{so} = D_{ijk}^{-1} \sigma_{hk}^{so} \end{cases}. \quad (6.7)$$

Conversely, in the case of the Hellinger-Reissner and of the complementary energy functionals the stresses $\hat{\sigma}_{ij}$, strains $\hat{\epsilon}_{ij}$, and displacements \hat{u}_i of the elastic auxiliary problem are the stresses, strains, and displacements of the original problem under the following assumptions: (a) linear elastic material behavior, (b) homogeneous boundary conditions, (c) external actions given only by the imposed non compatible strains θ_{ij}^o corresponding (through the inelastic part Φ_r of the constitutive law (3.9)) to the real stresses σ_{ij} solution of the nonlinear original problem. In other words, denoting with σ_{ij}^{so} and with ϵ_{ij}^{so} the elastic stresses and strains induced in the auxiliary problem by the above mentioned strains θ_{ij}^o , the following relations hold:

$$\begin{cases} \hat{\epsilon}_{ij} = \epsilon_{ij}^{so} + \theta_{ij}^o \\ \hat{\sigma}_{ij} = \sigma_{ij}^{so} \end{cases}, \quad \begin{cases} \epsilon_{ij}^{so} = D_{ijk}^{-1} \sigma_{hk}^{so} \\ \sigma_{ij}^{so} = D_{ijk} \epsilon_{hk}^{so} \end{cases}. \quad (6.8)$$

3 It is possible, using the principle of virtual work, to rewrite the functionals (6.1)–(6.4) in an alternative form (allowing to give them an energetic interpretation) of the type

$$F_{ext}[w] = F_{ext}^S[w] + F_{ext}^R[w] + F_{ext}^{SR}[w]. \quad (6.9)$$

In particular, in the case of extended total potential energy functional, the three terms of Eq. (6.9) take the form

$$F_{pe}^S[u_i] = \int_T \left\{ \frac{1}{2} \int_{\Omega} D_{ijk} \epsilon_{ij} \epsilon_{hk} d\Omega - \int_{\Omega} \bar{F}_i u_i d\Omega - \int_{\Gamma_p} \bar{p}_i u_i d\Gamma \right\} dt$$

$$F_{pe}^R[u_i] = \int_T \int_{\Omega} \Psi_r(\epsilon_{ij}) (\epsilon_{ij} - \epsilon_{ij}^s) d\Omega dt$$

$$F_{pe}^{SR}[u_i] = \frac{1}{2} \int_T \int_{\Omega} D_{ijk} \hat{\epsilon}_{ij} \hat{\epsilon}_{hk} d\Omega dt \quad (6.10)$$

where $F_{pe}^S[u_i]$ is the total potential energy functional of the elastic problem under the given external actions \bar{F}_i , \bar{p}_i of the original nonlinear problem (2.1), $F_{pe}^R[u_i]$ is the work done by the unknown nonequilibrated stresses $\sigma_{ij}^o = \Psi_r(\epsilon_{ij})$ for the strains $(\epsilon_{ij} - \epsilon_{ij}^s)$ where ϵ_{ij}^s is the elastic solution of the problem under the external actions \bar{F}_i , \bar{p}_i , \bar{u}_i , and $F_{pe}^{SR}[u_i]$ is the elastic energy of the elastic auxiliary problem (5.4)–(5.5) under the external actions

$$R(w) = \sigma_{ij}^o = \Psi_r(\epsilon_{ij}). \quad (6.11)$$

In the case of extended complementary energy functional the three terms of the functional (6.9) take the form

$$F_{ce}^S[\sigma_{ij}] = \int_T \left\{ \frac{1}{2} \int_{\Omega} D_{ijk}^{-1} \sigma_{ij} \sigma_{hk} d\Omega - \int_{\Gamma_u} n_j \sigma_{ij} \bar{u}_i d\Gamma \right\} dt$$

$$F_{ce}^R[\sigma_{ij}] = \int_T \int_{\Omega} \Phi_r(\sigma_{ij}) (\sigma_{ij} - \sigma_{ij}^s) d\Omega dt$$

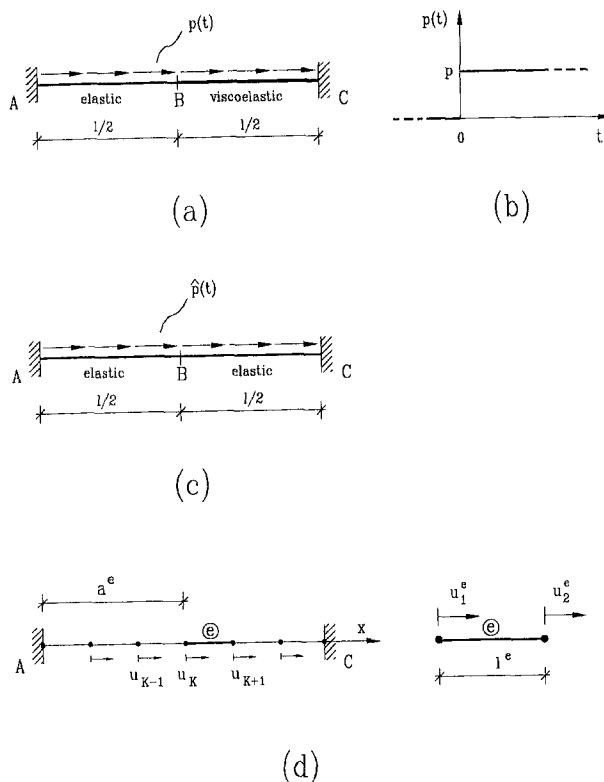


Fig. 2 Example of application of the extended total potential energy principle (Eqs. (6.9)–(6.10)). (a) The fixed-end elastic-viscoelastic rod considered subject to a uniformly distributed axial load $p(t)$; (b) the assumed time load function $p(t)$ (Heaviside function); (c) the elastic auxiliary problem with the relevant load $\hat{p}(t)$ (see Eq. (7.10)); (d) the adopted spatial finite element discretization with n^e two-node bar finite elements with linear shape functions.

$$F_{ce}^{SR}[\sigma_{ij}] = \frac{1}{2} \int_T \int_{\Omega} D_{ijk}^{-1} \hat{\sigma}_{ij} \hat{\sigma}_{hk} d\Omega dt \quad (6.12)$$

where $F_{ce}^S[\sigma_{ij}]$ is the complementary energy functional of the elastic problem under the given external actions \bar{F}_i, \bar{p}_i of the original nonlinear problem (2.1), $F_{ce}^R[\sigma_{ij}]$ is the work done by the unknown noncompatible strains $\theta_{ij}^o = \Phi_r(\sigma_{ij})$ for the stresses $(\sigma_{ij} - \sigma_{ij}^s)$ where σ_{ij}^s is the elastic solution of the problem under the external actions $\bar{F}_i, \bar{p}_i, \bar{u}_i$, and $F_{ce}^{SR}[\sigma_{ij}]$ is the elastic energy of the elastic auxiliary problem (5.4)–(5.5) under the external actions

$$R(w) = \theta_{ij}^o = \Phi_r(\sigma_{ij}). \quad (6.13)$$

Analogous relations hold for the extended Hu-Washizu and Hellinger-Reissner functionals, but are here omitted for brevity.

7 Illustrative Example

(a) Problem Description. As an illustrative example, the inelastic rod of Fig. 2 is considered with the aim of emphasizing the possibility of the method to be applied to general inelastic (provided that differentiable) constitutive laws such as the viscoelastic case and the possibility to allow for a temporal Ritz-type discretization for time-dependent problems (i.e., using shape functions defined over all the time interval T). In Fig. 2(a) the rod (clamped at its ends and with constant cross-section area A) has a linear elastic behavior with Young modulus E_0 in its first half-length $A-B$ while the constitutive law of the second half-length $B-C$ is linear viscoelastic of hereditary type as in Eq. (3.7):

$$\sigma(x; t) = H(0)\epsilon(x; t) + \int_0^t \frac{dH(t-\tau)}{d(t-\tau)} \epsilon(x; \tau) d\tau \quad (7.1)$$

where $H(0)$ represents the instantaneous elastic modulus, while $H(t-\tau)$ is the relaxation kernel here assumed according to the following three-parameter model (Kelvin-Voigt):

$$H(t-\tau) = E_{\infty} + (E_0 - E_{\infty}) \exp\left(-\frac{t-\tau}{T^*}\right) \quad (7.2)$$

where $E_0 \equiv H(0)$, E_{∞} is the asymptotic elastic modulus and T^* is the relaxation time (see, e.g., Christensen, 1982).

A constant distributed axial load $p(t)$ is applied at instant $t_0 = 0$ (Fig. 2(b)) when all stresses, strains, and displacements are assumed to be vanishing; besides $T/T^* = 50$ is assumed.

(b) Functional Construction. The extension of the total potential energy principle of Section 6.3 is used in the form (6.9)–(6.10), that is

$$F_{tpe} = F_{tpe}^S + F_{tpe}^R + F_{tpe}^{SR} \quad (7.3)$$

where, assuming as integrating operator \mathbf{K} the inverse of the elastic operator relevant to the elastic rod with Young modulus equal to E_0 over all the field $A-B-C$,

$$F_{tpe}^S[u] = \int_T \left\{ \frac{1}{2} \int_0^t E_0 A \left(\frac{\partial u(x; t)}{\partial x} \right)^2 dx - \int_0^t p(t) u(x; t) dx \right\} dt \quad (7.4)$$

$$F_{tpe}^R[u] = \int_T \int_{l/2} \left(\int_0^t \frac{dH(t-\tau)}{d(t-\tau)} \frac{\partial u(x; \tau)}{\partial x} d\tau \right) \times \left(\frac{\partial u(x; t)}{\partial x} - \frac{\partial u^s(x; t)}{\partial x} \right) A dx dt \quad (7.5)$$

$$F_{tpe}^{SR}[u] = \frac{1}{2} \int_T \int_0^t E_0 A \left(\frac{\partial \hat{u}(x; t)}{\partial x} \right)^2 dx dt \quad (7.6)$$

being $u = u(x; t)$ the unknown axial displacement function and $u^s(x; t)$ the elastic solution of the rod problem (with Young modulus E_0 over all the field $A-B-C$) under the axial load $p(t)$. It is worth noting that the above quoted (in F_{tpe}^{SR}) unknown function $\hat{u}(x; t)$ represents the solution of the following elastic auxiliary problem of the type (5.4)–(5.5) (see Fig. 2(c)) (here \hat{N} is the axial force):

$$\frac{\partial \hat{N}}{\partial x} = 0; \quad \hat{\epsilon} = \frac{\partial \hat{u}}{\partial x}; \quad \hat{N} = E_0 A \hat{\epsilon} - A \Psi_r(\epsilon) \quad (7.7)$$

where

$$\Psi_r(\epsilon) = \int_0^t \frac{dH(t-\tau)}{d(t-\tau)} \epsilon(x; \tau) d\tau. \quad (7.8)$$

The Eq. (7.7a) written in terms of the displacement $\hat{u}(x; t)$ becomes

$$\frac{\partial^2 \hat{u}}{\partial x^2} = -\frac{1}{E_0 A} \left[-A \frac{\partial}{\partial x} \left(\Psi_r \left(\frac{\partial \hat{u}}{\partial x} \right) \right) \right] \quad (7.9)$$

which gives the load $\hat{p}(t)$ of the auxiliary problem of Fig. 2(c) as the following:

$$\hat{p}(t) = -A \frac{\partial}{\partial x} \left(\Psi_r \left(\frac{\partial u}{\partial x} \right) \right). \quad (7.10)$$

In order to express, in the functional $F_{ipe}^{SR}[u]$, the displacement \hat{u} as a function of the unknown axial displacement u (of the original problem), the auxiliary elastic problem (Fig. 2(c)) has to be solved in closed form using the Green functions that are relevant to the elastic structural problem. In particular, for the elastic auxiliary rod of the example considered, the Green function giving the axial displacement at x due to a concentrated unit axial force at ξ , is

$$G(x, \xi) = \begin{cases} (l - \xi)x / (E_0 A l) & \text{for } x \leq \xi \\ \xi(l - x) / (E_0 A l) & \text{for } x \geq \xi \end{cases} \quad (7.11)$$

and then

$$\hat{u}(x; t) = \int_0^l G(x, \xi) \hat{p}(\xi) d\xi. \quad (7.12)$$

However, when the structural complexity of the elastic auxiliary problem does not allow to easily find the above Green functions, an alternative approach could be the use of the total potential energy principle, that is, the minimization of the functional

$$\begin{aligned} \bar{F}_{ipe}[\hat{u}] = & \frac{1}{2} \int_0^l E_0 A \left(\frac{\partial \hat{u}(x; t)}{\partial x} \right)^2 dx \\ & - \int_0^l \hat{u}(x; t) \hat{p}(x; t) dx \end{aligned} \quad (7.13)$$

after a space and time discretization of \hat{u} (that is equivalent to the stiffness matrix inversion of the discretized structure of the elastic auxiliary problem).

(c) Discretization and Problem Solution. Concerning the minimization of the extended total potential energy F_{ipe} of Eq. (7.3) relevant to the original problem, the rod is discretized with n^e two-node bar finite elements with linear shape functions $h_1^e = 1 - (x - a^e)/l^e$ and $h_2^e = (x - a^e)/l^e$ in the global coordinate x ($0 \leq x \leq l$), where a^e is the coordinate of the first node of element e (see Fig. 2(d)), being ns the total number of spatial degrees of freedom of the assemblage. Let $\bar{\mathbf{u}}^e(t) = [u_1^e(t), u_2^e(t)]$ be the vector of the nodal axial displacements of the element e and $\bar{\mathbf{h}}^e(x) = [h_1^e(x), h_2^e(x)]$ the vector of the two linear spatial shape functions, denoting, with $\bar{\mathbf{u}}(t) = [u_1(t), \dots, u_k(t), \dots, u_{ns}(t)]$ and \mathbf{A}^e the vector of the degrees-of-freedom of the assemblage and the element connectivity matrix, respectively, the following relations can be written:

$$u^e(x; t) = \bar{\mathbf{h}}^e(x) \mathbf{u}^e(t); \quad \mathbf{u}^e(t) = \mathbf{A}^e \mathbf{u}(t). \quad (7.14)$$

In the spirit of Ritz-type (i.e., over all field T) time discretization, each finite element degree-of-freedom $u_k(t)$, of the spatial discretization, can be written as a function of n temporal degrees-of-freedom, collected in the vector $\beta_k = [\beta_{k_1}, \dots, \beta_{k_{n_t}}]$, through n time shape functions, collected in the vector $\bar{\mathbf{m}}_k = [m_{k_1}(t), \dots, m_{k_{n_t}}(t)]$, that is

$$u_k(t) = \bar{\mathbf{m}}_k(t) \beta_k. \quad (7.15)$$

Therefore, after introducing a global unknown vector β , collecting the subvectors β_k , the vector $\mathbf{u}(t)$ can be written as follows:

$$\begin{aligned} \mathbf{u}(t) = \begin{bmatrix} u_1 \\ \vdots \\ u_{ns} \end{bmatrix} &= \begin{bmatrix} \bar{\mathbf{m}}_1 & & \\ & \ddots & \\ & & \bar{\mathbf{m}}_{ns} \end{bmatrix} \cdot \begin{bmatrix} \beta_1 \\ \vdots \\ \beta_{ns} \end{bmatrix} \\ &= \mathbf{M}(t) \beta. \end{aligned} \quad (7.16)$$

Then, the discretized functionals $F_{ipe}^S[\beta]$, $F_{ipe}^R[\beta]$ and $F_{ipe}^{SR}[\beta]$ of Eq. (7.3) assume the following forms:

$$\begin{aligned} F_{ipe}^S[\beta] = & \frac{1}{2} \hat{\beta} \left[\sum_e \int_T \int_{a^e}^{a^e+l^e} \bar{\mathbf{M}}(t) \bar{\mathbf{A}}^e \right. \\ & \times \frac{d\mathbf{h}^e(x)}{dx} E_0 A \frac{d\bar{\mathbf{h}}^e(x)}{dx} \mathbf{A}^e \mathbf{M}(t) dx dt \Big] \beta \\ & - \hat{\beta} \left[\sum_e \int_T \int_{a^e}^{a^e+l^e} p^e(x; t) \bar{\mathbf{M}}(t) \bar{\mathbf{A}}^e \mathbf{h}^e(x) dx dt \right] \end{aligned} \quad (7.17)$$

$$\begin{aligned} F_{ipe}^R[\beta] = & \hat{\beta} \left[\sum_e \int_T \int_{a^e}^{a^e+l^e} \bar{\mathbf{Q}}^e(t) \bar{\mathbf{A}}^e \right. \\ & \times \frac{d\mathbf{h}^e(x)}{dx} \frac{d\bar{\mathbf{h}}^e(x)}{dx} \mathbf{A}^e \mathbf{M}(t) A dx dt \Big] \beta \\ & - \hat{\beta} \left[\sum_e \int_T \int_{a^e}^{a^e+l^e} \bar{\mathbf{Q}}^e(t) \bar{\mathbf{A}}^e \right. \\ & \times \frac{d\mathbf{h}^e(x)}{dx} \frac{\partial u^e(x; t)}{\partial x} A dx dt \Big] \end{aligned} \quad (7.18)$$

$$\begin{aligned} F_{ipe}^{SR}[\beta] = & \frac{1}{2} \hat{\beta} \\ & \times \left[\int_T \int_0^l \left(\sum_e \int_{a^e}^{a^e+l^e} \frac{\partial^2 G(x, \xi)}{\partial x \partial \xi} \bar{\mathbf{Q}}^e(t) \bar{\mathbf{A}}^e \frac{d\mathbf{h}^e(\xi)}{d\xi} d\xi \right) \right. \\ & \times E_0 A \left(\sum_e \int_{a^e}^{a^e+l^e} \frac{d\bar{\mathbf{h}}^e(\xi)}{d\xi} \mathbf{A}^e \mathbf{Q}^e(t) \right. \\ & \times \left. \left. \frac{\partial^2 G(x, \xi)}{\partial x \partial \xi} d\xi \right) dx dt \right] \beta \end{aligned} \quad (7.19)$$

where

$$\mathbf{Q}^e(t) = \int_0^t \frac{dH^e(t - \tau)}{d(t - \tau)} \mathbf{M}(\tau) d\tau \quad (7.20)$$

with $H^e(t - \tau) \equiv H(t - \tau)$ of Eq. (7.2) for elements of the viscoelastic part $B-C$ of the rod and $H^e(t - \tau) \equiv 0$ for elements of the elastic part $A-B$ of the rod. It may be easily shown that the discretized form $F_{ipe}[\beta]$ of the functional $F_{ipe}[u]$ (Eq. (7.3)) can be written as follows:

$$F_{ipe}[\beta] = \frac{1}{2} \hat{\beta} \mathbf{L} \beta - \hat{\beta} \mathbf{b} \quad (7.21)$$

where \mathbf{L} is a symmetric definite positive matrix; this allows to find the unknown vector β through the solution of the system of linear equation

$$\mathbf{L} \beta = \mathbf{b}. \quad (7.22)$$

(d) Results. For the sake of simplicity, all the spatial degrees-of-freedom $u_k(t)$ are discretized with respect to the time using the same shape functions of exponential type, that is

$$\begin{aligned} \bar{\mathbf{m}}_1 = \dots = \bar{\mathbf{m}}_{ns} \\ = [1, \exp(-t/T^*), \exp(-2t/T^*), \dots]. \end{aligned} \quad (7.23)$$

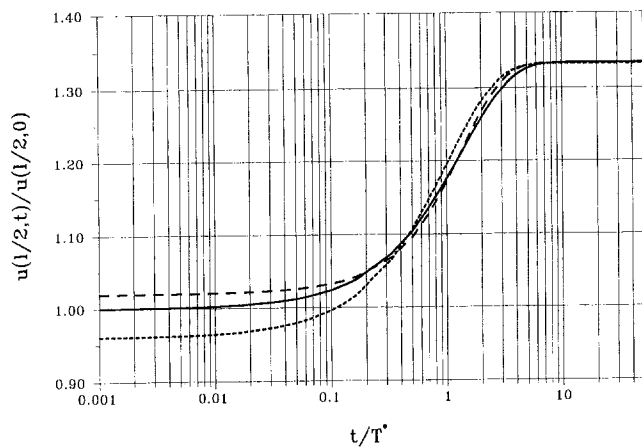


Fig. 3(a)

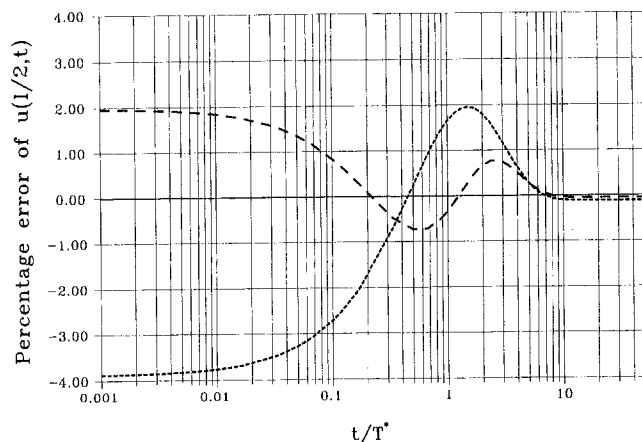


Fig. 3(b)

Fig. 3 Comparisons between the exact solution (solid line) of the problem of Fig. 2 and the numerical solutions for two (dotted line) or three (dashed line) degrees-of-freedom time discretizations. (a) Dimensionless axial displacement $u(l/2, t)$ of mid section B of the rod versus time t/T^* ; (b) percentage error of $u(l/2, t)$.

In Fig. 3 some of the numerical results obtained are compared with the exact solution with reference to a two or three-degree-of-freedom time discretization scheme, always assuming four two-node rod finite elements (two elements for both the elastic and viscoelastic part, respectively). The plots show a good approximation of the exact viscoelastic behavior of the rod, over all of interval T despite its wideness ($T/T^* = 50$) without the need, as in classical step-by-step methods, of its subdivision in many subintervals and without the need of the use of "difference-type" integration schemes.

8 Concluding Remarks

In this paper, for the inelastic continuum problem, four new principles are found despite the absence of a potential (which excludes the existence of variational formulations in the classical sense).

It is worth making the following remarks:

(a) Among the above principles only those with operator $\mathbf{K} \equiv \mathbf{S}^{-1}$ definite positive are minimum principles. This condition is fulfilled only by the two *one-field* operational formula-

tions (6.3)–(6.4) (extended total potential energy and extended complementary energy).

(b) As already said, the specialization of the constitutive law Eqs. (3.8)–(3.9) to the elastic case ($\Phi_e \equiv 0$ or $\Psi_e \equiv 0$) in the presence of time-independent external actions leads all the functionals to the classical ones of the theory of elasticity.

Analogously it may be shown that the specialization of Eqs. (3.8)–(3.9) to the incremental elastoplastic constitutive law leads, despite the absence of the differentiability of the constitutive law, to well-known classical and more recent variational formulations of the incremental elastoplastic problem. This has been shown for the total potential energy and complementary energy functionals by Carini (1996).

It is worth emphasizing that finding previous particular cases by the specialization of general formulations is not frequent when dealing with nonlinear variational formulations. On the contrary, this happens for the above-mentioned cases by virtue of the particular choice of the integrating operator adopted.

(c) The physical meaning of all the above-found extended functionals is always an energy as seen in Section 6. This energetic character of the functionals also depends on the choice made of Tonti's integrating operator \mathbf{K} which has always been chosen so that $\mathbf{K}\mathbf{N}(w)$ has the same dimension of w .

(d) When applied to time-dependent problems the above extended formulation allows for the use of the Ritz-type time discretization scheme (i.e., with shape functions defined over all time interval T), which leads to a good approximation of the exact solution as shown in the illustrative example of Section 7.

(e) A relatively straightforward generalization of the present study should be to materials whose elastic part of the constitutive law is nonlinear (hyperelastic material). Another possible generalization is to the case of large strains and displacements.

References

- Carini, A., 1996, "Colonnetti's minimum principle extension to generally non linear materials," *Int. J. Solids and Structures*, Vol. 33, pp. 121–144.
- Ceradini, G., 1966, "A maximum principle for the analysis of elastic-plastic systems," *Meccanica*, Vol. 1, pp. 77–82.
- Christensen, R. M., 1982, *Theory of viscoelasticity*, Academic Press.
- Colonnetti, G., 1918, "Sul problema delle coazioni elastiche," *Rend. Accad. Lincei*, Vol. 27, serie 5a, 2. sem.
- De Donato, O., and Franchi, A., 1973, "A modified gradient method for finite element elastoplastic analysis by quadratic programming," *Comp. Meth. Appl. Mech. Engrg.*, Vol. 2, pp. 107–131.
- Gurtin, M. E., 1964, "Variational principles in linear initial value problems," *Quar. App. Math.*, Vol. 12, pp. 252–256.
- Magri, F., 1974, "Variational formulation for every linear equation," *Int. J. Engng. Sci.*, Vol. 12, pp. 537–549.
- Maier, G., 1968, "A Quadratic programming approach for certain classes of nonlinear structural problems," *Meccanica*, Vol. 3, pp. 121–130.
- Maier, G., 1969, "Some theorems for plastic strains rates and plastic strains," *J. de Mécanique*, Vol. 8, pp. 5–19.
- Mura, T., 1987, *Micromechanics of defects in solids*, Martinus Nijhoff Publishers.
- Tonti, E., 1972, "A systematic approach to the search for variational principles," *Variational Methods in Engineering*, Department of Civil Engineering, University of Southampton, Proceedings of an Int. Conf. Southampton, U.K., Sept. 25.
- Tonti, E., 1973, "On the variational formulation for linear initial value problems," *Annali di Matematica Pura ed Applicata*, Serie quarta, Tomo XCV, pp. 331–359.
- Tonti, E., 1982, "A general solution of the inverse problem of calculus of Variations," *Hadronic J.*, Vol. 5, pp. 1404–1450.
- Tonti, E., 1984, "Variational formulation for every nonlinear problem," *Int. J. Engng. Sci.*, Vol. 22, No. 11–12, pp. 1343–1371.
- Yu, M., Moran, B., and Keer, L. M., 1992, "A Direct Analysis of Two-Dimensional Elastic-Plastic Rolling Contact," *ASME Journal of Tribology*, Vol. 115, pp. 227–236.
- Zarka, J., and Casier, J., 1979, "Elastic-plastic response of a structure to cyclic loading: Practical rules," *Mechanics Today*, S. Nemat-Nasser, ed., Vol. 6, pp. 93–198, Pergamon Press, New York.

Simulation of Rough, Elastic Contacts

J. J. Kalker

F. M. Dekking

E. A. H. Vollebregt

Delft University of Technology,
Faculty of Technical Mathematics
and Informatics, Mekelweg 4,
2628 CD Delft, The Netherlands

Frictionless rough contact problems have been studied in great detail by J. A. Greenwood and his co-workers. The only thing that actually seems missing is a simulated figure of the real contact between two rough bodies. Such a figure will be provided. Frictional rough elastic contact, on the other hand, seems to be terra incognita, and we intend to explore it. We will use two-dimensional rough bodies, because then we can simulate many asperities, and also because three-dimensional does not differ very much from two-dimensional in frictional contact, while finally the figures resulting from two-dimensional are clearer and more transparent as well as more realistic. On the other hand, two-dimensional calculations yield only qualitative results; for quantitative results one needs three-dimensional computations.

Introduction

In this paper we will wander through elastic half-space contact mechanics with rough surfaces. As usual, a distinction will be made between frictionless and frictional contact problems.

Frictionless rough elastic contact problems have been studied in great detail by J. A. Greenwood and his co-workers (see Johnson, 1985; Greenwood and Williamson, 1966; Greenwood, 1967). The only thing that actually seems missing is a simulated diagram of the real contact between two rough bodies.

Frictional rough elastic contact, on the other hand, seems to be terra incognita, and we intend to explore it qualitatively. We will use two-dimensional rough bodies, because then we can simulate many asperities, and also because three-dimensional does not differ very much from two-dimensional in frictional contact, while finally the figures resulting from two-dimensional are clearer and more transparent as well as more realistic.

All calculations were performed on a HP 9000-735, with the program CONTACT (Kalker, 1990) which was especially modified for problems of rough elastic bodies with and without friction.

Similar work has been performed by Carneiro Esteves e.a. (e.g., Carneiro et al., 1988). Carneiro concentrates on the description and filtering of the rough surface. In Kalker (1990) p. 201 is found a figure due to Carneiro dealing with the pressure distribution of frictionless, rough elastic cylinders.

1 Contact Problems Without and With Coulomb Friction

There are two basic problems in contact mechanics, viz.

- 1.1 Normal (frictionless) contact problems. In Kalker (1990) they are abbreviated by NORM.
- 1.2 Tangential (frictional) contact problems which in Kalker (1990) are abbreviated by TANG.

We will presently define these problems more precisely.

1.1 Normal Contact Problems. The potential contact area (A_c) is an arbitrarily given region of the contacting surfaces encompassing the actual contact.

Contributed by the Applied Mechanics Division of THE AMERICAN SOCIETY OF MECHANICAL ENGINEERS for publication in the ASME JOURNAL OF APPLIED MECHANICS.

Discussion on this paper should be addressed to the Technical Editor, Professor Lewis T. Wheeler, Department of Mechanical Engineering, University of Houston, Houston, TX 77204-4792, and will be accepted until four months after final publication of the paper itself in the ASME JOURNAL OF APPLIED MECHANICS.

Manuscript received by the ASME Applied Mechanics Division, June 15, 1995; final revision, Oct. 11, 1996. Associate Technical Editor: J. T. Jenkins.

THE PROBLEM READS:

GIVEN the tangential traction inside A_c , and the profile of the contacting bodies at A_c , while at every point of A_c frictionless contact conditions hold,

COMPLETED by classical well supported boundary conditions outside A_c

FIND the elastic field inside the bodies and on the surface. This problem is called NORM.

In this problem statement, two concepts are as yet undefined:

- Frictionless contact conditions state that outside the contact the surface traction vanishes, while inside the contact the normal traction component is compressive.
- Classical boundary conditions prescribe either the surface traction or the surface displacement, while well-supportedness means that the body as a whole, in its undeformed state, is kept rigidly into place.

The solution to this problem involves the computation of a variational inequality (in this case, a quadratic programming problem) (Fichera, 1964). From 1972 onwards there has been a spate of numerical solutions based on Fichera's variational inequality. CONTACT (see Kalker, 1990) solves the problem with a variant of an active set algorithm, which reads as follows:

NORM

- 1 Start with an estimate of the discretised contact area.
- 2 Compute the normal pressure.
- 3 Remove from the contact area all nodes with a non-compressive normal pressure.
- 4 If nodes have been removed by the last executed 3, go to 2, else go to 5.
- 5 Put all nodes at which penetration takes place into the contact area.
- 6 If nodes have been put into the contact area by the last executed 5, go to 2, or else READY.

1.2 Tangential Contact Problems. The tangential problem is incremental; a time step is discretized by Δt ; t and $(t - \Delta t)$ are important instants: viz. the present, and one step in the past.

A Cartesian coordinate system is introduced of which the origin lies in the centroid of the contact area (contact fixed coordinate system).

The bodies are numbered by i , with $i = 1, 2$ and $\mathbf{v}_i(t)$ is the velocity of the body in this coordinate system, at the origin.

Friction is according to Coulomb.

THE PROBLEM READS:

GIVEN the surface traction at A_c at time $(t - \Delta t)$, and the normal surface traction in A_c at the time t ;
the velocities $\mathbf{v}_i(t)$, $\mathbf{v}_i(t - \Delta t)$, $i = 1, 2$ are given;
Coulomb contact conditions with given traction bound prevail locally in A_c ;
the problem is completed by well-supported boundary conditions outside A_c ;
FIND the elastic field inside the bodies and on the surface.

This problem is called TANG.

One set of concepts have to be explained, viz. the Coulomb contact conditions:

- 1 A_c , outside the contact area, is free of traction;
- 2 inside the contact area, the tangential component of the traction is \mathbf{p}_t , with

$$|\mathbf{p}_t| \leq g \text{ where } g \text{ is the traction bound;}$$

- 3 the traction bound is a function of position. Usually it is related to the normal pressure p_n , by means of the coefficient of friction f , as follows:

$$g = fp_n.$$

The slip $\mathbf{s}(\mathbf{x})$ is defined as the velocity of the upper body 1 with respect to the lower body 2 at the point \mathbf{x} . We define the scalar function: $w(\mathbf{x})$ with the property that $|w(\mathbf{x})| = |\mathbf{s}(\mathbf{x})|$. The traction $\mathbf{p}(\mathbf{x})$ is the traction exerted on the upper body 1 at the point \mathbf{x} . $\mathbf{s}(\mathbf{x})$ should be opposite $\mathbf{p}_t(\mathbf{x})$, the tangential traction. Then we have

4

$w(\mathbf{x}) = 0$: no slip, i.e. area of adhesion

$w(\mathbf{x}) > 0$: slip has the correct sign. Area of slip.

$w(\mathbf{x}) < 0$: slip has the same sense as \mathbf{p}_t ; it is wrong.

The problem TANG was solved in a mathematical sense by Duvaut and Lions in 1972 (Duvaut and Lions, 1972). They proved a variational inequality-minimization problem for one incremental step of this problem.

From 1979 onwards several numerical methods were based on Duvaut and Lions, by means of which sophisticated incremental problems can be solved (complicated shift problems, impact, nonsteady-state and steady-state rolling).

The problem of Duvaut and Lions can be solved numerically by the following algorithm (CONTACT, originally from in 1982, and described in Kalker's book (Kalker, 1990, Ch. 4)). It is a variant of a so-called active set algorithm:

TANG

- 1 Given are the traction bound $g(\mathbf{x})$, the normal pressure in the contact area $p_n(\mathbf{x})$, as well as the contact area. These quantities do not change during the algorithm.
- 2 We start with complete adhesion $\mathbf{s}(\mathbf{x}) = 0$ ($w(\mathbf{x}) = 0$ in the entire contact area).
- 3 Compute the tangential traction, the slip, and the w -parameter from:

- In the adhesion area:

$$w(\mathbf{x}) = 0, \Rightarrow \mathbf{s}(\mathbf{x}) = 0$$

for the three unknowns w , and \mathbf{p}_t . Indeed, \mathbf{s} can be expressed in \mathbf{p}_t by an equation of the first degree.

- In the slip area: Solve the three nonlinear equations

$$|\mathbf{p}_t(\mathbf{x})| = g(\mathbf{x})$$

$$\mathbf{s}(\mathbf{x}) = -w(\mathbf{x})\mathbf{p}_t(\mathbf{x})/g(\mathbf{x})$$

for the unknowns $\mathbf{p}_t(\mathbf{x})$ and $w(\mathbf{x})$.

So we find \mathbf{p}_t and w in the entire contact area. Note that the contact area is found by the algorithm NORM.

In the slip area equations, the requirement " $w > 0$ " is hard to enforce. We drop it temporarily when we solve the slip area equations. It is taken care of in Step 5.

- 4 Move all \mathbf{x} with $|\mathbf{p}_t(\mathbf{x})| > g(\mathbf{x})$ from the adhesion area to the slip area. If there are such points, go to 3, or else go to 5.
- 5 Move all \mathbf{x} with $w(\mathbf{x}) < 0$ from the slip area to the adhesion area. If there are such points, go to 3, or else we are READY.

2 Discussion

The algorithm for NORM which was discussed above can solve all normal elastic contact problems. The algorithm TANG, however, does not seem to be completely reliable for the tangential contact problem for which it is intended, which is due to the difficulty of solving the nonlinear equations set up in its every Step 3. Also, the active set algorithm upon which our calculating schemes are built has been proved only for the transition of a SINGLE point from one region to the other, whereas we apply it using the transition of MANY points simultaneously.

There is another point to be mentioned in criticism of our algorithms. Intuitively one would suppose that a single application of NORM followed by a single application of TANG would solve an elastic contact problem. Such a process was indeed proposed and executed by Bentall and Johnson in 1967 (Bentall and Johnson, 1967). It is, however, an approximative process, as was pointed out by Panagiotopoulos in 1975 (Panagiotopoulos, 1975), who in the same paper proposed the process of alternately executing NORM and TANG, starting with NORM, until convergence hopefully occurs.

There is one set of circumstances in which the Panagiotopoulos process introduced above converges after one step and so reduces to the process of Bentall and Johnson (1967). It was discovered by de Pater in the late 1950s and described in his paper (Pater, 1962, p. 33). It is the case of material and geometric mirror-symmetry about the plane in which the contact area lies. Now, in the technical literature, the contacting bodies are often approximated by elastically symmetric half-spaces. The first to do so was Heinrich Hertz, the founder of modern contact mechanics (Hertz, 1882). This half-space hypothesis reads, in the case of elastic symmetry:

- For elastic calculations, the bodies are approximated by half-spaces; the boundary conditions are not changed.
- The elastic constants E_i , ν_i of both bodies are equal and constant.

Then it may be shown (de Pater did so) that NORM is independent of the tangential traction in A_c . TANG does depend on NORM, however, through the traction bound $g = fp_n$, and the solution of the complete contact problem may be found by executing NORM, followed by performing TANG. A notable application of elastically symmetric half-spaces is found in wheel-rail rolling contact theory.

We consider the convergence of CONTACT.

- (a) Elastic-Geometric Symmetry (three-dimensional).

We made a table of the total contact force for smooth wheel-rail theory as a function of the creep. The creep is defined in the first paragraphs of Section 5. This table contained 114,688 entries. CONTACT contains two methods of solution of TANG, a fast one due to Vollebregt (1995) and a slow one due to myself (Kalker, 1990). To calculate the table, we used Vollebregt's fast solver. NORM converged always. TANG failed four times. For those entries, we used the slow solver, which converged.

Concluding, we obtained the complete table, but not without complications. The failures occurred for slender contact areas.

(b) Elastic-Geometric Asymmetry (two-dimensional).

We made a program for two cylinders covered with smooth viscoelastic layers. The cylinders are pressed together, rolled over each other, and then for viscoelastic analysis, approximated by flat slabs. The cylinders have parallel axes, so that two-dimensional calculation by CONTACT is possible.

Many parameter combinations were tried. NORM converged always, and TANG and the Panagiotopoulos process diverged about once in 100,000 cases. When they diverged, it sufficed to perturb the discretization to obtain convergence.

Concluding, NORM converged always, and TANG and the Panagiotopoulos process also converged always, but not without complications.

CONTACT has been used to calculate contact problems with smooth surfaces. It may also be used to calculate contact problems covered by asperities by fully specifying the rough surface. Greenwood and his co-workers, see Greenwood and Williamson (1966), specify the rough surface by counting the asperities, measuring their height and curvature, and postulating their probability distribution function. It seems hard to generate a rough surface from these data, and indeed the question arises whether this is possible. At any rate, in the present paper we start from a given rough surface which is generated by a stochastic Fourier polynomial.

3 Model for a Rough Surface

It is remarkable that the standard work on rough surfaces (Thompson, 1982) does not contain a specification of a random process modeling a rough surface. In the more mathematical literature Gaussian and inverted chi squared processes are studied (Adler, 1981). We shall use a model which is a natural randomized version of the two-dimensional waviness described by Johnson Johnson, (1985, p. 402). We consider

$$z_{asp}(x, y) = \sum_{m=1}^M \sum_{n=1}^N a_{mn} \gamma^{m+n-2} \times \cos\left(\frac{2\pi mx}{l_x} + \varphi_{mn}\right) \cos\left(\frac{2\pi ny}{l_y} + \theta_{mn}\right)$$

on the rectangle $[0, l_x] \times [0, l_y]$.

The randomness resides in the triples $(a_{mn}, \varphi_{mn}, \theta_{mn})$ which for each frequency pair (m, n) give the amplitude a_{mn} which is uniformly distributed on $[0, A]$, and the phases φ_{mn} and θ_{mn} which are uniformly distributed on $[0, 2\pi]$. The three components of each triple are independent, and the triples are independent of each other. The parameter γ ($0 < \gamma \leq 1$) is a smoothing parameter which attenuates the higher frequencies.

The advantages of this random surface model are that it is flexible (choice of M , N , and γ), that it encompasses the single wavy surface ($M = N = 1$), that it is bounded (by MNA for all γ), and that it is easy to simulate. A disadvantage is that it seems very hard to obtain closed formulae for the center line average R_a and the height distribution or bearing area. However, we do have expressions for the root mean square roughness R_q and the surface autocovariance function $R(x, y)$.

Obviously the mean height $\int_0^{l_x} \int_0^{l_y} z(u, v) du dv$ equals 0.

Hence

$$R(x, y) = \lim_{L_1, L_2 \rightarrow \infty} \frac{1}{4L_1 L_2} \int_{-L_1}^{L_1} \int_{-L_2}^{L_2} z(u, v) z(u+x, v+y) du dv$$

$$= \frac{1}{l_x l_y} \int_0^{l_x} \int_0^{l_y} z(u, v) z(u+x, v+y) du dv$$

$$= \sum_{m=1}^M \sum_{n=1}^N \sum_{\tilde{m}=1}^M \sum_{\tilde{n}=1}^N a_{mn} a_{\tilde{m}\tilde{n}} \gamma^{m+n+\tilde{m}+\tilde{n}-4} \times Q_{m,\tilde{m},n,\tilde{n}}(x, l_x) Q'_{m,\tilde{m},n,\tilde{n}}(y, l_y)$$

where

$$Q_{m,\tilde{m},n,\tilde{n}}(x, l_x) = \frac{1}{l_x} \int_0^{l_x} \cos\left(\frac{2\pi mu}{l_x} + \varphi_{mn}\right) \times \cos\left(\frac{2\pi \tilde{m}(u+x)}{l_x} + \varphi_{\tilde{m}\tilde{n}}\right) du$$

and $Q'_{m,\tilde{m},n,\tilde{n}}(y, l_y)$ is similarly defined. Putting $t = u/l_x$ and $\alpha_{mn} = 2\pi \tilde{m}x/l_x$, we have

$$Q_{m,\tilde{m},n,\tilde{n}}(x, l_x) = \int_0^1 \cos(2\pi mt + \varphi_{mn}) \cos(2\pi \tilde{m}t + \alpha_{mn} + \varphi_{\tilde{m}\tilde{n}}) dt$$

$$= \frac{1}{2} \int_0^1 \{ \cos(2\pi(m + \tilde{m})t + \varphi_{mn} + \alpha_{mn} + \varphi_{\tilde{m}\tilde{n}}) + \cos(2\pi(m - \tilde{m})t + \varphi_{mn} - \alpha_{mn} - \varphi_{\tilde{m}\tilde{n}}) \} dt.$$

Since $m + \tilde{m} \geq 2$, the first part of the integrand always integrates to 0, and the second part too, unless $m = \tilde{m}$. We obtain that for all n, \tilde{n}

$$Q_{m,\tilde{m},n,\tilde{n}} = \begin{cases} 0 & m \neq \tilde{m} \\ \frac{1}{2} \cos(\varphi_{mn} - \alpha_{mn} - \varphi_{\tilde{m}\tilde{n}}) & m = \tilde{m} \end{cases}$$

We obtain a similar expression for $Q'_{m,\tilde{m},n,\tilde{n}}$, which is nonzero only if $n = \tilde{n}$. Hence the product of $Q_{m,\tilde{m},n,\tilde{n}}$ and $Q'_{m,\tilde{m},n,\tilde{n}}$ is nonzero only if both $\tilde{m} = m$ and $\tilde{n} = n$, and we obtain

$$R(x, y) = \frac{1}{4} \sum_{m=1}^M \sum_{n=1}^N a_{mn}^2 \gamma^{2m+2n-4} \cos\left(\frac{2\pi mx}{l_x}\right) \cos\left(\frac{2\pi ny}{l_y}\right).$$

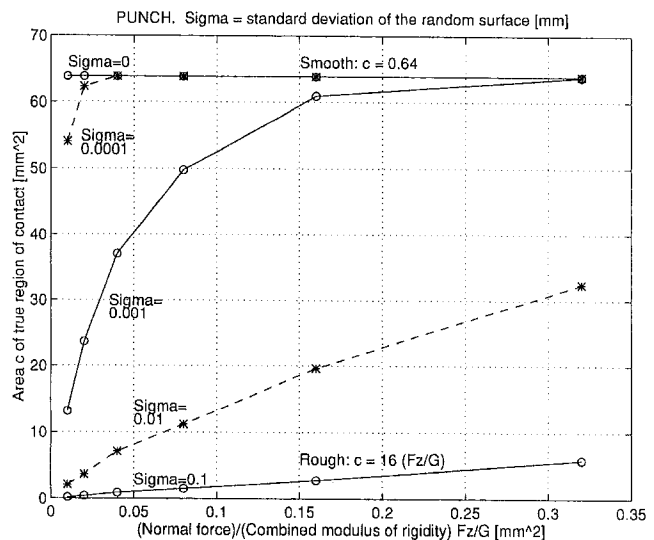


Fig. 1 $c-(F_z/G)$ diagrams of punch

Putting $x = y = 0$ we obtain the mean square roughness

$$R_q^2 = \frac{1}{4} \sum_{m=1}^M \sum_{n=1}^N a_{mn}^2 \gamma^{2m+2n-4}.$$

It is noteworthy that both $R(x, y)$ and R_q do not depend on the φ_{mn} and θ_{mn} .

4 Examples: Frictionless Contact Problems

We treat two frictionless contact problems as examples. They are three-dimensional.

Ex. 1 Frictionless Contact of a Smooth, Rigid Flat-Ended Circular Punch and a Rough, Elastic Half-Space. This is an example of the elastic contact of nominally flat rough surfaces; this problem is described and analyzed by Greenwood and Williamson (1966) and it is found in K. L. Johnson's book (Johnson, 1985, Sec. 13.4, p. 411 sqq).

Data:

Diameter circular punch	$D = 8.97 \text{ mm}$
Mean number of asperities	$\mu = 1/\text{mm}^2$
Decay factor	$\gamma = 0.8$
Circular punch	$G_1 = E_1 = \infty$
Poisson ratio of the half-space	$\nu_2 = 0.28 \text{ (steel)}$
E-modulus of the half-space	$E_2 = 1.02\text{e}5 \text{ N/mm}^2$
G-modulus of the half-space	$G_2 = E_2 / \{2(1 + \nu_2)\} = 40\,000 \text{ N/mm}^2$
Coefficient of friction	$f = 0$
Variance of rough surface	$\sigma^2 = R(0, 0) = R_q^2$
Standard deviation of rough surface	$\sigma = \sqrt{\sigma^2} = \sqrt{R_q^2}$

Ex. 2 Frictionless Contact of a Smooth Steel Sphere With a Rough, Steel Half-Space. The half-space assumption is adopted.

This is an example of the elastic contact of rough surfaces described and analyzed by Greenwood and Tripp (1967), which description may be found in Johnson's book (Johnson, 1985, Sec. 13.5, p. 416 sqq).

Data:

Diameter of sphere	$D = 1000 \text{ mm}$
Mean number asperities	$\mu = 1/\text{mm}^2$
Decay factor	$\gamma = 0.8$
Poisson ratio half-space and sphere, i.e. body i	$\nu_i = 0.28$
G-modulus half-space and sphere, i.e. body i	$G_i = 80,000 \text{ N/mm}^2$
Coefficient of friction	$f = 0$
Standard deviation of the surface	$\sigma = \sqrt{R_q}$

The results of the two examples are treated concurrently, so that a comparison is easily made.

Figures 1, 3, and 5 belong to the punch. Figures 2, 4, 6, and 7 belong to the sphere.

The approach of the middle surface (δ), the true area of contact (c), and the normal force divided by the combined modulus of rigidity (F_z/G) are plotted against each other, where the combined modulus of rigidity (G) is defined as:

$$\text{Combined modulus of rigidity: } G = 2G_1G_2/(G_1 + G_2)$$

In each plot of Figs. 1–6, five lines are shown (they may coincide); these lines correspond to the standard deviations σ of the surface. We have

$$\sigma = 0.1 \text{ (rough)}, 0.01, 0.001, 0.0001, 0 \text{ (perfectly smooth)}.$$

Let us first consider the area of the true contact c , plotted against F_z/G . Figure 1 relates to the punch, and Fig. 2 to the sphere. Concerning the sphere it is seen that three lines with $\sigma = 0, 0.0001, 0.001$ almost coincide. This indicates that these three σ 's correspond to an almost smooth surface. The common line has the equation

$$c = 135(F_z/G)^{2/3}.$$

Indeed, c is the area of the Hertzian contact region, which is proportional to b^2 where b is the radius of the contact region. F_z/G is proportional to b^3 , and this is in accordance with the above formula.

The lowest line, marked "rough" corresponds to $\sigma = 0.1$. We found:

$$c = 16(F_z/G)$$

that is, the area of the true region of contact is proportional to (F_z/G) .

The equations for $\sigma = 0$ and $\sigma = 0.1$ have a sound theoretical background. This is not so with the lines $\sigma = 0.01$, so that a curve fit of them would have no physical meaning.

The punch, Fig. 1, provides a different picture. Again $\sigma = 0.1$ yields the equation $c = 16(F_z/G)$, and it is remarkable that the factor 16 occurs in both formulae. We surmise that this factor is determined by the size of the potential contact area A_c , which is the same in both cases. Even more remarkable is the behaviour of the lines for $\sigma = 0, 0.0001, 0.001$. $\sigma = 0.001$ seems to be smooth-behaved only when $F_z/G > 0.32$, while $\sigma = 0.0001$ is smooth-behaved at $F_z/G > 0.04$. These boundaries are well defined, and differ approximately by a factor 10, as the corresponding σ 's do. We note, moreover, that the form of the curves for $\sigma = 0.0001, 0.001, 0.01$ are quite irregular, so that a curve fit would have no physical meaning.

We turn to Fig. 7, in which the true region of contact of the sphere is shown as a function of (F_z/G) . Here also it is quite clear that $\sigma = 0.001$ is nearly smooth, while $\sigma = 0.01$ appears to be rough, and $\sigma = 0.1$ very rough. We come back to Fig. 7 later on.

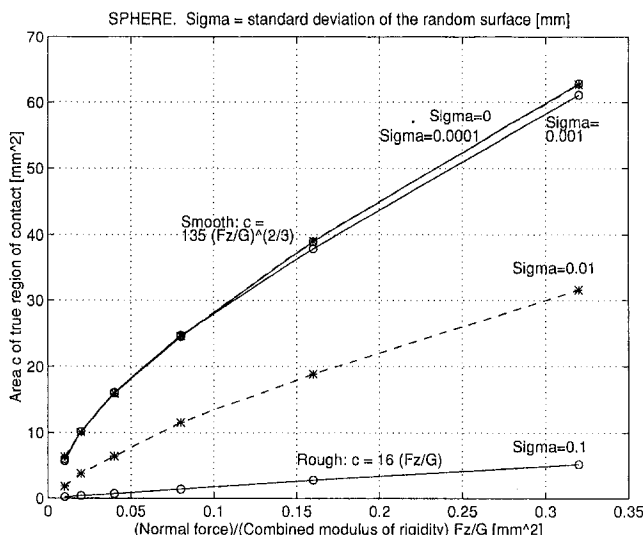


Fig. 2 $c-(F_z/G)$ diagrams of sphere

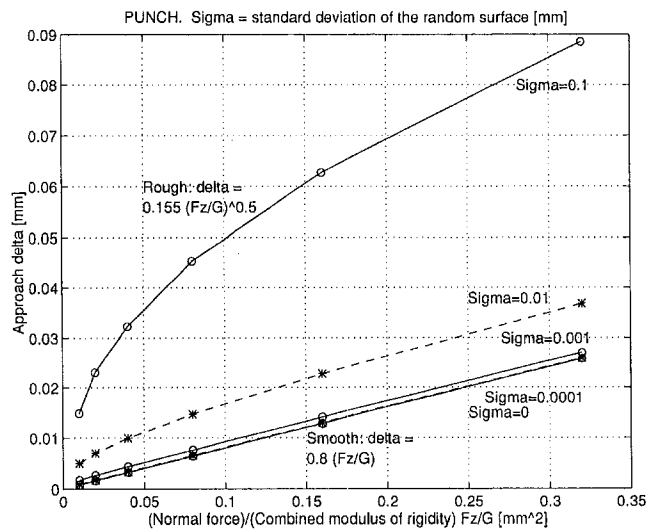


Fig. 3 δ -(F_z/G) diagrams of punch

In Figs. 3 and 4 the approach of the middle surfaces of the bodies σ are plotted against (F_z/G); Fig. 3 relates to the punch, Fig. 4 to the sphere. It is remarkable that the lines $\sigma = 0.1$ for sphere and punch almost coincide, and that the δ 's for $\sigma = 0.1$ are considerably larger than for $\sigma = 0$. Further, the δ 's for $\sigma = 0, 0.0001, 0.001$ are much closer for the sphere than for the punch; this behavior is similar to the c 's as a function of (F_z/G).

K. L. Johnson (Johnson, 1985) e.g., (13.54) has introduced the parameter $\alpha = \sigma/\delta_0$, where δ_0 is the approach of the smooth sphere. When $\alpha < 0.05$ the surface may be regarded as smooth.

The approach of the smooth sphere δ_0 is found from Fig. 4, $\sigma = 0$. It depends on (F_z/G). σ is likewise found from Fig. 4. Setting (F_z/G) = 0.32, we find $\delta_0 = 0.04$, and

$\sigma = 0$	$\Rightarrow \alpha = 0.0$	< 0.05 : ideally smooth surface
$\sigma = 0.0001$	$\Rightarrow \alpha = 0.00225$	< 0.05 : smooth surface
$\sigma = 0.001$	$\Rightarrow \alpha = 0.0225$	< 0.05 : smooth surface
$\sigma = 0.01$	$\Rightarrow \alpha = 0.25$	> 0.05 : rough surface
$\sigma = 0.1$	$\Rightarrow \alpha = 2.5$	> 0.05 : very rough surface

which is in accordance with what we found above. A similar theory for the punch does not seem to exist.

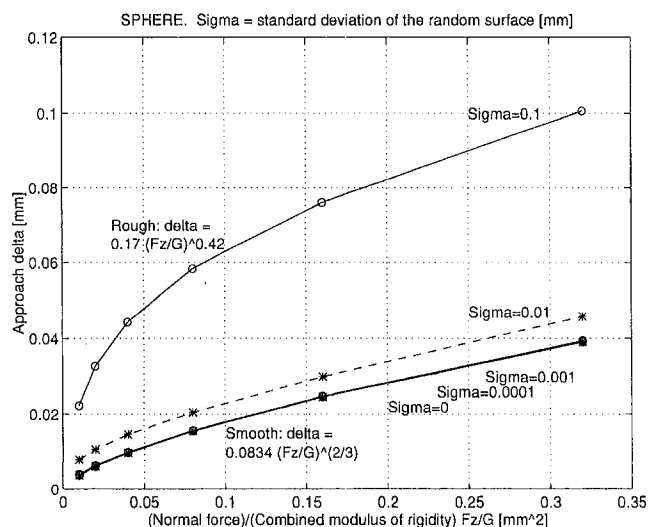


Fig. 4 δ -(F_z/G) diagrams of sphere

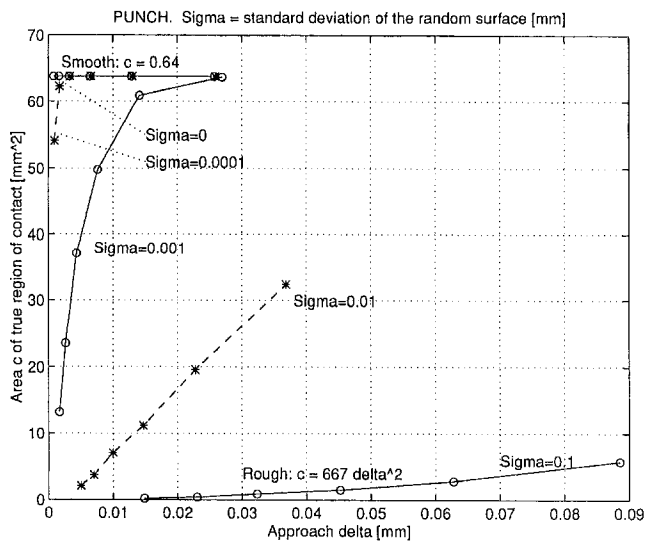


Fig. 5 c - δ diagrams of punch

We turn again to Fig. 7, in which the true region of contact is shown as a functional of the normal force parameter (F_z/G) and the standard deviation of the bodies σ . In particular we consider $\sigma^2 = 1e - 4$; this corresponds to $\sigma = 0.01$, while (F_z/G) runs from 0.16 mm² to 0.01 mm². The regions of contact have a definitely rough look.

It is interesting to compare this with Fig. 2, the c - (F_z/G) diagram of the sphere, where the curve for $\sigma = 0.01$ lies between the purely smooth curve $\sigma = 0$ and the very rough curve $\sigma = 0.1$. Also, the $\sigma = 0.01$ curve is not a straight line in the c - (F_z/G) diagram.

If we consider the $\sigma = 0.01$ line in the c - (F_z/G) diagram for the punch, however (Fig. 1), we see that it is an almost straight line for (F_z/G) > 0.04 . We conclude that the linear proportionality of c and (F_z/G) is strictly only verified for very rough surfaces, but for medium rough surfaces ($\sigma = 0.01$) only approximately. This holds both for punch and sphere.

Figures 5 and 6, which are in the c - δ diagrams for punch and sphere, do not add any new information. They have been added for completeness' sake.

5 Frictional Contact Problems in Rough Bodies

We had introduced a coordinate system with the origin in the centroid of contact (contact fixed coordinate system). v_i is

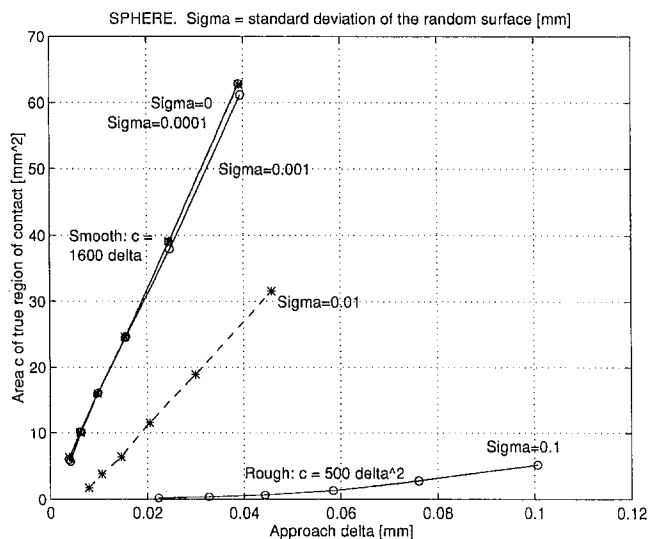


Fig. 6 c - δ diagrams of sphere

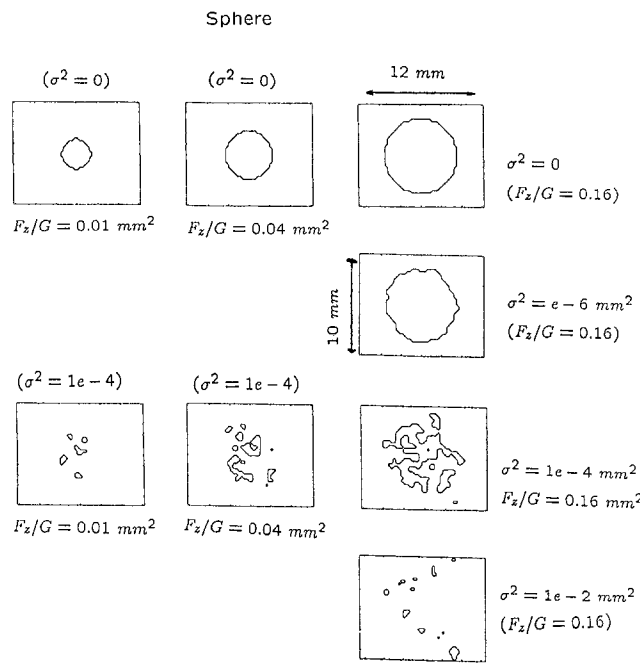


Fig. 7 True area of contact plotted against (F_z/G) and σ^2 (sphere)

the velocity of body i with respect to this coordinate system. The creep $\mathbf{k} = \mathbf{v}_1 - \mathbf{v}_2$ is the difference of the velocities, and $\mathbf{v} = -\frac{1}{2}(\mathbf{v}_1 + \mathbf{v}_2)$ is the rolling velocity, see Fig. 8(a).

- We speak of a shift when the rolling velocity vanishes: $\mathbf{v} = \mathbf{0}$, that is, when $\mathbf{v}_1 = -\mathbf{v}_2$, see Fig. 8(b).
- We speak of rolling when the rolling velocity does not vanish. Note that the creep can vanish (free rolling) ($\mathbf{k} = \mathbf{0}$), can be small ($|\mathbf{k}| \ll |\mathbf{v}|$), and can be large ($|\mathbf{k}|$ of order $|\mathbf{v}|$). Free rolling is often considered in the mechanics of undeformable bodies. Small creep is important in contact mechanics. It was shown by de Pater (Pater, 1962) that the traction distribution of rolling is determined by the so-called creepage $\epsilon \triangleq \mathbf{k}/|\mathbf{v}|$. Note that rolling with small creep is characterized by $|\epsilon| \ll 1$. When $|\epsilon|$ is small it may be shown that the contact area of smooth bodies is decomposed into a region where the slip of the bodies vanishes: The area of adhesion, while in the complementary region the slip is nonzero. One may say that rolling with small creepage is characterized by the presence of an area of adhesion, while rolling with large creepage is characterized by the absence of such an area. Rolling with large creep is referred to as "sliding." Slid-

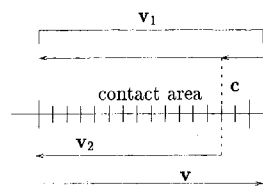


Fig. 8(a) Velocities \mathbf{v}_1 and \mathbf{v}_2 together with the creep \mathbf{k} and the rolling velocity \mathbf{v}

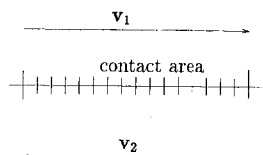


Fig. 8(b) The shift $\mathbf{v}_1 = -\mathbf{v}_2$ (rolling velocity $\mathbf{v} = \mathbf{0}$)

ing is also often considered in the mechanics of undeformable bodies. It is then also called "Rolling with Sliding."

5.1 An Example. Consider two sets of two cylinders with parallel axes, see Fig. 9(a).

All cylinders have the same radius R . The sets are called A and B . Set A is smooth, set B is rough. The cylinders of set A are brought into contact, as well as those of set B . A and B each form a two-dimensional system.

When $t < 0$ the cylinders are at rest. Then all cylinders are loaded with a constant moment about their axes, the two upper cylinders by M , the two lower cylinders by N , see Fig. 9(a). M and N are almost equal; they differ precisely so much that the cylinders start to roll. The total tangential force \mathbf{F} acting in the contact area is shown in Fig. 9(b), as well as the velocities \mathbf{v}_1 and \mathbf{v}_2 of the upper and the lower cylinders.

The traction distribution acting on the contact areas of set A and set B perform an evolution with the distance traversed as parameter, which is shown in Fig. 10; the smooth set A is shown left, the rough set B is shown right.

The contact area along the smooth cylinders a is six units wide. The distance traversed by the cylinders is, reading from top to bottom, 0, 1, 2, 3, 8 of the same units; the distance traversed between the upper four is easily read off from the motion of the highest asperity load of set B , see Fig. 10(b).

The Cattaneo traction distribution for smooth three dimensions (Cattaneo, 1938) constitutes the first tangential contact traction distribution in three dimension ever calculated (1938). Here, in Fig. 10(a), level 0 of the evolution we have the two-dimensional Cattaneo distribution for smooth cylinders. In Fig. 10(b) level 0 of the evolution we have the analogue for rough bodies. This state is reminiscent of the two-dimensional Cattaneo distribution.

The rough body distribution becomes maximal at the edge of the contact area. This effect, however, is diminished since the spacing of the loaded asperities increases towards the edges, so that effectively the traction diminishes near the edges of the contact regions. Also, the smooth traction distribution to the left has very steep flanges and high peaks near the edges of the contact area. This is typical of the no-slip Cattaneo solution. Next, the lower levels of the evolution are also very close to the no-slip solution smooth or rough. Finally, the asperity traction height is of a random nature, so that no fixed rule may be derived from a single instance of the value of the traction.

The three levels of the evolution below the Cattaneo traction distribution have traversed equal distances. The effect of the flow of the asperities from right to left is clearly seen. The highest peak moves from right to left; at the left edge, the asperities flow out of the contact area; new asperities move in at the right, and their loading increases initially from right to left.

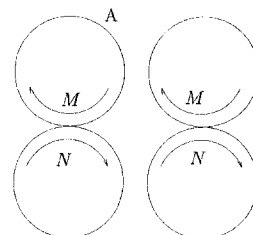


Fig. 9(a) Two sets of cylinders in contact, A and B ; equally loaded

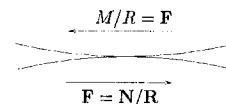


Fig. 9(b) Tangential forces acting near the contact area

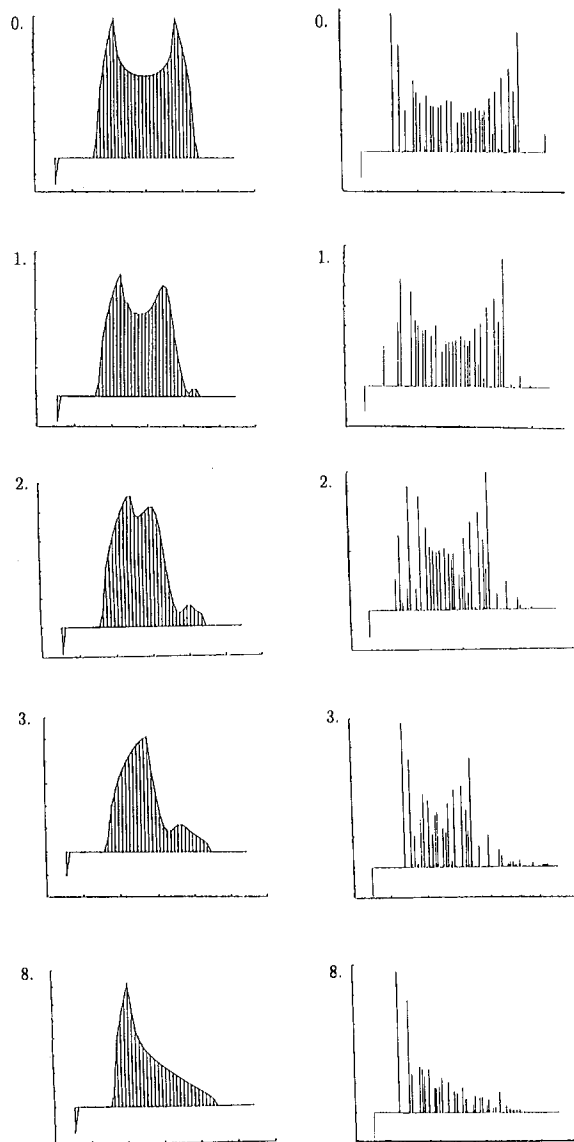


Fig. 10 Cylinder sets A (smooth) and B (rough, $\sigma = 0.1$) in transient rolling, from Cattaneo (level 0) to (approximately) steady-state (level 8)

The lowest level, at distance traversed = 8, represents an approximation of the limiting state of the evolution. For the smooth cylinders A this is the two-dimensional steady-state rolling situation. The smooth two-dimensional steady-state was first calculated analytically by F. C. Carter (Carter, 1926) in 1926.

The rough cylinders B do not reach a true limiting state; at the end of the evolution they perform a random walk about the stable equilibrium state. This equilibrium state is much like Carter's steady-state for smooth bodies, see Fig. 10(a), lowest level. The approximate limiting states of the evolutions of A and B are reached at the same distance traversed, viz. eight units, or, 1.33 contact widths traversed.

5.2 (Quasi-)Steady-State Rolling. The calculation of Fig. 10 consists of two parts, viz. the calculation of the initial state, followed by the calculation of the nonsteady-state tangential contact evolution. In Fig. 10, we use the Cattaneo distribution, smooth or rough, for the initial state.

If one is merely interested in (quasi-)steady-state rolling, it is better to start using the so-called direct method, which for smooth bodies gives the steady-state of rolling directly. This method also converges for rough bodies, but in order to obtain an acceptable steady-state it may be safe to perform a few steps

of the nonsteady-state tangential contact calculation. The results is a very fast algorithm, a direct generalization of the calculation of steady-state rolling for smooth bodies.

5.3 Miscellaneous Remarks on the Effect of Asperities in Technology.

Not long after the publication of Kalker in 1967, it was observed that the measured creep in the wheel-rail system was considerably smaller than that of Kalker (1967). It seemed that asperities were at the bottom of this, since, by them, the material near the surface would seem weakened. To verify this, it was of minor importance how the asperities were formed, as long as this weakening would seem to be present.

A sinusoidal, two-dimensional surface provided a good model. As a result, it was found, however, that the asperities had ABSOLUTELY NO effect on the creep. It turned later out that contamination was the cause of the effect.

Another technological problem involving asperities is rolling contact noise. D. J. Thompson (Thompson, 1993) investigated this phenomenon quantitatively. He confined himself to the normal effect of asperities, which, as is well known, have been investigated extensively by J. A. Greenwood and his co-workers.

Inertial effects are taken into account in the study of elastic waves and seismic effects. Elastic waves are studied in combating ground vibrations generated by road and rail traffic. Their frequency, however, is too small than that they can be caused by asperities.

Finally, asperities play a large, perhaps decisive, role in the study of friction and wear.

6 Conclusion

We have completed our hike through the field of elastic rough contacts.

As to frictionless contacts, we worked in three dimensions. We gave a number of pictures of the real area of contact, ranging from almost smooth to very rough. Also we gave a simulation of the connection between the real area and the approach on the one hand, and the roughness and the compressive force on the other hand.

As to frictional contact the *piece de resistance* is a well-documented simulation of nonsteady-state rolling. This was performed in two dimensions because more asperities could be considered, three-dimensional does not differ very much from two dimensions, and the resulting pictures are clearer.

References

- Adler, R. J., 1981, "Random field models in surface science," *Bull. Int. Statist. Inst.*, Vol. 49, pp. 669–681.
- Bentall, R. H., and Johnson, K. L., 1967, "Slip in the rolling contact of two dissimilar elastic rollers," *Int. Journal of Mechanical Sciences*, Vol. 9, pp. 389–404.
- Carter, F. C., 1926, "On the action of a locomotive driving wheel," *Proc. Roy. Soc. London*, Vol. A112, pp. 151–157.
- Pater, A. D. de, 1962, "On the reciprocal pressure between two bodies," *Proceedings Symposium Rolling Contact Phenomena*, J. B. Bidwell, ed., Elsevier, p. 33.
- Duvaut, G., and Lions, J.-L., 1972, *Les inéquations en mécanique et en physique*, Dunod, Paris.
- Carneiro Esteves, A., Seabra, J., and Berthe, D., 1988, "Roughness frequency analysis and particle depth," (Interface Dynamics) *Proceedings 14th Leeds-Lyon Symposium on Tribology*, D. Dowson, C. M. Taylor, M. Godet, and D. Berthe, eds., Elsevier.
- Fichera, G., 1964, "Problemi elastostatici con vincoli unilaterale: Il problema di Signorini con ambigue condizioni al contorno," *Mem. Accad. Nazionale dei Lincei Ser.*, Vol. 8, No. 7, pp. 91–140.
- Greenwood, J. A., and Tripp J. H., 1967, "The Elastic Contact of Rough Spheres," *ASME JOURNAL OF APPLIED MECHANICS*, Vol. 34, p. 153.
- Greenwood J. A., and Williamson, J. B. P., 1966, "Contact of nominally flat surfaces," *Proceedings Royal Society of London Vol. A295* p. 300.
- Hertz, H., 1882, "Über die Berührung fester elastischer Körper," *Journal reine und angewandte Mathematik (Crelle)*, Vol. 92, pp. 156–171.
- Johnson, K. L., 1985, *Contact Mechanics*, Cambridge University Press, Cambridge, UK.
- Kalker, J. J., 1990, *Three-dimensional Elastic Bodies in Rolling Contact*, Kluwer Academic Publishers, Dordrecht, The Netherlands.
- Panagiotopoulos, P. D., 1975, "A non-linear approach to the unilateral contact and friction boundary value problem in the theory of elasticity," *Ingenieur Archiv*, Vol. 44, pp. 421–432.

Thompson, T. R., ed., 1982, *Rough Surfaces*, Longman, London.

Kalker, J. J., 1967, "On rolling contact of two elastic bodies in the presence of dry friction," Ph.D. Thesis, Delft University of Technology, Delft, The Netherlands.

Cattaneo, C., 1938, "Sul contatto di due corpi elastici: distribuzione locale degli sforzi," *Accademia Nazionale Lincei, Rend. Ser. 6*, Vol. 27, pp. 342–348; 434–436; 474–478.

Thompson, D. J., 1993, "Wheel-rail noise generation," Parts I–V, *Journal of Sound and Vibration*, Vol. 161, pp. 387–481.

Vollebregt, E. A. H., 1995, "A Gauss-Seidel type solver for special convex programs, with application to frictional contact mechanics," *Journal of Optimization, Theory and Applications*, Vol. 87, pp. 47–67.

E. B. Crellin

F. Janssens

D. Poelaert

ESTEC Noordwijk.

W. Steiner

H. Troger¹

Technical University Vienna.

On Balance and Variational Formulations of the Equation of Motion of a Body Deploying Along a Cable

The equation of motion of a body moving along a vertically hanging cable by deploying the cable from the body or retrieving the cable in the body is derived. The derivation of the equation is given both by means of balance principles and a variational principle. Due to the fact that this system is not conservative the derivation by means of the variational principle requires the introduction of the Carnot energy loss concept. Its explanation is the main objective of this paper. The motion of the free falling folded string and a horizontally moving folded string modelling a whip are treated as examples.

1 Introduction

Tethered satellite systems (Beletsky and Levin, 1993; Proceedings, 1995), are systems of two or more satellites connected by one or several thin flexible cables moving on a space orbit. An important, but also delicate aspect of their dynamics occurs while the length of the deployed cable is changed. For this purpose equations of motion have been derived (Kohler et al., 1978; Beletsky and Levin, 1993) where, in the balance equations for the satellites, so-called rocket terms appear. They follow from the assumption that the changing mass distribution of parts of the system, due to deploying or retrieving the cable in the satellites, is essentially modeled by a continuous sequence of plastic impacts (Beletsky and Levin, 1993). However, a careful analysis (Crellin et al., 1995) of the equations given in Kohler et al. (1978) and Beletsky and Levin (1993) reveals that they are only valid if the motion of the cable at the satellites is a prescribed function of time. This, however, is a strong limitation of the applicability of these equations since, for example, the use of the equations of motion as derived in Kohler et al. (1978) and Beletsky and Levin (1993) is not possible for the free deployment of a subsatellite from a space shuttle due to the gravity gradient.

The purpose of this paper is to show that treating the mechanical model where the motion of the cable at the satellite is not prescribed but is itself an unknown, results in a number of fundamental problems, especially if a variational formulation of the equations of motion is used. Such a variational formulation is, first, convenient for a complicated satellite system, because it also supplies the boundary conditions for the cable, that is, the equations of motion of the satellites. Second, it is also necessary if one wants to have the equations of motion in weak form. The weak form of the equations is required in case a finite element discretization of the cable equations is needed for their numerical simulation (Steiner et al., 1995).

¹Address for correspondence: Institute of Mechanics, TU-WIEN, Wiedner Hauptstrasse 8-10/325, A-1040 Wien, Austria.

Contributed by the Applied Mechanics Division of THE AMERICAN SOCIETY OF MECHANICAL ENGINEERS for publication in the ASME JOURNAL OF APPLIED MECHANICS.

Discussion on the paper should be addressed to the Technical Editor, Professor Lewis T. Wheeler, Department of Mechanical Engineering, University of Houston, Houston, TX 77204-4792, and will be accepted until four months after final publication of the paper itself in the ASME JOURNAL OF APPLIED MECHANICS.

Manuscript received by the ASME Applied Mechanics Division, Aug. 22, 1995; final revision, July 19, 1996; Associate Technical Editor: S. W. Shaw.

In order to make the essential ideas of this paper as clear as possible we will treat a vertically hanging inextensible string with a body modeled as a point mass moving up and down under the action of a force N_0 acting between body and string by retrieving the string in the body or deploying it from the body. For the variational formulation of the equations of motion of such a system where the change of its mass distribution is modeled by plastic impacts, it is necessary to include the Carnot energy loss concept (Sommerfeld, 1943; Crellin et al., 1995). Its introduction and explanation will be one of the main points of this paper. As one illustrative example we apply the Carnot energy loss concept to derive the equations of motion of a falling folded string which is treated in Hamel (1949) and again in Steiner and Troger (1995) making use of balance principles. Finally we treat the horizontal motion of a folded string as a two-degree-of-freedom system. This last example has been used in the literature (Hamel, 1949; Rosenberg, 1991) to explain the crack of a whip.

2 Body Moving Along a Deploying or Retrieving Inextensible String

2.1 Derivation from Momentum Balance Equations.

We consider the vertical motion of a body with mass $m(t)$ hanging at the end of an *inextensible* string which remains always in the vertical position (Fig. 1). If, for example, the body is moving downward, a proper amount of string is deployed from the body. By the force N_0 acting between the body and the string, depending on its magnitude, either braked downward motion and deployment or upward motion and, hence, retrieval of the string in the body are possible. The force N_0 can be considered to model the force acting due to the storage or braking mechanism inside the body. We assume that the total length of the string is l . The mass $m(t)$ of the body, therefore, can be written

$$m(t) = m_0 + \mu(l - s_m(t)), \quad (1)$$

where m_0 is the constant mass of the body without the stored part of the string and μ is the mass per unit length of the string. By $s_m(t)$ we designate the position of the body (Fig. 1). Hence $l - s_m(t)$ is the length of string stored in the body.

The equation of motion of the body can be derived from the

linear momentum balance. Designating the linear momentum by $i(t)$ we have with $d/dt = (\quad)$

$$i(t) = (m_0 + \mu(l - s_m))\dot{s}_m, \\ i(t + dt) = (m_0 + \mu(l - s_m(t + dt)))\dot{s}_m(t + dt). \quad (2)$$

The momentum balance yields

$$i(t + dt) - i(t) = (mg - N)dt, \quad (3)$$

where N is the tension in the string at the location of the body. Expanding the expressions in (2), inserting into (3) and performing the limit $dt \rightarrow 0$ we obtain with (1)

$$m \frac{d\dot{s}_m}{dt} - \mu\dot{s}_m\dot{s}_m = mg - N, \quad (4)$$

or more generally

$$m \frac{d\dot{s}_m}{dt} = v_{rel} \frac{dm}{dt} - N + mg, \quad (5)$$

usually given in the literature. Here $v_{rel} = v_s - v_m = -\dot{s}_m$, where $v_s = 0$ is the absolute velocity of the string and $v_m = \dot{s}_m$ is the absolute velocity of the body. $\dot{m} = -\mu\dot{s}_m$ follows from (1). Now N_0 , the force transferred from the body to the string, must be related to the tension N in the string. To do this we have to distinguish the two different cases of downward and upward motion.

We consider first downward motion. For this purpose we write down the momentum balance of the differential string element just leaving the body. We obtain

$$i(t) = dm_s\dot{s}_m, \quad i(t + dt) = 0 \\ 0 - dm_s\dot{s}_m = (N_0 - N)dt$$

or

$$-\frac{dm_s}{dt}\dot{s}_m = N_0 - N. \quad (6)$$

The relation between dm_s and the change of the mass of the body follows from the principle of mass conservation

$$m(t) = m(t + dt) + dm_s,$$

from which follows with (1)

$$\frac{dm_s}{dt} = -\frac{dm}{dt} = \mu\dot{s}_m. \quad (7)$$

Inserting (7) into (6) results in

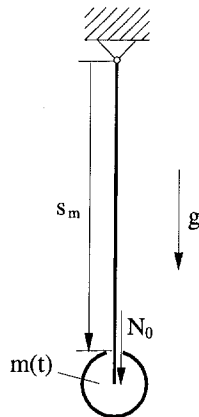


Fig. 1 Vertical motion of a body with mass $m(t)$ by deploying or retrieving a string depending on the size of the force N_0 , exerted from the body on the string

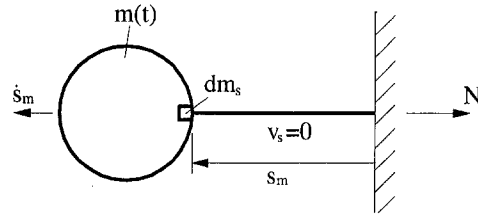


Fig. 2 In deployment the force N is necessary to pull the deploying string out of the body which moves with speed \dot{s}_m

$$N = N_0 - \dot{m}\dot{s}_m = N_0 + \mu\dot{s}_m^2. \quad (8)$$

We note from (8) that the string tension N must not only sustain the force N_0 but must also brake down the element dm_s from the speed of the body to zero speed. Inserting (8) into (4) we obtain for $\dot{s}_m(t) > 0$

$$m\dot{s}_m = -N_0 + mg. \quad (9)$$

If we prescribe $\dot{s}_m(t)$, then from (9) $N_0(t)$ can be calculated, since $m(t)$ is also known. If, on the other hand, $N_0(t)$ is prescribed, $\dot{s}_m(t)$ can be calculated using (1). If $N_0(t)$ is zero we have free deployment.

Now we consider upward motion. For this case $N = N_0$. The impact of the string element, entering the body, with the body is taken care of in the balance Eq. (4). Inserting $N = N_0$ into (4) the equation of motion

$$m(t)\dot{s}_m = \mu\dot{s}_m^2 - N_0 + mg \quad (10)$$

is obtained, which is valid if $\dot{s}_m(t) < 0$.

We note that there is an essential difference between the usual rocket problem and the cable problem considered here. In both problems a variable mass system is treated. However, in the rocket problem mass is ejected from the body whereas in the cable problem mass is pulled out of the body.

2.1.1 Discussion of the Different Values of N . We found that N is different for downward and upward motion. This has also been recognized in Crellin et al. (1995) for tethered satellite systems and in Steiner and Troger (1995) for the motion of a folded string.

The difference in N results in the two different sets of equations of motion (9) and (10) for downward and upward motion and can be best understood if one considers certain special motions. To make this important point of our investigation as clear as possible we, besides the vertical motion, consider also a horizontal motion of the body and the string, for which the difference in N is even better to understand.

1 The Free-Falling Body. In this case in (9) $N_0 = 0$ must be inserted. We see that N is not equal to zero but given by (8). This is the force necessary to reduce the speed of the element of the string, which is leaving the body, from the velocity of the body to velocity zero.

2 Upward Motion with Constant Speed. Then in (10) the left-hand side is zero and we see that N_0 not only has to sustain the weight but must also accelerate the element of the string entering the body to the speed of the body.

3 Horizontal Motion. A horizontal motion of the body without any action of N_0 is considered.

(a) Deployment. From Fig. 2 follows that for deployment a cable tension $N \neq 0$ is needed to pull the cable out of the body. With the momenta

$$i(t) = dm_s\dot{s}_m, \quad i(t + dt) = 0$$

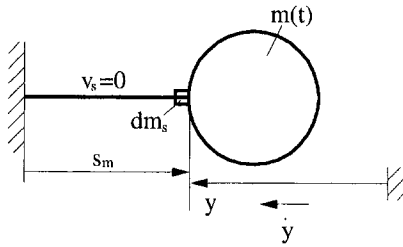


Fig. 3 In retrieval the tensionless string moves into the body which moves with velocity y

the linear momentum balance for the element dm_s is

$$0 - dm_s \dot{s}_m = -N dt.$$

Inserting $dm_s = \mu ds_m$ from (7) results in

$$N = \mu \dot{s}_m^2.$$

With $\dot{m} = -\mu \dot{s}_m$, following from (1), the equation of motion of the body (5) with $mg = 0$ and $v_{rel} = v_s - \dot{s}_m = -\dot{s}_m$ is

$$m(t) \ddot{s}_m = -\dot{s}_m (-\mu \dot{s}_m) - N = 0,$$

which shows that there is no rocket term in the body equation, such that the body performs an inertial motion.

(b) Retrieval. Since no tension is needed to retrieve the cable (the body moves into the cable (Fig. 3)) now $N = 0$. In order not to get confused with the signs of $s_m(t)$ we introduce for a moment an auxiliary variable $y(t) = l - s_m(t)$ (Fig. 3). Then also $m(t) = m_0 + \mu y(t)$ follows. The equation of motion (5) of the body now is

$$m \ddot{y} = v_{rel} \dot{m} = -\dot{y} \mu \dot{y} = -\mu \dot{y}^2. \quad (11)$$

Inserting into (11) $s_m(t)$ instead of $y(t)$ yields

$$m(t) \ddot{s}_m = \mu \dot{s}_m^2. \quad (12)$$

We see from (11) or (12) that given an initial velocity to the body, it will slow down while acquiring more mass from the cable.

2.2 Derivation From a Variational Principle. A straightforward variational formulation of the equations of motion immediately leads into problems because, for the considered motion, energy is not conserved. This follows from the fact that the velocity of the string at the body is discontinuous. For example, in the downward motion the speed of the string element leaving the body is instantly reduced to zero and hence its kinetic energy is annihilated without gaining another form of mechanical energy. This is also related to the fact that the rocket equation is based on a series of infinitesimal inelastic (plastic) impacts. In Sommerfeld (1943) (Exercise (Übungsaufgabe) 1.7) it is noted that for motions of this type

$$\frac{d}{dt} (T + V) \neq 0, \quad (13)$$

where T is the kinetic energy and V the potential energy. In Sommerfeld (1943), in order to have the equality sign in (13), the Carnot energy loss concept is introduced by adding a term $-\dot{W}$ to (13) by which the inelastic process can be included. Hence, instead of (13) one obtains

$$\frac{d}{dt} (T + V - W) = 0. \quad (14)$$

Similar consequences arise for the derivation of the equations of motion from a variational principle. We use the variational

principle of Hamilton Ostrogradskii (Lur'e, 1968) by means of which also nonconservative effects can be introduced

$$\delta' R = \delta S + \int_{t_0}^{t_1} \delta' W dt, \quad (15)$$

where the δ' indicates that there exists no quantity R the variation of which is δR . The action S in the time interval (t_0, t_1) in the sense of Hamilton is defined by

$$S = \int_{t_0}^{t_1} L dt \quad (16)$$

with

$$L = T - V \quad (17)$$

being Lagrange's function. Forces which cannot be derived from a potential are included in the second term in (15) by means of the virtual work principle.

For the moving body problem of Section 2 we write the variational principle adding a nonconservative Carnot force Q by means of the virtual work principle to obtain

$$\delta' R = \delta \int_{t_0}^{t_1} (T - V) dt + \int_{t_0}^{t_1} (Q - N_0) \delta s_m dt = 0 \quad (18)$$

where

$$T = \frac{1}{2} m \dot{s}_m^2, \quad V = -m g s_m - \frac{1}{2} \mu g s_m^2.$$

Inserting we obtain

$$\delta' R = \int_{t_0}^{t_1} (m \dot{s}_m \delta \dot{s}_m + \frac{1}{2} \delta m \dot{s}_m^2 + m g \delta s_m + \delta m g s_m + \mu g s_m \delta s_m + Q \delta s_m - N_0 \delta s_m) dt = 0.$$

The integration by parts yields with $\delta m = -\mu \delta s_m$

$$\delta' R = \int_{t_0}^{t_1} \left(-\frac{d}{dt} (m \dot{s}_m) + m g - \frac{1}{2} \mu \dot{s}_m^2 + Q - N_0 \right) \delta s_m dt + m \dot{s}_m \delta s_m \Big|_{t_0}^{t_1} = 0.$$

Since δs_m is arbitrary and vanishes at t_0 and t_1 , we may write the equation of motion

$$m \ddot{s}_m - \frac{1}{2} \mu \dot{s}_m^2 - m g = Q - N_0. \quad (19)$$

The same equation may be obtained directly from the Lagrangian (17), without performing any variation, but simply using the classical Lagrange equation for a discrete system

$$\frac{d}{dt} \left[\frac{\partial L}{\partial \dot{s}_m} \right] - \frac{\partial L}{\partial s_m} = Q - N_0. \quad (20)$$

The power developed by the nonconservative forces on coordinate s_m is by definition

$$\dot{H} = \dot{s}_m (Q - N_0) \quad (21)$$

if $H = T + V$ is the total energy of the system.

Using the results in Appendix A, with

$$|\dot{m}| = \mu |\dot{s}_m| \quad \text{and} \quad (v - u)^2 = \dot{s}_m^2$$

one obtains for the power developed by the Carnot losses and the applied force N_0 the expression

$$\dot{H} = -\frac{1}{2} \mu |\dot{s}_m| \dot{s}_m^2 - \dot{s}_m N_0. \quad (22)$$

Comparing the two expressions (21) and (22) for \dot{H} one deduces the generalised Carnot force

$$Q = -\frac{1}{2} \mu |\dot{s}_m| \dot{s}_m. \quad (23)$$

Hence we obtain by inserting (23) into (19) for the example of the falling body:

- for the downward motion ($\dot{s}_m > 0$):

$$m\dot{s}_m = -N_0 + mg$$

- for the upward motion ($\dot{s}_m < 0$):

$$m\dot{s}_m = \mu \dot{s}_m^2 - N_0 + mg.$$

These results confirm that our previous balance Eqs. (9) and (10) were properly written!

3 Example: Equation of Motion of the Falling Folded String

The equations of motion of the falling sharply folded inextensible string (Fig. 4) is treated in Hamel (1949) in Exercise (Aufgabe) 100. However, there it is treated as a conservative problem by means of the energy principle and the equation of motion derived must be questioned. An equation of motion under the assumption of plastic impacts at the fold is derived in Steiner and Troger (1995) by means of balance equations. Here we derive the equations of motion by means of (20). The system has one degree-of-freedom which we denote by y (Fig. 4). If the total length of the string is l then the relationship $2x = l + y$ holds. From the expression for the kinetic energy

$$T = \frac{1}{2} \mu (x - y)\dot{y}^2 = \frac{1}{4} \mu (l - y)\dot{y}^2$$

and the potential energy

$$V = -\frac{\mu g}{2} (4lx - l^2 - 2x^2) = -\frac{\mu g}{4} (l^2 + 2ly - y^2)$$

we obtain the Lagrangian

$$L = T - V = \frac{1}{4} \mu [(l - y)\dot{y}^2 + g(l^2 + 2ly - y^2)]. \quad (24)$$

The Carnot force Q follows from equating $\dot{H} = Q\dot{y}$ to

$$\dot{H} = -\frac{1}{2} |\dot{m}| (\Delta v)^2 = -\frac{1}{4} |\mu \dot{y}| \dot{y}^2 = -\frac{1}{4} \mu \dot{y}^2 \dot{y}, \quad (25)$$

given by (A.1), with $\dot{y} > 0$ for downward motion. Hence we have

$$Q = -\frac{1}{4} \mu \dot{y}^2. \quad (26)$$

In (25) \dot{m} has been calculated from $m = \frac{1}{2} \mu (l - y)$.

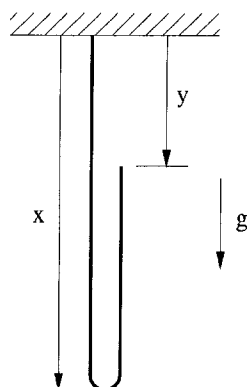


Fig. 4 Free-falling sharply folded inextensible string

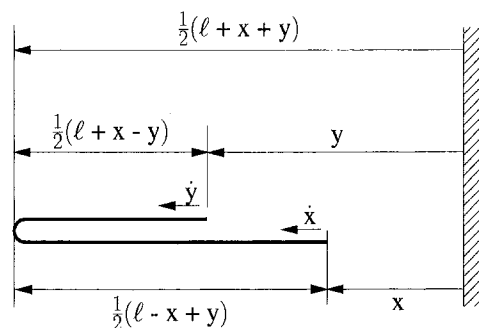


Fig. 5 Mechanical model of a whip with two degrees-of-freedom

Inserting (24) and (26) into (20) yields

$$\frac{d}{dt} \left(\frac{1}{2} \mu (l - y) \dot{y} \right) + \frac{1}{4} \mu \dot{y}^2 - \frac{1}{4} \mu g (2l - 2y) = -\frac{1}{4} \mu \dot{y}^2$$

or

$$\ddot{y} = g,$$

which has been also derived in Crellin et al. (1995) and Steiner and Troger (1995). This means that the falling part is really in free fall as is intuitively expected. When $y = l$, the velocity of the last point ($\sqrt{2gl}$) is finite and reduced instantaneously to zero.

4 Example: Equations of Motion of a Simple Model for a Whip

In Rosenberg (1991) equations of motion of a horizontally moving sharply folded string with two degrees-of-freedom are derived. They are considered as a model to explain the crack of a whip at the instant the folded string extends to its full length. The whipping effect is then explained by the infinite velocity of the last point. However, as it is shown in Steiner and Troger (1995), they contain again energy conservation as in Hamel (1949), since Lagrange's equations without the term Q introduced in (20) are used.

We consider now the motion of the folded string of Fig. 5 which has the two degrees-of-freedom $x(t)$ and $y(t)$ modeled as a nonconservative system as discussed above. The kinetic energy is

$$T = \frac{1}{4} \mu [(l - x + y)\dot{x}^2 + (l + x - y)\dot{y}^2].$$

In order to calculate the Q_i we have

$$|\dot{m}| = \frac{1}{2} \mu \left| \frac{d}{dt} (l - x + y) \right| = \frac{1}{2} \mu |\dot{x} - \dot{y}|$$

and

$$(v - u)^2 = (\dot{x} - \dot{y})^2.$$

Hence the Carnot dissipation (A.1) is given by

$$\dot{H} = -\frac{1}{2} |\dot{m}| (v - u)^2 = -\frac{1}{4} \mu |\dot{x} - \dot{y}| (\dot{x} - \dot{y})^2. \quad (27)$$

Setting

$$\dot{H} = Q_x \dot{x} + Q_y \dot{y}$$

we obtain from (27)

$$Q_x \dot{x} + Q_y \dot{y} = -\frac{1}{4} \mu |\dot{x} - \dot{y}| (\dot{x} - \dot{y}) \dot{x} + \frac{1}{4} \mu |\dot{x} - \dot{y}| (\dot{x} - \dot{y}) \dot{y}$$

or

$$Q_x = -\frac{\mu}{4}(\dot{x} - \dot{y})|\dot{x} - \dot{y}|$$

$$Q_y = -\frac{\mu}{4}(\dot{y} - \dot{x})|\dot{y} - \dot{x}|.$$

Obviously, this decomposition generates generalized forces Q_x , Q_y that preserve the symmetry in x and y . This procedure illustrates that for a multiple-degree-of-freedom system the two Carnot forces have to be identified from the single equation for the dissipated power. In this example, the symmetry in the problem leads to the correct split-up. In general one should choose the generalized coordinates such, that the Carnot dissipation (27) only depends on one of them. For example, using the coordinates

$$\xi_1 = \frac{1}{2}(l - x + y) \quad \text{and} \quad \xi_2 = \frac{1}{2}(l + x + y) \quad (28)$$

in (27) only one Carnot generalized force, in one variable ξ_1

$$Q_{\xi_1} = -2\mu|\dot{\xi}_1|\dot{\xi}_1$$

appears, whereas $Q_{\xi_2} = 0$. The physical interpretation of the coordinate transformation (28) is obvious from Fig. 5. If the linear change of velocities from $(\dot{\xi}_1, \dot{\xi}_2)$ to (\dot{x}, \dot{y}) is governed by, say, matrix \mathbf{A} then the change of generalized forces $(Q_{\xi_1}, 0)$ to (Q_x, Q_y) is governed by the transpose of the inverse of \mathbf{A} . A short derivation is given in Appendix B.

Inserting these results into (20) we obtain for $\dot{x} > \dot{y}$:

$$\begin{aligned} \frac{1}{2}\mu(l - x + y)\ddot{x} &= 0 \\ \frac{1}{2}\mu(l + x - y)\ddot{y} &= \frac{1}{2}\mu(\dot{x} - \dot{y})^2 \end{aligned} \quad (29)$$

and for $\dot{y} > \dot{x}$:

$$\begin{aligned} \frac{1}{2}\mu(l + x - y)\ddot{y} &= 0 \\ \frac{1}{2}\mu(l - x + y)\ddot{x} &= \frac{1}{2}\mu(\dot{x} - \dot{y})^2. \end{aligned} \quad (30)$$

The physical meaning of the system of Eqs. (29) and (30) is as follows: the faster moving part moves with its constant initial velocity, "looses" mass to the slower part and while doing so accelerates the slower part. The velocity v_c of the centre of mass of the system is set by the initial conditions, it remains constant during and after the unfolding motion as there are no external forces acting on the string. At the instant, the string extends fully, the velocity of the slower part has increased to the velocity of the center of mass. For instance, considering (30) with $x_0 = y_0 = 0$ and defining

$$\xi(t) = l + y(t) - x(t); \quad \xi_0 = l;$$

$$\dot{\xi}_0 = \dot{y}_0 - \dot{x}_0; \quad v_c = \frac{\dot{x}_0 + \dot{y}_0}{2}$$

one obtains a nonlinear differential equation $\xi\ddot{\xi} + \dot{\xi}^2 = 0$ which using the identity $\ddot{\xi} = \dot{\xi}(d\dot{\xi}/d\xi)$ (Rosenberg, 1991) can be integrated to yield

$$\begin{aligned} \xi^2(t) &= 2\xi_0\dot{\xi}_0 t + \xi_0^2 \\ y(t) &= y_0 t \\ x(t) &= l + y_0 t - \sqrt{2l\dot{\xi}_0 t + l^2}. \end{aligned}$$

When the string becomes stretched, $\xi = 2l$ and the corresponding time t^* is

$$t^* = \frac{3}{2} \frac{l}{y_0 - \dot{x}_0}.$$

The corresponding velocity of the string is

$$\dot{x}(t^*) = \dot{y}_0 - \dot{\xi}(t^*) = \dot{y}_0 - \frac{l\dot{\xi}_0}{\xi(t^*)} = v_c.$$

Hence, this model contains only finite discontinuities in velocity which go on as long as mass is exchanged between the folded parts. We further note that the tension in the whip remains bounded during deployment and suddenly drops at the end of deployment. It is not obvious that the sonic boom of a whip can be explained by this model as the discontinuity exists throughout the unfolding motion. Probably the model must be extended to a two-dimensional model including bending stiffness of the string, due to which an acceleration effect of the free part can be explained (Schagerl et al., 1997).

5 Conclusion

When a one-dimensional continuum moves with discontinuities in the velocity, the evolution of the discontinuity implies energy loss. The equations of motion must contain dissipative terms modeling this loss of energy. This problem was noticed when describing the dynamics of deploying/retrieving tether systems and is illustrated here on simple examples. The traditional explanation of the sonic boom generated by a whip given in the literature is questioned.

Acknowledgment

This research project has been supported by ESA under project DATES and the Austrian Science Foundation (FWF), under the project P10705-MAT. We also appreciate the comments of the referees which improved the clarity of the paper.

References

- Beletsky, V. V., and Levin, E. M., 1993, "Dynamics of Space Tether Systems," *Advances of the Astronautical Sciences*, Vol. 83, AAS Publications, San Diego, CA.
- Crellin, E. B., Janssens, F., and Poelaert D., 1995, "Deployment and Retraction of a Continuous Tether—The Equations Revisited," *Proceedings of the Fourth International Conference on Tethers in Space*, Science and Technology Corporation, Hampton, VA, pp. 1415–1423.
- Hamel, G., 1949, "Theoretische Mechanik," *Grundlehren der Mathematischen Wissenschaften*, Vol. 62, Springer-Verlag, Berlin, p. 643.
- Kohler, P., Maag, W., Wehrli, R., Weber, R., and Brauchli, H., 1978, "Dynamics of a System of two Satellites Connected by a Deployable and Extensible Tether of Finite Mass," ESTEC Contract No. 2992/76/NL/AK(SC).
- Lur'e, L., 1968, "Mécanique Analytique," Vols. 1 and 2, Masson & Cie, Paris.
- Proceedings of the Fourth International Conference on Tethers in Space*, 1995, Science and Technology Corporation, Hampton, VA.
- Rosenberg, R., 1991, "Analytical Dynamics of Discrete Systems," *Mathematical Concepts and Methods in Science and Engineering*, Vol. 4, third printing, Plenum Press, p. 322.
- Schagerl, M., Steindl, A., Steiner, W., and Troger, H., 1997, "On the paradoxon of the free falling folded chain," *Acta Mechanica*, in press.
- Steiner, W., Steindl, A., and Troger, H., 1995, "Dynamics of a Tethered Satellite System with Two Rigid Endbodies," *Proceedings of the Fourth International Conference on Tethers in Space*, Science and Technology Corporation, Hampton, VA, pp. 1367–1379.
- Steiner, W., and Troger, H., 1995, "On the equations of motion of a folded inextensible string," *Z. angew. Math. Phys.*, Vol. 46, pp. 960–970.
- Sommerfeld A., 1943, "Vorlesungen über Theoretische Physik," Vol. 1: Mechanik, Akademische Verlagsgesellschaft, Leipzig, p. 249.

APPENDIX A

Energy Loss for Inelastic Impact

We calculate the Carnot energy loss for the plastic impact of an infinitesimal mass $|dm|$ having velocity v against a body with finite mass M which is moving with velocity u . We assume that the impacting mass $|dm|$ is added to the body M at the location of the impact. The advantage of the introduction of the absolute value $|dm|$ is that one equation for the energy loss will be obtained which is valid both for retrieval and deployment.

The conservation of linear momentum yields

$$(M + |dm|)u' = Mu + |dm|v$$

where u' is the common velocity after the impact. Up to first order in $|dm|$, this law gives

$$u' = u + (v - u) \frac{|dm|}{M}.$$

The kinetic energy before impact is

$$T = \frac{1}{2} |dm| v^2 + \frac{1}{2} M u^2$$

and after impact, it becomes

$$T' = \frac{1}{2} (|dm| + M) u'^2$$

so that the kinetic energy loss up to first order in $|dm|$ is given by

$$dT = T' - T = -\frac{1}{2} |dm| (v - u)^2.$$

We may conclude that the instantaneous power dissipated in a succession of infinitesimal shocks is

$$\dot{T} = -\frac{1}{2} |\dot{m}| (v - u)^2 < 0.$$

We notice that the value of M plays no role in this power dissipation.

If external forces are present, they too contribute to the change in kinetic energy. When these forces derive from a potential V , we must write

$$\dot{T} = -\dot{V} - \frac{1}{2} |\dot{m}| (v - u)^2.$$

Hence, the total energy $H = T + V$ of the system is decreasing owing to Carnot dissipation

$$\dot{H} = -\frac{1}{2} |\dot{m}| (v - u)^2 < 0. \quad (\text{A.1})$$

APPENDIX B

Transformation of Carnot Forces

In coordinates $\mathbf{x}^T = (x_1, \dots, x_n)$ we designate the generalized Carnot forces $\mathbf{Q}_x^T = (Q_{x_1}, \dots, Q_{x_n})$ and in coordinates $\xi^T = (\xi_1, \dots, \xi_n)$, $\mathbf{Q}_\xi^T = (Q_{\xi_1}, \dots, Q_{\xi_n})$. Let the transformation between \mathbf{x} and ξ be given by

$$\mathbf{x} = \mathbf{A}\xi.$$

Expressing the Carnot dissipation \dot{H} by the generalized Carnot forces results in

$$\dot{H} = \mathbf{Q}_\xi^T \dot{\xi} = \mathbf{Q}_\xi^T \mathbf{A}^{-1} \dot{\mathbf{x}} = \mathbf{Q}_x^T \dot{\mathbf{x}}.$$

Hence we obtain

$$\mathbf{Q}_x^T = \mathbf{Q}_\xi^T \mathbf{A}^{-1}$$

or

$$\mathbf{Q}_x = (\mathbf{A}^{-1})^T \mathbf{Q}_\xi.$$

ERRATUM

The paper "Linear Complementary Formulations Involving Frictional Contact for Elasto-Plastic Deformable Bodies" by Maocheng Li, Desong Sha, and K. K. Tamma, which appeared in the March 1997 issue of the ASME *Journal of Applied Mechanics*, contained a typographical error. The last line in the Acknowledgment section (page 88) should have read "R. Namburu, and Jimmy Balsara" (not John Balsara).

M. Toya
Professor.

M. Aritomi
Associate Professor.

A. Chosa
Graduate Student.

Department of Mechanical Engineering,
Kagoshima University,
1-21-40, Korimoto, Kagoshima 890, Japan

Energy Release Rates for an Interface Crack Embedded in a Laminated Beam Subjected to Three-Point Bending

Asymmetric three-point bending of a layered beam with an interface crack is analyzed on the basis of the classical beam theory. Axial forces induced by bending in the parts of the beam above and below the delamination are determined by regarding the cracked part as two lapped beams hinged at both ends. The compliance and the energy release rate are then derived. Numerical analyses based on the finite element method are carried out, which show that delamination growth occurs in mixed mode, i.e., both the normal separation (mode I) and mutual sliding (mode II) of the crack surfaces contribute to the fracturing process. Finally the decomposition of the energy release rate into mode I and mode II components is made by combining the analysis of the energy release rates by Toya (1992) and the two-dimensional linear beam solutions by Suo and Hutchinson (1990).

1 Introduction

Delamination, or interface fracture, of a multilayered composite laminate is one of the major problems in the technology of structural composite materials and hence many literatures have been presented on the subject. In the theoretical investigation of the delamination of laminated beams, the classical Euler-Bernoulli theory (simple beam theory or strength of materials theory) has been found to be effective. For example, Kanninen (1973) derived the compliance of a double cantilever specimen based on the theory of beams on an elastic foundation. The energy release rate was then obtained by differentiating the compliance by crack length. Ashby et al. (1985) and Charalambides et al. (1989) analyzed a notched beam in which delamination spreads parallel to the beam axis from the notch root. The strength of materials approach has been also adopted for the end-notched laminated beams subjected to either three-point bending (Okusa, 1983a) or to uniform temperature change (Toya et al., 1992).

In practical application of layered plates or beams, delaminations are often observed to arise from, e.g., low-velocity normal impact and from manufacturing errors resulting in poor bonding. The situation where such a local delamination grows as a consequence of local buckling resulting from compressive loads parallel to layers has been considered by a number of investigators (e.g., Chai et al., 1981; Kachanov, 1988; Madenci and Westman, 1991). However, except the work of Maikuma et al. (1989), it seems little attention has been paid to the case where the embedded interface crack grows under bending moments.

In this paper we consider a model layered beam with an interface crack that is subjected to asymmetric three-point bending (cf. Fig. 1) on the basis of the classical beam theory. Axial forces are induced by bending in the parts of the beam over and

below the interface crack, the determination of which becomes a key to the solution of the problem. These axial forces are determined by regarding the delaminated beam as two lapped beams hinged at both ends. The compliance and the strain energy release rate are then derived (Section 2). Finite element computations are carried out to show the validity of the approach based on the simple beam theory (Section 3). The numerical analyses also reveal that delamination occurs in mixed mode, i.e., both the normal separation of the crack faces (mode I) and mutual sliding of the crack faces (mode II) contribute to fracturing process. In Section 4, the decomposition of the energy release rate into mode I and mode II components is made by combining the recent analyses by Toya (1992) concerning the components of the energy release rate of an interface crack and the analyses by Suo and Hutchinson (1990) for a split-beam element subjected to general loading conditions.

2 Theory

We consider a local delamination as shown in Fig. 1. The model beam is formed by bonding two isotropic and linearly elastic rectangular beams having the same length l and width b . Thicknesses and Young's moduli of the two layers are h_1 and E_1 for the upper strip and h_2 and E_2 for the lower strip, respectively. An interlaminar crack with length c is assumed to be embedded, the ends of the crack being distant a_L and a_R from the left and right-hand supports, respectively. A concentrated force P is applied at the distance d from the left support. The case when the point of load application lies on the cracked part (i.e., $a_L \leq d \leq l - a_R$) is considered first. As is shown in Fig. 1, the position of load application is distant c_L from the left-side edge of the crack and c_R from the right-hand edge ($c = c_L + c_R$). We imaginatively cut the beam at points B and D to isolate three elements AB , BD , and DF . We regard the cracked part BD as two lapped beams hinged at both ends (cf. Fig. 2). The action of the two hinges is to produce a compressive forces $-Z$ for the upper beam and extensional force Z for the lower beam, the magnitude of which is later determined from the compatibility condition for the longitudinal deformations of both beams.

Thus, by further imaginatively cutting the beam at the point of load application and by replacing the hinges with forces $\pm Z$, we have free-body diagrams for the upper and lower strips as

Contributed by the Applied Mechanics Division of THE AMERICAN SOCIETY OF MECHANICAL ENGINEERS for publication in the ASME JOURNAL OF APPLIED MECHANICS.

Discussion on the paper should be addressed to the Technical Editor, Professor Lewis T. Wheeler, Department of Mechanical Engineering, University of Houston, Houston, TX 77204-4792, and will be accepted until four months after final publication of the paper itself in the ASME JOURNAL OF APPLIED MECHANICS.

Manuscript received by the ASME Applied Mechanics Division, Oct. 18, 1995; final revision, May 24, 1996. Associate Technical Editor: S. W. Shaw.

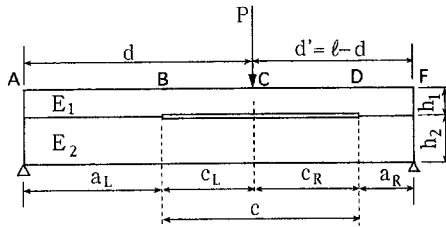


Fig. 1 Three-point bending of a laminated beam containing an interface crack

shown in Fig. 3, where the mutual beam reactions $q(x)$ is also taken into account. We assume that no frictional forces act on contact surfaces, so that $q(x)$ acts normal to the crack faces. In the figure, shearing forces αF_B and $\alpha' F_C$, bending moments M_{1B} and M_{1C} , and compressive forces Z are applied at the ends of the upper beam. Shearing forces βF_B and $\beta' F_C$, moments M_{2B} and M_{2C} , and extensional force Z likewise act for the lower beam. Here α , α' , β , and β' , are numerical constants which satisfy the condition $\alpha + \beta = 1$ and $\alpha' + \beta' = 1$. The conditions of equilibrium lead to following constraints:

$$\begin{aligned} F_B &= F_C = Pd'/l, \\ M_{1B} + M_{2B} &= Pd'a_L/l, \\ M_{1C} + M_{2C} &= Pdd'/l - Zh/2, \end{aligned} \quad (1)$$

where

$$d' = l - d, \quad h = h_1 + h_2. \quad (2)$$

The bending moments about the point x on the neutral axes of the upper and lower beams, M_{x1} and M_{x2} , are given as follows:

$$M_{x1} = M_1 + \alpha Pd'x/l + Zy + \int_0^x q(x')(x - x')dx', \quad (3)$$

$$M_{x2} = M_2 + \beta Pd'x/l - Zy - \int_0^x q(x')(x - x')dx', \quad (4)$$

where y is the deflection which is assumed to be identical for both beams, and

$$M_1 = M_{1B} - Zh_1/2, \quad M_2 = M_{2B} - Zh_2/2. \quad (5)$$

The equations of deflection are

$$D_1 d^2 y/dx^2 = -M_{x1}, \quad D_2 d^2 y/dx^2 = -M_{x2}, \quad (6)$$

with D_i ($i = 1, 2$) being flexural rigidity of the upper and lower beams, respectively, i.e., $D_i = E_i I_i$, $I_i = bh_i^3/12$, ($i = 1, 2$). Adding Eqs. (6)₁ and (6)₂, we have the deflection related to the point B ($x = 0$) as follows:

$$y_{BC} = s_1 x^3 + s_2 x^2 + s_3 x, \quad (7)$$

where

$$s_1 = -Pd'/(6Dl), \quad (8)$$

$$s_2 = -(Pa_L d'/l - \frac{1}{2}Zh)/(2D), \quad (9)$$

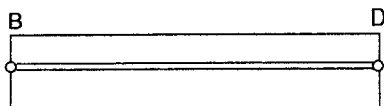


Fig. 2 Modeling by hinged lapped beams

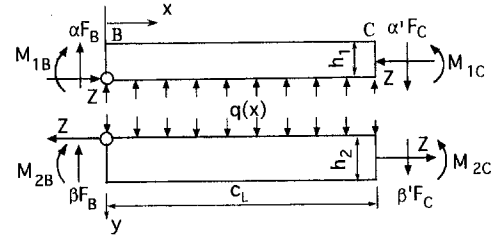


Fig. 3 Free-body diagram for the interval BC

with

$$D = D_1 + D_2. \quad (10)$$

The distribution of the reactive force is obtained as

$$q(x) = -Zd^2 y/dx^2 = -Z(6s_1 x + 2s_2). \quad (11)$$

Similarly, by taking the coordinate x' which is measured positive leftward with the origin at D, we have the deflection y_{CD} for the interval CD;

$$y_{CD} = s'_1 x'^3 + s'_2 x'^2 + s'_3 x', \quad (12)$$

where

$$s'_1 = -Pd/(6Dl), \quad (13)$$

$$s'_2 = -(Pa_R d/l - \frac{1}{2}Zh)/(2D). \quad (14)$$

For the bonded elements AB and DF, we have

$$y_{AB} = -Pd'x^3/(6D'l) + J_1 x, \quad (15)$$

$$y_{DF} = -Pdx'^3/(6D'l) + J'_1 x', \quad (16)$$

where D' is the flexural rigidity of the composite beam, the expression of which is given in Appendix A. The four unknown constants, s_3 , s'_3 , J_1 , and J'_1 are determined from the continuity conditions for the beam inclination and deflection at the points B, C, and D. They are given in Appendix B.

Finally, we determine the axial force Z from the condition that the length of the fiber along the upper surface of the crack should be equal to that along the lower surface. This condition leads to

$$\begin{aligned} \int_0^{c_L} \epsilon_1 dx + \int_0^{c_R} \epsilon'_1 dx' - \frac{Zc}{E_1 h_1 b} \\ = \int_0^{c_L} \epsilon_2 dx + \int_0^{c_R} \epsilon'_2 dx' + \frac{Zc}{E_2 h_2 b}, \end{aligned} \quad (17)$$

where, ϵ_1 and ϵ_2 denote the longitudinal strains of the upper and lower crack surface in the interval BC and ϵ'_i ($i = 1, 2$) denote those pertinent to the interval CD;

$$\epsilon_i = \frac{1}{2}(-1)^i h_i \frac{d^2 y_{BC}}{dx^2}, \quad \epsilon'_i = \frac{1}{2}(-1)^i h_i \frac{d^2 y_{CD}}{dx'^2} \quad (i = 1, 2). \quad (18)$$

Substitution of (18) into (17) leads to

$$\frac{Z}{P} = \frac{hfD_0}{c(4D + h^2 D_0)}, \quad (19)$$

where,

$$f = [d'(2a_L + c_L)c_L + d(c_R + 2a_R)c_R]/l, \quad (20)$$

$$D_0 = b/[(E_1 h_1)^{-1} + (E_2 h_2)^{-1}]. \quad (21)$$

By using the relation that can be readily verified,

$$D' = D + h^2 D_0 / 4, \quad (22)$$

Eq. (19) may be rewritten as

$$Z/P = f(1 - D/D')/(hc). \quad (23)$$

The deflection δ at the point of load application is given by

$$\delta = y_{AB}|_{x=a_L} + y_{BC}|_{x=c_L} = P\Phi, \quad (24)$$

where

$$\Phi = -\frac{1}{3l^2} \left(\frac{1}{D} - \frac{1}{D'} \right) [d^2(d' - c_R)^3 + d'^2(d - c_L)^3] - \frac{1}{4c} \left(\frac{1}{D} - \frac{1}{D'} \right) f^2 + \frac{d^2 d'^2}{3lD} \quad (25)$$

is the compliance of the cracked specimen.

Since the development of delamination is nothing more than the growth of the interface crack, the energy release rate becomes the most important parameter. For crack extension under constant force condition, the energy release rate at the left-hand crack-tip is given by

$$G_{a_L} = \frac{P^2}{2b} \frac{d\Phi}{dc_L} = \frac{P^2 c^2}{8b} \left(\frac{1}{D} - \frac{1}{D'} \right) \left[\frac{d'}{l} - \left(\frac{c_R}{c} \right)^2 \right]^2, \quad (26)$$

whereas the energy release rate at the right-hand crack-tip becomes

$$G_{a_R} = \frac{P^2 c^2}{8b} \left(\frac{1}{D} - \frac{1}{D'} \right) \left[\left(\frac{c_L}{c} \right)^2 - \frac{d}{l} \right]^2. \quad (27)$$

For example, if $c_L/c_R > d/d'$, then G_{a_L} is greater than G_{a_R} and crack extension at the left-hand tip occurs while the right-hand crack-tip remains stationary.

In the case where the point of load application lies outside of the cracked part of the beam ($d \leq a_L$), we have in a similar way as the foregoing analyses the axial force, the compliance and the energy release rates as follows:

$$\frac{Z}{P} = \frac{d}{hl} \left(1 - \frac{D}{D'} \right) (c + 2a_R) \quad (28)$$

$$\Phi = \frac{d^2 c^3}{12l^2} \left(\frac{1}{D} - \frac{1}{D'} \right) + \frac{d^2 d'^2}{3D'l}, \quad (29)$$

$$G_{a_L} = G_{a_R} = \frac{P^2 d^2 c^2}{8bl^2} \left(\frac{1}{D} - \frac{1}{D'} \right). \quad (30)$$

We see that when the point of load application is outside of the cracked part, both the compliance and the energy release rates are dependent only on the crack length but independent on the location (a_L or a_R) of the crack. It is expected that if the onset of delamination is stated as $G = G_c$ with G_c being a material constant, then unstable crack extension occurs simultaneously at both ends of the crack.

Maikuma et al. (1989) considered the simplest case where $d = d' = l/2$, $c_R = c_L = c/2$, $h_1 = h_2 = h/2$, $E_1 = E_2$. It is readily checked that in this case Eqs. (25) and (26) reduce to their solutions.

In passing, we note the statement by Suo and Hutchinson (1990) that the energy release rate for an interface crack subjected to pure bending moment (four-point bending) is identically zero. Their conclusion is also confirmed by our present method. We can readily check that the compliance of the beam

containing an interface crack coincides with that of an uncracked beam irrespective of the length of the crack. Hence, we are also led to the conclusion that the energy release rate is zero for four-point bending.

From (11), the beam reaction in the interval BC becomes

$$q(x) = (Z/D)[Pd'(x + a_L)/l - Zh/2], \quad (31)$$

for the case where the load point lies on the cracked part of the specimen. Hence, if

$$a' \equiv (Zh/l)/(2Pd') - a_L \quad (32)$$

is positive, then $q(x)$ takes negative values in the interval $0 \leq x \leq a'$. This means our solution is not consistent with the basic assumption that crack surfaces come into contact with one another everywhere and hence $q(x)$ should be positive. For example, for the case of $d = d' = l/2$, $c_R = c_L = c/2$, $h_1 = h_2 = h/2$, $E_1 = E_2$, we have

$$Z/P = 3(2l - c)/(16h), \quad a' = 5c/16 - l/8. \quad (33)$$

In this case $q(x)$ becomes negative near the crack-tip if c is larger than $2l/5$. However, as will be seen in the next section, in spite of this inconsistency in the sign of $q(x)$, the axial force, the compliance and the energy release rates predicted from the foregoing analyses agree well with the numerical results based on finite element method. In other words, the inaccuracy of $q(x)$ does not gravely affect the other physical quantities of interest.

It is also noted that the negative $q(x)$ implies the normal separation of the crack faces. Hence we expect that the delamination process generally occurs in mixed modes, in which both the normal separation (mode I) and mutual sliding of the two faces of the crack (mode II) contribute to the fracture of interface. In this case we can no longer regard G_{a_L} or G_{a_R} as pure mode II energy release rates. The decomposition of these total energy release rates into mode I and mode II components will be discussed in Section 4.

3 Analyses by Finite Element Method (FEM)

In this section we compare the theoretical results with those from FEM. The FEM program developed by Okusa (1983b) is utilized, by which mutual contact of crack faces may be readily analyzed. In this program, a rectangular four-nodes element, displacement function of which contains a term xy (x and y are coordinates parallel to sides of the rectangle), is used.

Materials chosen are acrylic resin with Young's modulus of $E_1 = 2.94$ GPa and Poisson's ratio of $\nu_1 = 0.345$ for the upper beam and aluminum with $E_2 = 73.5$ GPa and $\nu_2 = 0.35$ for the lower beam. We fix the beam dimensions as $l = 300$ mm, $b = 30$ mm, and $a_R = 50$ mm, and calculate the axial forces, the compliance, and the energy release rates as functions of the crack length c for several combinations of the thicknesses h_1 and h_2 . These thicknesses are chosen between 1 mm, 5 mm, and 10 mm. The unit load $P = 1$ N is applied at the center of the beam. Calculations are performed under plane stress condition.

After checking the accuracy by applying to a homogeneous uncracked slender beam we adopted discretization by five rectangular elements in the y -direction and 150 elements in the x -direction as a basic mesh division for each layer of the model composite beam. Mesh sizes are made smaller towards the crack tips, and the mesh with $\frac{1}{16}$ size of the basic rectangle is used in the small regions surrounding crack-tips. A schematic diagram of the finite element discretization is shown in Fig. 4.

Calculations are first made by assuming the mutual contact of the upper and lower crack surfaces. If tensile nodal forces are detected for nodes on the crack faces, the condition of contact is relaxed at these nodes at the second calculation. This procedure is repeated until no tensile nodal forces are detected at all nodes on the crack faces. We found that in many cases

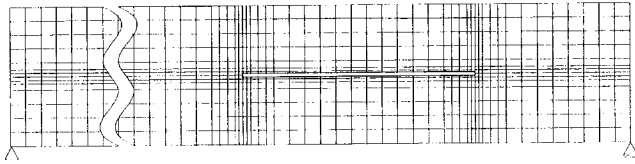


Fig. 4 Schematic diagram of the mesh division

normal separation of the crack faces occurred near the crack-tips, and hence the delamination occurred in mixed modes.

To obtain the components G_I and G_{II} of the total energy release rates, the finite element crack closure simulation (Rybicki and Kanninen, 1977) is performed. In this method, the nodal forces required to close the virtual crack extension, Δa , which is taken as the width of the element adjacent to the crack-tip, are computed using the local compliance method (cf. Armanios et al., 1986). Both components of the energy release rate are then given by

$$G_I = \frac{1}{2} \frac{Y \Delta v}{\Delta a}, \quad G_{II} = \frac{1}{2} \frac{X \Delta u}{\Delta a}, \quad (34)$$

where Y and X are the normal and tangential nodal forces required to hold two nodes together at the crack-tip, and the quantities Δv and Δu are the normal and tangential relative nodal displacements, respectively. The total energy release rate is given by the sum of both components.

The theoretical curves and numerical results for the axial force Z and the compliance Φ are shown in Figs. 5–6. These graphs show good agreement between the theory and numerical results, confirming the accuracy of the analyses based on the classical beam theory.

The energy release rates and their mode I and II components at the left and right-hand tip are shown in Figs. 7 and 8, respectively. (In Fig. 7(a), only the total energy release rate is shown; in this case there is no G_I component due to the perfect contact of the crack faces near the tip and hence G equals to G_{II} .) Again, we observe good agreement between the theory and numerical results. Equation (26) predicts that the energy release rate becomes zero when $c_R/c = (d'/l)^{1/2}$, ($c/l = 0.467$ in the present case). This prediction is well confirmed in Figs. 7(a)–(c). It is also noted that at these points the mode of crack growth changes from pure mode II to mixed mode type. We also see from Fig. 8(a) that G_I is negligibly small in comparison with G_{II} . Thus, it is concluded that for a relatively thick upper layer, the mode of delamination will occur in predominantly mode II for both crack tips.

4 Mode Partitioning of the Energy Release Rate

For the study of the criterion of the mixed mode fracture, it is desirable to separate the energy release rate into mode I and

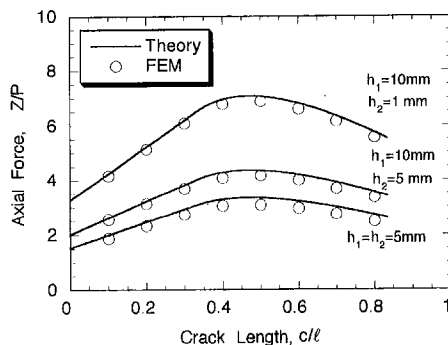


Fig. 5 Variation of axial force with crack length

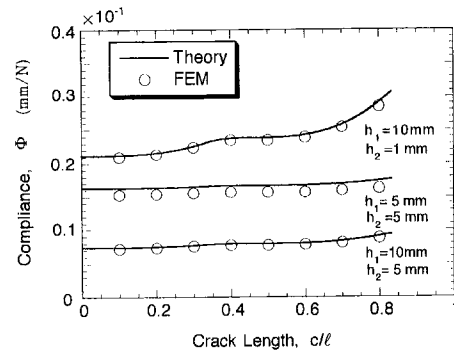


Fig. 6 Variation of compliance with crack length

mode II components. But with the previous analyses based on the compliance method we are unable to partition the energy release rate. It is clear that considerations based on the analyses of the near-crack-tip singular fields are needed to obtain each component.

By the aid of the complex factor in the notation by Suo and Hutchinson (1990), which is similar to the stress intensity factor introduced by Malyshev and Salganik (1965), singular stresses on the bond-line may be given as

$$\sigma_y + i\tau_{xy} = K(r/h_1)^{1/2}(2\pi r)^{1/2}, \quad (35)$$

where $K = K_I + iK_{II}$ (henceforth referred to as complex stress intensity factor) and r is the distance from the crack-tip. The height h_1 of the upper beam is chosen as the normalizing factor for r . Further,

$$\epsilon = \frac{1}{2\pi} \ln \frac{1 - \beta^*}{1 + \beta^*}, \quad (36)$$

where β^* is one of the two Dundurs' parameters,

$$\beta^* = \frac{\Gamma(\kappa_2 - 1) - (\kappa_1 - 1)}{\Gamma(\kappa_2 + 1) + (\kappa_1 + 1)}. \quad (37)$$

Subscripts 1 and 2 refer to the upper and lower beams as before, $\kappa_i = 3 - 4\nu_i$ for plane strain and $\kappa_i = (3 - \nu_i)/(1 + \nu_i)$ for plane stress, $\Gamma = \mu_1/\mu_2$, μ_i being shear modulus ($i = 1, 2$).

The normal component of the relative displacement of the two points of the upper and lower crack surfaces is given as

$$v = m \left[(K_I + 2\epsilon K_{II}) \cos \left(\epsilon \ln \frac{r}{2h_1} \right) - (K_{II} - 2\epsilon K_I) \sin \left(\epsilon \ln \frac{r}{2h_1} \right) \right] \sqrt{r}, \quad (38)$$

where

$$m = [(\kappa_1 + 1)/\mu_1 + (\kappa_2 + 1)/\mu_2] / [2\sqrt{2\pi} (1 + 4\epsilon^2) \cosh(\pi\epsilon)]. \quad (39)$$

With the definition of the complex stress intensity factor given by (35), the opening (mode I) and sliding (mode II) components of the energy, G_I^Δ and G_{II}^Δ , that are released during an incremental extension of an interface crack, Δa , were first calculated by Sun and Jih (1987). One of the present writers gave formulas of G_I^Δ and G_{II}^Δ in convenient forms as follows (Toya, 1992):

$$G_I^\Delta = (G/2)[1 + F(\epsilon) \cos(2\epsilon a' + \varphi(\epsilon) + \theta_0)]\Delta a, \quad (40)$$

$$G_{II}^\Delta = (G/2)[1 - F(\epsilon) \cos(2\epsilon a' + \varphi(\epsilon) + \theta_0)]\Delta a, \quad (41)$$

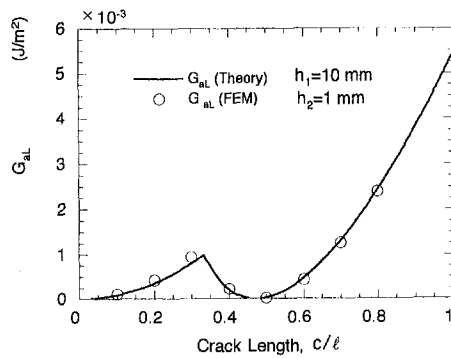


Fig. 7(a)

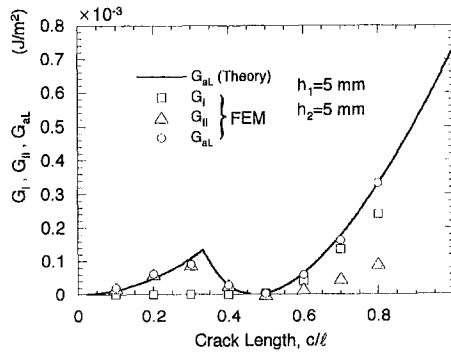


Fig. 7(b)

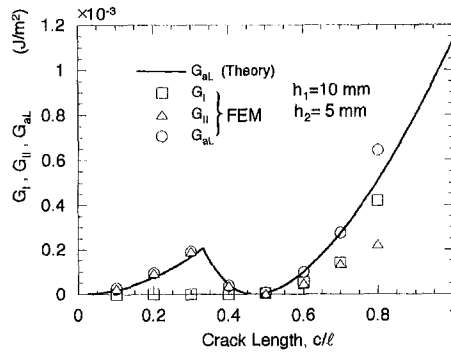


Fig. 7(c)

Fig. 7 Energy release rate at left-hand crack-tip, G_{II} , and its components: (a) $h_1 = 10$ mm, $h_2 = 1$ mm, (b) $h_1 = 5$ mm, $h_2 = 5$ mm, (c) $h_1 = 10$ mm, $h_2 = 5$ mm

where

$$F(\epsilon) = \left[\frac{\sinh(2\pi\epsilon)}{2\pi\epsilon(1 + 4\epsilon^2)} \right]^{1/2}, \quad (42)$$

$$a' = \ln[\Delta a / (2h_1)], \quad (43)$$

$$\varphi(\epsilon) = \sum_{n=0}^{\infty} \left(\tan^{-1} \frac{\epsilon}{1+n} - \tan^{-1} \frac{\epsilon}{\frac{1}{2}+n} \right), \quad (44)$$

$$\theta_0 = \begin{cases} \tan^{-1} [(1 - k^2 + 4\epsilon k)/k_0], & \text{for } k_0 > 0 \\ \tan^{-1} [(1 - k^2 + 4\epsilon k)/k_0] + \pi, & \text{for } k_0 \leq 0 \end{cases} \quad (45)$$

with

$$k = K_{II}/K_I, \quad k_0 = 2[k + \epsilon(k^2 - 1)]. \quad (46)$$

Values of $\varphi(\epsilon)$ are tabulated in Table I in Toya (1992). Espe-

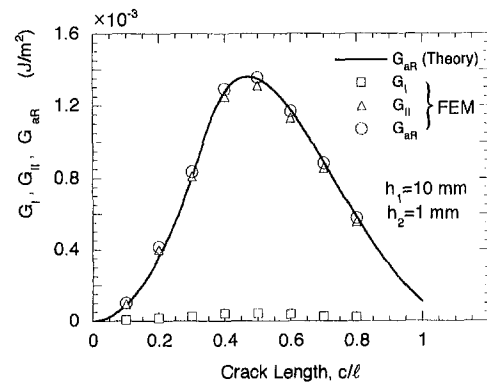


Fig. 8(a)

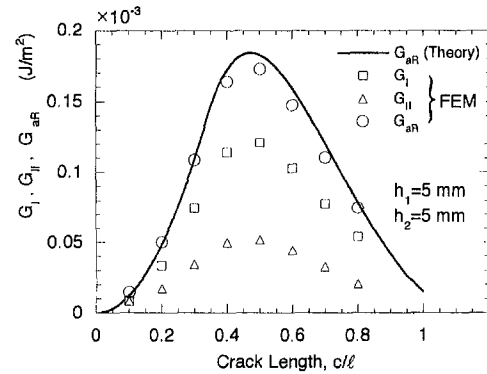


Fig. 8(b)

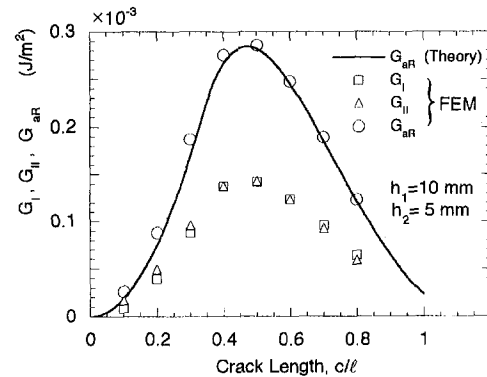


Fig. 8(c)

Fig. 8 Energy release rate at right-hand crack-tip, G_{II} , and its components: (a) $h_1 = 10$ mm, $h_2 = 1$ mm, (b) $h_1 = 5$ mm, $h_2 = 5$ mm, (c) $h_1 = 10$ mm, $h_2 = 5$ mm

cially when ϵ is small, say $|\epsilon| < 0.05$, the following approximation may be used:

$$\varphi(\epsilon) = -2\epsilon \ln 2 = -1.3863\epsilon. \quad (47)$$

Further, G is the total energy release rate (Malyshev and Salganik, 1965)

$$G = \left(\frac{\kappa_1 + 1}{\mu_1} + \frac{\kappa_2 + 1}{\mu_2} \right) (K_I^2 + K_{II}^2) / [16 \cosh^2(\pi\epsilon)]. \quad (48)$$

It is seen from (40), (41), and (43) that the conventional definition for the components of the energy release rates, i.e., $\lim_{\Delta a \rightarrow 0} G_i^\Delta / \Delta a$ ($i = I, II$), cannot be applied for interface cracks. Instead each component should be defined as

$$G_I = G_I^\Delta / \Delta a, \quad G_{II} = G_{II}^\Delta / \Delta a, \quad (49)$$

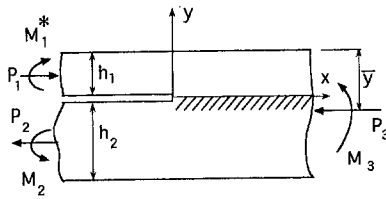


Fig. 9 Split-beam element under general loading condition

for some finite crack growth step size Δa . There is still no definite way of choosing a proper size of Δa , but the characteristic length of delamination process, e.g., the thickness of an adhesive layer could be suggested. We note that G_I and G_{II} calculated in the previous section are nothing more than these energy release rates with respect to the width of the element ($\Delta a = 0.125$ mm) adjacent to the crack tip.

Suo and Hutchinson (1990) gave formulas of K_I and K_{II} for the split beam with a unit width subjected to general stretching and bending as shown in Fig. 9. Their expressions are

$$K_I = \frac{p}{\sqrt{2}} \left[\frac{P_0}{\sqrt{A_0 h_1}} \cos \omega + \frac{M_0}{\sqrt{I h_1^3}} \sin (\omega + \gamma) \right], \quad (50)$$

$$K_{II} = \frac{p}{\sqrt{2}} \left[\frac{P_0}{\sqrt{A_0 h_1}} \sin \omega - \frac{M_0}{\sqrt{I h_1^3}} \cos (\omega + \gamma) \right], \quad (51)$$

where

$$P_0 = P_1 - C_1 P_3 - C_2 M_3 / h_1, \quad (52)$$

$$M_0 = M_1^* - C_3 M_3. \quad (53)$$

The constants p , A_0 , I , γ , and C 's are given in Appendix C. Further, ω is a real angular quantity that only depends on $\eta = h_1/h_2$ and Dundurs' parameters, α^* and β^* (cf. Appendix C for the definition of α^*). The function $\omega(\alpha^*, \beta^*, \eta)$ has been summarized in Tables 1–4 in Suo and Hutchinson (1990) for various α^* and β^* and $\eta = 0, 0.1, 0.5$ and 1 . Hence, substituting (50) and (51) into (40) and (41) we can obtain each component of the energy release rate.

We apply Suo and Hutchinson's results to our problem. In the case where the point of application of load is on the delaminated zone, we have

$$M_1^* = (D_1/bD)(Pa_L d'/l - \frac{1}{2}Zh), \quad (54)$$

$$M_3 = Pa_L d'/(bl), \quad (55)$$

for the left-hand tip of the delamination. Quantities M_1^* and M_3 for the right-hand crack-tip are obtained by replacing a_L and d'

in (54) and (55) with a_R and d , respectively. For both cases we readily see that

$$M_0 = -D_1 h P_0 / (2D). \quad (56)$$

Hence the ratio $k = K_{II}/K_I$ is identical for both crack tips and moreover it is independent of the crack length.

For the case where the point of force application is outside the delaminated zone, we have

$$M_1^* = (D_1/bD)[Pd(l - a_L)/l - \frac{1}{2}Zh], \quad (57)$$

$$M_3 = (Pd/bl)(l - a_L). \quad (58)$$

In this case we have also the same constant ratio of M_0/P_0 as given by (56). Thus, in view of (40), (41), and (43), we conclude that ratios G_{II}/G_I are the same for both crack-tips (except the case where one tip grows in pure mode II while the other does in mixed mode) and independent of the crack length and location of the applied load.

We also note that the total energy release rate given by (48) agrees with (27) and (30) under plane stress condition.

We now calculate K_{II}/K_I for the example models treated in the previous section. Since values of ω are given only for the case of $h_1 \leq h_2$ in Suo and Hutchinson (1990), we reverse the geometry of the model beams in order to apply their results. Namely we choose aluminum for the upper beam material and acrylic resin for the lower beam and reverse the direction of the applied force. For the aluminum/resin combination, Dundurs' parameters take the values $\alpha^* = 0.923$ and $\beta^* = 0.300$. By extrapolating the values in Tables in Suo and Hutchinson (1990), the angle ω is estimated to be $\omega \approx 45$ deg, 50 deg, 58 deg for $\eta = 1, 0.5$, and 0.1 , respectively. Using these values, we calculate K_I and K_{II} and substitute these into (38) to check the sign of v at $r = \Delta a$. If v is negative, pure mode II is implied. While if positive, this means mixed mode. In the latter case, each component of the energy release rate for the step size $\Delta a = 0.125$ mm is calculated from (40) and (41).

In the case of $h_1 = 10$ mm (acrylic resin) and $h_2 = 1$ mm (aluminum), we checked that v became negative for all crack lengths tested. This observation agrees with the computational results from FEM (cf. Fig. 7(a) and Fig. 8(a)) except the case of G_{a_R} at $c/l \approx 0.5$, where slight G_I component has been observed (Fig. 8(a)).

Ratios of G_I/G_{II} for the cases of $h_1 = h_2 = 5$ mm and $h_1 = 10$ mm, $h_2 = 5$ mm are compared with the numerical solutions in Table 1.

Since cracked and uncracked parts of the beam are required to be of infinite length in Suo and Hutchinson (1990), we cannot expect good correlation between the theory and numerical results for the cases of either short cracks or short uncracked parts of the beam (i.e., when $c \leq 5h$ or $a_L, a_R \leq 5h$). Except these cases, and the cases at $c/l \approx 0.5$, for which the energy release rate for the left-hand crack-tip is very small (cf. Fig. 7(b) and (c)), we observe that the ratios G_I/G_{II} based on FEM

Table 1 Comparison of the ratio G_I/G_{II} (percent)

c/l	$h_1 = 5$ mm (Acryl) $h_2 = 5$ mm (Al)				$h_1 = 10$ mm (Acryl) $h_2 = 5$ mm (Al)			
	left-hand tip		right-hand tip		left-hand tip		right-hand tip	
	FEM	theory	FEM	theory	FEM	theory	FEM	theory
0.1	0/100		58.1/41.9		0/100		34.5/65.5	
0.2	0/100		66.2/33.8		0/100		44.2/55.8	
0.3	0/100	0/100	68.6/31.4		0/100	0/100	48.0/52.0	
0.4	0/100		69.6/30.4		0/100		49.9/50.1	
0.5	91.0/9.0		70.0/30.0	74.2/25.8	65.9/34.1		49.8/50.2	55.4/44.6
0.6	71.4/28.6		69.8/30.2		50.7/49.3		50.1/49.9	
0.7	70.0/30.0	74.2/25.8	70.5/29.5		50.7/49.3	55.4/44.6	50.8/49.2	
0.8	72.1/27.9		72.5/27.5		65.2/34.8		52.1/47.9	

are nearly equal for both crack-tips, agreeing with the theoretical prediction. With regard to the values of G_I/G_{II} , the agreement between the theory and numerical calculations is also reasonable considering rather crude mesh division used in the FEM computations. The result suggests that the complex stress intensity factors may be determined with reasonable accuracy from the components of the energy release rate obtained from FEM by combining the works of Toya (1992) and Suo and Hutchinson (1990).

5 Concluding Remarks

Asymmetric three-point bending of a simply supported layered beam with an internal interface crack was analyzed based on the classical beam theory. Axial forces induced in the parts of the beam over and below the crack, the compliance, and the strain energy release rate were derived. The analyses were well confirmed by finite element computations, and hence the utility of a simple strength of materials approach to an interfacial crack in a laminate was ascertained.

Further, the decomposition of the energy release rate into mode I and mode II components was made by combining the analysis for the components of the energy release rates by Toya (1992) and the two-dimensional linear elasticity solutions by Suo and Hutchinson (1990) for a split-beam element subjected to general loading conditions. It was shown that the ratios of mode mix, G_I/G_{II} , with G_I and G_{II} defined in the present paper are the same for both crack-tips (except the case where one tip grows in pure mode II while the other does in mixed mode), and independent of the crack length and the location of the applied load. Theoretical values of the ratios of mode mix were also shown to be reasonably accurate using finite element analysis. We expect that the parameter of mode mixture G_I/G_{II} may be useful for the study of the criterion of the mixed mode delamination growth.

References

- Armanios, E. A., Regfield, L. W., and Reddy, A. D., 1986, "Design Analysis and Testing for Mixed-Mode and Mode II Interlaminar Fracture of Composites," *Composite Materials: Testing and Design*, J. M. Whitney, ed. ASTM STP 893, pp. 232–255.
- Ashby, M. F., Easterling, K. E., Harryson, R., and Maiti, K., 1985, "The Fracture and Toughness of Woods," *Proceedings of the Royal Society of London*, Vol. A398, pp. 261–280.
- Chai, H., Babcock, C. D., and Knauss, W. G., 1981, "One Dimensional Modeling of Failure in Laminated Plates by Delamination Buckling," *International Journal of Solids and Structures*, Vol. 17, pp. 1069–1083.
- Charalambides, P. G., Lund, J., Evans, A. G., and Mcmeeking, R. M., 1989, "A Test Specimen for Determining the Fracture Resistance of Bimaterial Interfaces," *ASME JOURNAL OF APPLIED MECHANICS*, Vol. 56, pp. 77–82.
- Kachanov, L. M., 1988, *Delamination Buckling of Composite Materials*, Kluwer Academic Publishers, Dordrecht, The Netherlands.
- Kanninen, M. F., 1973, "An Augmented Double Cantilever Beam Model for Studying Crack Propagation and Arrest," *International Journal of Fracture*, Vol. 9, pp. 83–92.
- Madenci, E., and Westman, R. A., 1991, "Local Delamination Buckling in Layered Systems," *ASME JOURNAL OF APPLIED MECHANICS*, Vol. 58, pp. 157–166.
- Maikuma, H., Gillespie, Jr., J. W., and Whitney, J. M., 1989, "Analysis and Experimental Characterization of the Center Notch Flexural Test Specimen for Mode II Interlaminar Fracture," *Journal of Composite Materials*, Vol. 23, pp. 756–786.
- Malyshev, B. M., and Salganik, R. L., 1965 "The Strength of Adhesive Joints Using the Theory of Cracks," *International Journal of Fracture*, Vol. 1, pp. 114–128.
- Okusa, K., 1983a, "Mode II Energy Release Rate for the End-Cracked Wood Beam," *Bulletin of Kagoshima University Forests*, No. 11, pp. 1–20.
- Okusa, K., 1983b "Studies on the shearing of Wood," *Bulletin of the Faculty of Agriculture, Kagoshima University*, No. 33, pp. 193–202.
- Rybicki, E. F., and Kanninen, M. F., 1977, "A Finite Element Calculation of Stress Intensity Factors by a Modified Crack Closure Integral," *Engineering Fracture Mechanics*, Vol. 9, pp. 931–938.
- Sun, C. T., and Jih, C. J., 1987, "On Strain Energy Release Rates for Interfacial Cracks in Bi-Material Media," *Engineering Fracture Mechanics*, Vol. 28, pp. 13–20.

Suo, Z., and Hutchinson, J. W., 1990, "Interface Crack between Two Elastic Layers," *International Journal of Fracture*, Vol. 43, pp. 1–18.

Toya, M., 1992, "On Mode I and Mode II Energy Release Rates of an Interface Crack," *International Journal of Fracture*, Vol. 56, pp. 345–352.

Toya, M., Miyawaki, T., and Kirioka, K., 1992, "Analyses of Delamination of Laminated Beams by Bending," *Proceedings of the Eighteenth International Symposium on Space Technology and Science*, T. Hashiguchi, ed., pp. 527–534.

APPENDIX A

The flexural rigidity of the composite beam is

$$D' = E_1 I_1' + E_2 I_2' \quad (A1)$$

where I_1' and I_2' are the second moment of inertia of the upper and lower beam with respect to the neutral axis of the composite beam, i.e.,

$$I_1' = bh_1^3/12 + (\bar{y} - h_1/2)^2 bh_1 \quad (A2)$$

$$I_2' = bh_2^3/12 + (h_1 + h_2/2 - \bar{y})^2 bh_2 \quad (A3)$$

with \bar{y} being the distance of the neutral axis from the top surface of the upper beam,

$$\bar{y} = \frac{E_1 h_1^2 + E_2 (h^2 - h_1^2)}{2(E_1 h_1 + E_2 h_2)} \quad (A4)$$

APPENDIX B

The four unknown constants, s_3 , s_3' , J_1 , and J_1' are determined from the following continuity conditions for the beam inclination and deflection:

$$\left. \frac{dy_{AB}}{dx} \right|_{x=a_L} = \left. \frac{dy_{BC}}{dx} \right|_{x=0} \quad \text{at } B, \quad (B1)$$

$$\left. \frac{dy_{BC}}{dx} \right|_{x=c_L} = - \left. \frac{dy_{CD}}{dx'} \right|_{x'=c_R} \quad \text{at } C, \quad (B2)$$

$$y_{AB}|_{x=a_L} + y_{BC}|_{x=c_L} = y_{CD}|_{x'=c_R} + y_{DF}|_{x'=a_R} \quad \text{at } C, \quad (B3)$$

$$\left. \frac{dy_{CD}}{dx'} \right|_{x'=0} = \left. \frac{dy_{DF}}{dx'} \right|_{x'=a_R} \quad \text{at } D. \quad (B4)$$

The solution of equations (B1) ~ (B4) are given as follows:

$$s_3 = \{Ac_L^2(c_L + 3d') + Bc_R^2(3d' - c_R)\}/(lD) \\ - s_2 c_L(c_L + 2d')/l - s_2' c_R(-c_R + 2d')/l \\ + 2(Ba_R^3 - Aa_L^3)/(lD') \quad (B5)$$

$$J_1 = s_3 + 3a_L^2 A/D' \quad (B6)$$

$$s_3' = \{-Ac_L^2(c_L - 3d) + Bc_R^2(3d + c_R)\}/(lD) \\ + s_2 c_L(c_L - 2d)/l - s_2' c_R(c_R + 2d)/l \\ - 2(Ba_R^3 - Aa_L^3)/(lD') \quad (B7)$$

$$J_1' = s_3' + 3a_R^2 B/D' \quad (B8)$$

with

$$A = Pd'/(6l), \quad B = Pd/(6l).$$

APPENDIX C

The constants appearing in (50) – (53) are defined as follows (Suo and Hutchinson, 1990):

$$\rho = \sqrt{\frac{1 - \alpha^{*2}}{1 - \beta^{*2}}} \quad (C1)$$

where

$$\alpha^* = \frac{\Gamma(\kappa_2 + 1) - (\kappa_1 + 1)}{\Gamma(\kappa_2 + 1) + (\kappa_1 + 1)}, \quad (C2)$$

is a Dundurs' parameter. Further, using the notations in the present paper,

$$A_0 = \frac{D_0 D_2}{b E_1 h_1 (D' - D_1)}, \quad \sin \gamma = \sqrt{\frac{(D' - D) D_1}{(D' - D_1) D}}, \quad (C3)$$

$$I = D_2 / (12 D), \quad C_1 = D_0 / (b E_2 h_2), \quad (C4)$$

$$C_2 = h_1 h D_0 / (2 D'), \quad C_3 = D_1 / D' \quad (C5)$$

under plane stress condition.

Coefficient of Restitution for Collinear Collisions of Elastic-Perfectly Plastic Spheres

C. Thornton

Civil Engineering Department,
Aston University,
Aston Triangle,
Birmingham B4 7ET, UK

Based on a simplified theoretical model for the normal contact interaction of two elastic-perfectly plastic spheres, an analytical solution is provided for the coefficient of restitution. The solution is expressed in terms of the ratio of impact velocity to yield velocity rather than in terms of material properties such as the yield stress which is difficult to reliably ascertain for many materials.

Introduction

A simplified theoretical model is presented for the normal contact interaction between two elastic-perfectly plastic spheres. The model was incorporated into the discrete element code TRUBAL by Thornton and Ning (1994) in order to numerically simulate a sphere impacting orthogonally with a target wall. From the results of the simulations a relationship was obtained between the coefficient of restitution and the impact velocity. In this paper we derive the analytical solution based on the same simplified theoretical model. Throughout the paper it is tacitly assumed that quasi-static contact mechanics theories are valid.

Theoretical Background

Elastic Loading. For two spheres of radii R_i and elastic properties E_i and ν_i ($i = 1, 2$) subjected to an applied force P , the Hertzian pressure distribution over the contact area of radius a is

$$p(r) = p_0 \left[1 - \left(\frac{r}{a} \right)^2 \right]^{1/2} \quad (1)$$

where

$$p_0 = \frac{3P}{2\pi a^2} \quad (2)$$

The contact normal force and contact radius are given by

$$P = \frac{4}{3} E^* R^{1/2} \alpha^{3/2} \quad (3)$$

and

$$a = \left(\frac{3PR^*}{4E^*} \right)^{1/3} \quad (4)$$

where α is the relative approach of the two particle centroids and

$$a^2 = R^* \alpha. \quad (5)$$

In the above equations

$$\frac{1}{E^*} = \frac{1 - \nu_1^2}{E_1} + \frac{1 - \nu_2^2}{E_2} \quad (6)$$

$$\frac{1}{R^*} = \frac{1}{R_1} + \frac{1}{R_2}. \quad (7)$$

Yield. If the relative impact velocity V is just large enough to initiate yield in one of the spheres then, using (3) and (5) we may write

$$\frac{1}{2} m^* V_y^2 = \int_0^{a_y} P d\alpha = \frac{8E^* a_y^5}{15R^{*2}} \quad (8)$$

where V_y , which we define as the yield velocity, is the relative impact velocity below which the interaction behavior is assumed to be elastic, a_y is the contact radius when yield occurs and m^* is related to the particle masses m_i by the equation

$$\frac{1}{m^*} = \frac{1}{m_1} + \frac{1}{m_2}. \quad (9)$$

Rearranging (8) we obtain

$$a_y = \left(\frac{15R^{*2} m^* V_y^2}{16E^*} \right)^{1/5}. \quad (10)$$

We now define a "contact yield stress" $\sigma_y = p_0(a_y)$. Using (2) and (4),

$$\sigma_y = \frac{2E^* a_y}{\pi R^*} \quad (11)$$

Substituting (10) and rearranging, we obtain

$$V_y = \left(\frac{\pi}{2E^*} \right)^2 \left(\frac{8\pi R^{*3}}{15m^*} \right)^{1/2} \sigma_y^{5/2} = 3.194 \left(\frac{\sigma_y^5 R^{*3}}{E^{*4} m^*} \right)^{1/2} \quad (12)$$

In the case of a sphere of density ρ impacting with a plane surface, $R^* = R$, $m^* = m$ and (12) reduces to

$$V_y = \left(\frac{\pi}{2E^*} \right)^2 \left(\frac{2}{5\rho} \right)^{1/2} \sigma_y^{5/2} = 1.56 \left(\frac{\sigma_y^5}{E^{*4} \rho} \right)^{1/2} \quad (13)$$

which was originally obtained by Davies (1949).

Plastic Loading. In order to model the post-"yield" behavior, it is necessary to make some simplifying assumptions. If plastic deformation occurs we assume a Hertzian pressure distribution with a cut-off corresponding to the contact yield

Contributed by the Applied Mechanics Division of THE AMERICAN SOCIETY OF MECHANICAL ENGINEERS for publication in the ASME JOURNAL OF APPLIED MECHANICS.

Discussion on this paper should be addressed to the Technical Editor, Professor Lewis T. Wheeler, Department of Mechanical Engineering, University of Houston, Houston, TX 77204-4792, and will be accepted until four months after final publication of the paper itself in the ASME JOURNAL OF APPLIED MECHANICS.

Manuscript received by the ASME Applied Mechanics Division, Nov. 28, 1995 final revision, Aug. 2, 1996. Associate Technical Editor: J. T. Jenkins.

stress σ_y defined by (11). After yield, the normal force is given by

$$P = P_e - 2\pi \int_0^{a_p} [\sigma(r) - \sigma_y] r dr \quad (14)$$

where P_e is the equivalent elastic force given by (4) which would result in the same total contact area and a_p is the radius of the contact area over which a uniform pressure is assumed, as indicated in Fig. 1. Integrating (14) we obtain

$$P = \pi a_p^2 \sigma_y + P_e \left[1 - \left(\frac{a_p}{a} \right)^2 \right]^{3/2} \quad (15)$$

Considering the conditions at yield, σ_y may be defined in terms of the normal force P_y and contact radius a_y as

$$\sigma_y = \frac{3P_y}{2\pi a_y^2} \quad (16)$$

or, according to Fig. 1,

$$\sigma_y = \frac{3P_e}{2\pi a^2} \left[1 - \left(\frac{a_p}{a} \right)^2 \right]^{1/2} \quad (17)$$

The contact radius is obtained from

$$a^3 = \frac{3R^*P_e}{4E^*} \quad (18)$$

Hence, combining (16), (17), and (18) we find that

$$\left[1 - \left(\frac{a_p}{a} \right)^2 \right] = \left(\frac{a_y}{a} \right)^2 \quad (19a)$$

or

$$a^2 = a_p^2 + a_y^2 \quad (19b)$$

which corresponds to the assumption of Bitter (1963). Substituting (19) and (18) into (15) we obtain

$$P = P_y + \pi \sigma_y (a^2 - a_y^2) \quad (20)$$

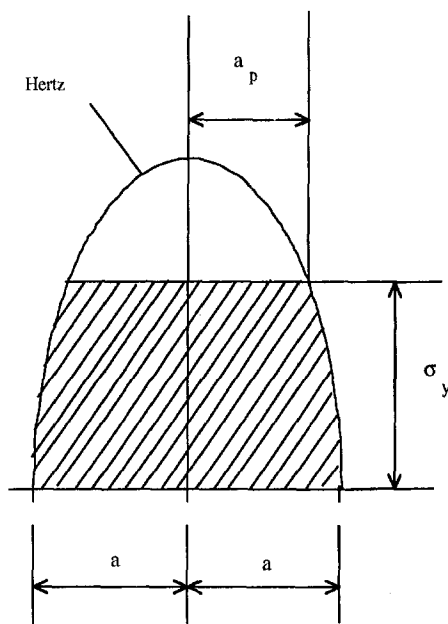


Fig. 1 Normal traction distribution

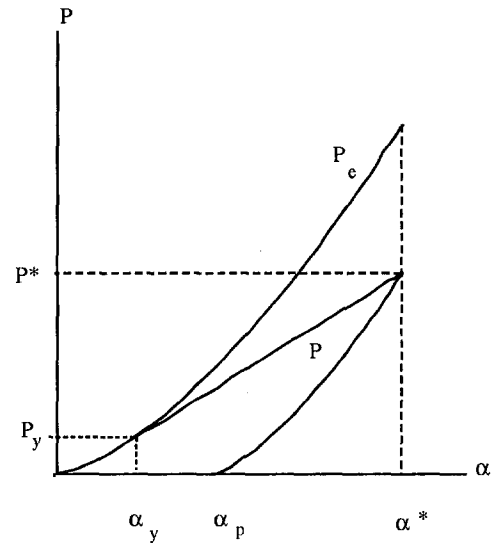


Fig. 2 Force-displacement relationship

Using the Hertzian substitution $a^2 = R^*\alpha$, where α is strictly the relative approach, the force-displacement relationship during plastic loading is given as

$$P = P_y + \pi \sigma_y R^* (\alpha - \alpha_y) \quad (21)$$

which is linear, as shown in Fig. 2.

Elastic Unloading. If plastic deformation occurs during the loading stage the contact curvature during unloading is $1/R_p^* < 1/R^*$ due to permanent deformation of the contact surfaces. During unloading the force-displacement behaviour is assumed to be elastic and is provided by the Hertzian equations but with a curvature $1/R_p^*$ corresponding to the point of maximum compression. At the point of unloading, the contact area developed by the actual maximum normal force P^* and reduced curvature $1/R_p^*$ is the same as that which would be generated by an equivalent elastic force P_e^* and a contact curvature $1/R^*$. Hence, from (18),

$$R_p^* P^* = R^* P_e^* \quad (22)$$

where

$$P_e^* = \frac{4}{3} E^* R^* \alpha^{3/2} \quad (23)$$

It can be seen from Fig. 2 that the linear plastic loading curve is tangential to the Hertzian curve at the yield point and, when extended, intersects the vertical axis at $P_0 < 0$. From (20) and (11) the plastic contact stiffness is defined as

$$k_N = \pi R^* \sigma_y = 2E^* a_y \quad (24)$$

Therefore,

$$\alpha^* = \frac{P^* - P_0}{\pi R^* \sigma_y} \quad (25)$$

and

$$P_0 = P_y - 2E^* a_y \alpha_y \quad (26)$$

Substituting (4) and (5),

$$P_0 = -\frac{P_y}{2} \quad (27)$$

and, hence,

$$\alpha^* = \frac{2P^* + P_y}{2\pi R^* \sigma_y} \quad (28)$$

$$a^{*2} = \left(\frac{2P^* + P_y}{2\pi \sigma_y} \right). \quad (29)$$

Combining (22), (23), and (28) leads to

$$R_p^* = \frac{4E^*}{3P^*} \left(\frac{2P^* + P_y}{2\pi \sigma_y} \right)^{3/2} \quad (30)$$

and, during elastic unloading,

$$P = \frac{4}{3} E^* R_p^{*1/2} (\alpha - \alpha_p)^{3/2} \quad (31)$$

where α_p is defined in Fig. 2.

Coefficient of Restitution

At impact velocities $V_i \leq V_y$ no plastic deformation occurs and, ignoring energy losses due to elastic wave motion in the two bodies, the coefficient of restitution $e = 1.0$. If the impact velocity $V_i > V_y$, the rebound kinetic energy is equal to the work done during elastic recovery. Thus

$$\frac{1}{2} m^* V_r^2 = \frac{2}{3} P^* (\alpha^* - \alpha_p) \quad (32)$$

where

$$(\alpha^* - \alpha_p) = \frac{a^{*2}}{R_p^*} \quad (33)$$

Hence, using (29) and (30)

$$\frac{1}{2} m^* V_r^2 = \frac{3P^{*2}}{10E^* a^*} \quad (34)$$

The coefficient of restitution is defined as $e = V_r/V_i$. Thus

$$e^2 = \frac{3P^{*2}}{5E^* a^* m^* V_i^2}. \quad (35)$$

The initial kinetic energy is equal to the work done during deceleration of the particles. Therefore, from inspection of Fig. 2,

$$\frac{1}{2} m^* V_i^2 = \frac{2}{3} P_y \alpha_y + \frac{1}{2} (P_y + P^*) (\alpha^* - \alpha_y). \quad (36)$$

Using (5), (16), and (28)

$$\alpha^* - \alpha_y = \frac{2P^* + P_y}{2\pi R^* \sigma_y} - \frac{3P_y}{2\pi R^* \sigma_y} = \frac{P^* - P_y}{\pi R^* \sigma_y}. \quad (37)$$

Therefore

$$\frac{1}{2} m^* V_i^2 = \frac{2}{3} P_y \alpha_y + \frac{P^{*2} - P_y^2}{2\pi R^* \sigma_y}. \quad (38)$$

Using (3) and (24) we obtain

$$\begin{aligned} \frac{1}{2} m^* V_i^2 &= \frac{2}{3} P_y \alpha_y + \frac{P^{*2}}{4E^* a_y} - \frac{1}{3} P_y \alpha_y \\ &= \frac{1}{12} m^* V_y^2 + \frac{P^{*2}}{4E^* a_y}, \end{aligned} \quad (39)$$

from which

$$P^{*2} = 2E^* a_y (m^* V_i^2 - \frac{1}{6} m^* V_y^2). \quad (40)$$

Substituting (40) into (35) the coefficient of restitution can be obtained from

$$e^2 = \frac{6a_y}{5a^*} \left[1 - \frac{1}{6} \left(\frac{V_y}{V_i} \right)^2 \right]. \quad (41)$$

Using the substitutions

$$a_y^2 = \frac{3P_y}{2\pi \sigma_y} \quad (42)$$

and

$$a^{*2} = \frac{2P^* + P_y}{2\pi \sigma_y} \quad (43)$$

we obtain

$$e^2 = \frac{6\sqrt{3}}{5} \left(\frac{P_y}{2P^* + P_y} \right)^{1/2} \left[1 - \frac{1}{6} \left(\frac{V_y}{V_i} \right)^2 \right]. \quad (44)$$

Combining (3), (8) and (40)

$$\frac{P^*}{P_y} = \left[\frac{6}{5} \left(\frac{V_i}{V_y} \right)^2 - \frac{1}{5} \right]^{1/2}. \quad (45)$$

Therefore, the general expression for the coefficient of restitution is

$$e = \left(\frac{6\sqrt{3}}{5} \right)^{1/2} \left[1 - \frac{1}{6} \left(\frac{V_y}{V_i} \right)^2 \right]^{1/2} \times \left[\frac{\left(\frac{V_y}{V_i} \right)}{\left(\frac{V_y}{V_i} \right) + 2\sqrt{\frac{6}{5} - \frac{1}{5} \left(\frac{V_y}{V_i} \right)^2}} \right]^{1/4} \quad (46)$$

with the yield velocity V_y defined by (12) or, in the special case of a sphere impacting a plane surface, by (13).

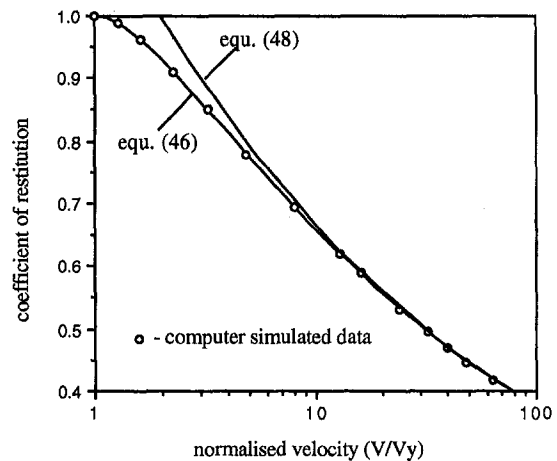


Fig. 3 Theoretical predictions of the coefficient of restitution given by the general Eq. (46), the approximation for high impact velocities (48) and \circ -computer simulated data (Thornton and Ning, 1994)

Equation (46) satisfies the condition $e = 1.0$ when $V_i = V_y$. At high velocities, $(V_y/V_i)^2 \rightarrow 0$ and (46) becomes

$$e = \left(\frac{6\sqrt{3}}{5}\right)^{1/2} \left[\frac{V_y}{V_y + \frac{2\sqrt{6}}{\sqrt{5}} V_i} \right]^{1/4}. \quad (47)$$

Taking $V_i \gg V_y$ we then obtain

$$e = \left(\frac{6\sqrt{3}}{5}\right)^{1/2} \left(\frac{\sqrt{5}}{2\sqrt{6}}\right)^{1/4} \left(\frac{V_y}{V_i}\right)^{1/4} = 1.185 \left(\frac{V_y}{V_i}\right)^{1/4}. \quad (48)$$

An alternative prediction was suggested by Stronge (1995) which may be written in the form

$$e = \frac{V_y}{V_i} \left[\frac{8}{5} \left(\frac{V_i}{V_y}\right)^2 - \frac{3}{5} \right]^{3/8}. \quad (49)$$

Inspection of (49) shows that, for $V_i \gg V_y$, the equation degenerates to

$$e = 1.193 \left(\frac{V_y}{V_i}\right)^{1/4} \quad (50)$$

and that, for $V_i = V_y$, $e = 1$. However, Stronge's (1995) equation (49) also predicts $e > 1$ for $V_y < V_i < 1.59 V_y$.

For the case of a sphere impacting a plane surface we may substitute for V_y using (13) to obtain

$$e = 1.324 \left(\frac{\sigma_y^5}{E^{*4} \rho} \right)^{1/8} (V_i)^{-1/4} \quad (51)$$

which was given by Thornton and Ning (1994). Johnson (1985) provided a similar expression to (51) except that the prefactor was 1.72 as a result of assuming that the plastic normal contact stiffness was twice that given by (24).

Figure 3 shows the dependence of the coefficient of restitution on the impact velocity according to the general expression (46). Superimposed on the figure is the prediction according to (48) and the numerical results obtained by Thornton and Ning (1994). It can be seen that (48) is only satisfactory for $V > 10V_y$. Equation (46) provides an analytical solution for the coefficient of restitution in the range $V_y < V < 10V_y$ which is relevant to many industrial and scientific areas.

References

- Bitter, J. G. A., 1963, "A Study of Erosion Phenomena, Part I," *Wear*, Vol. 6, pp. 5–21.
- Davies, R. M., 1949, "The Determinations of Static and Dynamic Yield Stresses Using a Steel Ball," *Proc. Roy. Soc., London*, Vol. A197, pp. 416–432.
- Johnson, K. L., 1985, *Contact Mechanics*, Cambridge University Press, Cambridge, UK, p. 363.
- Stronge, W., 1995, "Coupling of Friction and Internal Dissipation in Planar Collision of Compliant Bodies," *Proc. 2nd Int. Conf. on Contact Mechanics*, Raous, Jean, and Moreau, eds., Plenum Press, pp. 417–426.
- Thornton, C., and Ning, Z., 1994, "Oblique Impact of Elasto-Plastic Spheres," *Proc. 1st Int. Particle Technology Forum*, Vol. II, AIChE Publications, pp. 14–19.

Criticality of Damping in Multi-Degree-of-Freedom Systems

A. Bhaskar

Department of Engineering,
Trumpington Street,
Cambridge CB2 1PZ, UK

The concept of criticality in multi-degree-of-freedom systems is discussed. Sufficient conditions for overdamping, critical damping, and underdamping are derived in terms of the matrices appearing in the modal coordinates. It is noted that results available in the literature for the case of overdamping and mixed damping are erroneous. This has been pointed out by Bhaskar (1991, 1992) for the cases of overdamping and mixed damping, and by Barkwell et al. (1992) for the case of overdamping. The error in the proof of the conditions for overdamping is brought out. A sufficient condition for overdamping is presented. Results obtained for the symmetric systems are then generalized to the symmetrizable systems. Theorems on eigenvalue bounds are applied to establish criticality.

1 Introduction

For a single-degree-of-freedom vibratory system, the damping ratio ζ determines the boundary of oscillatory and nonoscillatory damped free motion. The value of damping ratio at this boundary (also known as critical damping) is 1. It has been observed (see for example, Meirovitch, 1975) that, in case of critical damping, free response of the system approaches the equilibrium configuration fastest.

Consider the free damped motion of a multi-degree-of-freedom system, governed by the following matrix differential equation:

$$\mathbf{M}\ddot{\mathbf{x}} + \mathbf{C}\dot{\mathbf{x}} + \mathbf{K}\mathbf{x} = \mathbf{0}, \quad (1)$$

where \mathbf{M} , \mathbf{C} , and \mathbf{K} are the mass, stiffness, and damping matrices of order $n \times n$, respectively and \mathbf{x} is the response vector of size $n \times 1$. In this section and the next, matrices \mathbf{M} , \mathbf{C} , and \mathbf{K} are assumed to be symmetric. In addition, it is also assumed that \mathbf{M} and \mathbf{C} are positive definite; while allowing for rigid-body modes, matrix \mathbf{K} is assumed to be positive definite or positive semi-definite. The case of semi-definite damping matrix is not straightforward and is omitted from the present discussion. Statements regarding criticality, similar to those for single-degree-of-freedom systems, can be given to each of the decoupled modes, when damping is classical (i.e., when the equations of motion decouple in the modal coordinates). For a general case of damping, criticality is expressed in terms of latent roots of the λ -matrix $(\lambda^2\mathbf{M} + \lambda\mathbf{C} + \mathbf{K})$. Analogy suggests that, for the case of multi-degree-of-freedom systems, these conditions could be expressed in terms of definiteness properties of the matrices involved. It is surprising that this problem was not addressed until as late as 1955 (Duffin).

Nicholson (1978) defined a system to be underdamped when all the modes are underdamped with a sufficient condition $c_{\max} \leq 2k_{\min}^{1/2}$, where c_{\max} is the largest eigenvalue of $(\mathbf{M}^{-1/2}\mathbf{C}\mathbf{M}^{-1/2})$ and k_{\min} is the smallest eigenvalue of $(\mathbf{M}^{-1/2}\mathbf{K}\mathbf{M}^{-1/2})$. Here $\mathbf{M}^{1/2}$ is the positive square root of \mathbf{M} . Muller (1979) gave a sufficient condition for a system to be underdamped as positive definiteness of $[4\mathbf{M}^{-1/2}\mathbf{K}\mathbf{M}^{-1/2} - (\mathbf{M}^{-1/2}\mathbf{C}\mathbf{M}^{-1/2})^2]$. This generalization was further improved by Inman and Andry (1980)

with a sufficient condition of underdamping as positive definiteness of $[2(\mathbf{M}^{-1/2}\mathbf{K}\mathbf{M}^{-1/2})^{1/2} - (\mathbf{M}^{-1/2}\mathbf{C}\mathbf{M}^{-1/2})]$. They then demonstrated that Muller's condition is a special case of their's, when matrices $(\mathbf{M}^{-1/2}\mathbf{K}\mathbf{M}^{-1/2})$ and $(\mathbf{M}^{-1/2}\mathbf{C}\mathbf{M}^{-1/2})$ commute but, they did not notice that, this is not the only case when the two conditions are equivalent. In fact, whenever the smallest eigenvalue of $2(\mathbf{M}^{-1/2}\mathbf{K}\mathbf{M}^{-1/2})^{1/2}$ is greater than the greatest eigenvalue of $(\mathbf{M}^{-1/2}\mathbf{C}\mathbf{M}^{-1/2})$, all the three criteria for underdamping, viz. those of Nicholson's (1978), Muller's (1979), and Inman's (1980) are equivalent. To show this, the following property of real, symmetric, and positive definite matrices is required:

If $a_1 \leq a_2 \leq \dots \leq a_n$ are the eigenvalues of a real, symmetric, and positive definite matrix \mathbf{A} and $b_1 \leq b_2 \leq \dots \leq b_n$ are the eigenvalues of another real, symmetric, and positive definite matrix \mathbf{B} and if $a_1 > b_n$, then $(\mathbf{A}^p - \mathbf{B}^p)$ is positive definite for any positive integer p .

This property can be readily proved using the min-max properties of Rayleigh quotients associated with the matrices \mathbf{A} , \mathbf{B} , \mathbf{A}^p , and \mathbf{B}^p and noting that the eigenvalues of \mathbf{A}^p are $a_1^p \leq a_2^p \leq \dots \leq a_n^p$ and those of \mathbf{B}^p are $b_1^p \leq b_2^p \leq \dots \leq b_n^p$.

It is now clear that replacing \mathbf{A} by $2(\mathbf{M}^{-1/2}\mathbf{K}\mathbf{M}^{-1/2})^{1/2}$ and \mathbf{B} by $(\mathbf{M}^{-1/2}\mathbf{C}\mathbf{M}^{-1/2})$, when $a_{\min} > b_{\max}$ (Nicholson's criterion essentially), Inman's criterion follows for $p = 1$ and Muller's for $p = 2$. Of the three criteria, Nicholson's is undoubtedly the most conservative. Using a result (Bellman, 1968) that whenever $\mathbf{A} - \mathbf{B}$ is positive definite (\mathbf{A} , \mathbf{B} non-negative), $(\mathbf{A}^{1/2} - \mathbf{B}^{1/2})$ is also positive definite (note that this implication is one way), we conclude that Inman's criterion is sharper than Muller's.

The three criteria presented in the literature involve matrices which appear in the governing equations expressed in the so-called pseudo-modal coordinates (coordinates obtained through the transformation $\mathbf{y} = \mathbf{M}^{-1/2}\mathbf{x}$, \mathbf{y} being the vector of generalized displacements in the pseudo-modal coordinates). In this paper, we have chosen to express the conditions of criticality in the modal coordinates (coordinates in which inertia and stiffness terms decouple) so that the equations for damped free motion are given by (see Meirovitch, 1975; Newland, 1989)

$$\ddot{\mathbf{q}} + \tilde{\mathbf{C}}\dot{\mathbf{q}} + \Lambda\mathbf{q} = \mathbf{0} \quad (2)$$

where $\tilde{\mathbf{C}} = \mathbf{U}^T\mathbf{C}\mathbf{U}$, \mathbf{U} being the modal matrix (corresponding to the undamped problem). Define two λ -matrices as $\mathbf{Q}(\lambda) \stackrel{\text{def}}{=} (\lambda^2\mathbf{M} + \lambda\mathbf{C} + \mathbf{K})$ and $\mathbf{R}(\lambda) \stackrel{\text{def}}{=} \mathbf{U}^T\mathbf{Q}(\lambda)\mathbf{U} = (\lambda^2\mathbf{I}_n + \lambda\tilde{\mathbf{C}} + \Lambda)$ whose $2n$ latent roots are given by $\det[\mathbf{Q}(\lambda)] = 0$ and

Contributed by the Applied Mechanics Division of THE AMERICAN SOCIETY OF MECHANICAL ENGINEERS for publication in the ASME JOURNAL OF APPLIED MECHANICS.

Discussion on this paper should be addressed to the Technical Editor, Professor Lewis T. Wheeler, Department of Mechanical Engineering, University of Houston, Houston, TX 77204-4792, and will be accepted until four months after final publication of the paper itself in the ASME JOURNAL OF APPLIED MECHANICS.

Manuscript received by the ASME Applied Mechanics Division, Nov. 19, 1992; final revision, Apr. 6, 1994. Associate Technical Editor: P. D. Spanos.

$\det [\mathbf{R}(\lambda)] = 0$, respectively. Since determinant of a product of matrices equals product of respective determinants, and since the rows and columns of the modal matrix \mathbf{U} are linearly independent so \mathbf{U} cannot be singular, we have $\det [\mathbf{R}(\lambda)] = 0 \Leftrightarrow \det [\mathbf{Q}(\lambda)] = 0$. This equivalence enables us to use matrices from the modal coordinates while arriving at conditions of criticality. These conditions are on the lines of those given by Inman et al. (1980), but the matrices taken in the present paper are coefficients from the equations of motion in the modal coordinates (in terms of $\mathbf{\Lambda}$ and $\tilde{\mathbf{C}}$), instead of the pseudo-modal coordinates used by Inman et al. (1980). Definitions presented there draw incorrect conclusions for the case of overdamping and mixed damping and this will be discussed later.

2 Conditions of Criticality in Terms of Definiteness of the Matrices

Sufficient conditions for a system to be critically damped, underdamped, or overdamped are presented as follows:

Condition 1 (Critical damping): *If $\tilde{\mathbf{C}} = 2\mathbf{\Lambda}^{1/2}$, the system described by (2) must be critically damped.*

Condition 2 (Underdamping): *If $(2\mathbf{\Lambda}^{1/2} - \tilde{\mathbf{C}})$ is positive definite, the system described by (2) must be underdamped.*

Condition 3 (Overdamping): *If $(\tilde{\mathbf{C}} - 2\mathbf{\Lambda}^{1/2}\mathbf{I}_n)$ is positive definite, the system described by (2) must be overdamped.*

Here Λ_{\max} denotes the maximum eigenvalue of $\mathbf{\Lambda}$. The first two conditions are essentially the same as those of Inman and Andry (1980). Discussions on these two cases are presented here again for the sake of completeness and also to present a background in order to contrast the situation of overdamping with that of underdamping.

2.1 Critical Damping. The condition presented above for critical damping requires that the modal damping matrix $\tilde{\mathbf{C}}$ be diagonal; i.e., damping must be classical. The i th equation can be written as

$$\ddot{q}_i + 2\Lambda_{ii}^{1/2}\dot{q}_i + \Lambda_{ii}q_i = 0. \quad (3)$$

Discriminant of the characteristic equation $(2\Lambda_{ii}^{1/2})^2 - 4\Lambda_{ii}$ is then equal to zero, and so latent roots of the λ -matrix $\mathbf{Q}(\lambda)$ are repeated and real.

2.2 Underdamping. Positive definiteness of $(2\mathbf{\Lambda}^{1/2} - \tilde{\mathbf{C}})$, $\tilde{\mathbf{C}}$ and $2\mathbf{\Lambda}^{1/2}$ requires, for all nonzero vectors \mathbf{x} , that $4(\mathbf{x}^T\mathbf{\Lambda}^{1/2}\mathbf{x})^2 > (\mathbf{x}^T\tilde{\mathbf{C}}\mathbf{x})^2$. Using Cauchy-Schwarz inequality for normalized vectors \mathbf{x} , one obtains $(\mathbf{x}^T\mathbf{\Lambda}^{1/2}\mathbf{x})^2 \leq \mathbf{x}^T\mathbf{\Lambda}\mathbf{x}$. To look into the nature of latent roots of the λ -matrix $\mathbf{R}(\lambda)$ we post multiply $\mathbf{R}(\lambda)$ by its unit right latent vector \mathbf{x} and premultiply by \mathbf{x}^T so that the latent roots are given by

$$\lambda = [-\mathbf{x}^T\tilde{\mathbf{C}}\mathbf{x} \pm \sqrt{(\mathbf{x}^T\tilde{\mathbf{C}}\mathbf{x})^2 - 4\mathbf{x}^T\mathbf{\Lambda}\mathbf{x}}]. \quad (4)$$

It then follows that the latent roots occur in complex-conjugate pairs, which is necessary and sufficient for underdamping to be observed.

2.3 Overdamping. An overdamped system is defined as the one whose *all* modes are overdamped. This means that the latent roots of the λ -matrix $\mathbf{Q}(\lambda)$ (or equivalently $\mathbf{R}(\lambda)$) must all be real and negative. The criterion for overdamping given by Inman et al. (1980), when expressed in modal coordinates, states that *the system must be overdamped if $(\tilde{\mathbf{C}} - 2\mathbf{\Lambda}^{1/2})$ is positive definite*. This result has been accepted and/or used by many authors (see Ahmadian et al., 1984; Gray, 1982; Inman et al., 1982, 1982a, 1982b, 1983, 1987, 1989; Liang et al., 1988; Nicholson et al., 1983, 1987, 1987a; Ross et al., 1990; Ulsoy, 1989; etc., for example). In the following discussions it is shown that this is incorrect through a counter-example. This

has been noted by Bhaskar (1991, 1992) and later by Barkwell et al. (1992).

- *A counter-example:* Consider the following matrices

$$\mathbf{\Lambda} = \begin{bmatrix} 1 & 0 & 0 \\ 0 & 2 & 0 \\ 0 & 0 & 3 \end{bmatrix} \times 10^2 \text{ and } \tilde{\mathbf{C}} = \begin{bmatrix} 22.0 & 1.0 & 1.0 \\ 1.0 & 32.0 & 1.0 \\ 1.0 & 1.0 & 36.0 \end{bmatrix}.$$

Both $\tilde{\mathbf{C}}$ and $(\tilde{\mathbf{C}} - \mathbf{C}_c)$ are positive definite since

$$\text{eig}(\tilde{\mathbf{C}}) = \{21.844 \quad 31.818 \quad 36.338\} \text{ and}$$

$$\text{eig}(\tilde{\mathbf{C}} - \mathbf{C}_c) = \{1.755 \quad 0.608 \quad 4.712\}$$

where $\text{eig}(\cdot)$ represents the eigenvalue of (\cdot) . Thus the criterion of Inman et al. (1980), would predict that none of the modes oscillate. This could be checked by computing latent roots of the associated λ -matrix $\mathbf{R}(\lambda)$, which can be shown to be equal to the eigenvalues of the constant matrix \mathcal{A} defined as

$$\mathcal{A} = \begin{bmatrix} \mathbf{0} & \mathbf{I}_n \\ -\mathbf{\Lambda} & -\tilde{\mathbf{C}} \end{bmatrix}. \quad (5)$$

If positive definiteness of $(\tilde{\mathbf{C}} - \mathbf{C}_c)$ were a sufficient condition for overdamping, *all* the eigenvalues of \mathcal{A} must be negative and real (a necessary and sufficient condition for overdamping). We observe that due to the presence of a complex conjugate pair of eigenvalues in

$$\text{eig}(\mathcal{A}) = \{-6.259 \quad -25.448 \quad -8.826$$

$$-14.185 \pm j1.040 \quad -21.097\},$$

one of the modes oscillates. Note that if $\mathbf{x}^T\tilde{\mathbf{C}}\mathbf{x} \geq \mathbf{x}^T(2\mathbf{\Lambda}^{1/2})\mathbf{x}$ for all \mathbf{x} , the discriminant in the above equation need not necessarily be positive, since $(\mathbf{x}^T\mathbf{\Lambda}^{1/2}\mathbf{x})^2 \leq \mathbf{x}^T\mathbf{\Lambda}\mathbf{x}$. However, the difference $[(\mathbf{x}^T\mathbf{\Lambda}\mathbf{x}) - (\mathbf{x}^T\mathbf{\Lambda}^{1/2}\mathbf{x})^2]$ is expected to be small (zero when \mathbf{x} is an eigenvector of the matrices $\mathbf{\Lambda}$ or $\mathbf{\Lambda}^{1/2}$) due to stationarity of Rayleigh-quotients around the eigenvectors. Thus if the eigenvector of the matrix $\mathbf{\Lambda}$ differs from the latent vector of the system by a small quantity δ (in the sense of an appropriate norm), the difference $[(\mathbf{x}^T\mathbf{\Lambda}\mathbf{x}) - (\mathbf{x}^T\mathbf{\Lambda}^{1/2}\mathbf{x})^2]$ would be of the order of δ^2 . In these cases, the approximation $(\mathbf{x}^T\mathbf{\Lambda}^{1/2}\mathbf{x})^2 \approx \mathbf{x}^T\mathbf{\Lambda}\mathbf{x}$ would closely hold. Hence if the inequality $\mathbf{x}^T\tilde{\mathbf{C}}\mathbf{x} > \mathbf{x}^T(2\mathbf{\Lambda}^{1/2})\mathbf{x}$ is a strong one, where \mathbf{x} is a unit latent vector of the system, it would outweigh in its favor as compared to the weak inequality $(\mathbf{x}^T\mathbf{\Lambda}^{1/2}\mathbf{x})^2 \leq \mathbf{x}^T\mathbf{\Lambda}\mathbf{x}$, so that the inequality $(\mathbf{x}^T\tilde{\mathbf{C}}\mathbf{x})^2 \geq 4\mathbf{x}^T\mathbf{\Lambda}\mathbf{x}$ would hold, and hence overdamping would be correctly predicted. It is, therefore, not surprising that the sufficiency conditions for overdamping based on the positive definiteness of $(\tilde{\mathbf{C}} - 2\mathbf{\Lambda}^{1/2})$, although not strictly correct, have been in use for so long. The reason clearly is the fact that due to stationarity of the Rayleigh-quotients associated with the matrices $\mathbf{\Lambda}$ and $\mathbf{\Lambda}^{1/2}$, counterexamples are hard to find. To study the behavior of latent roots of the system, while the difference $(\tilde{\mathbf{C}} - 2\mathbf{\Lambda}^{1/2})$ varies, consider the matrix $\tilde{\mathbf{C}}(\epsilon) = 2\mathbf{\Lambda}^{1/2} + \epsilon\mathbf{P}$ where \mathbf{P} is a constant positive definite matrix and ϵ is a positive scalar. Consider the scalar form $D(\epsilon) = [\mathbf{y}^T(2\mathbf{\Lambda}^{1/2} + \epsilon\mathbf{P})\mathbf{y}]^2 - 4\mathbf{y}^T\mathbf{\Lambda}\mathbf{y}$ where $\mathbf{y}(\epsilon)$ is a latent vector of the λ -matrix associated with the problem when $\tilde{\mathbf{C}} = \tilde{\mathbf{C}}(\epsilon)$. The discriminant $D(\epsilon, \mathbf{y}(\epsilon)) > 0$ for any $\epsilon > 0$ if

$$[a] \quad \partial D(\epsilon, \mathbf{y} = \mathbf{y}_0)/\partial \epsilon > 0 \quad \text{and}$$

$$[b] \quad D(\epsilon = 0, \mathbf{y} = \mathbf{y}_0) \geq 0$$

or,

$$[c] \quad \partial D[\epsilon, \mathbf{y}(\epsilon)]/\partial \epsilon > 0 \quad \text{and}$$

$$[d] \quad D(\epsilon = 0, \mathbf{y} = \mathbf{y}(0)) \geq 0.$$

In the first set of these conditions (i.e., [a] and [b]), the discriminant is a function of the parameter ϵ alone while the vector \mathbf{y} is held constant equal to \mathbf{y}_0 . These conditions, if correct, assure that the discriminant is positive for all positive values of ϵ when \mathbf{y} equals any arbitrary constant vector \mathbf{y}_0 (thus it is also positive when this arbitrary vector is a latent vector of the system). The second set of conditions (i.e., [c] and [d]), in contrast, treat the vector \mathbf{y} as a variable equal to the latent vector of the system while the parameter ϵ changes (the latent vector of the λ -matrix describing the system is a function of the matrix $\tilde{\mathbf{C}}(\epsilon)$, which in turn is a continuous function of ϵ due to Ostrowski's theorem on the continuity of eigenvalues; Wilkinson, 1965). If conditions [c] and [d] were correct, it would then follow, that the discriminant is always positive for all positive values of ϵ when vector \mathbf{y} assumes a value equal to a latent vector of the system, as ϵ varies.

Validity of conditions [a] and [d] could be shown as follows. The left-hand side of [a] equals $4\mathbf{y}_0^T \Lambda^{1/2} \mathbf{y}_0 \mathbf{y}_0^T \mathbf{P} \mathbf{y}_0 + 2\epsilon(\mathbf{y}_0^T \mathbf{P} \mathbf{y}_0)^2$ which is positive since the first term is a product of two quadratic forms of the positive definite matrices Λ and \mathbf{P} , and the second term is square of a positive definite quadratic form. When $\mathbf{y}(\epsilon)$ is treated as a variable equal to the latent vector of the system corresponding to the variable value of ϵ , the left-hand side of [d] equals zero since at $\epsilon = 0$ and $\mathbf{y} = \mathbf{y}(0)$, $\tilde{\mathbf{C}} = 2\Lambda^{1/2}$ and the latent vectors coincide with the eigenvectors of Λ (Caughey, 1965) (in fact, in the present formulation using modal coordinates, the matrix Λ is a diagonal matrix so that i th eigenvector is the i th basis vector \mathbf{e}_i). To examine the validity of [b], when the vector \mathbf{y} is kept constant, the left-hand side of [b] could be shown to be equal to

$$D(\epsilon = 0, \mathbf{y} = \mathbf{y}_0) = 4(\mathbf{y}_0^T \Lambda^{1/2} \mathbf{y}_0)^2 - 4\mathbf{y}_0^T \mathbf{y}_0 \mathbf{y}_0^T \Lambda \mathbf{y}_0$$

which is negative due to Cauchy-Schwarz inequality. Thus inequality [b] does not hold. Again it could be shown that the left-hand side of [c] may not be positive since the latent vector $\mathbf{y}(\epsilon)$ is no longer constant but varies with ϵ . Note that the left-hand side of [c] is different from that of [a], since derivatives of $\mathbf{y}(\epsilon)$ with respect to the parameter ϵ appear in the expression of [c]. Hence inequality [c] also does not hold.

In the reference (Inman et al., 1980) conditions [a] (the case when the vector \mathbf{y} has been held constant during differentiation) and [d] (the case when $\mathbf{y}(\epsilon)$ is a variable depending on the value of ϵ), have been taken as sufficient for positive definiteness of the discriminant, which is incorrect. The fallacy in the proof presented by Inman et al. (1980) lies in the fact that, while calculating rate of change of the scalar form, vector \mathbf{y} has been kept constant whereas for calculating its value at $\epsilon = 0$ it has been treated as a variable.

The variation of the qualitative behavior of the latent roots, while ϵ varies, is best illustrated through an example. The numerical values of Λ (hence \mathbf{C}_c) and $\mathbf{P} = [\tilde{\mathbf{C}}(\epsilon = 1) - \mathbf{C}_c]$ are taken to be the same as those in the counter-example presented in this section earlier. New values of the matrix $\tilde{\mathbf{C}}(\epsilon)$ are now generated by varying the scalar ϵ . The difference $\tilde{\mathbf{C}}(\epsilon) - 2\Lambda^{1/2} = \epsilon \mathbf{P}$ must now be positive definite for all positive values of ϵ , since ϵ is a positive scalar and \mathbf{P} is a positive definite matrix. Therefore, if the sufficient condition of overdamping presented in the reference (Inman et al., 1980) were correct, the overall system must always remain overdamped, no matter what the value of ϵ be (so long as it is positive). This is not true for the present set of numerical values since there exist complex branches in the trajectory of the latent roots (Fig. 1, in which $\epsilon \in [0, 2]$). Imaginary part of the latent roots is plotted as a function of ϵ in Fig. 2. Note that there exist intervals of values of ϵ for which latent roots possess a complex-conjugate pair. The numerical values of Λ and \mathbf{P} matrices chosen to generate these trajectories are such that the counter-example presented in the beginning of this section corresponds to $\epsilon = 1$.

Proof of sufficiency of condition 3: Condition 3 for overdamping presented here requires that $\mathbf{x}^T(\tilde{\mathbf{C}} - 2\Lambda^{1/2} \mathbf{I}_n)\mathbf{x} > 0$ for all arbitrary vectors \mathbf{x} . Separating the terms, one obtains

$$\min_{\mathbf{x}} (\mathbf{x}^T \tilde{\mathbf{C}} \mathbf{x} / \mathbf{x}^T \mathbf{x}) > (\mathbf{x}^T 2\Lambda^{1/2} \mathbf{x} / \mathbf{x}^T \mathbf{x}) = 2\Lambda_{\max}^{1/2}. \quad (6)$$

Since both sides of the inequality are positive, the quantities on both sides can be squared without changing direction of the inequality. Thus for an arbitrary unit vector \mathbf{x} ,

$$\min [(\mathbf{x}^T \tilde{\mathbf{C}} \mathbf{x})^2] = [\min (\mathbf{x}^T \tilde{\mathbf{C}} \mathbf{x})]^2 > 4\Lambda_{\max} = 4 \max (\mathbf{x}^T \Lambda \mathbf{x}). \quad (7)$$

This inequality implies overdamping since the discriminant in Eq. (4) is always positive.

2.4 Mixed Damping. A system is said to possess mixed damping if, and only if, in the damped free response, at least one mode oscillates and at least one does not. For this case the criterion of Inman et al. (1980) demands that the matrix $(2\Lambda^{1/2} - \tilde{\mathbf{C}})$ must be *indefinite*. It should be emphasized here that indefiniteness does not imply that the matrix could be either positive definite or negative definite. Rather it means that it must not be either. It follows then that at least one eigenvalue of $(2\Lambda^{1/2} - \tilde{\mathbf{C}})$ must be negative and at least one must be positive. It so turns out that indefiniteness of $(2\Lambda^{1/2} - \tilde{\mathbf{C}})$ is neither a necessary nor a sufficient condition for mixed damping (this has been discussed by Bhaskar (1991, 1992)). Necessity is violated by the counter-example presented in Section 2.3, since mixed damping is observed, although $(\tilde{\mathbf{C}} - 2\Lambda^{1/2})$ is positive definite for the example chosen there. The incorrectness of sufficiency is demonstrated through the following two counter-examples.

• *Counter-examples:* Consider the following modal damping matrix $\tilde{\mathbf{C}}$ and the critical damping matrix \mathbf{C}_c

$$\tilde{\mathbf{C}} = \begin{bmatrix} 19.5 & 1 & 1 \\ 1 & 25 & 1 \\ 1 & 1 & 30 \end{bmatrix} \quad \text{and}$$

$$\mathbf{C}_c = \begin{bmatrix} 20.0 & 0 & 0 \\ 0 & 28.284 & 0 \\ 0 & 0 & 34.641 \end{bmatrix}.$$

Eigenvalues of $(\tilde{\mathbf{C}} - \mathbf{C}_c)$ and those of $\tilde{\mathbf{C}}$ are then given by

$$\text{eig}(\tilde{\mathbf{C}} - \mathbf{C}_c) = \{-3.37 \quad -5.21 \quad +0.16\},$$

$$\text{eig}(\tilde{\mathbf{C}}) = \{19.26 \quad 24.92 \quad 30.32\}.$$

Thus matrix $(\tilde{\mathbf{C}} - \mathbf{C}_c)$ is indefinite and $\tilde{\mathbf{C}}$ is positive definite. The condition of Inman et al. (1980) predicts that damping must be of *mixed* type and that at least one mode must oscillate and at least one must not. However, we note that *all* the modes oscillate, since eigenvalues of the λ -matrix are given by

$$\text{eig}(\mathcal{A}) = \{-10.377 \pm j1.264, \\ -12.401 \pm j6.359, \quad -14.472 \pm j8.558\}$$

For the sake of completeness, the following example illustrates that the condition of Inman et al. (1980) predicts mixed damping although overdamping is actually observed. Consider

$$\Lambda = 10^3 \times \begin{bmatrix} 1 & 0 \\ 0 & 2 \end{bmatrix} \quad \text{and} \quad \tilde{\mathbf{C}} = \begin{bmatrix} 63.246 & 1 \\ 1 & 89.443 \end{bmatrix}.$$

Clearly, $(\mathbf{C} - \mathbf{C}_c)$ is indefinite since $\text{eig}(\mathbf{C} - \mathbf{C}_c) = \{\pm 1\}$. Again conditions of sufficiency of mixed damping presented by Inman et al. (1980) would predict that one of the modes oscillates and one of them does not. Eigenvalues of the associated

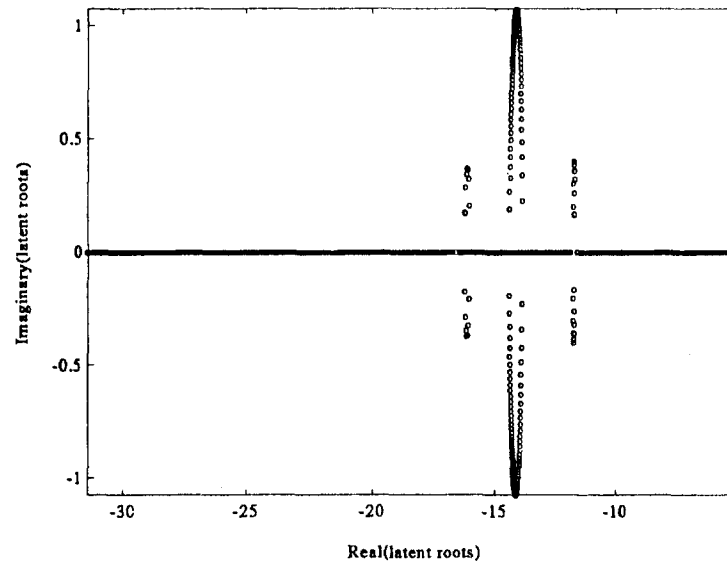


Fig. 1 Trajectory in the complex plane for the six latent roots of the system described in the counter-example of Section 2.3. The variable ϵ is the implicit parameter which varies along the trajectories.

matrix \mathcal{A} indicates overdamping, since $\text{eig}(\mathcal{A}) = \{-29.655, -35.443, -39.902, -47.690\}$.

3 Generalization to a Class of Nonconservative Systems

In the previous section, matrices \mathbf{M} , \mathbf{C} , and \mathbf{K} were assumed to be symmetric while \mathbf{M} and \mathbf{C} were assumed to be positive definite. In this section, results of the previous section are generalized to a class of systems known as the *symmetrizable systems*. With a suitable transformation, the equations of motion for this class of systems can be cast in terms of symmetric matrices and are discussed by Inman (1983). Results of Inman et al. (1980) are generalized by Ahmadian et al. (1984) and are again incorrect for the cases of overdamping and mixed damping. In the present study, these results are modified appropriately.

Assuming that the mass matrix is nonsingular, equations of motion can be expressed as

$$\mathbf{I}_n \ddot{\mathbf{x}} + \bar{\mathbf{C}} \dot{\mathbf{x}} + \bar{\mathbf{K}} \mathbf{x} = \mathbf{0} \quad (8)$$

where $\bar{\mathbf{C}} = \mathbf{M}^{-1}\mathbf{C}$ and $\bar{\mathbf{K}} = \mathbf{M}^{-1}\mathbf{K}$. No matrix is assumed to be symmetric at this stage which is why premultiplication by the inverse of mass matrix has been carried out, since preserving the symmetry is not the idea any more. It is now assumed that the matrices $\bar{\mathbf{C}}$ and $\bar{\mathbf{K}}$ are symmetrizable so that factorizations $\bar{\mathbf{C}} = \mathbf{S}_1 \mathbf{S}_2$ and $\bar{\mathbf{K}} = \mathbf{T}_1 \mathbf{T}_2$ are permissible (Inman, 1983), where matrices \mathbf{S}_1 and \mathbf{T}_1 are real, symmetric, and positive definite, while \mathbf{S}_2 and \mathbf{T}_2 need only be symmetric. The condition for symmetrizability demands that at least one factor in the above factorization be common and so it is assumed that $\mathbf{S}_1 = \mathbf{T}_1$. Transforming the coordinates according to $\mathbf{x}(t) = \mathbf{S}_1^{1/2} \mathbf{y}(t)$ and

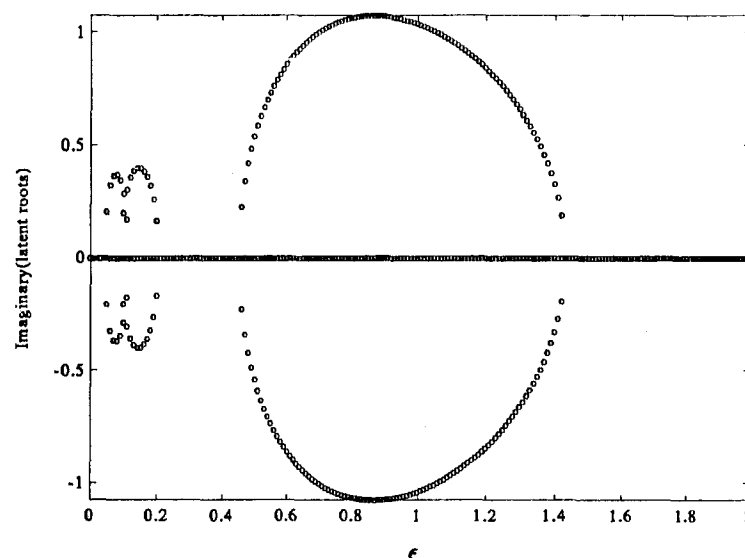


Fig. 2 Imaginary part of the latent roots as a function of ϵ . Note the existence of intervals of ϵ in which the imaginary part is nonzero indicating the presence of underdamped modes.

premultiplying by $\mathbf{S}^{-1/2}$, we recast the governing equations of motion (8) in terms of symmetric coefficient matrices as

$$\mathbf{I}_n \ddot{\mathbf{y}} + \mathbf{S}_1^{1/2} \mathbf{S}_2 \mathbf{S}_1^{1/2} \dot{\mathbf{y}} + \mathbf{S}_1^{1/2} \mathbf{T}_2 \mathbf{S}_1^{1/2} \mathbf{y} = \mathbf{0}. \quad (9)$$

Extension of the results obtained in the previous section is now straightforward.

Condition 4 (Critical damping): If $2(\mathbf{S}_1^{1/2} \mathbf{T}_2 \mathbf{S}_1^{1/2})^{1/2} = \mathbf{S}_1^{1/2} \mathbf{S}_2 \mathbf{S}_1^{1/2}$, then the system must be critically damped.

Condition 5 (Underdamping): If $2(\mathbf{S}_1^{1/2} \mathbf{T}_2 \mathbf{S}_1^{1/2})^{1/2} - (\mathbf{S}_1^{1/2} \mathbf{S}_2 \mathbf{S}_1^{1/2})$ is positive definite then the system must be underdamped.

Condition 6 (Overdamping): If $(\mathbf{S}_1^{1/2} \mathbf{S}_2 \mathbf{S}_1^{1/2}) - 2(\mathbf{S}_1^{1/2} \mathbf{T}_2 \mathbf{S}_1^{1/2})_{\max}^{1/2} \mathbf{I}_n$ is positive definite then the system must be overdamped.

Here $(\mathbf{S}_1^{1/2} \mathbf{T}_2 \mathbf{S}_1^{1/2})_{\max}$ represents the largest eigenvalue of the matrix $(\mathbf{S}_1^{1/2} \mathbf{T}_2 \mathbf{S}_1^{1/2})$. The first two of these conditions are identical to those presented by Ahmadian et al. (1984). The third condition presented there for overdamping states that, if $\mathbf{S}_1^{1/2} \mathbf{S}_2 \mathbf{S}_1^{1/2} - 2(\mathbf{S}_1^{1/2} \mathbf{T}_2 \mathbf{S}_1^{1/2})^{1/2}$ is positive definite, then the system must be overdamped, which is incorrect. The fourth condition presented there for mixed damping based on indefiniteness of $2(\mathbf{S}_1^{1/2} \mathbf{T}_2 \mathbf{S}_1^{1/2})^{1/2} - (\mathbf{S}_1^{1/2} \mathbf{S}_2 \mathbf{S}_1^{1/2})$ is also incorrect.

3.1 Conditions in Terms of Matrices in the Physical Coordinates. In this section, conditions in terms of matrices in the physical coordinates are derived. Unlike symmetric matrices, the quadratic form is not defined for a general case of real square arrays. Hence instead of definiteness of the matrices, conditions in terms of eigenvalues of the matrices are now presented. Substitution from the factorizations for $\tilde{\mathbf{C}}$ and $\tilde{\mathbf{K}}$, $\mathbf{S}_2 = \mathbf{S}_1^{-1} \tilde{\mathbf{C}}$ and $\mathbf{T}_2 = \mathbf{S}_1^{-1} \tilde{\mathbf{K}}$, into the expression $(\mathbf{S}_1^{1/2} \mathbf{S}_2 \mathbf{S}_1^{1/2}) - 2(\mathbf{S}_1^{1/2} \mathbf{T}_2 \mathbf{S}_1^{1/2})^{1/2}$ results in $\mathbf{S}_1^{-1/2} (\tilde{\mathbf{C}} - 2\tilde{\mathbf{K}}^{1/2}) \mathbf{S}_1^{1/2}$, which is a similarity transform on $(\tilde{\mathbf{C}} - 2\tilde{\mathbf{K}}^{1/2})$. Since similarity transforms preserve eigenvalues, definiteness properties can be expressed in terms of eigenvalues of matrices involving \mathbf{M} , \mathbf{C} , and \mathbf{K} . Conditions 4 to 6 can now be expressed as follows:

- (1) If $2(\mathbf{M}^{-1} \mathbf{K})^{1/2} = \mathbf{M}^{-1} \mathbf{C}$, the system must be critically damped.
- (2) If $[2(\mathbf{M}^{-1} \mathbf{K})^{1/2} - \mathbf{M}^{-1} \mathbf{C}]$ has its eigenvalues all positive then the system must be underdamped.
- (3) If $[\mathbf{M}^{-1} \mathbf{C} - 2(\mathbf{M}^{-1} \mathbf{K})_{\max}^{1/2} \mathbf{I}_n]$ has its eigenvalues all positive then the system must be overdamped.

Here $(\mathbf{M}^{-1} \mathbf{K})_{\max}$ represents the maximum eigenvalue of $(\mathbf{M}^{-1} \mathbf{K})$. Once again, the first two conditions presented here are identical to those by Ahmadian et al. (1984). The condition for overdamping presented there is based on definiteness of $[\mathbf{M}^{-1} \mathbf{C} - 2(\mathbf{M}^{-1} \mathbf{K})^{1/2} \mathbf{I}_n]$ which is incorrect and is consequently modified here. Again, counter-examples can be constructed for the cases of overdamping and mixed damping (Bhaskar 1992).

4 The Damping-Ratio Matrix

Analogy with a single-degree-of-freedom system suggests that the scalar quantity damping ratio could possibly be replaced by a matrix for a multi-degree-of-freedom system. An attempt of this can be found in Inman et al. (1987, 1989). A single matrix takes the role of damping ratios there and definiteness of the difference between this matrix and the identity matrix determines criticality for the system. However, we observe that the development of this matrix assumes the results of Inman et al. (1980), and consequently derives erroneous conclusions. In the following discussion, new results are presented in this light.

The damping ratio matrix \mathbf{Z} is defined as

$$\mathbf{Z} = \mathbf{C}_c^{-1/2} \tilde{\mathbf{C}} \mathbf{C}_c^{-1/2} \quad (10)$$

which is exactly the same as the definition presented by Inman (1989). The sufficient conditions of criticality, presented there, are in terms of definiteness of $(\mathbf{I}_n - \mathbf{Z})$. As expected, the conditions for overdamping and mixed damping are incorrect there. The sufficient conditions for criticality presented in the Section 2 and Section 3 can now be expressed in terms of the damping ratio matrix \mathbf{Z} as follows:

- (1) If $(\mathbf{I}_n - \mathbf{Z}) = \mathbf{0}$ then the system must be critically damped.
- (2) If the matrix $(\mathbf{I}_n - \mathbf{Z})$ is positive definite then the system must be underdamped.
- (3) If $\{\mathbf{Z} - \text{diag}(\Lambda_{\max}/\Lambda_{ii})^{1/2}\}$ is positive definite then the system must be overdamped.

5 Application of the Theorems on Eigenvalue Bounds

Some useful information can be derived by mere inspection of the terms on the diagonal of the matrix $(2\Lambda^{1/2} - \tilde{\mathbf{C}})$ and $(\tilde{\mathbf{C}} - 2\Lambda_{\max}^{1/2} \mathbf{I}_n)$. It turns out that if entries on the diagonal of $(2\Lambda^{1/2} - \tilde{\mathbf{C}})$ are all positive and if, it is diagonally dominant, then the system must be underdamped. Similarly, if the entries on the diagonal of $(\tilde{\mathbf{C}} - 2\Lambda_{\max}^{1/2} \mathbf{I}_n)$ are all positive and if, it is diagonally dominant, then the system must be overdamped. These results follow immediately by applying the well-known Gerschgorin's theorems (1931). In this section, \mathbf{A} denotes the matrix $(2\Lambda^{1/2} - \tilde{\mathbf{C}})$ which is a real and symmetric matrix.

Given that the entries on the diagonal of the matrix \mathbf{A} are all positive, it can be concluded that if the centers of the Gerschgorin discs fall on the positive real axis, and if \mathbf{A} is diagonally dominant, then none of the disks fall in the left half of the complex plane. Therefore, all the eigenvalues of \mathbf{A} must be in the right half of the complex plane. Hence the matrix \mathbf{A} must be positive definite, which is sufficient for underdamping of the system. On similar lines it could be shown that if another matrix say $\mathbf{B} = (\tilde{\mathbf{C}} - 2\Lambda_{\max}^{1/2} \mathbf{I}_n)$ is diagonally dominant and if, all the entries on its diagonal are positive, then the system must be overdamped. It is noted that all of these conditions are only sufficient but not necessary.

Conditions of the previous theorem may become stringent at times and a further refinement is possible using the following theorem due to Brauer (1946, 1947).

Theorem 1 (Brauer). Every eigenvalue of a matrix \mathbf{A} lies in the interior or on the boundary of at least one of the following $\frac{1}{2}n(n-1)$ Cassini ovals on the complex z -plane

$$|z - A_{ii}| |z - A_{jj}| \leq \sum_r |A_{ir}| \sum_s |A_{js}|, \quad i \neq j. \quad (11)$$

The proof can be found in Brauer (1946, 1947). The above condition may appear to be complicated, but a simple extension of the conclusions reached earlier on the basis of Gerschgorin's theorem can be obtained. For a real matrix (which is the case), the ovals must be symmetric about the real axis and about the line $x = (A_{ii} + A_{jj})/2$. The ovals for this situation intersect the real axis and satisfy $(x - A_{ii})(x - A_{jj}) = \sigma_i \sigma_j$ at the points of intersection on the x -axis, where $\sigma_i = \sum_{r=1}^{n-1} |A_{ir}|$. Solving the quadratic, the following roots are obtained:

$$x_{1,2} = (A_{ii} + A_{jj}) \pm (1/2) \sqrt{(A_{ii} - A_{jj})^2 + 4\sigma_i \sigma_j}. \quad (12)$$

Note that the discriminant is always positive, which is expected since the roots must remain real. In order that the ovals remain in the right half of the complex plane, both x_1 and x_2 must be positive, i.e. $(A_{ii} + A_{jj})^2 \geq (A_{ii} - A_{jj})^2 + 4\sigma_i \sigma_j$. Rearranging this inequality leads to

$$(A_{ii}/\sigma_i)(A_{jj}/\sigma_j) \geq 1, \quad \text{for all } i, j. \quad (13)$$

This result was obtained for general Hermitian matrices in Brauer (1947). It also follows from a more general theorem for complex matrices given in Brauer (1946). Here a simplified result is presented for the case of general real matrices (which may *not* necessarily be symmetric and hence not Hermitian). It should be noted that for asymmetric *real* matrices, Cassini ovals are symmetric about the real axis. The asymmetric formulation of Section 3 then allows us to apply these results to symmetrizable systems also.

Clearly, the condition in the inequality (13) is more relaxed than the one obtained through Gerschgorin's theorem, since whenever the latter is satisfied (i.e., diagonal dominance is observed), (13) is automatically satisfied. Inequality (13) allows the violation of dominance by at the most one row (or column). All that one needs to check is whether product of the smallest and the next smallest of the numbers (A_{ii}/σ_i) exceeds unity. When \mathbf{A} is replaced by $(2\Lambda^{1/2} - \bar{\mathbf{C}})$ in the previous discussion of this section, inequality (13) provides a sufficient condition for underdamping. Similarly, when $(\bar{\mathbf{C}} - 2\Lambda_{\max}^{1/2} \mathbf{I}_n)$ replaces \mathbf{A} , a sufficient condition for overdamping is obtained.

6 Coupling of Single-Degree-of-Freedom Oscillators

Consider a collection of single-degree-of-freedom oscillators, each of which is critically damped. These oscillators are then coupled through dashpots such that the mass elements only are connected through these new dashpots while the spring and the dashpots of the originally uncoupled oscillators remain grounded. If the statements of Ahmadian (1984), Inman et al. (1980, 1989) regarding overdamping were correct, it would imply that, coupling these individual oscillators via additional dashpot elements would *always* result in an overdamped system for any positive damping. This follows from the fact that in the equations of motion for the coupled system, the mass and stiffness matrices are diagonal and the damping matrix is such that $(\bar{\mathbf{C}} - 2\Lambda^{1/2})$ has terms on its diagonal greater than the sum of the absolute values of the terms off the diagonal. Applying Gerschgorin's theorem it is observed that none of the eigenvalues of $(\bar{\mathbf{C}} - 2\Lambda^{1/2})$ fall in the left half of the complex plane. This, as seen earlier, does not guarantee overdamping. Thus a collection of *overdamped oscillators may, in fact, exhibit underdamped modes when coupled through additional dashpot elements!* However, the condition of overdamping presented in this paper, offers a class of overdamped oscillators, which when coupled through further dashpot elements remain overdamped. This is expressed through the following lemma.

Lemma 1 *If each of the oscillators in a collection of single-degree-of-freedom oscillators with mass, dashpot constant, and stiffness for the i th oscillator as m_i , c_i and k_i is overdamped in such a way, that $(c_i/m_i) \geq \max_r 2(k_r/m_r)^{1/2}$ for all i , then coupling the oscillators with further dashpots of any arbitrary values always produces a coupled system which is overdamped.*

To prove this, consider a collection of n single-degree-of-freedom oscillators with mass, stiffness and dashpot constants as m_i , k_i and c_i associated to the i th oscillator. Since each of these is overdamped in the manner described above, we have

$$(c_i/m_i) - 2 \max_r (k_r/m_r)^{1/2} \geq 0 \quad \text{for all } i. \quad (14)$$

The dashpot connecting i th oscillator to the j th one is denoted by the dashpot constant equal to c_{ij} . Premultiplying by inverse of the mass matrix, elements of the matrix $(\bar{\mathbf{C}} - 2\mathbf{K}_{\max}^{1/2} \mathbf{I}_n)$ on its diagonal are obtained as

$$\bar{C}_{ii} - 2\mathbf{K}_{\max}^{1/2} = [c_i + \sum_{j=1}^n c_{ij}/m_i] - \max_r 2(k_r/m_r)^{1/2} \quad (15)$$

and those off the diagonal on the i th row and j th column as

$$\bar{C}_{ij} = -c_{ij}/m_i \quad \text{when } i \neq j. \quad (16)$$

Note that Eq. (16) is not symmetric in i and j so that $(\bar{\mathbf{C}} - 2\mathbf{K}_{\max}^{1/2} \mathbf{I}_n)$ is not symmetric. The conditions of symmetrizability of Section 3 are satisfied by the present class of systems since each of the matrices $\bar{\mathbf{C}}$ and \mathbf{K} have a common symmetric factor, viz. inverse of the mass matrix (which is diagonal). Since \mathbf{M} and \mathbf{K} are diagonal matrices, $(\mathbf{M}^{-1}\mathbf{K})_{\max} = \max_r (k_r/m_r)$ is the maximum eigenvalue of $(\mathbf{M}^{-1}\mathbf{K})$. Using conditions of Eq. (14); Eqs. (15) and (16) imply that $(\bar{\mathbf{C}} - 2\mathbf{K}_{\max}^{1/2} \mathbf{I}_n)$ is diagonally dominant. Using Gerschgorin's theorem and the conditions of overdamping stated in Section 3.1, it is concluded that the system must be overdamped. Two further special cases arise: *If a collection of overdamped oscillators is such that the ratio of stiffness to inertia or the ratio of dashpot constant to inertia is the same for each one of them, then coupling these oscillators with dashpots of any arbitrary value always results in an overdamped system.*

Application of Brauer's theorem, using Cassini-ovals as the basis for choosing regions of eigenvalue bounds, results in a more liberal condition. It could be shown after some algebra that the coupled system is overdamped if

$$(1 + \delta_i/\sigma_i)(1 + \delta_j/\sigma_j) \geq 1, \quad \text{for all } i, j \quad (17)$$

where, $\delta_i = [c_i/m_i - \max_r 2(k_r/m_r)^{1/2}]$, and $\sigma_i = \sum_{j=1}^{n'} c_{ij}$. It is easy to see that, inequality (17) always holds if the condition of Lemma 1 holds since δ_i is always positive for all i when the latter is satisfied.

Consider coupling the *underdamped* oscillators next. On the lines of Eqs. (15) and (16), elements of $2\mathbf{K}^{1/2} - \bar{\mathbf{C}}^{1/2}$ are given by

$$2\bar{K}_{ii}^{1/2} - \bar{C}_{ii} = 2(k_i/m_i)^{1/2} - [c_i + \sum_{j=1}^{n'} c_{ij}/m_i] \quad (18)$$

and

$$2\bar{K}_{ij}^{1/2} - \bar{C}_{ij} = c_{ij}/m_i, \quad i \neq j. \quad (19)$$

It could be seen in this instance that, if $2(k_i/m_i)^{1/2} - (c_i/m_i) > 2(\sum_{j=1}^{n'} c_{ij})/m_i$ then, the matrix $(2\mathbf{K}^{1/2} - \bar{\mathbf{C}}^{1/2})$ is diagonally dominant and has positive numbers on its diagonal. Hence $(2\mathbf{K}^{1/2} - \bar{\mathbf{C}}^{1/2})$ is positive definite. This leads to the following result.

Lemma 2 *If a collection of underdamped single-degree-of-freedom oscillators having mass, stiffness, and dashpot constant associated with the i th oscillator equal to m_i , k_i and c_i respectively, is connected through additional dashpots of constant c_{ij} that connect the i th oscillator to the j th one and which satisfy $2(k_i/m_i)^{1/2} - (c_i/m_i) > 2(\sum_{j=1}^{n'} c_{ij})/m_i$ then connecting the oscillators through such additional dampers always produces an underdamped system.*

Cassini-ovals can still relax the condition but they yield to a cumbersome result and thus it is omitted from the present discussion.

7 Conclusions

A set of sufficient conditions was presented for criticality in terms of matrices involved in the governing equations of motion, when they are expressed in the modal coordinates. This was later extended to the case of general asymmetric (but symmetrizable) systems. Similar conditions available in the literature for the cases of overdamping and mixed damping were found to be incorrect. This was shown through some counterexamples. The theorems on eigenvalue bounds were applied to infer criticality of a multi-degree-of-freedom system. This may lead to computational saving in practical applications. Two cases when underdamped oscillators remain underdamped, when coupled through additional dampers, and when overdamped oscillators remain overdamped, when coupled through

similar elements were discussed in the perspective of the sufficient conditions presented here. It is emphasized that all these conditions are only sufficient but not necessary. However, when the equations of motion decouple (i.e., when damping is classical), they become both necessary and sufficient.

Acknowledgments

I thank Dr. H. E. M. Hunt, Prof. D. E. Newland, and Dr. J. Woodhouse for numerous helpful discussions. Comments of an anonymous referee are gratefully acknowledged.

References

- Ahmadian, M., and Inman, D. J., 1984, "On the Nature of Eigenvalues of General Nonconservative Systems," *ASME JOURNAL OF APPLIED MECHANICS*, Vol. 51, pp. 193–194.
- Barkwell, L., and Lancaster, P., 1992, "Overdamped and Gyroscopic Vibrating Systems," *ASME JOURNAL OF APPLIED MECHANICS*, Vol. 59, pp. 176–181.
- Bellman, R., 1968, "Some Inequalities for the Square Root of a Positive Definite Matrix," *Linear Algebra and Its Applications*, Vol. 1, pp. 321–324.
- Bhaskar, A., 1991, Chapter 2 of Dissertation submitted to Trinity College, Cambridge, U.K., for the annual fellowship competition.
- Bhaskar, A., 1992, "Damping in Mechanical Vibrations: New Methods of Analysis and Estimation," Chapter 2 of Ph.D. thesis submitted to Cambridge University, Cambridge, U.K.
- Brauer, A., 1946, "Limits for the Characteristic Roots of a Matrix I," *Duke Mathematical Journal*, Vol. 13, pp. 387–395.
- Brauer, A., 1947, "Limits for the Characteristic Roots of a Matrix II," *Duke Mathematical Journal*, Vol. 14, pp. 21–26.
- Caughey, T. K., and O'Kelly, M. E. J., 1965, "Classical Normal Modes in Damped Linear Dynamic Systems," *ASME JOURNAL OF APPLIED MECHANICS*, Vol. 32, pp. 583–588.
- Duffin, R. J., 1955, "A Minimax Theory for Overdamped Networks," *Journal of Rational Mechanics and Analysis*, Vol. 4, pp. 221–233.
- Gerschgorin, S., 1931, "Über die Abgrenzung der Eigenwerte einer Matrix," *Izv. Akad. Nauk. SSSR, Ser. Fiz.-mat.*, Vol. 6, pp. 749–754.
- Gray, J. A., and Andry, A. N., 1982, "A simple Calculation of Critical Damping Matrix of a Linear Multi-degree-of-freedom System," *Mechanics Research Communications*, Vol. 9, No. 6, pp. 379–380.
- Inman, D. J., 1983, "Dynamics of Asymmetric Nonconservative Systems," *ASME JOURNAL OF APPLIED MECHANICS*, Vol. 50, pp. 199–203.
- Inman, D. J., and Andry, A. N., 1980, "Some Results on the Nature of Eigenvalues of Discrete Damped Linear Systems," *ASME JOURNAL OF APPLIED MECHANICS*, Vol. 47, pp. 927–930.
- Inman, D. J., 1989, *Vibration with Control, Measurement and Stability*, Prentice-Hall Int., Inc.
- Inman, D. J., and Jiang, B. L., 1987, "On Damping Ratios for Multiple-degree-of-freedom Linear Systems," *International Journal of Analytical & Experimental Modal Analysis*, Vol. 2, pp. 38–42.
- Inman, D. J., and Orabi, I., 1983, "An Efficient Method for Computing the Critical Damping Condition," *ASME JOURNAL OF APPLIED MECHANICS*, Vol. 50, pp. 679–682.
- Inman, D. J., and Andry, A. N., 1982, "A Procedure for Designing Overdamped Lumped Parameter Systems," *Shock and Vibration Bulletin*, Vol. 52, No. 5, pp. 49–53.
- Inman, D. J., 1982a, "Oscillatory Damped Distributed Systems," *Mechanics Research Communications*, Vol. 9, No. 2, pp. 101–107.
- Inman, D. J., and Andry, A. N., 1982b, "The Nature of Temporal Solutions of Damped Distributed Systems with Classical Normal Modes," *ASME JOURNAL OF APPLIED MECHANICS*, Vol. 49, pp. 867–870.
- Liang, Z., and Soong, T. T., 1988, "Bounds on Harmonically Forced Linear Systems," *ASME JOURNAL OF APPLIED MECHANICS*, Vol. 55, pp. 988–990.
- Meirovitch, L., 1975, *Elements of Vibration Analysis*, McGraw-Hill, New York.
- Muller, P. C., 1979, "Oscillatory Damped Systems," *Mechanics Research Communications*, Vol. 6, No. 2, pp. 81–85.
- Newland, D. E., 1989, *Mechanical Vibration Analysis and Computation*, Longman, Harlow, and John Wiley, New York.
- Nicholson, D. W., 1978, "Eigenvalue Bounds for Damped Linear Systems," *Mechanics Research Communications*, Vol. 5, No. 3, pp. 147–152.
- Nicholson, D. W., 1983, "Overdamping of a Linear Mechanical System," *Mechanics Research Communications*, Vol. 10, No. 2, pp. 67–76.
- Nicholson, D. W., 1987, "Eigenvalue Bounds for Linear Mechanical Systems with Nonmodal Damping," *Mechanics Research Communications*, Vol. 14, No. 2, pp. 115–122.
- Nicholson, D. W., 1987a, "Response Bounds for Nonclassically Damped Mechanical Systems under Transient Loads," *ASME JOURNAL OF APPLIED MECHANICS*, Vol. 55, pp. 430–433.
- Ross, A. D. S., and Inman, D. J., 1990, "Settling Time of Underdamped Linear Lumped Parameter Systems," *Journal of Sound and Vibration*, Vol. 140, No. 1, pp. 117–127.
- Ulsoy, A. G., 1989, "Utilization of Control Effort Constraints in Linear Controller Design," *ASME Journal of Dynamic Systems, Measurement and Control*, Vol. 111, pp. 378–381.
- Wilkinson, J. H., 1965, *The Algebraic Eigenvalue Problem*, Clarendon Press, Oxford, U.K.

Dynamic Analysis of the Axially Moving String Based on Wave Propagation

C. A. Tan
Associate Professor,
Mem. ASME.

S. Ying
Graduate Research Assistant.

Department of Mechanical Engineering,
Wayne State University,
Detroit, MI 48202

In this paper, we present an exact solution for the linear, transverse response of an axially moving string with general boundary conditions. The solution is derived in the frequency domain and interpreted in terms of wave propagation functions. The boundary effects are included by the use of compliance functions at the boundaries. The response in the time domain involves only several convolution integrals which can easily be obtained for many physical boundary conditions. A comparison of this method with an existing solution method shows that this method requires much less computation time. The transient response of the translating string with a spring or a dashpot at a boundary is presented. It is shown that complete wave absorption occurs at a boundary when that boundary has a dashpot with damping coefficient equal to the propagation speed of the reflected wave.

1 Introduction

Many mechanical devices use a slender, translating element as a means of transmitting power, material, or information. Examples include chain and belt drives, magnetic recording devices, band saws, and paper handling machinery. These structural elements are commonly termed as axially moving materials. The translating string model or the classical moving threadline theory (Swope and Ames, 1963) is the simplest that describes the dynamic response of many axially moving material systems. A literature summary on the vibration and stability of axially moving materials can be found in Wickert and Mote (1988).

The steady-state response of the axially moving string can easily be evaluated by several available techniques such as the modal analysis and Green's function method (Wickert and Mote, 1990) or the transfer function method (Yang and Tan, 1992). However, in many important industrial applications, such as the impact of chain drives during engagement with sprockets (Wang and Liu, 1991) or cables transporting materials (Wickert and Mote, 1991; Zhu and Mote, 1994), the axially moving material is continuously subjected to time-dependent forces and hence no steady-state solution exists for those problems.

Several solution techniques for the string problem have been reported in the literature. The classical D'Alembert's wave solution (Graff, 1975) is derived for an infinite or a semi-infinite nontranslating string. Hence, general boundary conditions cannot be considered in the analysis. Though the Green's function-modal analysis technique proposed by Wickert and Mote (1990) gives an exact solution, it involves a series expansion and, for second-order systems such as the translating string, many terms are needed for the convergence of the solution. Moreover, the method requires the knowledge of the system eigenfunctions and hence cannot be easily extended to systems with general boundary conditions. Nevertheless, the modal analysis technique gives a useful solution to the free and forced response

problems. The method of characteristics, which is useful for solving hyperbolic systems, provides an interesting interpretation of the response in terms of the physical phenomenon of wave propagation. However, it cannot be easily applied to systems with general boundary conditions. With an increasing demand of using axially moving structural elements in high precision machinery, development of vibration control techniques also relies on the availability of relatively simple response solution techniques. Despite the usefulness of the translating string model and the availability of existing solution methods, no simple solution for both the transient response and the active vibration control has been proposed.

The purpose of this paper is to apply the transfer function formulation and the concept of wave propagation (Perkins, 1990; Tan and Zhang, 1994) to derive an exact response solution for the axially moving string under general boundary conditions. The response is easily computed by evaluating several time-convolution integrals. It will be shown that the method does not require a knowledge of the system eigenfunctions and provides physical interpretations of the response in terms of wave propagation. This method has also proven to be useful in the design of active vibration control (Ying and Tan, 1996). In Section 2, the problem formulation is described, and the response of the axially moving string is given in Section 3. Interpretation of the solution in terms of wave propagation functions is provided in Sections 4 and 5. Results for the response of a string with a spring or a dashpot at a boundary are presented in Section 6.

2 Problem Formulation

Figure 1 shows an axially moving string of uniform density ρ and under constant tension P , traveling at a constant transport velocity V between two arbitrary boundaries separated by a distance L . The string is excited transversely by a distributed external force $F(X, T)$. By Hamilton's Principle, the equation of motion governing the transverse displacement $W(X, T)$ is (Archibald and Emslie, 1958)

$$\rho(W_{,TT} + 2VW_{,XT} + V^2W_{,XX}) - PW_{,XX} = F(X, T) \quad (1)$$

where $(\cdot)_{,T}$ denotes $\partial/\partial T(\cdot)$, $(\cdot)_{,X}$ denotes $\partial/\partial X(\cdot)$. Using the following nondimensional variables

Contributed by the Applied Mechanics Division of THE AMERICAN SOCIETY OF MECHANICAL ENGINEERS for publication in the ASME JOURNAL OF APPLIED MECHANICS.

Discussion on the paper should be addressed to the Technical Editor, Professor Lewis T. Wheeler, Department of Mechanical Engineering, University of Houston, Houston, TX 77204-4792, and will be accepted until four months after final publication of the paper itself in the ASME JOURNAL OF APPLIED MECHANICS.

Manuscript received by the ASME Applied Mechanics Division, May 5, 1995; final revision, Oct. 21, 1996; Associate Technical Editor: S. W. Shaw.

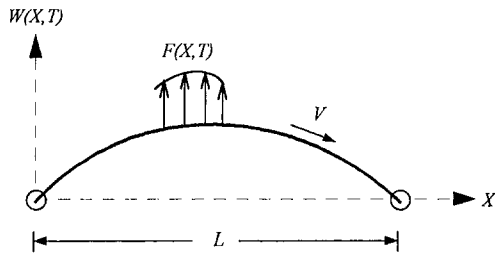


Fig. 1 A schematic of the axially moving string

$$x = \frac{X}{L}, \quad w = \frac{W}{L}, \quad f = \frac{FL}{P},$$

$$t = T\sqrt{\frac{P}{\rho L^2}}, \quad c = V\sqrt{\frac{\rho}{P}} \quad (2)$$

the normalized equation of motion is

$$w_{,tt}(x, t) + 2cw_{,xt}(x, t) - (1 - c^2)w_{,xx}(x, t) = f(x, t),$$

$$x \in (0, 1), \quad t \geq 0. \quad (3)$$

The initial conditions are specified as

$$w(x, t)|_{t=0} = u_0(x), \quad w_t(x, t)|_{t=0} = v_0(x), \quad x \in (0, 1) \quad (4)$$

and the boundary conditions of the string assume the general form

$$Mw(x, t)|_{x=0} = \gamma_{B0}(t), \quad t \geq 0 \quad (5a)$$

and

$$Nw(x, t)|_{x=1} = \gamma_{B1}(t), \quad t \geq 0 \quad (5b)$$

where M and N are second-order temporal-spatial, linear differential operators. When the transport speed exceeds the critical speed, $c \geq c_{cr} = 1$, the system experiences a buckling type of instability (Mote, 1965). In the present study, assume $c < 1$.

The basic wave propagation characteristics in the axially moving string can be understood by considering the homogeneous equation of (3) and introducing the change of variables

$$\zeta = x - (1 + c)t, \quad \eta = x + (1 - c)t. \quad (6)$$

$$G(x, \xi, s) = \begin{cases} \frac{e^{\lambda_2(x-\xi)} + \theta_0(s)e^{\lambda_2x-\lambda_1\xi} + \theta_1(s)e^{\lambda_2(1-\xi)-\lambda_1(1-x)} + \theta_0(s)\theta_1(s)e^{\lambda_2-\lambda_1(1+\xi-x)}}{2s(1 - \theta_0(s)\theta_1(s)e^{\lambda_2-\lambda_1})}, & x \geq \xi \\ \frac{\theta_0(s)e^{\lambda_2x-\lambda_1\xi} + \theta_0(s)\theta_1(s)e^{\lambda_2(1+x-\xi)-\lambda_1} + e^{-\lambda_1(\xi-x)} + \theta_1(s)e^{\lambda_2(1-\xi)-\lambda_1(1-x)}}{2s(1 - \theta_0(s)\theta_1(s)e^{\lambda_2-\lambda_1})}, & x \leq \xi \end{cases} \quad (11a)$$

The homogeneous “wave equation” of (3) then becomes

$$\frac{\partial^2 w(\zeta, \eta)}{\partial \zeta \partial \eta} = 0. \quad (7)$$

Based on the classical D'Alembert's solution for the non-translating string problem (Graff, 1975), the solution of (7), using (6), consists of disturbances propagating to the right at speed $1 + c$ and to the left at speed $1 - c$. These are the forward and backward propagating waves, respectively.

3 Response of the Axially Moving String

The response and spectrum of the axially moving string under specified initial conditions and external disturbances can be determined from the system transfer functions. Evaluation of transfer functions for one-dimensional distributed parameter systems has been presented by Yang and Tan (1992). Accord-

ingly, the Laplace transform of Eqns. (3)–(5) with respect to t gives

$$s^2\bar{w}(x, s) + 2cs\frac{\partial}{\partial x}\bar{w}(x, s) - (1 - c^2)\frac{\partial^2}{\partial x^2}\bar{w}(x, s) = \bar{f}_e(x, s) \quad (8a)$$

$$\bar{f}_e(x, s) = \bar{f}(x, s) + su_0(x) + v_0(x) + 2c\frac{\partial}{\partial x}u_0(x) \quad (8b)$$

$$\bar{M}\bar{w}(x, s)|_{x=0} = A_0(s)\bar{w}(0, s) + B_0(s)\bar{w}_{,x}(0, s) = \bar{\gamma}_{B0} + \bar{\gamma}_{I0} \equiv \bar{\gamma}_{I0}(s) \quad (8c)$$

$$\bar{N}\bar{w}(x, s)|_{x=1} = A_1(s)\bar{w}(1, s) + B_1(s)\bar{w}_{,x}(1, s) = \bar{\gamma}_{B1} + \bar{\gamma}_{I1} \equiv \bar{\gamma}_{I1}(s) \quad (8d)$$

where s is the complex Laplace transform variable, $\bar{w}(\cdot, s)$, $\bar{f}(\cdot, s)$ and $\bar{\gamma}_{Bj}(s)$ are the Laplace transform of $w(\cdot, t)$, $f(\cdot, t)$, and $\gamma_{Bj}(t)$, respectively, and $\bar{\gamma}_{Ij}(s)$ is a polynomial of s representing the initial conditions at the boundaries $x = 0, 1$. Henceforth, the index $j = 0, 1$ is used to denote the left and right boundaries, respectively. \bar{M} and \bar{N} are the operators M and N with their time derivative operators $\partial/\partial t$ and $\partial^2/\partial t^2$ replaced by s and s^2 , respectively.

From (6) and (7), the basic wave solution of the nondispersive string medium is of the form $e^{i(\omega t - kx)}$ where $k = \omega/v_p$ is the wave number and v_p is the phase velocity, or in complex notation, $e^{(st + \lambda x)}$ where λ is a complex wave number. From (8a), the characteristic roots of the homogeneous equation are

$$\lambda_1 = \frac{s}{1 - c}, \quad \lambda_2 = \frac{-s}{1 + c}. \quad (9)$$

Here, λ_1 and λ_2 are the complex wave numbers of the backward and forward propagating waves, respectively.

The exact response solution to (8a-d) is

$$\bar{w}(x, s) = \int_0^1 G(x, \xi, s)\bar{f}_e(\xi, s)d\xi + \sum_{j=0}^1 h_j(x, s)\bar{\gamma}_j(s) \quad (10)$$

where the closed-form transfer function $G(x, \xi, s)$ and the influence functions $h_j(x, s)$ of the translating string can be evaluated explicitly (Yang and Tan, 1992)

and

$$h_0(x, s) = \frac{e^{\lambda_2x} + \theta_1(s)e^{\lambda_2-\lambda_1(1-x)}}{1 - \theta_0(s)\theta_1(s)e^{\lambda_2-\lambda_1}} \quad (11b)$$

$$h_1(x, s) = \frac{e^{-\lambda_1(1-x)} + \theta_0(s)e^{\lambda_2x-\lambda_1}}{1 - \theta_0(s)\theta_1(s)e^{\lambda_2-\lambda_1}}. \quad (11c)$$

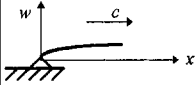
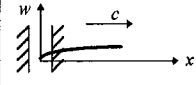
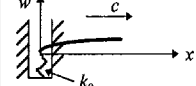
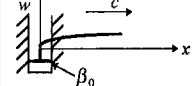
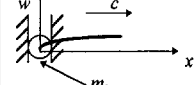
By (10) and (11b-c), the excitations $\bar{\gamma}_j(s)$ are

$$\bar{\gamma}_0(s) = \frac{\bar{\gamma}_{I0}(s)}{A_0(s) + \lambda_2 B_0(s)}, \quad (12a)$$

$$\bar{\gamma}_1(s) = \frac{\bar{\gamma}_{I1}(s)}{A_1(s) + \lambda_1 B_1(s)}. \quad (12b)$$

Note that (12a-b) represent normalizations since a spatial transform of $A_j\bar{w} + B_j\bar{w}_{,x}$ gives $(A_j + \lambda B_j)\bar{w}$, where \bar{w} is the spatial

Table 1 Types of boundary conditions and the corresponding compliance functions

Type	Diagram	Boundary Condition	Compliance Function
Fixed		$w(0, t) = 0$	$Z_0(s) = 0$
Free		$w_{,x}(0, t) = 0$	$Z_0(s) = \infty$
Spring		$k_0 w(0, t) - (1 - c^2) w_{,x}(0, t) = 0$	$Z_0(s) = \frac{-1}{k_0}$
Dashpot		$\beta_0 w_{,t}(0, t) - (1 - c^2) w_{,x}(0, t) = 0$	$Z_0(s) = \frac{-1}{s\beta_0}$
Mass		$m_0 w_{,tt}(0, t) - (1 - c^2) w_{,x}(0, t) = 0$	$Z_0(s) = \frac{-1}{s^2 m_0}$

transform of \bar{w} . Moreover, $\bar{\gamma}_0(s)$ is associated with λ_2 ; agreeing with the physics that only forward propagating waves are generated into the medium from the boundary at $x = 0$. Same reasoning can be applied to (12b). In (11a-c), the complex boundary coefficient functions are

$$\begin{aligned}\theta_0(s) &= -\frac{1 + (1 + c)sZ_0(s)}{1 - (1 - c)sZ_0(s)}, \\ \theta_1(s) &= -\frac{1 + (1 - c)sZ_1(s)}{1 - (1 + c)sZ_1(s)}\end{aligned}\quad (13)$$

where the complex compliance functions (displacement/force) $Z_j(s)$ are defined as

$$\begin{aligned}Z_0(s) &= \frac{-\bar{w}(0, s)}{(1 - c^2)\bar{w}_{,x}(0, s)}, \\ Z_1(s) &= \frac{\bar{w}(1, s)}{(1 - c^2)\bar{w}_{,x}(1, s)}.\end{aligned}\quad (14)$$

It should be noted that the exponential functions in (11a-c) represent delay functions in the time domain. For example, $e^{\lambda_2(x-\xi)}$ is associated with a forward propagating wave traveling from ξ (where the disturbance is applied) to x (where the response is measured). From (11a), the eigenvalues of the axially moving string system can be determined from the characteristic equation

$$1 - \theta_0(s)\theta_1(s)e^{\lambda_2-\lambda_1} = 0. \quad (15)$$

4 Interpretation of the Response in Terms of Wave Propagation

4.1 Type of Boundaries. When a wave is incident at a boundary, the wave is either completely, partially, or not reflected from the boundary. In this formulation, the wave propagation characteristics across a boundary are determined by $\theta_j(s)$. Table 1 lists a set of typical boundary conditions (shown for $x = 0$) and their corresponding compliance functions, where it is assumed that $w_{,x} = 0$ at $x = 0^-$. For the purpose of discussion, consider a backward propagating wave incident at the boundary $x = 0$. The physics of wave propagation at $x = 1$ can be interpreted in a similar manner. As the wave approaches $x = 0$, it is well known that an image (forward propagating) wave is generated such that the specific boundary condition can be satisfied (Graff, 1975). From (10), (11a-c), it can be shown that $\theta_0(s)$ is the displacement ratio of the reflected wave over the incident wave.

Consider the case of a fixed boundary condition at $x = 0$. This is an example of complete wave reflection. From Table 1, $Z_0(s) = 0$. Hence $\theta_0(s) = -1$. This is a well-known result stating that the wave is totally reflected and the signs of the displacements of the incident and reflected waves are opposite. From (15) and for the case of fixed-fixed boundary conditions, the eigenvalues of axially moving string are

$$R_k = ik\pi(1 - c^2), \quad k = \pm 1, \pm 2, \dots, i = \sqrt{-1}. \quad (16)$$

Note that $s = 0$ is not an eigenvalue because $\lim_{s \rightarrow 0} G(x, \xi, s)$ is finite.

Consider a free boundary condition at $x = 0$. This is an example of partial wave reflection. From Table 1, $Z_0(s) = \infty$, and from (13), $\theta_0(s) = (1 + c)/(1 - c)$, stating that the displacement ratio of the reflected wave over the incident wave equals the ratio of the propagation speeds. Note that, in order to satisfy the free end boundary condition $w_{,x}(0, t) = 0$, the displacement of the reflected wave must have the same sign as that of the incident wave.

Consider the boundary condition with a dashpot. From Table 1, $Z_0(s) = (-1/s\beta_0)$ where β_0 is the damping coefficient. The boundary coefficient function is

$$\theta_0(s) = \frac{(1 + c) - \beta_0}{(1 - c) + \beta_0}. \quad (17)$$

It is interesting to note that if $\beta_0 = 1 + c$ (speed of the forward propagating wave), no (forward propagating) wave will be reflected. In other words, the boundary absorbs all the wave energy. This phenomenon is noted by Hull (1994) for the longitudinal vibration problem of a bar with a viscous damper at one end. However, in that problem, both propagation speeds are equal and the conclusion that, for complete wave absorption, β_0 equals the propagation speed of the reflected wave cannot be drawn. It can also be shown that, for the axially moving string problem, the active boundary wave cancellation control (Chung and Tan, 1995) is equivalent to applying a passive

dashpot with the damping coefficient equals to $1 + c$ (if damper located at $x = 0$) or $1 - c$ (if damper located at $x = 1$).

4.2 Response in Terms of Propagation Functions. Based on (11a-c), the following propagation functions of the translating string are defined

$$G_D^+(x, \xi, s) = \frac{1}{2s} [e^{\lambda_2(x-\xi)} + \theta_0(s)e^{\lambda_2x-\lambda_1\xi}], \quad x > \xi \quad (18a)$$

$$G_D^-(x, \xi, s) = \frac{1}{2s} [\theta_1(s)e^{\lambda_2(1-\xi)-\lambda_1(1-x)} + \theta_0(s)\theta_1(s)e^{\lambda_2-\lambda_1(1+\xi-x)}], \quad x > \xi \quad (18b)$$

$$G_U^+(x, \xi, s) = \frac{1}{2s} [\theta_0(s)e^{\lambda_2x-\lambda_1\xi} + \theta_0(s)\theta_1(s)e^{\lambda_2(1+x-\xi)-\lambda_1}], \quad x < \xi \quad (18c)$$

$$G_U^-(x, \xi, s) = \frac{1}{2s} [e^{-\lambda_1(\xi-x)} + \theta_1(s)e^{\lambda_2(1-\xi)-\lambda_1(1-x)}], \quad x < \xi \quad (18d)$$

$$H_0^+(x, s) = e^{\lambda_2x} \quad (19a)$$

$$H_0^-(x, s) = \theta_1(s)e^{\lambda_2-\lambda_1(1-x)} \quad (19b)$$

$$H_1^+(x, s) = \theta_0(s)e^{\lambda_2x-\lambda_1} \quad (19c)$$

$$H_1^-(x, s) = e^{-\lambda_1(1-x)}. \quad (19d)$$

The G propagation functions represent wave disturbances in response to both external excitations and initial conditions, while the H propagation functions are wave disturbances in response to boundary excitations. Understanding the physical phenomena associated with these propagation functions is crucial to the dynamic analysis of the translating string system. Define the region to the right (left) of the applied force as downstream (upstream). In (18a-d), the subscripts D and U denote the downstream and upstream positions, respectively, while superscripts $+$ and $-$ denote the forward and backward directions of wave propagation, respectively. Moreover, the subscripts 0 and 1 in (19a-d) denote the boundaries at $x = 0$, 1 respectively. Using the G and H propagation functions, the transverse response of axially moving string is expressed as

$$\begin{aligned} \bar{w}(x, s) = & \theta_0(s)\theta_1(s)e^{\lambda_2-\lambda_1}\bar{w}(x, s) \\ & + \int_0^x [G_D^+(x, \xi, s) + G_D^-(x, \xi, s)]\bar{f}_e(\xi, s)d\xi \\ & + \int_x^1 [G_U^+(x, \xi, s) + G_U^-(x, \xi, s)]\bar{f}_e(\xi, s)d\xi \\ & + \sum_{j=0}^1 [H_j^+(x, s) + H_j^-(x, s)]\bar{\gamma}_j(s). \quad (20) \end{aligned}$$

In view of (20), the response consists of a resident wave (the first term) and propagating waves due to external excitations, initial conditions, and boundary conditions.

Consider the response to a unit impulse applied at ξ , under zero initial conditions and homogeneous boundary conditions. From (20)

$$\begin{aligned} \bar{w}(x, s) = & \theta_0(s)\theta_1(s)e^{\lambda_2-\lambda_1}\bar{w}(x, s) \\ & + [G_D^+(x, \xi, s) + G_D^-(x, \xi, s)], \quad x > \xi \quad (21a) \end{aligned}$$

$$\begin{aligned} \bar{w}(x, s) = & \theta_0(s)\theta_1(s)e^{\lambda_2-\lambda_1}\bar{w}(x, s) \\ & + [G_U^+(x, \xi, s) + G_U^-(x, \xi, s)], \quad x < \xi. \quad (21b) \end{aligned}$$

The G propagation functions are thus unit impulse response functions, which are time-delayed Heaviside functions in the time domain. In response to the applied impulse, $G_D^+(x, \xi, s)$

represents the propagation of the forward wave in the downstream region. From (18a), it is easy to see that $G_D^+(x, \xi, s)$ consists of a forward wave propagating directly from the applied source (the first term) and a forward wave which is reflected from the boundary $x = 0$ (the second term). This is illustrated in (a) and (b) of Table 2. Similarly, $G_D^-(x, \xi, s)$ represents the propagation of the backward wave in the downstream region. It consists of a backward wave reflected from $x = 1$ (the first term) and a backward wave propagating directly from the source and reflected from both boundaries (the second term); see (c) and (d) of Table 2. Similar physical meanings can be derived for G_U^+ , G_U^- and H propagation functions. The term $\theta_0(s)\theta_1(s)e^{\lambda_2-\lambda_1}\bar{w}(x, s)$ involves boundary coefficient functions and a delayed function. The inverse Laplace transform of this term gives $w_{01}(x, t - t_{d1})$ where $w_{01}(x, t - t_{d1})$ is the inverse Laplace transform of $\theta_0(s)\theta_1(s)\bar{w}(x, s)$ and the total time delay $t_{d1} = (1/(1+c)) + (1/(1-c))$ is the time required for a wave to propagate from the location x , reflected by both boundaries (separated by a distance $l = 1$), and back to x .

5 Construction of Propagation Functions Based on Wave Propagation

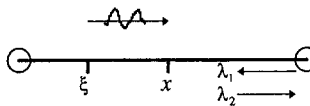
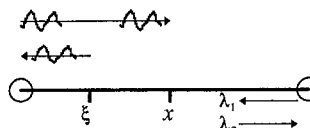
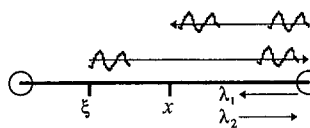
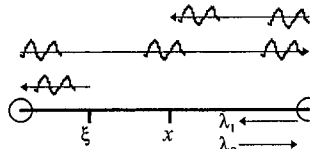
The representation of the response solution by (20) is based on consideration of physical phenomena (wave propagation). Hence the transverse response of the translating string system can be obtained once the propagation functions are constructed and there is no need to determine the system transfer functions. In this section, it is demonstrated how the wave propagation concept can be applied to construct the propagation functions. For the purpose of discussion, only the G functions for $x > \xi$ (see Table 2), i.e., G_D^+ and G_D^- , are considered. Construction of G functions for $\xi > x$ can be done in a similar manner.

Apply an external excitation at ξ . According to the classical D'Alembert's solution of the wave Eq. (3), the source produces two waves: one propagates along the translating string in the forward direction at speed $1 + c$ and the other propagates in the backward direction at speed $1 - c$. If a sensor is placed at position x , only four components of propagating waves will be measured between the time the excitation is applied and a time t_d later. These basic waves are illustrated in Table 2: (a) a forward wave propagating directly from the source at ξ to x , (b) a backward wave emanating from ξ is reflected from the left boundary and propagates forward to x , (c) a forward wave emanating from ξ is reflected from the right boundary and propagates back to x , (d) a backward wave emanating from ξ is reflected from both boundaries and then propagates backward to x . Each wave component can be expressed by a time delay function. For example, the wave component (a) involves a delay function $e^{\lambda_2(x-\xi)}$. The time delay t_d is given by

$$t_d = \frac{x - \xi}{1 + c} \quad (22)$$

since the distance and speed of wave propagation are $x - \xi$ and $1 + c$, respectively. The delay function $e^{\lambda_2(x-\xi)} = e^{-(x-\xi)/(1+c)s} = e^{-t_d s}$ corresponds to a forward wave and hence is part of G_D^+ in (18a). However, since the effect of an excitation is convoluted in the time domain, the time delay function should be multiplied by a factor $1/s$. (Note that the inverse Laplace transform of $(e - t_d s/s)$ is $\mathcal{H}(t - t_d)$, where $\mathcal{H}(\cdot)$ is the Heaviside function.) In addition, the strength of the excitation is split between the forward and backward propagating waves. This is indicated by the factor $\frac{1}{2}$ in (18a). Three of the basic waves illustrated in Table 2 are reflected from one or both boundaries. Each time a reflection occurs, the delay function is multiplied by $\theta_j(s)$. Based on the above discussion, the G propagation functions shown in (18a-d) can be constructed without reverting to the transfer function formulation.

Table 2 Interpretation of wave propagation functions ($x > \xi$ case)

Type	Components of Propagation Functions	Wave Propagation Phenomena
(a)	$e^{\lambda_2(x-\xi)}$	
(b)	$\theta_0(s)e^{\lambda_2x-\lambda_1\xi}$	
(c)	$\theta_1(s)e^{\lambda_2(1-\xi)-\lambda_1(1-x)}$	
(d)	$\theta_0(s)\theta_1(s)e^{\lambda_2-\lambda_1(1+\xi-x)}$	

The propagation functions H can be constructed by applying similar ideas. In either case of $x > \xi$ or $\xi > x$, there are only two basic wave components. Moreover, since the source comes from the boundary, no incident wave is considered at that boundary. Consider an excitation at $x = 0$ and a sensor placed at the position x . Two components of propagating waves will be measured between the time the excitation is applied and a time t_d later. They are (a) a forward wave propagating directly from the source to x , (b) a wave emanating from the source is reflected from the right boundary and propagates backward to x .

In summary, the propagation functions can be constructed based on following steps:

- 1 find λ_1, λ_2 , the complex wave numbers of the backward and forward waves, respectively;
- 2 determine the time delay t_d of each component of the delay functions;
- 3 determine the compliance functions $Z_j(s)$ based on the physical boundary conditions;
- 4 establish the complex boundary coefficient functions $\theta_j(s)$ based on λ_1, λ_2 and $Z_j(s)$; and
- 5 construct the propagation functions as a sum of appropriate delay functions.

By step 1, it is noted that this method is suitable for other hyperbolic systems with general boundary conditions. If the

system is nondispersive, the exponential functions, say $e^{\lambda_2(x-\xi)}$, can easily be inverted as time delay functions, and evaluation of the transient response poses no major difficulty. For dispersive systems, the analysis procedure outlined is still valid. However, the Laplace inversion does not lead to simple time-delay properties, and numerical inversion of (20) is required for the system response.

6 Examples and Results

Two sets of boundary conditions are considered to determine the exact transient response of the axially moving string by the present method. In all simulations, the left boundary is fixed and the right boundary is either spring-loaded (which becomes fixed when $k_1 \rightarrow \infty$) or has a dashpot. All computations were conducted using MATLAB® on a Sun Sparc 690MP Workstation. The transport speed c is chosen to be 0.3. An external force of a half-cycle sinusoidal impulse is applied at $d = 0.5$

$$f(x, t) = \delta(x - d)[\mathcal{H}(t) - \mathcal{H}(t - 0.125)](16\pi \cos 8\pi t) \quad (23)$$

The response in time domain can easily be derived from the results in the frequency domain. From (20), assuming zero initial conditions and homogeneous boundary conditions, the response to the point force (23) is

$$\begin{aligned} \bar{w}(x, s)(1 - \theta_0(s)\theta_1(s)e^{(\lambda_2-\lambda_1)}) \\ = \begin{cases} \left[\frac{e^{\lambda_2(x-d)} + \theta_0(s)e^{\lambda_2x-\lambda_1d} + \theta_1(s)e^{\lambda_2(1-d)-\lambda_1(1-x)} + \theta_0(s)\theta_1(s)e^{\lambda_2-\lambda_1(1+d-x)}}{2s} \right] \bar{f}_0(s), & d \leq x \\ \left[\frac{\theta_0(s)e^{\lambda_2x-\lambda_1d} + \theta_0(s)\theta_1(s)e^{\lambda_2(1+x-d)-\lambda_1} + e^{-\lambda_1(d-x)} + \theta_1(s)e^{\lambda_2(1-d)-\lambda_1(1-x)}}{2s} \right] \bar{f}_0(s), & x \leq d \end{cases} \quad (24) \end{aligned}$$

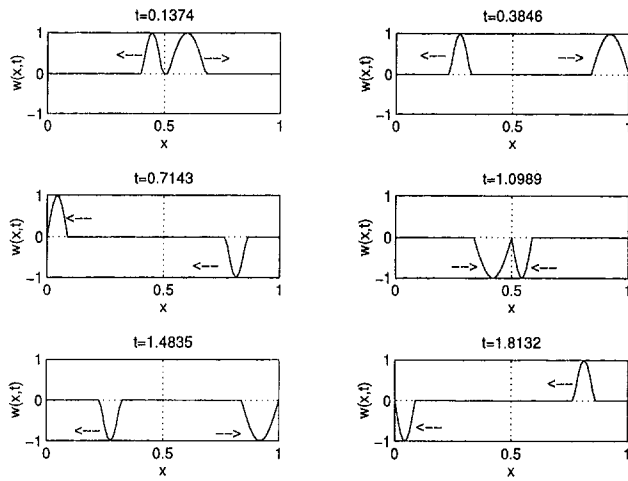


Fig. 2 Transient response of the axially moving string with fixed-fixed boundary conditions. Arrows indicate directions of wave propagation.

where

$$\bar{f}(x, s) = \delta(x - d) \bar{f}_0(s). \quad (25)$$

The exact response at any instant is obtained by inverting (24), which is straightforward, especially for the boundary conditions considered here. To see this, consider the second term on the right-hand side of (24) for $x \geq d$

$$e^{\lambda_2 x - \lambda_1 d} = e^{-(x/(1+c) + (d/(1-c)))s}. \quad (26)$$

The response in the time domain is then a delayed convolution of the excitation and $\theta_0(s)$ with the time delay $t_d = x/(1+c) + d/(1-c)$.

Figure 2 shows the wave propagation in the axially moving string with fixed-fixed boundaries. In this case, the boundary coefficient functions $\theta_0(s)$, $\theta_1(s)$ are -1 . It is readily seen that the speed of the forward wave is faster than the speed of the backward wave. Moreover, it is clearly seen that the reflected waves from the boundaries have the same shapes as the incident waves. To verify the usefulness of this solution, a comparison on the computation efficiency of this method with the modal analysis method (Wickert and Mote, 1990) was made for this problem, with 80 divisions in the x -domain. The string response was calculated for 150 time instants between $t = 0$ and $t = 0.206$. It was found that about 200 terms were needed in the modal analysis expansion series for close agreement with the exact solution. Moreover, our method required only 20 seconds of CPU time, while it took about 130 minutes using the modal analysis method with 200 terms in the expansion series. It should be noted that the computation time using the modal analysis method can be reduced if a closed-form expression of the Green's function or a table look-up method is used.

Figure 3 shows the wave propagation in the axially moving string with the right boundary supported by a spring ($k_1 = 5$). The wave incident at the spring boundary ($x = 1$) undergoes considerable distortion during the reflection process.

Figure 4 shows the exact response when the right boundary is supported by a dashpot. From (24), the exact response for this case is

$$\begin{aligned} w(x, t) &= \theta_0 \theta_1 w(x, t - t_d) + F(t - t_1) + \theta_0 F(t - t_2) \\ &\quad + \theta_1 F(t - t_3) + \theta_0 \theta_1 F(t - t_4), \quad d < x \\ w(x, t) &= \theta_0 \theta_1 w(x, t - t_d) + F(t - t_5) + \theta_0 F(t - t_6) \\ &\quad + \theta_1 F(t - t_7) + \theta_0 \theta_1 F(t - t_8), \quad d > x \end{aligned} \quad (27)$$

where $\theta_0(s) = -1$, $\theta_1(s) = ((1-c) - \beta_1)/((1+c) + \beta_1)$, are constants, and

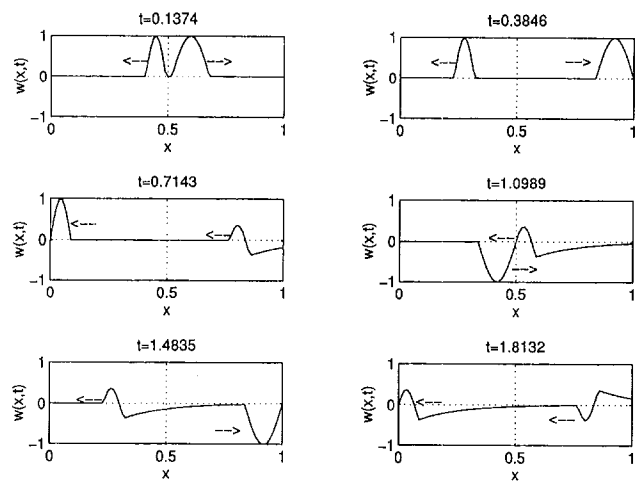


Fig. 3 Transient response of the axially moving string; the left boundary is fixed and the right boundary is spring-loaded. Arrows indicate directions of wave propagation.

$$F(t) = 2[\mathcal{H}(t) - \mathcal{H}(t - 0.125)] \sin(8\pi t) \quad (28a)$$

$$t_1 = \frac{x-d}{1+c}, \quad t_2 = \frac{x}{1+c} + \frac{d}{1-c},$$

$$t_3 = \frac{1-d}{1+c} + \frac{1-x}{1-c}, \quad t_4 = \frac{1}{1+c} + \frac{1+d-x}{1-c}$$

$$t_5 = \frac{d-x}{1-c}, \quad t_6 = \frac{x}{1+c} + \frac{d}{1-c},$$

$$t_7 = \frac{1-d}{1+c} + \frac{1-x}{1-c}, \quad t_8 = \frac{1+x-d}{1+c} + \frac{1}{1-c}. \quad (28b)$$

As we have discussed earlier, if the damping coefficient is chosen to be the speed of the reflected wave ($\beta_1 = 1 - c$ in this case), no wave can be reflected and the right boundary absorbs all the wave energy. This phenomenon is clearly illustrated in Fig. 4. Note that if the fixed boundary at $x = 0$ is replaced by a dashpot, then $\theta_0(s)$ is given by (17), which is again a constant. Hence, the solution in this case is also given by (27). It should be emphasized that the response solution (27) (or the general solution (20)) is valid for all time $t > 0$.

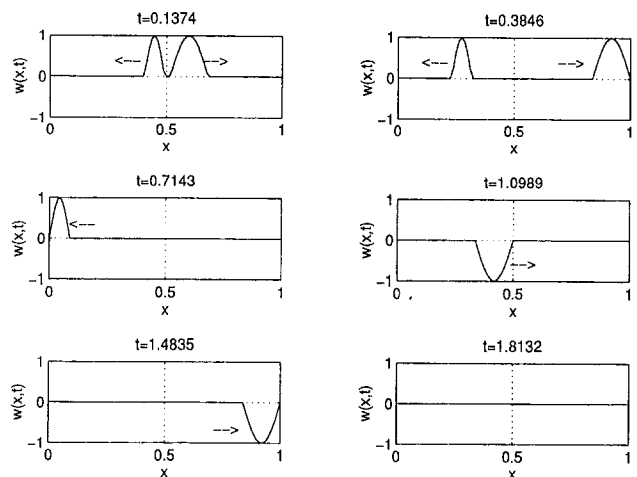


Fig. 4 Transient response of the axially moving string; the left boundary is fixed and the right boundary has a dashpot with damping coefficient equal to the backward propagation speed. Arrows indicate directions of wave propagation.

7 Conclusions

In this paper, the exact response of an axially moving string is presented based on wave propagation concept. In particular, the response solution may be expressed in terms of wave propagation functions which can be obtained by merely considering the wave propagation in the translating string. The response in the time domain is given in terms of the convolution of time-delayed excitation and boundary coefficient functions. The solution method has several important features: (i) it can include general boundary conditions; (ii) it does not require a knowledge of the system eigenfunctions; (iii) it requires much less computation time compared to the modal analysis method; (iv) it provides a physical interpretation of the response in terms of wave propagation. The formulation and numerical simulations indicate that complete wave absorption at a boundary occurs when the boundary has a dashpot with damping coefficient equal to the propagation speed of the reflected wave. The solution procedure outlined in this paper gives a new direction for evaluating the transient response of hyperbolic systems, in particular nondispersive systems.

Acknowledgment

The authors gratefully acknowledge the support of the National Science Foundation, General Motors Corporation, and the Institute of Manufacturing Research at Wayne State University for this research work.

References

- Archibald, F. R., and Emslie, A. G., 1958, "The Vibration of a String Having a Uniform Motion Along Its Length," *ASME JOURNAL OF APPLIED MECHANICS*, Vol. 25, pp. 347–348.

Chung, C. H., and Tan, C. A., 1995, "Active Vibration Control of the Axially Moving String by Wave Cancellation," *ASME Journal of Vibration and Acoustics*, Vol. 117, pp. 49–55.

Graff, K. F., 1975, *Wave Motion in Elastic Solids*, Ohio State University Press.

Hull, A. J., 1994, "A Closed Form Solution of a Longitudinal Bar With a Viscous Boundary Condition," *Journal of Sound and Vibration*, Vol. 169, No. 1, pp. 19–28.

Mote, C. D., Jr., 1965, "A Study of Band Saw Vibrations," *Journal of Franklin Institute*, Vol. 279, pp. 430–444.

Perkins, N. C., 1990, "Linear Dynamics of a Translating String on an Elastic Foundation," *ASME Journal of Vibration and Acoustics*, Vol. 112, pp. 2–7.

Swope, R. D., and Ames, W. F., 1963, "Vibrations of a Moving Threadline," *Journal of the Franklin Institute*, Vol. 275, No. 1, pp. 36–55.

Tan, C. A., and Zhang, L., 1994, "Dynamic Characteristics of a Constrained String Translating Across an Elastic Foundation," *ASME Journal of Vibration and Acoustics*, Vol. 116, pp. 318–325.

Wang, K. W., and Liu, S. P., 1991, "On the Noise and Vibration of Chain Drive Systems," *Shock and Vibration Digest*, Vol. 23, No. 4, pp. 8–13.

Wickert, J. A., and Mote, C. D., Jr., 1988, "Current Research on the Vibration and Stability of Axially Moving Materials," *Shock and Vibration Digest*, Vol. 50, No. 5, pp. 3–13.

Wickert, J. A., and Mote, C. D., Jr., 1990, "Classical Vibration Analysis of Axially Moving Continua," *ASME JOURNAL OF APPLIED MECHANICS*, Vol. 57, pp. 738–744.

Wickert, J. A., and Mote, C. D., Jr., 1991, "Traveling Load Response of an Axially-Moving String," *Journal of Sound and Vibration*, Vol. 149, pp. 267–284.

Yang, B., and Tan, C. A., 1992, "Transfer Functions of One-Dimensional Distributed Parameter Systems," *ASME JOURNAL OF APPLIED MECHANICS*, Vol. 59, pp. 1009–1014.

Ying, S., and Tan, C. A., 1996, "Active Vibration Control of the Axially Moving String Using Space Feedforward and Feedback Controllers," *ASME Journal of Vibration and Acoustics*, Vol. 118, pp. 306–312.

Zhu, W. D., and Mote, C. D., Jr., 1994, "Free and Force Response of an Axially Moving String Transporting a Damped Linear Oscillator," *Journal of Sound and Vibration*, Vol. 177, No. 5, pp. 591–610.

Nondimensional Parameters for Geometric Nonlinear Effects in Pressurized Cylinders With Axial Cracks

H. T. Budiman

P. A. Lagace¹

Technology Laboratory for Advanced Composites,
Department of Aeronautics and Astronautics,
Massachusetts Institute of Technology,
Cambridge, MA 02139

The effects of geometric nonlinearity on the response of axially cracked cylindrical shells under internal pressure are investigated in a general way. Using the Donnell-Mushtari-Vlasov nonlinear shell equations, the nonlinear response is shown to depend on two nondimensional parameters: the geometrical parameter λ , which is a function of the cylinder geometries and crack length, and the loading parameter η , which depends on the applied pressure, material properties, and cylinder geometries. To assess the applicability of such parameters, nonlinear analyses of different cylindrical configurations were performed using the STAGS finite element code. The results show that the two parameters are able to characterize the nonlinear response of such cylinders. Effects of nonlinearity are then presented in the form of an iso-nonlinear plot showing the percentage difference between the linear and nonlinear stress intensification factors. Using the iso-nonlinear plot, the importance of geometric nonlinearity can thus be assessed once the cylinder geometries, loading parameters, and material properties are known.

Introduction

The problem of thin cylindrical shells with axial cracks has been investigated for the past three decades (Folias, 1965; Copley and Sanders, 1967; Erdogan and Kibler, 1969) due to its relevance to the damage tolerance design of pressure vessels such as an aircraft fuselage. The response of a cracked shell is fundamentally different from that of a flat plate. In a cracked shell, the region surrounding the crack bulges (deforms out-of-plane) due to a combination of internal pressure and geometric coupling between the membrane and bending actions. The phenomenon is illustrated in Fig. 1 where bulging of the crack region in an axially cracked cylindrical shell is shown. This geometric coupling is a characteristic of any shell structure where bending and stretching deformations are coupled. Bulging causes an amplification of the stress intensity factor in a shell structure. This stress intensification in a cracked shell is therefore defined as the ratio of the stress intensity factor in a cracked shell to that of a cracked plate with the same crack geometry.

In general, there are two kinds of stress intensifications in thin, cracked plate/shell structures: the membrane stress intensification, which is uniform through-the-thickness, and the bending stress intensification, which varies linearly through-the-thickness. When the classical plate/shell theory is used to solve this problem, the angular distributions of the membrane and bending stress intensity factors with respect to the crack plane are different. This arises from the inability of the classical plate/shell theory to completely satisfy the stress-free boundary conditions along the crack face. The difference between the two

angular distributions suggests that the membrane and bending stress intensity factors cannot simply be combined by adding them. Some kind of interaction formula (Sanders, 1982) is needed to obtain the combined effects. However, it has been shown recently (Ansell, 1988) that the contribution of the bending stress intensity factor is less than 0.3 percent for thin plates/shells and can therefore be neglected for all practical purposes.

Folias (Folias, 1965) was the first to solve this crack problem and obtained the solutions for the membrane stress intensification. His solutions are based on the linear, shallow-shell equations. Folias claimed that the magnitude of the bending stress intensification is small and the contribution from the bending stress intensification can therefore be neglected. The final solution depends only on one geometrical parameter, λ :

$$\lambda = \frac{a}{\sqrt{Rh}} \sqrt{12(1-\nu^2)} \quad (1)$$

where a is the crack half-length, R is the shell radius, h is the shell thickness, and ν is the Poisson's ratio. The cylinder geometry is illustrated in Fig. 2.

Folias' original solution is valid only for small values of λ ($\lambda \ll 1$). Others (Copley and Sanders, 1967; Erdogan and Kibler, 1969) were able to obtain the solutions which are valid for larger values of λ (λ less than 8). The following simple equation was subsequently proposed by Folias (Folias, 1974a) to fit the numerical solution for the membrane (extensional) stress intensification, K^{ext} , and is valid within ± 6 percent for values of λ less than 8:

$$K^{\text{ext}} = \sqrt{1 + 0.317\lambda^2} \quad (2)$$

where λ is the geometrical parameter defined by Eq. (1).

Failure prediction methodology can then be developed by modifying the flat-plate failure prediction/correlation using Eq. (2) to take into account the stress intensification in the hoop direction due to bulging. This methodology has been developed for metallic cylinders (Folias, 1974a) as well as quasi-isotropic composite cylinders (Graves and Lagace, 1985; Ranniger et al., 1995). Comparison between the predictions and the experimen-

¹ Send all correspondence to this author at MIT 33-303, 77 Massachusetts Avenue, Cambridge, MA 02139.

Contributed by the Applied Mechanics Division of THE AMERICAN SOCIETY OF MECHANICAL ENGINEERS for publication in the ASME JOURNAL OF APPLIED MECHANICS.

Discussion on this paper should be addressed to the Technical Editor, Professor Lewis T. Wheeler, Department of Mechanical Engineering, University of Houston, Houston, TX 77204-4792, and will be accepted until four months after final publication of the paper itself in the ASME JOURNAL OF APPLIED MECHANICS.

Manuscript received by the ASME Applied Mechanics Division, 14, 1995; final revision, Sept. 26, 1996. Associate Technical Editor: J. W. Ju.

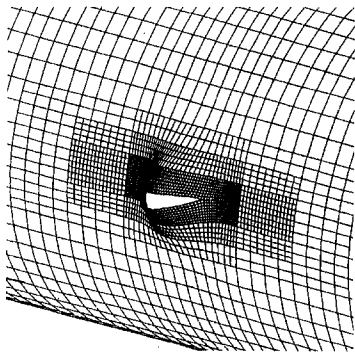


Fig. 1 Illustration of bulging of the crack face in an axially cracked cylinder (note: out-of-plane deformations are magnified 20 \times)

tal results performed on different cylinders is very good (Folias, 1974a; Ranniger et al., 1995). Such good agreement between the predicted and measured failure pressures was observed despite major assumptions imposed in deriving the stress intensification factors such as the assumptions on linearity, small deformation, and shell-shalowness.

However, such assumptions can be violated in practice. It can be shown from analyses that the maximum bulging displacement can be on the order of the cylinder thickness (Ansell, 1988; Riks, 1987). This implies that the response of an axially cracked cylinder is actually nonlinear to some degree. Ansell (Ansell, 1988) was the first to investigate the effects of geometric nonlinearity on the stress intensification factors in axially cracked cylindrical structures using the AB-AQUS finite element package. The configuration studied was the fuselage section of a SAAB 340 aircraft. The dependence of the stress intensification factors on the applied pressure was noted, thus illustrating the effects of geometric nonlinearity. Since then, others (Riks, 1987; Rankin, 1988) performed similar analyses for different cylindrical geometries using different finite element packages and found similar results. Recently, Chen and Schijve (1991) developed the membrane stress intensification expression based on some empirical geometrical parameters measured from experiments. In all cases, the magnitude of the nonlinear membrane stress intensification decreases as the pressure increases.

Despite such progress, the work performed in the literature to date has been case-specific in that the effects of nonlinearity have been investigated only for specific cylinders. Therefore, it is difficult to draw general conclusions on the significance of these effects. The present work addresses the nonlinearity issues in a more general way. Using the simplest nonlinear shell equations (the Donnell-Mushtari-Vlasov equations), the parameters of interest are extracted. Extensive finite element analyses are then performed to assess the applicability of this parameter. Error introduced by the assumption that nonlinearity is not important is shown in the form of an iso-nonlinear plot showing the percentage difference between the linear and the nonlinear stress intensification solutions as functions of the two proposed nondimensional parameters.

Approach

The overall goal of the work is to be able to predict the failure of axially cracked cylinders using flat plate fracture data. To accomplish this, the stress intensification factor discussed previously is needed to account for different structural responses of the two structures. This "structural factor" has been obtained for the linear case and has been used to modify a flat-plate fracture criterion to predict shell fracture (Folias, 1974; Graves and Lagace, 1985). Note that the geometric nonlinearity effects

due to bulging have been neglected in the derivation of the linear stress intensification factors.

The nonlinearity effects have been investigated only for specific cylinders and no general conclusions can be drawn from such analyses. The present work addresses the nonlinear effects in a general way. Using the Donnell-Mushtari-Vlasov nonlinear shell equations, nondimensional parameters are first derived. Finite element analyses of different cylinders are performed to verify the applicability of such parameters. The nonlinear stress intensification factors are obtained using the nodal release technique. An assessment of the nonlinear effects is then made by comparing the linear and the nonlinear solutions in the form of an iso-nonlinear plot.

Determination of the Governing Nondimensional Parameters

The Donnell-Mushtari-Vlasov (DMV) nonlinear shallow shell theory is used to obtain the parameters of interest. The DMV theory is strictly valid only for shallow shells but does include the effects of large deformation and moderate rotation (Yamaki, 1984). Other higher order nonlinear shell theories such as the Sanders nonlinear shell theory (Sanders, 1963), which is valid for the case of deep shells, can also be used and has been shown to yield the same results for the case where the crack is oriented in the axial direction (Budiman, 1996). The reason is that the size of the crack oriented in the axial direction does not influence the shallowness condition. However, when the crack is oriented in the circumferential direction, the size of the crack does influence the shallowness assumption. Therefore, the two theories are not expected to agree for this latter case and it is necessary the use the higher order theories that are valid for deep shells. Based on this reason, the generality of the approach outlined here for an axially cracked cylinder is not lost by using this simpler shell theory. Therefore, only the derivation using the DMV theory is presented here for the sake of simplicity.

The geometry of the cylindrical shells considered is shown in Fig. 2. For a cylindrical shell, the governing equations are (Yamaki, 1984)

$$\frac{1}{Eh} \nabla^4 F = \frac{1}{R} w_{,xx} + w_{,xy}^2 - w_{,xx} w_{,yy} \quad (3)$$

$$\frac{Eh^3}{12(1-\nu^2)} \nabla^4 w = -\frac{1}{R} F_{,xx} + F_{,xx} w_{,yy} + F_{,yy} w_{,xx} - 2F_{,xy} w_{,xy} + p \quad (4)$$

where F is the stress function, w is the out-of-plane displacement, p is the internal pressure, x is the axial coordinate, y is the hoop coordinate, E is the material modulus, and ν is the

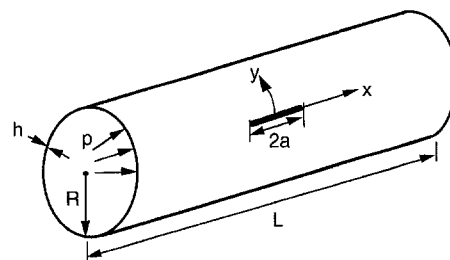


Fig. 2 Geometry of an axially cracked cylindrical shell under internal pressure

Poisson's ratio. It is convenient to perform nondimensionalization of Eqs. (3) and (4) via

$$\begin{aligned}x' &= ax \\y' &= ay \\w' &= \frac{\lambda^2 h}{[12(1 - \nu^2)]^{1/2}} w \\F' &= \left(\frac{Eh^3}{12(1 - \nu^2)} \right) F.\end{aligned}\quad (5)$$

In the nondimensionalization, a is the crack half-length, h is the cylinder thickness, λ is the nondimensional crack length given by Eq. (1), and E and ν are the material parameters. Henceforth, the primed quantities correspond to the physical variables and the unprimed quantities are dimensionless. In terms of these nondimensional parameters, the governing equations can be written as

$$\nabla^4 F - \lambda^4 w_{,xx} = \lambda^4 [w_{,xy}^2 - w_{,xx} w_{,yy}] \quad (6)$$

and

$$\begin{aligned}\nabla^4 w + F_{,xx} \\= F_{,xx} w_{,yy} + F_{,yy} w_{,xx} - 2F_{,xy} w_{,xy} + \lambda^2 \sqrt{12(1 - \nu^2)} \eta\end{aligned}\quad (7)$$

where λ is given by Eq. (1) and

$$\eta = \frac{p}{E \left(\frac{h}{R} \right)^2} \quad (8)$$

Unlike the linear theory, where only one parameter, λ , is needed to characterize the cylinder response, the nonlinear formulation requires *two* parameters: the geometrical parameter λ and the loading parameter η .

The η parameter is a measure of the "driving force" of the nonlinearity and can also be written as

$$\eta = \left(\frac{pR}{h} \right) \frac{1}{E} \frac{1}{\left(\frac{h}{R} \right)} \quad (9)$$

where each of the three components represents part of the physical "driving force" for nonlinear behavior. The "driving force" is directly proportional to the hoop stress (pR/h) since the higher this stress, the greater the out-of-plane deformation and thus the more nonlinear the response. The parameter is inversely proportional to the material (homogenized laminate) stiffness (E) since E is a measure of the material/structural resistance to deformation. It is also inversely proportional to the shell ratio (h/R) since, for a particular cylinder with a known radius, the smaller the magnitude of the shell ratio, the smaller the shell wall rigidity and thus more out-of-plane deformation occurs resulting in a more nonlinear response. The η parameter obtained via the equations is therefore consistent with that obtained by considering the physics of the situation.

Finite Element Models

The STAGS finite element code (Brogan et al., 1994) was used in the analyses. The shell element used was the 410 shell element which has six degrees-of-freedom per node: three displacements (u , v , w) and three rotations (ϕ_x , ϕ_y , ϕ_z). To simulate the biaxial stress state in the cylinders, internal pressure as well as axial forces at the end of the cylinders were applied. The length of the cylinder model was chosen so that the edge-effects from the end of the cylinders have negligible influence on the stress/strain fields in the region of interest.

There is no closed-form solution for the magnitude of the edge-effects in an axially cracked cylinder, so it was therefore assumed that a cylinder model with length corresponding with 25 times the crack size is adequate for this problem. By comparing the finite element solution with the available results in the literature for the linear case, this assumption is assessed and the cylinder length can be modified if necessary.

Other geometrical parameters of interest are the skin thickness, h , and the cylinder radius, R . The skin thickness of the crown of an aircraft fuselage is usually on the order of 1 to 2 mm (Niu, 1988). Two different thicknesses were thus chosen: a baseline thickness of 1.4 mm and the scaled-up thickness of 5.6 mm where the scaled-up thickness is exactly four times the baseline thickness. Although this choice is somewhat arbitrary, it can be shown from Eq. (1) that for this ratio and a constant value of R , the ratio of the crack length, $2a$, of the scaled-up model and that of the baseline model is exactly two.

The computation of stress intensity factor was accomplished using the nodal release technique (Rankin et al., 1994, Viz et al., 1995). This method was chosen due to its accuracy, simplicity, and compatibility with the STAGS code. This method has the advantage that no special finite element is needed to get accurate results. However, the use of this numerical technique in a nonlinear problem requires two separate analyses: one, to compute the nodal forces and, two, to compute the crack face separation distance as functions of the applied loads. This requirement may render this method inefficient for larger problems. Methods based on the energy-conservation integral (such as the J -integral) (Moran and Shih, 1987) or the crack closure integral (Potyondy et al., 1995) can also be used and may even be more efficient for larger problems. Nevertheless, the nodal release technique is still considered efficient for all the cases analyzed in the present work.

The procedure for the computation of the energy release rate is outlined briefly here. The detailed derivation can be found in Rankin et al. (1994) and in Viz et al. (1995). As briefly mentioned before, in order to use this technique to compute the nonlinear stress intensity factors, two separate finite element analyses are needed to compute the nodal forces and separation distances as functions of the applied loading. Each crack-tip in the finite element models is modeled using two different nodes (the master node and the slave node) which have the same coordinates and are constrained to move the same amount. In the first run, the general nodal forces (F_x , F_y , F_z , M_x , M_y , and M_z) at each crack-tip needed to ensure compatibility of the two crack-tip nodes are computed. In the second run, the crack-tip is moved a crack increment value Δ which is chosen a priori, thus allowing the two original crack-tip nodes to have independent degrees-of-freedom. The separation distances between the two nodes are then obtained. The nodal release technique is then used to compute the evolution of the energy release rate using the calculated nodal forces and separation distances. By knowing the energy release rate, the stress intensity factor can be computed using the Irwin formula (Rice, 1972).

As indicated, the crack increment, Δ , needs to be chosen a priori. In this work, Δ was chosen to be five percent of the half crack-length ($0.05a$) based on the results of a preliminary study on a large center-cracked panel loaded perpendicular to the crack plane. The numerical results obtained for such panels using the finite element method and the nodal release technique described here as well as the analytical solutions are shown in Table 1. The error is about 0.8 percent when the crack increment, Δ , is set to $0.05a$. Such error is considered acceptable and the Δ value of $0.05a$ was thus chosen.

In the nonlinear analysis, the nodal forces and the nodal separation distances are available only at discrete load steps which are not evenly spaced. To get a continuous solution, some kind of curve-fitting or interpolation is needed. The cubic-spline method (Press et al., 1989) was used to interpolate the discrete nodal forces and separation distances. The nodal release tech-

Table 1 Comparison between the numerical and analytical solutions for the mode I stress intensity factors of a large center-cracked panel ($\sigma = 100$ MPa, $2a = 20$ mm)

Δ/a	Calculated Stress Intensity Factor (MPa \sqrt{m})		
	Nodal-Release	Analytical	Error
0.025	17.80	17.73	0.4 percent
0.050	17.87	17.73	0.8 percent
0.100	17.97	17.73	1.4 percent

nique can then be used to obtain the evolution of the energy release rate and then the stress intensity factor once the continuous dependence of the nodal forces and that of the separation distances on the applied pressure are known. By taking the ratio of the stress intensity of the cracked shell to that of the cracked plate of the same crack length at each load step, the nonlinear stress intensifications were then obtained.

Results of Numerical Analyses

Three different stages of numerical analyses were performed. The initial stage was used to assess the accuracy and convergence of the finite element mesh used by comparing the linear membrane stress intensification factors obtained using STAGS with the numerical solutions available in the literature. It was also intended at this initial stage to investigate the influence of the edge effects from the cylinder ends and the validity of the chosen crack increment, Δ , before any nonlinear analyses were performed. The second stage was performed to assess the applicability of the proposed parameter, η , to characterize the nonlinear response of different cylinders. The third and final stage was intended to determine the severity of nonlinearity by comparing the linear and nonlinear membrane stress intensifications for cylinders analyzed. By knowing the differences between the linear and nonlinear solutions, an iso-nonlinear plot showing the percentage difference between the two solutions was then created.

In the first stage of the analyses, 12 cylinders with radius of 1.52 m, skin thickness of 1.4 mm, and λ values ranging from 1 to 12, corresponding to crack lengths of 51 mm to 612 mm, were analyzed. Only one-half of each cylinder had to be modeled due to symmetries in the applied loading and in the geometries with respect to the plane passing through and perpendicular to the middle of the crack. The finite element mesh of one such cylinder is shown in Fig. 3.

The stress intensification factors were computed using the nodal release technique and compared with the available numer-

ical solution obtained by Erdogan and Kibler (1969) which is based on the solution of coupled integral equations. Note that the Erdogan and Kibler numerical solutions are only available for values of λ less than 8. The comparison between the two solutions is shown in Fig. 4. The agreement is excellent. This indicates that the assumptions on the cylinder length discussed previously and the crack increment used are justified and the convergence of the finite element meshes is satisfactory.

After sufficient confidence with the finite element approach had been attained, the second stage of the analyses was started where different cylindrical configurations with λ equal to 3, 6, 9, and 12 were analyzed. The smaller values of λ (3 and 6) correspond to the range of λ investigated experimentally in the literature for isotropic and quasi-isotropic composite cylinders (Folias, 1978; Ranniger, Lagace and Graves, 1995), while the larger values of λ (9 and 12) correspond to the situation in a narrow-body fuselage structure. In an actual fuselage, an axial crack as large as 500 mm (~ 20 inches) may have to be considered since such size is usually dictated by the spacing between two adjacent crack arrest members.

The nonlinear analyses to obtain the nonlinear membrane stress intensification factors were performed for different values of crack size and skin thickness of the cylinder by keeping the cylinder radius constant. For each value of the geometrical parameter λ , nonlinear analyses were performed for different values of crack size and skin thickness while holding the cylinder radius constant at 1.52 m and 0.76 m. The largest cylinder ($R = 1.52$ m) corresponds to the geometries of a narrow-body fuselage. The other cylinder has a radius which is one-half this value.

The nonlinear membrane stress intensifications of different cylinders for the case of λ equal to 3 are shown in Fig. 5. In that figure, the membrane stress intensifications, K^{ext} , are shown to be strong functions of pressure and specific cylinder geometries. The linear membrane stress intensification factor, on the other hand, depends solely on λ and is therefore independent of the applied pressure. For all the cases shown in Fig. 5, the linear solution corresponds to the nonlinear results when the pressure, p , is equal to zero. In all of the cases studied, the magnitude of the membrane stress intensification decreases as the applied pressure increases. Geometric nonlinearity effects become more important as the pressure increases due to an increase in the driving force causing stiffening in the structural response. Further crack opening is constrained causing a decrease in the magnitude of the energy release rate and the stress intensity factor. This trend is consistent with the results from previous work (Ansell, 1988; Riks, 1987) where a similar trend was observed for the specific cylinders analyzed.

When the K^{ext} are presented as functions of η , the responses of different cylinders collapse nicely to a single curve as illustrated in Fig. 6. For small values of η ($\eta < 0.1$ for $\lambda = 3$),

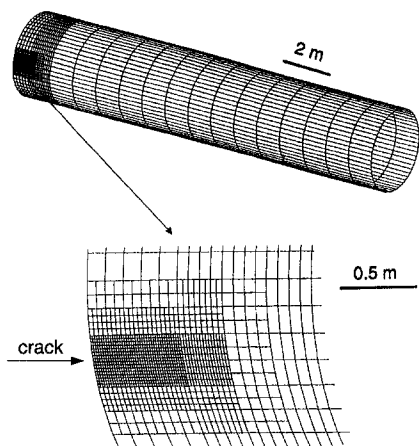


Fig. 3 Typical finite element mesh (case shown is cylinder with $R = 1.52$ m, $h = 1.4$ mm, $2a = 0.62$ m resulting in $\lambda = 12$)

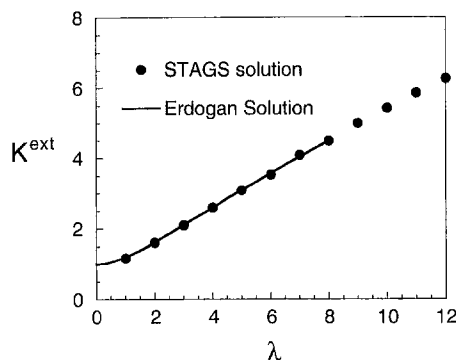


Fig. 4 Plot of the linear membrane stress intensification versus the geometrical parameter λ as computed using the STAGS code and the nodal release technique and using the Erdogan and Kibler numerical solution.

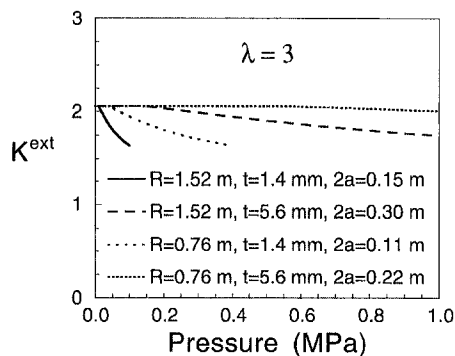


Fig. 5 Dependence of the membrane stress intensification factor (K^{ext}) on the internal pressure for different cylindrical configurations

K^{ext} is relatively constant and, therefore, the effects of nonlinearity are not important in that region. As the pressure is increased further (larger values of η), K^{ext} starts to deviate from the linear solution indicating that the nonlinear effects become more important. The same behavior is also observed for cylinders of different values of λ and is illustrated in Fig. 7.

The results of the analyses thus confirm the applicability of the nondimensional parameter η , obtained previously from the governing equations, in characterizing the nonlinear response of axially cracked cylinders. In general, the nonlinear response depends on the crack length (contained in λ) as well as on the applied loading (contained in η). For any cylinders, the longer the crack length (the higher the λ value) and the higher the applied loading (the higher the η value), the more nonlinear the response is.

In the third stage of the analysis, models of cylinders with different crack lengths were analyzed to assess the implications of the nonlinearity effects. The nonlinear analyses were performed on the same cylinder models analyzed in the first stage of the analyses (λ values ranging from 1 to 12). As previously mentioned, the purpose of these analyses is to create an iso-nonlinear plot where the severity of the nonlinearity can be readily determined from the cylinder geometries, material properties, crack length, and operating pressure.

The metric used to characterize the severity of nonlinearity is the percentage error between the magnitudes of the linear and nonlinear K^{ext} . For each value of λ , the error can be computed as

$$\text{Error} = \frac{K^{\text{ext}}_{\text{linear}} - K^{\text{ext}}_{\text{nonlinear}}}{K^{\text{ext}}_{\text{linear}}} \times 100. \quad (10)$$

The iso-nonlinear plot is depicted in Fig. 8 for λ values ranging from 1 to 12 where errors ranging from 5 to 40 percent are shown.

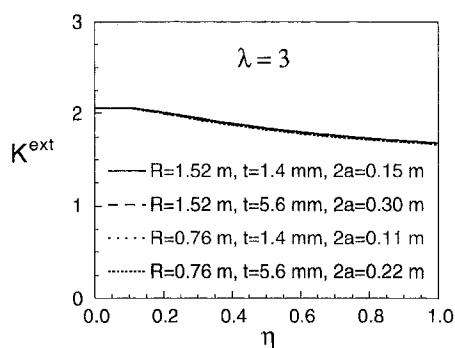


Fig. 6 Dependence of the membrane stress intensification factor (K^{ext}) on the loading parameter η

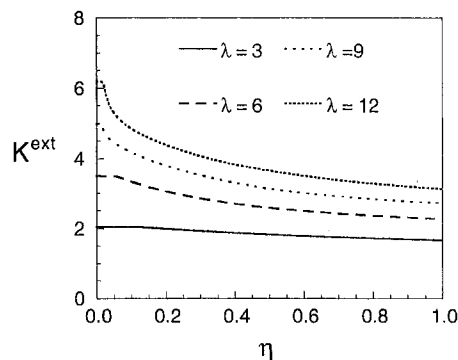


Fig. 7 Dependence of the membrane stress intensification factor (K^{ext}) on the loading parameter η for different values of the geometrical parameter λ

Values of λ less than 1 were not considered in creating the iso-nonlinear plot of Fig. 8. For a value of λ of 1, the magnitude of the linear K^{ext} is relatively small ($K^{\text{ext}} = 1.17$ from the numerical solution). Since K^{ext} is defined as the ratio between the stress intensity of a cracked shell to that of a cracked plate, its value cannot be less than 1. Therefore, the maximum percentage error for that case is only around 14 percent, irrespective of the value of the loading parameter η . Thus geometric nonlinearity effects are relatively insignificant for small crack lengths corresponding to values of λ less than 1.

Figure 8 can be readily used as a design chart to assess the degree of nonlinearity in any axially cracked cylinders. By knowing the geometries of the specific cylinders, the material properties, and the operating pressure, one can readily compute the magnitude of the two nondimensional parameters λ and η and use the iso-nonlinear plot to determine the importance of nonlinearity.

Implications

The stress intensification factor is a function of both the geometrical parameter λ and the loading parameter η as shown in Fig. 7. It is therefore important to consider both of these parameters in assessing the degree of nonlinearity for a particular case. The information provided by the iso-nonlinear plot shown in Fig. 8 is useful in this regard as it allows an assessment of the effects of geometric nonlinearity on any axially cracked cylindrical shells based on two nondimensional parameters λ and η . For example, for cylinders with constant crack length (constant value of λ), as pressure increases (η increases), the deviation from the linear solution increases, indicating more nonlinear response. Similarly, for a fixed pressure (constant value of η), as the crack grows (λ increases), the deviation

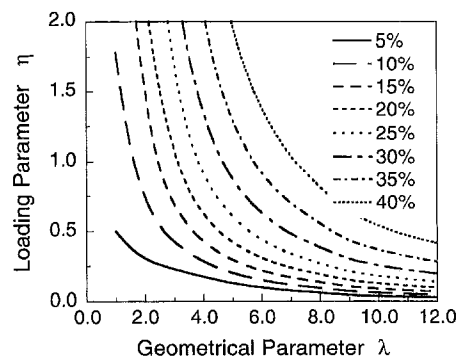


Fig. 8 Iso-nonlinear plot showing the percentage difference between the linear and nonlinear membrane stress intensifications as functions of the two nondimensional parameters

from the linear solution also increases. These observations show the importance of nonlinearity effects in the cylinder response.

Such information is particularly important to assess any "scale effects" in using experimental results obtained from laboratory-scale specimens to predict/assess the response/failure of a full-scale structure. For example, consider the case of two cylindrical shells of the same thickness, nondimensional crack length λ , and material but of different radii. Both cylinders are made of Aluminum 2024-T3 with a modulus (E) of 70 GPa and apparent toughness (K_c) of 100 MPa \sqrt{m} . The first cylinder is similar to the fuselage of a Boeing 737 airplane ($R = 2.0$ m, $h = 1.0$ mm) with a ratio of the radius to crown skin thickness on the order of 1000. The second cylinder is typical of a laboratory-scale test specimen with a radius-to-thickness ratio on the order of 100 ($R = 150$ mm, $h = 1.0$ mm). The maximum crack size considered in the larger cylinder is dictated by the spacing of two adjacent crack arrest members which is typically around 500 mm (Niu, 1988). In this example, it is assumed that a through-thickness axial crack of 250 mm long, corresponding to one-half the tear-strap spacing, is present in the fuselage. This yields a value of λ of 5. Axial cracks of different length can also be considered. For the smaller cylinder, the crack size for the same value of λ is approximately 68 mm. To compute the magnitude of the η -parameter using Eq. (9), the magnitude of the failure pressure p is needed. For metallic cylinders, the failure pressure p can be obtained from the linear-elastic fracture criterion. Therefore, Eq. (9) can be rewritten as

$$\eta = \left(\frac{K_c}{E} \right) \left(\frac{R}{h} \right) \frac{1}{\sqrt{\pi a}} \frac{1}{K^{\text{ext}}} \quad (11)$$

where K_c is the apparent material toughness in plane stress.

Note that to compute the magnitude of the η -parameter using Eq. (11), the magnitude of K^{ext} is also needed. Since the actual K^{ext} is nonlinear and is a function of both λ and η , the K^{ext} values obtained from the linear solution (which is only a function of λ) can be used as a first approximation. It has been shown in the previous section that the magnitude of the nonlinear K^{ext} is smaller than that obtained from the linear solution. By making this assumption, a conservative estimate of the η -parameter and the error for each cylinder can be made.

The computed η -parameters for the real fuselage and the laboratory-scale test specimens are equal to 1.53 and 0.22 corresponding to failure pressures of 45 kPa and 756 kPa, respectively. The error can be readily estimated using the iso-nonlinear plot (Fig. 8). For the real fuselage, the error is at least 35 percent. The error is around ten percent for the laboratory-scale test specimen. Therefore, it is clear that the nonlinear effects are more important in the larger cylinder.

Note that the failure pressure of the larger cylinder is lower than the ultimate design pressure for a Boeing 737 (around 110 kPa). The reason is that in determining the failure pressures in this sample problem, the upper bound value of the hoop stress [$\sigma_{\text{hoop}} = (pR/t)$] was used. In an actual fuselage, stiffening elements such as stringers and frames carry part of the loads, hence reducing the hoop stress in the skin. The reduction can be as high as 25 percent depending on a particular fuselage construction (Flugge, 1952). Furthermore, the magnitude of the plane stress toughness of Aluminum 2024-T3 used in this sample problem ($K_c = 100$ MPa \sqrt{m}) might be too low. Plane stress toughness for Aluminum 2024-T3 as high as 175 MPa \sqrt{m} has been noted by other author (Swift, 1987).

Despite those differences, this example illustrates the "danger" of using laboratory test results obtained from small specimens to predict the response of a full-scale structure. Neglecting the nonlinear effects in failure prediction of a large structure (such as an aircraft fuselage) can produce results which are too conservative due to different degrees of nonlinearity that operate at different scales.

Summary

Using the Donnell-Mushtari-Vlasov nonlinear shell equations and the finite element method, it has been shown that two nondimensional parameters can be used to characterize the nonlinear response of any axially cracked cylinders. The two parameters are the geometrical parameter λ , which depends on the specific cylinder geometries, and the loading parameter η , which depends on the applied pressure, the shell ratio h/R , and the material stiffness.

An iso-nonlinear plot showing the percentage difference between the membrane stress intensification factors obtained using the linear and nonlinear solutions as functions of λ and η has been presented. Such a plot is very useful in assessing the degree of nonlinearity in an axially cracked cylinder. By knowing the shell geometries, material properties, and loading conditions, one can readily compute the degree of nonlinearity with the help of the plot.

Using the iso-nonlinear plot, which shows the percentage difference between the linear and nonlinear stress intensification factors, one can also show the "danger" of directly translating experimental results obtained from "scaled" test specimens to predict the response of a full-scale structure due to different degrees of nonlinearity. The nonlinear effects are shown to be more significant in the full-scale structures than in the test specimens. The error introduced in the computation of the stress intensification factors is therefore larger in an actual fuselage and were shown in one particular example to be at least 35 percent.

Acknowledgment

This work is supported by the Aircraft Structures Branch of NASA Langley Research Center under grant NAG1-991. Suggestions and guidance of the contract monitor Dr. James H. Starnes, Jr. are gratefully acknowledged as are many stimulating discussions with Professor John W. Hutchinson of Harvard University.

References

- Ansell, H., 1988, "Bulging of Cracked Pressurized Aircraft Structure," Ph.D. thesis, Institute of Technology, Department of Mechanical Engineering, Linköping Institute of Technology, Sweden.
- Brogan, F. A., Rankin, C. C., and Cabiness, H. D., 1994, *STAGS User Manual*, LMSC P032594, Lockheed Palo Alto Research Laboratory.
- Budiman, H. T., 1996, "Mechanisms of Damage Tolerance and Arrest in Pressurized Composite Cylinders," Ph.D. thesis, Department of Aeronautics and Astronautics, Massachusetts Institute of Technology, Cambridge, MA.
- Chen, D., and Schijve, J., 1991, "Bulging of Fatigue Cracks in a Pressurized Aircraft Fuselage," *Aeronautical Fatigue: Key to Safety and Structural Integrity*, A. Kobayashi, ed., Proceeding of the 16th Symposium of the International Committee on Aeronautical Fatigue, Tokyo, Japan, pp. 277–316.
- Copley, L. G., and Sanders, J. L., 1969, "A Longitudinal Crack in Cylindrical Shell under Internal Pressure," *International Journal of Fracture Mechanics*, Vol. 5, No. 2, pp. 117–131.
- Erdogan, F., and Kibler, J. J., 1969, "Cylindrical and Spherical Shells with Cracks," *International Journal of Fracture Mechanics*, Vol. 5, No. 3, pp. 229–237.
- Flugge, W., 1952, "Stress Problems in Pressurized Cabins," NACA TN 2612.
- Folias, E. S., 1965, "An Axial Crack in Pressurized Cylindrical Shells," *International Journal of Fracture Mechanics*, Vol. 1, No. 2, pp. 104–113.
- Folias, E. S., 1969, "On the Effects of Initial Curvature on Cracked Flat Sheets," *International Journal of Fracture Mechanics*, Vol. 5, No. 4, pp. 327–346.
- Folias, E. S., 1974a, "Fracture in Pressure Vessels," *Thin Shell Structures: Theory, Experiment, and Design*, Y. C. Fung, and E. E. Sechler, eds., Prentice-Hall, Englewood Cliffs, NJ, pp. 483–518.
- Folias, E. S., 1974b, "On the Predictions of Catastrophic Failures in Pressurized Vessels," *Prospects of Fracture Mechanics*, G. C. Sih, H. C. van Elst, D. Broek, eds., Noordhoff International, Leyden, pp. 405–418.
- Folias, E. S., 1977, "Asymptotic Approximations to Crack Problems in Shells," *Mechanics of Fracture—Plates and Shells with Cracks*, G. C. Sih, ed., Noordhoff International, Leyden, pp. 117–160.
- Graves, M. J., and Lagace, P. A., 1985, "Damage Tolerance of Composite Cylinders," *Composite Structures*, Vol. 4, No. 1, pp. 75–91.
- Moran, B., and Shih, C. F., 1987, "Crack Tip and Associated Domain Integrals from Momentum and Energy Balance," *Engineering Fracture Mechanics*, Vol. 27, pp. 615–641.

- Niu, C. Y. M., 1988, *Airframe Structural Design*, Conmil Press, Ltd.
- Potyondy, D. O., Wawrzynck, P. A., Ingrassia, A. R., 1995, "Discrete Crack Growth Analysis Methodology for Through-Cracks in Pressurized Fuselage Structures," *International Journal for Numerical Methods in Engineering*, Vol. 38, No. 10, pp. 1611–1633.
- Press, W. H., Flannery, B. P., Teukolsky, S. A., and Vetterling, W. T., 1990, *Numerical Recipes: The Art of Scientific Computing*, Cambridge University Press, New York, pp. 86–89.
- Ranniger, C. U., Lagace, P. A., and Graves, M. J., 1995, "Damage Tolerance and Arrest Characteristics of Pressurized Graphite/Epoxy Tape Cylinders," *Composite Materials: Fatigue and Fracture—Fifth Volume*, ASTM STP 1230, ASTM, Philadelphia, PA, pp. 407–426.
- Rankin, C. C., Brogan, F. A., and Riks, E., 1993, "Some Computational Tools for the Analysis of Through Cracks in Stiffened Fuselage Shells," *Computational Mechanics*, Vol. 13, pp. 143–156.
- Rice, J. R., 1972, "Mathematical Analysis in the Mechanics of Fracture," *Fracture*, Vol. 2, H. Leibowitz, ed., Academic Press, New York.
- Riks, E., and den Rijer, P. J., 1987a, "A Finite Element Analysis of Cracks in a Thin Wall Circular Cylinder under Internal Pressure," NLR TR 87021 U, National Aerospace Laboratory, The Netherlands.
- Riks, E., 1987b, "Bulging Cracks in Pressurized Fuselages: a Numerical Study," NLR MP 87058 U, National Aerospace Laboratory, The Netherlands.
- Riks, E., Brogan, F. A., and Rankin, C. C., 1989, "Bulging Cracks in Pressurized Fuselage: A Procedure for Computation," *Analytical and Computational Models of Shells*, A. K. Noor, T. Belytschko, and J. Simo, eds., pp. 483–507.
- Sanders, J. L., Jr., 1963, "Nonlinear Theories for Thin Shells," *Quarterly for Applied Mathematics*, Vol. 21, pp. 21–36.
- Sanders, J. L., Jr., 1982, "Circumferential Through-Cracks in Cylindrical Shells under Tension," *ASME JOURNAL OF APPLIED MECHANICS*, Vol. 49, pp. 103–107.
- Swift, T., 1987, "Damage Tolerance in Pressurized Fuselages," *New Materials and Fatigue Resistant Aircraft Design*, D. L. Simpson, ed., Proceedings of the 14th Symposium of the International Committee on Aeronautical Fatigue, Ottawa, Canada, pp. 1–77.
- Viz, M. J., Potyondy, D., Zehnder, A., Rankin, C. C., and Riks, E., 1995, "Computation of Membrane and Bending Stress Intensity Factors for Thin, Cracked Plates," *International Journal of Fracture*, Vol. 72, No. 1, pp. 21–38.
- Yamaki, N., 1984, *Elastic Stability of Circular Cylindrical Shells* (North Holland Series in Applied Mathematics and Mechanics) Vol. 27, E. Becker, B. Budiansky, W. T. Koiter, and H. A. Lauwerier, eds., North Holland, Amsterdam.

Free-Edge Stress Singularity in a Two-Dimensional Unidirectional Viscoelastic Laminate Model

Sang Soon Lee

Senior Researcher,
Reactor Mechanical
Engineering Department,
Korea Atomic Energy Research Institute,
Taejeon, South Korea 305-600

This paper concerns the stress singularity at the interface corner between the perfectly bonded fiber and the matrix of a unidirectional two-dimensional laminate model subjected to a uniform transverse tensile strain. The matrix is assumed to be a linear viscoelastic material. The standard Laplace transform and the Mellin transform techniques are employed to get the characteristic equation and the order of singularity is obtained numerically for a given viscoelastic model. The time-domain boundary element method is used to investigate the behavior of stresses for the whole interface. It is shown that the order of singularity increases with time while the free-edge stress intensity factor is relaxed with time.

1 Introduction

The problem of a composite body consisting of two isotropic and elastic materials has received much attention (Bogy, 1968; Reedy, 1990; Tsai and Morton, 1991). It is well known that a stress singularity exists at the interface corner between bonded elastic quarter planes and such high stress intensification may lead to plastic deformation or interfacial edge cracks.

The fiber-matrix interface of a unidirectional laminate would suffer from a stress system in the vicinity of the free surface under a transverse tensile loading. In such a region two interacting free surface effects occur, and very large interface stresses can be produced. A stress singularity which exists at the interface corner between the fiber and the matrix might lead to fiber-matrix debonding. In this study, the stress singularity at the interface corner between the perfectly bonded fiber and the matrix of a unidirectional laminate model subjected to a uniform transverse tensile strain is investigated. At room temperature the matrix material remains in its initial elastic state through the entire loading period and hence it is not necessary to consider the time-dependent behavior of the stress-strain relations in performing the stress analysis of the composite material. In certain application, however, the temperature and time dependence of the loading may be such that the rheological behavior of the matrix may no longer be negligible. Hence, provision is made for a matrix assumed to be a linear viscoelastic material.

The viscoelastic interface problems have been studied by several investigators. Two studies (Weitsman, 1979; Delale and Erdogan, 1981) considered a pair of interfaces in which one material is elastic and the other is viscoelastic. The results exhibited a redistribution of the very large stresses near the edge of the interface, but no singularities were encountered because of the simplifying assumptions with regard to the modeling of joining structural members. Blanchard and Ghoniem (1988) used the Mellin transform technique and the elastic-viscoelastic correspondence principle to determine the relaxation of thermal

stress singularities in bonded viscoelastic quarter planes. As they indicated, however, numerical inversion of the Laplace transform is difficult because the operator's inherent unboundedness prevents explicit error control. It can be mentioned that such disadvantage limits the application of their approach.

In this study, the transformed characteristic equation for perfectly bonded elastic and viscoelastic materials is first derived, following Bogy, with the use of the Laplace transform with respect to time t and the Mellin transform with respect to r . This equation is inverted analytically for a given viscoelastic model into the time-dependent viscoelastic equation which is readily solved using standard numerical procedure. The time-domain boundary element method (BEM) is then employed to investigate the behavior of stresses at the interface of a unidirectional laminate model subjected to a uniform transverse tensile strain.

2 Stress Singularity at Interface Corner

The region near the interface corner between perfectly bonded elastic and viscoelastic quarter planes is shown in Fig. 1. In the following, a condition of plane strain is considered. The material properties in the upper viscoelastic quarter plane are referred to with a subscript "I" while those of the lower elastic plane are denoted by a subscript "II."

A solution of

$$\nabla^4 \Phi(r, \theta; t) = 0 \quad (1)$$

is to be found such that the normal stress, σ_θ , and shear stress, $\tau_{r\theta}$, vanish along $\theta = \pm(\pi/2)$, further that the displacements and stresses are continuous across the common interface line $\theta = 0$. The solution of this problem is facilitated by the Laplace transform, defined as

$$\Phi^*(r, \theta; p) = \int_0^\infty \Phi(r, \theta; t) e^{-pt} dt \quad (2)$$

where Φ^* denotes the Laplace transform of Φ and p is the transform parameter. Then Eq. (1) can be rewritten using Eq. (2) as follows:

$$\nabla^4 \Phi^*(r, \theta; p) = 0. \quad (3)$$

By definition, the stresses in the Laplace transformed space are found from the stress function Φ^* in the following manner:

Contributed by the Applied Mechanics Division of THE AMERICAN SOCIETY OF MECHANICAL ENGINEERS for publication in the ASME JOURNAL OF APPLIED MECHANICS.

Discussion on this paper should be addressed to the Technical Editor, Professor Lewis T. Wheeler, Department of Mechanical Engineering, University of Houston, Houston, TX 77204-4792, and will be accepted until four months after final publication of the paper itself in the ASME JOURNAL OF APPLIED MECHANICS.

Manuscript received by the ASME Applied Mechanics Division, Jan. 4, 1996; final revision, Sept. 12, 1996. Associate Technical Editor: J. M. Daniel.

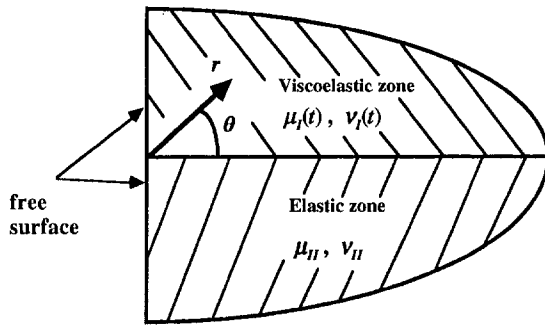


Fig. 1 Region near the interface corner between perfectly bonded elastic and viscoelastic quarter planes

$$\begin{aligned}\sigma_{rr}^* &= \frac{1}{r} \Phi_{,r}^* + \frac{1}{r^2} \Phi_{,\theta\theta}^* \\ \sigma_{\theta\theta}^* &= \Phi_{,rr}^* \\ \tau_{r\theta}^* &= \frac{1}{r^2} \Phi_{,\theta}^* - \frac{1}{r} \Phi_{,r\theta}^*\end{aligned}\quad (4)$$

and the displacements can be shown to be given by

$$\begin{aligned}u_{r,r}^* &= \frac{1}{2p\mu^*(p)} \left[\frac{1}{r} \Phi_{,r}^* + \frac{1}{r^2} \Phi_{,\theta\theta}^* - p\nu^*(p) \nabla^2 \Phi^* \right] \\ u_{\theta,r}^* - \frac{u_{\theta}^*}{r} + \frac{u_{r,\theta}^*}{r} &= \frac{1}{p\mu^*(p)} \left[\frac{1}{r^2} \Phi_{,\theta}^* - \frac{1}{r} \Phi_{,r\theta}^* \right]\end{aligned}\quad (5)$$

where σ_{ij}^* and u_i^* are the Laplace transformed stresses and displacements, respectively, and μ^* and ν^* are Laplace transforms of the shear relaxation modulus $\mu(t)$ and the viscoelastic Poisson's ratio $\nu(t)$.

Combining these equations with the traction-free boundary condition (at $\theta = \pm(\pi/2)$)

$$\sigma_{\theta\theta}^* = \tau_{r\theta}^* = 0 \quad (6)$$

and the interface conditions at $\theta = 0$

$$\begin{aligned}(\sigma_{\theta\theta}^*)_I &= (\sigma_{\theta\theta}^*)_{II} \\ (\tau_{r\theta}^*)_I &= (\tau_{r\theta}^*)_{II} \\ (u_r^*)_I &= (u_r^*)_{II} \\ (u_{\theta}^*)_I &= (u_{\theta}^*)_{II},\end{aligned}\quad (7)$$

one can solve the problem.

The boundary value problem represented by (3) to (7) is conveniently solved with the aid of the Mellin transform, defined as

$$\begin{aligned}\bar{\Phi}^*(s, \theta; p) &= \int_0^\infty \Phi^*(r, \theta; p) r^{s-1} dr \\ \bar{\sigma}_{ij}^*(s, \theta; p) &= \int_0^\infty \sigma_{ij}^*(r, \theta; p) r^{s+1} dr \\ \bar{u}_i^*(s, \theta; p) &= \int_0^\infty u_i^*(r, \theta; p) r^s dr.\end{aligned}\quad (8)$$

Typical solutions for the model shown in Fig. 1 are chosen of the form

$$\begin{aligned}\bar{\Phi}^*(s, \theta; p) &= a_I(s, p) \sin(s\theta) + b_I(s, p) \cos(s\theta) \\ &+ c_I(s, p) \sin[(s+2)\theta]\end{aligned}$$

$$+ d_I(s, p) \cos[(s+2)\theta]$$

$$\begin{aligned}\bar{\Phi}_{II}^*(s, \theta; p) &= a_{II}(s, p) \sin(s\theta) + b_{II}(s, p) \cos(s\theta) \\ &+ c_{II}(s, p) \sin[(s+2)\theta] \\ &+ d_{II}(s, p) \cos[(s+2)\theta]\end{aligned}\quad (9)$$

where subscripts "I" and "II" denote the upper viscoelastic zone and the lower elastic zone, respectively.

The relations between stresses, displacements, and stress functions are given as follows:
for the upper viscoelastic zone

$$\begin{aligned}(\bar{\sigma}_{rr}^*)_I &= \left[\frac{d^2}{d\theta^2} - s \right] \bar{\Phi}_I^* \\ (\bar{\sigma}_{\theta\theta}^*)_I &= s(s+1) \bar{\Phi}_I^* \\ (\bar{\tau}_{r\theta}^*)_I &= (s+1) \frac{d}{d\theta} \bar{\Phi}_I^* \\ (\bar{u}_r^*)_I &= \frac{1}{2p\mu_I^*(s+1)} \\ &\times \left[s(1+p\nu_I^*s) \bar{\Phi}_I^* - (1-p\nu_I^*) \frac{d^2}{d\theta^2} \bar{\Phi}_I^* \right] \\ (\bar{u}_{\theta}^*)_I &= \frac{1}{2p\mu_I^*(s+1)(s+2)} \\ &\times \left[(s+p\nu_I^*s^2 - 2(s+1)^2) \frac{d}{d\theta} \bar{\Phi}_I^* \right. \\ &\left. - (1-p\nu_I^*) \frac{d^3}{d\theta^3} \bar{\Phi}_I^* \right];\end{aligned}\quad (10)$$

for the lower elastic zone

$$\begin{aligned}(\bar{\sigma}_{rr}^*)_{II} &= \left[\frac{d^2}{d\theta^2} - s \right] \bar{\Phi}_{II}^* \\ (\bar{\sigma}_{\theta\theta}^*)_{II} &= s(s+1) \bar{\Phi}_{II}^* \\ (\bar{\tau}_{r\theta}^*)_{II} &= (s+1) \frac{d}{d\theta} \bar{\Phi}_{II}^* \\ (\bar{u}_r^*)_{II} &= \frac{1}{2\mu_{II}(s+1)} \\ &\times \left[s(1+\nu_{II}s) \bar{\Phi}_{II}^* - (1-\nu_{II}) \frac{d^2}{d\theta^2} \bar{\Phi}_{II}^* \right] \\ (\bar{u}_{\theta}^*)_{II} &= \frac{1}{2\mu_{II}(s+1)(s+2)} \\ &\times \left[(s+\nu_{II}s^2 - 2(s+1)^2) \frac{d}{d\theta} \bar{\Phi}_{II}^* \right. \\ &\left. - (1-\nu_{II}) \frac{d^3}{d\theta^3} \bar{\Phi}_{II}^* \right].\end{aligned}\quad (11)$$

Substituting Eq. (9) into (10) and (11) and combining these equations with the transformed boundary conditions (at $\theta = \pm(\pi/2)$)

$$(\bar{\sigma}_{\theta\theta}^*)_I = (\bar{\tau}_{r\theta}^*)_I = (\bar{\sigma}_{\theta\theta}^*)_{II} = (\bar{\tau}_{r\theta}^*)_{II} = 0 \quad (12) \quad \text{where}$$

and the transformed interface conditions (at $\theta = 0$)

$$\begin{aligned} (\bar{\sigma}_{\theta\theta}^*)_I &= (\bar{\sigma}_{\theta\theta}^*)_{II}, (\bar{\tau}_{r\theta}^*)_I = (\bar{\tau}_{r\theta}^*)_{II} \\ (\bar{u}_r^*)_I &= (\bar{u}_r^*)_{II}, (\bar{u}_\theta^*)_I = (\bar{u}_\theta^*)_{II} \end{aligned} \quad (13)$$

one can get the following homogeneous system of eight equations:

$$\begin{aligned} & -\sin\left(\frac{s\pi}{2}\right)a_I + \cos\left(\frac{s\pi}{2}\right)b_I \\ & + \sin\left(\frac{s\pi}{2}\right)c_I - \cos\left(\frac{s\pi}{2}\right)d_I = 0 \\ & \cos\left(\frac{s\pi}{2}\right)a_{II} + \sin\left(\frac{s\pi}{2}\right)b_{II} - \left(1 + \frac{2}{s}\right)\cos\left(\frac{s\pi}{2}\right)c_I \\ & - \left(1 + \frac{2}{s}\right)\sin\left(\frac{s\pi}{2}\right)d_I = 0 \\ & \sin\left(\frac{s\pi}{2}\right)a_{II} + \cos\left(\frac{s\pi}{2}\right)b_{II} - \sin\left(\frac{s\pi}{2}\right)c_{II} \\ & - \cos\left(\frac{s\pi}{2}\right)d_{II} = 0 \\ & \cos\left(\frac{s\pi}{2}\right)a_{II} - \sin\left(\frac{s\pi}{2}\right)b_{II} - \left(1 + \frac{2}{s}\right)\cos\left(\frac{s\pi}{2}\right)c_{II} \\ & + \left(1 + \frac{2}{s}\right)\sin\left(\frac{s\pi}{2}\right)d_{II} = 0 \\ & b_I + d_I - b_{II} - d_{II} = 0 \end{aligned}$$

$$sa_I + (s+2)c_I - sa_{II} - (s+2)c_{II} = 0$$

$$\begin{aligned} & \frac{sb_I}{p\mu_I^*} + \frac{1}{p\mu_I^*} [s + 4(1 - p\nu_I^*)]d_I \\ & - \frac{sb_{II}}{\mu_{II}} - \frac{1}{\mu_{II}} [s + 4(1 - \nu_{II})]d_{II} = 0 \\ & - \frac{sa_I}{p\mu_I^*} + \frac{1}{p\mu_I^*} [s + 2 - 4(1 - p\nu_I^*)]c_I \\ & + \frac{sa_{II}}{\mu_{II}} - \frac{1}{\mu_{II}} [s + 2 - 4(1 - \nu_{II})]c_{II} = 0. \end{aligned} \quad (14)$$

A nontrivial solution to the equation exists only if the determinant of the coefficient matrix vanishes. This occurs when s satisfies the following characteristic equation:

$$\begin{aligned} & \left[(m_1(p) - m_2(p)) \cos^2\left(\frac{s\pi}{2}\right) - m_1(p)(s+1)^2 \right]^2 \\ & + m_3^2(p) \cos^2\left(\frac{s\pi}{2}\right) \sin^2\left(\frac{s\pi}{2}\right) \\ & - m_2^2(p)(s+1)^2 = 0 \end{aligned} \quad (15)$$

$$m_1(p) = 2\left(\frac{1}{\mu_{II}} - \frac{1}{p\mu_I^*}\right)$$

$$m_2(p) = \frac{4}{\mu_{II}}(1 - \nu_{II}) - \frac{4}{p\mu_I^*}(1 - p\nu_I^*)$$

$$m_3(p) = \frac{4}{\mu_{II}}(1 - \nu_{II}) + \frac{4}{p\mu_I^*}(1 - p\nu_I^*). \quad (16)$$

Equation (15) has a form identical with that of two bonded, elastic quarter planes if $p\mu_I^*$ and $p\nu_I^*$ are associated with the elastic constants μ_I and ν_I . The calculation of roots of Eq. (15) actually can be reduced to two transformed material parameters $\alpha^*(p)$ and $\beta^*(p)$ which are associated with Dundurs' parameters α_D , β_D (1969). In plane strain, $p\alpha^*(p)$ and $p\beta^*(p)$ are defined as follows:

$$\begin{aligned} p\alpha^*(p) &= \frac{p\mu_I^*(1 - \nu_{II}) - \mu_{II}(1 - p\nu_I^*)}{p\mu_I^*(1 - \nu_{II}) + \mu_{II}(1 - p\nu_I^*)} \\ p\beta^*(p) &= \frac{p\mu_I^*(1 - 2\nu_{II}) - \mu_{II}(1 - 2p\nu_I^*)}{2[p\mu_I^*(1 - \nu_{II}) + \mu_{II}(1 - p\nu_I^*)]} \end{aligned} \quad (17)$$

For the problem of two dissimilar bonded elastic quarter planes, it can be easily verified that transformed material parameters $\alpha^*(p)$ and $\beta^*(p)$ are inverted into Dundurs' parameters α_D , β_D .

The time-dependent behavior of the problem is recovered by inverting Eq. (15) into the real time space. In order to examine the viscoelastic behavior at the interface corner of two bonded, elastic, and viscoelastic quarter planes, the viscoelastic model characterized by a standard solid shear relaxation modulus and a constant Poisson's ratio is taken as follows:

$$\begin{aligned} \mu_I(t) &= g_0 + g_1 \exp(-\lambda t) \\ \nu_I(t) &= \nu_0 \end{aligned} \quad (18)$$

where subscript "I" represents the viscoelastic zone, $\mu(t)$ is shear relaxation modulus, and ν is Poisson's ratio.

Introducing Eq. (18) into (16) and rearranging the resulting equation, we have

$$\begin{aligned} & [A^*(p) + B^*(p) + C^*(p)] \cos^4\left(\frac{s\pi}{2}\right) \\ & - [2A^*(p) + B^*(p)](s+1)^2 \cos^2\left(\frac{s\pi}{2}\right) \\ & + A^*(p)(s+1)^4 + D^*(p) \cos^2\left(\frac{s\pi}{2}\right) \sin^2\left(\frac{s\pi}{2}\right) \\ & - C^*(p)(s+1)^2 = 0 \end{aligned} \quad (19)$$

where

$$\begin{aligned} A^*(p) &= 4\left[\frac{p\mu_I^{*2}}{\mu_{II}^2} - 2\frac{\mu_I^*}{\mu_{II}} + \frac{1}{p}\right] \\ B^*(p) &= -16\left[\frac{p\mu_I^{*2}}{\mu_{II}^2}(1 - \nu_{II}) - \frac{\mu_I^*}{\mu_{II}}(1 - p\nu_I^*)\right. \\ & \quad \left. - \frac{\mu_I^*}{\mu_{II}}(1 - \nu_{II}) + \left(\frac{1}{p} - \nu_I^*\right)\right] \end{aligned}$$

$$\begin{aligned}
C^*(p) &= 16 \left[\frac{p\mu_l^{*2}}{\mu_n^2} (1 - \nu_n)^2 - 2 \frac{\mu_l^*}{\mu_n} (1 - p\nu_l^*)(1 - \nu_n) \right. \\
&\quad \left. + \left(\frac{1}{p} - 2\nu_l^* + p\nu_l^{*2} \right) \right] \\
D^*(p) &= 16 \left[\frac{p\mu_l^{*2}}{\mu_n^2} (1 - \nu_n)^2 + 2 \frac{\mu_l^*}{\mu_n} (1 - p\nu_l^*)(1 - \nu_n) \right. \\
&\quad \left. + \left(\frac{1}{p} - 2\nu_l^* + p\nu_l^{*2} \right) \right]
\end{aligned}$$

$$\begin{aligned}
\mu_l^* &= \frac{g_0}{p} + \frac{g_1}{p + \lambda} \\
\nu_l^* &= \frac{\nu_0}{p}
\end{aligned} \quad (20)$$

Equation (19) can be inverted analytically as follows:

$$\begin{aligned}
C(t) &= 16 \left[(1 - \nu_n)^2 \frac{g_0^2 + (2g_0g_1 + g_1^2 - \lambda g_1^2 t) e^{-\lambda t}}{\mu_n^2} \right. \\
&\quad \left. - 2 \frac{\mu_l(t)}{\mu_n} (1 - \nu_0)(1 - \nu_n) + (1 - \nu_0)^2 \right] \\
D(t) &= 16 \left[(1 - \nu_n)^2 \frac{g_0^2 + (2g_0g_1 + g_1^2 - \lambda g_1^2 t) e^{-\lambda t}}{\mu_n^2} \right. \\
&\quad \left. + 2 \frac{\mu_l(t)}{\mu_n} (1 - \nu_0)(1 - \nu_n) + (1 - \nu_0)^2 \right] \quad (22)
\end{aligned}$$

It can be easily verified that Eq. (21) for $t = 0$ and $t \rightarrow \infty$ is identical with that reported by Bogy (1968).

Equation (17) is inverted analytically as follows:

$$\alpha(t) = \eta_1[\eta_2 + \eta_3 \exp(-\varphi t)] \quad (23)$$

$$\beta(t) = \eta_4[\eta_5 + \eta_6 \exp(-\varphi t)] \quad (24)$$

where

$$\begin{aligned}
\eta_1 &= \frac{g(0)(1 - \nu_n) - \mu_n(1 - \nu_0)}{[g(0)(1 - \nu_n) + \mu_n(1 - \nu_0)]} \\
\eta_2 &= \frac{[g(0)(1 - \nu_n) + \mu_n(1 - \nu_0)][g_0(1 - \nu_n) - \mu_n(1 - \nu_0)]}{[g(0)(1 - \nu_n) - \mu_n(1 - \nu_0)][g_0(1 - \nu_n) + \mu_n(1 - \nu_0)]} \\
\eta_3 &= 1 - \frac{[g(0)(1 - \nu_n) + \mu_n(1 - \nu_0)][g_0(1 - \nu_n) - \mu_n(1 - \nu_0)]}{[g(0)(1 - \nu_n) - \mu_n(1 - \nu_0)][g_0(1 - \nu_n) + \mu_n(1 - \nu_0)]} \\
\eta_4 &= \frac{g(0)(1 - 2\nu_n) - \mu_n(1 - 2\nu_0)}{2[g(0)(1 - \nu_n) + \mu_n(1 - \nu_0)]} \\
\eta_5 &= \frac{[g(0)(1 - \nu_n) + \mu_n(1 - \nu_0)][g_0(1 - 2\nu_n) - \mu_n(1 - 2\nu_0)]}{[g(0)(1 - 2\nu_n) - \mu_n(1 - 2\nu_0)][g_0(1 - \nu_n) + \mu_n(1 - \nu_0)]} \\
\eta_6 &= 1 - \frac{[g(0)(1 - \nu_n) + \mu_n(1 - \nu_0)][g_0(1 - 2\nu_n) - \mu_n(1 - 2\nu_0)]}{[g(0)(1 - 2\nu_n) - \mu_n(1 - 2\nu_0)][g_0(1 - \nu_n) + \mu_n(1 - \nu_0)]}
\end{aligned}$$

$$[A(t) + B(t) + C(t)] \cos^4 \left(\frac{s\pi}{2} \right)$$

$$- [2A(t) + B(t)](s + 1)^2 \cos^2 \left(\frac{s\pi}{2} \right)$$

$$+ A(t)(s + 1)^4 + D(t) \cos^2 \left(\frac{s\pi}{2} \right) \sin^2 \left(\frac{s\pi}{2} \right)$$

$$- C(t)(s + 1)^2 = 0 \quad (21)$$

where

$$A(t) = 4 \left[\frac{g_0^2 + (2g_0g_1 + g_1^2 - \lambda g_1^2 t) e^{-\lambda t}}{\mu_n^2} - 2 \frac{\mu_l(t)}{\mu_n} + 1 \right]$$

$$\begin{aligned}
B(t) &= -16 \left[(1 - \nu_n) \frac{g_0^2 + (2g_0g_1 + g_1^2 - \lambda g_1^2 t) e^{-\lambda t}}{\mu_n^2} \right. \\
&\quad \left. - \left(\frac{\mu_l(t)}{\mu_n} - 1 \right) (1 - \nu_0) - \frac{\mu_l(t)}{\mu_n} (1 - \nu_n) \right]
\end{aligned}$$

$$\varphi = \frac{g_0(1 - \nu_n) + \mu_n(1 - \nu_0)}{[g(0)(1 - \nu_n) + \mu_n(1 - \nu_0)]} \lambda \quad (25)$$

As shown by Dundurs (1969), three types of behavior can occur, giving the following characteristics in the vicinity of the free surface of the interface:

- (a) for material combinations where $|\alpha(t)| < 2|\beta(t)|$ no stress singularity arises,
- (b) for material combinations where $\alpha(t) = 2\beta(t) \neq 0$ a weak singularity of the form $\ln(r)$ occurs, and
- (c) for cases where $|\alpha(t)| > 2|\beta(t)|$ a singularity of the form $r^{-\lambda}$ occurs, where λ is a positive constant.

In this paper, only the case which leads to a singularity of the form $r^{-\lambda}$ will be considered.

Roots of Eq. (21) with $-2 < \text{Re}(s) < -1$ are of interest since they produce solutions with unbounded stresses and vanishing displacements as $r \rightarrow 0$ (Bogy, 1968). The calculation of the zeros of Eq. (21) must be carried out numerically for given values of the material properties. For $0 < \nu_l, \nu_n < 0.5$, there is at most one root s_1 with $-2 < \text{Re}(s) < -1$, and that root is real. A more detailed discussion of the root of Eq. (21) is presented in Bogy (1968).

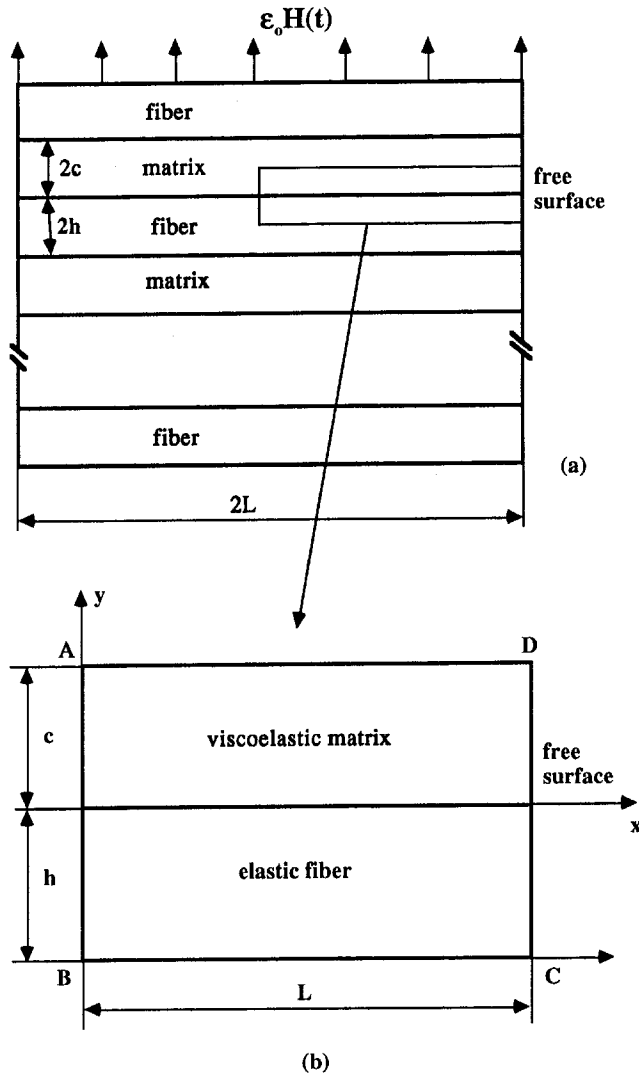


Fig. 2 Idealized unidirectional laminate model

3 Boundary Element Evaluation of Intensity of Stress Singularity for Unidirectional Laminate Model

Figure 2(a) shows a unidirectional laminate subjected to a transverse tensile strain $\epsilon_0 H(t)$, idealized as an infinite layered solid, and Figure 2(b) represents the two-dimensional plane-strain model for analysis of the microstresses at the interface corner between the fiber and matrix. Here $H(t)$ represents a Heaviside unit step function. It is assumed that the fibers are linearly elastic while the matrix is linearly viscoelastic. Typical values of fiber volume fraction range from 0.5–0.6 for fiber-reinforced laminated systems that are currently in use. In this study, fiber volume fraction is taken as 0.5. The fiber and matrix are considered to be perfectly bonded, with no defects or cracks.

Assuming that no body forces exist, the boundary integral equations for the analysis model under a transverse tensile strain can be written as follows:

for the matrix zone

$$c_{ij}^m(\mathbf{y})u_j^m(\mathbf{y}, t) + \int_{S^m} \left[u_j^m(\mathbf{y}', t) T_{ij}^m(\mathbf{y}, \mathbf{y}'; 0+) + \int_{0+}^t u_j^m(\mathbf{y}', t-t') \frac{\partial T_{ij}^m(\mathbf{y}, \mathbf{y}'; t')}{\partial t'} dt' \right] dS^m(\mathbf{y}')$$

$$= \int_{S^m} \left[t_j^m(\mathbf{y}', t) U_{ij}^m(\mathbf{y}, \mathbf{y}'; 0+) + \int_{0+}^t t_j^m(\mathbf{y}', t-t') \frac{\partial U_{ij}^m(\mathbf{y}, \mathbf{y}'; t')}{\partial t'} dt' \right] dS^m(\mathbf{y}'); \quad (26)$$

for the fiber zone

$$c_{ij}^f(\mathbf{y})u_j^f(\mathbf{y}, t) + \int_{S^f} u_j^f(\mathbf{y}', t) T_{ij}^f(\mathbf{y}, \mathbf{y}') dS^f(\mathbf{y}') = \int_{S^f} t_j^f(\mathbf{y}', t) U_{ij}^f(\mathbf{y}, \mathbf{y}') dS^f(\mathbf{y}') \quad (27)$$

where superscripts “m” and “f” represent the matrix and fiber zone, respectively, u_i and t_i denote displacement and traction, and S is the boundary of the given domain. The arguments (\mathbf{y}, t) imply that the variables are dependent upon both the position \mathbf{y} and the time t . $c_{ij}(\mathbf{y})$ is dependent only upon the local geometry of the boundary. For \mathbf{y} on a smooth surface, the free-term $c_{ij}(\mathbf{y})$ is simply a diagonal matrix $0.5 \delta_{ij}$. U_{ij}^m and T_{ij}^f represent the elastic fundamental solutions. The viscoelastic fundamental solutions U_{ij}^m and T_{ij}^m can be obtained by applying the elastic-viscoelastic correspondence principle to the elastic fundamental solutions.

Closed-form integrations of Eqs. (26) and (27) are not, in general, possible and therefore numerical quadrature must be used. Approximations are required in both time and space. In this study, Eqs. (26) and (27) are solved in a step-by-step fashion in time by using the modified Simpson's rule for the time integrals and employing the standard BEM for the surface integrals (Lee and Westmann, 1995). The resulting systems of equations are obtained in the matrix form as follows:

for the matrix zone

$$[\mathbf{H}^1 \mathbf{H}^{12}] \begin{Bmatrix} \mathbf{u}^1 \\ \mathbf{u}^{12} \end{Bmatrix} = [\mathbf{G}^1 \mathbf{G}^{12}] \begin{Bmatrix} \mathbf{t}^1 \\ \mathbf{t}^{12} \end{Bmatrix} + \{\mathbf{R}\}, \quad (28)$$

for the fiber zone

$$[\mathbf{H}^2 \mathbf{H}^{21}] \begin{Bmatrix} \mathbf{u}^2 \\ \mathbf{u}^{21} \end{Bmatrix} = [\mathbf{G}^2 \mathbf{G}^{21}] \begin{Bmatrix} \mathbf{t}^2 \\ \mathbf{t}^{21} \end{Bmatrix}. \quad (29)$$

In Eqs. (28) and (29), superscripts “1” and “2” represent the viscoelastic matrix zone and elastic fiber zone, respectively, while “12” and “21” represent the common interface. \mathbf{H} and \mathbf{G} are influence matrices and \mathbf{R} is the hereditary effect due to the viscoelastic history.

The equilibrium and continuity conditions at the common interface give

$$\mathbf{u}^{21} = \mathbf{u}^{12} \\ \mathbf{t}^{12} = -\mathbf{t}^{21}. \quad (30)$$

Incorporating Eq. (30) into Eqs. (28) and (29) results in the follow matrix equation:

$$\begin{bmatrix} \mathbf{H}^1 & \mathbf{H}^2 & \mathbf{0} & \mathbf{G}^{12} \\ \mathbf{0} & \mathbf{H}^{21} & \mathbf{H}^2 & -\mathbf{G}^{21} \end{bmatrix} \begin{Bmatrix} \mathbf{u}^1 \\ \mathbf{u}^{12} \\ \mathbf{u}^2 \\ \mathbf{u}^{21} \end{Bmatrix} = \begin{bmatrix} \mathbf{G}^1 & \mathbf{0} \\ \mathbf{0} & \mathbf{G}^2 \end{bmatrix} \begin{Bmatrix} \mathbf{t}^1 \\ \mathbf{t}^2 \end{Bmatrix} + \begin{Bmatrix} \mathbf{R} \\ \mathbf{0} \end{Bmatrix}. \quad (31)$$

The above Eq. (31) can be solved by taking account of the external boundary conditions. Due to the symmetry of the model (Fig. 2(b)), the shear stresses on every boundary surface are

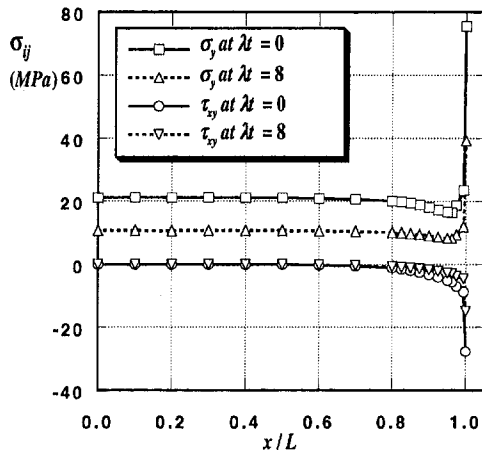


Fig. 3 Distribution of normal stress and shear stress on the interface at times $\lambda t = 0$ and 8.

zero. The resulting boundary conditions for the analysis model are given as follows:

$$\begin{aligned} \tau_{xy} &= 0, & u_x &= 0 & \text{along A-B} \\ \tau_{xy} &= 0, & u_y &= 0 & \text{along B-C} \\ \sigma_{xx} &= 0, & \tau_{xy} &= 0 & \text{along C-D} \\ \tau_{xy} &= 0, & u_y &= (c + h)\epsilon_0 & \text{along D-A.} \end{aligned} \quad (32)$$

Applying the above boundary conditions to Eq. (31) and solving the final system of equations at each time step lead to determination of all boundary and interface displacements and tractions. In order to examine the viscoelastic behavior along the interface line of the analysis model subjected to a transverse tensile strain $\epsilon_0 H(t)$, the viscoelastic model characterized by Eq. (18) is employed. The numerical values used in this example are as follows:

$$\begin{aligned} \mu(0) &= 10^3 \text{ MPa} \\ \mu(\infty) &= 0.5 \times 10^3 \text{ MPa} \\ \nu_0 &= 0.35 \\ \lambda &= 0.1/\text{min} \\ \mu_{II} &= 10^5 \text{ MPa} \\ \nu_{II} &= 0.2 \\ c/h &= 1 \\ L/h &= 12.5 \\ \epsilon_0 &= 0.01 \end{aligned} \quad (33)$$

where superscript “II” represents the elastic fiber zone, μ is the shear modulus, and ν is the Poisson’s ratio.

A suitable mesh density was determined for the analysis based upon the results of a convergence study for mesh refinement. The refined mesh was used near the interface corner. The boundary element discretization consisting of 36 line elements was employed. In this study, quadratic shape functions were used to describe both the geometric and functional variations. Viscoelastic stress profiles were plotted along interface to investigate the nature of stresses. Figure 3 shows the distribution of normal stress σ_y and shear stress τ_{xy} on the interface at nondimensional times $\lambda t = 0$ and 8. The results exhibit the relaxation of the interface stresses and large gradients are observed in the vicinity of the free surface.

The singular stress levels near the free-edge can be characterized by two parameters: the order of the singularity and the free-edge stress intensity factor. The order of singularity must be determined from the roots of the characteristic Eq. (21).

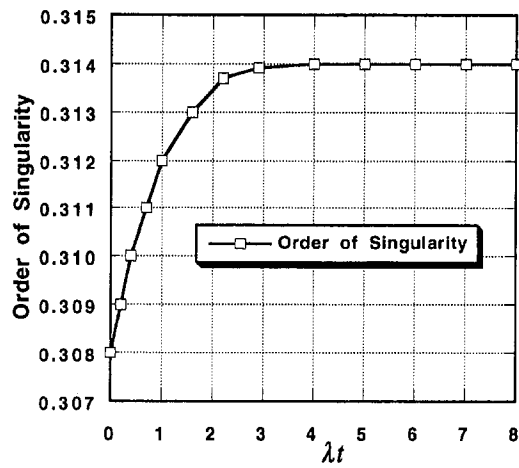


Fig. 4 Variation of the order of the singularity with time

The free-edge stress intensity factor was defined first by Wang and Choi (1982). In this study, the free-edge stress intensity factor is normalized by the quantity $h^{-(s_1+2)}$, giving it stress units, as follows:

$$K_{ij} = \lim_{r \rightarrow 0} \left(\frac{r}{h} \right)^{s_1+2} \sigma_{ij}(r, 0; t). \quad (34)$$

Figure 4 shows the variation of the order of singularity with time for the material properties given by Eq. (33). Since the contrast in shear moduli between the two materials becomes much greater with time, the order of singularity increases with time. For the purpose of comparison, it is interesting to consider two elastic cases for the viscoelastic matrix zone with shear moduli $\mu_I(0)$ and $\mu_I(\infty)$, respectively; i.e., the viscoelastic matrix material of Fig. 2(b) is replaced by an elastic material with $\mu_I(0)$ and $\mu_I(\infty)$ and the elastic fiber zone remains unchanged. At the initial instant of time $\lambda t = 0$, the order of singularity in Fig. 4 is identical with that for an analysis model consisting of elastic matrix with $\mu_I(0)$ and elastic fiber with μ_{II} . At greater times, the order of singularity in Fig. 4 approaches that for the analysis model consisting of elastic matrix with $\mu_I(\infty)$ and elastic fiber with μ_{II} . Figure 5 shows the variation of the free-edge stress intensity factor. It is shown that the free-edge stress intensity factor is relaxed with time while the order of singularity increases with time. It is, however, unclear how these competing effects will effect failure or fiber-matrix debonding.

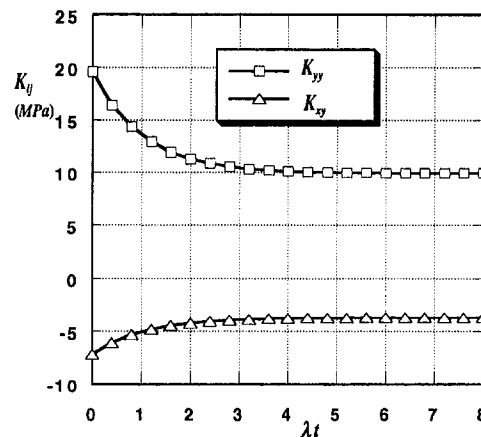


Fig. 5 Relaxation of free-edge stress intensity with time

4 Conclusions

The singular stresses at the interface corner between fiber and matrix of a unidirectional two-dimensional laminate model subjected to a uniform transverse tensile strain have been investigated by using the time-domain boundary element method. Numerical results show that very large stress gradients are present at the interface corner and such stress singularity dominates a very small region relative to layer thickness. It is also shown that the order of singularity increases with time while the free-edge stress intensity factor is relaxed with time. Since the exceedingly large stresses at the interface corner cannot be borne by matrix materials, local yielding or fiber-matrix debonding can occur in the vicinity of free surface.

References

- Blanchard, J. P., and Ghoniem, N. H., 1989, "Relaxation of Thermal Stress Singularities in Bonded Viscoelastic Quarter Planes," *ASME JOURNAL OF APPLIED MECHANICS*, Vol. 56, pp. 756–762.

- Bogy, D. B., 1968, "Edge-Bonded Dissimilar Orthogonal Elastic Wedges Under Normal and Shear Loading," *ASME JOURNAL OF APPLIED MECHANICS*, Vol. 35, pp. 460–466.
- Delale, F., and Erdogan, F., 1981, "Viscoelastic Analysis of Adhesively Bonded Joints," *ASME JOURNAL OF APPLIED MECHANICS*, Vol. 48, pp. 331–338.
- Dundurs, J., 1969, discussion, *ASME JOURNAL OF APPLIED MECHANICS*, Vol. 36, pp. 650–652.
- Lee, S. S., and Westmann, R. A., 1995, "Application of High-Order Quadrature Rules to Time-Domain Boundary Element Analysis of Viscoelasticity," *Int. J. Numerical Methods in Engineering*, Vol. 38, pp. 607–629.
- Reedy, E. D., Jr., 1990, "Intensity of the Stress Singularity at the Interface Corner Between a Bonded Elastic and Rigid Layer," *Engineering Fracture Mechanics*, Vol. 36, pp. 575–583.
- Tsai, M. Y., and Morton, J., 1991, "The Stresses in a Thermally Loaded Bimaterial Interface," *Int. J. Solids and Structures*, Vol. 28, pp. 1053–1075.
- Wang, S. S., and Choi, I., 1982, "Boundary Layer Effects in Composite Laminates, Part 2: Free-Edge Stress Solutions and Basic Characteristics," *ASME JOURNAL OF APPLIED MECHANICS*, Vol. 49, pp. 549–560.
- Weitsman, Y., 1979, "Interfacial Stresses in Viscoelastic Adhesive-Layers Due to Moisture Sorption," *Int. J. Solids and Structures*, Vol. 15, pp. 701–713.

Shakedown Analysis for Trusses and Frames

Pham Duc Chinh¹

Institute of Mechanics,
224 Doi can,
Hanoi, Vietnam

The kinematic method is applied to study the shakedown behavior of certain bar structures subjected to variable loads. For trusses, the possible elastic instability of a thin bar in compression is taken into account. In the case of frames, the possibility of formulating the problem in generalized variables is explored. The result implies that the methods available in plastic limit analysis, such as the method of hinge mechanisms, can be developed for use in shakedown analysis of the structures.

1 Introduction

Applications of shakedown theory in structural analysis meet certain difficulties, as its mathematical apparatus is much more complicated in comparison with that of its special case—the plastic limit theory. Nevertheless, efforts have been made toward implementing the static (mainly) and kinematic theorems to solve various practical problems (see, e.g., Koiter, 1963; Martin, 1975; Maier and Munro, 1982; König, 1987; Pham and Stumpf, 1994; and the references therein). The kinematic approach, which is popular and successful in solving elastic problems by the finite element scheme and in limit plastic analysis, seems not to be in such a stage regarding the shakedown theory, and therefore deserves further attentions. The difficulty comes from the complexity of the kinematic theorem, which involves time integrals over loading processes (the static theorem does not suffer this problem). Based on engineering sense and to avoid difficulty, it is widely accepted in practice to consider separately perfect-incremental and alternating plasticity collapse modes. Perhaps the most rigorous mathematical justifications of the separated criteria are laid down in the monograph of König (1987). The perfect-incremental criterium is derived from the assumption that the plastic strains at every point of the body should change both proportionally and monotonously during a cycle. In reality, a deformation process may be very complex and is not proportional nor monotonous and mixed modes of collapse are possible. Up to the present we do not have a general reduced form (based on rigorous proof) of the kinematic theorem with separated inadaptation modes (which were equivalent to Koiter's original theorem) although we have it for a restricted class of problems (Pham and Stumpf, 1994). An alternative approach in certain circumstances is to formulate the static theorem in a discretized standard form and then derive the dual problem using the tool of convex analysis as suggested in Corradi and Zavelani (1974), Maier and Munro (1982), and Kamenjarzh and Weichert (1992). However, since the formulation is derived from the static one, in our opinion, not much can be expected from the advantage of it over the original static formulation. To explore the possible advantage of the kinematic approach over the static one in appropriate circumstances it is our belief that we should start directly from the original kinematic theorem—the same way we go with

finite element elasticity from the minimum energy principle and in limited analysis with the respective kinematic theorem.

In recent works (Pham, 1993; Pham and Stumpf, 1994) we have succeeded in transforming Koiter's kinematic theorem (Koiter, 1963) into a simpler applicable form, which does not involve time integrals but is equivalent to the original one, for bar structures in the axial and bending deformation mode. Let k_s denote the largest coefficient (called the shakedown safety factor), the external agencies multiplied by which would still keep the structure shakedown, then the reduced kinematic theorem for the bars can be given formally as (Pham, 1993; Pham and Stumpf, 1994)

$$k_s^{-1} = \max \{I, A\}, \quad (1)$$

where

$$I = \sup_{\epsilon^p \in C} \frac{\int_V \max_{t_x} \sigma^e(\mathbf{x}, t_x) \epsilon^p(\mathbf{x}) dV}{\int_V \sigma_Y |\epsilon^p| dV}, \quad (2)$$

$$A = \sup_{x, t, t'} \frac{\sigma^e(\mathbf{x}, t) - \sigma^e(\mathbf{x}, t')}{2\sigma_Y}, \quad (3)$$

and where $\sigma^e(\mathbf{x}, t)$ denotes the fictitious elastic axial stress response of the structure $V(\mathbf{x} \in V)$ to the external agencies in the assumption of its perfectly-elastic behavior, which is confined to a certain bounded loading domain \mathcal{L} ; $\epsilon^p(\mathbf{x})$ —axial plastic strain; σ_Y —yield stress; and C is the set of compatible plastic strain fields.

As the bars are assumed in the axial and bending deformation mode, only the axial components of the stress and strain are present, while the other ones are secondary and can be disregarded. However, the stress and strain can vary across any section of the bars as well as along their axes. Usually it is presumed that the cross-sections of the bars remain planar and orthogonal to their axes during deformation, so the set C of compatible strain fields should be restricted by that kinematic constraint. The plastic strain rate field need not satisfy compatibility conditions but does not appear explicitly in the expression of the reduced theorem (1)–(3).

It can be seen that term (2) is responsible for incremental collapse (the compatible plastic deformation increment over a cycle $\epsilon^p \neq 0$), while the term (3) represents the alternating plasticity collapse.

Generally there is no simple transformation of (1)–(3) in generalized variables (moments, curvatures, etc.).

In the reduced form (1)–(3), the shakedown theorem is very near to the corresponding limit theorem, which through the limit safety factor k_s can be stated as

¹ Also at the Department of Mechanical Engineering, The University of Sydney, Sydney, Australia.

Contributed by the Applied Mechanics Division of THE AMERICAN SOCIETY OF MECHANICAL ENGINEERS for publication in the ASME JOURNAL OF APPLIED MECHANICS.

Discussion on the paper should be addressed to the Technical Editor, Professor Lewis T. Wheeler, Department of Mechanical Engineering, University of Houston, Houston, TX 77204-4792, and will be accepted until four months after final publication of the paper itself in the ASME JOURNAL OF APPLIED MECHANICS.

Manuscript received by the ASME Applied Mechanics Division, Jan. 30, 1996; final revision, July 5, 1996. Associate Technical Editor: R. Becker.

$$\hat{k}_s^{-1} = \sup_{\epsilon^p \in C} \frac{\int_V \sigma^e(\mathbf{x}) \cdot \epsilon^p(\mathbf{x}) dV}{\int_V \sigma_Y |\epsilon^p| dV}. \quad (4)$$

We have known that the shakedown design is more conservative than the limit plastic design, which is much simpler. The similarity between (4) and (1)–(3) makes us hope that the methods available in solving the former can be developed for use in solving the latter.

In plastic limit analysis of frames, one can work with plastic hinges. In shakedown analysis, complex distributions of residual stresses across the bar sections may be involved and contribute implicitly to the complexity of (1)–(3).

2 Trusses Under Quasi-Static Loading

Consider a truss structure composed of n pin-connected bars. The bars of lengths l_i carry axial forces $P_i(t)$ ($i = 1, \dots, n$), which are limited by the yield conditions $|P_i| \leq P_i^Y$. Let ϵ_i denote the strain of i -bar. The fictitious elastic reactions $\{P_i^e(t)\}$ of the bars to external agencies are confined to \mathcal{L} :

$$P_i^L \leq P_i^e(t) \leq P_i^U, \quad i = 1, \dots, n. \quad (5)$$

In this particular case, the reduced kinematic theorem (1)–(3) yields

$$k_s^{-1} = \max \{I, A\}, \quad (6)$$

$$I = \sup_{\{\epsilon_i\} \in C} \frac{\sum_{i=1}^n l_i \cdot \max \{P_i^U \epsilon_i, P_i^L \epsilon_i\}}{\sum_{i=1}^n l_i \cdot P_i^Y |\epsilon_i|}, \quad (7)$$

$$A = \max_i \frac{P_i^U - P_i^L}{2P_i^Y}. \quad (8)$$

For comparison, the corresponding safety factor in limit analysis has the form (according to (4))

$$\hat{k}_s^{-1} = \sup_{\{\epsilon_i\} \in C} \frac{\sum_{i=1}^n l_i \cdot P_i^e \epsilon_i}{\sum_{i=1}^n l_i \cdot P_i^Y |\epsilon_i|}. \quad (9)$$

If a bar is sufficiently thin, such that $P_i^Y > P_i^b$, where P_i^b denotes the Euler buckling force for the bar, the compression force in the bar can never reach P_i^Y , but is restricted by the smaller force P_i^b . So the formulae (6)–(8) should be modified accordingly. As the instability at P_i^b can contribute toward the incremental collapse mode (through I) but does not affect the alternating plasticity collapse mode (described by A), the safety factor k_{sb} for the problem can be given as

$$k_{sb}^{-1} = \max \{I_{sb}, A\}, \quad (10)$$

$$I_{sb} = \sup_{\{\epsilon_i\} \in C} \frac{\sum_{i=1}^n l_i \cdot \max \{P_i^U \epsilon_i, P_i^L \epsilon_i\}}{\sum_{i=1}^n l_i \cdot D_i^b(\epsilon_i)}, \quad (11)$$

$$A = \max_i \frac{P_i^U - P_i^L}{2P_i^Y}, \quad (12)$$

$$D_i^b(\epsilon_i) = \begin{cases} P_i^Y \epsilon_i, & \epsilon_i \geq 0 \\ \min \{-P_i^Y \epsilon_i, -P_i^b \epsilon_i\}, & \epsilon_i < 0 \end{cases} \\ = \max \{P_i^Y \epsilon_i, \min \{-P_i^Y \epsilon_i, -P_i^b \epsilon_i\}\}. \quad (13)$$

3 Shakedown of Frames in Bending

Consider an n -bar frame with local longitudinal coordinate axes lying along the axes of the bars (beams): $0 \leq x_i \leq l_i$, $i = 1, \dots, n$. The beams may be variable (but symmetric about the bending axis) cross sections. The bending planes of the beams are fixed and the compatible axial strain has the form

$$\epsilon_i(x_i, z) = z \cdot \kappa_i(x_i), \quad -h_i(x_i) \leq z \leq h_i(x_i) \\ i = 1, \dots, n, \quad (14)$$

z is the coordinate normal to and originated from the bending axis in the bending plane, κ_i is the curvature change of the bar axis.

Respectively, the fictitious elastic axial stress σ_i^e and bending moment M_i^e of the i -beam are related by

$$\sigma_i^e(x_i, z, t) = z \cdot \frac{M_i^e(x_i, t)}{J_i^0}, \quad (15)$$

J_i^0 is the second moment of area of the bar cross section.

The fictitious elastic bending moment response to external agencies is confined to \mathcal{L} :

$$M_i^L(x_i) \leq M_i^e(x_i, t) \leq M_i^U(x_i), \quad i = 1, \dots, n. \quad (16)$$

Substitution of (14)–(16) into (1)–(3) yields the relations in generalized variables:

$$k_s^{-1} = \max \{I, A\}, \quad (17)$$

$$I = \sup_{\{\kappa_i\} \in C} \frac{\sum_{i=1}^n \int_0^{l_i} \max \{M_i^U(x_i) \kappa_i(x_i), M_i^L(x_i) \kappa_i(x_i)\} dx_i}{\sum_{i=1}^n \int_0^{l_i} M_i^Y(x_i) |\kappa_i(x_i)| dx_i}, \quad (18)$$

$$A = \max_{i, x_i} \frac{M_i^U(x_i) - M_i^L(x_i)}{2M_i^E(x_i)}, \quad (19)$$

where M_i^Y is the yield moment and M_i^E is the elastic limit moment (the moment at beginning of plastic deformations at the extreme fibers) of the beam.

Correspondingly, the limit safety factor for frames has the form (according to (4))

$$\hat{k}_s^{-1} = \sup_{\{\kappa_i\} \in C} \frac{\sum_{i=1}^n \int_0^{l_i} M_i^e(x_i) \kappa_i(x_i) dx_i}{\sum_{i=1}^n \int_0^{l_i} M_i^Y(x_i) |\kappa_i(x_i)| dx_i}. \quad (20)$$

The similarity between (17)–(19) and (20) (in particular, between (18) representing the incremental collapse and (20)) implicates that the methods available in limit analysis of frames (see, e.g., Neal and Symonds, 1952; Hodge, 1959; Lubliner, 1990) can be developed for use there as well (in particular, the method of mechanisms with plastic hinges).

For example, consider a uniform beam $0 \leq x \leq L$ (Fig. 1(a)) clamped at both ends A and C , and subjected to a quasi-static load $P(t)$ at the midpoint B of the beam, such that

$$P^L \leq P(t) \leq P^U. \quad (21)$$

The fictitious elastic moment response of the beam to the external load is

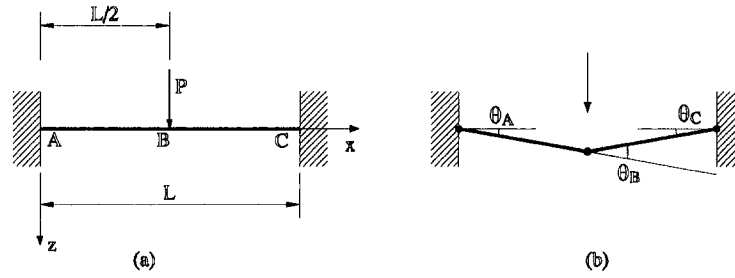


Fig. 1 (a) A beam clamped at both ends and subjected to a variable load at the midpoint; (b) an incremental collapse mechanism with the plastic hinges at A, B, and C

$$M^e(x, t) = \begin{cases} P(t) \cdot \left(\frac{x}{2} - \frac{L}{8} \right), & 0 \leq x \leq \frac{L}{2} \\ P(t) \cdot \left(\frac{3L}{8} - \frac{x}{2} \right), & \frac{L}{2} \leq x \leq L. \end{cases} \quad (22)$$

The loading domain \mathcal{L} is determined from (21) and (22):

$$\begin{aligned} M^L(x) &\leq M^e(x, t) \leq M^U(x), & (23) \\ M^L &= P^U \left(\frac{x}{2} - \frac{L}{8} \right), \quad M^U = P^L \left(\frac{x}{2} - \frac{L}{8} \right), & 0 \leq x \leq \frac{L}{4}, \\ M^L &= P^L \left(\frac{x}{2} - \frac{L}{8} \right), \quad M^U = P^U \left(\frac{x}{2} - \frac{L}{8} \right), & \frac{L}{4} \leq x \leq \frac{L}{2}, \\ M^L &= P^L \left(\frac{3L}{8} - \frac{x}{2} \right), \quad M^U = P^U \left(\frac{3L}{8} - \frac{x}{2} \right), & \frac{L}{2} \leq x \leq \frac{3L}{4}, \\ M^L &= P^U \left(\frac{3L}{8} - \frac{x}{2} \right), \quad M^U = P^L \left(\frac{3L}{8} - \frac{x}{2} \right), & \frac{3L}{4} \leq x \leq L. \end{aligned} \quad (24)$$

We come to (17). A is determined from (19) and (24)

$$A = \max_x \frac{M^U(x) - M^L(x)}{2M^E} = \frac{(P^U - P^L) \cdot L}{16M^E}. \quad (25)$$

To evaluate I in (18), we look for kinematically admissible incremental mechanisms $\kappa(x)$. There are only two possible mechanisms with the plastic hinges at A, B, C and the angle increment $\theta_B > 0$ or $\theta_B < 0$ (see Fig. 1(b)), which can be given as ($\delta(x)$ is the Dirac function)

$$\begin{aligned} \kappa(x) &= \theta_A \cdot \delta(x) + \theta_B \cdot \delta(x - L/2) + \theta_C \cdot \delta(x - L), \\ \theta_A &= \theta_C = -\theta_B/2, \quad \theta_B > 0 \quad \text{or} \quad \theta_B < 0. \end{aligned} \quad (26)$$

Substituting (26) into (18) and taking into account (24), one finds

Finally,

$$\begin{aligned} k_s^{-1} &= \text{Max} \{I, A\} \\ &= \text{Max} \left\{ \frac{P^U \cdot L}{8M^Y}, \frac{-P^L \cdot L}{8M^Y}, \frac{(P^U - P^L) \cdot L}{16M^E} \right\}. \end{aligned} \quad (28)$$

Shakedown theory is not restricted to quasi-static loading, but extended to general dynamic loading (Pham, 1992, 1996), the most important class of which might be the quasi-periodic dynamic one, as it is relatively easy to be described and supposed to model the wind, wave, and transport loads acting upon practical structures. Formulae (17)–(19) are still valid with a quasi-periodic dynamic response $M^e(x, t)$ taking the place of the quasi-static one in (16). For example, we take again the structure in Fig. 1 under a quasi-periodic dynamic loading,

$$P(t) = p_1 \sin \omega t + p_0, \quad (29)$$

where p_0, p_1, ω are arbitrary quasi-static functions of time, such that

$$p_0^L \leq p_0(t) \leq p_0^U, \quad 0 \leq p_1(t) \leq p_1^U,$$

$$0 \leq \omega(t) \leq \omega_1 < \omega_I, \quad (30)$$

ω_I is the principal natural frequency of the beam. Denote

$$\alpha = \left(\frac{m\omega^2}{EJ} \right)^{1/4}, \quad \alpha_1 = \left(\frac{m\omega_1^2}{EJ} \right)^{1/4}, \quad (31)$$

where m, E, J are the density, Young's modulus, and moment of inertia of the beam, respectively.

The fictitious elastic moment response of the beam to the external load is

$$\begin{aligned} I &= \sup_{\theta_B} \frac{\max \{M_A^U \theta_A, M_A^L \theta_A\} + \max \{M_B^U \theta_B, M_B^L \theta_B\} + \max \{M_C^U \theta_C, M_C^L \theta_C\}}{M^Y (|\theta_A| + |\theta_B| + |\theta_C|)} \\ &= \sup_{\theta_B} \frac{\max \left\{ P^U \frac{\theta_B}{2}, P^L \frac{\theta_B}{2} \right\} + \max \{P^U \theta_B, P^L \theta_B\} + \max \left\{ P^U \frac{\theta_B}{2}, P^L \frac{\theta_B}{2} \right\}}{M^Y \cdot 2|\theta_B|} = \text{Max} \left\{ \frac{P^U \cdot L}{8M^Y}, \frac{-P^L \cdot L}{8M^Y} \right\}. \end{aligned} \quad (27)$$

$$M^e = \begin{cases} p_1 \sin \omega t \frac{(\cos \alpha x + \operatorname{ch} \alpha x) \left(\cos \frac{\alpha L}{2} - \operatorname{ch} \frac{\alpha L}{2} \right) + (\sin \alpha x + \operatorname{sh} \alpha x) \left(\sin \frac{\alpha L}{2} + \operatorname{sh} \frac{\alpha L}{2} \right)}{4\alpha \left(\operatorname{sh} \frac{\alpha L}{2} \cos \frac{\alpha L}{2} + \sin \frac{\alpha L}{2} \operatorname{ch} \frac{\alpha L}{2} \right)} \\ + p_0 \cdot (x/2 - L/8), 0 \leq x \leq L/2, \\ p_1 \sin \omega t \frac{[\cos \alpha(x-L) + \operatorname{ch} \alpha(x-L)] \left(\cos \frac{\alpha L}{2} - \operatorname{ch} \frac{\alpha L}{2} \right) - [\sin \alpha(x-L) + \operatorname{sh} \alpha(x-L)] \left(\sin \frac{\alpha L}{2} + \operatorname{sh} \frac{\alpha L}{2} \right)}{4\alpha \left(\operatorname{sh} \frac{\alpha L}{2} \cos \frac{\alpha L}{2} + \sin \frac{\alpha L}{2} \operatorname{ch} \frac{\alpha L}{2} \right)} \\ + p_0 \cdot (3L/8 - x/2), L/2 \leq x \leq L. \end{cases} \quad (32)$$

Following the steps as those from (22) to (28) we get

$$k_s^{-1} = \operatorname{Max} \{I, A\}, \quad (33)$$

$$A = \frac{p_1^U}{M^E} \cdot \frac{\max \left\{ \operatorname{ch} \frac{\alpha_1 L}{2} - \cos \frac{\alpha_1 L}{2}, \sin \frac{\alpha_1 L}{2} \operatorname{sh} \frac{\alpha_1 L}{2} \right\}}{2\alpha_1 \left(\operatorname{sh} \frac{\alpha_1 L}{2} \cos \frac{\alpha_1 L}{2} + \sin \frac{\alpha_1 L}{2} \operatorname{ch} \frac{\alpha_1 L}{2} \right)} + \frac{(p_0^U - p_0^L) \cdot L}{16M^E}, \quad (34)$$

$$I = \max \left\{ \frac{p_1^U}{M^Y} \cdot \frac{\operatorname{ch} \frac{\alpha_1 L}{2} - \cos \frac{\alpha_1 L}{2} + \sin \frac{\alpha_1 L}{2} \operatorname{sh} \frac{\alpha_1 L}{2}}{4\alpha_1 \left(\operatorname{sh} \frac{\alpha_1 L}{2} \cos \frac{\alpha_1 L}{2} + \sin \frac{\alpha_1 L}{2} \operatorname{ch} \frac{\alpha_1 L}{2} \right)} + \frac{p_0^U \cdot L}{8M^Y}, \right. \\ \left. - \frac{p_1^U}{M^Y} \cdot \frac{\operatorname{ch} \frac{\alpha_1 L}{2} - \cos \frac{\alpha_1 L}{2} + \sin \frac{\alpha_1 L}{2} \operatorname{sh} \frac{\alpha_1 L}{2}}{4\alpha_1 \left(\operatorname{sh} \frac{\alpha_1 L}{2} \cos \frac{\alpha_1 L}{2} + \sin \frac{\alpha_1 L}{2} \operatorname{ch} \frac{\alpha_1 L}{2} \right)} - \frac{p_0^L \cdot L}{8M^Y} \right\}, \quad (35)$$

which determines the limits on the shakedown load for the structure.

4 Asymmetric Beams

The concept of generalized stress and strain (moments, curvatures, . . .) is useful not only in elasticity, but also in plastic limit analysis of beams and arches and frames (Prager, 1959). In shakedown theory, and generally in elastoplastic analysis of the structures (except the simple cases of trusses and ideal sandwich beams), additional complexities may arise from possible local distributions of residual stresses and plastic strains, which should be treated specifically. In the previous section we are able to give a simple formula for the shakedown factor of symmetric beams in the generalized variables. In this section we study bending of the beams, whose cross sections are asymmetric about the bending axis. Symptoms of difficulties have already been observed in Pham and Stumpf (1994) concerning the symmetric bars under combined axial and bending loads. For simplicity of notations, we take a single beam ($0 \leq x \leq l$), but the result also applies to the frames composed of beams as in the previous section in the respective sense. As in (15), the fictitious elastic axial stress σ^e and bending moment M^e are related by

$$\sigma^e(x, z, t) = z \cdot \frac{M^e(x, t)}{J^0}, \quad h^-(x) \leq z \leq h^+(x), \quad (36)$$

with $z = 0$ being the elastic bending axis (J^0 is the second moment of area of the section relative to this axis), the external agencies being such that M^e is restricted by

$$M^L(x) \leq M^e(x, t) \leq M^U(x). \quad (37)$$

As the beam is asymmetric, the bending axes change their positions in the cross sections during plastic deformations; so instead of (14), the compatible plastic axial deformation field ϵ should have the form

$$\epsilon(x, z) = [z - c(x)] \cdot \kappa(x), \quad h^-(x) \leq c(x) \leq h^+(x), \quad (38)$$

with $c(x)$ being a function of the axial coordinate.

Now, substituting (21)–(23) into (1)–(3) one can get

$$k_s^{-1} = \operatorname{Max} \{I, A\}, \quad (39)$$

$$I = \sup_{\kappa \in C, h^- \leq c \leq h^+} \frac{\int_0^l U(M^U, M^L, \kappa, c) dx}{\int_0^l D(\kappa, c) dx}, \quad (40)$$

$$A = \max_x \frac{M^U(x) - M^L(x)}{2M^E(x)}, \quad (41)$$

where ($S^0(x)$ is the area of the cross section and σ_Y is the yield stress in tension)

$$U = \int_{S^0} \max_{t_x} \sigma^e(x, z, t_x) \epsilon(x, z) dS \\ = \int_{S^0} \max_{t_x} \left[(z - c) z \frac{M(x, t_x)}{J^0} \kappa \right] dS, \quad (42)$$

$$D = \int_{S^0} \sigma_Y |\epsilon| dS = \int_{S^0} \sigma_Y |z - c| |\kappa| dS. \quad (43)$$

Let $S(z_1, z_2)$ denote the area of the part of the cross section that lies between the lines $z = z_1$ and $z = z_2$, which are orthogonal to the bending plane. $F(z_1, z_2)$ and $J(z_1, z_2)$ are, respectively, the static moment and second moment of area of the part relative to the axis $z = 0$. We calculate (42) and (43)

$$D = \left[\int_{S(h^-, c)} (c - z) dS + \int_{S(c, h^+)} (z - c) dS \right] \cdot \sigma_Y |\kappa| \\ = [S(h^-, c) \cdot c - F(h^-, c) \\ + F(c, h^+) - S(c, h^+) \cdot c] \cdot \sigma_Y |\kappa| \quad (44)$$

$$\begin{aligned}
U &= \frac{1}{J^0} \left[\int_{S(h^-, 0)} (z - c) z dS + \int_{S(c, h^+)} (z - c) z dS \right] \\
&\times \max \{ M^U \kappa, M^L \kappa \} \\
&+ \frac{1}{J^0} \int_{S(0, c)} (z - c) z dS \cdot \min \{ M^U \kappa, M^L \kappa \} \\
&= \frac{1}{J^0} [J(h^-, 0) - c \cdot F(h^-, 0) + J(c, h^+) \\
&- c \cdot F(c, h^+)] \cdot \max \{ M^U \kappa, M^L \kappa \} \\
&+ \frac{1}{J^0} [J(0, c) - c \cdot F(0, c)] \cdot \min \{ M^U \kappa, M^L \kappa \} \\
&\quad (c \geq 0); \quad (45)
\end{aligned}$$

$$\begin{aligned}
U &= \frac{1}{J^0} \left[\int_{S(h^-, c)} (z - c) z dS + \int_{S(0, h^+)} (z - c) z dS \right] \\
&\times \max \{ M^U \kappa, M^L \kappa \} \\
&+ \frac{1}{J^0} \int_{S(c, 0)} (z - c) z dS \cdot \min \{ M^U \kappa, M^L \kappa \} \\
&= \frac{1}{J^0} [J(h^-, c) - c \cdot F(h^-, c) + J(0, h^+) \\
&- c \cdot F(0, h^+)] \cdot \max \{ M^U \kappa, M^L \kappa \} \\
&+ \frac{1}{J^0} [J(c, 0) - c \cdot F(c, 0)] \cdot \min \{ M^U \kappa, M^L \kappa \} \\
&\quad (c < 0). \quad (46)
\end{aligned}$$

Comparing (17)–(19) with (39)–(41), we see that in the latter appears a new variable $c(x)$ in addition to the generalized kinematic variable $\kappa(x)$. In the case of symmetric beams $c(x) \equiv 0$, the latter formulae reduce to the former. If the upper bound method of plastic hinge mechanisms is applied, at a hinge section the variable $c(x)$ is determined from the yield condition for the section. Generally, however, exact $c(x)$ together with $\kappa(x)$ should be found from the optimization problem (39)–(41), (44)–(46). The ultimate presence of the variable $c(x)$ in the formulae contributes to difficulties of shakedown analysis in comparison with limit analysis, for which a rigid plastic analysis with plastic hinges is sufficient to determine the exact limit load.

In summary, we have not yet a general reduced form of shakedown kinematic theorem with separated incremental and alternating plasticity collapse modes; however, we have such a form for trusses and frames. Certain similarity of the reduced form with the kinematic theorem in limit analysis suggests that the methods available in solving the latter can be developed to study the former. However, there are differences that we should be careful about. In limit analysis, rigid plastic schemes are sufficient to determine the collapse load, while in shakedown analysis the elastoplastic state of the structures should be taken into account. Shakedown analysis applies also to dynamic loading problems (here we would like to make an emphasis on quasi-periodic dynamic loading), which lie outside the framework of limit analysis.

This study is concerned with the shakedown of bar structures. A more general aspect of the kinematic method is addressed in Pham and Stumpf (1994) and Pham (1996, 1997).

Acknowledgments

This work is supported by the Program of Fundamental Research in Natural Science.

References

- Corradi, L., and Zavelani, A., 1974, "A linear programming approach to shakedown analysis of structures," *Comput. Math. Mech. Engng.*, Vol. 3, p. 37.
- Hodge, P. G., Jr., 1959, *Plastic Analysis of Structures*, McGraw-Hill, New York.
- Kamenjarzh, J., and Weichert, D., 1992, "On kinematic upper bounds for the safety factor in shakedown theory," *Int. J. Plasticity*, Vol. 8, pp. 827–837.
- Koiter, W. T., 1963, "General theorems for elastic-plastic solids," *Progress in solids mechanics* I. N. Sneddon and R. Hill eds., North-Holland, Amsterdam, pp. 165–221.
- König, J. A., 1987, *Shakedown of elastic-plastic structures*, Elsevier, Amsterdam.
- Lubliner, J., 1990, *Plasticity theory*, McMillan, New York.
- Maier, G., and Monro, J., 1982, "Mathematical programming applications to engineering plastic analysis," *Appl. Mech. Rev.*, Vol. 35, pp. 1631–1643.
- Martin, J. B., 1975, *Plasticity: Fundamentals and General Results*, M.I.T. Press, Cambridge, MA.
- Neal, B. G., and Symonds, P. S., 1952, *Proc. Inst. Civ. Engrs.*, Vol. 1, p. 58.
- Pham, D. C., 1992, "Extended shakedown theorems for elastic plastic bodies under quasiperiodic dynamic loading," *Proc. R. Soc. Lond.*, Vol. A439, pp. 649–658.
- Pham, D. C., 1993, "Shakedown of bars subjected to cycles of loads and temperature," *Int. J. Solids Structures*, Vol. 30, pp. 1173–1179.
- Pham, D. C., and Stumpf, H., 1994, "Kinematical approach to shakedown analysis of some structures," *Q. Appl. Math.*, Vol. 52, pp. 707–719.
- Pham, D. C., 1996, "Dynamic shakedown and a reduced kinematic theorem," *Int. J. Plasticity*, Vol. 12, pp. 1055–1068.
- Pham, D. C., 1997, "Reduced forms of shakedown kinematic theorem for elastic-perfectly plastic," *Proc. Royal Soc. Lond.*, in press.
- Prager, W., 1959, *An introduction to plasticity*, Addition-Wesley.

M. J. Adams¹

B. J. Briscoe

G. M. Corfield

C. J. Lawrence

T. D. Papathanasiou

Department of Chemical Engineering
and Chemical Technology,
Imperial College of Science, Technology
and Medicine,
London, UK

An Analysis of the Plane-Strain Compression of Viscoplastic Materials

A theoretical analysis for the plane-strain compression of viscoplastic materials with a Tresca wall boundary condition is described. The analysis is based upon the incorporation of a viscoplastic associated flow rule into the cycloidal solution originally developed for rigid-perfectly plastic materials. The evolution of the calculated stress field suggests that the influence of strain rate hardening is similar to that reported previously for strain hardening. The calculated strain fields are elliptical in form and are consistent with those measured for a viscoplastic paste. Previous analyses of the compression of viscoplastic materials have employed the lubrication approximation for fluid flows with a resulting kinematic inconsistency in the predicted velocity fields.

1 Introduction

Zienkiewicz and Goodhale (1974) have examined the deformation of elasto-viscoplastic materials under large imposed strains when the elastic components may be neglected. They showed that such deformations could be usefully considered in terms of a non-Newtonian flow rule with the viscosity being a function of the current strain rates. In particular, on the basis of a viscoplastic associated flow proposed by Perzyna (1966) they were able to derive a constitutive relationship which is equivalent to that for a Bingham fluid where the flow stress is given as the sum of a plastic and a viscous component. The Herschel-Bulkley (1926) fluid is a more general form for this class of materials where the viscous component is given by a power-law term.

A common means of measuring the material parameters for the above "plastic fluids" is by compression between parallel platens. This is termed "squeeze flow" and is similar to the upsetting technique used for metals. Squeeze flow has been analysed using the lubrication approximation to the Navier-Stokes equation (Covey and Stanmore, 1981). However, this leads to an inconsistency in the calculated velocity field (Lipscombe and Denn, 1984; Adams et al., 1994). An unyielded region is predicted that is centred upon the midplane, parallel to the platens, with flow regions developed between this region and the surfaces of the platens (Fig. 1). In order to maintain continuity, the unyielded region would have to extend during closure of the platens which would violate the yield condition. This arises because of the difficulty in introducing a three-dimensional yield criterion into fluid dynamics analyses; the lubrication solution is based upon prescribing a critical shear stress for plastic flow to be instituted.

The plane-strain compression of plastically deforming materials between two parallel plates has been the subject of a number of studies. In the case of rigid-perfectly plastic materials, Prandtl (1923) obtained an analytical expression for the stress field (the cycloidal solution) while a corresponding velocity

solution was derived by Nadai (see Hill, 1950). Collins and Meguid (1977) extended these solutions for materials that exhibit both isotropic and anisotropic strain-hardening behavior. In this paper, we will describe how the solution may be adapted for viscoplastic materials which avoids the inconsistency associated with the lubrication solution.

2 Formulation

The coordinate system is shown in Fig. 2 for platens of width $l (=2L)$, instantaneous gap $h (=2H)$, and a constant closure velocity $u (=2U)$. Tresca wall boundary conditions are assumed such that the wall shear stress (τ_w) is given by

$$\tau_w = mk \quad (1)$$

where m is the interfacial friction factor ($0 \leq m \leq 1$) and k is the bulk shear yield stress which is a function of the strain rates (see later). The reduced yield criterion may be written in terms of the normal stress σ_x and σ_y in the following form:

$$\sigma_{xy} = \frac{1}{2}(\sigma_x - \sigma_y) = g(\tau_{xy}, y) = \pm[k^2 - \tau_{xy}^2]^{1/2} \quad (2)$$

where g is a function of the shear stress, τ_{xy} , which is dependent on y but not on x . This corresponds to the limiting field condition when the width of the compressed material is much greater than its height.

The associated flow rule may be expressed as

$$\tan 2\phi = \frac{-s_{xy}}{\tau} = -\frac{1}{2} \frac{\sigma_x - \sigma_y}{\tau_{xy}} = -\frac{1}{2} \frac{e_x - e_y}{e_{xy}} \quad (3)$$

where e_x , e_y , and e_{xy} are components of the strain rate tensor. From Eqs. (1), (2), and (3), together with the equilibrium and continuity conditions, the following relationships for the stress and velocity components may be obtained (see Collins and Meguid, 1977):

$$\sigma_y = \frac{\tau_w}{H} x + C_1 \quad (4)$$

where C_1 is a constant of integration.

$$\sigma_x = \frac{\tau_w}{H} x + C_1 + 2(k^2 - \tau_{xy}^2)^{1/2} \quad (5)$$

$$\tau_{xy} = \frac{-\tau_w}{H} y \quad (6)$$

¹ Visiting Professor from Unilever Research Ltd., Port Sunlight Laboratory.

Contributed by the Applied Mechanics Division of THE AMERICAN SOCIETY OF MECHANICAL ENGINEERS for publication in the ASME JOURNAL OF APPLIED MECHANICS.

Discussion on this paper should be addressed to the Technical Editor, Professor Lewis T. Wheeler, Department of Mechanical Engineering, University of Houston, Houston, TX 77204-4792, and will be accepted until four months after final publication of the paper itself in the ASME JOURNAL OF APPLIED MECHANICS.

Manuscript received by the ASME Applied Mechanics Division, Feb. 15, 1996; final revision, Aug. 12, 1996. Associate Technical Editor: R. Becker.

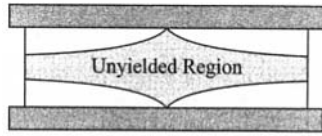


Fig. 1 Schematic of a squeeze flow rheometer

$$v_y = \frac{-U}{H} y \quad (7)$$

$$v_x = \frac{U}{H} x - \left(\frac{2U}{H} \right) \int \cot 2\phi dy \quad (8)$$

The forms given by (4)–(8) are valid for $x > 0$ with suitable symmetry for $x < 0$. The viscoplastic constitutive flow rule proposed by Perzyna (1966) may be written as follows:

$$e_{ij} = \gamma \langle \phi(F) \rangle \frac{\partial f}{\partial \sigma_{ij}} \quad (9)$$

where γ represents the fluidity which has units of reciprocal time, ϕ is a material function that defines the strain-rate dependency, σ_{ij} is the total stress tensor, $F = 0$ is the static yield function, f is the dynamic yield criterion defining the viscoplastic overstress, and $\langle \cdot \rangle$ are Macaulay's brackets. We will consider the general case where $\phi(F)$ is taken as being equal to $F^{1/n}$. Inversion of this function leads to a relationship that is analogous to a Herschel-Bulkley fluid, thus

$$k = k_0 \left\{ 1 + \left[\frac{(I_2^{vp})^{1/2}}{\gamma} \right]^n \right\} \quad (10)$$

where k_0 is the static shear yield stress and k is the corresponding dynamic value. The second invariant of the viscoplastic strain rate tensor, $I_2^{vp} = (\frac{1}{2} e_{ij} e_{ij})$, is given by

$$4I_2^{vp} = 2 \left[\left(\frac{\partial v_y}{\partial y} \right)^2 + \left(\frac{\partial v_x}{\partial x} \right)^2 \right] + \left[\frac{\partial v_y}{\partial x} + \frac{\partial v_x}{\partial y} \right]^2 \quad (11)$$

where e_{ij} is defined as

$$\left(\frac{\partial v_i}{\partial x_j} + \frac{\partial v_j}{\partial x_i} \right) \text{ and } I_2^{vp} = \gamma^2 = \left(\frac{\partial v_x}{\partial y} \right)^2 \text{ in simple shear flow.}$$

We see from (10) that γ may be regarded as a characteristic shear rate for the material.

If $(I_2^{vp})^{1/2} \ll \gamma$, the material is perfectly plastic, with constant yield stress, whereas for the opposite extreme, the material behaves as a purely viscous power-law fluid and the static yield stress is unimportant. This is illustrated in Fig. 3.

Now using (7) and (8) in (11) we obtain

$$(I_2^{vp})^{1/2} = \frac{2U}{H} |\csc 2\phi| \quad (12)$$

where, from Fig. 4, it may be seen that

$$\phi = \frac{1}{2} \cos^{-1} \left(\frac{\tau_{xy}}{k} \right) \quad (13)$$

and consequently (12) becomes

$$(I_2^{vp})^{1/2} = \frac{2U}{H} \left(1 - \frac{\tau_w^2 y^2}{k^2 H^2} \right)^{-1/2} \quad (14)$$

Substituting (14) into (10) and setting $y/H = y^*$ we obtain

$$k = k_0 \left\{ 1 + \left[\frac{2U}{\gamma H} \right]^n \left(1 - \frac{\tau_w^2 y^{*2}}{k^2} \right)^{-n/2} \right\} \quad (15)$$

which is an implicit nonlinear equation relating k to y^* .

At the boundaries $y^* = \pm 1$, $\tau_w = mk$ (Fig. 5) and hence

$$\tau_w = mk_0 \left\{ 1 + \left[\frac{2U}{\gamma H} \right]^n (1 - m^2)^{-n/2} \right\} \quad (16)$$

is determined explicitly from (15). By assigning values of m , k_0 , U , γ , n , H a value of τ_w may be calculated using Eq. (16) which may be substituted in (15) to obtain the function $k(y^*)$.

Taking the mean value of $\sigma_x (\pm L)$ as zero gives the following result using (5) and (16)

$$\int_{-H}^{+H} \sigma_x (\pm L) dy = 2mk_0 L \left\{ 1 + \left[\frac{2U}{\gamma H} \right]^n (1 - m^2)^{-n/2} \right\} + 2H(C_1 + C_2) = 0 \quad (17)$$

where $C_2 = \int_{-1}^{+1} (k^2 - \tau_{xy}^2)^{1/2} dy^*$ is not a function of x or y .

Thus from (17) we may obtain an expression for the integration constant C_1 ,

$$C_1 = (-mk_0 L/H) \left\{ 1 + \left[\frac{2U}{\gamma H} \right]^n (1 - m^2)^{-n/2} \right\} - C_2 \quad (18)$$

Substitution of (18) into (4) gives the pressure distribution

$$p(x) = -\sigma_y = (mk_0/H) \left\{ 1 + \left[\frac{2U}{\gamma H} \right]^n (1 - m^2)^{-n/2} \right\} \times (L - x) + C_2 \quad (19)$$

The mean imposed pressure over the platen surface, \bar{p} , is then given by

$$\bar{p} = -\frac{1}{L} \int_0^L \sigma_y dx = (mk_0 L/2H) \times \left\{ 1 + \left[\frac{2U}{\gamma H} \right]^n (1 - m^2)^{-n/2} \right\} + C_2 \quad (20)$$

The first term on the RHS of (20) may be seen as a direct effect of boundary friction, while C_2 represents a constant offset in the pressure related to the dynamic yield stress at the edge of the material sample.

The velocity fields are given by (7) and (8) with (13):

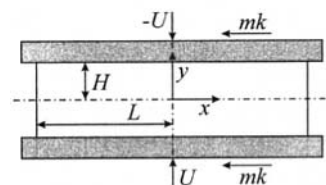


Fig. 2 The squeeze flow nomenclature

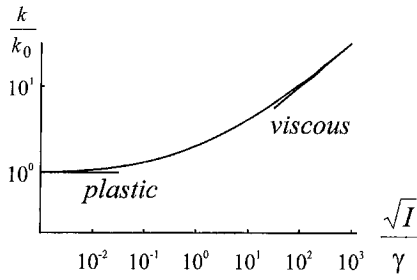


Fig. 3 The Herschel-Bulkley constitutive model; a log-log plot of k/k_0 versus $I^{1/2}/\gamma$

$$v_y = \frac{-U}{H} y = -Uy^* \quad (21)$$

$$v_x = \frac{U}{H} x - \left(\frac{2U}{H} \right) \int \cot 2\phi dy$$

$$= \frac{U}{H} x + \left(\frac{2U}{H} \right) \int_0^{y^*} \frac{\tau_{xy}}{(k^2 - \tau_{xy}^2)^{1/2}} dy + C_3 \quad (22)$$

where C_3 is a further constant of integration.

Since the value of k is not constant, the integral in (22) is not readily evaluated in closed form. We temporarily denote the y -dependent part of the velocity by

$$v_x^*(y^*) = -2U \int_0^{y^*} \cot 2\phi dy^* \quad (23)$$

The integration constant in the velocity profile solution may then be derived from global conservation of mass which requires that

$$\int_0^1 v_x dy^* = \frac{Ux}{H} \quad (24)$$

Hence from (22) we obtain

$$C_3 = - \int_0^1 v_x^*(y^*) dy^* \quad (25)$$

Thus, the x component of the velocity is given by using (25) and (23) in (22)

$$v_x = \frac{U}{H} x - 2U \left[\int_0^{y^*} \cot 2\phi dy^* - \int_0^1 \int_0^{y^*} \cot 2\phi dy^* dy^* \right] \quad (26)$$

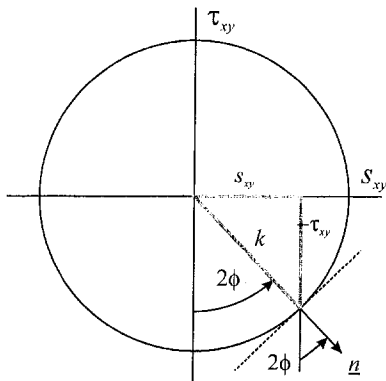


Fig. 4 The static yield surface (for $x > 0, y > 0$)

Displacement fields may be obtained by time integration of the velocities (21) and (26). We note that since (v_y) (21) is linear in y and independent of x , material elements retain their vertical position relative to the platen separation, id est. $y^* = \text{constant}$ for a material element. The x -component of displacement is given by integration of (26) in which the RHS is a function of x, y^* and time (t). Since y^* is constant for a material element, time integration is relatively straightforward.

$$X(t) = \int_0^t v_x(X, Y, t) dt \quad (27)$$

$$Y(t) = \int_0^t v_y(Y, t) dt \quad (28)$$

In evaluating the analysis, we see the importance of a dimensionless parameter $\Omega = 2U/\gamma H_0$ which may be regarded as the Weissenberg number, a ratio of the characteristic shear rate of the flow ($2U/H_0$) to the characteristic shear rate of the material, γ . The other key dimensionless constants are the slip parameter m and the flow index n . The independent variables may be taken as $y^* = y/H, x^* = x/H$ and H/H_0 which serves as a measure of a dimensionless time, where H_0 is the initial thickness. The solution to the implicit equation for the flow stress (15) was obtained using a simple numerical routine. The solutions for the pressure distribution, velocity and displacement fields were arrived at by successive evaluation using numerical integration.

3 Discussion

Given the assumptions of the analysis, that the strain rates are independent of x and the incompressibility condition, as the "time" and/or the deformation progresses, a given material element will maintain the same relative distance from the platen and plane of symmetry, hence y^* is incorporated as a dimensionless geometric parameter. By plotting the dimensionless ratio k/k_0 as a function of y^* (Fig. 6) we may visualize the variation of the yield stress throughout the material strip as a function of m , the interfacial friction factor and deformation ratio (H/H_0). When a strain-rate-dependent solid is initially compressed, the plastic response will predominate within the bulk. However, as time proceeds, i.e., at larger deformations, the viscous response will become significant provided that a critical shear strain rate has been achieved. This is exemplified in Fig. 6 which shows profiles from an analysis carried out at a moderate velocity (such that $\Omega = 1$) with $n = 0.2$ and $m = 0.1$ (Fig. 6(a)). If the analysis is now repeated with $m = 0.9$ (Fig. 6(b)) the flow stresses are no longer linear due to the effect of reduced slip at the walls (increasing the wall shear stresses); we note the sharp increase in the value of k/k_0 as y^* approaches unity. If the value of m is now reset to 0.1 but the platen velocity is increased by two orders of magnitude ($\Omega = 100$) the flow stresses are once again linear (Fig. 6(c)), however, the corresponding flow stresses have significantly increased. This reflects the strain-rate-dependent nature of the constitutive model. Figure 6(d) has been calculated for $m = 0.9$ and again a marked increase in the stress variation may be observed. Examination of (15) and (16) shows that viscous

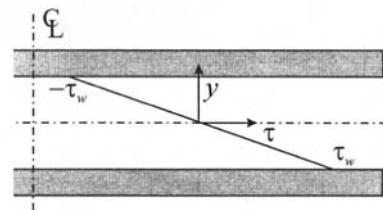


Fig. 5 Schematic, diagram of the boundary condition

effects are significant only if Ω is of order unity or larger; if Ω is small, the material is perfectly plastic. When viscous effects are present, the degree of inhomogeneity is determined first by m and then by n . If m is small, there is near perfect slip and deformation is nearly homogeneous. If m is large, there is significant boundary friction leading to shear deformation and inhomogeneity; the degree of inhomogeneity thus increases with m and n .

The behavior of the through-thickness yield stress ratio is very similar in form to that shown by Collins and Meguid (1977) for isotropic strain-hardening materials. For a small value of the interfacial friction factor, the wall stress boundary condition is close to frictionless so that the material deforms almost homogeneously. Thus the response is essentially that which would be obtained from a conventional cycloidal analysis for a rigid-perfectly plastic material at an appropriate value of the yield stress. At a constant closure velocity, the effective strain rate increases as the deformation proceeds leading to an increase in the dynamic yield stress. At large values of the friction factor, approaching the fully rough condition, there is a significant departure from homogeneous deformation with

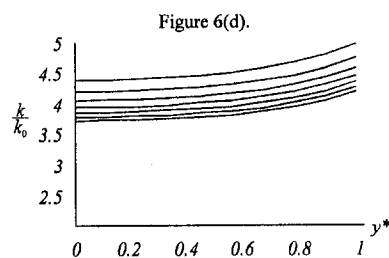
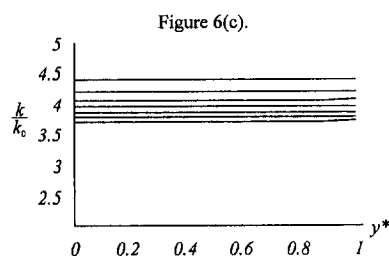
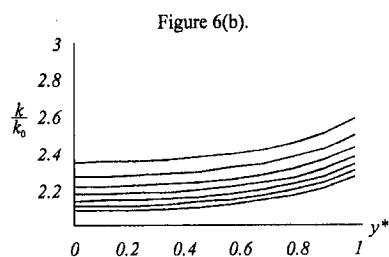
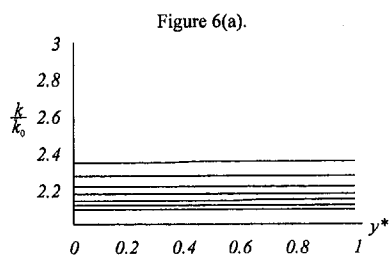


Fig. 6 Variation of the flow stress through the thickness, as a function of H/H_0 . Note higher flow stress corresponds to smaller H/H_0 : values 0.9, 0.8, 0.7, 0.6, 0.5, 0.4, 0.3. (a) $\Omega = 1$, $m = 0.1$, (b) $\Omega = 1$, $m = 0.9$, (c) $\Omega = 100$, $m = 0.1$, (d) $\Omega = 100$, $m = 0.9$. The flow index $n = 0.2$.

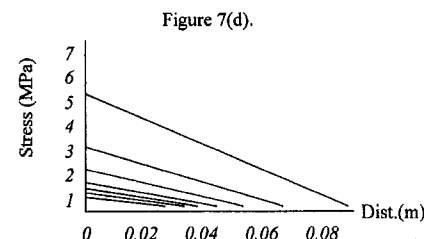
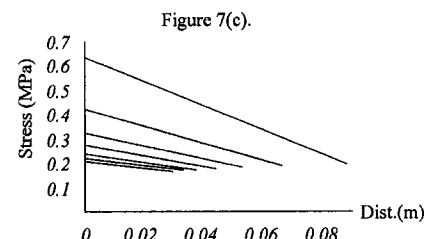
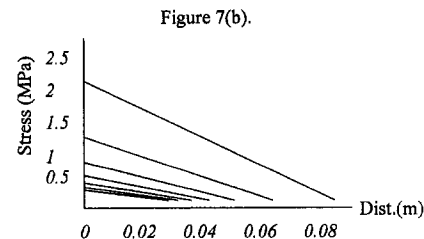
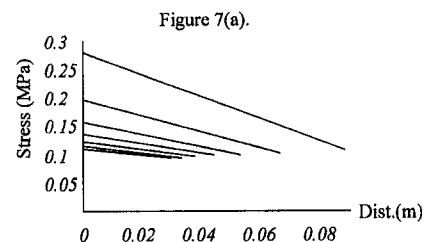


Fig. 7 Pressure distribution as a function of radial distance (x). Higher pressures correspond to smaller values of H/H_0 as in Fig. 6. (a) $\Omega = 1$, $m = 0.1$, (b) $\Omega = 1$, $m = 0.9$, (c) $\Omega = 100$, $m = 0.1$, (d) $\Omega = 100$, $m = 0.9$.

larger strain rates, and hence flow stresses, generated near the platens.

Figure 7 shows the pressure distribution as a function of radial distance plotted for the same values of interfacial friction and platen velocity as in Fig. 6. In each case, the pressure is a linear decreasing function of position with a finite positive value at the edge of the specimen corresponding to the local yield stress. This edge yield stress depends upon the shear rate (Ω)

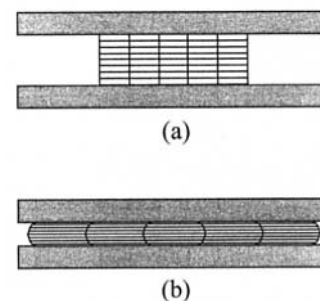


Fig. 8 An analytically generated deformed mesh

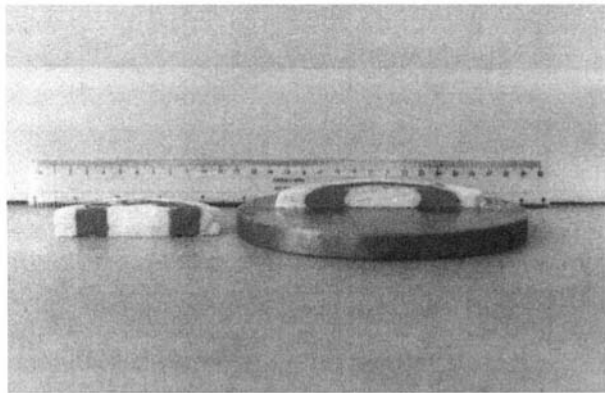


Fig. 9 Potato paste before and after the deformation process

while the peak pressure in the center of the specimen is strongly affected by both Ω and m . Smaller values of m give a more homogeneous pressure distribution, while larger values lead to very high pressures and strong gradients.

An example of the strain field generated at a high value of the friction factor is given in Fig. 8. Figure 8(b) shows the elliptical distortion as would be expected from a cycloidal solution. That is, the material is fully yielded across the thickness. This is in marked contrast to the partially yielded response predicted by the lubrication solution. It should be pointed out here that the lubrication analysis has been carried out by applying the no-slip wall boundary condition, which would be equivalent to a friction factor equal to unity. As discussed by Collins and Meguid (1977), for strain-hardening materials, this condition corresponds to an unbounded yield stress at the platen walls which physically would have to be treated in terms of a wall boundary layer. This is exactly the behavior that is observed for viscoplastic particulate suspensions (Adams et al., 1993). In these cases, the high local strain rates cause the particles to migrate away from the walls, generating a depleted lubricating layer. The wall stress boundary conditions employed for such materials are essentially Tresca in nature although there may be a slip velocity dependence once a critical wall shear

stress has been exceeded. The current analysis would require significant extension to take account of such slip velocity effects.

The quality of the predictions obtained from this analysis is exemplified via the displacement profiles. Figure 9 shows a photograph of potato paste before and after deformation in an axisymmetric squeeze flow geometry. This compares well with the analytically generated mesh (Fig. 8) based upon the relevant material parameters. Even though it is not possible to make quantitative comparisons between the axisymmetric experiment and the current (two-dimensional) model, the qualitative similarity to Fig. 8, which is based upon the same material parameters, is compelling.

Acknowledgment

This research was supported by the Unilever Research scheme "Optimisation of Solid Food Processing," and by X. Weert.

References

- Adams, M. J., Briscoe, B. J., and Kamyab, M., 1993, "The Deformation and Flow of Highly Concentrated Dispersions," *Colloid Interface Science*, Vol. 44, pp. 141–182.
- Adams, M. J., Edmondson, B., Caughey, D. G., and Yayha, R., 1994, "An experimental and theoretical study of the squeeze-film deformation and flow of elastoplastic fluids," *Journal of Non-Newtonian Fluid Mechanics*, Vol. 51, pp. 61–78.
- Collins, I. F., and Meguid, S. A., 1977, "On the Influence of Hardening and Anisotropy on the Plane-Strain Compression of Thin Metal Strip," *ASME JOURNAL OF APPLIED MECHANICS*, Vol. 44, pp. 271–278.
- Covey, G. H., and Stanmore, B. R., 1981, *Journal of Non-Newtonian Fluid Mechanics*, Vol. 8, pp. 337–356.
- Herschel, W. H., and Bulkley, R., 1926, *Proceedings of the American Society for the Testing of Materials*, Vol. 26, p. 612.
- Hill, R., 1950, *The Mathematical Theory of Plasticity*, Oxford University Press, Oxford, UK.
- Lipscombe, G. G., and Denn, M. M., 1984, "Flow of Bingham fluids in complex geometries," *Journal of Non-Newtonian Fluid Mechanics*, Vol. 14, pp. 337–346.
- Perzyna, P., 1966, "Fundamental problems in viscoplasticity," *Advances in Applied Mechanics*, Vol. 9, pp. 244–377.
- Prandtl, L., 1923, *Zeitschrift für angewandte Mathematik und Mechanik*, Vol. 3, pp. 401–426.
- Zienkiewicz, O. C., and Goodhale, P. N., 1974, "Flow of plastic and viscoplastic Solids with special reference to extrusion and forming processes," *International Journal of Numerical Methods in Engineering*, Vol. 8, pp. 3–16.

A Brief Note is a short paper that presents a specific solution of technical interest in mechanics but which does not necessarily contain new general methods or results. A Brief Note should not exceed 1500 words *or equivalent* (a typical one-column figure or table is equivalent to 250 words; a one line equation to 30 words). Brief Notes will be subject to the usual review procedures prior to publication. After approval such Notes will be published as soon as possible. The Notes should be submitted to the Technical Editor of the JOURNAL OF APPLIED MECHANICS. Discussions on the Brief Notes should be addressed to the Editorial Department, ASME, United Engineering Center, 345 East 47th Street, New York, N. Y. 10017, or to the Technical Editor of the JOURNAL OF APPLIED MECHANICS. Discussions on Brief Notes appearing in this issue will be accepted until two months after publication. Readers who need more time to prepare a Discussion should request an extension of the deadline from the Editorial Department.

Contact Pressures as an Elastic Roller Crosses a Scratch

J. A. Greenwood¹

The Westergaard method of plane elastic analysis is used to obtain an exact solution to the problem of an elastic roller crossing a gap, intended to represent a scratch, on a rigid half-space.

There is considerable interest in what happens to the stress distribution when a roller in a roller bearing crosses a scratch. We show here that a related problem, that of an elastic roller crossing a scratch on a rigid half-space, possesses a rather simple exact solution.

The Westergaard complex variable method for plane-strain elasticity is ideally suited to the study of frictionless contact problems between half-spaces. Although the formulation of the method and the determination of the internal stresses involve complicated algebra (Westergaard, 1939), the result is that an analytic function $f(z)$ exists such that on the surface of the half-space $z = x + 0i$ the real part of $f(z)$ is the contact stress (i.e., minus the contact pressure) while the imaginary part is the surface slope (actually the slope multiplied by half the plane-strain elastic modulus, $\frac{1}{2}E' \partial v / \partial x$). Thus, $f(x)$ must be purely imaginary outside the contact region, while inside the contact, its imaginary part must take prescribed values appropriate to the contact geometry. Westergaard shows that the stress function representing a point load P at the origin is simply $f(z) = -iP / \pi z$, from which it follows that for any stress function $f(z)$ the total load can be found from the coefficient of z^{-1} in the expansion of $f(z)$. In applying the method, it is frequently necessary to recall that the functions $f(z) = z^{1/2}$ and $z^{-1/2}$ are real for $y = 0$, $x > 0$ and purely imaginary for $y = 0$, $x < 0$, and that in passing from $x > 0$ to $x < 0$ in the upper half-plane the first

changes from $x^{1/2}$ to $+i|x|^{1/2}$ and the second from $x^{-1/2}$ to $-i|x|^{-1/2}$.

Westergaard shows that the stress function for the Hertz problem of the contact between a rigid roller of radius R and an elastic half-space is $f(z) = -iK[z - \sqrt{z^2 - b^2}]$, since this is pure imaginary (no contact pressure) for $y = 0$, $|x| > b$, while for $y = 0$, $|x| < b$ the imaginary part is $-Kx$, which will annul the initial slope due to the shape of the roller provided that $K = E'/2R$. The real part is then $-K\sqrt{b^2 - x^2}$, giving the usual contact pressures. For z large we have $f(z) \sim -iKb^2/2z$, so that the load is $W = \frac{1}{2}\pi Kb^2$; this may be verified by direct integration of the contact pressures.

Central Scratch

We wish to extend Westergaard's solution to the case of an elastic roller in contact with a rigid half-space, where part of the half-space is missing (a "scratch"). We examine first a centrally located scratch, extending from $x = -a$ to $x = +a$ when the contact region extends between $\pm b$; of course $a < b$. Consider the stress function

$$f(z) = -iKz \left[1 - \sqrt{\frac{z^2 - b^2}{z^2 - a^2}} \right]. \quad (1)$$

On the real axis the square root is real except for $a < |x| < b$, so contact pressures are restricted to these regions and are equal to $p(x) = K|x|\sqrt{(b^2 - x^2)/(x^2 - a^2)}$. In the contact regions the slope is $(1/2)E'(\partial v / \partial x) = -Kx$ as in the Hertz solution above, so that again we require $K = E'/2R$. For z large we have $f(z) \sim -iK(b^2 - a^2)/2z$, so the total load is $W = (1/2)\pi K(b^2 - a^2)$. Thus, the presence of a scratch extending from $-a$ to $+a$ increases the size of the contact region according to the simple rule

$$b^2 = b_H^2 + a^2 \quad (2)$$

where b_H is the Hertzian half-width. What is more important, it leads to stress singularities at the edges of the scratch, as shown in Fig. 1(a).

The surface slope in the noncontact regions is equal to

$$\frac{1}{2}E' \frac{\partial v}{\partial x} = Kx \left[\sqrt{\frac{b^2 - x^2}{a^2 - x^2}} - 1 \right] \quad (3)$$

¹ University Engineering Department, University of Cambridge, Trumpington Street, Cambridge CB2 1PZ, U.K.

Contributed by the Applied Mechanics Division of THE AMERICAN SOCIETY OF MECHANICAL ENGINEERS for publication in the ASME JOURNAL OF APPLIED MECHANICS. Manuscript received by the ASME Applied Mechanics Division, Aug. 10, 1995; final revision, Mar. 5, 1996. Associate Technical Editor: J. T. Jenkins.

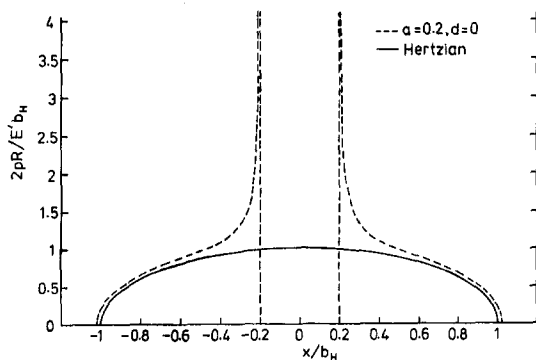


Fig. 1(a) Roller crossing a central scratch: pressures

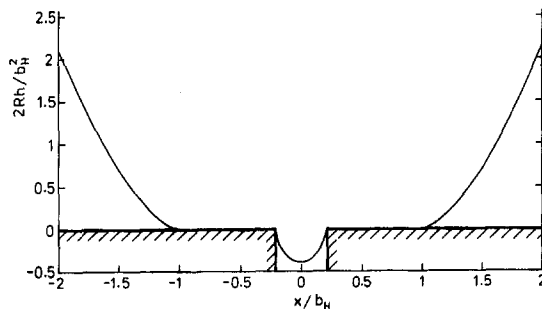


Fig. 1(b) Roller crossing a central scratch: shape

from which the deflection is found to be

$$v = \frac{1}{2R} \left[(a^2 - x^2) - \sqrt{(a^2 - x^2)(b^2 - x^2)} \right. \\ \left. - (b^2 - a^2) \sinh^{-1} \sqrt{\frac{a^2 - x^2}{b^2 - a^2}} \right] \quad \text{for } |x| < a \quad (4)$$

and the *shape* of the deformed roller is the same expression omitting the first term. Note that (inevitably) the roller surface is *vertical* at the edges of the scratch, so that this solution is valid only if the scratch edges are vertical (see Fig. 1(b)). For completeness we give the *shape* for $x > b$:

$$h = \frac{1}{2R} \left[+\sqrt{(x^2 - a^2)(x^2 - b^2)} \right. \\ \left. - (b^2 - a^2) \sinh^{-1} \sqrt{\frac{x^2 - b^2}{b^2 - a^2}} \right] \quad (5)$$

$$\frac{b-c}{2a} \int_{-\pi/2}^{\pi/2} \sqrt{\left(1 + \frac{a}{(b+d)} \sin \theta\right) \left(1 - \frac{a}{(c-d)} \sin \theta\right)} d\theta = \int_{-\pi/2}^{\pi/2} \sqrt{\left(1 + \frac{a}{(b+d)} \sin \theta\right) \left(1 - \frac{a}{(c-d)} \sin \theta\right)} \sin \theta d\theta \quad (11)$$

Scratch at any Location

Suppose now that the scratch is offset from the centre of the roller. On the basis of the above solution, we expect the presence of an off-center scratch to lead to an increase in the contact width, but by differing amounts on the two sides. Accordingly,

for a scratch of width $2a$ centred at $x = d$ we suppose contact to extend from $x = -b$ to $x = +c$. Consider the stress function

$$f(z) = -iK \left[z - (z-e) \sqrt{\frac{(z+b)(z-c)}{(z-d+a)(z-d-a)}} \right] \quad (6)$$

Provided that $-b < (d-a) < (d+a) < c$, the square root will be real for $x > c$, for $(d-a) < x < (d+a)$, and for $x < -b$ so that contact is restricted to the two regions $-b < x < (d-a)$ and $(d+a) < x < c$.

For large z the square root behaves like

$$\sqrt{\quad} \sim 1 + (b-c+2d)/2z$$

so that

$$f(z) \sim -iK [z - \{(z-e) + (b-c+2d)/2 + O(z^{-1})\}]$$

and for a finite load we must have

$$e = d + (b-c)/2 \quad (7)$$

From the next term in the expansion of $f(z)$ the total load is found to be

$$W = \frac{\pi E'}{16R} [(b+c)^2 + 4e(b-c) - 4a^2] \quad (8)$$

or, more conveniently,

$$\left(\frac{b+c}{2}\right)^2 = b_H^2 + a^2 + e(c-b) \quad (9)$$

where b_H is again the Hertzian half-width for the same load.

However, an extra condition needs to be imposed: the combination of the original roller shape and the displacement gives a constant "gap" over *each* of the two contact regions, but as yet the "gaps" are unequal, so that only one of them can be set to zero to give contact. Equal gaps requires that

$$\int_{d-a}^{d+a} \frac{\partial(v+h)}{\partial x} dx = 0 \quad \text{i.e.,} \\ \int_{d-a}^{d+a} \left[(x-e) \sqrt{\frac{(c-x)(b+x)}{a^2 - (x-d)^2}} \right] dx = 0$$

from which we obtain e in terms of b , c , a and d :

$$e \int_{d-a}^{d+a} \sqrt{\frac{(c-x)(b+x)}{a^2 - (x-d)^2}} dx \\ = \int_{d-a}^{d+a} x \sqrt{\frac{(c-x)(b+x)}{a^2 - (x-d)^2}} dx \quad (10)$$

Since $e-d = (b-c)/2$ this equation relates the three variables b/a , c/a and d/a .

Setting $x = d + a \sin \theta$ converts it to a form suitable for numerical integration:

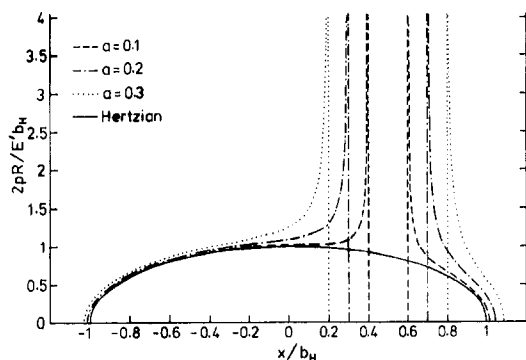


Fig. 2 Offset scratch ($d = 0.5$) of varying width

Table 1 Exact results: (b, c) for $b_H = 1$

$d \backslash a$	0.1	0.2	0.4
0.1	1.0045, 1.0055	1.0180, 1.0219	1.0706, 1.0847
0.3	1.0038, 1.0071	1.0153, 1.0274	1.0603, 1.1053
0.5	1.0033, 1.0099	1.0133, 1.0302	1.0525, 1.1374
0.7	1.0029, 1.0161	1.0117, 1.0592	1.0459, 1.1911

$$p(x) = \frac{E'}{2R} \left[|x - e| \sqrt{\frac{(b+x)(c-x)}{(x-d)^2 - a^2}} \right] \quad \text{for} \quad -b < x < d - a; \quad d + a < x < c \quad (12)^2$$

Note that $(c - b)$ is usually small, so that the increase in contact width is much the same as for the central scratch (and so small); but there is always a slight shift to the side containing the scratch. Figure 2 shows the pressure distributions for the cases $d = 0.5$, $a = 0.1, 0.2, 0.3$, and the corresponding Hertzian pressures.

Narrow Scratch

If a is small, an approximate solution is readily found. Expanding the square root in (11) in series and integrating term by term gives, writing $k_1 = a/(b + d)$, $k_2 = a/(c - d)$:

$$\frac{c-b}{2a} \left[1 - \left(\frac{k_1 + k_2}{4} \right)^2 \right] = \frac{k_2 - k_1}{4} \left[1 + \frac{3}{2} \left(\frac{k_1 + k_2}{4} \right)^2 \right]. \quad (13)$$

Using this together with (9) enables b and c to be found by iteration on a hand calculator. The approximation works well for scratches of plausible widths which are not too eccentric: for example, with $d = 0.5$, $a = 0.2$, and $b_H = 1$, the answers agree with the table to four decimals.

Discussion

In many contact problems the extension from a single elastic body to two is trivial, requiring only the replacement of the plane strain modulus of the single elastic body, E' , by the "contact modulus" E^* , combining the elasticities of the two bodies according to $E^{*-1} = E_1'^{-1} + E_2'^{-1}$ (see, e.g., Johnson, 1985). Thus, for example, the Hertzian pressure distribution $p(x) = (E'/2R)\sqrt{b^2 - x^2}$ becomes simply $p(x) = (E^*/2R)$

² The factor $|x - e|$ is mathematically misleading, and gives the correct result only because the point $x = e$ never lies inside a contact region. The sign changes are actually due to the square root.

$\times \sqrt{b^2 - x^2}$. But this requires both bodies to behave elastically as half-spaces. Treating a *roller* as a half-space is legitimate; and the same would be true for a *shallow* scratch. But our solution requires the scratch to have vertical edges, in order to avoid contact with the bulge which appears on the roller, and this is not acceptable. In practice, the edges of the scratch will deform (by much more than the same points of an elastic half-space), reducing the singularities in contact pressure to an unknown extent. Equally, the presence of the scratch will change the size of the contact area even when the scratch is not in the contact, a feature quite absent from our solution. So unfortunately, this analysis does not give any information about the practical problem of an elastic roller crossing a scratch on an elastic half-space. We can only hope that perhaps it may be of use in the development of a computer program designed for the real problem.

References

- Johnson, K. L., 1985, *Contact Mechanics*, Cambridge University Press, Cambridge, UK.
- Westergaard, H. M., 1939, "Bearing Pressures and Cracks," *ASME JOURNAL OF APPLIED MECHANICS*, Vol. 6, pp. A49-A53.

On the Problem of Equilibrium Length of a Bridged Crack

N. Morozov³, M. Paukshto³, and N. Ponikarov³

A solution is given for a partially bridged straight crack in orthotropic elastic material in particular unidirectionally fiber-reinforced brittle composite. The problem of crack with constant bridging forces is solved by use the complex potentials. By use of Novogilov's fracture criterion the estimation of the bridged part of crack and full length of equilibrium crack is obtained.

1 Introduction

The toughness of brittle solids such as ceramics can be increased considerably by the use of fibers which bridge microcracks. Experiments show that cracks being normal to fibers spread rectilinearly and can be bridged either partially or fully.

Nemat-Nasser and Hori (1987) have obtained a complete solution for a fully or partially bridged straight crack in a transversely isotropic elastic material. But that solution contains such a parameter as the length of a bridged part of a crack which was not known in advance. This length may be obtained from the strength criteria of a fiber (Budiansky et al., 1995) and a matrix (Novozhilov, 1969; Morozov and Paukshto, 1994). According to the criterion the average stress near the crack-tip can be no greater than the matrix strength. The averaging should be used over size peculiar to the given material. This is the distance between fibers for a unidirectionally fiber-reinforced composite and a straight crack. The model gives the opportunity to estimate the critical length of equilibrium crack.

³ St. Petersburg State University, 198904 St Petersburg, Russia.

Contributed by the Applied Mechanics Division of THE AMERICAN SOCIETY OF MECHANICAL ENGINEERS for publication in the ASME JOURNAL OF APPLIED MECHANICS. Manuscript received by the ASME Applied Mechanics Division, Nov. 13, 1995; final revision, Mar. 24, 1996. Associate Technical Editor: X. Markenscoff.

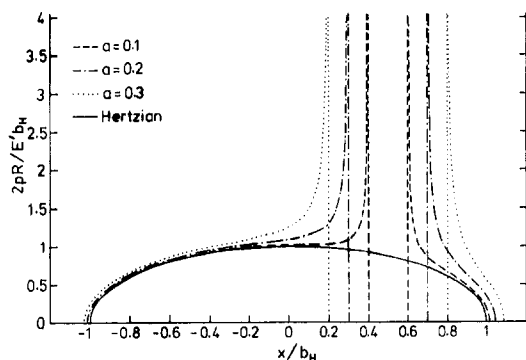


Fig. 2 Offset scratch ($d = 0.5$) of varying width

Table 1 Exact results: (b, c) for $b_H = 1$

$d \backslash a$	0.1	0.2	0.4
0.1	1.0045, 1.0055	1.0180, 1.0219	1.0706, 1.0847
0.3	1.0038, 1.0071	1.0153, 1.0274	1.0603, 1.1053
0.5	1.0033, 1.0099	1.0133, 1.0302	1.0525, 1.1374
0.7	1.0029, 1.0161	1.0117, 1.0592	1.0459, 1.1911

$$p(x) = \frac{E'}{2R} \left[|x - e| \sqrt{\frac{(b+x)(c-x)}{(x-d)^2 - a^2}} \right] \quad \text{for} \quad -b < x < d - a; \quad d + a < x < c \quad (12)^2$$

Note that $(c - b)$ is usually small, so that the increase in contact width is much the same as for the central scratch (and so small); but there is always a slight shift to the side containing the scratch. Figure 2 shows the pressure distributions for the cases $d = 0.5$, $a = 0.1, 0.2, 0.3$, and the corresponding Hertzian pressures.

Narrow Scratch

If a is small, an approximate solution is readily found. Expanding the square root in (11) in series and integrating term by term gives, writing $k_1 = a/(b + d)$, $k_2 = a/(c - d)$:

$$\frac{c-b}{2a} \left[1 - \left(\frac{k_1 + k_2}{4} \right)^2 \right] = \frac{k_2 - k_1}{4} \left[1 + \frac{3}{2} \left(\frac{k_1 + k_2}{4} \right)^2 \right]. \quad (13)$$

Using this together with (9) enables b and c to be found by iteration on a hand calculator. The approximation works well for scratches of plausible widths which are not too eccentric: for example, with $d = 0.5$, $a = 0.2$, and $b_H = 1$, the answers agree with the table to four decimals.

Discussion

In many contact problems the extension from a single elastic body to two is trivial, requiring only the replacement of the plane strain modulus of the single elastic body, E' , by the "contact modulus" E^* , combining the elasticities of the two bodies according to $E^{*-1} = E_1'^{-1} + E_2'^{-1}$ (see, e.g., Johnson, 1985). Thus, for example, the Hertzian pressure distribution $p(x) = (E'/2R)\sqrt{b^2 - x^2}$ becomes simply $p(x) = (E^*/2R)$

² The factor $|x - e|$ is mathematically misleading, and gives the correct result only because the point $x = e$ never lies inside a contact region. The sign changes are actually due to the square root.

$\times \sqrt{b^2 - x^2}$. But this requires both bodies to behave elastically as half-spaces. Treating a *roller* as a half-space is legitimate; and the same would be true for a *shallow* scratch. But our solution requires the scratch to have vertical edges, in order to avoid contact with the bulge which appears on the roller, and this is not acceptable. In practice, the edges of the scratch will deform (by much more than the same points of an elastic half-space), reducing the singularities in contact pressure to an unknown extent. Equally, the presence of the scratch will change the size of the contact area even when the scratch is not in the contact, a feature quite absent from our solution. So unfortunately, this analysis does not give any information about the practical problem of an elastic roller crossing a scratch on an elastic half-space. We can only hope that perhaps it may be of use in the development of a computer program designed for the real problem.

References

- Johnson, K. L., 1985, *Contact Mechanics*, Cambridge University Press, Cambridge, UK.
- Westergaard, H. M., 1939, "Bearing Pressures and Cracks," *ASME JOURNAL OF APPLIED MECHANICS*, Vol. 6, pp. A49-A53.

On the Problem of Equilibrium Length of a Bridged Crack

N. Morozov³, M. Paukshto³, and N. Ponikarov³

A solution is given for a partially bridged straight crack in orthotropic elastic material in particular unidirectionally fiber-reinforced brittle composite. The problem of crack with constant bridging forces is solved by use the complex potentials. By use of Novogilov's fracture criterion the estimation of the bridged part of crack and full length of equilibrium crack is obtained.

1 Introduction

The toughness of brittle solids such as ceramics can be increased considerably by the use of fibers which bridge microcracks. Experiments show that cracks being normal to fibers spread rectilinearly and can be bridged either partially or fully.

Nemat-Nasser and Hori (1987) have obtained a complete solution for a fully or partially bridged straight crack in a transversely isotropic elastic material. But that solution contains such a parameter as the length of a bridged part of a crack which was not known in advance. This length may be obtained from the strength criteria of a fiber (Budiansky et al., 1995) and a matrix (Novozhilov, 1969; Morozov and Paukshto, 1994). According to the criterion the average stress near the crack-tip can be no greater than the matrix strength. The averaging should be used over size peculiar to the given material. This is the distance between fibers for a unidirectionally fiber-reinforced composite and a straight crack. The model gives the opportunity to estimate the critical length of equilibrium crack.

³ St. Petersburg State University, 198904 St Petersburg, Russia.

Contributed by the Applied Mechanics Division of THE AMERICAN SOCIETY OF MECHANICAL ENGINEERS for publication in the ASME JOURNAL OF APPLIED MECHANICS. Manuscript received by the ASME Applied Mechanics Division, Nov. 13, 1995; final revision, Mar. 24, 1996. Associate Technical Editor: X. Markenscoff.

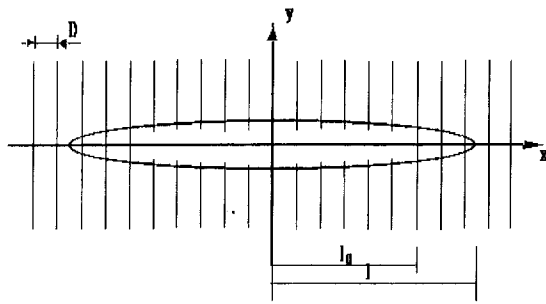


Fig. 1 The bridged crack

2 Crack in Orthotropic Media

Let us consider a partially bridged crack (Fig. 1). The fibers are broken in the middle part of crack, but they provide crack surfaces interaction near crack tips. A bridging law was obtained by Budiansky et al. (1995) and can be written in following form:

$$\frac{\sigma}{\sigma_A} = \begin{cases} \left(\frac{\sigma_A}{\sigma_S} \right) \left(\frac{u_y}{a} \right) & \text{for } u_y \leq u_D \\ \sqrt{\left(\frac{u_y}{a} \right)^2 + \left(\frac{\sigma_D}{\sigma_A} \right)^2} - \left(\frac{\sigma_S}{\sigma_A} \right) \left(\frac{\sigma_D}{\sigma_A} \right) & \text{for } u_y \geq u_D, \end{cases} \quad (1)$$

$$u_D = a \left(\frac{\sigma_S}{\sigma_A} \right) \left(\frac{\sigma_D}{\sigma_A} \right).$$

Here σ is an applied stress, u_y is a crack-opening displacement, and a is a fiber radius, σ_A , σ_D , σ_S are functions of fiber and matrix elastic moduli, fiber volume concentration, debonding toughness and sliding shear stress, respectively.

This relation can be approximated by a step function. The value of a bridging force is taken to be

$$\sigma_c = \begin{cases} c\sigma_f & \text{for } u_y \leq u_0 \\ 0 & \text{for } u_y \geq u_0 \end{cases} \quad (2)$$

where c is the fiber volume concentration and σ_f is the fiber strength. The critical crack-opening displacement u_0 is determined from (1) if σ_f is given.

So, we get the following problem: straight crack of length l in infinite orthotropic media, placed in-plane of orthotropy is externally loaded by constant stress σ_y^∞ . The constant compressing bridging forces σ_c are applied near the crack tips. Let Oxy be a rectangular Cartesian coordinate system with x , y defining the axes of symmetry of an orthotropic solid. The crack is located along Ox . Hooke's law becomes

$$\begin{aligned} \epsilon_x &= a_{11}\sigma_x + a_{12}\sigma_y + a_{16}\tau_{xy} \\ \epsilon_y &= a_{12}\sigma_x + a_{22}\sigma_y + a_{26}\tau_{xy} \\ \gamma_{xy} &= a_{16}\sigma_x + a_{26}\sigma_y + a_{66}\tau_{xy}. \end{aligned} \quad (3)$$

The bridging forces, denoted by σ_c , are equal to $\sigma_c(x) = \sigma_c H(|x| - l_0)$, where the step-function H is zero for nonpositive values of its argument and l_0 is the length of unbridged part of the crack.

This problem can be solved (Liebowitz, 1968) by use of the complex potentials. Let $z_1 = x + s_1y$, $z_2 = x + s_2y$, where s_i are purely imaginary roots of a characteristic equation

$$a_{11}s^4 + (2a_{12} + a_{66})s^2 + a_{22} = 0, \quad \text{Im}(s) > 0. \quad (4)$$

The stress σ_y and crack-opening displacement u_y becomes

$$\sigma_y = 2 \text{Re}(\Phi(z_1) + \Psi(z_2)),$$

$$u_y = 2 \text{Re}(q_1\phi(z_1) + q_2\psi(z_2)) \quad (5)$$

where Φ and Ψ are analytic functions of their arguments without cross-cut, $\phi'(z) = \Phi(z)$, $\psi'(z) = \Psi(z)$,

$$q_1 = \frac{a_{12}s_1^2 + a_{22} - a_{26}s_1}{s_1}, \quad q_2 = \frac{a_{12}s_2^2 + a_{22} - a_{26}s_2}{s_2}. \quad (6)$$

The potentials Φ and Ψ obtain the following forms:

$$\begin{aligned} \frac{s_2 - s_1}{s_2} \Phi_1(z_1) &= \frac{\sigma_y^\infty}{2} + \frac{1}{2\pi i \sqrt{z_1^2 - l^2}} \int_{-l}^l \frac{\sqrt{\tau^2 - l^2}}{\tau - z_1} \sigma_c(\tau) d\tau \\ \frac{s_1 - s_2}{s_1} \Psi(z_2) &= \frac{s_2 - s_1}{s_2} \Phi(z_2). \end{aligned} \quad (7)$$

By setting $y = 0$, $x \geq 0$ we obtain

$$\begin{aligned} \frac{s_2 - s_1}{s_2} \Phi_1(x) &= \frac{\sigma_c}{2} + \frac{1}{2} \frac{x}{\sqrt{x^2 - l^2}} \left(\sigma_y^\infty - \frac{2\sigma_c}{\pi} \arccos \frac{l_0}{l} \right) \\ &\quad - \frac{\sigma_c}{2\pi} \left(\arcsin \frac{l^2 - l_0x}{l(l_0 - x)} + \arcsin \frac{l^2 + l_0x}{l(l_0 + x)} \right). \end{aligned} \quad (8)$$

The potential ϕ can be obtained by the second integration:

$$\begin{aligned} \frac{s_2 - s_1}{s_2} \phi_1(x) &= \frac{\sigma_c x}{2} + \frac{1}{2} \left(\sigma_y^\infty - \frac{\sigma_c}{\pi} \arccos \frac{l_0}{l} \right) \sqrt{x^2 - l^2} \\ &\quad + \frac{\sigma_c}{2\pi} \left((x - l_0) \arcsin \frac{l^2 - l_0x}{l(l_0 - x)} \right. \\ &\quad \left. + (x + l_0) \arcsin \frac{l^2 + l_0x}{l(l_0 + x)} \right). \end{aligned} \quad (9)$$

The potential must be produced into a half-plane $x \geq 0$, ($\text{Re}(z) \geq 0$). We denote by $[\phi]$ the discontinuity of a function: $[\phi(x)] = \phi^+(x) - \phi^-(x)$, where an index “+” or “-” symbolizes the top or bottom surface cracks, respectively. Then

$$\begin{aligned} \frac{s_2 - s_1}{s_2} [\phi_1(x)] &= \left\{ \left(\sigma_y^\infty - \frac{2\sigma_c}{\pi} \arccos \frac{l_0}{l} \right) \sqrt{x^2 - l^2} \right. \\ &\quad \left. + \frac{\sigma_c}{2\pi} ((x - l_0)F(x, l_0) - (x + l_0)F(x, -l_0)) \right\} i. \end{aligned} \quad (10)$$

Function F is given by the form

$$F(x, l_0) = \ln \frac{l^2 - l_0x - \sqrt{(l^2 - l_0^2)(l^2 - x^2)}}{l^2 - l_0x + \sqrt{(l^2 - l_0^2)(l^2 - x^2)}}. \quad (11)$$

By substituting (8) and (10) into (5) we then obtain the solution to the problem:

$$\begin{aligned} \sigma_y(x, 0) &= \sigma_c + \frac{x}{\sqrt{x^2 - l^2}} \left(\sigma_y^\infty - \frac{2\sigma_c}{\pi} \arccos \frac{l_0}{l} \right) \\ &\quad - \frac{\sigma_c}{\pi} \left(\arcsin \frac{l^2 - l_0x}{l(l_0 - x)} + \arcsin \frac{l^2 + l_0x}{l(l_0 + x)} \right) \\ u_y(x, 0) &= \frac{2}{E^*} \left(\sigma_y^\infty - \frac{2\sigma_c}{\pi} \arccos \frac{l_0}{l} \right) \sqrt{x^2 - l^2} \\ &\quad + \frac{\sigma_c}{\pi E^*} ((x - l_0)F(x, l_0) + (x + l_0)F(x, -l_0)) \\ &\quad |x| < l. \end{aligned} \quad (12)$$

In (12), E^* is defined by

$$E^* = \left(a_{22} \operatorname{Re} \left(i \frac{s_1 + s_2}{s_1 s_2} \right) \right)^{-1} = \frac{1}{\sqrt{\frac{a_{11} a_{22}}{2}} \sqrt{\frac{a_{22}}{a_{11}} + \frac{2a_{12} + a_{66}}{2a_{11}}}}. \quad (13)$$

For a solid reinforced by laminae or fibers,

$$E^* \approx c E_f + (1 - c) E_m. \quad (14)$$

Near the crack tip the following asymptotic form is deduced:

$$\begin{aligned} \sigma_y(\xi, 0) &\approx \frac{1}{2} \sigma_c + \frac{1}{\sqrt{2}} \sqrt{\frac{l}{\xi}} \left(\sigma_y^\infty - \frac{2\sqrt{2}\sigma_c}{\pi} \sqrt{\frac{\Delta}{l}} \right) \\ &\quad + \frac{\sigma_c}{\pi} \arcsin \frac{\Delta - \xi}{\Delta + \xi} \\ u_y(\xi^*, 0) &\approx \frac{2\sqrt{2}}{E^*} \sqrt{l\xi^*} \left(\sigma_y^\infty - \frac{2\sqrt{2}\sigma_c}{\pi} \sqrt{\frac{\Delta}{l}} \right) \frac{4\sigma_c}{\pi E^*} \sqrt{\Delta\xi^*} \\ &\quad + \frac{\sigma_c}{\pi E^*} (\Delta - \xi^*) \ln \frac{(\sqrt{\Delta} - \sqrt{\xi^*})^2}{(\sqrt{\Delta} + \sqrt{\xi^*})^2} \end{aligned} \quad (15)$$

where

$$\Delta = l - l_0, \quad x = l + \xi, \quad x = l - \xi^*.$$

It is suggested that $\Delta/l \ll 1$ and $\xi/l \ll 1$. As will be shown, these conditions are satisfied with sufficient accuracy in the problem under consideration.

3 Fracture Criterion

A cracks expansion may be represented as a step-wise process. When the average normal stress in the element between neighbor ligaments exceeds some limiting value (matrix strength), the matrix material will distract and the crack will move forward on the step. The stress field should be taken to be the corresponding to a homogeneous orthotropic solid. The fracture criterion takes the form

$$\frac{1}{D} \int_0^D \sigma_y d\xi = \sigma_m \quad (16)$$

where D is the distance between neighbor fibers and σ_m is the matrix strength. Set $\alpha = \Delta/D$ and insert the asymptotic form for σ_y (15) into (16) we obtain

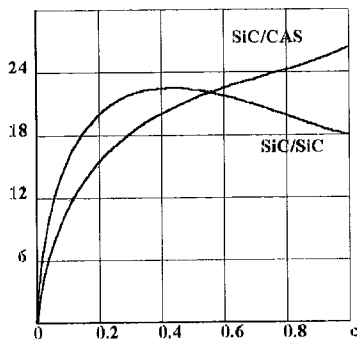


Fig. 2 The length of the bridged part of a crack

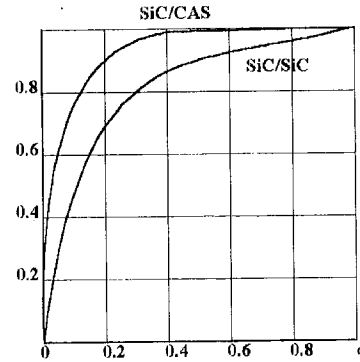


Fig. 3 The estimation of the full length of a crack

$$\begin{aligned} 2 \frac{\sigma_y^\infty}{\sigma_c} \sqrt{\frac{2l_k}{D}} &= 2 \left(\frac{\sigma_m}{\sigma_c} - 1 \right) + \frac{4}{\pi} \sqrt{\alpha} \\ &\quad + (1 + \alpha) \left(1 - \frac{2}{\pi} \arcsin \frac{\alpha - 1}{\alpha + 1} \right). \end{aligned} \quad (17)$$

The condition for the breaking of the fibers in the unbridged part of crack is that

$$u_y(\Delta, 0) = \frac{2}{E^*} \left(\sigma_y^\infty \sqrt{l_c \Delta} - \frac{2}{\pi} \sigma_c \Delta \right) = u_0. \quad (18)$$

To simplify the notation let us take

$$l_g = \frac{4}{\pi} \frac{E^* \sigma_c u_0}{\sigma_c^2}; \quad \beta = \frac{u_0}{D} \frac{E^*}{\sigma_c}; \quad U^2 = \frac{\pi}{4} \frac{\beta}{\alpha} \quad (19)$$

then (18) may be written as

$$2 \frac{\sigma_y^\infty}{\sigma_c} \sqrt{\frac{2l_k}{D}} = \frac{\beta}{\sqrt{\alpha}} + \frac{4}{\pi} \sqrt{\alpha} \quad (20)$$

or

$$2 \sqrt{\frac{l_k}{l_g}} = U + \frac{1}{U}. \quad (21)$$

It is clear that $l_k > l_g$.

Subtracting (20) from (17) we obtain

$$\begin{aligned} \beta &= 2\sqrt{\alpha} \left(\frac{\sigma_m}{c\sigma_f} - 1 \right) \\ &\quad + \sqrt{\alpha} (1 + \alpha) \left(1 - \frac{2}{\pi} \arcsin \frac{\alpha - 1}{\alpha + 1} \right). \end{aligned} \quad (22)$$

Here β is an explicit function of the material parameters, i.e., it has prescribed value. Consequently, (22) is an algebraic equation for α . A numerical solution is shown in Fig. 2.

If we consider the crack not only of critical length, but also of any one equilibrium, then the sign “=” in Eq. (16) is replaced by “≤” and Eqs. (18), (20), (21) do not change. As a consequence, we obtain the following estimate of the crack length:

$$l_g \leq l \leq l_k \quad (23)$$

Values l_g and l_k can be computed from the forms

$$l_k = \lambda \frac{D\sigma_f^2}{\sigma_{\infty}^2}, \quad l_g = \kappa l_k \quad (24)$$

$$\lambda = c^2 \left(\frac{2}{\pi} \beta + \frac{4}{\pi^2} \alpha + \frac{1}{4} \frac{\beta^2}{\alpha} \right) \quad (25)$$

$$\kappa = \frac{4U^2}{(1 + U^2)^2} \quad (26)$$

In conclusion, the results of the calculation for two specific materials, namely silicon carbide fibers in calcium aluminosilicate glass ceramic matrix and a silicon carbide fiber in a silicon carbide matrix, are given. Data for the material are presented in Table 1 (Budiansky et al., 1995). In Fig. 3 we have shown the factors λ and κ according to (26) as a function of fiber concentration.

References

- Budiansky, B., Evans, A. G., and Hutchinson, 1995, "Fiber-matrix debonding effects on cracking in aligned fiber ceramic composites," *Int. J. Solids Structures*, Vol. 32, No. 3–4, pp. 315–328.
- Morozov, N., and Paukshto, M., 1994, *Discrete and hybrid models of fracture mechanics*, St. Petersburg State University, St. Petersburg, Russia. in Russian.
- Libowitz, H., ed., 1968, *Fracture*, Academic Press, New York.
- Nemat-Nasser, S., and Hori, M., 1987, "Toughening by partial or full bridging of cracks in ceramics and fiber reinforced composites," *Mechanics of Materials*, Vol. 6, pp. 245–269.
- Novozhilov, V. V., 1969, "On the foundation of a theory of equilibrium cracks in elastic solids," *Prikl. Math. Mech.*, Vol. 33, No. 5, pp. 797–812 (in Russian, see also English translation: *Applied Math. Mech.*, 1969, Vol. 33, No. 5, pp. 777–790).

Simultaneous Triangularization of the Coefficients of Linear Systems

W. C. Lee^{4,6} and F. Ma^{5,6}

1 Introduction

The coefficient matrices in the equation of motion of a linear nonconservative system may consist of arbitrary square matrices lacking any properties of symmetry and definiteness. An efficient way to analyze such a system is to reduce its coefficient matrices simultaneously to upper triangular forms. The purpose of this brief note is to present some criteria for simultaneous triangularization, and to expound a consequent procedure for constructing the triangularizing transformation.

The equation of motion of an n -degree-of-freedom linear nonconservative system can be written as

$$A\ddot{\mathbf{x}} + B\dot{\mathbf{x}} + C\mathbf{x} = \mathbf{g}(t), \quad (1)$$

where A , B , and C are arbitrary square matrices of order n . These coefficient matrices need not possess any of the familiar properties of symmetry or definiteness. The displacement $\mathbf{x}(t)$ and external excitation $\mathbf{g}(t)$ are n -dimensional vectors. In traditional applications, equations of the above type arise chiefly in

the area of vehicle dynamics. The use of control devices in structures in recent years, however, has permitted linear nonconservative systems to manifest themselves on a widespread scale (Soong, 1990). In theory, it is always possible to investigate a linear nonconservative system with the state-space approach. Additionally, alternative methods have been proposed for the analysis of system (1) in its second-order formulation. These various approaches were recently discussed by Ma and Caughey (1995). It was pointed out that conversion of system (1) to first-order form could increase the computational effort and diminish the physical insight. On the other hand, methods applicable directly to system (1) could be rather restrictive. An efficient method for the analysis of system (1) involves simultaneous reduction of A , B , and C to upper triangular matrices by a common similarity transformation. Necessary and sufficient conditions for the existence of a triangularizing transformation were presented by Caughey and Ma (1993) in the language of Lie algebra. Without disputing the relative merits of other techniques, the aim of this paper is to document additional criteria for simultaneous triangularization that are comprehensible and practical. A procedure for constructing the triangularizing transformation is also described.

2 Qualitative Criteria

A family of square matrices of order n constitutes a Lie algebra L if, for all P, Q in L , the commutator product $[P, Q] = PQ - QP$ also belongs to L . The notation $L(P_1, P_2, \dots, P_k)$ is employed to denote the Lie algebra generated by the matrices P_1, P_2, \dots, P_k . A Lie algebra L is associated with its derived sequence, defined inductively as follows:

$$L^{(0)} = L, \quad (2)$$

$$L^{(n+1)} = \{[S, T]: S, T \in L^{(n)}\}, \quad n \geq 0. \quad (3)$$

A Lie algebra L is said to be solvable if there exists an integer m such that $L^{(m)} = \{0\}$. The class of solvable Lie algebra includes the class of pairwise commuting matrices, where $L^{(1)} = \{0\}$. As explained by Caughey and Ma (1993), a necessary and sufficient condition under which the coefficient matrices A , B , and C can be reduced simultaneously to upper triangular forms is the following.

Criterion 1. The linear nonconservative system (1) is triangularizable if and only if the coefficient matrices A , B , and C generate a solvable Lie algebra.

The above criterion involves computation of $L^{(m)}$, where m is not specified beforehand. To develop a mathematically equivalent criterion that is more specific, the concept of adjoint representation of a matrix is needed (Bauerle and de Kerf, 1990). In the space of square matrices of order n , a natural basis e_{ij} ($i, j = 1, 2, \dots, n$) can be chosen such that each member e_{ij} is itself a square matrix of order n with 1 as the ij th element and 0 elsewhere. Any square matrix $A = [a_{ij}]$ of order n may be expanded in the natural basis in such a way that

$$A = \sum_{i=1}^n \sum_{j=1}^n a_{ij} e_{ij}. \quad (4)$$

Let the double subscript of e_{ij} be rearranged sequentially so that $e_1 = e_{11}, e_2 = e_{12}, \dots, e_n = e_{1n}, e_{n+1} = e_{21}, e_{n+2} = e_{22}, \dots, e_{n+n} = e_{2n}, \dots, e_{n^2} = e_{nn}$. The adjoint representation of a square matrix A of order n , denoted by adA , is a square matrix of order n^2 whose j th column may be computed from the sequence of commutator products

$$[A, e_j] = Ae_j - e_jA = \sum_{i=1}^{n^2} C_{ij}^j e_i, \quad j = 1, 2, \dots, n^2. \quad (5)$$

The i th element of the j th column of adA , or its ij th element, is simply given by C_{ij}^j ($i, j = 1, 2, \dots, n^2$). Algorithms for the

⁴ Postdoctoral Fellow.

⁵ Professor of Applied Mechanics. Mem. ASME.

⁶ Department of Mechanical Engineering, University of California, Berkeley, CA 94720.

Contributed by the Applied Mechanics Division of THE AMERICAN SOCIETY OF MECHANICAL ENGINEERS for publication in the ASME JOURNAL OF APPLIED MECHANICS. Manuscript received by the ASME Applied Mechanics Division, Jan. 3, 1996; final revision, Aug. 9, 1996. Associate Technical Editor: W. K. Liu.

$$l_k = \lambda \frac{D\sigma_f^2}{\sigma_{\infty}^2}, \quad l_g = \kappa l_k \quad (24)$$

$$\lambda = c^2 \left(\frac{2}{\pi} \beta + \frac{4}{\pi^2} \alpha + \frac{1}{4} \frac{\beta^2}{\alpha} \right) \quad (25)$$

$$\kappa = \frac{4U^2}{(1 + U^2)^2} \quad (26)$$

In conclusion, the results of the calculation for two specific materials, namely silicon carbide fibers in calcium aluminosilicate glass ceramic matrix and a silicon carbide fiber in a silicon carbide matrix, are given. Data for the material are presented in Table 1 (Budiansky et al., 1995). In Fig. 3 we have shown the factors λ and κ according to (26) as a function of fiber concentration.

References

- Budiansky, B., Evans, A. G., and Hutchinson, 1995, "Fiber-matrix debonding effects on cracking in aligned fiber ceramic composites," *Int. J. Solids Structures*, Vol. 32, No. 3–4, pp. 315–328.
- Morozov, N., and Paukshto, M., 1994, *Discrete and hybrid models of fracture mechanics*, St. Petersburg State University, St. Petersburg, Russia. in Russian.
- Libowitz, H., ed., 1968, *Fracture*, Academic Press, New York.
- Nemat-Nasser, S., and Hori, M., 1987, "Toughening by partial or full bridging of cracks in ceramics and fiber reinforced composites," *Mechanics of Materials*, Vol. 6, pp. 245–269.
- Novozhilov, V. V., 1969, "On the foundation of a theory of equilibrium cracks in elastic solids," *Prikl. Math. Mech.*, Vol. 33, No. 5, pp. 797–812 (in Russian, see also English translation: *Applied Math. Mech.*, 1969, Vol. 33, No. 5, pp. 777–790).

Simultaneous Triangularization of the Coefficients of Linear Systems

W. C. Lee^{4,6} and F. Ma^{5,6}

1 Introduction

The coefficient matrices in the equation of motion of a linear nonconservative system may consist of arbitrary square matrices lacking any properties of symmetry and definiteness. An efficient way to analyze such a system is to reduce its coefficient matrices simultaneously to upper triangular forms. The purpose of this brief note is to present some criteria for simultaneous triangularization, and to expound a consequent procedure for constructing the triangularizing transformation.

The equation of motion of an n -degree-of-freedom linear nonconservative system can be written as

$$A\ddot{\mathbf{x}} + B\dot{\mathbf{x}} + C\mathbf{x} = \mathbf{g}(t), \quad (1)$$

where A , B , and C are arbitrary square matrices of order n . These coefficient matrices need not possess any of the familiar properties of symmetry or definiteness. The displacement $\mathbf{x}(t)$ and external excitation $\mathbf{g}(t)$ are n -dimensional vectors. In traditional applications, equations of the above type arise chiefly in

the area of vehicle dynamics. The use of control devices in structures in recent years, however, has permitted linear nonconservative systems to manifest themselves on a widespread scale (Soong, 1990). In theory, it is always possible to investigate a linear nonconservative system with the state-space approach. Additionally, alternative methods have been proposed for the analysis of system (1) in its second-order formulation. These various approaches were recently discussed by Ma and Caughey (1995). It was pointed out that conversion of system (1) to first-order form could increase the computational effort and diminish the physical insight. On the other hand, methods applicable directly to system (1) could be rather restrictive. An efficient method for the analysis of system (1) involves simultaneous reduction of A , B , and C to upper triangular matrices by a common similarity transformation. Necessary and sufficient conditions for the existence of a triangularizing transformation were presented by Caughey and Ma (1993) in the language of Lie algebra. Without disputing the relative merits of other techniques, the aim of this paper is to document additional criteria for simultaneous triangularization that are comprehensible and practical. A procedure for constructing the triangularizing transformation is also described.

2 Qualitative Criteria

A family of square matrices of order n constitutes a Lie algebra L if, for all P, Q in L , the commutator product $[P, Q] = PQ - QP$ also belongs to L . The notation $L(P_1, P_2, \dots, P_k)$ is employed to denote the Lie algebra generated by the matrices P_1, P_2, \dots, P_k . A Lie algebra L is associated with its derived sequence, defined inductively as follows:

$$L^{(0)} = L, \quad (2)$$

$$L^{(n+1)} = \{[S, T]: S, T \in L^{(n)}\}, \quad n \geq 0. \quad (3)$$

A Lie algebra L is said to be solvable if there exists an integer m such that $L^{(m)} = \{0\}$. The class of solvable Lie algebra includes the class of pairwise commuting matrices, where $L^{(1)} = \{0\}$. As explained by Caughey and Ma (1993), a necessary and sufficient condition under which the coefficient matrices A , B , and C can be reduced simultaneously to upper triangular forms is the following.

Criterion 1. The linear nonconservative system (1) is triangularizable if and only if the coefficient matrices A , B , and C generate a solvable Lie algebra.

The above criterion involves computation of $L^{(m)}$, where m is not specified beforehand. To develop a mathematically equivalent criterion that is more specific, the concept of adjoint representation of a matrix is needed (Bauerle and de Kerf, 1990). In the space of square matrices of order n , a natural basis e_{ij} ($i, j = 1, 2, \dots, n$) can be chosen such that each member e_{ij} is itself a square matrix of order n with 1 as the ij th element and 0 elsewhere. Any square matrix $A = [a_{ij}]$ of order n may be expanded in the natural basis in such a way that

$$A = \sum_{i=1}^n \sum_{j=1}^n a_{ij} e_{ij}. \quad (4)$$

Let the double subscript of e_{ij} be rearranged sequentially so that $e_1 = e_{11}, e_2 = e_{12}, \dots, e_n = e_{1n}, e_{n+1} = e_{21}, e_{n+2} = e_{22}, \dots, e_{n+n} = e_{2n}, \dots, e_{n^2} = e_{nn}$. The adjoint representation of a square matrix A of order n , denoted by adA , is a square matrix of order n^2 whose j th column may be computed from the sequence of commutator products

$$[A, e_j] = Ae_j - e_jA = \sum_{i=1}^{n^2} C_{ij}^j e_i, \quad j = 1, 2, \dots, n^2. \quad (5)$$

The i th element of the j th column of adA , or its ij th element, is simply given by C_{ij}^j ($i, j = 1, 2, \dots, n^2$). Algorithms for the

⁴ Postdoctoral Fellow.

⁵ Professor of Applied Mechanics. Mem. ASME.

⁶ Department of Mechanical Engineering, University of California, Berkeley, CA 94720.

Contributed by the Applied Mechanics Division of THE AMERICAN SOCIETY OF MECHANICAL ENGINEERS for publication in the ASME JOURNAL OF APPLIED MECHANICS. Manuscript received by the ASME Applied Mechanics Division, Jan. 3, 1996; final revision, Aug. 9, 1996. Associate Technical Editor: W. K. Liu.

computation of adA are available (Bauerle and de Kerf, 1990) but will not be addressed herein. A square matrix A is said to be nilpotent if $A^r = 0$ for some r . If A is nilpotent, then $ad A$ is also nilpotent but the reverse is not true. It is known that a Lie algebra L is solvable if and only if each element in $L^{(1)}$ has a nilpotent adjoint representation (Sagle and Walde, 1973). When this assertion is applied to system (1), a necessary and sufficient condition for simultaneous triangularization of A , B , and C can be readily obtained.

Criterion 2. The linear nonconservative system (1) is triangularizable if and only if each element in $L^{(1)}(A, B, C)$ has an adjoint representation that is nilpotent.

The above criterion is more specific than Criterion 1 since examination of only $L^{(1)}$ is needed. On the other hand, Criterion 2 requires calculation of the adjoint representations of matrices in $L^{(1)}$. An immediate corollary of the above criterion is that system (1) is triangularizable if each element in $L^{(1)}(A, B, C)$ is a nilpotent matrix. However, this is only a sufficient and not a necessary condition. Sometimes it is useful to know when a system cannot be triangularized. It can be shown that if a Lie algebra L is solvable, then there exists a common eigenvector among all elements in L (Bauerle and de Kerf, 1990). That means if system (1) is triangularizable, there must be a common eigenvector among all elements in $L(A, B, C)$. An upshot at this stage is the following statement.

Criterion 3. If there is not a common eigenvector among elements of the Lie algebra generated by the coefficient matrices A , B , and C , then the linear nonconservative system (1) is not triangularizable.

It is now quite clear that only a small subclass of linear nonconservative systems can be triangularized. The above criterion will be used in the next section for constructing a triangularizing similarity transformation.

Example 1. Consider a two-degree-of-freedom structure of the form (1), with

$$A = \begin{bmatrix} 1 & 0 \\ 0 & 1 \end{bmatrix}, \quad B = \begin{bmatrix} 4 & -6 \\ 3 & -5 \end{bmatrix}, \quad C = \begin{bmatrix} -5 & 7 \\ -3 & 5 \end{bmatrix}. \quad (6)$$

The Lie algebra and the derived sequence generated by A , B , and C are $L^{(0)}(A, B, C) = \{0, A, B, C, nD, -nD\}$, $L^{(1)}(A, B, C) = \{0, nD, -nD\}$ ($n = 3, 9, 12, 27, 36, \dots$) where the matrix D is given by

$$D = \begin{bmatrix} -1 & 1 \\ -1 & 1 \end{bmatrix}. \quad (7)$$

Adjoint representation of the matrix nD is

$$ad nD = n \begin{bmatrix} 0 & 1 & 1 & 0 \\ -1 & -2 & 0 & 1 \\ -1 & 0 & 2 & 1 \\ 0 & -1 & -1 & 0 \end{bmatrix}. \quad (8)$$

Since $(ad nD)^3 = 0$ for all n , each element of $L^{(1)}(A, B, C)$ has an adjoint representation that is nilpotent. Hence from Criterion 2 the structure is triangularizable. Define a coordinate transformation $\mathbf{x} = T\mathbf{q}$, for which

$$T = \begin{bmatrix} 1 & 2 \\ 1 & 1 \end{bmatrix}. \quad (9)$$

The transformed equation of motion becomes

$$T^{-1}AT\ddot{\mathbf{q}} + T^{-1}BT\dot{\mathbf{q}} + T^{-1}CT\mathbf{q} = T^{-1}\mathbf{g}(t) \quad (10)$$

with coefficient matrices

$$T^{-1}AT = \begin{bmatrix} 1 & 0 \\ 0 & 1 \end{bmatrix}, \quad T^{-1}BT = \begin{bmatrix} -2 & 0 \\ 0 & 1 \end{bmatrix},$$

$$T^{-1}CT = \begin{bmatrix} 2 & 1 \\ 0 & -2 \end{bmatrix}. \quad (11)$$

According to Criterion 3, there exists a common eigenvector among A , B , C , nD , and $-nD$ ($n = 3, 9, 12, 27, 36, \dots$). After calculating and comparing the eigenvectors of B and C , it is observed that $[1, 1]^T$ is a common eigenvector among matrices in $L^{(0)}(A, B, C)$.

3 Construction of Triangularizing Transformation

Based upon Criterion 3, a procedure for determining a triangularizing similarity transformation for system (1) will be given. The procedure itself may be regarded as a constructive criterion for assessing triangularizability, since the procedure cannot be carried through unless the coefficient matrices are simultaneously reducible to upper triangular forms. The abstract theory associated with this method is described by Sagle and Walde (1973).

In exposition of this method, it is convenient to start by assuming that the coefficient matrices A , B , and C of system (1) are simultaneously triangularizable and nonsingular. Since $L(A, B, C)$ contains the coefficient matrices themselves, by Criterion 3 there exists a common eigenvector among A , B , and C . Denote this common eigenvector of order n by \mathbf{u}_1 . Choose linearly independent vectors $\tilde{\mathbf{u}}_2^1, \tilde{\mathbf{u}}_3^1, \dots, \tilde{\mathbf{u}}_n^1$ so that together with \mathbf{u}_1 they constitute a basis of the n -dimensional space. For each $\tilde{\mathbf{u}}_j^1$ ($j = 2, 3, \dots, n$), unique scalars $a_{ij}^1, b_{ij}^1, c_{ij}^1$ ($i, j = 1, 2, \dots, n$) can be determined so that

$$A\tilde{\mathbf{u}}_j^1 = a_{1j}^1\mathbf{u}_1 + \sum_{i=2}^n a_{ij}^1\tilde{\mathbf{u}}_i^1, \quad B\tilde{\mathbf{u}}_j^1 = b_{1j}^1\mathbf{u}_1 + \sum_{i=2}^n b_{ij}^1\tilde{\mathbf{u}}_i^1,$$

$$C\tilde{\mathbf{u}}_j^1 = c_{1j}^1\mathbf{u}_1 + \sum_{i=2}^n c_{ij}^1\tilde{\mathbf{u}}_i^1. \quad (12)$$

Define three matrices of order $n-1$ by $A_1 = [a_{ij}^1]$, $B_1 = [b_{ij}^1]$ and $C_1 = [c_{ij}^1]$ ($i, j = 2, 3, \dots, n$). From Criterion 3, it can be deduced that there is a common eigenvector among A_1 , B_1 and C_1 (Sagle and Walde, 1973). Denote this common eigenvector of order $n-1$ by \mathbf{u}_2^* . Transform \mathbf{u}_2^* into a vector \mathbf{u}_2 of order n by $\mathbf{u}_2 = D_1\mathbf{u}_2^*$, where $D_1 = [\tilde{\mathbf{u}}_2^1, \tilde{\mathbf{u}}_3^1, \dots, \tilde{\mathbf{u}}_n^1]$ is an $n \times (n-1)$ matrix consisting of the vectors $\tilde{\mathbf{u}}_j^1$ ($j = 2, 3, \dots, n$) as columns.

With \mathbf{u}_1 and \mathbf{u}_2 specified, one then proceeds to choose linearly independent vectors $\tilde{\mathbf{u}}_3^2, \tilde{\mathbf{u}}_4^2, \dots, \tilde{\mathbf{u}}_n^2$ so that together with \mathbf{u}_1 and \mathbf{u}_2 they constitute a basis of the n -dimensional space. For each $\tilde{\mathbf{u}}_j^2$ ($j = 3, 4, \dots, n$), unique scalars $a_{ij}^2, b_{ij}^2, c_{ij}^2$ ($i, j = 1, 2, \dots, n$) can be found such that

$$A\tilde{\mathbf{u}}_j^2 = a_{1j}^2\mathbf{u}_1 + a_{2j}^2\mathbf{u}_2 + \sum_{i=3}^n a_{ij}^2\tilde{\mathbf{u}}_i^2,$$

$$B\tilde{\mathbf{u}}_j^2 = b_{1j}^2\mathbf{u}_1 + b_{2j}^2\mathbf{u}_2 + \sum_{i=3}^n b_{ij}^2\tilde{\mathbf{u}}_i^2,$$

$$C\tilde{\mathbf{u}}_j^2 = c_{1j}^2\mathbf{u}_1 + c_{2j}^2\mathbf{u}_2 + \sum_{i=3}^n c_{ij}^2\tilde{\mathbf{u}}_i^2. \quad (13)$$

Define three matrices of order $n-2$ by $A_2 = [a_{ij}^2]$, $B_2 = [b_{ij}^2]$ and $C_2 = [c_{ij}^2]$ ($i, j = 3, 4, \dots, n$). It can be deduced that there is a common eigenvector among A_2 , B_2 , and C_2 . Denote this common eigenvector of order $n-2$ by \mathbf{u}_3^* . Transform \mathbf{u}_3^* into a vector \mathbf{u}_3 of order n by $\mathbf{u}_3 = D_2\mathbf{u}_3^*$, where $D_2 = [\tilde{\mathbf{u}}_3^2, \tilde{\mathbf{u}}_4^2, \dots, \tilde{\mathbf{u}}_n^2]$ is an $n \times (n-2)$ matrix. Thus \mathbf{u}_1 , \mathbf{u}_2 , and \mathbf{u}_3 are now specified. Inductively, one can compute the remaining vectors $\mathbf{u}_4, \mathbf{u}_5, \dots, \mathbf{u}_n$ in an analogous fashion. The

matrix $T = [\mathbf{u}_1, \mathbf{u}_2, \dots, \mathbf{u}_n]$ defines a similarity transformation such that $T^{-1}AT$, $T^{-1}BT$ and $T^{-1}CT$ are upper triangular. The overall procedure for determining the triangularizing transformation T amounts to constructing its columns sequentially. An algorithmic approach to this procedure was discussed by Lee (1995).

Upon reduction of its coefficient matrices to upper triangular forms, system (1) may be solved by the method of back-substitution. Solving a triangularized system by back-substitution may be looked upon as solving n uncoupled equations with additional nonhomogeneous terms which originate from the off-diagonal elements of the triangularized coefficient matrices. These extra nonhomogeneous terms can be treated physically as internal excitation, as opposed to the external excitation $\mathbf{g}(t)$. Concepts of this type may be useful in an attempt to formulate a theory of coupling for linear nonconservative systems (Lee, 1995). Among other things, simultaneous reduction of A , B , and C to triangular forms is certainly more general than simultaneous reduction of the same coefficient matrices to diagonal forms. Compared to direct numerical integration of system (1), simultaneous triangularization offers the possibility of generating analytical solutions.

Example 2. A linear nonconservative system of the form (1) is defined by

$$A = \begin{bmatrix} 2.750 & 1.750 & -1.750 & 1.375 \\ 5.400 & 5.000 & -5.400 & 6.100 \\ 4.150 & 1.750 & -3.150 & 7.975 \\ 3.600 & 0.000 & -3.600 & 8.400 \end{bmatrix}, \quad (14)$$

$$B = \begin{bmatrix} 2.500 & 2.500 & -0.500 & 0.250 \\ 6.600 & 5.000 & -6.600 & 5.900 \\ 4.100 & 2.500 & -2.100 & 4.150 \\ 6.400 & 0.000 & -6.400 & 10.600 \end{bmatrix}, \quad (15)$$

$$C = \begin{bmatrix} 4.100 & 1.500 & -1.100 & 0.150 \\ 2.900 & 7.500 & -2.900 & 0.850 \\ -0.350 & 2.250 & 3.350 & -1.275 \\ -2.300 & 0.500 & 2.300 & 0.050 \end{bmatrix}. \quad (16)$$

It can be seen that $\mathbf{u}_1 = [1, 0, 1, 0]^T$ is a common eigenvector among A , B , and C . Choose linearly independent vectors $\hat{\mathbf{u}}_2^1 = [0, 1, 0, 1]^T$, $\hat{\mathbf{u}}_3^1 = [1, 1, 0, 0]^T$, $\hat{\mathbf{u}}_4^1 = [1, 0, 0, 0]^T$ so that \mathbf{u}_1 , $\hat{\mathbf{u}}_2^1$, $\hat{\mathbf{u}}_3^1$ and $\hat{\mathbf{u}}_4^1$ constitute a basis. Upon calculating A_1 , B_1 , and C_1 , it is found that a common eigenvector among them is $\mathbf{u}_2^* = [-0.667, 0, 1]^T$. Define a 4×3 matrix $D_1 = [\hat{\mathbf{u}}_2^1, \hat{\mathbf{u}}_3^1, \hat{\mathbf{u}}_4^1]$. Transform \mathbf{u}_2^* into a vector \mathbf{u}_2 by $\mathbf{u}_2 = D_1 \mathbf{u}_2^* = [1, -0.667, 0, -0.667]^T$. In a similar fashion, $\mathbf{u}_3 = [0, 1, 0, 0]^T$ and $\mathbf{u}_4 = [2, 0, 0, 0]^T$ can be determined. The transformation matrix is $T = [\mathbf{u}_1, \mathbf{u}_2, \mathbf{u}_3, \mathbf{u}_4]$. Upon triangularization of the system, the coefficient matrices become

$$T^{-1}AT = \begin{bmatrix} 1.000 & -2.333 & 1.750 & 8.300 \\ 0.000 & 3.000 & 0.000 & -10.800 \\ 0.000 & 0.000 & 5.000 & 3.600 \\ 0.000 & 0.000 & 0.000 & 4.000 \end{bmatrix}, \quad (17)$$

$$T^{-1}BT = \begin{bmatrix} 2.000 & -0.333 & 2.500 & 8.200 \\ 0.000 & 1.000 & 0.000 & -19.200 \\ 0.000 & 0.000 & 5.000 & 0.400 \\ 0.000 & 0.000 & 0.000 & 8.000 \end{bmatrix}, \quad (18)$$

$$T^{-1}CT = \begin{bmatrix} 3.000 & -1.000 & 2.250 & -0.700 \\ 0.000 & 4.000 & -0.750 & 6.900 \\ 0.000 & 0.000 & 7.000 & 10.400 \\ 0.000 & 0.000 & 0.000 & 1.000 \end{bmatrix}. \quad (19)$$

4 Conclusions

Criteria for simultaneous reduction of the coefficient matrices of a linear nonconservative system to upper triangular forms have been presented. The coefficient matrices A , B , and C are

simultaneously triangularizable if and only if $L(A, B, C)$ is solvable. Equivalently, these coefficient matrices are simultaneously reducible if and only if each element in $L^{(1)}(A, B, C)$ has an adjoint representation that is nilpotent. A sufficient condition for simultaneous triangularization is that each element in $L^{(1)}(A, B, C)$ be a nilpotent matrix. On the other hand, if there is not a common eigenvector among elements in $L(A, B, C)$, then system (1) is not triangularizable. The last criterion has been employed in the construction of a triangularizing transformation. Simultaneous reduction of A , B , and C to triangular forms is more general than simultaneous reduction of the same coefficient matrices to diagonal forms. Compared to direct numerical integration of system (1), simultaneous triangularization offers the possibility of generating analytical solutions.

Acknowledgment

This research has been supported in part by the National Science Foundation under Grant No. MSS-8657619. Opinions, findings, and conclusions expressed in this paper are those of the authors and do not necessarily reflect the views of the National Science Foundation.

References

- Bauerle, G. G. A., and de Kerf, E. A., 1990, *Finite and Infinite Dimensional Lie Algebras and Applications in Physics*, North-Holland, Amsterdam, pp. 2, 10–12, 52–54, 64–70.
- Caughey, T. K., and Ma, F., 1993, "Complex Modes and Solvability of Nonclassical Linear Systems," *ASME JOURNAL OF APPLIED MECHANICS*, Vol. 60, pp. 26–28.
- Lee, W. C., 1995, "Analysis and Stability of Nonconservative Systems," doctoral dissertation, Department of Mechanical Engineering, University of California at Berkeley, Berkeley, CA, pp. 6–21.
- Ma, F., and Caughey, T. K., 1995, "Analysis of Linear Nonconservative Vibrations," *ASME JOURNAL OF APPLIED MECHANICS*, Vol. 62, pp. 685–691.
- Sagle, A. A., and Walde, R. E., 1973, *Introduction to Lie Groups and Lie Algebras*, Academic Press, New York, pp. 210–212, 220.
- Soong, T. T., 1990, *Active Structural Control: Theory and Practice*, Longman, Essex, UK, p. 8.

Stress Field Around Holes in Antiplane Shear Using Complex Variable Boundary Element Method

S. I. Chou⁷

1 Introduction

The problem of the stress field around two circular inclusions in an infinity medium under remote uniform, longitudinal shear has recently been investigated by Honein et al. (1992). Numerical results for stresses around two circular holes, and around two circular inclusions disturbing the uniform remote shear have been given. A similar problem was solved earlier by Goree and Wilson (1967), Budiansky and Carrier (1984), and Steif (1989).

As is well known, the antiplane shear problem in elastostatics can be reduced to the solution of Laplace equation in terms of

⁷ Department of Engineering Mechanics, University of Nebraska-Lincoln, Lincoln, NE 68588-0347.

Contributed by the Applied Mechanics Division of THE AMERICAN SOCIETY OF MECHANICAL ENGINEERS for publication in the ASME JOURNAL OF APPLIED MECHANICS. Manuscript received by the ASME Applied Mechanics Division, Apr. 17, 1996; final revision, June 10, 1996. Associate Technical Editor: X. Markenscoff.

matrix $T = [\mathbf{u}_1, \mathbf{u}_2, \dots, \mathbf{u}_n]$ defines a similarity transformation such that $T^{-1}AT$, $T^{-1}BT$ and $T^{-1}CT$ are upper triangular. The overall procedure for determining the triangularizing transformation T amounts to constructing its columns sequentially. An algorithmic approach to this procedure was discussed by Lee (1995).

Upon reduction of its coefficient matrices to upper triangular forms, system (1) may be solved by the method of back-substitution. Solving a triangularized system by back-substitution may be looked upon as solving n uncoupled equations with additional nonhomogeneous terms which originate from the off-diagonal elements of the triangularized coefficient matrices. These extra nonhomogeneous terms can be treated physically as internal excitation, as opposed to the external excitation $\mathbf{g}(t)$. Concepts of this type may be useful in an attempt to formulate a theory of coupling for linear nonconservative systems (Lee, 1995). Among other things, simultaneous reduction of A , B , and C to triangular forms is certainly more general than simultaneous reduction of the same coefficient matrices to diagonal forms. Compared to direct numerical integration of system (1), simultaneous triangularization offers the possibility of generating analytical solutions.

Example 2. A linear nonconservative system of the form (1) is defined by

$$A = \begin{bmatrix} 2.750 & 1.750 & -1.750 & 1.375 \\ 5.400 & 5.000 & -5.400 & 6.100 \\ 4.150 & 1.750 & -3.150 & 7.975 \\ 3.600 & 0.000 & -3.600 & 8.400 \end{bmatrix}, \quad (14)$$

$$B = \begin{bmatrix} 2.500 & 2.500 & -0.500 & 0.250 \\ 6.600 & 5.000 & -6.600 & 5.900 \\ 4.100 & 2.500 & -2.100 & 4.150 \\ 6.400 & 0.000 & -6.400 & 10.600 \end{bmatrix}, \quad (15)$$

$$C = \begin{bmatrix} 4.100 & 1.500 & -1.100 & 0.150 \\ 2.900 & 7.500 & -2.900 & 0.850 \\ -0.350 & 2.250 & 3.350 & -1.275 \\ -2.300 & 0.500 & 2.300 & 0.050 \end{bmatrix}. \quad (16)$$

It can be seen that $\mathbf{u}_1 = [1, 0, 1, 0]^T$ is a common eigenvector among A , B , and C . Choose linearly independent vectors $\hat{\mathbf{u}}_2^1 = [0, 1, 0, 1]^T$, $\hat{\mathbf{u}}_3^1 = [1, 1, 0, 0]^T$, $\hat{\mathbf{u}}_4^1 = [1, 0, 0, 0]^T$ so that \mathbf{u}_1 , $\hat{\mathbf{u}}_2^1$, $\hat{\mathbf{u}}_3^1$ and $\hat{\mathbf{u}}_4^1$ constitute a basis. Upon calculating A_1 , B_1 , and C_1 , it is found that a common eigenvector among them is $\mathbf{u}_2^* = [-0.667, 0, 1]^T$. Define a 4×3 matrix $D_1 = [\hat{\mathbf{u}}_2^1, \hat{\mathbf{u}}_3^1, \hat{\mathbf{u}}_4^1]$. Transform \mathbf{u}_2^* into a vector \mathbf{u}_2 by $\mathbf{u}_2 = D_1 \mathbf{u}_2^* = [1, -0.667, 0, -0.667]^T$. In a similar fashion, $\mathbf{u}_3 = [0, 1, 0, 0]^T$ and $\mathbf{u}_4 = [2, 0, 0, 0]^T$ can be determined. The transformation matrix is $T = [\mathbf{u}_1, \mathbf{u}_2, \mathbf{u}_3, \mathbf{u}_4]$. Upon triangularization of the system, the coefficient matrices become

$$T^{-1}AT = \begin{bmatrix} 1.000 & -2.333 & 1.750 & 8.300 \\ 0.000 & 3.000 & 0.000 & -10.800 \\ 0.000 & 0.000 & 5.000 & 3.600 \\ 0.000 & 0.000 & 0.000 & 4.000 \end{bmatrix}, \quad (17)$$

$$T^{-1}BT = \begin{bmatrix} 2.000 & -0.333 & 2.500 & 8.200 \\ 0.000 & 1.000 & 0.000 & -19.200 \\ 0.000 & 0.000 & 5.000 & 0.400 \\ 0.000 & 0.000 & 0.000 & 8.000 \end{bmatrix}, \quad (18)$$

$$T^{-1}CT = \begin{bmatrix} 3.000 & -1.000 & 2.250 & -0.700 \\ 0.000 & 4.000 & -0.750 & 6.900 \\ 0.000 & 0.000 & 7.000 & 10.400 \\ 0.000 & 0.000 & 0.000 & 1.000 \end{bmatrix}. \quad (19)$$

4 Conclusions

Criteria for simultaneous reduction of the coefficient matrices of a linear nonconservative system to upper triangular forms have been presented. The coefficient matrices A , B , and C are

simultaneously triangularizable if and only if $L(A, B, C)$ is solvable. Equivalently, these coefficient matrices are simultaneously reducible if and only if each element in $L^{(1)}(A, B, C)$ has an adjoint representation that is nilpotent. A sufficient condition for simultaneous triangularization is that each element in $L^{(1)}(A, B, C)$ be a nilpotent matrix. On the other hand, if there is not a common eigenvector among elements in $L(A, B, C)$, then system (1) is not triangularizable. The last criterion has been employed in the construction of a triangularizing transformation. Simultaneous reduction of A , B , and C to triangular forms is more general than simultaneous reduction of the same coefficient matrices to diagonal forms. Compared to direct numerical integration of system (1), simultaneous triangularization offers the possibility of generating analytical solutions.

Acknowledgment

This research has been supported in part by the National Science Foundation under Grant No. MSS-8657619. Opinions, findings, and conclusions expressed in this paper are those of the authors and do not necessarily reflect the views of the National Science Foundation.

References

- Bauerle, G. G. A., and de Kerf, E. A., 1990, *Finite and Infinite Dimensional Lie Algebras and Applications in Physics*, North-Holland, Amsterdam, pp. 2, 10–12, 52–54, 64–70.
- Caughey, T. K., and Ma, F., 1993, "Complex Modes and Solvability of Nonclassical Linear Systems," *ASME JOURNAL OF APPLIED MECHANICS*, Vol. 60, pp. 26–28.
- Lee, W. C., 1995, "Analysis and Stability of Nonconservative Systems," doctoral dissertation, Department of Mechanical Engineering, University of California at Berkeley, Berkeley, CA, pp. 6–21.
- Ma, F., and Caughey, T. K., 1995, "Analysis of Linear Nonconservative Vibrations," *ASME JOURNAL OF APPLIED MECHANICS*, Vol. 62, pp. 685–691.
- Sagle, A. A., and Walde, R. E., 1973, *Introduction to Lie Groups and Lie Algebras*, Academic Press, New York, pp. 210–212, 220.
- Soong, T. T., 1990, *Active Structural Control: Theory and Practice*, Longman, Essex, UK, p. 8.

Stress Field Around Holes in Antiplane Shear Using Complex Variable Boundary Element Method

S. I. Chou⁷

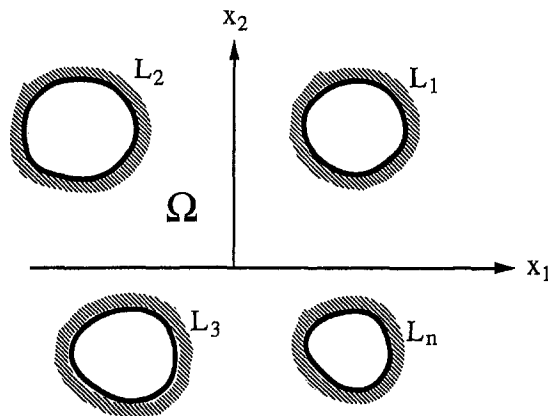
1 Introduction

The problem of the stress field around two circular inclusions in an infinity medium under remote uniform, longitudinal shear has recently been investigated by Honein et al. (1992). Numerical results for stresses around two circular holes, and around two circular inclusions disturbing the uniform remote shear have been given. A similar problem was solved earlier by Goree and Wilson (1967), Budiansky and Carrier (1984), and Steif (1989).

As is well known, the antiplane shear problem in elastostatics can be reduced to the solution of Laplace equation in terms of

⁷ Department of Engineering Mechanics, University of Nebraska-Lincoln, Lincoln, NE 68588-0347.

Contributed by the Applied Mechanics Division of THE AMERICAN SOCIETY OF MECHANICAL ENGINEERS for publication in the ASME JOURNAL OF APPLIED MECHANICS. Manuscript received by the ASME Applied Mechanics Division, Apr. 17, 1996; final revision, June 10, 1996. Associate Technical Editor: X. Markenscoff.

Fig. 1 Infinite plane Ω exterior to n holes

the transverse displacement. It can thus be solved by using the complex variable boundary element method (CVBEM), which was developed extensively by Hromadka and Lai (1986), and is shown to be an effective numerical method for the solution of potential problems. It is particularly suitable for the solution of problems involving an infinite region, such as the one to be considered here.

In most problems, the stress field is of interest and is determined by numerical differentiation using the boundary values of displacement found. This usually yields less accurate results. As shown by Hromadka and Yen (1988), one natural remedy to this problem is to use higher order interpolation function for the element, which, however, requires more analytical and numerical work. In this paper, it is shown that the antiplane shear problem of an infinite medium with holes can be formulated in terms of the derivatives of displacement, and thus, the stresses on the boundaries found directly without recourse to numerical differentiation. In the same line of thought, Choi and Kwak (1989) considered the formation of a boundary integral equation in terms of unknown derivatives by integration by parts of the Cauchy integral; however, their method is substantially different from what is to be presented here.

As numerical examples, the problems of two holes considered by Honein et al. (1992) are solved using the present method.

2 Formulation of the Problem

The antiplane deformation is defined by the displacement field

$$u_1 = u_2 = 0; \quad u \equiv u_3 = u_3(x_1, x_2), \quad (1)$$

with a nonvanishing stress field given by

$$\sigma_{13} = \sigma_{31} = \mu \frac{\partial u}{\partial x_1}, \quad \sigma_{23} = \sigma_{32} = \mu \frac{\partial u}{\partial x_2}, \quad (2)$$

where μ is the shear modulus. The problem is thus two-dimensional, and $u(x_1, x_2)$ satisfies the Laplace equation.

Consider the problem of an infinite medium Ω exterior to n traction-free circular holes bounded by contours L_k , $k = 1, 2, \dots, n$, Fig. 1. At infinity, the medium is under uniform shear $\sigma_{32}^\infty = \tau$; $\sigma_{31}^\infty = 0$, or equivalently under the displacement $u^\infty = \tau x_2 / \mu_2 + c$, where c denotes rigid-body displacement. Let the stress field σ'_{32} and σ'_{31} in the medium be given as

$$\sigma'_{31} = \sigma_{31}^\infty + \sigma_{31}, \quad \sigma'_{32} = \sigma_{32}^\infty + \sigma_{32}, \quad (3)$$

and the displacement u' as

$$u' = u^\infty + u, \quad (4)$$

where σ_{31} , σ_{32} , and u are quantities due to the presence of holes. The problem becomes the solution of the following problem:

$$\nabla^2 u = 0 \text{ in } \Omega,$$

$$\frac{\partial u}{\partial n} = -\frac{\tau}{\mu} n_2 \text{ on } L_k, \quad u \rightarrow 0 \text{ as } x_1^2 + x_2^2 \rightarrow \infty. \quad (5)$$

Here $\mathbf{n} = (n_1, n_2)$ is the outward unit vector on the hole contours.

Let

$$\phi = \frac{\partial u}{\partial x_2}, \quad \psi = \frac{\partial u}{\partial x_1}. \quad (6)$$

It is easily shown that the problem (5) is reduced to the following equivalent problem:

$$\nabla^2 \phi = 0; \quad \nabla^2 \psi = 0 \text{ in } \Omega$$

$$n_1 \psi + n_2 \phi = -\frac{\tau}{\mu} \text{ on } L_k; \quad \phi, \psi \rightarrow 0 \text{ as } x_1^2 + x_2^2 \rightarrow \infty, \quad (7)$$

with the conditions of single-valueness of displacement given by

$$\int_{L_k} (\psi dx_1 + \phi dx_2) = 0, \quad k = 1, 2, \dots, n. \quad (8)$$

The functions ϕ , ψ are harmonic and can be shown to be conjugate of each other. They are the real and imaginary parts

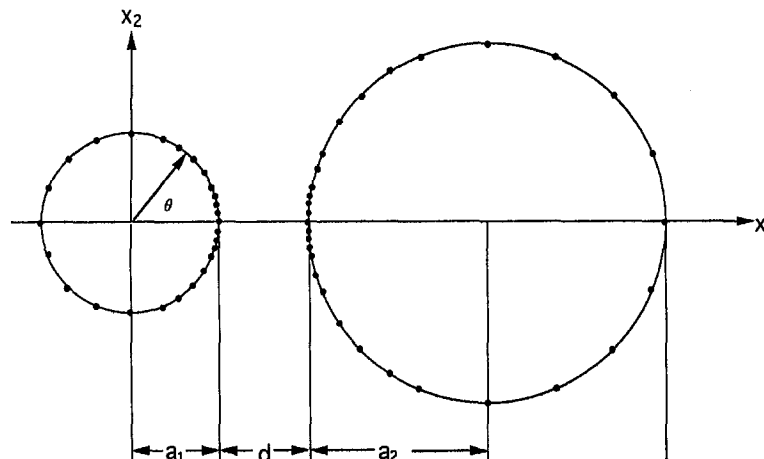


Fig. 2 Schematic representation of nodes for two circular holes

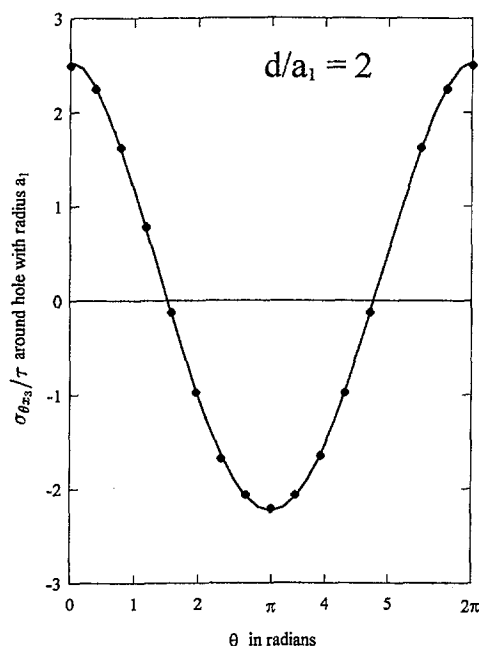


Fig. 3 $\sigma_{\theta z_3}/\tau$ around hole with radius a_1 versus θ for $d/a_1 = 2$

of an analytic function $\omega(z) = \phi + i\psi$ of a complex variable $z = x_1 + ix_2$. It is well known that a function harmonic in a multiply connected region does not necessarily possess a single-valued conjugate function; however, it is shown in Henrici (1986) that Eqs. (8) are the necessary and sufficient conditions that such a function exists.

For $\omega(z)$ analytic in Ω including the point at infinity and continuous in $\Omega + L$, the Cauchy integral formula states that

$$\omega(z) - \omega(\infty) = \frac{1}{2\pi i} \int_L \frac{\omega(\zeta)}{\zeta - z} d\zeta, \quad z \in \Omega. \quad (9)$$

Here $L = L_1 + L_2 + \dots + L_n$, with the positive direction of L chosen in such way that Ω lies to the left, and $\omega(\infty) = 0$ for the problem under consideration.

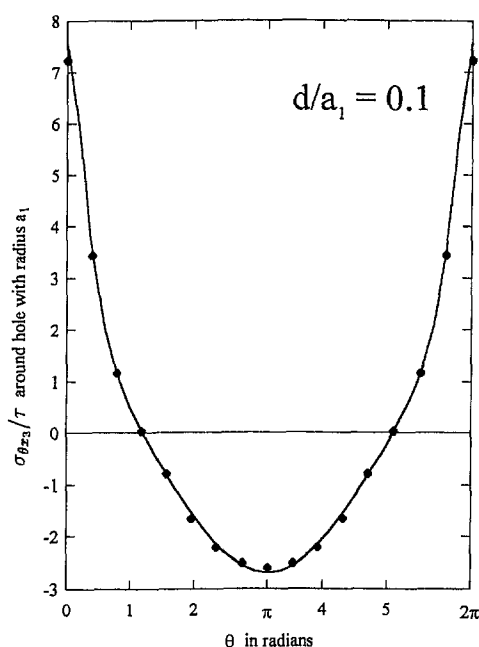


Fig. 4 $\sigma_{\theta z_3}/\tau$ around hole with radius a_1 versus θ for $d/a_1 = 0.1$

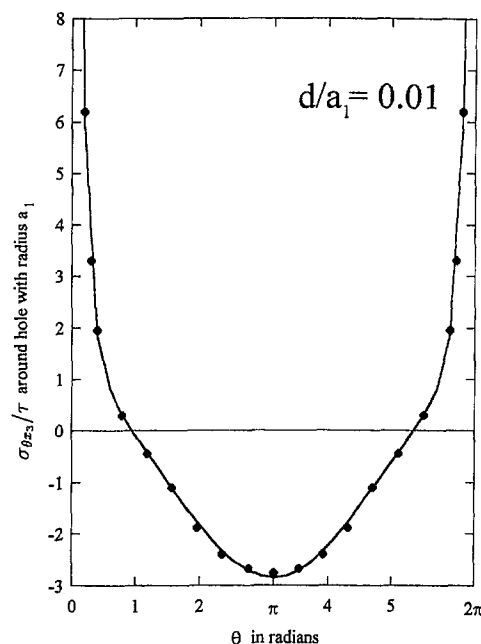


Fig. 5 $\sigma_{\theta z_3}/\tau$ around hole with radius a_1 versus θ for $d/a_1 = 0.01$

The boundary values of ϕ and ψ , and hence the stresses, around the holes can thus be found by using the CVBEM. Each contour L_k is subdivided into m_k elements $\Gamma_{k,j}$, and the analytic function $\omega(z)$ is approximated by the interpolating function $\alpha_{k,j}(z)$ on each element $\Gamma_{k,j}$. Equation (9) then gives the approximate function $\hat{\omega}(z)$ of $\omega(z)$ as follows:

$$\hat{\omega}(z) = \frac{1}{2\pi i} \sum_{k=1}^n \sum_{j=1}^{m_k} \int_{\Gamma_{k,j}} \frac{\alpha_{k,j}(\zeta)}{\zeta - z} d\zeta, \quad z \in \Omega. \quad (10)$$

Let $z \in \Omega$ approach a nodal point $z_{k,j}$ of all contours L_k . Equating the real and imaginary parts of both sides of (10) yields

$$\{\hat{\Phi}\} = \mathbf{C}_R\{\hat{\Phi}\} + \mathbf{D}_R\{\hat{\Psi}\}, \quad (11)$$

$$\{\hat{\Psi}\} = \mathbf{C}_I\{\hat{\Phi}\} + \mathbf{D}_I\{\hat{\Psi}\}. \quad (12)$$

Here \mathbf{C}_R , \mathbf{C}_I , \mathbf{D}_R , and \mathbf{D}_I are matrices whose values depend only on the configuration of the contours; $\{\hat{\Phi}\}$, $\{\hat{\Psi}\}$ and $\{\tilde{\Phi}\}$, $\{\tilde{\Psi}\}$ are vectors whose elements are, respectively, the approximate nodal values $\hat{\phi}_{k,j}$, $\hat{\psi}_{k,j}$ and the specified nodal values $\tilde{\phi}_{k,j}$, $\tilde{\psi}_{k,j}$ of ϕ and ψ .

In most engineering problems, either $\{\tilde{\Phi}\}$ or $\{\tilde{\Psi}\}$, but not both, is given on the contours. If, for example, $\{\tilde{\Psi}\}$ is given on the contours, there exist two methods for estimating $\{\hat{\Phi}\}$: collocate implicitly the unknown nodal values by setting $\{\hat{\Phi}\} = \{\tilde{\Phi}\}$ in (11) and solve for $\{\hat{\Phi}\}$; collocate explicitly the known nodal values by setting $\{\hat{\Psi}\} = \{\tilde{\Psi}\}$ in (12) and solve for $\{\hat{\Phi}\}$. Hromadka and Lai (1986) show that the implicit collocation can give more accurate results and is preferred.

3 Numerical Procedure and Examples

The contours L_k is subdivided into m_k elements, and the matrices \mathbf{C}_R , \mathbf{C}_I , \mathbf{D}_R , and \mathbf{D}_I are generated. For the problem (7), ϕ and ψ are related on a contour L_k , and, consequently, either one can be chosen as unknown. At a nodal point $z_{k,j}$ with outward unit normal $\mathbf{n} = (n_1, n_2)$, for $n_1 \neq 0$,

$$\tilde{\psi}_{k,j} = -\left(\frac{\tau}{\mu} + n_2 \tilde{\phi}_{k,j}\right) / n_1, \quad (13)$$

and the j th equation in (11) is chosen for implicit collocation with $\tilde{\phi}_{k,j}$ as unknown; while, for $n_1 = 0$,

$$\tilde{\phi}_{k,p} = -\frac{\tau}{\mu n_2}, \quad (14)$$

which is known, and the p th equation in (12) is selected for implicit collocation with $\tilde{\psi}_{k,p}$ the unknown. In this way, a set of algebraic equations is composed from (11) and (12) with the form

$$\{\hat{\mathbf{X}}\} = \mathbf{A}^T \{\tilde{\mathbf{X}}\} + \mathbf{B}^T \{\tilde{\mathbf{Y}}\}. \quad (15)$$

Here $\{\hat{\mathbf{X}}\}$ consists of unknown values $\hat{\phi}_{k,j}$ or $\hat{\psi}_{k,j}$; $\{\tilde{\mathbf{X}}\}$ with elements $\tilde{\phi}_{k,j}$ or $\tilde{\psi}_{k,j}$; and $\{\tilde{\mathbf{Y}}\}$ contains all the known values. Letting $\{\hat{\mathbf{X}}\} = \{\tilde{\mathbf{X}}\} = \{\mathbf{X}\}$ in (15), a set of algebraic equations

$$\mathbf{A}\{\mathbf{X}\} = \{\mathbf{b}\} \quad (16)$$

is obtained.

The Eq. (16) is solved, subjected to the conditions of single-valuedness of displacement (8):

$$\mathbf{C}^T \{\mathbf{X}\} = \{\mathbf{d}\} \quad (17)$$

where \mathbf{C} has the form

$$\mathbf{C} = \begin{bmatrix} \mathbf{c}_1 & \mathbf{0}_1 & \cdots & \mathbf{0}_1 \\ \mathbf{0}_2 & \mathbf{c}_2 & \cdots & \mathbf{0}_2 \\ \vdots & \vdots & \cdots & \vdots \\ \mathbf{0}_n & \mathbf{0}_n & \cdots & \mathbf{c}_n \end{bmatrix}, \quad (18)$$

with \mathbf{c}_k a vector of order m_k ; $\mathbf{0}_k$ a null vector of order m_k . Imposing condition (17) on Eq. (16) using the Lagrange multiplier $\boldsymbol{\lambda} = \{\lambda_1, \lambda_2, \dots, \lambda_n\}^T$ yields

$$\begin{bmatrix} \mathbf{A} & \mathbf{C} \\ \mathbf{C}^T & \mathbf{0} \end{bmatrix} \begin{bmatrix} \{\mathbf{X}\} \\ \{\boldsymbol{\lambda}\} \end{bmatrix} = \begin{bmatrix} \{\mathbf{b}\} \\ \{\mathbf{d}\} \end{bmatrix}. \quad (19)$$

Here $\mathbf{0}$ is a null matrix of order $n \times n$. Equation (19) is a set of algebraic equations which can be solved using any standard numerical package.

Although the numerical procedure presented can be applied to the solution of a stress field around any number of holes of different configuration, the problem of two circular holes whose centers lie on the x_1 -axis considered by Honein et al. (1992) is solved as examples.

The contours of each hole are subdivided into 36 elements with elements much finer near the point $(a_1, 0)$ and the direct opposite point $(a_1 + d, 0)$ which are known to be the singular points, Fig. 2. Numerical results for $\sigma_{\theta\theta}/\tau$ around the hole with radius a_1 for $a_2/a_1 = 2$ are superimposed on the results of Honein et al. (1992) using the solid dots: $d/a_1 = 2$ in Fig. 3; $d/a_1 = 0.1$ in Fig. 4; $d/a_1 = 0.01$ in Fig. 5. The numerical results compare well with the analytical results, except at the point $(a_1, 0)$ for cases $d/a_1 = 0.1$ and $d/a_1 = 0.01$, where the results obtained have an error of about 4.5 percent and 11 percent, respectively. The larger error at the point $(a_1, 0)$ as $d/a_1 \rightarrow 0$ is to be expected, since it is harder and harder to attain numerical accuracy as the two holes approach each other.

References

- Budiansky, B., and Carrier, G. F., 1984, "High Shear Stresses in Stiff-Fiber Composites," *ASME JOURNAL OF APPLIED MECHANICS*, Vol. 51, pp. 733–735.
- Choi, J. H., and Kwak, B. M., 1989, "A Boundary Integral Equation Formulation in Derivative Unknowns for Two-Dimensional Potential Problems," *ASME JOURNAL OF APPLIED MECHANICS*, Vol. 56, pp. 617–623.
- Gore, J. G., and Wilson, H. B., Jr., 1967, "Transverse Shear Loading in An Elastic Matrix Containing Two Circular Cylindrical Inclusions," *ASME JOURNAL OF APPLIED MECHANICS*, Vol. 34, pp. 511–513.
- Henrici, P., 1986, *Applied and Computational Complex Analysis*, Vol. III, John Wiley and Sons, New York.
- Honein, E., Honein, T., and Herrmann, G., 1992, "On Two Circular Inclusions in Harmonic Problems," *Quarterly of Applied Mathematics*, Vol. L, pp. 479–499.
- Hromadka, T. V., and Lai, C., 1986, *The Complex Variable Boundary Element Method in Engineering Analysis*, Springer-Verlag, New York.

- Hromadka, T. V., and Yen, C. C., 1988, "Extension of the CVBEM to Higher-Order Trial Functions," *Applied Mathematical Modelling*, Vol. 12, pp. 619–626.
- Steif, P. S., 1989, "Shear Stress Concentration Between Holes," *ASME JOURNAL OF APPLIED MECHANICS*, Vol. 56, pp. 719–712.

On Pala's Method for Plastic Bending With Torsion

P. Oberweis⁸ and M. Zyczkowski⁹

Handelman (1944) and Hill (1948) considered the general case of longitudinal homogeneity of the perfectly plastic stress state in a prismatic bar. It corresponds to simultaneous biaxial bending, tension, and torsion. In the above papers the Prandtl stress function was employed, whereas the relevant equation in terms of displacements was derived by Piechnik (1961) and Piechnik and Życzkowski (1961). Advantages of numerical integration of Piechnik's equation were pointed out by Miller and Malvern (1967).

In the simpler case of uniaxial bending with torsion of a prismatic bar with bisymmetric cross section, the Handelman-Hill equation may be reduced to

$$\begin{aligned} \frac{\partial}{\partial x} \left\{ |y| \frac{\partial u}{\partial x} \left[1 - \left(\frac{\partial u}{\partial x} \right)^2 - \left(\frac{\partial u}{\partial y} \right)^2 \right]^{-1/2} \right\} \\ + \frac{\partial}{\partial y} \left\{ |y| \frac{\partial u}{\partial y} \left[1 - \left(\frac{\partial u}{\partial x} \right)^2 - \left(\frac{\partial u}{\partial y} \right)^2 \right]^{-1/2} \right\} + A = 0, \end{aligned} \quad (1)$$

where $A = (2/\sqrt{3})(\dot{\theta}/|\dot{\varrho}|)$; $\dot{\theta}$ and $\dot{\varrho}$ denote rate of twist and rate of curvature, respectively; x and y are measured along the symmetry axes of the cross section; and z is measured along the axis of the bar. Further, u is the Prandtl stress function, defined by

$$\tau_{xz} = -k \frac{\partial u}{\partial y}, \quad \tau_{yz} = k \frac{\partial u}{\partial x}; \quad (2)$$

the normal stress is then given by

$$\sigma_z = \pm k \sqrt{3} \sqrt{1 - \left(\frac{\partial u}{\partial x} \right)^2 - \left(\frac{\partial u}{\partial y} \right)^2}, \quad (3)$$

obtained from the Huber-Mises-Hencky yield condition, and k denotes the yield-point stress in simple shear. Equation (1) holds also for monosymmetric sections with x being the axis of symmetry bent in the plane yz ; otherwise shifting of the axis of discontinuity along y would take place, and this is not indicated in (1). Hill (1948) derived his equation for the general case of shifting and rotation of the neutral axis turning in the limit state into the discontinuity axis, but this case will not be considered here. Notation of the present paper follows that used

⁸ Assistant, 1. Institut für Mechanik, Technische Universität, 10623 Berlin, Germany.

⁹ Professor, Instytut Mechaniki i Podstaw Konstrukcji Maszyn Politechniki Krakowskiej, 31-155 Kraków, Poland.

Contributed by the Applied Mechanics Division of THE AMERICAN SOCIETY OF MECHANICAL ENGINEERS for publication in the ASME JOURNAL OF APPLIED MECHANICS. Manuscript received by the ASME Applied Mechanics Division, Nov. 28, 1995; final revision, Sept. 17, 1996. Associate Technical Editor: W. J. Drugan.

$$\tilde{\phi}_{k,p} = -\frac{\tau}{\mu n_2}, \quad (14)$$

which is known, and the p th equation in (12) is selected for implicit collocation with $\tilde{\psi}_{k,p}$ the unknown. In this way, a set of algebraic equations is composed from (11) and (12) with the form

$$\{\hat{\mathbf{X}}\} = \mathbf{A}''\{\tilde{\mathbf{X}}\} + \mathbf{B}''\{\tilde{\mathbf{Y}}\}. \quad (15)$$

Here $\{\hat{\mathbf{X}}\}$ consists of unknown values $\hat{\phi}_{k,j}$ or $\hat{\psi}_{k,j}$; $\{\tilde{\mathbf{X}}\}$ with elements $\tilde{\phi}_{k,j}$ or $\tilde{\psi}_{k,j}$; and $\{\tilde{\mathbf{Y}}\}$ contains all the known values. Letting $\{\hat{\mathbf{X}}\} = \{\tilde{\mathbf{X}}\} = \{\mathbf{X}\}$ in (15), a set of algebraic equations

$$\mathbf{A}\{\mathbf{X}\} = \{\mathbf{b}\} \quad (16)$$

is obtained.

The Eq. (16) is solved, subjected to the conditions of single-valuedness of displacement (8):

$$\mathbf{C}^T\{\mathbf{X}\} = \{\mathbf{d}\} \quad (17)$$

where \mathbf{C} has the form

$$\mathbf{C} = \begin{bmatrix} \mathbf{c}_1 & \mathbf{0}_1 & \cdots & \mathbf{0}_1 \\ \mathbf{0}_2 & \mathbf{c}_2 & \cdots & \mathbf{0}_2 \\ \vdots & \vdots & \cdots & \vdots \\ \mathbf{0}_n & \mathbf{0}_n & \cdots & \mathbf{c}_n \end{bmatrix}, \quad (18)$$

with \mathbf{c}_k a vector of order m_k ; $\mathbf{0}_k$ a null vector of order m_k . Imposing condition (17) on Eq. (16) using the Lagrange multiplier $\boldsymbol{\lambda} = \{\lambda_1, \lambda_2, \dots, \lambda_n\}^T$ yields

$$\begin{bmatrix} \mathbf{A} & \mathbf{C} \\ \mathbf{C}^T & \mathbf{0} \end{bmatrix} \begin{bmatrix} \mathbf{X} \\ \boldsymbol{\lambda} \end{bmatrix} = \begin{bmatrix} \mathbf{b} \\ \mathbf{d} \end{bmatrix}. \quad (19)$$

Here $\mathbf{0}$ is a null matrix of order $n \times n$. Equation (19) is a set of algebraic equations which can be solved using any standard numerical package.

Although the numerical procedure presented can be applied to the solution of a stress field around any number of holes of different configuration, the problem of two circular holes whose centers lie on the x_1 -axis considered by Honein et al. (1992) is solved as examples.

The contours of each hole are subdivided into 36 elements with elements much finer near the point $(a_1, 0)$ and the direct opposite point $(a_1 + d, 0)$ which are known to be the singular points, Fig. 2. Numerical results for $\sigma_{\theta\theta_3}/\tau$ around the hole with radius a_1 for $a_2/a_1 = 2$ are superimposed on the results of Honein et al. (1992) using the solid dots: $d/a_1 = 2$ in Fig. 3; $d/a_1 = 0.1$ in Fig. 4; $d/a_1 = 0.01$ in Fig. 5. The numerical results compare well with the analytical results, except at the point $(a_1, 0)$ for cases $d/a_1 = 0.1$ and $d/a_1 = 0.01$, where the results obtained have an error of about 4.5 percent and 11 percent, respectively. The larger error at the point $(a_1, 0)$ as $d/a_1 \rightarrow 0$ is to be expected, since it is harder and harder to attain numerical accuracy as the two holes approach each other.

References

- Budiansky, B., and Carrier, G. F., 1984, "High Shear Stresses in Stiff-Fiber Composites," *ASME JOURNAL OF APPLIED MECHANICS*, Vol. 51, pp. 733–735.
- Choi, J. H., and Kwak, B. M., 1989, "A Boundary Integral Equation Formulation in Derivative Unknowns for Two-Dimensional Potential Problems," *ASME JOURNAL OF APPLIED MECHANICS*, Vol. 56, pp. 617–623.
- Gore, J. G., and Wilson, H. B., Jr., 1967, "Transverse Shear Loading in An Elastic Matrix Containing Two Circular Cylindrical Inclusions," *ASME JOURNAL OF APPLIED MECHANICS*, Vol. 34, pp. 511–513.
- Henrici, P., 1986, *Applied and Computational Complex Analysis*, Vol. III, John Wiley and Sons, New York.
- Honein, E., Honein, T., and Herrmann, G., 1992, "On Two Circular Inclusions in Harmonic Problems," *Quarterly of Applied Mathematics*, Vol. L, pp. 479–499.
- Hromadka, T. V., and Lai, C., 1986, *The Complex Variable Boundary Element Method in Engineering Analysis*, Springer-Verlag, New York.

- Hromadka, T. V., and Yen, C. C., 1988, "Extension of the CVBEM to Higher-Order Trial Functions," *Applied Mathematical Modelling*, Vol. 12, pp. 619–626.
- Steif, P. S., 1989, "Shear Stress Concentration Between Holes," *ASME JOURNAL OF APPLIED MECHANICS*, Vol. 56, pp. 719–712.

On Pala's Method for Plastic Bending With Torsion

P. Oberweis⁸ and M. Zyczkowski⁹

Handelman (1944) and Hill (1948) considered the general case of longitudinal homogeneity of the perfectly plastic stress state in a prismatic bar. It corresponds to simultaneous biaxial bending, tension, and torsion. In the above papers the Prandtl stress function was employed, whereas the relevant equation in terms of displacements was derived by Piechnik (1961) and Piechnik and Życzkowski (1961). Advantages of numerical integration of Piechnik's equation were pointed out by Miller and Malvern (1967).

In the simpler case of uniaxial bending with torsion of a prismatic bar with bisymmetric cross section, the Handelman-Hill equation may be reduced to

$$\begin{aligned} \frac{\partial}{\partial x} \left\{ |y| \frac{\partial u}{\partial x} \left[1 - \left(\frac{\partial u}{\partial x} \right)^2 - \left(\frac{\partial u}{\partial y} \right)^2 \right]^{-1/2} \right\} \\ + \frac{\partial}{\partial y} \left\{ |y| \frac{\partial u}{\partial y} \left[1 - \left(\frac{\partial u}{\partial x} \right)^2 - \left(\frac{\partial u}{\partial y} \right)^2 \right]^{-1/2} \right\} + A = 0, \end{aligned} \quad (1)$$

where $A = (2/\sqrt{3})(\dot{\theta}/|\dot{\varrho}|)$; $\dot{\theta}$ and $\dot{\varrho}$ denote rate of twist and rate of curvature, respectively; x and y are measured along the symmetry axes of the cross section; and z is measured along the axis of the bar. Further, u is the Prandtl stress function, defined by

$$\tau_{xz} = -k \frac{\partial u}{\partial y}, \quad \tau_{yz} = k \frac{\partial u}{\partial x}; \quad (2)$$

the normal stress is then given by

$$\sigma_z = \pm k \sqrt{3} \sqrt{1 - \left(\frac{\partial u}{\partial x} \right)^2 - \left(\frac{\partial u}{\partial y} \right)^2}, \quad (3)$$

obtained from the Huber-Mises-Hencky yield condition, and k denotes the yield-point stress in simple shear. Equation (1) holds also for monosymmetric sections with x being the axis of symmetry bent in the plane yz ; otherwise shifting of the axis of discontinuity along y would take place, and this is not indicated in (1). Hill (1948) derived his equation for the general case of shifting and rotation of the neutral axis turning in the limit state into the discontinuity axis, but this case will not be considered here. Notation of the present paper follows that used

⁸ Assistant, 1. Institut für Mechanik, Technische Universität, 10623 Berlin, Germany.

⁹ Professor, Instytut Mechaniki i Podstaw Konstrukcji Maszyn Politechniki Krakowskiej, 31-155 Kraków, Poland.

Contributed by the Applied Mechanics Division of THE AMERICAN SOCIETY OF MECHANICAL ENGINEERS for publication in the ASME JOURNAL OF APPLIED MECHANICS. Manuscript received by the ASME Applied Mechanics Division, Nov. 28, 1995; final revision, Sept. 17, 1996. Associate Technical Editor: W. J. Drugan.

by Pala (1994) with some small changes, namely with the introduction of absolute values in (1) and in the definition of A , which is necessary for the correct description of the problem.

Equation (1) is an elliptic nonlinear partial differential equation with the boundary condition $u = 0$ along the contour of a simply connected cross section. Many numerical solutions of this equation were reviewed by Życzkowski (1981) and Pala (1994), but it is difficult to find an analytical solution. Probably the only one known as yet is

$$u = C|h - y|, \quad \tau_{xz} = -C \operatorname{sign} y, \quad \sigma_z = \pm k\sqrt{3}\sqrt{1 - C^2}. \quad (4)$$

Indeed, substituting into (1) we obtain

$$-C \operatorname{sign} y(1 - C^2)^{-1/2} + A = 0, \quad (5)$$

hence

$$C = \pm \frac{A}{\sqrt{1 + A^2}} = \pm \frac{2\dot{\theta}}{\sqrt{3\dot{\theta}^2 + 4\dot{\theta}^2}}, \quad (6)$$

and the boundary condition is satisfied for a strip (very long rectangle) $-h \leq y \leq h$ bent in the plane at its smaller stiffness. The above solution was derived earlier by some other way: by Rzhantsyn (1949) directly from basic equations of plasticity, and by Życzkowski (1981) from the general displacement equation.

In order to find other analytical solutions, Pala (1994) proposed to introduce an auxiliary function ϕ defined by the following transformation:

$$\begin{aligned} \frac{\partial \phi}{\partial x} &= y u_x (1 - u_x^2 - u_y^2)^{-1/2}, \\ \frac{\partial \phi}{\partial y} &= y u_y (1 - u_x^2 - u_y^2)^{-1/2}, \end{aligned} \quad (7)$$

(with a shorter notation for partial derivatives), obtaining for ϕ the equation

$$\frac{\partial^2 \phi}{\partial x^2} + \frac{\partial^2 \phi}{\partial y^2} + A = 0, \quad (8)$$

for which many analytical solutions are known.

Pala's idea is unquestionably too optimistic. One cannot expect a complicated nonlinear partial differential equation to be replaced exactly and in a general manner by a linear one. The author defines ϕ by its partial derivatives (7) without checking the Schwarz condition. Since, in general, formulae (7) will not satisfy this condition, namely

$$\partial \phi_x / \partial y \neq \partial \phi_y / \partial x, \quad (9)$$

the function ϕ may not exist at all: for various integration paths one would obtain various values of ϕ at the same point x, y . And, vice versa, if a function ϕ is constructed, then the relevant stress function u should be found from two differential formulae (6) in Pala's paper; generally, they also will not satisfy the Schwarz condition and the function u will not exist. Hence, in general, the method proposed is not correct, as pointed out by Shield (1995).

However, there may exist some exceptional cases in which the Pala method can successfully be used. Consider the example of a bar with elliptical cross section mentioned in his paper. The function ϕ for such a section is given by the author but with a mistake. Having corrected this mistake to satisfy the boundary condition we obtain

$$\phi = \frac{A}{4} \left[\frac{a^2 - b^2}{a^2 + b^2} (x^2 - y^2) - (x^2 + y^2) \right], \quad (10)$$

(numerator and denominator of the first term are interchanged). Formulae (7) give here

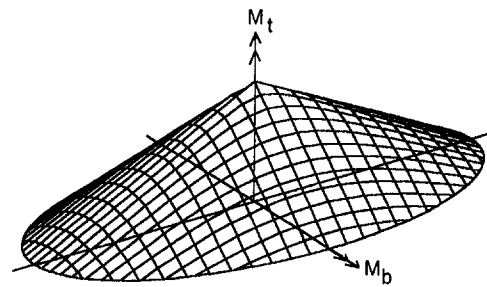


Fig. 1 Stress function for the particular case of an elliptical section

$$\begin{aligned} u_x &= \frac{-Ab^2x}{\sqrt{A^2b^4x^2 + [A^2a^4 + (a^2 + b^2)^2]y^2}}, \\ u_y &= \frac{-Aa^2y}{\sqrt{A^2b^4x^2 + [A^2a^4 + (a^2 + b^2)^2]y^2}}, \end{aligned} \quad (11)$$

and the Schwarz condition leads to the equation

$$A^2a^4 + (a^2 + b^2)^2 = A^2a^2b^2. \quad (12)$$

Hence, if the semi-axis b is larger than the semi-axis a (ellipse subject to bending in the plane of larger moment of inertia), we obtain

$$A = \pm \frac{a^2 + b^2}{a\sqrt{b^2 - a^2}}. \quad (13)$$

In this very particular case Pala's solution is correct. Integrating either of Eqs. (7) we obtain the same result for the stress function, satisfying the boundary condition $u = 0$ along the contour,

$$u = a \left(1 - \sqrt{\frac{x^2}{a^2} + \frac{y^2}{b^2}} \right). \quad (14)$$

Indeed, the Handelman-Hill equation is then satisfied. In the case under consideration, ((13) and (14)), we have

$$\begin{aligned} &\left[1 - \left(\frac{\partial u}{\partial x} \right)^2 - \left(\frac{\partial u}{\partial y} \right)^2 \right]^{1/2} \\ &= (a^2 + b^2) |y| / \left(Aab^2 \sqrt{\frac{x^2}{a^2} + \frac{y^2}{b^2}} \right), \end{aligned} \quad (15)$$

and (7) is satisfied both for positive and negative y . Pure bending of this elliptic section corresponds to a discontinuity line along $y = 0$, whereas pure torsion, along $x = 0$ (both these special, but well-known cases are outside the scope of the present solution). In the combined case under consideration these discontinuity lines have shrunk just to one point $x = y = 0$ (Fig. 1). Of course, this solution does not allow to construct a plastic interaction curve, since for each ellipse we have just one point of such a curve, given by (13), and the relevant expressions for bending moment and torque.

In general, Pala's method is not correct. For example, as mentioned above, it does not correctly describe pure torsion of an elliptical bar, considered by Życzkowski (1964), since (13) is not satisfied for this case. Also, other classical solutions of the problem of elastic torsion (isosceles triangle, circle with circular incision) do not satisfy the Schwarz conditions for the auxiliary function ϕ , hence the solution (14) is probably the only one to be obtained by Pala's method.

In other cases Pala's method may be considered as approximate, but it would be difficult to estimate the approximation errors: for a given shape of the cross section the solution of Eq. (8) is unique, but the construction of the relevant Prandtl's

stress function u depends on the path of integration of the differential formulae resulting from (7). Both bending and twisting moments depend on u and hence the errors depend on the quite arbitrary choice of integration path.

References

- Handelman, G. H., 1944, "A Variational Principle for a State of Combined Plastic Stress," *Quarterly of Applied Mathematics*, Vol. 1, pp. 351–353.
- Hill, R., 1948, "A Variational Principle of Maximum Plastic Work in Classical Plasticity," *Quarterly Journal of Mechanics and Applied Mathematics*, Vol. 1, pp. 18–28.
- Miller, P. M., and Malvern, L. E., 1967, "Numerical Solution of Piechnik's Equation for the Combined Bending and Torsion of Rigid-Plastic Bars," *Proceedings 10th Midwestern Conference of Solid Mechanics*, Colorado State Univ., pp. 571–580.
- Pala, Y., 1994, "Analytical Solution of Hill's Equation," *ASME JOURNAL OF APPLIED MECHANICS*, Vol. 61, pp. 1000–1001.
- Piechnik, S., 1961, "The Influence of Bending on the Limit State of a Circular Bar Subject to Torsion," *Archiwum Mechaniki Stosowanej*, Vol. 13, pp. 77–106.
- Piechnik, S., and Życzkowski, M., 1961, "On the Plastic Interaction Curve for Bending and Torsion of a Circular Bar," *Archiwum Mechaniki Stosowanej*, Vol. 13, pp. 669–692.
- Rzhanitsyn, A. R., 1949, "Structural Analysis With Plastic Properties of Materials Taken Into Account," Stroyizdat, Moskva, in Russian.
- Shield, R. T., 1995, discussion on Pala's paper, *ASME JOURNAL OF APPLIED MECHANICS*, Vol. 62, p. 553.
- Życzkowski, M., 1964, "Some Particular Solutions of the Problem of Plastic Torsion," *Bulletin de l'Academie Polonaise, Serie Sciences Techniques*, Vol. 12, pp. 79–87.
- Życzkowski, M., 1981, *Combined Loadings in the Theory of Plasticity*, PWN—Nijhoff, Warszawa, Aalphen aan den Rijn.

Elastic Tensile Stresses Beneath Perfectly Plastic Indentation Fields

D. M. Stump^{10,12} and V. G. Hart^{11,12}

1 Introduction

The stress field beneath an indenter is very complex. Far from the indenter, the field is elastic and compressive by equilibrium requirements. The field is also compressive directly under the indenter and, if the load is large enough, the material can deform plastically. If the material under the indenter is perfectly plastic, then an elastic transition region surrounds this plastic zone. The stresses within this transition zone are complicated and may even be tensile rather than compressive. This note considers the elastic stresses in the transition region surrounding a perfectly plastic indenter field.

Sneddon (1951) has studied the elastic stresses occurring under a strip length $2a$ of uniform pressure p_0 applied to a half-plane. A compressive stress parallel to the free surface occurs everywhere in the half-space below the strip. This note determines the stresses in the elastic transition regions beneath truncated-wedge plastic indentation fields (Hill, 1950), and there is an interesting contrast with the purely elastic case.

¹⁰ Department of Civil Engineering.

¹¹ Department of Mathematics.

¹² The University of Queensland, St. Lucia QLD 4072, Australia.

Contributed by the Applied Mechanics Division of THE AMERICAN SOCIETY OF MECHANICAL ENGINEERS for publication in the ASME JOURNAL OF APPLIED MECHANICS. Manuscript received by the ASME Applied Mechanics Division, Jan. 4, 1996; final revision, June 11, 1996. Associate Technical Editor: R. Becker.

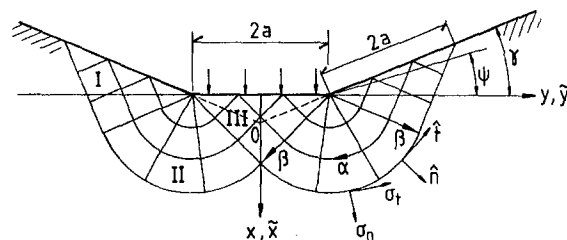


Fig. 1 Schematic drawing of the slip-line field for the truncated wedge

2 The Plastic Field

The plastic field geometry of the truncated wedge (Hill, 1950, p. 255) is shown in Fig. 1. The Prandtl field is folded through an additional angle γ so that the total opening half-angle of the wedge is $\theta_0 = \pi/2 + \gamma$. Let $2a$ be the length of the uniform strip of pressure with the resultant downward force P . The yield strength in shear is k . The field consists of constant stress regions I and III combined with centered fans II, where the polar angle ψ is measured from the corner of the strip, as shown in Fig. 1. The mean normal stress in the three regions is given by

$$\left. \begin{aligned} p &= -k \text{ (Region I),} \\ p &= -k \left(1 - \frac{\pi}{2} + 2\gamma - 2\psi \right) \text{ (Region II),} \\ p &= -k(1 + \pi + 2\gamma) \text{ (Region III).} \end{aligned} \right\} \quad (1)$$

The load on the indenter (Hill, 1950, p. 255) is

$$P = 2ak(2 + \pi + 2\gamma). \quad (2)$$

For the purpose of this approximate analysis, the boundary to the plastic region is shown in Fig. 1, even though, as Hill (1950) points out, this is not necessarily the physical boundary which would develop under a monotonically increasing indenter load. The normal σ_{nn} and shear σ_{nt} tractions exerted by the plastic region on the elastic region exterior to Region I are

$$\sigma_{nn} = \sigma_{nt} = -k. \quad (3)$$

Region II exerts the tractions

$$\left. \begin{aligned} \sigma_{nn} &= -k \left(1 - \frac{\pi}{2} + 2\gamma - 2\psi \right), \\ \sigma_{nt} &= -k. \end{aligned} \right\} \quad (4)$$

3 The Elastic Region

The forces in the truncated wedge can be approximated by using the eigenvalue series as described by Buchwald (1965) in terms of complex stress potentials $\Omega(z)$ and $\omega(z)$. The complex variable $z = \bar{x}/a + i\bar{y}/a$ is measured from the "vertex" center O on Fig. 1. The series solutions are

$$\Omega(z) = A_0 \log(z) + \sum_{n=1}^N c_n z^{-\beta_n} + \sum_{n=N+1}^{\infty} [c_n z^{-\beta_n} + \bar{c}_n z^{-\bar{\beta}_n}] \quad (5)$$

and

$$\omega(z) = -A_0 \log(z) + \sum_{n=1}^N c_n \hat{a}_n z^{-\beta_n} + \sum_{n=N+1}^{\infty} [c_n \hat{a}_n z^{-\beta_n} + \bar{c}_n \hat{a}_n z^{-\bar{\beta}_n}]. \quad (6)$$

Here $A_0 = -P/[4\theta_0 + 2\sin(2\theta_0)]$ is a constant determined by the resultant load P (Timoshenko and Goodier, 1970). The first sum in each expression is carried out over the N positive real eigenvalues ($\beta_1, \beta_2, \dots, \beta_N$) that are solutions to the equation

stress function u depends on the path of integration of the differential formulae resulting from (7). Both bending and twisting moments depend on u and hence the errors depend on the quite arbitrary choice of integration path.

References

- Handelman, G. H., 1944, "A Variational Principle for a State of Combined Plastic Stress," *Quarterly of Applied Mathematics*, Vol. 1, pp. 351–353.
- Hill, R., 1948, "A Variational Principle of Maximum Plastic Work in Classical Plasticity," *Quarterly Journal of Mechanics and Applied Mathematics*, Vol. 1, pp. 18–28.
- Miller, P. M., and Malvern, L. E., 1967, "Numerical Solution of Piechnik's Equation for the Combined Bending and Torsion of Rigid-Plastic Bars," *Proceedings 10th Midwestern Conference of Solid Mechanics*, Colorado State Univ., pp. 571–580.
- Pala, Y., 1994, "Analytical Solution of Hill's Equation," *ASME JOURNAL OF APPLIED MECHANICS*, Vol. 61, pp. 1000–1001.
- Piechnik, S., 1961, "The Influence of Bending on the Limit State of a Circular Bar Subject to Torsion," *Archiwum Mechaniki Stosowanej*, Vol. 13, pp. 77–106.
- Piechnik, S., and Życzkowski, M., 1961, "On the Plastic Interaction Curve for Bending and Torsion of a Circular Bar," *Archiwum Mechaniki Stosowanej*, Vol. 13, pp. 669–692.
- Rzhanitsyn, A. R., 1949, "Structural Analysis With Plastic Properties of Materials Taken Into Account," Stroyizdat, Moskva, in Russian.
- Shield, R. T., 1995, discussion on Pala's paper, *ASME JOURNAL OF APPLIED MECHANICS*, Vol. 62, p. 553.
- Życzkowski, M., 1964, "Some Particular Solutions of the Problem of Plastic Torsion," *Bulletin de l'Academie Polonaise, Serie Sciences Techniques*, Vol. 12, pp. 79–87.
- Życzkowski, M., 1981, *Combined Loadings in the Theory of Plasticity*, PWN—Nijhoff, Warszawa, Aalphen aan den Rijn.

Elastic Tensile Stresses Beneath Perfectly Plastic Indentation Fields

D. M. Stump^{10,12} and V. G. Hart^{11,12}

1 Introduction

The stress field beneath an indenter is very complex. Far from the indenter, the field is elastic and compressive by equilibrium requirements. The field is also compressive directly under the indenter and, if the load is large enough, the material can deform plastically. If the material under the indenter is perfectly plastic, then an elastic transition region surrounds this plastic zone. The stresses within this transition zone are complicated and may even be tensile rather than compressive. This note considers the elastic stresses in the transition region surrounding a perfectly plastic indenter field.

Sneddon (1951) has studied the elastic stresses occurring under a strip length $2a$ of uniform pressure p_0 applied to a half-plane. A compressive stress parallel to the free surface occurs everywhere in the half-space below the strip. This note determines the stresses in the elastic transition regions beneath truncated-wedge plastic indentation fields (Hill, 1950), and there is an interesting contrast with the purely elastic case.

¹⁰ Department of Civil Engineering.

¹¹ Department of Mathematics.

¹² The University of Queensland, St. Lucia QLD 4072, Australia.

Contributed by the Applied Mechanics Division of THE AMERICAN SOCIETY OF MECHANICAL ENGINEERS for publication in the ASME JOURNAL OF APPLIED MECHANICS. Manuscript received by the ASME Applied Mechanics Division, Jan. 4, 1996; final revision, June 11, 1996. Associate Technical Editor: R. Becker.

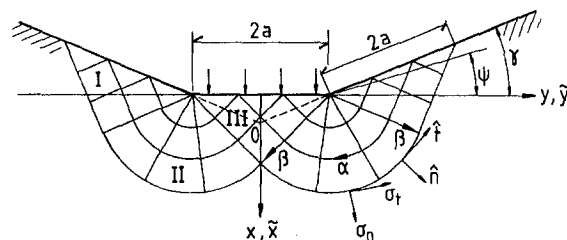


Fig. 1 Schematic drawing of the slip-line field for the truncated wedge

2 The Plastic Field

The plastic field geometry of the truncated wedge (Hill, 1950, p. 255) is shown in Fig. 1. The Prandtl field is folded through an additional angle γ so that the total opening half-angle of the wedge is $\theta_0 = \pi/2 + \gamma$. Let $2a$ be the length of the uniform strip of pressure with the resultant downward force P . The yield strength in shear is k . The field consists of constant stress regions I and III combined with centered fans II, where the polar angle ψ is measured from the corner of the strip, as shown in Fig. 1. The mean normal stress in the three regions is given by

$$\left. \begin{aligned} p &= -k \text{ (Region I),} \\ p &= -k \left(1 - \frac{\pi}{2} + 2\gamma - 2\psi \right) \text{ (Region II),} \\ p &= -k(1 + \pi + 2\gamma) \text{ (Region III).} \end{aligned} \right\} \quad (1)$$

The load on the indenter (Hill, 1950, p. 255) is

$$P = 2ak(2 + \pi + 2\gamma). \quad (2)$$

For the purpose of this approximate analysis, the boundary to the plastic region is shown in Fig. 1, even though, as Hill (1950) points out, this is not necessarily the physical boundary which would develop under a monotonically increasing indenter load. The normal σ_{nn} and shear σ_{nt} tractions exerted by the plastic region on the elastic region exterior to Region I are

$$\sigma_{nn} = \sigma_{nt} = -k. \quad (3)$$

Region II exerts the tractions

$$\left. \begin{aligned} \sigma_{nn} &= -k \left(1 - \frac{\pi}{2} + 2\gamma - 2\psi \right), \\ \sigma_{nt} &= -k. \end{aligned} \right\} \quad (4)$$

3 The Elastic Region

The forces in the truncated wedge can be approximated by using the eigenvalue series as described by Buchwald (1965) in terms of complex stress potentials $\Omega(z)$ and $\omega(z)$. The complex variable $z = \bar{x}/a + i\bar{y}/a$ is measured from the "vertex" center O on Fig. 1. The series solutions are

$$\Omega(z) = A_0 \log(z) + \sum_{n=1}^N c_n z^{-\beta_n} + \sum_{n=N+1}^{\infty} [c_n z^{-\beta_n} + \bar{c}_n z^{-\bar{\beta}_n}] \quad (5)$$

and

$$\begin{aligned} \omega(z) &= -A_0 \log(z) + \sum_{n=1}^N c_n \hat{a}_n z^{-\beta_n} \\ &\quad + \sum_{n=N+1}^{\infty} [c_n \hat{a}_n z^{-\beta_n} + \bar{c}_n \hat{a}_n z^{-\bar{\beta}_n}]. \end{aligned} \quad (6)$$

Here $A_0 = -P/[4\theta_0 + 2 \sin(2\theta_0)]$ is a constant determined by the resultant load P (Timoshenko and Goodier, 1970). The first sum in each expression is carried out over the N positive real eigenvalues ($\beta_1, \beta_2, \dots, \beta_N$) that are solutions to the equation

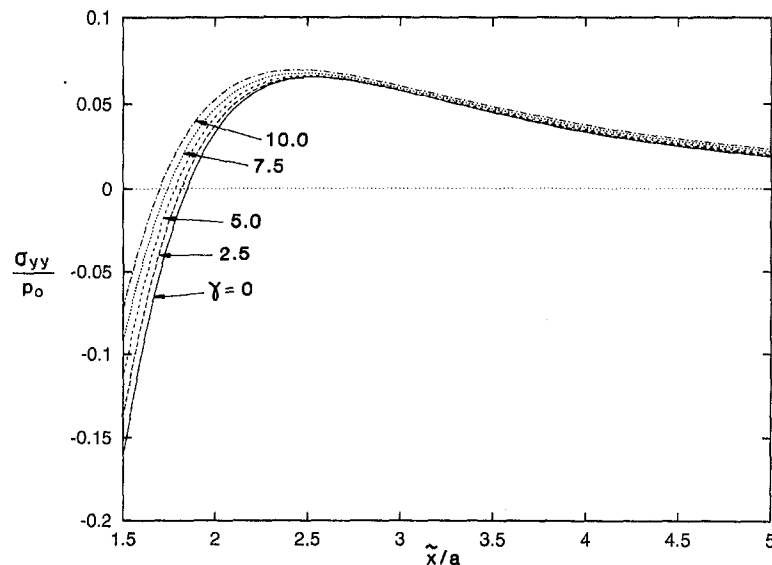


Fig. 2 The stress σ_{yy}/p_0 versus \tilde{x}/a for various wedge angles γ

$$\sin(2\beta_i\theta_0) + \beta_i \sin(2\theta_0) = 0, \quad (7)$$

and the remaining sum is carried out over the set of complex conjugate roots with positive real parts. The coefficients c_n , the first N of which are purely real, are obtained by boundary matching the tractions from the plastic region, and

$$\hat{a}_n = \beta_n \cos(2\theta_0) - \cos(2\theta_0\beta_n). \quad (8)$$

The complex potentials (5) and (6) are substituted into the formula

$$\sigma_{nn} - i\sigma_{nt} = \Omega'(z) + \bar{\Omega}'(\bar{z}) - e^{2i\theta} \{ \bar{z}\Omega''(z) + \omega'(z) \} \quad (9)$$

where $z = (\tilde{r}/a)e^{i\theta}$, and (\tilde{r}, θ) are polar coordinates measured from O . Equation (9) is separated into real and imaginary parts, and a least-squares fitting method is used to enforce these expressions at equally spaced points along the boundary. It was found that 15 coefficients and 40 fitting points were sufficient to obtain a solution. The series convergence decreases with increasing angle γ since the vertex approaches the plastic boundary and only small values of γ are considered. The complicated nature of the boundary along which tractions are prescribed yields a slowly convergent series which does not satisfy particularly well the prescribed tractions at some locations along the boundary. However, these inaccuracies are localized and die away quickly with distance from the boundary.

4 Results

Figure 2 shows a plot of the normalized tensile stress σ_{yy}/p_0 , where $p_0 = P/2a$ is the uniform pressure under the indenter, versus \tilde{x}/a along the line beneath the center of the indenter for several values of γ . This result differs from Sneddon's elastic result in a major way. Our stress in the elastic transition region starts out compressive and then reaches a maximum tensile value before decaying to zero with increasing \tilde{x}/a . This is in contrast to the elastic solution for $\gamma = 0$ which always gives a compressive σ_{yy} everywhere in the half-space beneath the indenter. Our peak tensile stress is $\sigma_{yy} \sim 0.068p_0$. The region of positive σ_{yy} is a lenticular shaped region with the center lying about $2.5a$ below the indenter. These results compare favorably with unpublished independent finite element calculations for a variety of different materials.

Acknowledgment

This work was supported by the Australian Research Council Small Grant Program.

References

- Buchwald, V. T., 1965, "Eigenfunctions of plane elastostatics III: The wedge," *J. Austral. Math. Soc.*, Vol. 5, pp. 241–257.
- Hill, R., 1950, *Plasticity*, Oxford University Press, Oxford, UK.
- Sneddon, I. N., 1951, *Fourier Transforms*, McGraw-Hill, New York, pp. 407–408.
- Timoshenko, S. P., and Goodier, J. N., 1970, *Theory of Elasticity*, 3rd ed., McGraw-Hill, New York, pp. 109–110.

A Kelvin Theorem and Partial Work of Impulsive Forces

A. P. Ivanov¹³

A rigid body under the action of several impulsive forces is considered. A Kelvin theorem provides a simple rule to calculate the total work done by all impulsive forces, but it is not necessarily applicable to the independent work done by each impulse. It is shown that there exist two cases when the partial work can be determined by the same Kelvin formula. Otherwise, the problem has no algebraic solution.

A problem in classical impact theory is to determine the work done by a given impulsive force \mathbf{F} which acts during a short interval $(t', t' + \tau)$ when the impulse is applied to a point A of the body. It was solved by Kelvin and Tait (1867, Art. 308):

$$W = \frac{1}{2} \mathbf{I}(\mathbf{U} + \mathbf{V}), \quad \mathbf{I} = \int_{t'}^{t'+\tau} \mathbf{F}(s) ds \quad (1)$$

where \mathbf{U}, \mathbf{V} denote initial and final velocities of point A .

It is important that the result does not depend on the specific form of function $\mathbf{F}(t)$. The original proof of formula (1) is

¹³ Professor, Moscow State Academy of Device and Information, Moscow, Stromynka 20, Russia.

Contributed by the Applied Mechanics Division of THE AMERICAN SOCIETY OF MECHANICAL ENGINEERS for publication in the ASME JOURNAL OF APPLIED MECHANICS. Manuscript received by the ASME Applied Mechanics Division, Nov. 28, 1995; final revision, May 15, 1996. Associate Technical Editor: S. W. Shaw.

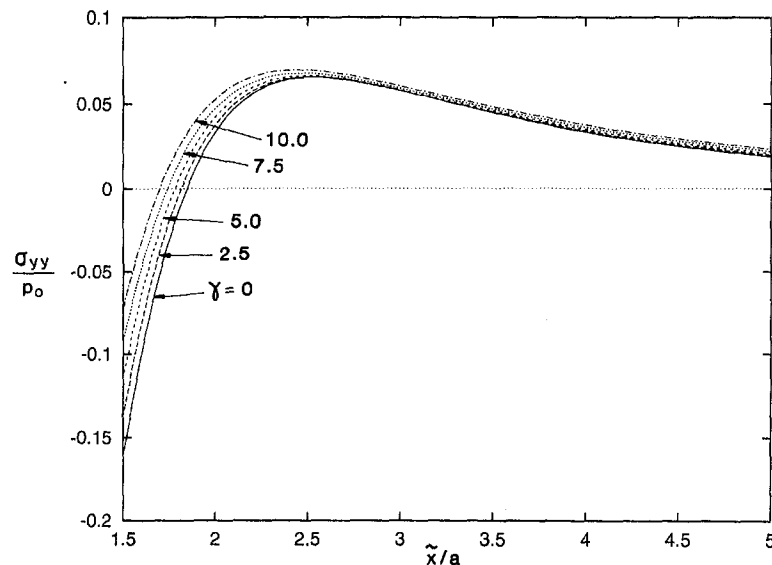


Fig. 2 The stress σ_{yy}/p_0 versus \tilde{x}/a for various wedge angles γ

$$\sin(2\beta_i\theta_0) + \beta_i \sin(2\theta_0) = 0, \quad (7)$$

and the remaining sum is carried out over the set of complex conjugate roots with positive real parts. The coefficients c_n , the first N of which are purely real, are obtained by boundary matching the tractions from the plastic region, and

$$\hat{a}_n = \beta_n \cos(2\theta_0) - \cos(2\theta_0\beta_n). \quad (8)$$

The complex potentials (5) and (6) are substituted into the formula

$$\sigma_{nn} - i\sigma_{nt} = \Omega'(z) + \bar{\Omega}'(\bar{z}) - e^{2i\theta}\{\bar{z}\Omega''(z) + \omega'(z)\} \quad (9)$$

where $z = (\tilde{r}/a)e^{i\theta}$, and (\tilde{r}, θ) are polar coordinates measured from O . Equation (9) is separated into real and imaginary parts, and a least-squares fitting method is used to enforce these expressions at equally spaced points along the boundary. It was found that 15 coefficients and 40 fitting points were sufficient to obtain a solution. The series convergence decreases with increasing angle γ since the vertex approaches the plastic boundary and only small values of γ are considered. The complicated nature of the boundary along which tractions are prescribed yields a slowly convergent series which does not satisfy particularly well the prescribed tractions at some locations along the boundary. However, these inaccuracies are localized and die away quickly with distance from the boundary.

4 Results

Figure 2 shows a plot of the normalized tensile stress σ_{yy}/p_0 , where $p_0 = P/2a$ is the uniform pressure under the indenter, versus \tilde{x}/a along the line beneath the center of the indenter for several values of γ . This result differs from Sneddon's elastic result in a major way. Our stress in the elastic transition region starts out compressive and then reaches a maximum tensile value before decaying to zero with increasing \tilde{x}/a . This is in contrast to the elastic solution for $\gamma = 0$ which always gives a compressive σ_{yy} everywhere in the half-space beneath the indenter. Our peak tensile stress is $\sigma_{yy} \sim 0.068p_0$. The region of positive σ_{yy} is a lenticular shaped region with the center lying about $2.5a$ below the indenter. These results compare favorably with unpublished independent finite element calculations for a variety of different materials.

Acknowledgment

This work was supported by the Australian Research Council Small Grant Program.

References

- Buchwald, V. T., 1965, "Eigenfunctions of plane elastostatics III: The wedge," *J. Austral. Math. Soc.*, Vol. 5, pp. 241–257.
- Hill, R., 1950, *Plasticity*, Oxford University Press, Oxford, UK.
- Sneddon, I. N., 1951, *Fourier Transforms*, McGraw-Hill, New York, pp. 407–408.
- Timoshenko, S. P., and Goodier, J. N., 1970, *Theory of Elasticity*, 3rd ed., McGraw-Hill, New York, pp. 109–110.

A Kelvin Theorem and Partial Work of Impulsive Forces

A. P. Ivanov¹³

A rigid body under the action of several impulsive forces is considered. A Kelvin theorem provides a simple rule to calculate the total work done by all impulsive forces, but it is not necessarily applicable to the independent work done by each impulse. It is shown that there exist two cases when the partial work can be determined by the same Kelvin formula. Otherwise, the problem has no algebraic solution.

A problem in classical impact theory is to determine the work done by a given impulsive force \mathbf{F} which acts during a short interval $(t', t' + \tau)$ when the impulse is applied to a point A of the body. It was solved by Kelvin and Tait (1867, Art. 308):

$$W = \frac{1}{2}\mathbf{I}(\mathbf{U} + \mathbf{V}), \quad \mathbf{I} = \int_{t'}^{t'+\tau} \mathbf{F}(s)ds \quad (1)$$

where \mathbf{U}, \mathbf{V} denote initial and final velocities of point A .

It is important that the result does not depend on the specific form of function $\mathbf{F}(t)$. The original proof of formula (1) is

¹³Professor, Moscow State Academy of Device and Information, Moscow, Stromynka 20, Russia.

Contributed by the Applied Mechanics Division of THE AMERICAN SOCIETY OF MECHANICAL ENGINEERS for publication in the ASME JOURNAL OF APPLIED MECHANICS. Manuscript received by the ASME Applied Mechanics Division, Nov. 28, 1995; final revision, May 15, 1996. Associate Technical Editor: S. W. Shaw.

valid in any impact conditions, but one should make certain efforts to realize this generality. In particular, Stronge (1992) claimed the Kelvin theorem to be correct only in some particular cases. The detailed and exhaustive proof of formula (1) can be found in a number of textbooks, the most famous of them by Routh (1905, Art. 346).

Furthermore, in the case where there are several impulses \mathbf{I}_k ($k = 1, 2, \dots, n$), which are applied to the same body at different points A_k , their total work can be determined by analogy with (1) (see Kelvin and Tait, Art. 309 or Routh, Art. 384):

$$W = \frac{1}{2} \sum_k \mathbf{I}_k (\mathbf{U}_k + \mathbf{V}_k) \quad (2)$$

where velocities $\mathbf{U}_k, \mathbf{V}_k$ are related to A_k . It appears that formula (2) is calculated by summation of the work done by each of the impacts. However, *in general, none of the terms in (2) equals the partial work done by the corresponding impulse and only their total is equal to the total work*. This statement is contained (without proof) in Kelvin and Tait (Art. 309). The present paper is devoted to the analysis of partial work.

First of all we prove relation (2). We assume the change in position of the body is negligible during the impacts. Then the total work W equals to the change of kinetic energy:

$$W = \Delta T = \frac{1}{2} M (\mathbf{V}^* - \mathbf{U}^*)^2 + \frac{1}{2} (\mathbf{J} \Omega - \omega) - \frac{1}{2} (\mathbf{J} \omega, \omega) \quad (3)$$

where $\mathbf{U}^*, \mathbf{V}^*$ denote the initial and final velocities of the center of mass G ; ω, Ω are the initial and final angular velocities, M is the mass, and \mathbf{J} is the inertia tensor. The equations of impulsive motions have the form

$$\begin{aligned} M(\mathbf{V}^* - \mathbf{U}^*) &= \sum_k \mathbf{I}_k, \\ \mathbf{J}(\Omega - \omega) &= \sum_k \mathbf{r}_k \times \mathbf{I}_k, \quad \mathbf{r}_k = GA_k. \end{aligned} \quad (4)$$

Formulas (3), (4) imply that

$$W = \frac{1}{2} \sum_k \mathbf{I}_k \cdot (\mathbf{V}^* + \mathbf{U}^*) + \frac{1}{2} \sum_k (\mathbf{I}_k, (\Omega + \omega) \times \mathbf{r}_k) \quad (5)$$

which is equivalent to Eq. (2) since by the Euler formula $\mathbf{U}_k = \mathbf{U}^* + \omega \times \mathbf{r}_k$. As regards the work done by a particular impulse \mathbf{I}_j , this has no kinematical interpretation and is calculated by integrating the following relation:

$$\begin{aligned} dW_j &= (\mathbf{u}_j, d\mathbf{i}_j) = (\mathbf{u}^* + \omega^* \times \mathbf{r}_j, d\mathbf{i}_j), \\ \mathbf{i}_j(t) &= \int_{t'}^t \mathbf{F}_j(s) ds \end{aligned} \quad (6)$$

where $\mathbf{u}^* = \mathbf{u}^*(t)$, $\omega^* = \omega^*(t)$ are the velocity of the center of mass and the angular velocity, respectively, $\mathbf{i}_j = \mathbf{i}_j(t)$ — moving impulse of the j th force. According to (4), relation (6) may be transformed to

$$\begin{aligned} dW_j &= (\mathbf{U}_j, d\mathbf{i}_j) + M^{-1} \left(\sum_k \mathbf{i}_k, d\mathbf{i}_j \right) \\ &\quad + (\mathbf{J}^{-1} (\sum_k \mathbf{r}_k \times \mathbf{i}_k), \mathbf{r}_j \times d\mathbf{i}_j) \end{aligned} \quad (7)$$

Formula (7) shows that the value of W_j depends on the character of impulsive forces, i.e., it can not be calculated without specification of the functions $\mathbf{i}_k(t)$. We can determine conditions when W_j can be expressed in a simple formula similar to (1), namely

$$W_j = \frac{1}{2} (\mathbf{I}_j, \mathbf{U}_j + \mathbf{V}_j). \quad (8)$$

The right-hand side in (8) due to (4) can be written in the form

$$\begin{aligned} \frac{1}{2} (\mathbf{I}_j, \mathbf{U}_j + \mathbf{V}_j) &= (\mathbf{U}_j, \mathbf{I}_j) + \frac{1}{2M} \left(\sum_k \mathbf{I}_k, \mathbf{I}_j \right) \\ &\quad + \frac{1}{2} (\mathbf{J}^{-1} (\sum_k \mathbf{r}_k \times \mathbf{I}_k), \mathbf{r}_j \times \mathbf{I}_j). \end{aligned} \quad (9)$$

Equation (8) is valid if and only if the integral of the right-hand side of formula (7) equals the right-hand side of formula (9). This condition has the following form:

$$\begin{aligned} (\mathbf{U}_j, \mathbf{V}_j) &+ \int_{t'}^{t'+\tau} dt \int_{t'}^t \sum_k [M^{-1} (\mathbf{F}_k(s), \mathbf{F}_j(t)) \\ &\quad + (\mathbf{J}^{-1} (\mathbf{r}_k \times \mathbf{F}_k(s)), \mathbf{r}_j \times \mathbf{F}_j(t))] ds \\ &= (\mathbf{U}_j, \mathbf{V}_j) + \frac{1}{2} \int_{t'}^{t'+\tau} dt \int_{t'}^t \sum_k [M^{-1} (\mathbf{F}_k(s), \mathbf{F}_j(t)) \\ &\quad + (\mathbf{J}^{-1} (\mathbf{r}_k \times \mathbf{F}_k(s)), \mathbf{r}_j \times \mathbf{F}_j(t))] ds. \end{aligned} \quad (10)$$

The domains of integration in formula (10) are the square with the side τ and right triangle which is half of this square while the integrands are similar. The correctness of this formula depends on the actual form of functions $\mathbf{F}_i(t)$. It is wrong in general but some particular cases of practical value exist when it is true. Note that formula (10) is valid if for all $s, t \in (t', t' + \tau)$ and for all $k \neq j$

$$\begin{aligned} M^{-1} (\mathbf{F}_k(s), \mathbf{F}_j(t)) &+ (\mathbf{J}^{-1} (\mathbf{r}_k \times \mathbf{F}_k(s)), \mathbf{r}_j \times \mathbf{F}_j(t)) \\ &= M^{-1} (\mathbf{F}_k(t), \mathbf{F}_j(s)) + (\mathbf{J}^{-1} (\mathbf{r}_k \times \mathbf{F}_k(t)), \mathbf{r}_j \times \mathbf{F}_j(s)). \end{aligned} \quad (11)$$

There exist two cases when condition (11) is satisfied; these are connected with a restriction for the direction of impulsive forces and their values.

(i) If the impulsive forces satisfy the following conditions

$$\begin{aligned} \mathbf{F}_j(t) \perp \mathbf{F}_k(s) &+ M(\mathbf{J}^{-1} (\mathbf{r}_k \times \mathbf{F}_k(s)) \times \mathbf{r}_j), \\ \forall s, t, \forall k \neq j, \end{aligned} \quad (12)$$

then both sides of formula (11) vanish. These conditions are fulfilled provided the directions of the impulsive forces are compatible with positions of points A_k . In particular, formulas (12) are correct if the j th impulsive force has constant direction which is parallel to \mathbf{r}_j while each of vectors \mathbf{F}_k with $k \neq j$ is orthogonal to that direction. The similar conclusion can be made in the case any force \mathbf{F}_k with $k \neq j$ is parallel to \mathbf{r}_k while \mathbf{F}_j is orthogonal to all of these vectors, and

(ii) if all impulsive forces have constant directions and there exist a scalar function $\varphi(t)$ and vectors \mathbf{l}_k (which may have arbitrary length) such that

$$\mathbf{F}_k(t) = \varphi(t) \mathbf{l}_k \quad (k = 1, 2, \dots, n). \quad (13)$$

The first of these cases is related to a rather strong restriction for directions of the impulsive forces but these forces might act nonsimultaneously in any order. On the contrary, in the second case all the forces must be synchronous but their direction might be nonorthogonal.

Remark 1. In practice, impulsive forces are associated with mechanical collisions of rigid bodies. In the absence of friction, the impulsive reaction is orthogonal to the body surface at the point of contact. Thus conditions (i) concern the possible location of such points in the case of multiple collision (see Example 1 below). Conditions (ii) may be applied to the collision of two bodies by means of separately calculating the normal and tangential components of the reaction (see Example 2).

Remark 2. In general, when neither of the conditions (i) or (ii) are fulfilled, the value W_j cannot be determined by means of any algebraic formula. Then the calculation of the double integral in the left-side part of formula (10) is necessary. In

particular, the result will depend on the order in which the impulsive forces are applied.

Example 1. Examine the collision without friction of a rigid body with two other bodies. The impulsive forces are collinear with normal vectors $\mathbf{n}_{1,2}$ to the body surface at contact points $A_{1,2}$. The condition (12) has form

$$(\mathbf{n}_1, \mathbf{n}_2) + M(\mathbf{J}^{-1}(\mathbf{r}_2 \times \mathbf{n}_2), \mathbf{r}_1 \times \mathbf{n}_1) = 0. \quad (14)$$

For instance, if at least one of vectors \mathbf{n}_1 or \mathbf{n}_2 is collinear to the corresponding radius vector $\mathbf{r}_{1,2}$ then Eq. (14) requires orthogonality of \mathbf{n}_1 and \mathbf{n}_2 . In the case where a horseshoe hits the ground at two points simultaneously, the vectors \mathbf{n}_1 and \mathbf{n}_2 are collinear, and Eq. (14) coincides with the definition of *center of percussion* (see Routh, Art. 120).

Example 2. Consider the point collision of a rigid body with a massive barrier. The impulsive reaction can be presented as the sum of normal reaction and friction, both forces are

applied at the same contact point A . The work done by the normal reaction can be calculated by the formula

$$W_n = \frac{1}{2} I_n (U_n + V_n) \quad (15)$$

in the following two cases:

- (i) the line GA is normal to the barrier and for any friction law;
- (ii) unidirectional sliding and Coulomb friction and for any orientation of the body.

Note that the second of these cases was discovered by Stronge (1992); he showed that these conditions are satisfied only if during the impulse the changes in velocity are planar.

References

- Kelvin, W. T., and Tait, P. G., 1867, *Treatise on Natural Philosophy*, Vol. 1, Part 1, Clarendon Press, Oxford, UK.
- Routh E. J., 1905, *Dynamics of a System of Rigid Bodies*, 7th ed., Part 1, McMillan, London.
- Stronge, W. J., 1992, "Energy Dissipated in Planar Collision," *ASME JOURNAL OF APPLIED MECHANICS*, Vol. 59, pp. 681–682.

Finite Strain Elastostatics With Stiffening Materials: A Constrained Minimization Model

S. J. Hollister^{14,17} J. E. Taylor,^{15,17}
P. D. Washabaugh^{16,17}

Finite strain elastostatics is expressed for general anisotropic, piecewise linear stiffening materials, in the form of a constrained minimization problem. The corresponding boundary value problem statement is identified with the associated necessary conditions. Total strain is represented as a superposition of variationally independent constituent fields. Net stress-strain properties in the model are implicit in terms of the parameters that define the constituents. The model accommodates specification of load fields as functions of a process parameter.

Introduction

Familiar models for finite strain elastostatics rely on the designation of a proper potential function. The alternative approach described in this note has the form of a constrained minimization problem, where the effective potential is synthesized from individually designated terms each having the form for an elastic-locking material. The quantity being minimized is suggestive of *potential energy*. Also, components of the load vector fields are stated as independent functions of a scalar parameter (process or evolution parameter), and so it is possible within the model to represent general load path. This feature may be exploited to advantage in the design of a test program that is to provide data for the identification of values for the material properties parameters in the model. In the context of the nonlin-

ear problem, each independent load path may provide independent information for the identification of a given material.

The Constitutive Model

Our objective in this section is to establish the above-described model for the finite strain elastostatics of structures composed of nonlinear, stiffening material. This model is expressed in a form consistent with interpretations in continuum mechanics for an arbitrarily inhomogeneous and anisotropic material. The results obtained in what follows are applicable to one, two, or three-dimensional problems in the analysis of any structure having material properties consistent with the present general characterization.

Essentially the same device as the one described in Taylor (1994) is used here to construct the modeling of nonlinear constitutive properties. As was done there, we introduce the notion (following Prager, 1964) of an elastic-locking material, which can be described in terms of a given scalar function $h(\epsilon_{ij})$ and specified \bar{h} as follows:

$$\epsilon_{ij} = \begin{cases} C_{ijkl} \tau_{kl} & \text{when } h(\epsilon_{ij}) < \bar{h} \\ \hat{\epsilon}_{ij} = \text{Arg} [h(\epsilon_{ij}) = \bar{h}] & \text{otherwise} \end{cases} \quad (1)$$

τ_{kl} represents the second Piola-Kirchhoff stress, and compliance tensor C_{ijkl} is independent of the deformation process. A typical stress-strain curve for one dimension is sketched in Fig. 1. For the general locking material of (1), $h(\epsilon_{ij})$ is restricted to functions such that $h(\epsilon_{ij}) - \bar{h} = 0$ defines a closed convex surface (the *locking surface*) in the space of field ϵ_{ij} , and the notation $\hat{\epsilon}_{ij}$ introduced in (1) identifies states on that surface. In the context of a simple locking material, statement (1) represents linear behavior for all strain states corresponding to points interior to this surface. Strain states outside the surface are inadmissible. (This construction for elastic/locking materials is similar in form to the more familiar model for elastic/perfectly plastic material, but with the role of stress and strain interchanged and the yield surface replaced by a locking surface.)

To proceed with the description of the general model, total strain, ϵ_{ij}^T , is defined here in a form that amounts to a composition of a set of such elastic/locking constituents, say ϵ_{ij}^β , combined with a strictly linear component $\hat{C}_{ijkl} \tau_{kl}$. Thus, for each point x in the closed interval Ω_0 which defines the body the total strain is expressed as

$$\epsilon_{ij}^T = \sum_{\beta=1}^{N_A} \epsilon_{ij}^\beta + \hat{C}_{ijkl} \tau_{kl} \quad x \in \Omega_0. \quad (2)$$

¹⁴ Assistant Professor of Surgery and Mechanical Engineering and Applied Mechanics, Orthopedic Research Laboratories, Mem. ASME.

¹⁵ Professor of Aerospace Engineering and Applied Mechanics, Department of Aerospace Engineering.

¹⁶ Associate Professor of Aerospace Engineering, Department of Aerospace Engineering, Mem. ASME.

¹⁷ University of Michigan, Ann Arbor, MI 48109.

Contributed by the Applied Mechanics Division of THE AMERICAN SOCIETY OF MECHANICAL ENGINEERS for publication in the ASME JOURNAL OF APPLIED MECHANICS. Manuscript received by the ASME Applied Mechanics Division, Oct. 10, 1995; final revision, Sept. 5, 1996. Associate Technical Editor: J. N. Reddy.

particular, the result will depend on the order in which the impulsive forces are applied.

Example 1. Examine the collision without friction of a rigid body with two other bodies. The impulsive forces are collinear with normal vectors $\mathbf{n}_{1,2}$ to the body surface at contact points $A_{1,2}$. The condition (12) has form

$$(\mathbf{n}_1, \mathbf{n}_2) + M(\mathbf{J}^{-1}(\mathbf{r}_2 \times \mathbf{n}_2), \mathbf{r}_1 \times \mathbf{n}_1) = 0. \quad (14)$$

For instance, if at least one of vectors \mathbf{n}_1 or \mathbf{n}_2 is collinear to the corresponding radius vector $\mathbf{r}_{1,2}$ then Eq. (14) requires orthogonality of \mathbf{n}_1 and \mathbf{n}_2 . In the case where a horseshoe hits the ground at two points simultaneously, the vectors \mathbf{n}_1 and \mathbf{n}_2 are collinear, and Eq. (14) coincides with the definition of *center of percussion* (see Routh, Art. 120).

Example 2. Consider the point collision of a rigid body with a massive barrier. The impulsive reaction can be presented as the sum of normal reaction and friction, both forces are

applied at the same contact point A . The work done by the normal reaction can be calculated by the formula

$$W_n = \frac{1}{2} I_n (U_n + V_n) \quad (15)$$

in the following two cases:

- (i) the line GA is normal to the barrier and for any friction law;
- (ii) unidirectional sliding and Coulomb friction and for any orientation of the body.

Note that the second of these cases was discovered by Stronge (1992); he showed that these conditions are satisfied only if during the impulse the changes in velocity are planar.

References

- Kelvin, W. T., and Tait, P. G., 1867, *Treatise on Natural Philosophy*, Vol. 1, Part 1, Clarendon Press, Oxford, UK.
- Routh E. J., 1905, *Dynamics of a System of Rigid Bodies*, 7th ed., Part 1, McMillan, London.
- Stronge, W. J., 1992, "Energy Dissipated in Planar Collision," *ASME JOURNAL OF APPLIED MECHANICS*, Vol. 59, pp. 681–682.

Finite Strain Elastostatics With Stiffening Materials: A Constrained Minimization Model

S. J. Hollister^{14,17} J. E. Taylor,^{15,17}
P. D. Washabaugh^{16,17}

Finite strain elastostatics is expressed for general anisotropic, piecewise linear stiffening materials, in the form of a constrained minimization problem. The corresponding boundary value problem statement is identified with the associated necessary conditions. Total strain is represented as a superposition of variationally independent constituent fields. Net stress-strain properties in the model are implicit in terms of the parameters that define the constituents. The model accommodates specification of load fields as functions of a process parameter.

Introduction

Familiar models for finite strain elastostatics rely on the designation of a proper potential function. The alternative approach described in this note has the form of a constrained minimization problem, where the effective potential is synthesized from individually designated terms each having the form for an elastic-locking material. The quantity being minimized is suggestive of *potential energy*. Also, components of the load vector fields are stated as independent functions of a scalar parameter (process or evolution parameter), and so it is possible within the model to represent general load path. This feature may be exploited to advantage in the design of a test program that is to provide data for the identification of values for the material properties parameters in the model. In the context of the nonlin-

ear problem, each independent load path may provide independent information for the identification of a given material.

The Constitutive Model

Our objective in this section is to establish the above-described model for the finite strain elastostatics of structures composed of nonlinear, stiffening material. This model is expressed in a form consistent with interpretations in continuum mechanics for an arbitrarily inhomogeneous and anisotropic material. The results obtained in what follows are applicable to one, two, or three-dimensional problems in the analysis of any structure having material properties consistent with the present general characterization.

Essentially the same device as the one described in Taylor (1994) is used here to construct the modeling of nonlinear constitutive properties. As was done there, we introduce the notion (following Prager, 1964) of an elastic-locking material, which can be described in terms of a given scalar function $h(\epsilon_{ij})$ and specified \bar{h} as follows:

$$\epsilon_{ij} = \begin{cases} C_{ijkl} \tau_{kl} & \text{when } h(\epsilon_{ij}) < \bar{h} \\ \hat{\epsilon}_{ij} = \text{Arg} [h(\epsilon_{ij}) = \bar{h}] & \text{otherwise} \end{cases} \quad (1)$$

τ_{kl} represents the second Piola-Kirchhoff stress, and compliance tensor C_{ijkl} is independent of the deformation process. A typical stress-strain curve for one dimension is sketched in Fig. 1. For the general locking material of (1), $h(\epsilon_{ij})$ is restricted to functions such that $h(\epsilon_{ij}) - \bar{h} = 0$ defines a closed convex surface (the *locking surface*) in the space of field ϵ_{ij} , and the notation $\hat{\epsilon}_{ij}$ introduced in (1) identifies states on that surface. In the context of a simple locking material, statement (1) represents linear behavior for all strain states corresponding to points interior to this surface. Strain states outside the surface are inadmissible. (This construction for elastic/locking materials is similar in form to the more familiar model for elastic/perfectly plastic material, but with the role of stress and strain interchanged and the yield surface replaced by a locking surface.)

To proceed with the description of the general model, total strain, ϵ_{ij}^T , is defined here in a form that amounts to a composition of a set of such elastic/locking constituents, say ϵ_{ij}^β , combined with a strictly linear component $\hat{C}_{ijkl} \tau_{kl}$. Thus, for each point x in the closed interval Ω_0 which defines the body the total strain is expressed as

$$\epsilon_{ij}^T = \sum_{\beta=1}^{N_A} \epsilon_{ij}^\beta + \hat{C}_{ijkl} \tau_{kl} \quad x \in \Omega_0. \quad (2)$$

¹⁴ Assistant Professor of Surgery and Mechanical Engineering and Applied Mechanics, Orthopedic Research Laboratories, Mem. ASME.

¹⁵ Professor of Aerospace Engineering and Applied Mechanics, Department of Aerospace Engineering.

¹⁶ Associate Professor of Aerospace Engineering, Department of Aerospace Engineering, Mem. ASME.

¹⁷ University of Michigan, Ann Arbor, MI 48109.

Contributed by the Applied Mechanics Division of THE AMERICAN SOCIETY OF MECHANICAL ENGINEERS for publication in the ASME JOURNAL OF APPLIED MECHANICS. Manuscript received by the ASME Applied Mechanics Division, Oct. 10, 1995; final revision, Sept. 5, 1996. Associate Technical Editor: J. N. Reddy.

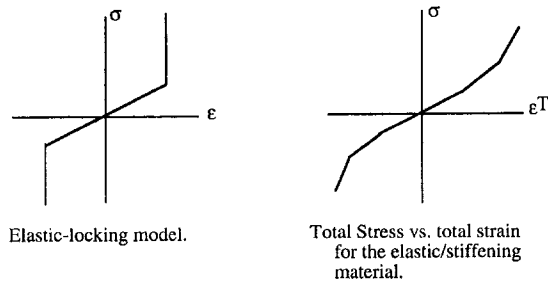


Fig. 1 Typical stress-strain curves according to (1) and (2), for the one-dimensional continuum

Again, each constituent ϵ_{ij}^β in (2) has the form of the elastic/locking material defined in (1), and the number N_A of them is arbitrary. Of course, it is possible that at some point in the loading process all elements ϵ_{ij}^β in this expression become locked. The last term in (2) provides that in this event the total stress-total strain relation is linear for subsequent increase in strain. Between the initial stage of deformation and this fully evolved state, the stress-strain behavior is piecewise linear; this is indicated in Fig. 1 as it would appear for the one-dimensional case. Finally, the finite strain deformation kinematics is described in terms of the Green-Lagrange strain tensor, i.e., total strain is given in terms of displacement u_k by¹⁸

$$\epsilon_{ij}^T = \frac{1}{2}(u_{i,j} + u_{j,i} + u_{k,i}u_{k,j}) \quad x \in \Omega_o. \quad (3)$$

Here the notation is to represent differentiation taken with respect to coordinates X_i of the undeformed structure.

Behavior predicted using the present stiffening material model is similar to what is realized for *fibred collagenous* materials. Typically such "soft tissue bio-material" is composed of wavy collagen fibrils that deform readily until they become straightened, at which point the material becomes substantially stiffer. A simple mechanical analog for this structure exists in the biomechanics literature; e.g., Frisen et al. (1969) and Kwan and Woo (1989). However, their models, which are in effect special cases of (1, 2) expressed for one-dimensional problems, are not readily extended to cover two-dimensional and three-dimensional anisotropic continua.

Our formulation for the continuum analysis is expressed in a form that facilitates prediction of the evolution of structural system behavior with the loading process. As was indicated in the Introduction, the loads themselves are stated in terms of a general "loading program," and it will be confirmed that the formulation is applicable for all load programs that are monotone in the process parameter (see, e.g., Taylor, 1996); the parameter is symbolized here by scalar α . The formulation comprises a statement for elastostatics suited to modeling the general nonlinear material described above, and it is expressed here via the following extremum problem statement:

$$\min_{\alpha, \tau, \epsilon, u} \int_{\Omega_o} \left\{ \frac{1}{2} \hat{C}_{ijkl} \tau_{ij} \tau_{kl} + \frac{1}{2} \sum_{\beta} L_{ijkl}^{\beta} \epsilon_{ij}^{\beta} \epsilon_{kl}^{\beta} - b_i(\alpha) u_i \right\} dV_o - \int_{\Gamma_{ot}} t_i(\alpha) u_i dS_o \quad [P]$$

subject to

$$\alpha - \bar{\alpha} \leq 0 \quad (C1)$$

$$\frac{1}{2}(u_{i,j} + u_{j,i} + u_{k,i}u_{k,j}) - (\hat{C}_{ijkl} \tau_{kl} + \sum_{\beta} \epsilon_{ij}^{\beta}) = 0 \quad x \in \Omega_o \quad (C2)$$

$$h^{\beta}(\epsilon_{ij}^{\beta}) - \bar{h}^{\beta} \leq 0 \quad \forall x \in \Omega_o; \quad \forall \beta \in I_A = \{\beta | \beta = 1, 2, \dots, N_A\}. \quad (C3)$$

Note that minimization in problem [P] reflects variation inde-

pendently with respect to "process parameter" α , and fields τ_{ij} , ϵ_{ij} , and u_k within their admissible sets (admissibility of u_k follows from the conventional requirement for *kinematically admissible displacement*, and so on). Symbols Ω_o and Γ_o identify the domain of the given structure and its loaded boundary, respectively, in the undeformed state. The load program expressed by body force $b_i(\alpha)$ and boundary traction $t_i(\alpha)$ are specified, as are the material properties \hat{C}_{ijkl} , $L_{ijkl}^{\beta} = [C_{ijkl}^{\beta}]^{-1}$, $h^{\beta}(\epsilon_{ij}^{\beta})$, and \bar{h}^{β} . The set of *admissible load programs* consistent with problem statement [P] is identified below. Note that compared to constructions used in more familiar expressions of the "min principle," this characterization of load program amounts to a generalization, one for which the statement of proportional loading appears as a special case.

The constrained minimization problem [P] expresses (formally) what amounts to a generalized version of the "minimum potential energy characterization" for the elastostatics analysis of continuum structures. Accordingly, in what follows an equilibrium boundary value problem statement is identified as part of the "necessary conditions associated with this extremum problem." Also, the constitutive character described via (1) and (2) is incorporated within [P] in implicit form, and this is to be confirmed as well. The compatibility requirement (3) appears in explicit form as constraint (C2) in our model, (C3) simply states the locking limit constraint for each element field, and (C1) expresses an upper bound on process parameter α .

Before proceeding to consider these qualities in detail, we note that this convex, nonsmooth constrained minimization problem is substantiated in terms of established results in the mathematics of nonlinear programming (Clarke, 1983). Uniqueness of the solution to [P] can be confirmed directly as well, using arguments similar to those exploited in conventional modeling of hyperelasticity (e.g., Gurtin, 1981). Also, the min problem form [P] comprises a proper and convenient setting for the development of means for computational solution.

As part of the detailed interpretation of formulation [P], necessary conditions for a minimum of the (constrained) general potential energy objective are examined next. The equations of stationarity with respect to the parameter α , stress τ_{ij} , the β th constituent ϵ_{ij}^{β} of (2), and displacement u_i , are (after some simplification)

$$-\frac{\partial}{\partial \alpha} \left[\int_{\Omega_o} b_i(\alpha) u_i dV_o + \int_{\Gamma_{ot}} t_i(\alpha) u_i dS_o \right] + \Lambda = 0 \quad (4)$$

$$\hat{C}_{rskl}(\tau_{kl} - \lambda_{kl}) = 0 \quad \text{in } \Omega_o \quad (5)$$

$$L_{rskl}^{\beta} \epsilon_{kl}^{\beta} - \lambda_{rs} + \mu^{\beta} \frac{\partial h^{\beta}}{\partial \epsilon_{rs}^{\beta}} = 0 \quad \text{in } \Omega_o, \quad \forall \beta \in I_A \quad (6)$$

$$(\lambda_{ij} F_{mi})_{,j} + b_m(\alpha) = 0 \quad \text{in } \Omega_o \quad (7)$$

$$\lambda_{ij} F_{mi} n_j - t_m(\alpha) = 0 \quad \text{on } \Gamma_{ot}. \quad (7B)$$

Here Λ , λ_{ij} , and μ^{β} are multipliers associated respectively with constraints (C1-3) of [P], and $F_{mi} := \partial x_m / \partial X_i$ represents the deformation gradient tensor. According to the Kurash-Kuhn-Tucker condition $\Lambda \geq 0$. At the same time, generally the derivative of compliance w.r.t. process parameter α differs from zero and so $\Lambda > 0$. In other words, satisfaction of necessary condition (4) implies that compliance is monotone increasing in α . Thus it is clear that formulation [P] is valid only for load programs $b_i(\alpha)$; $t_i(\alpha)$ belonging to the set for which this monotonicity requirement is met.

To continue with the interpretation, from (5) $\lambda_{ij} = \tau_{ij}$, and so $\tau_{ij} \neq 0$ implies through the complementarity requirement associated with (C2) that the total strain is compatible (the constraint (C2) is active). Also, λ_{ij} may be eliminated from (6) to obtain

¹⁸ The development is expressed for Cartesian coordinates without loss of generality.

$$\tau_{rs} = L_{rskl}^{\beta} \epsilon_{kl}^{\beta} + \mu^{\beta} \frac{\partial h^{\beta}}{\partial \epsilon_{rs}^{\beta}} \quad \forall \beta \in I_A \quad (8)$$

and from (7) and (7B) to find

$$(\tau_{ij} F_{mj})_{,j} + b_m = 0 \quad \text{in } \Omega_o \quad (9)$$

$$\tau_{ij} F_{mj} n_j - t_m = 0 \quad \text{in } \Gamma_{ot}. \quad (9B)$$

Thus, loads $b_i(\alpha)$; $t_i(\alpha)$ are equilibrated by total stress τ_{ij} , as should be expected. For the interpretation of (8), in order to distinguish locked fields from the rest, the set I_A of all β indexing constituent fields ϵ_{ij}^{β} is represented in terms of subsets as follows: $I_{AE} = \{\beta \in I_A; h(\epsilon_{ij}^{\beta}) < \bar{h}^{\beta}\}$ and $I_{AL} = \{\beta \in I_A; h^{\beta}(\epsilon_{ij}^{\beta}) = \bar{h}^{\beta}\}$.

Then, since $h^{\beta} < \bar{h}^{\beta}$ implies $\mu^{\beta} = 0$, it follows from (8) that

$$\tau_{rs} = L_{rskl}^{\beta} \epsilon_{kl}^{\beta} \quad \forall \beta \in I_{AE}. \quad (10)$$

In other words, all fields ϵ_{kl}^{β} satisfying the condition that their strain state lies *within* the locking constraint surface are uniformly consistent with total stress τ_{ij} , in a form that corresponds to a simple linear stress-strain relation.

On the other hand, with $h^{\beta} = \bar{h}^{\beta}$ and $\mu^{\beta} > 0$, the result from (8) is

$$\tau_{rs} = L_{rskl}^{\beta} \hat{\epsilon}_{kl}^{\beta} + \mu^{\beta} \frac{\partial h^{\beta}}{\partial \epsilon_{rs}^{\beta}} \bigg|_{\epsilon_{rs}^{\beta}} \quad \forall \beta \in I_{AL} \quad (11)$$

where consistent with the notation introduced earlier, $\hat{\epsilon}_{rs}^{\beta}$ symbolizes strain state on the locking surface. (Note that I_{AE} and I_{AL} intersect on $I_{AC} := \{\beta \in I_A; h^{\beta} = \bar{h}^{\beta} \text{ and } \mu^{\beta} = 0\}$, and $I_A = I_{AE} \cup I_{AE} \cup I_{AC}$.) The second term in (11) may be viewed as a "stress relaxation" associated with the strain constraint $h^{\beta}(\epsilon_{ij}^{\beta}) \leq \bar{h}^{\beta}$. Also, Eq. (11) provides for the evaluation of (multiplier) μ^{β} for those constituent fields having strain state on the locking surface.

To summarize, the interpretation just given provides that the necessary conditions associated with formulation [P] correspond to the requirements of equilibrium, compatibility, and the general form of piecewise linear constitutive relations that was introduced at the beginning of this section. In other words, stationarity in [P] is identified with the general equilibrium boundary value problem statement for finite strain analysis of continuum structures composed of such materials.

Closure

Formulation [P] can be viewed as a generalization of the classical minimum potential energy characterization for finite strain elastostatics in terms of energy potentials. "Total energy" appearing in the objective of [P] sums the norm measures of

the individual constituent fields, which are arbitrary in number, and each of these fields is specified independently in terms of the designated form of its locking surface, the value in the locking constraint that sets the location of that surface, and the various tensors \hat{C}_{ijkl} and L_{ijkl}^{β} . Net material behavior reflects the aggregate effect of the constituent properties, and so matching of the model to a particular material requires designation of all these attributes.

The following points also may be of interest: (1) The approach reflected in the structure of [P] admits extension to an even more versatile form, one where each constituent is itself represented by a potential function (e.g., see Taylor, 1996). (2) The formulation given here may be viewed as a *mixed model* (both stress and deformation fields are represented); this is facilitated by the representation of total strain in the form of its decomposition (2). (3) While it may be argued that formulation [P] is related to the Hu-Washizu principle (see, e.g., Reddy (1984)), in fact it is distinct in the two respects that it has the form of a min problem rather than a stationarity principle, and it makes use of the decomposition of total strain per (2). (4) The present characterization for finite strain analysis of the nonlinear continuum provides a convenient base for the formulation of the optimal material properties design problem (a treatment for optimal design of nonlinear material but modeled with linear deformation kinematics is given in Bendsøe, et al. (1995), and for trusses in Taylor and Washabaugh (1994).

References

- Bendsøe, M. P., Guedes, Jose M., Plaxton, S., and Taylor, J. E., 1996, "Optimization of Structure and Material Properties for Solids Composed of Softening Material," *International Journal of Solids & Structures*, Vol. 33, pp. 1799–1813.
- Clarke, F. H., 1983, *Optimization and Nonsmooth Analysis*, Wiley-Interscience, New York.
- Frisen, M., Magi, M., Sonnerup, L., and Viidik, A., 1969, "Rheological Analysis of Soft Collagenous Tissue: Part I. Theoretical consideration," *Journal of Biomechanics*, Vol. 2, pp. 13–20.
- Gurtin, M. E., 1981, *Topics in Finite Elasticity*, Society for Industrial and Applied Mathematics, Philadelphia, PA.
- Kwan, J. K., and Woo, S. L.-Y., 1989, "A Structural Model to Describe the Nonlinear Stress-Strain Behavior for Parallel Fibered Collagenous Tissues," *ASME Journal of Biomechanical Engineering*, Vol. 11, pp. 361–363.
- Prager, W., 1964, "On Elastic, Perfectly Locking Materials," *Proceedings, 11th International Congress of Applied Mechanics*, H. Gortler, ed., Munich, Springer-Verlag, Berlin.
- Reddy, J. N., 1984, *Energy and Variational Methods in Applied Mechanics*, John Wiley and Sons, New York.
- Taylor, J. E., and Washabaugh, P. D., 1994, "Analysis and Design of Trussed Structures Made of Elastics/Stiffening Materials," *Structural Optimization*, Vol. 8, pp. 1–8.
- Taylor, J. E., 1994, "A Global Extremum Principle in Mixed Form for Equilibrium Analysis with Elastic/Stiffening Material: a Generalized Minimum Potential Energy Principle," *ASME JOURNAL OF APPLIED MECHANICS*, Vol. 61, pp. 914–918.
- Taylor, J. E., 1997, "Generalized Potential Formulations for Elastostatics of Constitutively Nonlinear Structures Under Generalized Loading," *International Journal of Mechanical Sciences*, Vol. 39, No. 5, pp. 537–548.